Iron and Cobalt Based Heterogeneous Catalysts for the Conversion of CO2 to Hydrocarbons

Owen, Rhodri

Award date:
2014

Awarding institution:
University of Bath

Iron and Cobalt Based Heterogeneous Catalysts for the Conversion of CO_2 to Hydrocarbons

Rhodri Ellis Owen

A thesis submitted for the degree of Doctor of Philosophy

Department of Chemistry

University of Bath

January 2014

COPYRIGHT

Restrictions

This thesis may be made available for consultation within the University library and may be photocopied or lent to other libraries for the purposes of consultation

Signed .....

Date .....

Contents

Acknowledgements

First and foremost I would like to express my sincere gratitude to Dr. Matthew Jones for all of his excellent supervision and support throughout the course of my PhD. He has always been willing to help me with any problem I have faced and has genuinely made my PhD a very enjoyable experience. I must also thank Dr. Davide Mattia, Dr. Pawel Plucinski and Dr. Sofia Pascu for all of their guidance and supervision over the last three years. I will honestly miss the friendly environment of our CO_2 group meetings.

I wish to also express an enormous thank you to Dr. Justin O'Byrne for all of his help with multiple aspects of my work. His unfaltering willingness help me with any problem, simple or complex, will always be remembered and appreciated.

Glyn Griffiths is gratefully acknowledged for all of his help with all of the life cycle assessment work. His friendly personality made the collaboration a very enjoyable experience.

Thanks are also due to the EPSRC and University of Bath for their financial support.

Thanks go to all of the members of the Jones, Davidson, Pascu and Mattia groups past and present. A special mention to Carlo, Stuart, Ready and Marek, it was a pleasure to share an office with you. Thanks to Heather, Paul, Sarah, George and everyone else in the new office for keeping me company and sane while I finished off writing my thesis. A special thank you to Lois, Tom and Ben for their friendship over the years. Dan Minett is also thanked for all of his help in the lab over the years.

I must also express my gratitude to all of my friends outside of academia who have always been there when I needed to relax and take my mind off work.

Thank you very much to my Mum and Dad who have always been incredibly supportive of me in whatever I have done.

Last but by no means least I would also like to say a huge thank you to Megan for all of her support and endless patience throughout the course of my PhD (and before). I really appreciate everything you've done for me.

Abstract

Hydrocarbons, currently derived from crude oil, represent a vital source of fuel as well as an important feedstock in many chemical processes. As a result the dwindling crude oil supply is likely to have a significant impact on society. When combined with the long timescale and large cost associated with their substitution it becomes obvious that a new route for hydrocarbon production is essential. CO_2 has been gaining significant attention as a possible feedstock due, in part, to its low cost and renewable nature. The work reported within this thesis focuses on the development of catalysts that are active for both the reverse water gas shift (RWGS) reaction and the Fischer-Tropsch (FT) process simultaneously allowing the direct conversion of CO_2 to hydrocarbons.

Chapter 1 outlines the research carried out to date on the conversion of CO_2 to hydrocarbon products as reported in the literature. A more detailed discussion on the motivation behind this work is given along with an introduction to both the reverse water-gas shift reaction and the Fischer-Tropsch process with a review of the literature associated with both processes. The aims of the work conducted within this thesis are contained at the end of this chapter.

Chapter 2 details the experimental procedures used for the reported catalyst studies. The construction of each of the reactors used is given along with information on the components used. The characterisation methods utilised are introduced and the equipment and conditions used are detailed. Full information on the product analysis is also reported within this chapter.

Chapter 3 reports the results obtained from an investigation into the utilisation of magnesium oxide as a possible catalyst support for iron, cobalt and nickel based catalysts for CO_2 hydrogenation. The use of both palladium and potassium as potential promoters for Fe-MgO and Co-MgO catalysts was also investigated and reported along with the use of mixed MgO-SiO_2 supports for a potassium and palladium promoted iron system.

Chapter 4 investigates in the use of palladium as a potential promoter for use in conjunction with an iron-silica catalyst. This three component system was further optimised for the production of heavier hydrocarbons and a higher CO_2 conversion by the variation of both iron and palladium loading. The environmental impact associated with the preparation of each catalyst was assessed and compared relative to the improved performance through the use of life cycle assessment.

Chapter 5 looks at the use of copper, zinc and gallium as possible promoters for the formation of hydrocarbons from CO_2 over an iron-silica catalyst system. The study was extended to include further metals from Group 11 and Group 13 in order to determine how their promotional

ability varied as you descend each group. The effect of promoter loading was also studied for the indium and gold containing systems.

Chapter 6 includes further studies into the effects of the silica support properties on the performance of an iron-silica catalyst. Further investigations included the influence of reaction conditions such as WHSV, pressure and temperature. From these studies information on activation energies, mass transfer limitations and reaction mechanisms was derived.

Chapter 7 outlines the investigations into the use of cobalt as the main catalyst component for CO_2 hydrogenation. The influence of support properties as well as the effects of introducing a range of different noble, alkali and transition metal promoters was studied. These systematic studies allowed the development and optimisation of a cobalt-based CO_2 hydrogenation catalyst that showed a high CO_2 conversion combined with a good selectivity towards C_2+ hydrocarbons.

Abbreviations

Abbreviation	Definition
ASF	Anderson-Schulz-Flory
BET	Brunauer-Emmet-Teller
BPR	Back pressure regulator
CAMERE	Carbon dioxide hydrogenation to form methanol *via* the reverse water-gas shift
CCS	Carbon capture and storage/sequestration
CCU	Carbon capture and utilisation/usage
CNT	Carbon nanotube
CO_2	Carbon dioxide
CO_2LO	Carbon dioxide to lower olefins
CSTR	Continuously stirred tank reactor
DME	Dimethyl ether
DRIFTS	Diffuse reflectance infrared Fourier transform spectroscopy
EDS/EDX	Energy dispersive X-ray spectroscopy
EIA	Energy Information Administration
FE-SEM	Field emission Scanning electron microscopy
FF	Fossil fuels
FID	Flame ionisation detector
FT	Fischer-Tropsch
FTO	Fischer-Tropsch to olefins
FU	Functional unit
GC	Gas chromatography
GHG	Greenhouse gas
GWP	Global warming potential
HC	Hydrocarbon
HTFT	High temperature Fischer-Tropsch
IPCC	International Panel for Climate Change
ISO	International Standards Organisation
LCA	Life cycle assessment/analysis
LCI	Life cycle inventory
LTFT	Low-temperature Fischer-Tropsch
MFC	Mass flow controller
MS	Mass spectrometry
MTG	Methanol to gasoline
MTO	Methanol to olefins
NEXAFS	Near edge reflectance infrared Fourier transform structure spectroscopy
NRL	Naval Research Laboratory
OSC	Oxygen storage capacity
PGM	Platinum group metal
pXRD	Powder X-ray diffraction
RF	Response factor
RT	Retention time
RWGS	Reverse water-gas shift
SCCM	Standard cubic centimetres
SEM	Scanning electron microscopy
TCD	Thermal conductivity detector
TEM	Transmission electron microscopy
TGA	Thermogravimetric analysis
WHSV	Weight hourly space velocity
WGS	Water-gas shift
XPS	X-ray photoelectron spectroscopy

Publications

Cobalt Catalysts for the Conversion of CO_2 to Light Hydrocarbons at Atmospheric Pressure

Rhodri E. Owen, Justin P. O'Byrne, Davide Mattia, Pawel Plucinski, Sofia I. Pascu and Matthew D. Jones.

Chem. Commun., **2013**, *49*, 11683-11685

Promoter Effects on Iron-Silica Fischer-Tropsch Nanocatalysts: Conversion of Carbon Dioxide to Lower Olefins and Hydrocarbons at Atmospheric Pressure

Rhodri E. Owen, Justin P. O'Byrne, Davide Mattia, Pawel Plucinski, Sofia I. Pascu and Matthew D. Jones.

ChemPlusChem, **2013**, *78*, 1536-1544

Using Life Cycle Assessment to Measure the Environmental Performance of Catalysts and Directing Research in the Conversion of CO_2 into Commodity Chemicals: A Look at the Potential for Fuels from 'Thin-Air'

O. Glyn Griffiths, Rhodri E. Owen, Justin P. O'Byrne, Davide Mattia, Matthew D. Jones and Marcelle C. McManus.

RSC Adv., **2013**, *3*, 12244-12254

Investigations into the Kinetics of CO_2 Hydrogenation for the Formation of Hydrocarbons over Iron-Silica Catalysts

Rhodri E. Owen, Justin P. O'Byrne, Davide Mattia, Pawel Plucinski, Sofia I. Pascu and Matthew D. Jones.

(Manuscript in Preparation)

ChemComm

RSC Publishing

COMMUNICATION

View Article Online
View Journal | View Issue

Cite this: *Chem. Commun.*, 2013, **49**, 11683

Received 5th September 2013,
Accepted 29th October 2013

DOI: 10.1039/c3cc46791k

www.rsc.org/chemcomm

Cobalt catalysts for the conversion of CO_2 to light hydrocarbons at atmospheric pressure†

Rhodri E. Owen,[a] Justin P. O'Byrne,[b] Davide Mattia,[b] Pawel Plucinski,[b] Sofia I. Pascu[a] and Matthew D. Jones*[a]

A series of cobalt heterogeneous catalysts have been developed that are effective for the conversion of CO_2 to hydrocarbons. The effect of the promoter and loadings have been investigated.

One of the "holy grails" for the catalysis community for the 21st century remains the development of robust and cheap systems for the upgrading of CO_2. With the dwindling supply of oil derived chemical feedstocks coupled with uncertainties of supply, now is unequivocally the time to act.[1] The "shale-gas boom" in the US (and Europe) remains, to date, a temporary life-line rather than a long-term solution. Therefore, it is of paramount importance to find a sustainable alternative. We and several other groups across the world have already taken up this research challenge – mainly utilising iron promoted systems for the conversion of CO_2 to hydrocarbons (HCs).[2] Far less attention has been applied to cobalt containing catalysts; this is largely due to their preference to form CH_4.[3] One of the first examples of this catalysis was in 1950 by Miller with a series of activated cobalt systems.[4] In more recent years examples of active catalysts include those of Somorjai who have prepared cobalt nanoparticles on MCF-17 mesoporous silica with the major products being CH_4 and CO.[5] It is observed that platinum can act as a promoter for such processes. Willauer and co-workers have investigated a Co–Pt/Al_2O_3 system for the conversion of CO_2 to HCs.[6] The lowest selectivity to CH_4 being 93.1% (T = 220 °C, P = 275 psi, $H_2:CO_2$ 1 : 1) higher selectivities towards CH_4 where observed with $H_2:CO_2$ ratios of 2 : 1 and 3 : 1. It was hypothesised that changing this ratio lowered the methanation ability of the catalysts and conversely favoured chain growth.

In this paper we report the utilisation of a new series of cobalt-containing heterogeneous catalysts for the conversion of CO_2 to HCs at atmospheric pressure. The catalysts were prepared by the wet impregnation of the appropriate metal salts on the silica support.†[7] The catalysts were characterised by TEM, SEM, XPS and pXRD.† From XPS and pXRD the cobalt is present as Co_3O_4. Initial catalytic results are shown in Table 1, the cobalt only system (entry 1) gave good conversion but to predominately CH_4, analogous to literature precedent.[4–6] It has been shown that the addition of a noble metals has a beneficial effect upon the catalysis.[8] It has also previously been shown that adding alkali metals with cobalt increases selectivity to heavier HCs (for traditional FT reaction).[9] Furthermore, in traditional FT catalysis the olefin–paraffin ratio increases with addition of alkali metals.[10] Thus, we tested a range of Co:Pd:K systems Table 1 entries 2–9 with palladium present to aid CO production and potassium to increase selectivity to heavier HCs. A cobalt loading of 20 wt% was found to be optimal in terms of conversion but with higher loadings producing lower quantities of CH_4. Increasing potassium loading was found to reduce selectivity towards CH_4 and led to an increased yield of heavier HCs, this occurs at the cost of conversion with high potassium loadings leading to lower CO_2 conversion. Comparing entries 1 *vs.* 4 *vs.* 9 it is clear that for this system there is no advantage, in-terms of selectivity, adding palladium to the catalyst. Comparing entries 1 and 9 there is a dramatic reduction in conversion, with a concurrent increase in selectivity to heavier HCs. As expected the palladium containing systems produced lower level of olefins, entry 4 *vs.* 9, compared to the potassium promoted system.

The pore diameter of the SiO_2 was varied (60, 250, 500 Å) Table 1 entry 4 (60 Å) *vs.* Table 2 entries 1 and 2. Generally as the pore diameter is increased the HC yield decreases, however a noticeable increase in selectivity away from CH_4 is observed. However, the same trend is not observed for the 20 wt%Co/1 wt%K/SiO_2 system. Noteworthy, is that the large pore diameter silica appears to facilitate the formation of slightly larger crystalline phases, which maybe related to the enhanced selectivity.†[11] To assess the potential to scale-up this catalyst system a larger particle size support was utilised, Table 2 entry 3. There was a reduction in conversion compared to the 35–70 μm material (Table 1, entry 4) potentially due to diffusional effects; HC distribution was however observed to remain similar. The removal of all promoters, giving a 20 wt%Co/SiO_2_500 catalyst (Table 2 entry 8) resulted in almost exclusively CH_4 formation as observed with the use of 60 Å pore size silica (Table 1, entry 1) showing the use of larger pore size silica alone

[a] *Department of Chemistry, University of Bath, Claverton Down, Bath BA2 7AY, UK. E-mail: mj205@bath.ac.uk; Fax: +44 (0)1225 386231; Tel: +44 (0)1225 384908*
[b] *Department of Chemical Engineering, University of Bath, Claverton Down, Bath BA2 7AY, UK*

† Electronic supplementary information (ESI) available: Synthesis, characterisation details and tentative mechanism. See DOI: 10.1039/c3cc46791k

Owen, R. E., O'Byrne, J. P., Mattia, D., Plucinski, P., Pascu, S. I. and Jones, M. D. (2013), Promoter Effects on Iron–Silica Fischer–Tropsch Nanocatalysts: Conversion of Carbon Dioxide to Lower Olefins and Hydrocarbons at Atmospheric Pressure. ChemPlusChem, 78: 1536–1544. doi: 10.1002/cplu.201300263

O. Glyn Griffiths, Rhodri E. Owen, Justin P. O'Byrne, Davida Mattia, Matthew D. Jones and Marcelle C. McManus (2013) Using life cycle assessment to measure the environmental performance ofcatalysts and directing research in the conversion of CO2 into commodity chemicals: a look at the potential for fuels from 'thin-air'. RSC Advances 30(3) p.12244-12254 DOI: 10.1039/C3RA41900B

1 Introduction

Atmospheric carbon dioxide (CO_2) levels have continued to increase annually according to the International Panel for Climate Change (IPCC).[1] This continuous rise in CO_2 emissions can largely be attributed to anthropogenic factors originating from the increased consumption of fossil fuels since the industrial revolution in the mid 1700's. CO_2 levels increased 80% between 1970 and 2004[1] with the atmospheric concentration recently passing the symbolic 400 ppm mark (40% higher than the pre-industrial level[2]). CO_2, a greenhouse gas (GHG), is an established cause for these rising global temperatures. This can lead to a number of negative environmental effects such as the melting of the polar ice sheets,[3] increased desertification of the tropics,[4] rising sea levels[5] and ocean acidification to name but a few. Baseline CO_2 emissions are predicted to continue this increase from current levels (approximately 30 $GtCO_2$) up to 57 $GtCO_2$ by 2050 if no measures to reduce release are implemented.[6]

Global warming is a recognised worldwide problem and as a result many governments have pledged to reduce the long-term emissions of GHGs in an attempt to combat the problem. The majority of current CO_2 emissions are however from developed and societally dependent technologies. With carbon emitters intrinsic in their usage the emissions from these sources are unlikely to see any large decrease in the foreseeable future.

Several possibilities are currently being considered and investigated to reduce CO_2 emissions. The first and most obvious suggestion is the replacement of fossil fuels by carbon neutral energy sources such as renewable energy (solar, wind and hydro) and nuclear power. Nuclear power possesses large capital costs and when combined with its unpopular reputation in public opinion it seems an unlikely alternative. With the insatiably high demand for energy in some developing countries, such as India and China, CO_2 emissions from fossil fuel based power is set to continue to increase.

Another possibility is carbon capture and storage/sequestration (CCS) where waste CO_2 from power plants or other large point sources is captured and its release into the atmosphere prevented. The storage generally involves the transportation of the captured CO_2 to a suitable location where it is injected into geological formations. While CSS is one of the more developed processes for reducing emission of CO_2 with many plants planned and already in operation[7] it does possess several problems. For one, it is not suitable for all types of carbon emissions, sites must be close to safe sequestration sites, CO_2 concentrations must be high and it is not suited to small to medium sized sources. Many risks are also associated with CCS such as the possibility of leakage of storage reservoirs and unknown effects on the environment.[2] High cost and high energy demands also decrease the appeal of CSS as a solution to rising CO_2 levels. It is estimated that an extra 30% of fuel is required to capture the CO_2 (transportation and

sequestration requires further energy)[2] resulting in significantly reduced efficiency in reduction of CO_2 emissions.

The most promising possibility is carbon capture and utilisation/usage (CCU). This is where the captured CO_2 is used either directly or utilised as a carbon feedstock for the production of chemicals and fuels. CO_2 has for a long period been thought of as an unwanted waste product but with its low cost and availability in large quantities at point sources combined with the socio-political pressure for companies to reduce the amount released there are increasing attempts to consider it as a resource and a business opportunity.

The low (or even negative) cost of CO_2 has already seen it used as a refrigerant, in the food industry and as a feedstock in a limited number of processes such as the synthesis of urea for nitrogen fertilizer and plastic production, synthesis of salicylic acid for the pharmaceutical industry and for polycarbonate production. These uses are, however well established and unlikely to grow much further. Polycarbonate, for example is most important large volume CO_2 based polymer (2.9 million tonnes in 2009) and is expected to grow at a rate of 3-5% over the next few years which will lead to a use of 0.1-0.2 Mt a^{-1} by 2020 which equates to 0.005% of the estimated amount of CO_2 available.[6] This value is not significant enough to have an impact on the reduction in CO_2 emissions. As a result new target products are needed.

Fossil fuels (FF) provide 81 % of the global primary energy supply.[8] Studies by the International Energy Agency estimate that they will remain the main energy source up to 2050 and beyond.[6] Table 1.1 shows the percentage share of global energy consumption for 2011.[2] Crude oil was found to be the most important primary energy resource and largest contributor with a share of approximately 31 %. The remaining share is dominated by two other FF sources, coal and natural gas with 28 % and 22 % contributions respectively.

Table 1.1 – The fuel shares of global consumption in 2011[2]

	Percentage share of global energy
Crude Oil	30.8
Coal	28.3
Natural Gas	22.1
Nuclear	4.6
Hydro-electrical	6.0
Traditional Biomass	6.7
Other (renewables)	1.5

Fossil fuels are a finite resource, Table 1.2 summarises the estimated reserves in 2010.[2] The International Energy Agency research suggests that conventional oil (non-conventional oil

consists of heavy crude oil with a density > 1000 kg m^{-3}, oil sand and oil shale) may have already reached its peak in 2006.[9] The dwindling supplies of conventional oil combined with the limited availability of non-conventional oil are predicted to have a significant influence on oil prices. The US Energy Information Administration (EIA) predicts[10] that it is likely that price of oil will double over the next few decades with a 2035 price of $210 per barrel likely. Combined with its heavy usage as a fuel, crude oil also provides a range of hydrocarbons that are essential raw materials for a variety of chemical industries.

Table 1.2 - The fuel reserves and consumption in 2010[2]

Fuel Type	Consumption (10^9 toe a^{-1})	Reserves (10^9 toe)
Conventional Crude Oil	3.9	169
Non-Conventional Crude Oil[a]		48
Conventional Natural Gas	2.9	172
Non-Conventional Natural Gas[b]		3
Coal	3.9	508

[a] – Oil sand, oil shale and high density oil (>1000 kg m^{-3}) [b] – Shale gas.

For all the reasons above hydrocarbons traditionally derived from crude oil are the ideal targets for synthesis from CO_2. The use of crude oil based fuel is approximately 3 billion tons per year which is theoretically equivalent to almost all of the CO_2 emitted by FF power plants. When combined with the crude oil consumed as feedstocks for the chemical industry this gives a value large enough to have an impact on total CO_2 emissions. While CO_2 will be produced from the combustion of the synthesised FF since they are prepared from CO_2 the overall influence on the environment in terms of CO_2 emissions will be greatly reduced provided energy for the process is also derived from renewable sources.

CO_2 is the end product of the combustion of any carbon source and as a result is relatively stable lying in a potential energy well with a standard enthalpy of formation of -393.51 $kJmol^{-1}$. The oxygen moieties in CO_2 demonstrate a weak Lewis basicity while the carbon atom is electrophilic. This has resulted in the majority of CO_2 activation reactions relying on the nucleophilic attack of this central carbon. CO_2 can also be activated by adsorption on solid surfaces. While there are several possibilities for the activation of CO_2 all require the thermodynamic energy barrier that exists to be overcome and as such require the input of energy. If a more environmentally friendly process with a net reduction in CO_2 emissions relative to current processes for hydrocarbon production is to be achieved energy cannot be derived from FF sources. To obtain a sustainable process the energy must be obtained from renewable sources.

Renewable energy sources have long been termed ‘alternative energy’ however their use has increased so much recently that the Economist[11] has called for this term to be dropped as renewable power becomes the norm. Hydroelectric plants provide 16 % of the world’s power, wind farms currently provide 2 % of the world’s power and their capacity is expected to double over the next few years. The real potential in the renewable energy sector, however, lies in photovoltaics. While currently only contributing 0.25 % of the world’s energy supply it showed a growth of 86 % in the last year alone due to large reductions in cost as the technology develops. The price per watt has dropped from $77 in 1977 down to $0.74 in 2013. Conventional, FF fuelled power station construction costs currently come in at approximately $5 per watt.

The main problem stunting the growth of renewable energies such as wind and solar has the potential to actually be solved when they are used as the energy source for CO_2 conversion. When relying on wind or the sun as your source of energy the reliability of supply is a crucial factor and as a result energy must be stored during times of low demand and high production to be used at peak times or when only low electricity production is possible in order to be able to give a constant energy supply. A range of different techniques are currently being studied as possibilities to store this power. Storage of compressed air in the ground, pumping of water into reservoirs are two techniques being considered but are generally considered too inefficient. The direct conversion to chemical energy is the most attractive process.

While hydrogen may appear an obvious choice as target chemical for production problems with storage (compression or liquefaction require energy) and transport reduce its attractiveness. It also has a low volumetric energy density even when liquefied relative to other possible targets (Table 1.3).[12] Liquid hydrocarbons on the other hand exhibit a high volumetric energy density, can be stored and transported easily and with the existing demand, infrastructure and distribution make an excellent chemical store for excess electricity. As such the synthesis of hydrocarbons from CO_2 and H_2 has begun to attract increasing attention.

Table 1.3 - The volumetric energy densities of different possible chemical energy carriers. Adapted from [2, 12]

Chemical energy Carrier	Volumetric energy density (GJ m^{-3})
Diesel	35.9
Ethanol	21.2
Compressed Natural Gas[a]	8.5
Liquefied Natural Gas[b]	21.0
Compressed Hydrogen[c]	4.7
Liquefied Hydrogen[d]	8.5

[a]: 273.15 K, 2 0MPa. [b]: 113.15 K, 0.1 MPa. [c]: 273.15 K, 70 MPa. [d]: 20.15 K, 0.1 MPa.

The hydrogenation of CO_2 to hydrocarbons can be achieved *via* a number of different direct or indirect routes. Direct routes generally form lower value products such as the Sabatier reaction, which involves the direct hydrogenation of CO_2 to form methane.[7] Methanation reactions however, have a large hydrogen consumption and provide the same storage problems as hydrogen. Indirect routes can either be achieved using multistep processes or through the use of hybrid catalysts that are active for both steps.[7] Indirect pathways first convert CO_2 to a more reactive intermediate such as methanol or carbon monoxide (CO), this intermediate can then be converted to the end products *via* the Methanol to Gasoline (MTG) process or Fischer-Tropsch (FT) synthesis. While the methanol mediated route is possible, the Fischer-Tropsch route is preferable with a vast amount of information available on FT catalysts with several plants currently running based on a CO feedstock.[13] The first step involves another well-known reaction, the conversion of CO_2 to CO through the reverse water-gas shift (RWGS) reaction. It is this CO meditated method that is currently attracting the majority of the attention with the US Naval Research Laboratory (NRL), one of the most advanced CO_2 to hydrocarbon processes, preferring this route.[14]

The CO_2 source used as a feedstock for the hydrogenation reactions must be as pure as possible in order to obtain maximum efficiencies from the overall process as any contaminants in the stream may negatively affect catalyst performance. Flue gas presents itself as a mostly untapped carbon source; the separation of CO_2 from other components, such as water which has been shown to have a negative effect on both RWGS and FT processes, has posed a challenge.[15] Recent work by Jess *et al.*[16] has shown that this CO_2 can be separated from the flue gas with reasonable energy consumption. Other options include capture directly from the atmosphere, again work by Jess *et al.*[16] showed this to be possible with reasonable energy consumption. Not all of the CO_2 emitted from fossil fuel combustion is released into the atmosphere. Vast quantities are dissolved into the ocean causing rising acidity resulting in many

negative environmental effects. This has caused the ocean to have concentrations of CO_2 approximately 140 times greater than that available from the atmosphere. As a result there is currently a great deal of interest in obtaining CO_2 from seawater. The US NRL has based their program for the development of a technology for converting CO_2 to jet fuel on obtaining CO_2 from seawater.[14]

In order to optimise the process both in terms of economic factors and sustainability the hydrogen used must be obtained from renewable sources. There are a range of different techniques currently being investigated for the renewable production of hydrogen. These processes include bio-routes involving cyanobacteria and green algae,[17] electrolysis of water[18] powered by either wind or solar energy and even the use of 'Stranded hydrogen', H_2 formed as a by-product of industrial processes that currently has no use (for example in Japan it is currently estimated[6] that oil refineries are producing 4.7 billion cubic meters of 'waste' H_2).

One technology for renewable hydrogen production that is of particular interest the application of CO_2 hydrogenation is the process currently under development by Rau *et al.*[19] The group has developed and demonstrated on a lab scale a process which removes and stores CO_2 whilst also generating carbon negative renewable H_2. The technology relies on the acidity produced from the electrolysis of seawater to accelerate the dissolution of abundant silicate minerals producing renewable H_2. The remaining electrolyte solution containing a high concentration of OH^- anions can then be used to capture CO_2, either from waste gases or the atmosphere in the form of carbonates. Although so far only performed at lab scale the simplicity of the process combined by its use of widely available starting materials mean scale up to an efficient capacity is entirely possible with work currently continuing to this end.

In summary CO_2 levels are rising rapidly with many negative environmental consequences. New technologies are desperately needed to reduce the amount released into the atmosphere. Although CCS is attracting a lot of attention its high costs and relatively small effect on CO_2 concentrations means other techniques need to be developed further. CDU is one of the most promising techniques currently being studied as it has the ability to have a significant effect on CO_2 levels. The formation of hydrocarbons is the most ideal target due to their high demand and ability to fit right into current infrastructure. When developing such a process the sources of energy and other reactants must be considered carefully in order for the process to be as sustainable and environmentally friendly as possible.

1.1 The Forward and Reverse Water-Gas Shift Reactions

The water-gas shift (WGS) reaction was first reported in 1888.[20] It is the combination of carbon monoxide and water to give carbon dioxide and hydrogen. The mildly exothermic reaction is shown in Equation 1.1.

$$H_2O + CO \rightleftharpoons CO_2 + H_2$$

Equation 1.1 – The water-gas shift reaction

Since its initial discovery the WGS reaction has become increasingly important in industrial applications. Its current primary use is in the production of high purity hydrogen for hydrogen fed industrial processes. The Haber process, for example, requires a source of hydrogen and a low concentration of CO (a common contaminant in H_2 production). As such the WGS reaction is employed as it reduces the CO concentration whilst also producing hydrogen.[20] Recently there has been a renewed interest in the reaction for use in conjunction with fuel cell power generation.[21] The WGS reaction provides the ideal means for CO removal from the hydrogen required as a fuel, which can be harmful to the platinum electrode.[22] With the envisioned use of small-scale fuel cells in transportation, more efficient catalysts are required.

The WGS reaction is also an important process in Fischer-Tropsch chemistry. Iron based catalysts, one of the most common metals used for the FT, have phases that are also WGS active resulting in process becoming one of the most important side reactions.[23] This WGS activity can be either beneficial or detrimental to the FT process depending on the reaction feed-gas. Water is produced as one of the main products in FT synthesis; this can then react with CO from the CO/H_2 feed-gas to produce further H_2 and CO_2. If the CO/H_2 ratio of the feed-gas is high this is beneficial to the process as the produced hydrogen helps to develop the optimal ratio. Cobalt catalysts, another of the most commonly used metals for the FT process is not WGS active.[24] As a result many attempts to impart WGS activity have been attempted using promoters known to be WGS active to try and recreate the *in situ* H_2 formation observed in the analogues iron systems.[25] The presence of such promoters has, however, been shown to undesirably affect the product selectivity of the cobalt based catalysts.

Although the WGS reaction can be useful under certain conditions, such as a hydrogen lean synthesis gas, work has shown that it can also begin to compete with the Fischer-Tropsch reaction. Work by Pirola *et al*.[26] showed that at higher temperatures, on catalysts with high iron loading, the formation of CO_2 *via* WGS becomes the predominant reaction and greatly reduces conversion to hydrocarbons.

The WGS reaction is an equilibrium reaction and at higher temperatures the slightly endothermic reverse water-gas shift (RWGS) reaction, shown in Equation 1.2, begins to become favorable.

$$H_2 + CO_2 \rightleftharpoons CO + H_2O,\ \Delta H = +41.2 kJmol^{-1}$$

Equation 1.2 – The reverse water-gas shift reaction

Generally, the RWGS reaction has been seen as an unfavourable reaction, producing CO that can be highly detrimental to some systems. As a result the majority of WGS catalysts are designed to work at as low a temperature as possible to direct the reaction towards the formation of H_2 and CO_2. The RWGS reaction has however begun to attract increasing attention recently. It is seen as a key reaction in carbon dioxide utilisation. The hydrogenation of CO_2 is the first step in a range of different processes for the formation of many commercially important chemicals. For example the CAMERE (CArbon dioxide hydrogenation to form MEthanol *via* the REverse water-gas shift reaction) process currently generating interest[27] uses the RWGS reaction to produce methanol *via* the conversion of CO_2 to CO. The formation of syngas (CO/H_2) from CO_2 *via* RWGS reaction also opens the door to a whole range of hydrocarbons with many syngas fed processes already well know and industrially used.[28]

Given the high stability of CO_2, a large amount of energy is needed for its hydrogenation to CO and H_2O. The reaction is thermodynamically favoured at higher temperatures. The equilibrium for the process can also be forced to the right and towards the formation of CO by increasing the concentration of either reactant. Increasing the CO_2 concentration forces the complete consumption of H_2, while high amounts of H_2 will increase the consumption of CO_2. It is the latter of these two options that will be most useful for CO_2 utilisation as it encourages CO_2 consumption while ensuring that H_2 is still present to give a syngas (CO/H_2) product stream ready for use in the consecutive process.

The removal of products upon formation should also help force the equilibrium to the right. A catalyst active for both the RWGS reaction and the following consumption of CO/H_2 to the final product would be beneficial for this reason. As soon as CO is formed it could be consumed forcing the further conversion of CO_2 to CO. An alternative or possibly complimentary process would be the removal of water, also formed during the RWGS, with its removal having a similar effect to the consumption of CO. Water removal could be achieved using a number of different processes such as a desiccant bed or a membrane permoselective to water.[7]

1.1.1 Catalysts for the Forward and Reverse Water-Gas Shift Reaction

In general, for reversible reactions, heterogeneous catalyst that produce good rates of reaction in the forward process also show a high rate of reaction in the reverse process.[29] This proves to be true for the WGS reaction with the majority of catalysts active in the direct WGS process also effective for the reverse reaction.

Copper based catalysts are one of the most commonly used systems industrially for the WGS reaction. In these commercial catalysts zinc oxide is generally used as a structural stabiliser and promoter.[30] The Cu/ZnO catalysts are often supported on Al_2O_3 as despite alumina's inactivity it has been found to improve catalyst dispersion and prevent sintering.[31] $Cu/ZnO/Al_2O_3$ systems have been employed industrially since the 1960s and are used effectively in both low (180-250 ^oC) and mid (220-350 ^oC) temperature processes.[32] They have shown activity at temperatures as low as 200 ^oC.[33] The systems have been the subject of extensive studies with much emphasis based on catalyst preparation techniques[22] kinetics[34] and reaction mechanisms.[35] Improved catalyst activity has also been reported upon the addition of alkali metals[36] and manganese.[32] The $Cu/ZnO/Al_2O_3$ systems do possess some drawbacks. They are highly susceptible to poisoning[31] and are also pyrophoric.[7]

Iron oxide catalysts are another of the most widely studied and used WGS catalysts.[20] Iron oxide-chromium oxide catalysts have been used extensively in industry. They were employed prior to the discovery of copper based systems and are typically used at higher temperatures in the 310-450 ^oC range. The systems are based on magnetite (Fe_3O_4), the main iron phase along with hematite (Fe_2O_3) thought to be responsible for the WGS activity observed in FT synthesis. When used alone the rapid thermal sintering of the iron oxide species can greatly reduce the catalyst's lifetime. Chromium oxide (Cr_2O_3) is regularly employed as a structural promoter for the system helping to prevent the sintering of the magnetite. The ratio of iron oxide to chromium oxide varies but generally a 12:1 Fe:Cr ratio is utilised.[31] While the iron-chromium oxide systems show a lower activity than the copper based catalysts they are far more tolerant to poisoning.[31]

Many attempts have been made to improve the performance of the standard iron oxide – chromium oxide catalysts. Work by Rhodes *et al.*[37] focused on the effects of adding a range of different promoters in addition to the iron and chromium oxides. Their studies showed that the addition of 2 wt% of Hg, Ag, Cu and Ba can improve catalyst performance. While Cr_2O_3 is used industrially, low activity and the environmental concerns associated with its use has led to several studies investigating the use of a range of replacement dopants that can be more environmentally friendly while also improving catalyst performance. Natesakhawat *et al.*[38] found after testing a range of different metals, that aluminium in the form of its oxide, Al_2O_3 proved effective for the stabilisation of the active iron species. Although activity was not as high as the analogous iron-chromium system the addition of small amounts of copper to the system could improve catalyst activity further. Work by Júnior *et al.*[39] has also shown that the replacement of Cr_2O_3 with vanadium oxide leads to a catalyst system with an activity much higher than that observed for a commercially available iron and chromium oxide sample.

Iron oxide, specifically Fe_2O_3, has also begun to attract attention as a possible support for WGS catalysis. Basińska *et al.* reported that ruthenium supported on iron oxide gave a good CO conversion with a very low methane selectivity.[40] The main focus of iron oxide supported

catalysts has been on the use of gold. Gold has been gaining significant attention in the field of heterogeneous catalysis since the discovery of the catalytic activity of gold nano-particles by Haruta *et al.*[41] The ability of these systems to oxidise carbon monoxide at very low temperatures has resulted in gold-based catalysts being studied with increasing interest for the WGS reaction. A range of different supports have been investigated such as Fe_2O_3, TiO_2[42] and CeO_2.[43] It is thought that the success of these supports can be attributed to their reducibility with non-reducible supports such as Al_2O_3 proving far less successful.[42] Au/Fe_2O_3 systems have shown conversions of over 80 % to CO at 200 ^oC even at high hourly space velocities.[44] These systems have also been reported active at temperatures below 150 ^oC.[45]

Another catalytic support generating a great deal of interest currently is cerium dioxide. The high oxygen storage capacity (OSC) is thought to play an important role in the support's suitability for the WGS shift reaction. The majority of work has focused on the use of platinum group metals (PGMs).[46] Studies have shown that platinum supported on CeO_2 outperforms both palladium and rhodium[47] and as a result Pt/CeO_2 catalysts have been the focus of the majority of studies.[48] These investigation have led to the development of a $2wt\%Pt/CeO_2$ catalyst by NexTech materials[49] that is reported to have a higher activity than conventional copper based WGS catalysts in the medium temperature range with high stability while also being non-pyrophoric. While PGMs have been the focus of the research, a range of other metals have also been studied such as iron, cobalt,[50] nickel and copper.[32] Nickel and copper catalysts showed an increased activity over CeO_2 alone and exhibited a higher thermal stability relative to the more traditional Cu/ZnO based catalyst systems allowing for a wider range of operating temperatures.[32] The nickel systems were shown to possess a similar catalytic activity to Pd/CeO_2. While cobalt and iron catalysts supported on ceria have been shown to be effective for WGS catalysis their activity was lower than that observed for the copper and nickel systems.[50]

Although copper, iron oxide and ceria catalysts represent the main focus of research into WGS catalysis other more novel catalyst systems are still receiving attention. In particular NiMo-sulfide[51] and CoMo-sulfide[52] catalysts are promising systems for industrial use as both show a high catalytic activity and possess a high sulfur tolerance. Catalyst performance can be improved further by the addition of alkali metals such as potassium to the NiMo-S[53] and CoMo-S[54] systems. The potassium addition can modify the properties of the support (typically Al_2O_3) affecting the reducibility of the molybdenum species present.[53-54] Mo^{IV} and Mo^{V} are thought to play an important role in catalytic activity and as such this change in reducibility can be advantageous. Alkali metal addition can adversely affect the catalyst stability. Cobalt based catalyst systems have also been successful when used in conjunction with V, W,[21] Cr[55] and Mn[56] oxides.

Investigations into the RWGS reaction have generally focused on the same catalyst systems as those studied for the direct WGS process. Copper based catalyst systems have been shown to be effective for the process[57] with mixed Cu/ZnO systems again the focus of

research.[58] More extensive research has also been conducted on the use of ZnO/Al_2O_3 systems not containing copper.[59] Iron oxide systems have also been studied in conjunction with Cr_2O_3[60] with other oxides such as V_2O_5[61] and SiO_2[62] also proving successful replacements for Cr_2O_3. PGMs such as platinum and palladium have proved particularly successful as catalysts[29, 63] especially when supported on reducible supports such as TiO_2[64] and CeO_2.[65] The performance of platinum systems has also been improved with promotion using the alkaline earth metals Mg and Ca.[66]

1.1.2 Mechanisms of the Forward and Reverse Water-Gas Shift Reactions

As vast number of reports have focused on the mechanism of the forward and reverse water gas shift reactions[67] but it still remains a controversial area. Most groups agree that the reaction proceeds *via* one of two mechanisms. These are the surface redox/oxygen adatom and the associative/formate decomposition mechanism.

The surface redox mechanism begins with the dissociative adsorption of a CO_2 molecule to give a surface bound CO and O. Hydrogen present in the reaction mixture is also dissociatively adsorbed to give surface hydrogen species. The carbon monoxide then desorbs from the surface to give gaseous carbon monoxide and the oxygen reacts with hydrogen species present to give water. The reactions involved in the mechanism are summarised in Equation 1.3[68] where *a* represents an adsorbed species.

$$CO_{2(g)} \rightleftharpoons CO_a + O_a$$

$$CO_a \rightleftharpoons CO_{(g)}$$

$$H_{2(g)} \rightleftharpoons 2H_a$$

$$H_a + O_a \rightleftharpoons OH_a$$

$$H_a + OH_a \rightarrow H_2O_a$$

$$H_2O_a \rightleftharpoons H_2O_{(g)}$$

Equation 1.3 – The redox mechanism for the WGS reaction[68]

Despite much research it still remains unclear as to the precise mechanism of OH_a formation. It is either the elementary step shown above in Equation 1.3 or the water catalysed process shown in Equation 1.4.[68]

$$H_2O_a + O_a \rightleftharpoons 2OH_a$$

$$H_a + OH_a \rightleftharpoons H_2O$$

$$\text{Net:} \quad H_a + O_a \rightleftharpoons OH_a$$

Equation 1.4 – Water catalysed formation of OH_a[68]

Mechanistic studies by Fujita *et al.*[58] over Cu/ZnO catalysts strongly suggested that the RWGS reaction proceeds *via* the redox mechanism. They concluded that the CO_2 oxidised the Cu(0) surface to form Cu(I) with a surface bound oxygen and CO. This oxidation of the surface with CO_2 was determined to be the rate-determining step. Hadden *et al.*[69] showed that carbon monoxide can be formed from CO_2 on the surface of copper without the addition of any hydrogen to the reactant gas mixture. This strongly supports the redox mechanism as the formate mechanism cannot account for the formation of CO in absence of hydrogen. Further work has shown that the rate of dissociation of CO_2 is nearly equal to the rate of the RWGS reaction. Kinetic studies based on the redox mechanism by Ernst *et al.* match well with their experimental work providing further support for this mechanism.[68]

Some authors favour the formate decomposition mechanism whereby carbon monoxide is formed through a formate intermediate. Hydrogen dissociatively adsorbs to the catalysts surface and reacts with gaseous carbon dioxide to give a formate. This intermediate then decomposes to form a surface bound CO and OH. The CO desorbs and the OH forms water through the addition of another surface bound hydrogen. This mechanism is summarised in Equation 1.5[67c]

$$H_{2(g)} \rightleftharpoons 2H_a$$

$$CO_{2(g)} + H_a \rightleftharpoons HCOO_a$$

$$HCOO_a \rightleftharpoons CO_a + OH_a$$

$$OH_a + H_a \rightleftharpoons H_2O_a$$

$$H_2O_a \rightleftharpoons H_2O_{(g)}$$

Equation 1.5 – The formate decomposition mechanism[67c]

Mechanistic studies conducted on a Cu/SiO_2 catalyst have shown that rate of production of carbon monoxide increased with concentration of the formate species on the catalyst surface.[70] This strongly suggests that the formate plays an important role in CO formation. When rate expressions based on the formate mechanism have been employed to explain experimental results they tend to fit results relatively well[71] whereas, in the majority of cases, redox-based kinetics cannot be used to explain the observed behaviour.[70]

It has been suggested, in an attempt to explain both mechanisms shortfalls, that both are in fact occurring at the same time.[67c] However, as yet, no strong evidence has been reported to support this hypothesis.

While the redox and formate mechanisms have attracted the vast majority of attention in this field a third possible mechanism has also been suggested.[72] The mechanism is an associative mechanism similar to the formate pathway discussed previously except the key

intermediate is a carbonate species. It is suggested that gaseous CO_2 reacts with a surface oxygen species forming a surface carbonate. This surface carbonate can then react with gaseous hydrogen to form CO and a surface hydroxide species.[73] This mechanism is summarised in Equation 1.6. Recent work by Goguet *et al.* supports this mechanism, studies over a Pt/CeO_2 catalyst revealed that the rate determining step is the formation of a reaction intermediate that does not require the presence of hydrogen, most likely a carbonate.[74]

$$2OH^-_a \rightleftharpoons H_2O_{(g)} + O^{2-}_a$$

$$CO_{2(g)} + O^{2-}_a \rightleftharpoons CO_3^{2-}_a$$

$$CO_3^{2-}_a + H_{2(g)} \rightleftharpoons CO_a + 2OH^-_a$$

$$H_{2(g)} \rightleftharpoons 2H_a$$

$$2H_a + O_a \rightleftharpoons H_2O_a$$

$$H_2O_a \rightleftharpoons H_2O_{(g}$$

Equation 1.6 – The carbonate mechanism[73]

1.2 The Fischer-Tropsch Process

Fischer-Tropsch (FT) synthesis was developed more than 85 years ago, signalled by the application for a patent entitled 'Production of liquid hydrocarbons *via* hydrogenation of carbon monoxide over metal catalysts'[75] by Franz Fischer and Hans Tropsch. Since then it has developed into a commercial process being employed in many plants across the world.[76] With oil prices at an all-time high research into FT synthesis is still of great importance. Problems with catalyst activity and selectivity mean there is still much to be done before it becomes more viable than traditional methods for production of petrochemicals.

As implied by the patent title, FT synthesis involves the hydrogenation of carbon monoxide into hydrocarbons over metal catalysts. The process mainly produces linear paraffins and α-olefins with a wide distribution of carbon chain lengths. Equation 1.7 and Equation 1.8 show the two main reactions responsible for the production of the primary reaction products from the process.

$$(2n+1)H_2 + nCO \rightarrow C_nH_{(2n+2)} + nH_2O$$

Equation 1.7 – Formation of paraffins *via* the Fischer-Tropsch process

$$2nH_2 + nCO \rightarrow C_nH_{2n} + nH_2O$$

Equation 1.8 – Formation of olefins *via* the Fischer-Tropsch process

Although linear hydrocarbons represent the majority of the products, depending on the catalyst used and the reaction conditions employed, various other products are possible.[77] Highly branched hydrocarbons only represent a small proportion of the products due to steric restrictions during their formation.[23] Under appropriate conditions oxygenated by-products such as aldehydes, ketones and alcohols are obtainable. Equation 1.9 shows the side reaction responsible for the production of the main oxygenated species, alcohols.[78]

$$2nH_2 + nCO \rightarrow C_nH_{(2n+2)}O + (n-1)H_2O$$

Equation 1.9 – Formation of alcohols *via* the Fischer-Tropsch process

The Fischer-Tropsch process can be separated into two modes of operation depending on the reaction temperature. These two modes are defined as high temperature Fischer-Tropsch (HTFT) and low temperature Fischer-Tropsch (LTFT). The process used depends greatly on the desired product as well as the catalyst being employed. Generally the LTFT is used in a temperature range of 200-300 ^{o}C and produces high molecular weight hydrocarbon waxes as well as the main components of diesel.[79] HTFT on the other hand operates at temperatures greater than 300 ^{o}C and the majority of products can be accounted for by linear low weight olefins and gasoline.[80]

A large proportion of the attention on the Fischer-Tropsch process is focused on the formation of fuel. This can be attributed to a few key reasons. Oil and gas reverses are dwindling and combined with political troubles this is leading to large increases in price. An alternative source of fuel is needed and Fischer-Tropsch chemistry is one of the most promising sources from non-petroleum based supplies. Even with current industrial processes FT synthesis becomes economically viable when oil prices rise above US $30 per barrel[81] (price at time of writing is over $95 and set to rise).[82]

The levels of harmful chemicals such as sulfur and aromatic hydrocarbons in fuel is strictly controlled[78] and whereas fuel formed by traditional crude oil based methods tend to have high levels of these undesired compounds fuel produced by Fischer-Tropsch synthesis is much cleaner and possesses no sulfur or aromatic hydrocarbons. As such it can not only be used as a standalone fuel but can be added to petrol and diesel obtained through traditional methods in order to reduce these levels to within the acceptable limits.[83]

1.2.1 Catalysts

The catalysts most suited towards the Fischer-Tropsch process have been found to share a few similar characteristics.[84] These can be condensed into two main requirements.

1. They must be active for hydrogenation reactions
2. The conditions that thermodynamically favour metal carbonyl formation are similar to the pressures and temperatures needed for Fischer-Tropsch chemistry.

The Group 8, 9 and 10 metals iron, ruthenium, cobalt, rhodium, iridium, nickel, palladium and platinum are found to match these characteristics best and are consequently used most often.[24] Although all show some activity it varies greatly between each metal. A study conducted by Vannice *et al.* showed that on an alumina support activity decreased in the order: Ru > Fe > Co > Rh > Ni > Pd > Pt > Ir.[85] Other metals such as chromium and molybdenum have also been tested by Sasol but show much lower activity.[78]

The metal employed also has a significant influence on the product distribution with Vannice's work also showing the average molecular weight of the hydrocarbon decreases in the order Ru > Fe > Co > Rh > Ni > Ir > Pt > Pd.[86] From these results it is possible to conclude that although palladium may be active enough for the Fischer-Tropsch process the average molecular weight of products may be too low with the opposite true for iridium. This leaves ruthenium, iron, cobalt, rhodium and nickel as the only truly viable catalysts as they show both sufficient activity and a suitable product distribution.

Ruthenium presents itself as the obvious choice for use as a catalyst in Fischer-Tropsch synthesis as it shows the highest activity and best product distribution. It works at low temperatures (100 ^{o}C) and, at high pressures (1000-2000 bar), can produce hydrocarbons with exceptionally high molecular weights.[87] It does, however, possess a few major drawbacks, at

lower pressures (< 100 bar) product selectivity can shift mainly to methane.[88] Its main drawback is its availability, its very rare nature has resulted in prices approximately 31,000 times higher than that of iron as is shown in Table 1.4.

Table 1.4 – Relative prices of metals[78]

Metal	Price Ratio
Iron	1
Cobalt	230
Nickel	250
Ruthenium	31,000
Rhodium	570,000

Although nickel is far cheaper than ruthenium and rhodium and within acceptable costs it does possess a few characteristics, which make it unsuitable for Fischer-Tropsch catalysis. At practical temperatures the product distribution shifts almost entirely to methane with little to no heavier hydrocarbons being produced.[89] At higher temperatures the production of volatile nickel compounds can also occur leading to a loss of active metal and eventual deactivation of catalyst.[23]

Although much research has focused on ruthenium and nickel and continues to do so, it is iron and cobalt that have been used most widely, this is due to an acceptable compromise between price, activity and product distribution. Cobalt and iron where the first two metals originally suggested by Fischer and Tropsch[75] and to this day remain the only catalysts used on an industrial scale.[28]

Both cobalt and iron have their advantages and disadvantages, which should be used depends greatly on what products are desired, what temperature and pressure you are able to operate at and costs. Cobalt is 230 times more expensive than iron (see Table 1.4) but this is partially counteracted by its higher resistance to catalyst deactivation than the equivalent iron catalyst and so needs replacing less often.[24]

Generally cobalt based catalysts give higher yields as at higher conversions more water is produced by the Fischer-Tropsch process which has a much greater negative affect on iron than cobalt due to iron's higher water gas shift activity[90] (see Section 1.1 for further details). At low temperatures the maximum chain growth probability for each metal is approximately equivalent.[79] However, when the temperature is increased cobalt's selectivity shifts towards methane whereas iron gives good product selectivity over a wider range of temperatures and pressures.[23]

The narrow operating conditions for cobalt based catalysts mean they are generally employed only in LTFT. Iron on the other hand is used industrially in both the HTFT and LTFT processes.[28]

1.2.1.1 Cobalt-based Fischer-Tropsch catalysts

During Fischer-Tropsch synthesis a range of different cobalt species can be present on the catalyst surface. These vary from cobalt carbides, cobalt oxides and cobalt-support mixed oxides to metallic cobalt.[24] It is currently believed that metallic cobalt is the active species in Fischer-Tropsch catalysis. This is based on several pieces of experimental evidence; metallic cobalt phases have been detected in all investigated FT active cobalt catalysts. The carbdisation of this metallic cobalt to cobalt carbide results in a reduced catalytic activity and a higher selectivity to methane.[91] Unsupported cobalt has been shown to be active under reaction conditions[92] whereas the other main species detected such as oxides are not. The other species present may, however, affect the rates of side reactions such as olefins isomerisation, the WGS reaction and hydrogenolysis.

The cobalt-based catalysts employed for the FT process generally tend to consist of an active cobalt phase dispersed over an inorganic oxide support. The active metallic cobalt species are usually formed by *in situ* reduction of cobalt oxides already deposited on the catalyst support under a hydrogen atmosphere. The reduction proceeds *via* a two-step process as shown in Equation 1.10 and Equation 1.11 with the overall process shown in Equation 1.12.[93]

$$Co_3O_4 + H_2 \rightarrow 3CoO + H_2O$$

Equation 1.10 – Reduction of Co_3O_4 to CoO in the presence of hydrogen.

$$3CoO + 3H_2 \rightarrow 3Co^0 + 3H_2O$$

Equation 1.11 – Reduction of CoO to metallic cobalt in the presence of hydrogen.

$$Co_3O_4 + 4H_2 \rightarrow 3Co^0 + 4H_2O$$

Equation 1.12 – The overall reduction of Co_3O_4 to Co^0 in the presence of hydrogen.

The activity and selectivity of supported metallic cobalt is dependent on a range of different factors such as particle size the nature of the metallic cobalt formed during the reduction phase. Depending on the temperature of reduction and composition of the reducing gas different phases of metallic cobalt may be formed with both Co (fcc) and Co (hcp) appearing to perform differently under reaction conditions.[94]

The size of the formed metallic cobalt nano-particles has been found to have a large influence on the performance of catalyst systems both in terms of activity[95] and product

selectivity.[96] Recent studies by Park *et al*. have shown that generally as the particle size of the cobalt oxide precursor is increased the ease and degree of reducibility to metallic cobalt is increased.[97] When a range of cobalt particle sizes were investigated[95] (2.6 nm - 27 nm) selectivity towards heavier (C_5+) hydrocarbons was found to generally increase with larger cobalt particle sizes. Activity proceeds *via* a maximum at *ca*. 6 nm. The turnover frequency shows little variation above this 6 nm size. Larger sized nano-particles tend to show a more stable behaviour with increasing time on stream[97] this can likely be attributed to the increased ease of oxidation of small particles to inactive oxides in the presence of water.[98]

The main function of the inorganic support is to disperse the cobalt and stabilise the active metallic cobalt metal particles.[24] The Fischer-Tropsch process is highly exothermic and so the catalyst support also plays an important role in dissipating the heat released during reaction which can cause catalyst deactivation. The use of supports also helps to prevent temperature gradients in fixed-bed reactors.

The porous structure of the inorganic supports can also have an impact on the size of the formed cobalt particles,[99] which in turn can effect both the activity and product distribution of the catalyst.[95] It has been suggested that the electronic properties of the support material could also be used to alter activity. Ishihara *et al.* have shown that a more electron donating support enriches the electron density of the cobalt metal phase which consequently makes it easier to break the C–O bond of the adsorbed carbon monoxide.[100]

Iglesia and co-workers conducted investigations into the effects of several widely used supports on the activity of cobalt based Fischer-Tropsch catalysts.[101] It was found that at pressures of 5 bar, which favour high conversions and high selectivity to liquid (C_5+) hydrocarbons the nature of the metal oxide support used had little effect on either the activity or selectivity of the catalyst system. Work conducted by Reuel *et al.* however showed that at lower conversion the nature of support can have a large effect on selectivity and activity.[102] It was found that catalytic activity decreased in the order TiO_2 > Al_2O_3 > SiO_2 > unsupported cobalt. Other work has also shown large differences between catalysts prepared on different supports under lower conversions.

Silica is one of the most widely used catalysts supports and its effects on catalyst activity and selectivity have been widely investigated. The interaction between cobalt and the silica support has found to be relatively weak which leads to the oxides generally being easier to reduce. This higher reducibility has a positive effect on catalytic activity as more of the active metallic cobalt can be formed. The main disadvantage of using silica over other supports is the lower cobalt distribution observed, which can negatively affect the overall activity.[24]

The physical properties of the silica support and their effects on the catalyst performance have also been investigated with the majority of studies focusing on the effects of silica pore size.[99, 103] Recent work by Song and Li has shown that pore size has a large effect on both C_5+ selectivity and activity.[104] Both are found to initially increase with increasing pore

diameter before finally decreasing. The optimum pore size for a desirable product distribution was found to be between 60 and 100 Å.

Alumina is also widely used in Fischer-Tropsch chemistry as a catalyst support material particularly with cobalt based catalysts. Its properties as a support vary greatly from those of silica with one of the greatest variations being its more acidic nature. It has been shown to interact very strongly with cobalt. This strong interaction can lead to the formation of undesirable cobalt aluminate spinels that are inactive for the Fischer-Tropsch process and so reduce catalyst activity.[105]

Xiong *et al*. investigated the effects of increasing pore diameter of the Al_2O_3 support in cobalt-based catalysts.[106] It was found that the increasing pore size led to the formation of larger crystallite Co_3O_4. These bigger oxide particles meant fewer active sites this combined with lower reducibility culminated in reduced Fischer-Tropsch activity. Recent work by Liu *et al*. has shown that the morphology, the size and shape, of the Al_2O_3 particles used as a support can also lead to a large difference in catalyst performance.[107] Nanostructured Al_2O_3 was observed to give up to a 20-30 % increase in CO conversion over commercial Al_2O_3 with the alumina nanorods performing best.

Studies by Reuel and co-workers showed the use of titania (TiO_2) to be one of the most effective supports when combined with cobalt for use as a Fischer-Tropsch catalyst.[102] As a result of these studies it has been attracting significant attention. Further work has shown that TiO_2 supported systems tend to combine this higher activity with higher selectivities to C_5+ hydrocarbons than the analogous Al_2O_3 and SiO_2 supported systems.[108] This is possibly due to an increase in Co_3O_4 particle size and easier reduction of cobalt oxide phases as reported by de la Osa.[109] It should be noted that due to the reducible nature of the titanium oxide support the catalysts are prone to strong metal support interactions.[110] Recent work has shown that this reducibility can also lead to the formation of TiO_x ($x < 2$) which can lead to the encapsulation of active metal nanoparticles by titanium oxides.[111]

The use of carbon supported cobalt systems for FT catalysis have been the focus of many studies. While several have reported the use of activated carbon[112] the majority have focused on the use of more well defined carbon species. For example recent studies have shown that the use of mesoporous carbon is more suited and a better performing support for cobalt catalysts than the more traditionally utilised activated carbon.[113] A vast quantity of research has investigated the use of carbon nanotubes (CNTs) as possible supports with results showing an improved performance over activated carbon.[114] Non-promoted cobalt catalysts supported on CNTs have also been shown to give remarkably high selectivities to C_5+ hydrocarbons.[115] The performance of CNT supported catalysts can be improved further using an acid treatment before cobalt loading.[116] Their low interaction with the metal nano-particles makes them an ideal choice for the investigation of particle size effects.[95]

A range of other catalyst supports have also been investigated with several beneficial properties observed. Recent work by de Jong *et al*. compared cobalt catalysts supported on Al_2O_3 and niobia (Nb_2O_5) and found several benefits for its use over Al_2O_3.[117] A higher selectivity towards C_5+ hydrocarbons was observed and a lower cobalt loading was required to obtain the same activity per mass of catalyst. The use of ZrO_2 as a lone support has also been investigated with the low interaction between the ZrO_2 support and cobalt phases playing an important role in high activity and C_5+ selectivity.[118]

1.2.1.1.1 Noble metal promotion of cobalt catalysts

The most commonly used promoters for cobalt based Fischer-Tropsch catalysis are noble metals such as ruthenium, rhodium and platinum. Their introduction can influence several properties which are key to increasing the catalyst activity. These properties range from an increase in reducibility of the precursor Co_3O_4 to better cobalt dispersions across the catalyst surface.[24]

With metallic cobalt being the active species in FT catalysis its formation from the reduction of cobalt oxide precursors becomes important in the production of active catalysts. Work done by Tsubaki has shown that the introduction of small amounts of ruthenium greatly increases the reducibility of cobalt oxides and as a result gives a much higher activity without any significant change in the product distribution.[119] Rhenium,[120] rhodium[121] platinum[122] and iridium[24] have been found to give similar results but with smaller increases in activity.

Although the addition of platinum and palladium have also been shown to increase the reducibility of cobalt oxides its effect on overall activity is almost insignificant relative to the increase in activity due to the increased cobalt dispersion observed.[123] It is believed that the introduction of noble metals leads to a higher number of cobalt oxide nucleation sites which gives a higher dispersion of cobalt.

1.2.1.1.2 Metal oxide promotion of cobalt catalysts

The introduction of metal oxides as promoters has also been widely investigated. The addition of these oxides can affect catalyst performance in several ways. They can modify the texture, porosity and mechanical strength, reduce the formation of cobalt-support mixed oxides as well as affecting cobalt dispersion and reducibility. Among the most frequently employed are ZrO_2, MnO_2, CeO_2 and La_2O_3.

Zirconia promotion has different effects depending on the main support used, for example when introduced with an alumina support no increase in reducibility or dispersion is observed.[124] On silica based cobalt catalyst zirconia reduces the interaction between the cobalt and silica increasing both the reducibility and dispersion.[125] Zirconia addition has also been shown to increase selectivity towards C_5+ hydrocarbons.[126] Similar enhancements in activity and selectivity are observed for cobalt systems supported on activated carbon.[112]

The addition of MnO_2 has been shown to have a significant effect on the activity[127] and selectivity[128] of cobalt catalysts. Improved dispersion of cobalt phases has been observed upon the introduction of small amounts of MnO_2.[24] Although the formation of mixed cobalt-manganese oxides are often observed they, unlike most cobalt-support mixed oxides, can still be reduced to form active species.[129] The inclusion of MnO_2 has, however, been shown to have a negative effect on the reducibility of the cobalt oxides present.[130]

Although zirconia and manganese dioxide represent the focus of the majority of studies on the addition of oxide promoters a range of others have also been investigated and shown promising properties. Cerium oxide addition has been shown to increase cobalt dispersion and direct selectivity towards alkenes.[131] Lanthanum oxide addition can shift hydrocarbon selectivity towards heavier liquid hydrocarbons with little effect observed on catalytic activity.[132] The addition of TiO_2 in low loadings as a promoter for cobalt catalysts has also been investigated.[133] Addition was found to improve conversion rate and increase selectivity towards heavier, liquid hydrocarbons.

1.2.1.2 Iron-based Fischer-Tropsch catalysts

After activation of iron based Fischer-Tropsch catalysts a range of different iron species can be formed; which are produced is heavily dependent on the reaction conditions. The most commonly observed consist of a range of iron oxides, iron carbides and metallic iron.[134] Unlike cobalt Fischer-Tropsch catalysts the actual active phase of the iron-based systems is still a topic of on-going discussion.

Mössbauer spectroscopy investigations conducted by Raupp and Delgass showed an almost linear correlation between activity of the catalyst and carburization.[135] Several other groups have also published results that support these observations.[136] This has led to a belief that the iron carbides, Hagg carbide (Fe_5C_2) more specifically, are mainly responsible for the activity observed. Reports suggesting the activity of other iron phases have also been published[137] with Fe_3O_4 another species suggested to be the main active component in Fischer-Tropsch catalysis based on experimental observation.[138]

Based on these observations Niemantsverdriet and van der Kraan proposed several models to explain the catalytic activity.[139] Of these the carbide model has become the most widely accepted. For this system it is assumed that metallic iron is inactive for the Fischer-Tropsch process. The active phase is said to consist of active surface carbides located on a bulk iron carbide structure. It is the state of this bulk that controls the number of active sites, and hence catalytic activity.

As with cobalt catalysts the iron based systems tend to consist of an active iron phase deposited on an inorganic support. It is introduced for the same main reasons as in cobalt systems, to disperse the iron phase and stabilise it. Similar supports are used with the two most

popular again being silica and alumina. A range of other oxides have also been investigated such as titania, magnesia and zirconia.[140]

Of these supports silica is the most widely used, this can be attributed to a number of key factors.[81] It has been found to increase catalyst activity by up 40% over unsupported iron and has been shown to be up to 50% more active than an equivalent alumina catalyst.[141] Work by Bukur *et al.* has shown that introduction of SiO_2 can also have a large effect on product distribution as it tends to promote side reactions such as olefin hydrogenation and isomerisation.[142]

Silica can have a large effect on the iron phases formed before and during reaction. Work by Zhang *et al.* has shown that without a support present only hematite (α-Fe_2O_3) is formed, in the presence of silica however a range of oxides are formed including mixed silica-iron-oxides.[143] Although the Fe_2SiO_4 formed is inactive and so reduces overall activity, the presence of other iron oxide phases appears to have an overall beneficial effect.

Alumina is widely used in cobalt systems but has several features that prevent it being used as extensively in iron systems. Al_2O_3 has been found to inhibit the reduction of iron species which can prevent the formation of active species and decrease the catalysts affectivity.[141] The use of alumina as a support can also increase selectivity towards the generally undesired low weight hydrocarbons. Work by Wan *et al.* has shown that when used in conjunction with silica several beneficial results can be observed.[144] The correct ratio of alumina to silica can increase overall activity for Fischer-Tropsch synthesis. This is thought to be due to unfavourable SiO_2-iron interactions being minimised in the presence of Al_2O_3.

1.2.1.2.1 Noble metal promotion of iron catalysts

Although not as widely employed as in cobalt-based catalysts research has been conducted into the use of noble metals as promoters in iron Fischer-Tropsch catalysts. The introduction of platinum into iron systems has been shown to increase the catalytic activity.[145] It is believed that this increase in activity is due to an increase in proportion of iron carbide formed in its presence.[145] The use of platinum has received the most attention of the noble metals mainly due to its effect on product distribution. Its introduction decreases the formation of methane and shifts selectivity towards heavier hydrocarbons.

Work has also been conducted on the use of palladium on iron based Fischer-Tropsch catalysts. LuO *et al.* have shown that with palladium an increase in activity is observed although not to the same extent as that shown by platinum.[146] Palladium promotion has little effect on average molecular weight but can direct towards paraffins. Other noble metals such as ruthenium[147] and rhodium[148] have been investigated as promoters and show an increased activity although again, not to the same extent as that observed with platinum.[149]

1.2.1.2.2 Alkali promotion of iron catalysts

One of the most widely reported and successful methods for increasing the effectiveness of iron-based catalysts is the introduction of alkali metals. The effect of alkali metal introduction varies greatly between each metal. Generally, Group I metals lithium, caesium, rubidium can be considered as inhibitors as their introduction leads to a decrease in activity over un-promoted iron.[150] The addition of sodium and potassium is highly beneficial and leads to a large increase in overall activity.[151] Ngantsoue-hoc *et al.* showed that with the introduction of equal amounts of each metal the percentage conversion of CO increased in the order Cs < Rb < Li < un-promoted iron < Na < K.[150]

The promotional effects of Group II metals were also investigated by Luo *et al*.[152] It was found that iron based catalysts promoted by alkali earths have a higher activity over un-promoted iron but do not reach the effectiveness of potassium-iron catalysts. It was found that magnesium had the greatest activity enhancement followed by barium, beryllium and finally calcium. The results obtained also showed that calcium and magnesium were capable of suppressing water gas shift activity below that observed for un-promoted iron.

Work by Dry *et al*. on the correlation between the basicity of catalyst surfaces of alkali promoted systems and the activity has led to a belief that the promotional effects are largely due to an increase in basicity.[153] Their work showed that basicity increased in the order K > Na > Ca > Li > Ba. This corresponds with the increase in activity observed with the promoted catalysts.

Potassium, due to its higher activity, has led to it becoming the most used of the alkali promoters and is currently employed industrially.[154] Although its introduction reduces iron dispersion[155] Dry *et al.* showed that its presence greatly increases the strength of CO chemisorption and decreases the strength of H_2 adsorption.[156] It is believed that this leads to the higher average molecular weight observed in the products.[157]

1.2.1.2.3 Promotion of iron catalyst by other metals

Metals other than alkali and noble metals are often used in iron based catalysts. Of these, copper, manganese and zinc are used most widely. Iron based catalysts employed industrially tend to be based upon these promoters (as well as alkali promoters).[158]

Copper is a common promoter in iron Fischer-Tropsch chemistry as it increases catalyst activity and shifts selectivity towards longer/heavier hydrocarbons.[23] Its introduction can also help prevent the loss of active surface area, a process known as sintering. Copper has been found to play a direct role in altering the surface chemistry of the catalyst surface.[159] This change leads to an increased reducibility of the iron oxide species present. Although the precise active species in iron catalysts is not known its formation is thought to require the reduction of iron oxide and as such an increase in reducibility leads to an increase in activity.

Manganese is industrially used as a promoter as it has been shown to have several important effects on iron based catalysts. It increases the active surface area and improves iron dispersion.[160] Although initial activity is slightly hampered by its presence it restrains the reoxidation of iron carbides, which improves catalyst stability.[161] Manganese has also been found to suppress the undesired formation of methane and force selectivity towards light olefins and heavy hydrocarbons.[161]

1.2.2 Mechanisms

The mechanism for the Fischer-Tropsch process has attracted a lot of attention over its 85-year lifetime. An accurate mechanism is essential in order to develop an understanding into the kinetics of the processes involved and understand how the alteration of reaction conditions could lead to a shift in conversion or selectivity towards desired products.

Fischer conducted the first mechanistic work whilst initial investigations into Fischer-Tropsch catalysis were being under taken. He developed a range of different mechanisms that could go some way to explaining the product distributions that were being observed.[162] It was only once the process was fully established with hydrocarbons as the main reaction product that he came up with the first widely accepted mechanism known as the 'carbide mechanism'.[163]

A version of this mechanism, slightly modified by Craxford and Ridel[164] is represented in Equation 1.13 to Equation 1.16. Initially CO from the syn-gas is adsorbed on the surface (Equation 1.13). It then dissociates in the presence of either CO or H_2 to form H_2O or CO_2 (Equation 1.14 and Equation 1.15). CO_2 and H_2O then rapidly desorb and a chemisorbed carbon is formed. This carbon then reacts directly with H_2 to give a chemisorbed methylene (CH_2) moiety. This then acts as a monomer in a polymerisation[165] reaction that forms saturated and unsaturated hydrocarbons (Equation 1.16).

$$M + CO \rightarrow M\text{-}CO$$

Equation 1.13 – Adsorption of CO onto the catalyst surface

$$M\text{-}CO + CO \rightarrow M\text{-}C + CO_2$$

Equation 1.14 – Dissociation of adsorbed CO in the presence of CO

$$M\text{-}CO + H_2 \rightarrow M\text{-}C + H_2O$$

Equation 1.15 – Dissociation of adsorbed CO in the presence of H_2

$$M\text{-}C + H_2 \rightarrow M\text{-}CH_2 \rightarrow\rightarrow \text{Hydrocarbons}$$

Equation 1.16 – Formation of methylene monomer and subsequent polymerisation resulting in the formation of hydrocarbons

This basic mechanism was further adapted based on experimental evidence by Brady and Pettit to give another modified version known as the 'alkyl mechanism'.[166] This version has become the most widely accepted mechanism for the formation of hydrocarbons from the Fischer-Tropsch process.[78] It is essentially an extended version of that proposed by Craxford and Ridel.

It is suggested that both the CO and H_2 components of the syn-gas are chemisorbed to the surface and then dissociated to form carbide, oxy and hydride surface species. The oxo groups are then generally lost by a reaction with either H_2 or CO to from water and CO_2 respectively. These initial steps are shown in Figure 1.1.

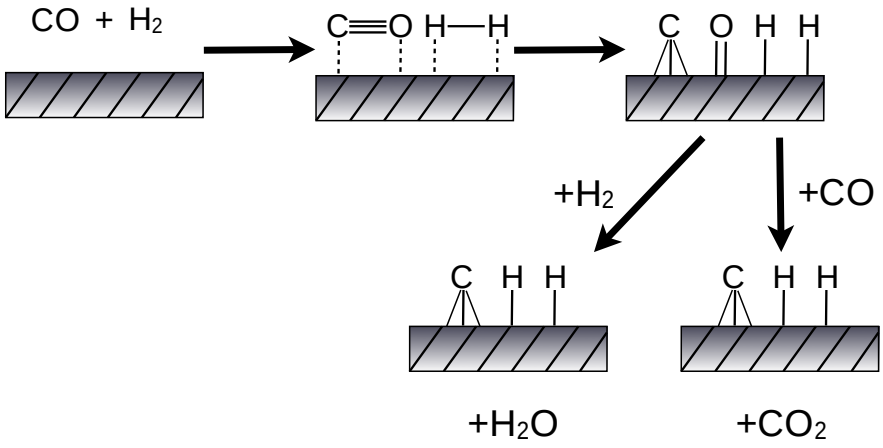

Figure 1.1 – The formation of carbide, oxy and hydride species

The surface carbides are then hydrogenated by the hydride species also present on the surface. The addition of one hydride forms a methyne which when hydrogenated again forms a methylene group.[167] This hydrogenation can continue to form a methyl group that can then be hydrogenated one final time to form methane (shown in Figure 1.2). It is these methyne, methylene and methyl groups that play the main role in the formation of heavier hydrocarbons with their formation generally accepted as the rate limiting step of the reaction.[168]

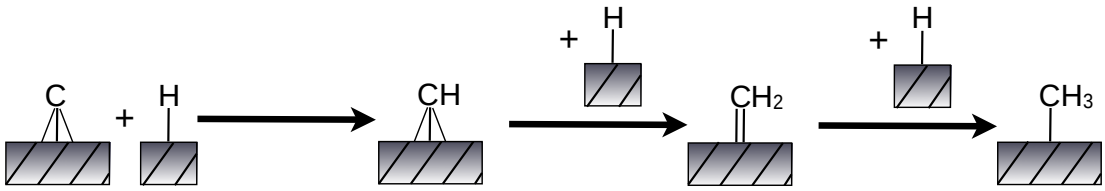

Figure 1.2 – Hydrogenation of carbide species as proposed in the 'alkyl mechanism'

The process of hydrocarbon growth is again based on the polymerisation of the methylene species. The alkyl mechanism suggests that this chain growth is initiated by the reaction of a methylene group with either a hydride or methyl species as shown in Figure 1.3.[162] The chain growth then continues by the coupling of the growing chain with another neighbouring methylene group. This then continues until β-hydride elimination gives linear olefins or until it is hydrogenated by a hydride species to give linear paraffins.

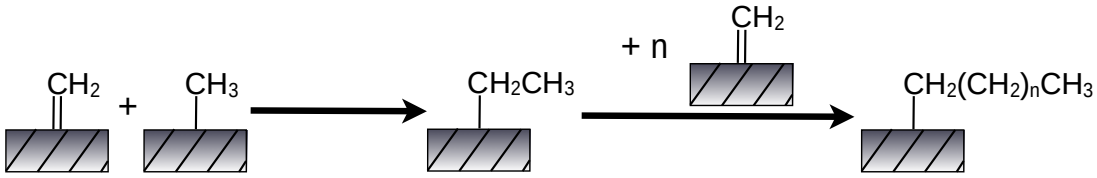

Figure 1.3 – Chain growth in the alkyl mechanism

Although the alkyl mechanism is the most widely accepted several others have been developed based on similar principles. The two most highly rated of these are the alkenyl/vinyl[169] and the Dry[81] mechanisms. Both rely on the formation of carbides and a methylene monomer but the method of chain growth varies in both.

The alkenyl/vinyl mechanism proposes the formation of vinyl species by the coupling of a methylidene and methyne groups present on the catalysts surface[167] as shown in Figure 1.4. Chain growth then proceeds by the insertion of a methylene group followed by an isomerisation step to reform a metal bound vinyl (also shown in Figure 1.4). Termination then occurs by the addition of a surface hydride to the methyne group of the growing hydrocarbon.

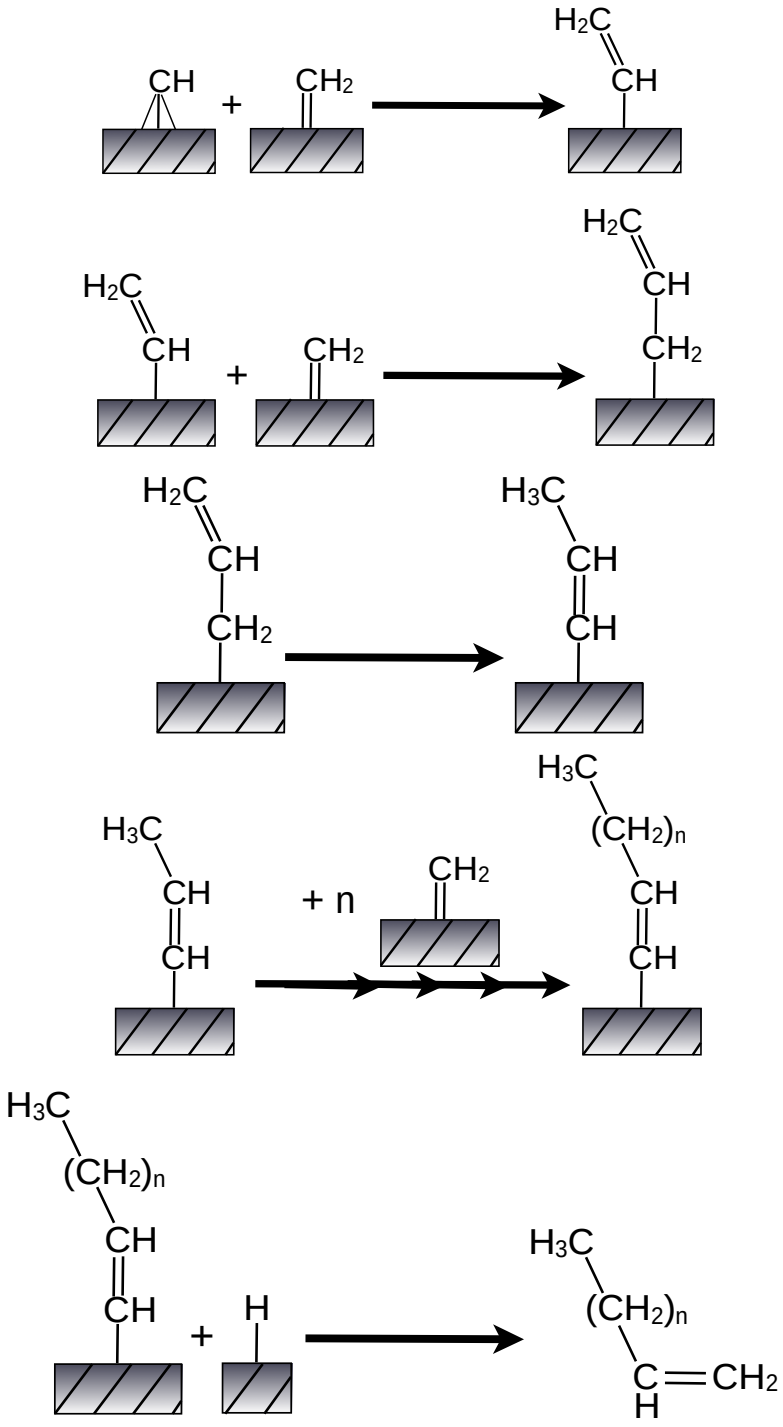

Figure 1.4 – Hydrocarbon formation *via* the vinyl mechanism

One of the more recent carbide based mechanisms is that proposed by Dry.[170] He suggested that in order for a mechanism to be accepted it should be capable of explaining all the unique characteristics possessed by the hydrocarbons produced by the Fischer-Tropsch process. While most previously proposed mechanisms satisfactorily explain most features such as why the majority of formed hydrocarbons are linear and with a lower ratio of paraffins to olefins than predicted by thermodynamics there are features that are not explained.

One aspect that could not be mechanistically explained is why branching is found to be predominantly monomethyl and less likely to occur as the chain length increases. Several other mechanisms had attempted to explain this phenomenon and although monomethyl branching could be explained the reason behind why branching decreases for longer hydrocarbons could not be found. In an attempt to explain this characteristic a new mechanism was suggested with one key difference. It was assumed that there is a two-point attachment to the catalyst surface at the end of the growing hydrocarbon chain as opposed to the normal single-point attachment.

The formation of methylene groups on the catalyst surface proceeds by the same process shown in Figure 1.2. The first part of chain growth then begins through the combination of two methylene species to form a metallocyclopropane. Growth then proceeds by the insertion of a methylene group to form a metallocyclobutane that rearranges to form the metallocyclopropane (shown in Figure 1.5).[171]

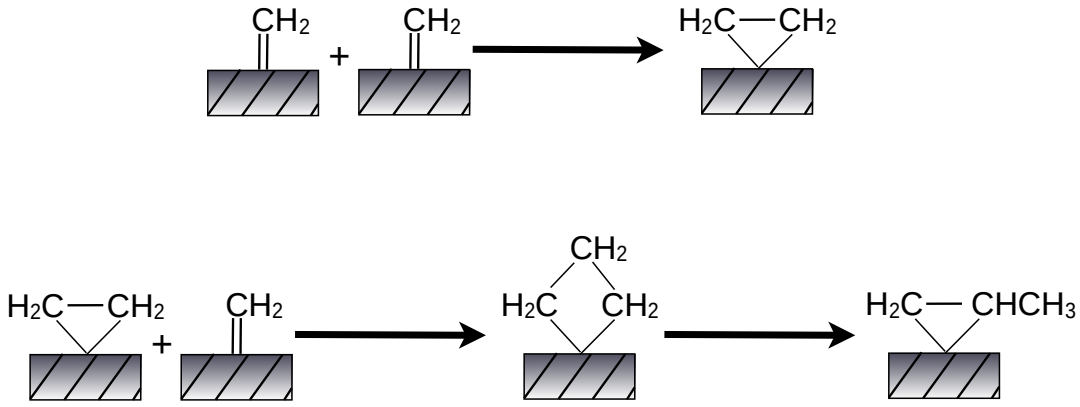

Figure 1.5 – Formation of metallopropane followed by CH_2 insertion

After the insertion of an initial methylene species into the metallocyclopropane bonds **a** and **b** (see Figure 1.6) are no longer equivalent. Due to steric reasons the next methylene unit is more likely to insert into bond **a** rather than bond **b**. As chain length increases the steric bulk at **a** increases, reducing the probability of insertion into bond **b** accounting for why monomethyl branching is found less frequently in longer hydrocarbons. Figure 1.6 shows the products formed when a methylene group inserts into bonds **a** and **b**.

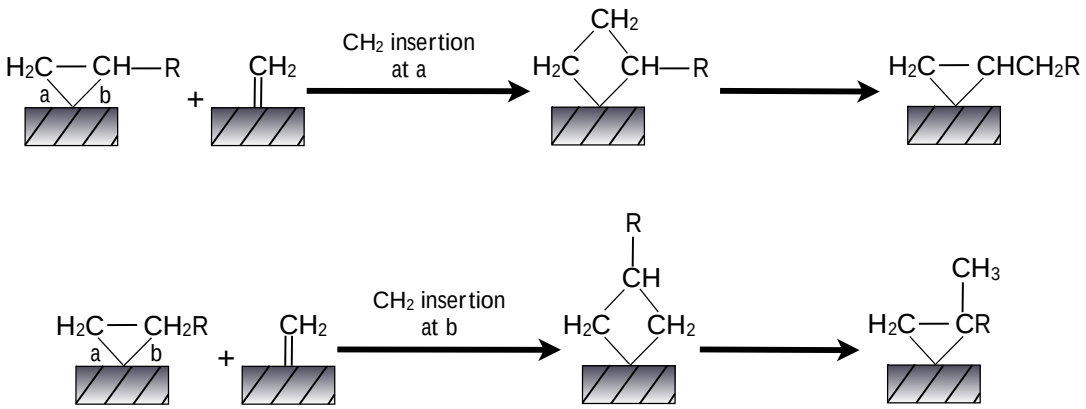

Figure 1.6 – CH_2 insertion at bonds a and b during the Dry mechanism

The insertion process shown in Figure 1.6 can repeat and chain growth can continue or desorption of products can occur to give a linear terminal olefin (product of insertion at **a**) or a monomethyl branched olefin (product of insertion at **b**). Termination can also occur by hydrogenation to give paraffins.

While these carbide mechanisms are the most widely accepted processes for the formation of hydrocarbons through the Fischer-Tropsch process[78] they do possess a few problems. One of the more significant of these problems is the lack of an explanation for the formation of oxygenated products such as alcohols, ketones and aldehydes. In an attempt to explain their formation several oxygen containing mechanisms have been proposed.[172] Of these the two most widely accepted are the enol[171] and carbonyl insertion mechanisms.[137]

The carbonyl insertion mechanism (also called the Pichler-Schulz[173] mechanism) is based on the insertion of a CO molecule into a growing alkyl chain. The formation of a methylene group occurs by the insertion of carbon monoxide into a metal hydride followed by hydrogenation as shown in the first step[162] of Figure 1.7. Chain growth then proceeds by the hydrogenation of this methylene group to form a methyl species as shown in the second step of Figure 1.7. It is this species that CO initially inserts into. The intermediate is then hydrogenated to form the beginnings of an alkyl chain. The alkyl chain then grows in length as process repeats until termination.

Termination can occur through several pathways as shown in the third step of Figure 1.7. The carbonyl containing alkyl chain can react with a single metal hydride to form an aldehyde that can then be further hydrogenated to form an alcohol. Alternatively the alkyl chain can dissociate and form olefins that can be further hydrogenated to give paraffins.[162]

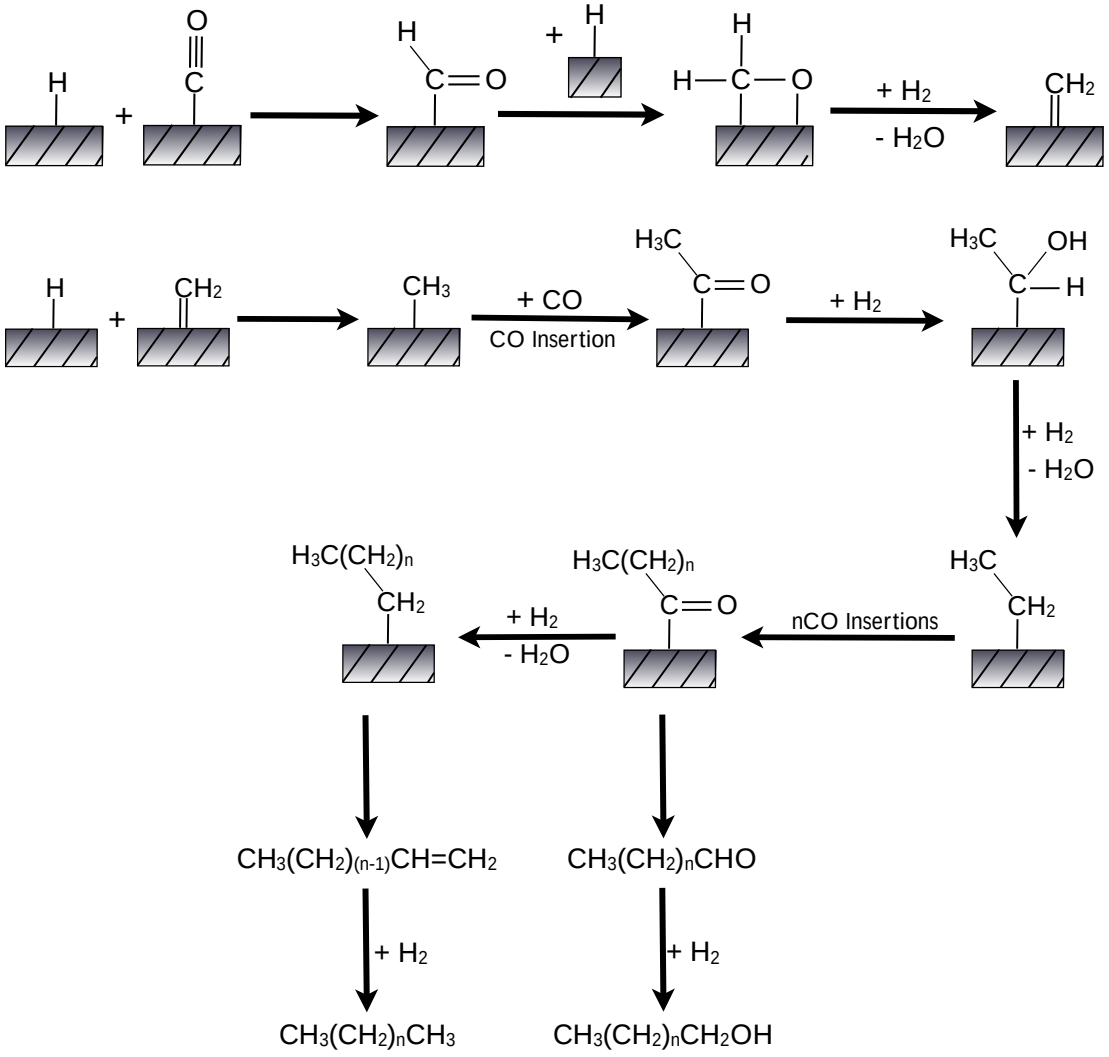

Figure 1.7 - The carbonyl insertion mechanism.

The enol mechanism was first suggested by Storch and Anderson in 1951[174] and further backed up by experimental work utilising radioactive tracers by Emmett *et al.* in 1953.[175] It proposes that CO chemisorbed to the surface of a catalyst is hydrogenated to form surface bound hydroxyl-carbenes. Chain growth then begins by a condensation reaction between two adjacent hydroxyl-carbenes to form the intermediate seen in Figure 1.8.[171] Hydrogenation of one of the carbene groups in this intermediate then forms a methyl group to complete the step. This process of condensation followed by hydrogenation repeats to form hydrocarbons of increasing length. Termination then occurs to give oxygenated products.

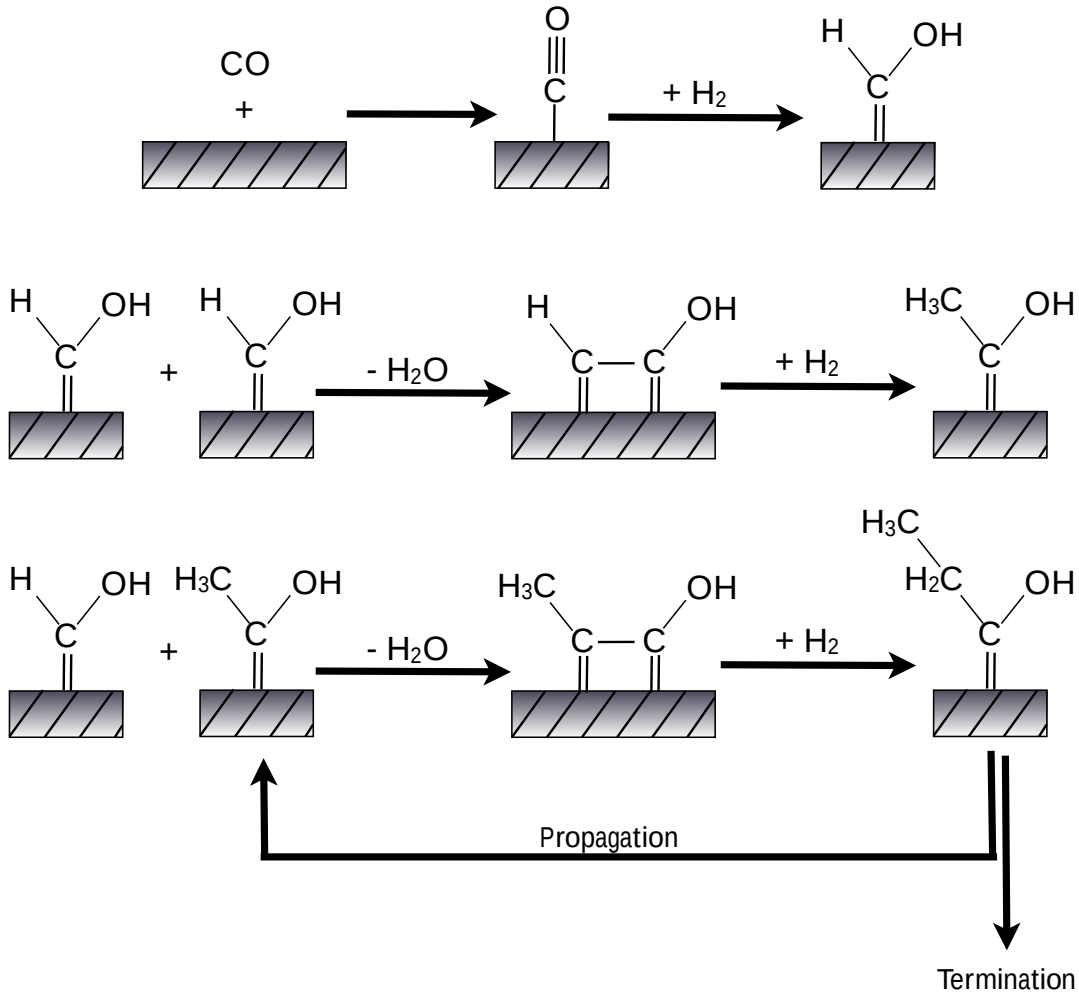

Figure 1.8 – The Enol mechanism suggested by Storch and Anderson

All mechanisms discussed previously possess problems, either not relating well enough to the experimental product distributions[176] or kinetics[177] or not matching some thermodynamic information[178] and as a result the exact mechanism is still highly debated. Experimental findings have led to the polymerisation of adjacent surface bound methylene groups becoming widely accepted,[179] it is however, the exact formation of these groups and their insertion into growing chains that divides opinion. Generally speaking, the majority accept that the alkyl mechanism accounts for the formation of hydrocarbons[78] and that the CO insertion mechanism accounts for the formation of oxygenated products.[180]

1.2.3 Selectivity and Product Distribution of the Fischer-Tropsch Process

Hydrocarbons formed through the Fischer-Tropsch process have been found to share a range of characteristics.[170] Irrespective of type the formed, products are generally linear. The olefin to paraffin ratio is lower than predicted by thermodynamics with selectivity towards olefins greatly exceeding 50%. Of the olefins formed the vast majority are terminal (α) and their proportion

decreases with increasing carbon chain length. A large amount of branched products are also formed but most are monomethyl in nature and while dimethyl products are produced the quantity is much lower.[78]

The conditions employed in the Fischer-Tropsch synthesis can have a significant influence on the distribution of products. Although one of the largest influences on products formation is the composition of the catalyst (as discussed in Section 1.2.1) other factors such as reaction conditions can also play a large role. Of these reaction conditions the effects of temperature, pressure, space velocity and H_2/CO ratios have the largest influence.

Work on the effects of temperature on Fischer-Tropsch synthesis has shown that for both iron[181] and cobalt[24] based catalysts increased temperature results in a shift of product selectivity towards the lighter hydrocarbons with methane formation greatly increased. An increase in the olefin to paraffin ratio has also been associated with higher temperatures although the relationship is somewhat complex.[78]

The effect of pressure has also been shown to have a large influence on the product distribution of the Fischer-Tropsch process. Most studies have shown that an increase in reaction pressure leads to the formation of heavier hydrocarbons.[182] Oxygenated species that account for only a small fraction of products in reactions conducted at lower pressures over most fractions become increasingly more common as pressure increases.

Many experiments have been conducted investigating the alteration of H_2/CO ratios of the feed-gas. Increasing the content of H_2, i.e. increasing the ratio, has been found to give much lighter hydrocarbons. Unsurprisingly, in this more reductive environment the olefin to paraffin ratio is greatly reduced. Bukur *et al*.[181] found that an increase in H_2/CO ratio of 0.3 to 4 gave a drop in olefin to paraffin ratio of 6 to 1.

The space velocity of the reactant gases, which is directly related to residence time, has been shown to effect the product distribution.[24, 78] It has been observed that by decreasing the space velocity, and so increasing residence time, the average molecular weight of hydrocarbons increases while the olefin to paraffin ratio decreases.

The effects above give a brief introduction into the factors affecting the selectivity of Fischer-Tropsch products, the influences of each parameter can be greatly influenced by the catalyst used and its composition. Table 1.5 (adapted from work by Van Der Laan[78]) summarises these influences.

Table 1.5[78] – The influence of reaction conditions on product distribution and selectivity in the Fischer-Tropsch process

Parameter	Chain Length	Chain Branching	Olefin Selectivity	Alcohol Selectivity	Methane Selectivity
Temperature	↓	↑	*	↓	↑
Pressure	↑	↓	*	↑	↓
H_2/CO Ratio	↓	↑	↓	↓	↑
Space Velocity	*	*	↑	↑	↓

Note: ↑ indicates an increase with increasing parameter, ↓ denotes a decrease with increasing parameter and * indicates a complex relationship.

Although, as shown in Section 1.2.2, the mechanism of the Fischer-Tropsch process is not fully understood it is widely agreed that chain growth proceeds in a stepwise fashion as proposed in all mechanisms discussed. If, as suspected, the hydrocarbon proceeds *via* the insertion of CH_2 monomers then the distribution of the products chain lengths can be predicted based on the simplified reaction growth scheme shown in Figure 1.9.[183]

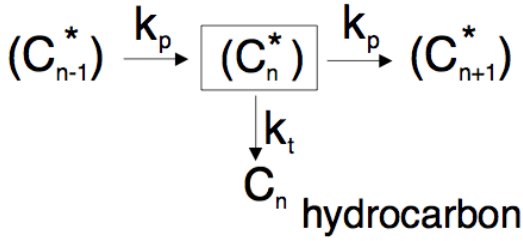

Figure 1.9 – A simplified reaction scheme for hydrocarbon chain growth during the Fischer-Tropsch process

Using this simplified reaction growth scheme the product distribution can be described by the Anderson-Schulz-Flory (ASF) distribution,[184] Equation 1.17. where m_n is the mole fraction of a hydrocarbon with carbon chain length n. This distribution describes the product range based on a single parameter, the chain growth probability, α.

$$m_n = (1-\alpha)\alpha^{(n-1)}$$

Equation 1.17 – The Anderson Schulz Flory distribution

α is defined in Equation 1.18 where R_p is the rate of propagation and R_t the rate of termination.

$$\alpha = \frac{R_p}{R_p + R_t}$$

Equation 1.18 – Equation showing the relationship between α and rates of termination and propagation

The distribution of products using the ASF distribution is entirely dependent on the relationship between the rate of propagation and termination. This dependence on the value of α is shown in Figure 1.10.

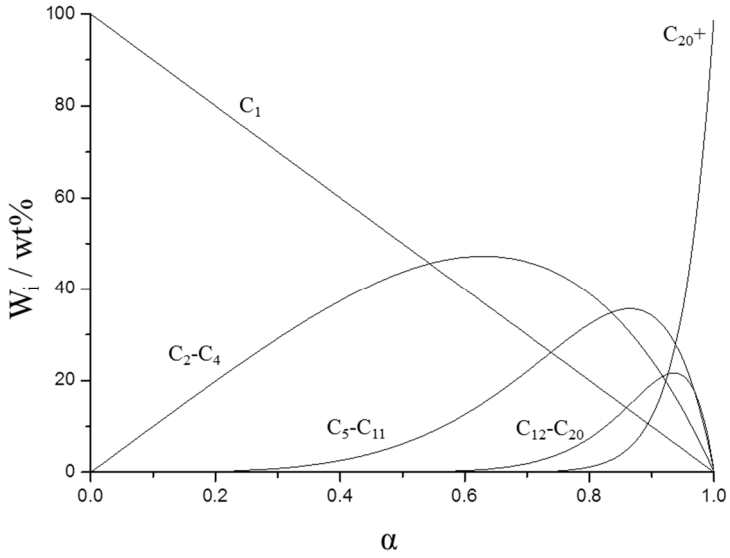

Figure 1.10 – A plot showing the relationship between α and product distribution.

The chain growth probability value is influenced by a several different factors. Dry *et al.*[185] found that generally α is 0.7-0.8 for cobalt based catalysts and 0.5-0.7 for iron systems. Temperature, pressure and synthesis gas composition have also been shown to influence the chain growth probability

Although the ASF distribution is widely used to explain product distributions it has been reported to show deviations from experimental results. This is presumed to be due the fact that in practice a range of different products, such as paraffins, olefins, alcohols, aldehydes etc. are formed, the ASF however assumes the formation of a single type of product and as a result a single termination mechanism.[78]

Glebov and Kliger modified the original ASF distributions to take into account the formation of multiple species.[183] Figure 1.11 shows the reaction scheme the new model was based upon. It still assumes that chain growth occurs from the same stepwise mechanism shown in Figure 1.9 but gives multiple termination routes for different products.

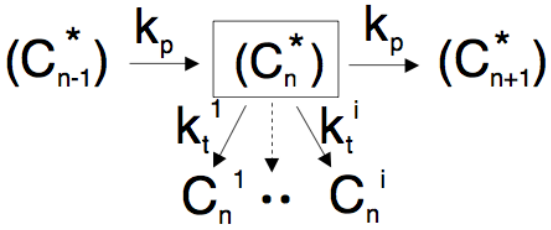

Figure 1.11 – Simplified reaction scheme for chain growth with multiple possible termination steps

As shown in Figure 1.11 the formation of each type of hydrocarbon (paraffin, olefin, alcohols etc.) is given a different termination rate constant from k_t^1 to k_t^i. Based on this Glebov and Kliger[183] modified the ASF equation to give Equation 1.19 where α is defined as the rate constant of propagation over the rate constant of propagation plus the sum of all rate constants of termination as shown in
Equation 1.20.

$$\sum^{i} m_n^i = (1-\alpha)\alpha^{(n-1)}$$

Equation 1.19 – Glebov and Kliger's modified ASF distribution.

$$\alpha = \frac{k_p}{k_p + \sum_i k_t^i}$$

Equation 1.20 – The relationship between α and the rate constants.

With the use of Glebov and Kliger's modified ASF distribution values much closer to experimental results can be obtained. Deviations have been reported, these could be due to analytical difficulties[88] or non-steady state conditions[186] found in the reactor systems. More advanced models are still being developed in an attempt to eliminate these deviations.[187]

1.2.4 Catalyst Deactivation

Over an extended period of time the activity of both iron and cobalt catalysts tend to degrade due to deactivation of the catalyst. What causes this loss in activity is widely debated but can be split into four main mechanisms.

A mechanism often reported for both iron and cobalt Fischer-Tropsch catalysts is based on the oxidation of active species. Water is formed in high quantities in Fischer-Tropsch reactions and it is widely believed that this water can then oxidise active species into inactive oxides. Work has been conducted on the effects of water on both cobalt[188] and iron[189] catalysts and has been shown to have a significant effect. In the case of iron an increase in the water

content led to the formation of more Fe_3O_4 indicating that under typical Fischer-Tropsch conditions water can oxidise active iron species into inactive oxides.[190] Work conducted by Jacobs *et al*.[188] suggested that water oxidised the metallic cobalt into inactive cobalt and cobalt-support oxides. It has also been suggested that in iron systems[137] active carbide species could also be converted into inactive carbide species which would also lead to a reduction in catalyst activity. Recent research has suggested that the oxidation of metallic cobalt by water only plays a small role under commercially relevant conditions.[191]

Another mechanism thought to play an important role in catalyst deactivation is surface reconstruction.[192] This most commonly occurs through the combination of active metal particles through a process known as sintering, conglomeration of larger catalyst particles has however also been observed in certain systems.[193] In order for the sintering of active nanoparticles to occur the catalyst must reach a temperature equal to half of the nanoparticles bulk melting point, a value defined as the Tammann temperature. At temperatures above this value surface atoms become mobile, which can result in catalyst sintering. Although general Fischer-Tropsch operating conditions are below this local temperatures can reach much higher values due to the exothermic nature of the reactions occurring.[137]

Recent work by Bezemer and co-workers[194] has shown a direct correlation between water content and the sintering of a Fischer-Tropsch catalyst suggesting that the sintering of active nanoparticles could be playing an important role in the deactivation of catalyst systems observed in the presence of water, in combination with the oxidation of active species as discussed earlier. Deactivation models incorporating water assisted sintering correlate well with experimental studies providing further evidence to support this theory.[195] Catalyst sintering has been suggested as the main source of catalyst deactivation in several studies[195-196] it can be reduced by the introduction of support materials such as silica and alumina as they stabilise the active species preventing sintering of the active nanoparticles.

Research into the deactivation of catalysts has also shown that in iron[197] and cobalt[198] systems carbonaceous species can become deposited on the catalyst surface. Graphitic carbon, coke and amorphous carbon have all been found deposited on the surface of used catalysts.[137] The formation of this bulk carbon is thought to occur mainly *via* the Boudouard reaction, Equation 1.21.[78] These inactive carbon species can prevent the interaction between reactant gases and the active catalyst surface and so reduce activity. It has been shown in cobalt catalysts that this mechanism is unlikely to be solely responsible for the decrease in catalytic activity observed.[199]

$$2CO \rightarrow C + CO_2$$

Equation 1.21 - The formation of bulk carbon *via* the Boudouard reaction.

Many studies have been conducted on regeneration procedures for catalyst systems affected by carbon deposition. Hydrogenation studies have been shown to reduce the amount of carbon deposited on the catalyst surface[200] but with little effect on catalyst activity. Oxygen-reduction treatments have proven quite effective in restoring catalyst activity with commercially used cobalt-based catalyst systems able to obtain lifetimes in the order of years when oxidative-reduction treatments are used.[201] These oxidative treatments can sometimes influence catalyst morphology resulting in catalyst systems that behave differently before and after regeneration. Some have reported improved catalyst performance with improved product selectivity[71] whereas others have reported significant decreases in catalytic activity[200] suggesting that the catalyst and conditions of the oxidative-reductive treatments play an important role in the regeneration procedure's success and effectiveness.

The extent of carbon deposition on a catalyst's surface can be reduced by the addition of other components to the catalyst system. DFT studies[202] have shown that the addition of noble metals such as platinum and ruthenium can reduce the formation of carbonaceous species. Less traditional (not cobalt or iron based) catalysts more tolerant to carbon such as molybdenum carbide based systems are also being investigated as a method to combat deactivation problems caused by catalyst coking.[203]

The final mechanism for catalyst deactivation is catalyst poisoning. Most industrial feed gases contain traces of sulfur and nitrogen based compounds that can cause poisoning and result in a reduced catalytic activity.[204] Poisoning by nitrogen containing poisons are less severe than that caused by sulfur containing poisons and can generally be removed by catalyst hydrogenation.[201] Sulfur based poisons when present above a certain threshold level can, however, irreversibly poison catalyst systems.[205]

The majority of papers covering the deactivation of catalysts in the Fischer-Tropsch process have found that one single mechanism is unlikely to be responsible for the observed deactivation. It is generally believed that several of the mechanisms are occurring simultaneously, dependent on the catalyst composition and reaction conditions.

1.3 Hydrogenation of CO_2

A range of methods are currently being investigated for the conversion of CO_2 to value added hydrocarbons.[206] While both photocatalystic and electrocatalytic methods have gained a great deal of interest, generating promising results, the field is still in its infancy and they do not currently give sufficient selectivity towards heavier, higher valued hydrocarbons and yields tend to be relatively low.[207] Thermochemical conversion of CO_2 has been known for several decades and at the moment is the most successful method used for production of heavier hydrocarbons.

Relative to the thermochemical hydrogenation of carbon monoxide, CO_2 has received very little attention, this is mainly due to its perceived high chemical stability. Of the papers published the mechanism employed for CO_2 conversion can generally bit split into three main categories; direct hydrogenation,[208] the methanol mediated and the non-methanol mediated approach.[209] Other than the direct hydrogenation process, which tends to form only short low value products, both involve two steps; first the conversion of CO_2 into a more reactive intermediate followed by the reaction of this intermediate to form hydrocarbons.

1.3.1 Conversion of CO_2 to Methanol and the Methanol Mediated Mechanism for the Formation of Hydrocarbons

Carbon dioxide can be converted to methanol *via* Equation 1.22. The replacement of CO with CO_2 for methanol formation has been gaining increasing attention over the last few decades.[210] Higher pressures favour the formation of methanol. The exothermic nature of the reaction means a lower reaction temperature should also favour the formation of methanol. At higher temperatures the endothermic RWGS reaction (see Section 1.1) can compete with methanol formation producing carbon monoxide. In fact a range of further reaction products are observed such as CO, hydrocarbons and higher alcohols[211] and as a result a selective catalyst is needed if methanol is desired as the sole product.

$$CO_2 + 3H_2 \rightarrow CH_3OH + H_2O,\ \Delta_R H^0_{298} = -90.7\ kJ\ mol^{-1}$$

Equation 1.22 – Hydrogenation of CO_2 for the formation of methanol

The majority of studies for methanol formation have focused on the use of catalysts already known to work for the CO to methanol process. The bulk of the investigated systems contain copper and zinc as the main components together with a range of promoters/modifiers such as silica[212] gallium, zirconia, alumina and chromium.[213] The addition of Ga_2O_3 improves specific activity while ZrO_2, Al_2O_3 and SiO_2 improve the copper dispersion.[214] The formation of water can however inhibit the formation of methanol and as such in order to obtain better performing catalysts water must either be removed or new catalysts, not sensitive to water, specific for methanol formation must be developed.

To this end several new catalysts are currently being investigated. Liang and co-workers have recently reported the use of a Pd-ZnO catalyst supported on carbon nanotubes (CNTs) as an effective catalyst for the formation of methanol from carbon dioxide.[215] They found that the use of CNTs as a catalyst support over the more traditional Al_2O_3 aided an increased dispersion of palladium and increased adsorption of hydrogen. Mixed Pd-Ga_2O_3 have also proved successful for methanol production.[216]

1.3.1.1 Formation of hydrocarbons from methanol

The conversion of methanol to hydrocarbons has been known since the early 1980s when it was discovered that methanol could be converted to hydrocarbons over a ZSM-5 zeolite catalyst. [217] Investigations into the reaction steps indicated that methanol was first being converted into dimethyl ether (DME) which is then dehydrogenated to form alkenes. An interruption of the reaction at this point leads to the production of light olefins, the so called methanol to olefins (MTO) process developed by Mobil. If the reaction is allowed to continue however these lower olefins can react further to form a mixture of higher olefins, paraffins aromatics and naphthenes so called the methanol to gasoline (MTG) process.[218] Both the MTO and MTG processes have been shown to be industrially viable.[218]

A range of further zeolites have since been shown to be active for the process with the range of catalysts investigated summarised in a review by Stöcker.[219] While the significant majority of studies have focused on the use of various zeolites a range of non-zeolytic materials have also proved successful.

1.3.1.2 Catalyst systems for the methanol mediated formation of hydrocarbons from CO_2

Several studies have investigated the combination of typical methanol producing catalysts, usually based on zinc or copper, with zeolite supports in an attempt to combine both the hydrogenation of CO_2 to methanol and the MTG/MTO process in order to produce a catalyst capable of converting CO_2 directly to hydrocarbons.[220]

Fujiwara and co-workers investigated the use of a Cu-Zn-Cr catalyst on a zeolite support.[221] They found that the catalyst was active for the formation of hydrocarbons from CO_2. Their work suggested that the Cu-Zn-Cr oxide component was active for the formation of CO and methanol and the zeolite active for the formation of hydrocarbons from the formed methanol *via* DME.[221]

Rongxian *et al*. investigated the effect of metal promoters and the influence of the zeolite support on a Fe-Zn-M/zeolite (where M = Cr, Mn, Zr, Al and La) catalyst and its ability for the hydrogenation of carbon dioxide for the formation of *iso*-alkanes.[222] Of the promotional metals investigated zirconia was found to be most effective for the formation of the desired *iso*-alkanes. The zeolite employed as a catalyst support also greatly influenced product selectivity

with the medium to strong nature of the HY zeolite's acidity playing an important role in its performance as the best support for iso-alkane synthesis.[222]

Studies by Ni and co-workers on the resulting optimised Fe-Zn-Zr/HY catalyst investigated the reaction mechanism.[223] They found that while the RWGS reaction is involved in the formation of CO it is not part of the overall reaction mechanism and is instead simply an undesired side reaction. Their investigations showed that the first step is the formation of methanol directly from CO_2 with the Fe-Zn-Zr being the active component of the catalyst for this process. The zeolite component of the catalyst is then responsible for the formation of C_1 to C_5 hydrocarbons through the MTG process. The zeolite is also active as a catalyst for the formation of *i*-C_5 through the dimerization of C_2 and C_3 hydrocarbons. The formation of C_1-C_4 hydrocarbons, albeit in small quantities, upon the removal of the zeolite support also indicates that the Fe-Zn-Zr component also shows limited activity for the MTG process.[223] The processes involved are summarised in Figure 1.12

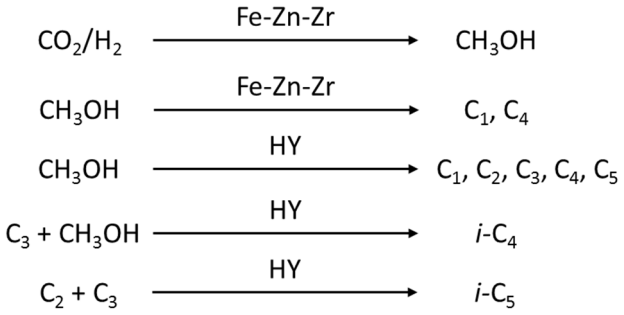

Figure 1.12 – The reaction mechanism for CO_2 hydrogenation to hydrocarbons over the Fe-Zn-Zr/zeolite catalyst as proposed by [223]

Despite the extensive research into composite catalysts such as those discussed above this approach currently still yields mainly short chained alkanes.

1.3.2 Methanation of CO_2 and the Direct Hydrogenation Mechanism for the Formation of Hydrocarbons

1.3.2.1 Methanation of CO_2

The catalytic hydrogenation of CO_2 to methane is often called the Sabatier reaction after its discoverer Paul Sabatier. Equation 1.23 shows the overall process. The methanation of CO_2 has several important uses namely the formation of compressed natural gas as well as being used as a feedstock for the formation of syngas. With the renewed interest in "fracking" there is now also a significant amount of attention going into developing uses of the large quantities of methane being formed through this process. For example, Audi are currently investigating

running cars utilising methane as a fuel.[224] One of the most interesting uses of the conversion of the Sabatier reaction is for the storage of excess energy formed from renewable sources (wind, solar and hydro).[214a] The reaction is also being studied by the National Aeronautics and Space Administration (NASA) as a possible source of water (which can also be split to give oxygen and hydrogen) and fuel from the carbon dioxide atmosphere on Mars as well as a possibility for the recycling of CO_2 given off in respiration by humans aboard the international space station.[225]

$$CO_2 + 2H_2 \rightarrow CH_4 + H_2O,\ \Delta_R H^0_{298} = -252.9\ kJ\ mol^{-1}$$

Equation 1.23 – The Sabatier reaction

The methanation of CO_2 is thermodynamically favourable although significant kinetic limitations mean that a catalyst is required in order to achieve acceptable conversions and selectivities.[226] Extensive investigations have been conducted on heterogeneous catalysts for the thermochemical hydrogenation of CO_2 to methane.

Catalysts based on nickel supported on inorganic oxides have been the most widely investigated systems for the Sabatier reaction. While all Group 8 metals show activity for CO_2 methanation economic factors have resulted in nickel receiving the majority of attention.[227] The nature of the support and the extent of interaction with the nickel has been shown to have a significant impact on catalyst performance and as such extensive research has been conducted on the effects of support on catalysis.[206]

Amorphous silica supported nickel catalysts have been shown to be active for methane production form CO_2 with a range of studies conducted.[227-228] The nature of the silica used can influence performance with Du *et al*. showing that a MCM-41 supported system shows greatly enhanced catalyst performance over amorphous silica.[225] The method used for catalyst preparation also influences the performance of Ni-SiO_2 catalysts, this is likely due to the effects on dispersion[229] with the nickel particle size appearing to have little to no effect on the intrinsic catalyst activity.[230]

The use of alumina as a catalyst support has also proven a successful for nickel based catalysts.[231] The strong interaction between Al_2O_3 and nickel can result in the formation of mixed oxides such as $NiAl_2O_4$ which can affect nickel reducibility and hence catalyst performance. Studies on the effect of nickel loading by Kester *et al*. showed that the interaction between nickel and Al_2O_3 is sufficiently strong as to form two distinct sites for methanation, one consisting of nickel crystallites the other a less reactive mixed alumina-nickel oxide.[232] As loading is increased the proportion of the less reactive sites is reduced.

A series of silica-alumina composites supports were synthesised and tested by Chang *et al*.[233] They found that while effective for CO_2 methanation the effectiveness of the catalysts

prepared varied greatly depending on the calcination and reduction temperatures used before catalyst tests. Generally hydrogenation activity decreased with increasing alumina content.

Two other oxides attracting interest as nickel supports are ZrO_2 and CeO_2. ZrO_2 has been shown to significantly promote the methanation of CO through an increased ability to adsorb CO and a hydrogen spillover phenomenon, the effect of ZrO_2 is however not as significant for CO_2 methanation.[234] The combination of ceria and zirconia as a mixed oxide catalyst support ($Ce_{0.75}Zr_{0.28}O_2$) has however proved very successful with high conversions and a 99.1 % selectivity to methane.[235] This improved catalyst performance can be attributed to the high oxygen storage capacity of the mixed oxide as well as the enhanced nickel dispersion.

The inclusion of addition metals (Fe, Zr, Y and Mg) to mesoporous nickel alumina xerogels have been investigated.[236] Methane yield was observed to decrease in the order Fe > Zr > Ni > Y > Mg.

Nickel-based catalysts can suffer from major drawbacks. One of the most troublesome is the formation of volatile nickel carbonyls due to the interaction of nickel nano-particles and CO at low temperatures.[237] This can result in the loss of the active component and deactivation of the catalyst. Another option for CO_2 methanation is the use of the more expensive noble metals ruthenium, rhodium,[238] palladium[226] and platinum.[239]

Of the noble metals studied the use of ruthenium has proved most effective with catalyst supported on Al_2O_3,[240] SiO_2[241] and CeO_2[242] successful. Recent studies have shown that ruthenium nano-particles supported on TiO_2 are capable of 100 % CH_4 selectivity at 160 ^oC when the particle size distribution is carefully controlled at *ca*. 2.5 nm.[243] This occurs at 200 ^oC lower than the same system if nano-particle size distribution is allowed to broaden.

Despite the relative simplicity of the Sabatier reaction some controversy still exists over the exact reaction mechanism. Several studies have reported that the process first involves the conversion CO_2 to CO followed by the hydrogenation of CO to methane. Kinetic studies on Ru/TiO_2 catalysts have indicated that CO is a key intermediate in the formation of methane which would support the CO mediated mechanism.[244] Formate species were also observed in these studies.

The second mechanism reported for CO_2 methanation involves the direct hydrogenation of CO_2 to methane without passing through a CO intermediate. FTIR studies conducted by Schild *et al*. indicated that CO_2 is rapidly adsorbed to the catalyst surface and a formate species formed.[245] This is formate is then hydrogenated to methane without further observable intermediates.

1.3.2.2 Direct hydrogenation of CO_2 to C_2+ hydrocarbons

Some literature suggests that the Sabatier reaction proceeds *via* a direct hydrogenation process and while the formation of methane in this manner accounts for the great majority of literature published on the direct hydrogenation of CO_2 for the formation of hydrocarbons the formation

of C_2+ hydrocarbons *via* the direct hydrogenation of CO_2 has also been reported although these instances are rare.[208, 246] Kinetic studies by Fiato *et al.* indicated that C_2+ hydrocarbons are formed through a direct hydrogenation mechanism over laser generated iron-carbide catalysts.[247] Further kinetic studies over a potassium promoted iron catalyst also showed that C_2+ hydrocarbons are formed *via* a direct hydrogenation mechanism although this work indicated that only a small portion of HCs are actually formed through this mechanism with the vast majority formed by the RWGS and FT reactions as discussed in detail in the next section.[208]

1.3.3 Conversion of CO_2 to Hydrocarbons Based on the RWGS Reaction and FT Synthesis

Carbon dioxide can be converted to hydrocarbons through a process involving two reaction steps. The first step is the reduction of carbon dioxide to carbon monoxide *via* the reverse water-gas shift reaction (discussed in detail in Section 1.1). The formed carbon monoxide can then be converted to hydrocarbons through the Fischer-Tropsch process (discussed in detail in Section 1.2). The processes involved are shown in Equation 1.24 and Equation 1.25.

$$CO_2 + H_2 \rightleftharpoons CO + H_2O,\ \Delta_R H^0_{298} = 41\ kJ\ mol^{-1}$$

Equation 1.24 – The reverse water-gas shift reaction

$$CO + 2H_2 \rightarrow (-CH_2-) + H_2O,\ \Delta_R H^0_{298} = -152\ kJ\ mol^{-1}$$

Equation 1.25 – The Fischer-Tropsch process

Due to the fact that the CO_2 must first be reduced to CO the hydrogenation of CO_2 consumes 50 % more hydrogen relative to the Fischer-Tropsch process. As a result twice as much water is also formed as a by-product which can negatively affect the performance of catalysts.[15] The endothermic nature of the RWGS reaction means that in order to get acceptable CO_2 conversion values higher temperatures than generally employed in Fischer-Tropsch synthesis are required. These high temperatures can, however, affect the product selectivity of FT catalysts. The formation of methane is thermodynamically favoured and as such catalysts must be developed that catalyse both the RWGS reaction and FT process but show a limited activity for the undesired direct hydrogenation of CO_2 to methane. In order to obtain optimal CO_2 conversion values the rate of the FT process should also be higher than that of the RWGS reaction meaning that any CO formed is rapidly consumed further aiding the formation of more CO.

This combined RWGS-FT process has been attracting the most attention of all the possible CO_2 to HCs routes and is the favoured method of the U.S. Navy who have been investigating the formation of jet fuel through this process.[207, 248] The widely available

literature on both FT and WGS catalysts mean that a range of already available research can be applied in order to aid catalyst development.

The desired product selectivity can generally be separated into two groups; short chained olefins and longer chained, liquid hydrocarbons. Long chained hydrocarbons are a desired target as they can act as a direct replacement for transport fuels with all the infrastructure for their distribution and use already in place. The second group, the lower (C_2-C_4) olefins, represent an important building block for many industrial processes such as the production of polymers, solvents, drugs, cosmetics and detergents.[249] They can also be used to form jet fuel and other liquid hydrocarbons using an acid catalysed oligamerisation process.[158]

As the production of hydrocarbons is essentially a modification of the FT process generally research has focused on the same type of catalysts that have been used successfully for the CO fed version. The vast majority of research has focused on the use of iron and cobalt based system, the only two metals used industrially for FT synthesis. Research has focused on the optimisation of these catalysts in order to increase conversion and direct selectivity away from methane and towards more valuable products.

1.3.3.1 Initial studies into the use of FT catalysts for CO_2 hydrogenation

Most of the initial studies into the use of Fischer-Tropsch based catalysts for the hydrogenation of CO_2 focused on the use of supported nickel catalysts.[250] These studies generally found that while it was possible to convert CO_2 to hydrocarbons using these systems[251] the product distribution showed a very high selectivity to methane.[252] Syn-gas fed Fischer-Tropsch studies on nickel based catalysts have shown that the temperatures normally employed in FT synthesis tend to shift product selectivity to almost entirely methane.[89] It is likely that under the relatively high temperatures required to form CO *via* the RWGS reaction nickel simply acts as a methanation catalysts and does not promote the growth of longer hydrocarbon chains normally seen in FT chemistry. The other possibility is that methane formation is occurring through the direct hydrogenation of CO_2, the detection of CO in the product stream makes this unlikely.

Studies by Vance *et al*. found that through the variation of support and reaction conditions the product selectivity could be somewhat shifted away from methane to CO but no C_2+ hydrocarbons were formed.[253] The large quantities of carbon monoxide being formed during reaction prompted an investigation into reaction mechanism by Weatherbee *et al*.[252] The mechanism proposed consisted of a combination of the redox mechanism of the RWGS reaction (see Section 1.1.2) for the formation of CO followed by the carbide mechanism of the FT process (see Section 1.2.2) for the conversion of CO into hydrocarbons. Kinetic studies based on this model were found to match observations well.

An extended study by Weatherbee and Bartholomew investigated the use of cobalt, iron and ruthenium catalysts supported on SiO_2 as well as nickel.[250] They found that while the

ruthenium-based system also formed only methane and carbon monoxide as products both iron and cobalt based systems showed the formation of C_2+ hydrocarbons.

1.3.3.2 Iron-based catalysts for CO_2 hydrogenation

Iron and cobalt catalysts are the only two metals utilised industrially for the FT process[28] and of these two metals iron has so far showed the most promise in the field of CO_2 hydrogenation. It is well known as an active component in FT catalysis (See Section 1.2) and, unlike cobalt based catalysts, is also widely used as a catalyst in both the WGS and RWGS reactions (See Section 1.1). While this WGS activity is sometimes seen as a disadvantage in FT catalysis as it competes with the FT reaction for the consumption of CO, under CO_2 hydrogenation conditions it is advantageous as it aids the conversion of CO_2 to CO *via* the RWGS reaction.

Whereas cobalt catalysts tend to only be utilised at lower temperatures (200-240 ^oC) iron catalysts are also used in the high temperature Fischer-Tropsch process (HTFT).[254] At these higher temperatures (300-350 ^oC) the iron catalysts are still capable of good product selectivity whereas cobalt mainly produces methane.[255] This better tolerance to higher temperatures is significant when catalysts are being employed in CO_2 hydrogenation as the endothermic nature of the first step (the RWGS reaction) means higher temperatures lead to higher equilibrium CO_2 conversion values.

Because of these facts iron-based catalyst have attracted the majority of attention in the field of CO_2 hydrogenation for the formation of hydrocarbons.[209] The majority of research conducted thus far has focused on the use of FT-type catalysts. Several studies have been conducted investigating the influence of CO_2 introduction into a traditional CO/H_2 fed FT reactions over iron-based catalysts as well as investigations on the effect of catalyst performance when switching the CO/H_2 to a CO_2/H_2 only stream.[256]

Increasing the concentration of CO_2 in a CO/H_2 feed has been shown to have a negative influence on the performance of an iron-based FT catalyst with a decreased rate of CO_2 conversion observed.[257] This decrease in rate has been attributed to a competition between the adsorption of CO and CO_2 over the active catalyst sites as demonstrated by temperature-programmed desorption studies.[257] Despite the low CO partial pressures when the feed is switched from CO/H_2 to CO_2/H_2, due to the equilibrium constraints of the RWGS reaction, iron-based catalyst are still observed to maintain a very similar product distribution for both feeds.[258] This provides good experimental evidence that HCs are being formed through the same process (FT synthesis) with both reaction feeds.

Early publications by Weatherbee and Bartholomew have shown that SiO_2 supported iron catalysts are active for the hydrogenation of CO_2 for the formation of hydrocarbons.[250] Despite its activity under the reaction conditions studied the Fe/SiO_2 system only produced HCs with a chain length of up to C_5 with a high preference (> 77 %) for the formation of the undesired product methane.[250] A similarly poor selectivity was observed by Dorner and co-

workers for iron supported on Al_2O_3.[259] While increasing iron loading did increase CO_2 conversion no effect was observed on product selectivity. Both systems also showed a low selectivity to olefin products with the majority of HCs formed being alkanes.

Iron-based catalysts utilised in FT synthesis frequently contain additives to promote structural and chemical properties while also stabilising the active components. In an attempt to combat the problems encountered when supported iron is used alone as a catalyst for CO_2 hydrogenation a range of different dopants have been investigated in an attempt to direct selectivity towards the desired products and increase CO_2 conversion.

The addition of potassium to iron-based catalyst systems for CO_2 hydrogenation has one of the most significant effects on the catalyst performance. Since initial work conducted by Lee and co-workers in 1988 showed that its incorporation into an unsupported iron system could both increase conversion and increase selectivity to hydrocarbon products over CO it has attracted a significant amount of attention in the literature.[260] In combination with the increased HC yield the potassium promoted catalyst systems also show a much higher selectivity towards heavier hydrocarbons with the relative amount of methane formed dropping drastically. The amount of unsaturated HCs produced was also significantly boosted with the olefin/paraffin ratio increasing from 0.9 to 6.4 with the addition of 3 at % potassium.[260] Further studies have shown that the same effect can be obtained by the addition of potassium to supported Fe/Al_2O_3 systems.[261] Ho Choi *et al*. showed that increasing potassium loading could also lead to a further improvement in catalyst performance both in terms of CO_2 conversion and product selectivity.[262] However, when the K/Fe molar ratio was increased above 0.5 to 1 little further improvement was observed suggesting this value is close to the optimal loading under the reaction conditions studied.

While the potassium promoted catalysts do show a high conversion and good selectivity little attention has been shown to the catalyst stability. Studies conducted by Hwang and co-workers has shown that a significant reduction (*ca.* 37 %) is observed over a 850 h period.[263] They found that the catalyst deactivation was mainly due to carbonaceous deposits, the catalyst performance could, however, be restored using a simple oxidative-reduction treatment. Lee *et al*. conducted a similar study again on a $Fe\text{-}K/Al_2O_3$, and found the catalyst deactivated significantly with time on stream.[264] While they also found that one of the main causes for catalyst deactivation was coke deposition they observed that a phase change of the active component of the catalyst to the inactive carbide Fe_3C also played an important role.[264]

While the role of potassium as a promoter for iron catalyst both in the FT process and the hydrogenation of CO_2 is not fully understood Dry *et al*. suggested that potassium acts as an electronic promoter.[156] They proposed that the potassium present donates electron density to the vacant d orbital of the iron enhancing the strength of binding and dissociative adsorption of CO while also lowering the H_2 adsorption ability. The reduced H_2 binding strength results in a reduced concentration of H_2 at the catalyst's surface leading to a less reductive environment and

as such an increase in alkene formation and a reduction in methane formation is observed. It is likely that a similar process is also responsible for the improved performance observed for CO_2 hydrogenation.[207] Chio *et al*. also demonstrated that potassium's introduction increased the chemisorption strength of CO_2 which would also aid the formation of CO, further improving the CO_2 conversion.[262]

The majority of Fe-K catalysts have been studied on an alumina support as it performs best both in terms of conversion and product selectivity. Dorner and co-workers reported that the improvement in certain catalysts containing both K and Al_2O_3 may be due to the formation of a potassium-aluminium mixed oxide which is either catalytically active or plays an important role in catalysis.[259] The presence of a potassium alanate ($KAlH_4$) phase was detected with a Fe-K/Al_2O_3 catalyst. This $KAlH_4$ phase can act as a hydrogen reservoir and a centre of H_2 activation which can improve catalyst performance.[259] This potassium alanate model is suggested to aid catalyst performance in conjunction with the electronic benefits and does not compete with that model.

The addition of a range of other alkali metals (lithium, sodium, potassium, rubidium and caesium) has also been investigated.[265] While lithium and sodium were shown to enhance catalyst performance both in terms of CO_2 conversion and selectivity to C_2+ hydrocarbons it was not to the same extent as that observed upon the addition of an equal amount of potassium. The addition of rubidium and caesium resulted in a slightly larger increase in CO_2 conversion relative to potassium inclusion this, however, occurred at the cost of HC selectivity with both metals increasing selectivity to methane compared to potassium addition.

Manganese is another dopant that has received significant attention in the field of Fischer-Tropsch catalysis with its promotional abilities in combination with iron known for some time.[266] Studies have shown that the addition of manganese to iron-based catalysts utilised in CO_2 hydrogenation can also be beneficial.[209] Lee *et al.* were one of the first groups to study the effects of manganese addition to iron catalysts with their studies focusing on its introduction into an unsupported iron-based CO_2 hydrogenation catalyst.[267] They found that, at high pressure (1013 kPa), the inclusion of manganese led to a slight increase in CO_2 conversion combined with a suppression of methane formation and a subsequent increase in chain growth probability. The same effect was observed for a co-precipitated Fe-Mn system investigated by Nam *et al.* with their work also showing a significant increase in selectivity to alkenes when manganese was also present in the system.[268]

Manganese's addition to a supported iron-based catalyst (Fe/Al_2O_3) has also been shown to result in the same promotional effect.[259] While increasing the manganese loading initially leads to a further improvement in performance over doping can result in a reversal of the promotional effect with selectivity shifting back towards undesirable products. This reduction in promotional ability at higher loadings has been attributed to the blocking of active sites with higher manganese content.[259]

The effect of manganese addition to iron-based catalysts has been reported to be two-fold with it acting both as a structural promoter and influencing the system through electronic effects.[207] Manganese has been shown to increase the surface basicity[269] and both aid the reduction of the irons species and their carburization.[267]

One of the most effective catalysts reported thus far for CO_2 hydrogenation is an Fe/Al_2O_3 catalyst promoted with a combination of both manganese and potassium.[259] The addition of both potassium and manganese simultaneously was initially shown to be successful for CO_2 hydrogenation over a silicalite-2 support with increasing potassium and manganese loadings resulting in improved catalyst performance.[270] Dorner and co-workers investigated the addition of the same promoters over an alumina support.[259] Similar effects were observed with the introduction of both potassium and manganese resulting in a significant increase in CO_2 conversion, HC yield and olefin/paraffin ratio whilst also reducing selectivity to methane. An optimal catalyst composition was found to be 17wt%Fe/12wt%Mn/8wt%K/Al_2O_3, which gave a CO_2 conversion of over 40 % and a methane selectivity of 26 % that remains one of the lowest values reported (290 ^oC, 13.6 atm, H_2:CO_2 3:1). The chain growth reported for this catalyst composition was found to be only slightly below that reported for comparable iron-based catalysts used in the FT process.[207]

The addition of copper to an iron-based CO_2 hydrogenation catalyst has also been shown to significantly improve the catalyst performance in a similar manner to that observed upon manganese addition.[206] Ando *et al*. showed that its introduction to an unsupported iron system resulted in a significant increase in CO_2 conversion and shifted HC selectivity away from methane and towards heavier HC products.[271] An increase in olefin content of the HC products is also reported.

The improved catalyst performance can likely be attributed to the increased reducibility of the iron species of the catalyst when copper is present.[272] An increased dispersion and ease of carburization are also likely to play a role.[273] Copper is active for the RWGS reaction and as such may also act as an active site for the initial reduction of CO_2 to CO which could also partially account for the improved catalyst performance.[274] When copper is reduced to its metallic form, as observed under reaction conditions,[271] it also provides active sites for the dissociative adsorption of hydrogen.[272]

As with the analogous manganese promoted systems the combination of copper with potassium as a second promoter has also been investigated. Studies by Yan *et al*. showed that the addition of potassium to an unsupported Fe-Cu catalyst system could further reduce selectivity towards methane and increase the selectivity towards heavier, more desirable hydrocarbons.[275] The effect of support addition was found to vary depending on the inorganic oxide used. Silica addition increased selectivity towards methane whereas alumina addition was found to enhance the catalyst performance.[275]

Catalyst optimisation studies have shown that increasing potassium loading can further increase the chain growth probability while also increasing selectivity to unsaturated hydrocarbon products.[275] A Fe-Cu-Al-K composition of 100:6.6:15.7:6 by weight ratio was found to perform best with a methane selectivity of 15 % reported for this catalyst system with a CO_2 conversion of *ca*. 40 % (300 ^oC, 10 atm, H_2:CO_2 3:1) making it one of the best performing CO_2 hydrogenation catalysts reported.[276]

Long-term tests on the Fe-Cu-K/Al_2O_3 catalyst over a period of 2000 h showed that after 1500 h on stream both CO_2 conversion and selectivity began to decrease.[276] XRD, XPS and Mössbauer spectroscopy techniques suggested that although carbon deposition was present is was not the main contributing factor in catalyst deactivation and it was in fact the growth of crystallite size resulting from component separation that was mainly responsible.[276] As a result the catalytic activity of the deactivated Fe-Cu-K-Al catalyst could not be regained by reduction or oxidative-reduction treatments.

The addition of zinc to an unsupported iron catalyst has been shown to improve its CO_2 hydrogenation ability.[268] The inclusion of zinc results in an increased CO_2 conversion and HC yield while also improving the product selectivity. Methane selectivity is greatly reduced and the percentage of unsaturated products can be increased from 6 % up to 70 %. While zinc's introduction is beneficial to catalyst performance its content should be kept low as if the Fe:Zn ratio is decreased below 9:1 the promotional effect begins to be reduced.[268]

Ceria is a highly active catalyst for both the low temperature WGS and RWGS reactions and as such has been generating a great deal of interest in this area (See Section 1.1.1). As the CO_2 present in the reaction stream must first be converted to CO *via* the RWGS reaction the use of ceria as a dopant for iron-based CO_2 hydrogenation catalysts has gained attention. Pérez-Alonso and co-workers studied the effects of ceria addition to an unsupported iron catalyst used for CO_2 hydrogenation they found that while the addition of ceria did not significantly change the overall performance of the catalyst system it did reduce the time needed for the system to reach stationary-state conditions.[277]

Dorner *et al*. studied what effect the addition of ceria had on a co-precipitated Fe-Mn/Al_2O_3 catalyst when used for CO_2 hydrogenation.[278] They found that the introduction of low loadings of ceria (2 wt%) led to a small improvement in CO_2 conversion with a slight reduction in methane selectivity. If the ceria loading was increased above this point, however, the promotional ability was reversed with lower CO_2 conversion and higher selectivity for methane observed.[278] It was found that the addition of ceria resulted in the formation of ceria particles on the surface of the iron catalysts and as such when ceria loading was increased it reduced the availability of chain growth sites.[278]

In an attempt to prevent the blocking of active sites by ceria particles the addition of ceria to an alumina support followed by a calcination step prior to the addition of the active catalyst components was tested with a Fe-Mn-K/Al_2O_3 catalyst.[279] It was found that if added in

this manner, thus preventing the ability of ceria to block active sites, an improvement in catalyst performance could be obtained with a 22 % increase in CO_2 conversion combined with a reduction in selectivity to methane and an increase in unsaturated hydrocarbons.[279]

A range of other metals have also been investigated as potential promoters for the iron-based CO_2 hydrogenation catalysts. They have not, however, received as much attention as those discussed thus far. Nam and co-workers studied the use of chromium and vanadium as dopants for unsupported iron catalysts.[268] Chromium addition was found to result in an increased CO_2 conversion but this occurred in conjunction with an increase in methane selectivity. Vanadium addition gave a reduced CO_2 conversion relative to the non-promoted iron system, there was however, an increase in selectivity to C_2+ HCs and unsaturated products.[268]

The addition of various loadings of lanthanum to alumina for use as a catalyst support for a potassium promoted iron catalyst has shown that it can be successfully used to enhance catalyst performance.[280] The modification of Al_2O_3 with lanthanum resulted in an increased CO_2 conversion, HC yield and selectivity to lower olefins. Methane selectivity was also found to be reduced. The effects could be increased further with increasing lanthanum loading until 4 wt%. Above this point the promotional ability begins to be reversed.[280]

The use of zirconium has also attracted some attention both as a support[281] (discussed in more detail later) and as a dopant.[282] The addition of zirconium to an Fe-Cu-Zn catalyst was found to result in enhanced CO_2 adsorption and higher hydrocarbon yields. Little effect was however observed in terms of hydrocarbon distribution.[282]

Nobel metals have been investigated extensively for iron-based FT catalysts[145-148] but have only received limited attention in the field of CO_2 hydrogenation. The addition of ruthenium to an Fe-K/Al_2O_3 catalyst was investigated by Lee and co-workers.[283] They found that the inclusion of ruthenium resulted in an increased CO_2 conversion and lower methane selectivity. A reduction in C_2-C_4 hydrocarbons was also observed with a much higher selectivity to heavier, longer chained hydrocarbon. This has been explained by the ruthenium component promoting the readsorption of olefin products which results in an increase in the length of the product hydrocarbon chain. As a result of this readsorption of products a slight deviation in ASF distribution is observed.[283] When the addition of ruthenium was investigated on a Fe-Cu-K/Al_2O_3 by Niemelä *et al*. they found no benefit in terms of CO_2 conversion or selectivity.[282] To this author's knowledge no further investigations using noble metal promoters have been conducted with iron-based CO_2 hydrogenation catalysts.

As already discussed iron-based catalysts are often supported on inorganic oxides as this tends to increase dispersion and aid catalyst stability. The catalyst performance both in terms of CO_2 conversion and product selectivity is greatly dependent on the supporting material used. Riedel and co-workers studied the influence of different supports on the performance of a

non-promoted iron catalyst and found that CO_2 conversion increased in the order $SiO_2 < TiO_2 < Al_2O_3$ with the selectivity towards methane found to decrease in the same order.[258]

The same order was also observed by Wang *et al*. for potassium promoted iron catalyst only their study was extended to also included the use of mesoporous carbon (meso-C), carbon nanotubes (CNTs) and ZrO_2.[281b] They found all three of the new supports gave a CO_2 conversion value similar to or greater than that of the alumina with the recorded CO_2 conversion values increasing in the order; $SiO_2 < TiO_2 < Al_2O_3 \sim$ Meso-C $<$ CNT $< ZrO_2$. Despite this increase in CO_2 conversion the product selectivity was not observed to follow the same trend with the Meso-C, CNT and ZrO_2 all giving a higher methane selectivity than the alumina supported system. The methane selectivity was observed to decrease in the order; $SiO_2 >$ Meso-C $>$ CNT $> TiO_2 > ZrO_2 > Al_2O_3$.[281b]

A similar trend was also observed for Al_2O_3, TiO_2 and ZrO_2 using non-promoted iron catalysts by Suo and co-workers.[281a] Investigations into the use of CNTs as a support for a Fe-K-Mn catalyst showed that the replacement of the more traditional Al_2O_3 support resulted in an increased CO_2 conversion, this however occurred at the cost of methane selectivity which was seen to increase when CNTs were utilised.[248] This matches the results observed by Wang *et al*. for an Fe-K catalyst.[281b]

A limited number of studies have also been conducted on the utilisation of mixed oxide supports for iron-based systems. The introduction of MgO in addition to Al_2O_3 as a support for an Fe-K catalyst showed both an increased conversion and an improved selectivity to heavier hydrocarbons and unsaturated products.[284] This is believed to be due to the increased basicity of the catalyst when MgO is used combined with the higher iron dispersion when Al_2O_3 is used. An Al_2O_3:MgO ratio of 80:20 was found to be optimal both in terms of CO_2 conversion and methane selectivity.[284]

Zeolites have also successfully been used as supports for iron-based CO_2 hydrogenation catalysts although these systems tend to form hydrocarbons through the methanol mediated mechanism discussed in Section 1.3.1.1 rather that the RWGS-FT process.

1.3.3.3 Cobalt-based catalysts for CO_2 hydrogenation

Cobalt catalysts are widely employed for CO fed FT processes, see Section 1.2.1.1. Despite their higher relative cost compared to iron-based systems their higher activity, greater selectivity to heavier hydrocarbons and increased stability make them the best performing in terms of performance-to-cost ratio. Properties seen as advantageous in the CO fed FT process such as low water-gas shift activity can however hinder their ability as catalysts for CO_2 hydrogenation. When utilised for FT synthesis cobalt catalysts are generally used at lower temperatures than iron-based systems in order to direct selectivity to heavier hydrocarbons,[285] these low temperatures are, however, not well suited to the formation of CO *via* the RWGS reaction which generally requires higher temperatures.

Despite these shortcomings cobalt-based systems are the second most studied catalysts for CO_2 hydrogenation after iron-based systems. Most studies have focused on the use of traditional FT based catalysts for CO_2 hydrogenation. A wide range of investigations into the effects of CO_2 introduction into CO/H_2 feeds have been completed in an attempt to gain a better understanding of how CO_2 effects the performance of the catalyst relative to a CO/H_2 only feed gas.

1.3.3.3.1 Effects of CO_2 introduction into a CO/H_2 feed over Co-based catalysts

When cobalt catalyst are tested under regular FT conditions with an CO/H_2 feed gas they generally perform well showing high CO conversions/activities as well as selectivity to heavy hydrocarbons with a good chain growth probability as determined from ASF plots. When the CO present in these reaction streams begins to be replaced with CO_2 the catalyst performance alters with significantly different results obtained from CO_2/H_2 streams compared with CO/H_2 feed gas.

Yao and co-workers investigated the influence of introducing increasing amounts of CO_2 to a CO/H_2 stream over a typical FT based cobalt catalyst; Co/TiO_2.[286] They found that both CO and CO_2 are readily hydrogenated over the Co/TiO_2 catalyst under standard FT reaction conditions. They in-fact observed higher conversions for systems containing more CO_2 perhaps indicating a higher reactivity for CO_2 over the catalyst being studied. The product selectivity was found to be strongly dependent on the amount of CO_2 present within the feed gas. For a purely CO/H_2 feed a high selectivity to heavier hydrocarbons was observed however with increasing CO_2 content the product distribution shifted towards methane with the pure CO_2/H_2 stream resulting in a CH_4 selectivity of approximately 90 %. Both the CO/H_2 and CO_2/H_2 only systems were found to follow the ASF distribution with only an exception for the C_1 point indicating that CO_2 hydrogenation was occurring through the combination of RWGS and FT reactions.

When a similar study was conducted over a Co/Al_2O_3 catalyst by Visconti *et al* they also found both CO and CO_2 were readily hydrogenated over the cobalt based catalyst with the CO_2 containing feed showing a higher reactivity than CO.[287] The selectivities observed for the CO/H_2 and CO_2/H_2 fed reactions were also drastically different with a regular FT distribution for CO but over a 90 % selectivity to methane for the CO_2 fed reaction. FTIR spectroscopy studies were conducted under both feeds with no evidence for the involvement of any different surface species in CO and CO_2 hydrogenation observed with the CO_2 hydrogenation appearing to hydrogenate through the same mechanism with a CO intermediate. They speculated that the drastically different product distributions could be attributed to the low strength of adsorption of CO_2 relative to CO with this resulting in a different atomic H/C ratio on the catalyst surface. The higher H/C ratio with the CO_2/H_2 feed inhibits chain growth due to the relatively high hydrogen concentration favouring the formation of methane.

The results obtained from mixed $CO/CO_2/H_2$ vary greatly from those observed by Yao *et al.*,[286] Visconti *et al.* found that in the presence of CO, CO_2 simply acted as an inert diluting gas. No significant change in product selectivity was observed when the CO_2 in the $CO/CO_2/H_2$ system was replaced by N_2.[287] This behaviour has been attributed to a competition between CO and CO_2 for adsorption on the catalyst surface. Gnanamani and co-worker's study of the effects of CO_2 over a $Co\text{-}Pt/Al_2O_3$ catalyst revealed the same trend with CO_2 acting as an inert gas in the presence of CO.[288] This was again attributed to the competition between CO and CO_2 for adsorption sites on the catalyst surface.

Riedel and Schaub investigated the effect of CO_2 addition to the CO/H_2 stream over several different cobalt catalysts containing several promoters such as ruthenium, platinum, lanthanum oxide and zirconia oxide supported on alumina and silica.[289] They found that the effect of CO_2 addition can depend on catalyst composition. For the majority of the catalysts studied CO_2 simply acted as a diluent as observed by Visconti[287] and Gnanamani.[288] However, for one of the catalyst systems studied the addition of CO_2 had a negative effect on the Fischer-Tropsch performance. This indicates that the composition of the catalyst can affect how the inclusion of CO_2 in the feed stream can affect the performance. This could be the reason behind the drastically different results obtained for the Co/TiO_2 system studied by Yao and co-workers.[286] Unfortunately Riedel and Schaub conducted no reactions using a CO_2/H_2 only feed without CO present and as such the effects of the promoters studied on the performance of the cobalt catalysts for CO_2 hydrogenation cannot be determined.

Zhang *et al.* studied the effect of CO_2 addition to the CO/H_2 stream over $Co\text{-}Pt/Al_2O_3$ and Co/SiO_2 catalysts and again noticed a significant difference between the products formed depending on whether the feed contained CO or CO_2 as the carbon source.[290] For all studies conducted with a CO_2/H_2 feed products consisted of greater than 70 % methane and although this is one of the lowest methane selectivity values reported for CO_2 hydrogenation over cobalt catalysts it is still significantly higher than that observed for the CO/H_2 fed reaction. Based on their results Zhang and co-workers concluded that in order to explain the exceptionally high methane selectivity for CO_2 fed reactions there must be a second reaction pathway for the conversion of CO_2, but not CO, to methane.

It was assumed that the hydrogenation and breaking of the two C-O bonds present in CO_2 rather than the one present in CO provides the source of the different reaction pathways. CO hydrogenation is proposed to proceed *via* the addition of an adsorbed H as shown in Equation 1.26.

$$C\text{-}O_a + 2H_a \rightarrow [H\text{-}C\cdots O\text{-}H]_a \rightarrow H\text{-}C_a + O\text{-}H_a$$

Equation 1.26 – Mechanism for breaking C-O bond in CO as proposed by Zhang *et al.*[290]

In the case of CO_2 hydrogenation the process is presumed to be more complex as there are two C-O bonds that must be broken. The first step (shown in Equation 1.27) involves the addition of an adsorbed H as with CO, there however still remains a second C-O bond.

$$O\text{-}C\text{-}O_a + 2H_a \rightarrow [H\text{-}C\cdots O\text{-}H]_a \rightarrow [H\text{-}C]_a + O\text{-}H_a$$
$$\qquad\qquad\qquad\qquad\quad |\qquad\qquad\quad |$$
$$\qquad\qquad\qquad\qquad\quad O\qquad\qquad\quad O$$

Equation 1.27 – Mechanism for breaking of first C-O bind in CO_2 as proposed by Zhang *et al.*[290]

From Equation 1.27 the next step is the hydrogenation of the above intermediate *via* Equation 1.28 to produce methane through a surface bond methanol intermediate.

$$[H\text{-}C\text{-}O]_a + 3H_a \rightarrow [H_3\text{-}C\text{-}O\text{-}H]_a + 2H_a \rightarrow CH_4 + H_2O$$

Equation 1.28 – Formation of methane from the surface bond $[H\text{-}C\text{-}O]_a$ species[290]

Based on their experimental results they reported that *ca*. 75 % of CO_2 hydrogenation occurs through the mechanism reported in Equation 1.27 and Equation 1.28 with the remainder proceeding *via* the formation of CO followed by the regular FT process. It is this remaining 25 % that accounts for the formation of the C_2+ hydrocarbons observed in the product stream.

1.3.3.3.2 Hydrogenation of CO_2 over Co-based catalysts

Although the effect of CO_2 addition to CO/H_2 fed reactions represents the majority of studies conducted over cobalt-based catalysts a range of studies have also been conducted using exclusively CO_2/H_2 feed gases. These studies generally focus on the use of FT type catalysts in an attempt to produce HCs from just CO_2 and H_2 with no additional reactants.

Akin *et al*. studied a co-precipitated Co/Al_2O_3 system as a possible catalyst for hydrocarbon formation.[291] Initial catalyst studies revealed that the catalyst was effective for CO_2 hydrogenation forming CO, CH_4 and a limited amount of C_2+ HCs. Increasing the temperature up to 540 K was found to lead to a higher CO_2 conversion with larger quantities of all products being formed. This is most likely due to the increased rate of CO formation *via* the RWGS reaction at higher temperatures.[291] Increasing the quantity of H_2 relative to CO_2 in the reaction feed led to a higher CO_2 conversion, although under the reaction conditions chosen for these studies it was not possible to determine the effect on HC distribution. The kinetic studies based on this data suggested that the reaction proceeded *via* the RWGS reaction followed by the FT process with the carbide mechanism for the later matching best with the experimental data more extensive studies are, however, required.[291]

Das and co-workers studied what effect the calcination temperature had on a Co/Al_2O_3 catalyst when utilised for the hydrogenation of CO_2 and compared it to an unsupported cobalt system also calcined at a range of temperatures.[292] They found that the use of Al_2O_3 inhibited

the reducibility of the cobalt oxide species; this can most likely be attributed to the interaction between the cobalt oxide and alumina support. This is further confirmed by the fact that higher calcination temperatures which would lead to stronger cobalt oxide-support interactions resulted in an increased reduction temperature. When the calcination temperature of the Co/Al_2O_3 catalyst is increased above 473 K a reduction in CO_2 conversion is observed with a concurrent decrease in selectivity towards methane. While this is likely partially attributable to the increased cobalt oxide-support interactions the same trend is also observed for the unsupported cobalt catalysts suggesting there is also a contribution from the larger nano-particles formed at higher calcination temperatures.[292] The Al_2O_3 supported cobalt systems showed a higher CO_2 conversion relative to the unsupported system.

One of the most comprehensive studies on CO_2 hydrogenation over cobalt-based catalysts has been conducted by Dorner *et al*. using a platinum promoted Co/Al_2O_3 catalyst.[293] They found the system to be active for CO_2 hydrogenation with only a slight (5 %) drop in conversion observed relative to a CO/H_2 fed catalyst system. The CO_2/H_2 fed system did however produce large quantities of methane (98 %). In order to determine if the alteration of the CO_2/H_2 feed ratio could shift this selectivity towards the more valuable C_2+ hydrocarbons a range of ratios (1:3, 1:2 and 1:1) were tested. They found that the selectivity to C_2-C_4 products could be increased up to 7 % as the relative content of CO_2 in the system was increased from 1:3 to 1:1. This did, however, occur at the cost of CO_2 conversion which drops significantly as the hydrogen content of the feed gas is decreased. There is also a slight increase in olefin content in the 1:1 fed system relative to the 1:3 test. This can most likely be attributed to the reduced quantity of H_2 present, which results in the formation of olefins becoming more favoured.

In addition to investigations into the effect of feed gas composition they also studied the effect of reaction pressure on the system. They found that as the reaction pressure was decreased from 450 psi to 150 psi the CO_2 conversion value decreased dramatically. This lowering of pressure did result in an increased selectivity towards longer chained hydrocarbons. Little to no selectivity towards olefins was observed.[293]

An increasing time on stream (TOS) was observed to lead to a reduction in selectivity towards methane. Doner *et al*. hypothesised that this could either be due a change in catalyst morphology or the deactivation of a particular site.[293] It is suggested, based on their results, that methane and C_2+ HCs are being formed over two separate active sites with the one responsible for methane formation more susceptible to deactivation by carbon deposition. This means that with increasing time on stream the amount of methane produced is gradually being reduced by deactivation of the methanation site and as such a shift in selectivity to C_2+ HCs is observed. Dorner and co-workers do, however, acknowledge that further *in situ* studies are required to fully confirm this.

The two active site hypothesis is backed up by the break between C_1 and longer hydrocarbon in the ASF plot of product distribution. Breaks in ASF plots such as this, known as the double alpha phenomenon, are typical for systems containing two active sites.[294] The break observed between C_1 and higher hydrocarbons is not typical for HCs produced by the FT process and as such suggests that HC formation is not occurring *via* the FT process and instead *via* the direct hydrogenation of CO_2.[293] This is further supported by the lack of CO observed in the product stream, something that would be expected if HC formation was occurring through the RWGS reaction followed by FT synthesis.

The hydrogenation of CO_2 over SiO_2 supported cobalt systems has also been investigated recently by Somorjai *et al*.[295] They prepared Co/SiO_2 catalysts that showed cobalt nanoparticles with a narrow particle size distribution using colloidal techniques.[295b] These catalysts were used to investigate the effect of cobalt particle size on CO_2 hydrogenation. They found the Co/SiO_2 systems to be active for the hydrogenation of CO_2 for the production CO and methane only with a strong preference for methane. The turn over frequency was observed to steadily increase as the average nanoparticle size increased. Cobalt particle diameter was however shown to have little effect on product selectivity.[295a]

Somorjai and co-workers also studied the use of bimetallic Co-Pt nanoparticles supported on MCF-17.[296] The bimetallic Co-Pt catalysts were compared to analogous Co and Pt only catalysts and studied under reaction conditions using a range of techniques such as TEM, XPS and near edge X-ray absorption fine structure (NEXAFS) spectroscopy. They found that the addition of platinum to the system aided the reduction of the cobalt oxide species as has been observed previously.[24] When tested for CO_2 hydrogenation all catalyst proved successful for CO_2 hydrogenation producing CO, CH_4 and trace amounts of C_2+ HCs. The Co-Pt system, despite showing a similar conversion to the Co-only system showed a significantly different product distribution. The HC selectivity was significantly reduced with CO formed almost exclusively. This is similar to the selectivity observed for the Pt only catalyst system. *In situ* studies indicated that under reduction conditions the platinum present in the bimetallic Co-Pt nanoparticles segregates to the surface, this would explain the 'Pt-like' performance of the catalyst as access to cobalt is limited.

Das *et al.* studied the hydrogenation of CO_2 over cobalt supported on Al_2O_3, SiO_2 and MgO.[297] All catalysts showed activity for the formation of CO and methane with a strong preference for CH_4. Activity was found to decrease in the order $Co/Al_2O_3 > Co/MgO > Co/SiO_2$ showing that the support has a significant influence on catalyst performance. *In situ* DRIFTS on both the Co/Al_2O_3 and Co/MgO systems indicated the presence of adsorbed formate species and chemisorbed CO whereas the Co/SiO_2 catalyst only showed the presence of chemisorbed CO and no formate species. This indicates that the support plays an important role in the formation of formate species on the catalyst surface. The formate formation does however appear to be independent of CO_2 conversion and CH_4 selectivity.[297]

It has been suggested that the high selectivity towards methane and limited formation of C_2+ hydrocarbon over cobalt-based catalysts is likely due to the limited RWGS activity of cobalt-based catalysts.[208] Studies by Keyser and co-workers showed that the addition of MnO as promoter with cobalt-based catalysts using in FT synthesis resulted in an increased WGS activity.[298] In an attempt to increase the RWGS activity of cobalt catalysts Riedel *et al*. studied the use of a Co-MnO-Pt/SiO_2 catalyst for CO_2 hydrogenation.[258] They envisioned that the increased RWGS activity of the catalyst would allow the formation of CO which could then in turn be converted to heavier hydrocarbons by the FT process.

While the studied Co-MnO-Pt/SiO_2 showed activity for CO_2 hydrogenation the selectivity to methane was still high at 95 %. This is likely due to the fact that even with CO formation the partial pressures formed would remain low and as such would be insufficient to establish a FT regime rather than CO_2 methanation.[258]

1.3.3.4 Mixed iron-cobalt catalysts for CO_2 hydrogenation

In order to determine if the known RWGS activity of iron based catalysts[209] could be combined with the high chain growth properties of the cobalt based catalyst systems observed under FT conditions bimetallic iron and cobalt catalysts have begun to attract attention. Although several studies have been conducted on mixed Co-Fe catalyst systems for CO hydrogenation *via* the FT process[299] the number of studies on these mixed systems in the field of CO_2 hydrogenation is so far limited.

Park and co-workers were the first to study mixed Fe-Co catalysts for CO_2 hydrogenation in an attempt to develop a catalyst with a high CO_2 conversion and good selectivity towards heavier hydrocarbons.[300] They studied an Fe-Co/Al_2O_3 system with a 2:1 Fe:Co ratio and found that the combination of Fe and Co gave a slightly higher CO_2 conversion than the analogous Fe-Ni/Al_2O_3 and Fe/Al_2O_3 systems. Despite the selectivity towards C_2+ being slightly higher than Fe-Ni/Al_2O_3 it did not outperform the Fe/Al_2O_3 system indicating there is no advantage in terms of hydrocarbon selectivity for the addition of cobalt.

Tihay *et al*. prepared a range of unsupported Co-Fe mixed catalysts with differing Co/Fe ratios and tested their ability for CO_2 hydrogenation.[301] XRD studies showed that the catalysts consisted of both a Co-Fe alloy and a cobalt magnetite mixed oxide spinel phase. The catalyst containing the highest iron content (Fe:Co ratio; 4:1) showed the highest CO_2 conversion and lowest selectivity to methane. When cobalt content was increased beyond this point a large drop in conversion and selectivity to C_2+ HCs is observed.

After reaction under a CO_2/H_2 feed XRD studies show that a large proportion of the spinel phase was converted to iron carbide. The extent of the conversion of the spinel phase appears to affect the catalyst performance with the catalyst containing the highest amount of iron showing the least attacked spinel phase resulting in the highest CO_2 conversion and best selectivity [301]

While these studies showed limited success only catalysts with high Co/Fe ratios (1-4) were investigated. A more systematic study was recently conducted by Satthawong and co-workers.[302] They investigated the effect of Fe:Co ratios on a Fe-Co/Al_2O_3 catalyst system including Co/Fe ratios significantly lower than studied previously (0.17 and 0.1). They found under CO_2 hydrogenation conditions the introduction of any cobalt loading to the Fe/Al_2O_3 system increased CO_2 conversion as previously observed by Park *et al.*[300] For catalyst containing a Co/Fe ratio of 0.17 and above cobalt's inclusion also resulted in an increased methane selectivity, however the bimetallic system containing the lowest content of cobalt (Co/Fe ratio; 0.1) a reduction in methane selectivity in conjunction with the higher CO_2 conversion was observed.

The addition of a small quantity of potassium to each bimetallic Fe-Co/Al_2O_3 system resulted in a further increase in CO_2 conversion[302] as has been previously witnessed with iron only catalysts utilised for CO_2 hydrogenation. Methane selectivity showed a further drop upon its inclusion. The Fe-Co-K/Al_2O_3 catalyst (Co/Fe ratio; 0.1) showed a methane selectivity of 18 %, significantly lower than that observed for the analogous Fe/Al_2O_3 system (80 %) and one of the lowest methane selectivity values reported for CO_2 hydrogenation catalysts.

1.4 Aim of Thesis

The primary aim of this thesis was the experimental investigation of heterogeneous iron and cobalt based catalysts for the hydrogenation of CO_2 into hydrocarbons. As discussed in the previous sections while both metals have been utilised for this purpose previously each show potential for further improvement. The iron-based catalysts, when used alone, tend to show a poor product selectivity and relatively low conversion, cobalt based systems on the other hand can show high conversion but selectivity tends to be almost exclusively towards methane. This aim was to be achieved through the following objectives.

1) The design and construction of purpose-built fixed-bed reactors capable of testing heterogeneous catalysts under a range of conditions

2) The preparation of a range of different catalyst systems utilising a range of different supports and co-catalysts/promoters.

3) The characterisation of these catalyst systems to determine the composition and species present as well as the effects of changing supports and the introduction of promoters.

4) The testing and optimisation of the prepared catalyst systems for CO_2 hydrogenation.

1.5 References

[1] IPCC, *Climate change 2007: Synthesis Report. Contribution of Working Groups I, II and III to the Fourth Assesment Report of the Intergovernmental Panel on Climate Change*, Cambridge University Press, **2007**.

[2] P. Kaiser, R. B. Unde, C. Kern, A. Jess, *Chem. Ing. Tech.* **2013**, *85*, 489-499.

[3] P. Lemke, J. Ken, R. B. Alley, I. Allison, J. Carrasco, G. Flato, Y. Fujii, G. Kaser, P. Mote, R. H. Thomas, T. Zhang, *Observations: Changes in Snow, Ice and Frozen Ground. In: Climate Change 2007: The Physical Basis*, Cambridge University Press, Cambridge, **2007**.

[4] K. E. Trenberth, P. D. Jones, P. Ambenje, R. Bojariu, D. Easterling, A. Klein Tank, D. Parker, F. Rahimzadeh, J. A. Renwick, M. Rusticucci, B. Soden, P. Zhai, *Observations: Surface and Atmospheric Climate Change, In: Climate Change 2007: The Physical Science Basis*, Cambridge University Press, Cambridge, **2007**.

[5] N. L. Bindoff, J. Willebrand, V. Artale, A. Cazenave, J. Gregory, S. Gulev, K. Hanawa, C. Le Quéré, S. Levitus, Y. Nojiri, C. K. Shum, L. D. Talley, A. Unnikrishnan, *Observations: Oceanic Climate Change and Sea Level, In: Climate Change 2007: The Physical Science Basis*, Cambridge University Press, Cambridge, **2007**.

[6] G. Centi, G. Iaquaniello, S. Perathoner, *ChemSusChem* **2011**, *4*, 1265-1273.

[7] G. Centi, S. Perathoner, *Catal. Today* **2009**, *148*, 191-205.

[8] IEA, *Statistics: CO2 Emissions from Fuel Combustion*, International Energy Agency, **2011**.

[9] IEA, *World Energy Outlook*, International Energy Agency, Paris, **2010**.

[10] *See http://www.eia.gov/ (accessed August 2013).*

[11] G. Carr, in *Alternative Energy Will no Longer be Alternative, The Economist: The World in 2013*, **2012**.

[12] B. Elvers, *Handbook of Fuels: Energy Sources for Transportation*, Wiley-VCH, Weinheim, **2008**.

[13] R. L. Espinoza, A. P. Steynberg, B. Jager, A. C. Vosloo, *Appl. Catal., A* **1999**, *186*, 13-26.

[14] (a) D. R. Hardy, T. Coffey, *Vol. US 7,420,004 B2* (Ed.: The_United_States_Of_America_As_Represented_By_The_Secretary_Of_The_Navy), **2008**; (b) *See http://www.nrl.navy.mil/media/news-releases/2012/fueling-the-fleet-navy-looks-to-the-seas (Accessed August 2013).*

[15] C. N. Satterfield, R. T. Hanlon, S. E. Tung, Z. M. Zou, G. C. Papaefthymiou, *Ind. Eng. Chem. Prod. R. D.* **1986**, *25*, 407-414.

[16] A. Jess, P. Kaiser, C. Kern, R. B. Unde, C. von Olshausen, *Chem. Ing. Tech.* **2011**, *83*, 1777-1791.

[17] (a) S. Manish, R. Banerjee, *Int. J. Hydrogen Energy* **2008**, *33*, 279-286; (b) S. Meher Kotay, D. Das, *Int. J. Hydrogen Energy* **2008**, *33*, 258-263.

[18] R. Abe, *J. Photochem. Photobiol., C* **2010**, *11*, 179-209.

[19] (a) G. H. Rau, S. A. Carroll, M. J. Bourcier, M. M. Smith, R. D. Aines, *Proc. Natl. Acad. Sci. U. S. A.* **2013**, *110*, 10095-10100; (b) G. H. Rau, *Environ. Sci. Technol.* **2010**, *45*, 1088-1092.

[20] C. Ratnasamy, J. P. Wagner, *Catal. Rev.* **2009**, *51*, 325-440.

[21] A. Faur Ghenciu, *Curr. Opin. Solid St. M.* **2002**, *6*, 389-399.

[22] Y. Tanaka, T. Utaka, R. Kikuchi, K. Sasaki, K. Eguchi, *Appl. Catal., A* **2003**, *238*, 11-18.

[23] H. Schulz, *Appl. Catal., A* **1999**, *186*, 3-12.

[24] A. Y. Khodakov, W. Chu, P. Fongarland, *Chem. Rev.* **2007**, *107*, 1692-1744.

[25] C. A. Chanenchuk, I. C. Yates, C. N. Satterfield, *Energ. Fuel* **1991**, *5*, 847-855.
[26] C. Pirola, C. L. Bianchi, A. Di Michele, S. Vitali, V. Ragaini, *Catal. Commun.* **2009**, *10*, 823-827.
[27] (a) O. S. Joo, K. D. Jung, Y. Jung, in *Stud. Surf. Sci. Catal., Vol. Volume 153* (Eds.: S. E. Park, S. J. Chang, K. W. Lee), Elsevier, **2004**, pp. 67-72; (b) O. S. Joo, K. D. Jung, I. Moon, A. Y. Rozovskii, G. I. Lin, S. H. Han, S. J. Uhm, *Ind. Eng. Chem. Res.* **1999**, *38*, 1808-1812.
[28] R. L. Espinoza, A. P. Steynberg, B. Jager, A. C. Vosloo, *Appl. Catal., A* **1999**, *186*, 13-26.
[29] S. S. Kim, K. H. Park, S. C. Hong, *Fuel Process. Technol.* **2013**, *108*, 47-54.
[30] M. S. Spencer, *Top. Catal.* **1999**, *8*, 259-266.
[31] C. Rhodes, G. J. Hutchings, A. M. Ward, *Catal. Today* **1995**, *23*, 43-58.
[32] Y. Li, Q. Fu, M. Flytzani-Stephanopoulos, *Appl. Catal., B* **2000**, *27*, 179-191.
[33] F. M. Gottschalk, G. J. Hutchings, *Appl. Catal.* **1989**, *51*, 127-139.
[34] K. M. V. Bussche, G. F. Froment, *J. Catal.* **1996**, *161*, 1-10.
[35] G. C. Chinchen, M. S. Spencer, K. C. Waugh, D. A. Whan, *J. Chem. Soc., Faraday Trans. 1* **1987**, *83*, 2193-2212.
[36] K. Klier, C. W. Young, J. G. Nunan, *Ind. Eng. Chem. Fund.* **1986**, *25*, 36-42.
[37] C. Rhodes, B. Peter Williams, F. King, G. J. Hutchings, *Catal. Commun.* **2002**, *3*, 381-384.
[38] S. Natesakhawat, X. Wang, L. Zhang, U. S. Ozkan, *J. Mol. Catal. A: Chem.* **2006**, *260*, 82-94.
[39] I. L. Júnior, J. M. M. Millet, M. Aouine, M. do Carmo Rangel, *Appl. Catal., A* **2005**, *283*, 91-98.
[40] A. Basinska, L. Kepinski, F. Domka, *Appl. Catal., A* **1999**, *183*, 143-153.
[41] M. Haruta, H. Kageyama, N. Kamijo, T. Kobayashi, F. Delannay, in *Stud. Surf. Sci. Catal., Vol. Volume 44* (Ed.: T. Inui), Elsevier, **1989**, pp. 33-42.
[42] H. Sakurai, A. Ueda, T. Kobayashi, M. Haruta, *Chem. Commun.* **1997**, *0*, 271-272.
[43] D. Andreeva, I. Ivanov, L. Ilieva, M. V. Abrashev, *Appl. Catal., A* **2006**, *302*, 127-132.
[44] D. Andreeva, V. Idakiev, T. Tabakova, A. Andreev, R. Giovanoli, *Appl. Catal., A* **1996**, *134*, 275-283.
[45] S. Kudo, T. Maki, T. Fukuda, K. Mae, *Catalysts* **2011**, *1*, 175-190.
[46] (a) T. Bunluesin, R. J. Gorte, G. W. Graham, *Appl. Catal., B* **1998**, *15*, 107-114; (b) X. Wang, R. J. Gorte, J. P. Wagner, *J. Catal.* **2002**, *212*, 225-230.
[47] B. I. Whittington, C. J. Jiang, D. L. Trimm, *Catal. Today* **1995**, *26*, 41-45.
[48] (a) F. C. Meunier, D. Tibiletti, A. Goguet, S. Shekhtman, C. Hardacre, R. Burch, *Catal. Today* **2007**, *126*, 143-147; (b) G. Jacobs, L. Williams, U. Graham, D. Sparks, B. H. Davis, *J. Phys. Chem. B* **2003**, *107*, 10398-10404; (c) X. Liu, W. Ruettinger, X. Xu, R. Farrauto, *Appl. Catal., B* **2005**, *56*, 69-75.
[49] A. Goguet, F. C. Meunier, D. Tibiletti, J. P. Breen, R. Burch, *J. Phys. Chem. B* **2004**, *108*, 20240-20246.
[50] S. Hilaire, X. Wang, T. Luo, R. J. Gorte, J. Wagner, *Appl. Catal., A* **2001**, *215*, 271-278.
[51] A. A. Andreev, V. J. Kafedjiysky, R. M. Edreva-Kardjieva, *Appl. Catal., A* **1999**, *179*, 223-228.
[52] H. Wang, Y. Lian, Q. Zhang, Q. Li, W. Fang, Y. Yang, *Catal. Lett.* **2008**, *126*, 100-105.
[53] D. Nikolova, R. Edreva-Kardjieva, T. Grozeva, *Reac. Kinet. Mech. Cat.* **2011**, *103*, 71-86.
[54] Y. Lian, R. Xiao, W. Fang, Y. Yang, *J. Nat. Gas Chem.* **2011**, *20*, 77-83.

[55] R. G. Copperthwaite, F. M. Gottschalk, T. Sangiorgio, G. J. Hutchings, *Appl. Catal.* **1990**, *63*, L11-L16.
[56] G. J. Hutchings, R. G. Copperthwaitet, F. M. Gottschalk, R. Hunter, J. Mellor, S. W. Orchard, T. Sangiorgio, *J. Catal.* **1992**, *137*, 408-422.
[57] (a) C. S. Chen, W. H. Cheng, S. S. Lin, *Catal. Lett.* **2000**, *68*, 45-48; (b) G. C. Chinchen, M. S. Spencer, K. C. Waugh, D. A. Whan, *Appl. Catal.* **1987**, *32*, 371-372; (c) C. S. Chen, W. H. Cheng, S. S. Lin, *Appl. Catal., A* **2004**, *257*, 97-106; (d) R. A. Koeppel, A. Baiker, A. Wokaun, *Appl. Catal., A* **1992**, *84*, 77-102.
[58] S. I. Fujita, M. Usui, N. Takezawa, *J. Catal.* **1992**, *134*, 220-225.
[59] (a) O. S. Joo, K. D. Jung, *Bull. Kor. Chem. Soc.* **2003**, *24*, 86-90; (b) S. W. Park, O. S. Joo, K. D. Jung, H. Kim, S. H. Han, *Appl. Catal., A* **2001**, *211*, 81-90.
[60] S. W. Park, O. S. Joo, K. D. Jung, H. Kim, S. H. Han, *Korean J. Chem. Eng.* **2000**, *17*, 719-722.
[61] A. G. Kharaji, M. A. Takassi, A. Shariati, *Int. Proc. Chem., Bio. Envir. Eng.* **2012**, *30*, 118-123.
[62] J. Kaspar, M. Graziani, A. M. Rahman, A. Trovarelli, E. J. S. Vichi, E. C. da Silva, *Appl. Catal., A* **1994**, *117*, 125-137.
[63] D. J. Pettigrew, D. L. Trimm, N. W. Cant, *Catal. Lett.* **1994**, *28*, 313-319.
[64] S. S. Kim, H. H. Lee, S. C. Hong, *Appl. Catal., A* **2012**, *423-424*, 100-107.
[65] A. Goguet, F. Meunier, J. P. Breen, R. Burch, M. I. Petch, A. Faur Ghenciu, *J. Catal.* **2004**, *226*, 382-392.
[66] M. C. Roman-Martinez, D. Cazorla-Amorós, A. Linares-Solano, C. S.-M. n. de Lecea, *Appl. Catal., A* **1994**, *116*, 187-204.
[67] (a) D. C. Grenoble, M. M. Estadt, D. F. Ollis, *J. Catal.* **1981**, *67*, 90-102; (b) T. van Herwijnen, W. A. de Jong, *J. Catal.* **1980**, *63*, 83-93; (c) T. Salmi, R. Hakkarainen, *Appl. Catal.* **1989**, *49*, 285-306.
[68] K. H. Ernst, C. T. Campbell, G. Moretti, *J. Catal.* **1992**, *134*, 66-74.
[69] R. A. Hadden, H. D. Vandervell, K. C. Waugh, G. Webb, *Catal. Lett.* **1988**, *1*, 27-33.
[70] C. S. Chen, W. H. Cheng, *Catal. Lett.* **2002**, *83*, 121-126.
[71] A. N. Pour, M. R. Housaindokht, S. F. Tayyari, J. Zarkesh, *J. Nat. Gas Chem.* **2010**, *19*, 362-368.
[72] E. Ortelli, J. Weigel, A. Wokaun, *Catal. Lett.* **1998**, *54*, 41-48.
[73] V. Arunajatesan, B. Subramaniam, K. W. Hutchenson, F. E. Herkes, *Chem Eng. Sci.* **2007**, *62*, 5062-5069.
[74] A. Goguet, S. O. Shekhtman, R. Burch, C. Hardacre, F. C. Meunier, G. S. Yablonsky, *J. Catal.* **2006**, *237*, 102-110.
[75] F. Fischer, H. Tropsch, *Vol. DE484337(c)*, **1925**.
[76] D. Leckel, *Energ. Fuel* **2009**, *23*, 2342-2358.
[77] M. E. Dry, *Catal. Today* **1990**, *6*, 183-206.
[78] G. P. Van Der Laan, A. A. C. M. Beenackers, *Catal. Rev.* **1999**, *41*, 255-318.
[79] B. Jager, R. Espinoza, *Catal. Today* **1995**, *23*, 17-28.
[80] M. E. Dry, *Catal. Today* **2002**, *71*, 227-241.
[81] A. A. Adesina, *Appl. Catal., A* **1996**, *138*, 345-367.
[82] *See http://www.oil-price.net/ (accessed August 2013).*
[83] Z. Jiang, T. Xiao, V. L. Kuznetsov, P. P. Edwards, *Philos. Trans. R. Soc. London, A* **2010**, *368*, 3343-3364.
[84] H. Schulz, *Appl. Catal., A* **1999**, *186*, 3-12.
[85] M. A. Vannice, *J. Catal.* **1975**, *37*, 449-461.
[86] M. A. Vannice, *J. Catal.* **1977**, *50*, 228-236.
[87] A. K. Datye, J. Schwank, *J. Catal.* **1985**, *93*, 256-269.

[88] R. C. Everson, E. T. Woodburn, A. R. M. Kirk, *J. Catal.* **1978**, *53*, 186-197.
[89] M. A. Vannice, *J. Catal.* **1976**, *44*, 152-162.
[90] J. A. Amelse, L. H. Schwartz, J. B. Butt, *J. Catal.* **1981**, *72*, 95-110.
[91] Z. Pan, M. Parvari, D. Bukur, *Top. Catal.* **2013**, 1-9.
[92] J. J. C. Geerlings, M. C. Zonnevylle, C. P. M. de Groot, *Surf. Sci.* **1991**, *241*, 315-324.
[93] B. Ernst, S. Libs, P. Chaumette, A. Kiennemann, *Appl. Catal., A* **1999**, *186*, 145-168.
[94] M. K. Gnanamani, G. Jacobs, W. D. Shafer, B. H. Davis, *Catal. Today* **2013**, *215*, 13-17.
[95] G. L. Bezemer, J. H. Bitter, H. P. C. E. Kuipers, H. Oosterbeek, J. E. Holewijn, X. Xu, F. Kapteijn, A. J. van Dillen, K. P. de Jong, *J. Am. Chem. Soc.* **2006**, *128*, 3956-3964.
[96] S. Rane, Ø. Borg, E. Rytter, A. Holmen, *Appl. Catal., A* **2012**, *437–438*, 10-17.
[97] J. Y. Park, Y. J. Lee, P. R. Karandikar, K. W. Jun, K. S. Ha, H. G. Park, *Appl. Catal., A* **2012**, *411–412*, 15-23.
[98] Z. J. Wang, S. Skiles, F. Yang, Z. Yan, D. W. Goodman, *Catal. Today* **2012**, *181*, 75-81.
[99] A. Y. Khodakov, A. Griboval-Constant, R. Bechara, V. L. Zholobenko, *J. Catal.* **2002**, *206*, 230-241.
[100] T. Ishihara, K. Eguchi, H. Arai, *J. Mol. Catal.* **1992**, *72*, 253-261.
[101] E. Iglesia, S. L. Soled, R. A. Fiato, *J. Catal.* **1992**, *137*, 212-224.
[102] R. C. Reuel, C. H. Bartholomew, *J. Catal.* **1984**, *85*, 78-88.
[103] A. M. Saib, M. Claeys, E. van Steen, *Catal. Today* **2002**, *71*, 395-402.
[104] D. Song, J. Li, *J. Mol. Catal. A: Chem.* **2006**, *247*, 206-212.
[105] G. Jacobs, P. M. Patterson, Y. Zhang, T. Das, J. Li, B. H. Davis, *Appl. Catal., A* **2002**, *233*, 215-226.
[106] H. Xiong, Y. Zhang, S. Wang, J. Li, *Catal. Commun.* **2005**, *6*, 512-516.
[107] C. Liu, J. Li, Y. Zhang, S. Chen, J. Zhu, K. Liew, *J. Mol. Catal. A: Chem.* **2012**, *363-364*, 335-342.
[108] S. Storsæter, B. Tøtdal, J. C. Walmsley, B. S. Tanem, A. Holmen, *J. Catal.* **2005**, *236*, 139-152.
[109] A. R. de la Osa, A. De Lucas, A. Romero, J. L. Valverde, P. Sánchez, *Catal. Today* **2011**, *176*, 298-302.
[110] T. O. Eschemann, J. H. Bitter, K. P. de Jong, *Catal. Today* **2013**.
[111] V. A. de la Pena O'Shea, M. Consuelo Alvarez Galvan, A. E. Platero Prats, J. M. Campos-Martin, J. L. G. Fierro, *Chem. Commun.* **2011**, *47*, 7131-7133.
[112] T. Wang, Y. J. Ding, J. M. Xiong, W. M. Chen, Z. D. Pan, Y. Lu, L. W. Lin, in *Stud. Surf. Sci. Catal., Vol. Volume 147* (Eds.: B. Xinhe, X. Yide), Elsevier, **2004**, pp. 349-354.
[113] L. Chen, G. Song, Y. Fu, J. Shen, *J. Colloid Interface Sci.* **2012**, *368*, 456-461.
[114] M. Zaman, A. Khodadi, Y. Mortazavi, *Fuel Process. Technol.* **2009**, *90*, 1214-1219.
[115] G. L. Bezemer, A. van Laak, A. J. van Dillen, K. P. de Jong, in *Stud. Surf. Sci. Catal., Vol. Volume 147* (Eds.: B. Xinhe, X. Yide), Elsevier, **2004**, pp. 259-264.
[116] M. Trépanier, A. Tavasoli, A. K. Dalai, N. Abatzoglou, *Fuel Process. Technol.* **2009**, *90*, 367-374.
[117] J. den Otter, K. de Jong, *Top. Catal.* **2013**, 1-6.
[118] X. Zhang, H. Su, X. Yang, *J. Mol. Catal. A: Chem.* **2012**, *360*, 16-25.
[119] N. Tsubaki, S. Sun, K. Fujimoto, *J. Catal.* **2001**, *199*, 236-246.
[120] T. K. Das, G. Jacobs, P. M. Patterson, W. A. Conner, J. Li, B. H. Davis, *Fuel* **2003**, *82*, 805-815.

[121] H. F. J. van 't Blik, D. C. Koningsberger, R. Prins, *J. Catal.* **1986**, *97*, 210-218.
[122] K. M. Cook, S. Poudyal, J. T. Miller, C. H. Bartholomew, W. C. Hecker, *Appl. Catal., A* **2012**, *449*, 69-80.
[123] D. Schanke, S. Vada, E. A. Blekkan, A. M. Hilmen, A. Hoff, A. Holmen, *J. Catal.* **1995**, *156*, 85-95.
[124] F. Rohr, O. A. Lindvåg, A. Holmen, E. A. Blekkan, *Catal. Today* **2000**, *58*, 247-254.
[125] A. Feller, M. Claeys, E. v. Steen, *J. Catal.* **1999**, *185*, 120-130.
[126] L. A. Bruce, G. J. Hope, J. F. Mathews, *Appl. Catal.* **1983**, *8*, 349-358.
[127] S. Colley, R. G. Copperthwaite, G. J. Hutchings, M. Van der Riet, *Ind. Eng. Chem. Res.* **1988**, *27*, 1339-1344.
[128] A. Dinse, M. Aigner, M. Ulbrich, G. R. Johnson, A. T. Bell, *J. Catal.* **2012**, *288*, 104-114.
[129] Z. J. L. R. J. Chen, J. G. S. Y. Han, *Acta Physico-chimica Sinica* **2002**, *3*, 014.
[130] G. L. Bezemer, P. B. Radstake, U. Falke, H. Oosterbeek, H. P. C. E. Kuipers, A. J. van Dillen, K. P. de Jong, *J. Catal.* **2006**, *237*, 152-161.
[131] B. Ernst, L. Hilaire, A. Kiennemann, *Catal. Today* **1999**, *50*, 413-427.
[132] J. S. Ledford, M. Houalla, A. Proctor, D. M. Hercules, L. Petrakis, *J. Phys. Chem.* **1989**, *93*, 6770-6777.
[133] A. M. Venezia, V. La Parola, L. F. Liotta, G. Pantaleo, M. Lualdi, M. Boutonnet, S. Järås, *Catal. Today* **2012**, *197*, 18-23.
[134] Y. Jin, A. K. Datye, *J. Catal.* **2000**, *196*, 8-17.
[135] G. B. Raupp, W. N. Delgass, *J. Catal.* **1979**, *58*, 361-369.
[136] (a) W. Ning, N. Koizumi, H. Chang, T. Mochizuki, T. Itoh, M. Yamada, *Appl. Catal., A* **2006**, *312*, 35-44; (b) M. D. Shroff, D. S. Kalakkad, K. E. Coulter, S. D. Kohler, M. S. Harrington, N. B. Jackson, A. G. Sault, A. K. Datye, *J. Catal.* **1995**, *156*, 185-207.
[137] E. de Smit, B. M. Weckhuysen, *Chem. Soc. Rev.* **2008**, *37*, 2758-2781.
[138] D. Mahajan, P. Gutlich, J. Ensling, K. Pandya, U. Stumm, P. Vijayaraghavan, *Energ. Fuel* **2003**, *17*, 1210-1221.
[139] J. W. Niemantsverdriet, A. M. van der Kraan, *J. Catal.* **1981**, *72*, 385-388.
[140] J. Galuszka, T. Sang, J. A. Sawicki, *J. Catal.* **1992**, *136*, 96-109.
[141] D. B. Bukur, C. Sivaraj, *Appl. Catal., A* **2002**, *231*, 201-214.
[142] D. B. Bukur, X. Lang, D. Mukesh, W. H. Zimmerman, M. P. Rosynek, C. Li, *Ind. Eng. Chem. Res.* **1990**, *29*, 1588-1599.
[143] C. H. Zhang, H. J. Wan, Y. Yang, H. W. Xiang, Y. W. Li, *Catal. Commun.* **2006**, *7*, 733-738.
[144] H. J. Wan, B. S. Wu, C. H. Zhang, B. T. Teng, Z. C. Tao, Y. Yang, Y. L. Zhu, H. W. Xiang, Y. W. Li, *Fuel* **2006**, *85*, 1371-1377.
[145] J. Xu, C. Bartholomew, J. Sudweeks, D. Eggett, *Top. Catal.* **2003**, *26*, 55-71.
[146] M. Luo, R. O'Brien, B. Davis, *Catal. Lett.* **2004**, *98*, 17-22.
[147] J. W. Niemantsverdriet, D. P. Aschenbeck, F. A. Fortunato, W. N. Delgass, *J. Mol. Catal.* **1984**, *25*, 285-293.
[148] M. M. Bhasin, W. J. Bartley, P. C. Ellgen, T. P. Wilson, *J. Catal.* **1978**, *54*, 120-128.
[149] G. L. Ott, T. Fleisch, W. N. Delgass, *J. Catal.* **1979**, *60*, 394-403.
[150] W. Ngantsoue-Hoc, Y. Zhang, R. J. O'Brien, M. Luo, B. H. Davis, *Appl. Catal., A* **2002**, *236*, 77-89.
[151] M. E. Dry, T. Shingles, C. S. van H. Botha, *J. Catal.* **1970**, *17*, 341-346.
[152] M. Luo, B. H. Davis, *Appl. Catal., A* **2003**, *246*, 171-181.
[153] M. E. Dry, G. J. Oosthuizen, *J. Catal.* **1968**, *11*, 18-24.
[154] M. E. Dry, *J. Chem. Technol. Biotechnol.* **2002**, *77*, 43-50.

[155] H. Arakawa, A. T. Bell, *Ind. Eng. Chem. Proc. D. D.* **1983**, *22*, 97-103.
[156] M. E. Dry, T. Shingles, L. J. Boshoff, G. J. Oosthuizen, *J. Catal.* **1969**, *15*, 190-199.
[157] R. J. O'Brien, L. Xu, R. L. Spicer, S. Bao, D. R. Milburn, B. H. Davis, *Catal. Today* **1997**, *36*, 325-334.
[158] C. H. Zhang, Y. Yang, B. T. Teng, T. Z. Li, H. Y. Zheng, H. W. Xiang, Y. W. Li, *J. Catal.* **2006**, *237*, 405-415.
[159] E. de Smit, F. M. F. de Groot, R. Blume, M. Havecker, A. Knop-Gericke, B. M. Weckhuysen, *Phys. Chem. Chem. Phys.* **2010**, *12*, 667-680.
[160] N. Lohitharn, J. G. Goodwin Jr, *J. Catal.* **2008**, *257*, 142-151.
[161] Z. Tao, Y. Yang, C. Zhang, T. Li, M. Ding, H. Xiang, Y. Li, *J. Nat. Gas Chem.* **2007**, *16*, 278-285.
[162] B. H. Davis, *Catal. Today* **2009**, *141*, 25-33.
[163] F. Fischer, *Brennstoff Chemie* **1926**, *7*, 97-99.
[164] S. R. Craxford, E. K. Rideal, *J. Chem. Soc.* **1939**, 1604-1614.
[165] S. R. Craxford, *Trans. Faraday Soc.* **1946**, *42*, 576-580.
[166] R. C. Brady, R. Pettit, *J. Am. Chem. Soc.* **1980**, *102*, 6181-6182.
[167] P. M. Maitlis, H. C. Long, R. Quyoum, M. L. Turner, Z. Q. Wang, *Chem. Commun.* **1996**, 1-8.
[168] M. Arsalanfar, A. A. Mirzaei, H. Atashi, H. R. Bozorgzadeh, S. Vahid, A. Zare, *Fuel Process. Technol.* **2012**, *96*, 150-159.
[169] P. M. Maitlis, R. Quyoum, H. C. Long, M. L. Turner, *Appl. Catal., A* **1999**, *186*, 363-374.
[170] M. E. Dry, *Appl. Catal., A* **1996**, *138*, 319-344.
[171] B. H. Davis, *Fuel Process. Technol.* **2001**, *71*, 157-166.
[172] (a) M. Zhuo, A. Borgna, M. Saeys, *J. Catal.* **2013**, *297*, 217-226; (b) W. Y. Mao, Q. W. Sun, W. Y. Ying, D. Y. Fang, *J. Fuel Chem. Tech.* **2013**, *41*, 314-321.
[173] H. Pichler, H. Schulz, *Chem. Ing. Tech.* **1970**, *42*, 1162-1174.
[174] R. B. Anderson, R. A. Friedel, H. H. Storch, *J. Chem. Phys.* **1951**, *19*, 313-319.
[175] W. K. Hall, R. J. Kokes, P. H. Emmett, *J. Am. Chem. Soc.* **1960**, *82*, 1027-1037.
[176] J. T. Kummer, T. W. DeWitt, P. H. Emmett, *J. Am. Chem. Soc.* **1948**, *70*, 3632-3643.
[177] R. A. van Santen, A. J. Markvoort, *ChemCatChem* **2013**, *5*, 3384-3397.
[178] L. C. Browning, P. H. Emmett, *J. Am. Chem. Soc.* **1952**, *74*, 1680-1682.
[179] S. J. Trepanier, J. N. L. Dennett, B. T. Sterenberg, R. McDonald, M. Cowie, *J. Am. Chem. Soc.* **2004**, *126*, 8046-8058.
[180] M. Claeys, E. van Steen, in *Stud. Surf. Sci. Catal., Vol. Volume 152* (Eds.: S. Andro, D. Mark), Elsevier, **2004**, pp. 601-680.
[181] D. B. Bukur, S. A. Patel, X. Lang, *Appl. Catal.* **1990**, *61*, 329-349.
[182] Z. Yan, Z. Wang, D. B. Bukur, D. W. Goodman, *J. Catal.* **2009**, *268*, 196-200.
[183] L. S. Glebov, G. A. Kliger, *Russ. Chem. Rev.* **1994**, *63*, 185.
[184] A. Tavakoli, M. Sohrabi, A. Kargari, *Chem. Eng. J.* **2008**, *136*, 358-363.
[185] M. E. Dry, *J. Mol. Catal.* **1982**, *17*, 133-144.
[186] G. A. Huff, C. N. Satterfield, *Ind. Eng. Chem. Proc. D. D.* **1985**, *24*, 986-995.
[187] T. Bhatelia, W. Ma, B. Davis, G. Jacobs, G. Drabukur, *Chem. Eng.Trans.* **2011**, *25*, 707-712.
[188] G. Jacobs, P. M. Patterson, Y. Zhang, T. Das, J. Li, B. H. Davis, *Appl. Catal., A* **2002**, *233*, 215-226.
[189] P. J. van Berge, J. van de Loosdrecht, S. Barradas, A. M. van der Kraan, *Catal. Today* **2000**, *58*, 321-334.

[190] V. Pendyala, G. Jacobs, J. Mohandas, M. Luo, H. Hamdeh, Y. Ji, M. Ribeiro, B. Davis, *Catal. Lett.* **2010**, *140*, 98-105.
[191] D. J. Moodley, A. M. Saib, J. van de Loosdrecht, C. A. Welker-Nieuwoudt, B. H. Sigwebela, J. W. Niemantsverdriet, *Catal. Today* **2011**, *171*, 192-200.
[192] N. E. Tsakoumis, M. Rønning, Ø. Borg, E. Rytter, A. Holmen, *Catal. Today* **2010**, *154*, 162-182.
[193] S. J. Park, J. W. Bae, G. I. Jung, K. S. Ha, K. W. Jun, Y. J. Lee, H. G. Park, *Appl. Catal., A* **2012**, *413–414*, 310-321.
[194] G. L. Bezemer, T. J. Remans, A. P. van Bavel, A. I. Dugulan, *J. Am. Chem. Soc.* **2010**, *132*, 8540-8541.
[195] M. Sadeqzadeh, S. Chambrey, S. Piché, P. Fongarland, F. Luck, D. Curulla-Ferré, D. Schweich, J. Bousquet, A. Y. Khodakov, *Catal. Today* **2013**.
[196] A. Tavasoli, S. Karimi, S. Taghavi, Z. Zolfaghari, H. Amirfirouzkouhi, *J. Nat. Gas Chem.* **2012**, *21*, 605-613.
[197] J. P. Reymond, P. Mériaudeau, S. J. Teichner, *J. Catal.* **1982**, *75*, 39-48.
[198] A. M. Saib, D. J. Moodley, I. M. Ciobîcă, M. M. Hauman, B. H. Sigwebela, C. J. Weststrate, J. W. Niemantsverdriet, J. van de Loosdrecht, *Catal. Today* **2010**, *154*, 271-282.
[199] D. J. Moodley, J. van de Loosdrecht, A. M. Saib, M. J. Overett, A. K. Datye, J. W. Niemantsverdriet, *Appl. Catal., A* **2009**, *354*, 102-110.
[200] J. M. G. Carballo, E. Finocchio, S. García-Rodriguez, M. Ojeda, J. L. G. Fierro, G. Busca, S. Rojas, *Catal. Today* **2013**, *214*, 2-11.
[201] F. G. Botes, J. W. Niemantsverdriet, J. van de Loosdrecht, *Catal. Today* **2013**.
[202] N. Balakrishnan, B. Joseph, V. R. Bhethanabotla, *Appl. Catal., A* **2013**, *462–463*, 107-115.
[203] D. V. N. Vo, V. Arcotumapathy, B. Abdullah, A. A. Adesina, *J. Chem. Technol. Biotechnol.* **2013**, *88*, 1358-1363.
[204] D. J. Duvenhage, N. J. Coville, *Appl. Catal., A* **2006**, *298*, 211-216.
[205] D. E. Sparks, G. Jacobs, M. K. Gnanamani, V. R. R. Pendyala, W. Ma, J. Kang, W. D. Shafer, R. A. Keogh, U. M. Graham, P. Gao, B. H. Davis, *Catal. Today* **2013**.
[206] W. Wang, S. Wang, X. Ma, J. Gong, *Chem. Soc. Rev.* **2011**, *40*, 3703-3727.
[207] R. W. Dorner, D. R. Hardy, F. W. Williams, H. D. Willauer, *Energy Environ. Sci.* **2010**, *3*, 884-890.
[208] T. Riedel, G. Schaub, K. W. Jun, K. W. Lee, *Ind. Eng. Chem. Res.* **2001**, *40*, 1355-1363.
[209] P. S. Sai Prasad, J. W. Bae, K. W. Jun, K. W. Lee, *Catal. Surv. Asia.* **2008**, *12*, 170-183.
[210] J. Ma, N. Sun, X. Zhang, N. Zhao, F. Xiao, W. Wei, Y. Sun, *Catal. Today* **2009**, *148*, 221-231.
[211] T. Inui, T. Takeguchi, *Catal. Today* **1991**, *10*, 95-106.
[212] T. C. Schilke, I. A. Fisher, A. T. Bell, *J. Catal.* **1999**, *184*, 144-156.
[213] M. Saito, T. Fujitani, M. Takeuchi, T. Watanabe, *Appl. Catal., A* **1996**, *138*, 311-318.
[214] (a) G. Centi, E. A. Quadrelli, S. Perathoner, *Energy Environ. Sci.* **2013**, *6*, 1711-1731; (b) M. Saito, K. Murata, *Catal. Surv. Asia.* **2004**, *8*, 285-294.
[215] X. L. Liang, X. Dong, G. D. Lin, H. B. Zhang, *Appl. Catal., B* **2009**, *88*, 315-322.
[216] S. Collins, D. Chiavassa, A. Bonivardi, M. Baltanás, *Catal. Lett.* **2005**, *103*, 83-88.
[217] D. Mignard, C. Pritchard, *Chem. Eng. Res. Des.* **2006**, *84*, 828-836.
[218] F. J. Keil, *Microporous Mesoporous Mater.* **1999**, *29*, 49-66.

[219] M. Stöcker, *Microporous Mesoporous Mater.* **1999**, *29*, 3-48.
[220] M. Fujiwara, R. Kieffer, H. Ando, Q. Xu, Y. Souma, *Appl. Catal., A* **1997**, *154*, 87-101.
[221] M. Fujiwara, R. Kieffer, H. Ando, Y. Souma, *Appl. Catal., A* **1995**, *121*, 113-124.
[222] B. Rongxian, T. Yisheng, H. Yizhuo, *Fuel Process. Technol.* **2004**, *86*, 293-301.
[223] X. Ni, Y. Tan, Y. Han, N. Tsubaki, *Catal. Commun.* **2007**, *8*, 1711-1714.
[224] in *The Economist*, **April 2013**.
[225] G. Du, S. Lim, Y. Yang, C. Wang, L. Pfefferle, G. L. Haller, *J. Catal.* **2007**, *249*, 370-379.
[226] J. N. Park, E. W. McFarland, *J. Catal.* **2009**, *266*, 92-97.
[227] W. Wei, G. Jinlong, *Front. Chem. Sci. Eng.* **2011**, *5*, 2-10.
[228] J. L. Falconer, A. E. Zağli, *J. Catal.* **1980**, *62*, 280-285.
[229] F. W. Chang, M. T. Tsay, S. P. Liang, *Appl. Catal., A* **2001**, *209*, 217-227.
[230] D. Baudouin, U. Rodemerck, F. Krumeich, A. d. Mallmann, K. C. Szeto, H. Ménard, L. Veyre, J. P. Candy, P. B. Webb, C. Thieuleux, C. Copéret, *J. Catal.* **2013**, *297*, 27-34.
[231] F. W. Chang, M. S. Kuo, M. T. Tsay, M. C. Hsieh, *Appl. Catal., A* **2003**, *247*, 309-320.
[232] K. B. Kester, E. Zagli, J. L. Falconer, *Appl. Catal.* **1986**, *22*, 311-319.
[233] F. W. Chang, M. T. Tsay, M. S. Kuo, *Thermochim. Acta* **2002**, *386*, 161-172.
[234] D. C. D. da Silva, S. Letichevsky, L. E. P. Borges, L. G. Appel, *Int. J. Hydrogen Energy* **2012**, *37*, 8923-8928.
[235] F. Ocampo, B. Louis, A. C. Roger, *Appl. Catal., A* **2009**, *369*, 90-96.
[236] S. Hwang, U. Hong, J. Lee, J. Baik, D. Koh, H. Lim, I. Song, *Catal. Lett.* **2012**, *142*, 860-868.
[237] M. Agnelli, M. Kolb, C. Mirodatos, *J. Catal.* **1994**, *148*, 9-21.
[238] A. Karelovic, P. Ruiz, *Appl. Catal., B* **2012**, *113–114*, 237-249.
[239] K. P. Yu, W. Y. Yu, M. C. Kuo, Y. C. Liou, S. H. Chien, *Appl. Catal., B* **2008**, *84*, 112-118.
[240] A. Beuls, C. Swalus, M. Jacquemin, G. Heyen, A. Karelovic, P. Ruiz, *Appl. Catal., B* **2012**, *113–114*, 2-10.
[241] S. Scirè, C. Crisafulli, R. Maggiore, S. Minicò, S. Galvagno, *Catal. Lett.* **1998**, *51*, 41-45.
[242] S. Sharma, Z. Hu, P. Zhang, E. W. McFarland, H. Metiu, *J. Catal.* **2011**, *278*, 297-309.
[243] T. Abe, M. Tanizawa, K. Watanabe, A. Taguchi, *Energy Environ. Sci.* **2009**, *2*, 315-321.
[244] M. Marwood, R. Doepper, A. Renken, *Appl. Catal., A* **1997**, *151*, 223-246.
[245] C. Schild, A. Wokaun, A. Baiker, *J. Mol. Catal.* **1990**, *63*, 243-254.
[246] U. Rodemerck, M. Holeňa, E. Wagner, Q. Smejkal, A. Barkschat, M. Baerns, *ChemCatChem* **2013**, *5*, 1948-1955.
[247] R. A. Fiato, E. Iglesia, G. W. Rice, S. L. Soled, in *Stud. Surf. Sci. Catal., Vol. Volume 114* (Eds.: T. Inui, M. Anpo, K. Izui, S. Yanagida, T. Yamaguchi), Elsevier, **1998**, pp. 339-344.
[248] R. W. Dorner, D. R. Hardy, F. W. Williams, H. D. Willauer, *Advances in CO2 conversion and utilization; Chapter 8 Catalytic CO2 Hydrogenation to Feedstock Chemicals for Jet Fuel Synthesis Using Multi-Walled Carbon Nanotubes as Support*, American Chemical Society, Washington, DC, **2010**.
[249] B. Hu, S. Frueh, H. F. Garces, L. Zhang, M. Aindow, C. Brooks, E. Kreidler, S. L. Suib, *Appl. Catal., B* **2013**, *132–133*, 54-61.
[250] G. D. Weatherbee, C. H. Bartholomew, *J. Catal.* **1984**, *87*, 352-362.

[251] G. D. Weatherbee, C. H. Bartholomew, *J. Catal.* **1981**, *68*, 67-76.
[252] G. D. Weatherbee, C. H. Bartholomew, *J. Catal.* **1982**, *77*, 460-472.
[253] C. K. Vance, C. H. Bartholomew, *Appl. Catal.* **1983**, *7*, 169-177.
[254] M. E. Dry, *Catal. Today* **2002**, *71*, 227-241.
[255] H. Schulz, *Appl. Catal., A* **1999**, *186*, 3-12.
[256] T. Riedel, H. Schulz, G. Schaub, K. W. Jun, J. S. Hwang, K. W. Lee, *Top. Catal.* **2003**, *26*, 41-54.
[257] D. Chun, H. T. Lee, J. I. Yang, H. J. Kim, J. H. Yang, J. C. Park, B. K. Kim, H. Jung, *Catal. Lett.* **2012**, *142*, 452-459.
[258] T. Riedel, M. Claeys, H. Schulz, G. Schaub, S. S. Nam, K. W. Jun, M. J. Choi, G. Kishan, K. W. Lee, *Appl. Catal., A* **1999**, *186*, 201-213.
[259] R. W. Dorner, D. R. Hardy, F. W. Williams, H. D. Willauer, *Applied Catalysis A: General* **2010**, *373*, 112-121.
[260] M. D. Lee, J. F. Lee, C. S. Chang, *Bull. Chem. Soc. Jpn.* **1989**, *62*, 2756-2758.
[261] (a) M. J. Choi, J. S. Kim, H. K. Kim, S. B. Lee, Y. Kang, K. W. Lee, *Korean J. Chem. Eng.* **2001**, *18*, 646-651; (b) S. C. Lee, J. H. Jang, B. Y. Lee, T. Jeong, S. J. Choung, in *Stud. Surf. Sci. Catal., Vol. Volume 153* (Eds.: S. E. Park, J. S. Chang, K. W. Lee), Elsevier, **2004**, pp. 185-188.
[262] P. H. Choi, K. W. Jun, S. J. Lee, M. J. Choi, K. W. Lee, *Catal. Lett.* **1996**, *40*, 115-118.
[263] J. S. Hwang, K. W. Jun, K. W. Lee, *Appl. Catal., A* **2001**, *208*, 217-222.
[264] S. C. Lee, J. S. Kim, W. C. Shin, M. J. Choi, S. J. Choung, *J. Mol. Catal., A: Chem.* **2009**, *301*, 98-105.
[265] Z. You, W. Deng, Q. Zhang, Y. Wang, *Chin. J. Catal.* **2013**, *34*, 956-963.
[266] J. Venter, M. Kaminsky, G. L. Geoffroy, M. A. Vannice, *J. Catal.* **1987**, *103*, 450-465.
[267] M. D. Lee, J. F. Lee, C. S. Chang, T. Y. Dong, *Appl. Catal.* **1991**, *72*, 267-281.
[268] S. S. Nam, S. J. Lee, H. Kim, K. W. Jun, M. J. Choi, K.-W. Lee, *Energ. Convers. Manage.* **1997**, *38*, *Supplement*, S397-S402.
[269] T. Li, Y. Yang, C. Zhang, X. An, H. Wan, Z. Tao, H. Xiang, Y. Li, F. Yi, B. Xu, *Fuel* **2007**, *86*, 921-928.
[270] L. Xu, Q. Wang, D. Liang, X. Wang, L. Lin, W. Cui, Y. Xu, *Appl. Catal., A* **1998**, *173*, 19-25.
[271] H. Ando, Q. Xu, M. Fujiwara, Y. Matsumura, M. Tanaka, Y. Souma, *Catal. Today* **1998**, *45*, 229-234.
[272] T. Herranz, S. Rojas, F. J. Pérez-Alonso, M. Ojeda, P. Terreros, J. L. G. Fierro, *Appl. Catal., A* **2006**, *311*, 66-75.
[273] S. Li, S. Krishnamoorthy, A. Li, G. D. Meitzner, E. Iglesia, *J. Catal.* **2002**, *206*, 202-217.
[274] (a) K. H. Ernst, C. T. Campbell, G. Moretti, *J. Catal.* **1992**, *134*, 66-74; (b) N. Schumacher, A. Boisen, S. Dahl, A. A. Gokhale, S. Kandoi, L. C. Grabow, **2005**, *229*, 265-275.
[275] S. R. Yan, K. W. Jun, J. S. Hong, M. J. Choi, K. W. Lee, *Appl. Catal., A* **2000**, *194–195*, 63-70.
[276] J. Hong, J. S. Hwang, K. Jun, J. C. Sur, K. W. Lee, *Appl. Catal., A* **2001**, *218*, 53-59.
[277] F. J. Pérez-Alonso, M. Ojeda, T. Herranz, S. Rojas, J. M. González-Carballo, P. Terreros, J. L. G. Fierro, *Catal. Commun.* **2008**, *9*, 1945-1948.
[278] R. W. Dorner, D. R. Hardy, F. W. Williams, H. D. Willauer, *Catal. Commun.* **2010**, *11*, 816-819.
[279] R. W. Dorner, D. R. Hardy, F. W. Williams, H. D. Willauer, *Catal. Commun.* **2011**, *15*, 88-92.

[280] S. S. Nam, G. Kishan, M. W. Lee, M. J. Choi, K. W. Lee, *Appl. Organomet. Chem.* **2000**, *14*, 794-798.
[281] (a) Z. H. Suo, Y. Kou, J. Z. Niu, W. Z. Zhang, H. L. Wang, *Appl. Catal., A* **1997**, *148*, 301-313; (b) J. Wang, Z. You, Q. Zhang, W. Deng, Y. Wang, *Catal. Today* **2013**, *215*, 186-193.
[282] M. Niemelä, M. Nokkosmäki, *Catal. Today* **2005**, *100*, 269-274.
[283] S.-C. Lee, J.-H. Jang, B.-Y. Lee, J.-S. Kim, M. Kang, S.-B. Lee, M.-J. Choi, S.-J. Choung, *Journal of Molecular Catalysis A: Chemical* **2004**, *210*, 131-141.
[284] G. Kishan, M. W. Lee, S. S. Nam, M. J. Choi, K. W. Lee, *Catal. Lett.* **1998**, *56*, 215-219.
[285] D. Leckel, *Energ. Fuel* **2009**, *23*, 2342-2358.
[286] Y. Yao, D. Hildebrandt, D. Glasser, X. Liu, *Ind. Eng. Chem. Res.* **2010**, *49*, 11061-11066.
[287] C. G. Visconti, L. Lietti, E. Tronconi, P. Forzatti, R. Zennaro, E. Finocchio, *Appl. Catal., A* **2009**, *355*, 61-68.
[288] M. K. Gnanamani, W. D. Shafer, D. E. Sparks, B. H. Davis, *Catal. Commun.* **2011**, *12*, 936-939.
[289] T. Riedel, G. Schaub, *Top. Catal.* **2003**, *26*, 145-156.
[290] Y. Zhang, G. Jacobs, D. E. Sparks, M. E. Dry, B. H. Davis, *Catal. Today* **2002**, *71*, 411-418.
[291] A. N. Akin, M. Ataman, A. E. Aksoylu, Z. I. Önsan, *React. Kinet. Catal. Lett.* **2002**, *76*, 265-270.
[292] T. Das, S. Sengupta, G. Deo, *Reac. Kinet. Mech. Cat.* **2013**, *110*, 147-162.
[293] R. W. Dorner, D. R. Hardy, F. W. Williams, B. H. Davis, H. D. Willauer, *Energ. Fuel* **2009**, *23*, 4190-4195.
[294] C. M. Masuku, D. Hildebrandt, D. Glasser, *Chem Eng. Sci.* **2011**, *66*, 6254-6263.
[295] (a) G. Melaet, A. Lindeman, G. Somorjai, *Top. Catal.* **2013**, 1-8; (b) V. Iablokov, S. K. Beaumont, S. Alayoglu, V. V. Pushkarev, C. Specht, J. Gao, A. P. Alivisatos, N. Kruse, G. A. Somorjai, *Nano Lett.* **2012**, *12*, 3091-3096.
[296] S. Alayoglu, S. Beaumont, F. Zheng, V. Pushkarev, H. Zheng, V. Iablokov, Z. Liu, J. Guo, N. Kruse, G. Somorjai, *Top. Catal.* **2011**, *54*, 778-785.
[297] T. Das, G. Deo, *J. Mol. Catal. A: Chem.* **2011**, *350*, 75-82.
[298] M. J. Keyser, R. C. Everson, R. L. Espinoza, *Appl. Catal., A* **1998**, *171*, 99-107.
[299] A. A. Mirzaei, R. Habibpour, E. Kashi, *Appl. Catal., A* **2005**, *296*, 222-231.
[300] S. E. Park, S. S. Nam, M. J. Choi, K. W. Lee, *Energy Convers. Manage.* **1995**, *36*, 573-576.
[301] F. Tihay, A. C. Roger, G. Pourroy, A. Kiennemann, *Energ. Fuel* **2002**, *16*, 1271-1276.
[302] R. Satthawong, N. Koizumi, C. Song, P. Prasassarakich, *Journal of CO_2 Utilisation* **2013**, *3-4*, 102-106.

2 Materials and Methods

The heterogeneous catalysts studied within this thesis were prepared using several preparation techniques. The method used for the preparation of each catalyst is discussed briefly in each chapter with full details given Section 2.7. Catalysts were analysed using a range of different characterisation techniques, the details of equipment used and conditions are given in Section 2.1.

Information on the all reactors used for catalyst testing along with the general testing procedures is given in Sections 2.2 and 2.3. Product analysis was conducted using gas chromatography. The full details of the equipment and procedures used are given in Section 2.4. Details of any other calculations reported within this thesis are given in Section 2.5.

2.1 Characterisation Methods

2.1.1 Scanning Electron Microscopy (SEM)

Scanning electron microscopy, often abbreviated to SEM, is a method of electron microscopy that scans a sample with a focused beam of electrons allowing for analysis of the catalyst morphology on a nm scale.

Powdered catalyst samples were prepared by supporting on carbon tape. SEM analysis was carried out on a JEOL 6480LV at 5-25 kV acceleration voltage.

2.1.2 Transmission Electron Microscopy (TEM)

Transmission electron microscopy, often abbreviated to TEM, is another method of electron microscopy. A beam of electrons is transmitted through a thin piece of sample with an image formed from the interaction with the sample as it passes through and allows analysis of catalyst morphology.

Powdered catalysts samples for TEM analysis were prepared by dispersion in ethanol before being deposited on a copper or nickel grid. TEM analysis was conducted on a JEOL 1200 operated at 120 kV. Particle sizes were measured and the distributions calculated using ImageJ software.

2.1.3 Energy Dispersive X-ray Spectroscopy (EDX/EDS)

Energy dispersive X-ray spectroscopy, often abbreviated to EDX or EDS, is a technique used to analyse the X-rays given off by a sample when excited, normally by a high-energy beam of electrons. The X-rays given off when stimulated by a beam of electrons are characteristic for each element and allows the analysis of the composition of the sample under investigation.

EDX studies were conducted *in situ* during SEM analysis on a JEOL 6480LV. Sample preparation was the same as that used for SEM as detailed in Section 2.1.1.

2.1.4 Powder X-ray Diffraction (pXRD/XRD)

Powder X-ray diffraction, abbreviated to pXRD or just XRD, is a method of determining the crystalline phases present in the bulk material. X-rays are fired at a powdered samples and the diffraction pattern recorded. From the position of the peaks present the crystalline compounds present can be identified using a database of know materials. The crystalline particle size may also be determined using XRD based on the broadening of the diffraction peaks. Full details of this procedure are given in Section 2.5.1.

Generally XRD samples were run on a BRUKER D8-Advance diffractometer set up in capillary mode in the 2θ range of 4 – 60 ^{o} with a step size of 0.0164 ^{o} and a time per step of 0.6 s. Cu Kα (λ = 1.5406 Å) radiation was used for all samples.

For analysis of crystalline size the method of diffraction pattern acquisition was changed slightly. The BRUKER D8 was set in flat-plate mode with a step size of 0.0164 ^{o} and a time per step of 0.6 s.

2.1.5 Thermogravimetric Analysis (TGA)

Thermogravimetric analysis, abbreviated to TGA, is a method of thermal analysis in which the change in mass of a sample may be monitored over a range of temperatures allowing the investigation of sample decomposition or oxidation.

The TGA results reported within this thesis were recorded on two different instruments. The first was a Perkin Elmer TGA 7 instrument over a temperature range of 45 to 600 ^{o}C at a heating rate of 10 ^{o}C min^{-1} under static air. The second instrument used was a Mettler Toledo TGA/DSC 1 analysed over a 50 to 600 ^{o}C temperature range at a heating rate of 10 ^{o}C min^{-1} under an air flow of *ca*. 25 ml min^{-1}.

2.1.6 N_2 Physisorption Analysis

N_2 physisorption experiments were conducted in order to determine the surface area of the catalysts used. This was done through the use of the Brunauer-Emmett-Teller (BET) theory, Equation 2.1.

$$\frac{P}{V(P_0 - P)} = \left(\frac{c-1}{V_{mon}c}\right).\left(\frac{P}{P_0}\right) + \left(\frac{1}{V_{mon}c}\right)$$

Equation 2.1 – The BET equation

All N_2 physisorption experiments were carried out using a BELSORP mini-II gas adsorption instrument. All samples were first pre-treated under vacuum for 420 minutes at 300 ^{o}C before measurements. All data were collected at 77 K and analysed in the P/P_0 range of 0.05-0.3.

2.1.7 X-Ray Photoelectron Spectroscopy (XPS)

X-ray photoelectron spectroscopy, abbreviated to XPS, is a quantitative, surface sensitive, spectroscopic technique used to analyse the surface composition of a sample. From the data obtained it is also possible to determine the chemical and electronic state of each element present.

The XPS data reported within this thesis were recorded on three different spectrometers; (1) A Kratos AXIS Ultra-DLD photoelectron spectrometer housed at Cardiff University with monochromatic Al-K_α radiation, samples run by Dr. David Morgan. (2) A VG Escalab 250 with monochromatic Al-K_α radiation located at Leeds University, samples run by Dr. Benjamin Johnson (3) A Kratos AXIS 165 spectrometer with a monochromatic Al-K_α X-ray gun, located at the Materials & Surface Science Institute, University of Limerick. Samples run by Dr. Fathima Laffir.

All survey scans were conducted from 0-1200 eV (binding energy) with a 1 eV step size and a dwell of 50 ms. More detailed spectra were collected with a step size of 0.05 eV with a dwell of 100 ms with exception of the results recorded in the University of Leeds where a step size of 0.25 eV and a dwell of 100 ms was used. All spectra were calibrated to the C 1s line at 284.8 eV. The XPS detection limit was estimated to be *ca.* 0.1 at%.

2.1.8 Raman Spectroscopy

Raman spectroscopy is a spectroscopic technique which can yield information on the species present in the sample providing they are Raman active. Raman spectra reported within this thesis were all collected on a Renishaw InVia Raman microscope with a laser beam emitting at 530 nm. The collection optic was set at 50X objective.

2.2 Catalyst Testing Rigs

The choice of reactor for catalyst testing is important for the process being studied.[1] The chosen design must be simple and cost effective whilst also providing reliable results that are representative of what may be achieved when scaled up. Although many types of reactor are used in the commercial Fischer-Tropsch process the majority of catalyst tests reported are conducted in two forms of reactor, the tubular fixed bed reactor and the stirred tank reactor.[2]

Each reactor possesses advantages and disadvantages and as such the choice of which to use must be carefully considered. The main problem with using a stirred tank reactor is the separation of reaction products and changing of exhausted catalyst.[3] A stirred tank reactor consists of a tank of fine catalyst powder suspended in a liquid that is continuously agitated. Heavier hydrocarbons formed though the Fischer-Tropsch process can build up and cause clogging as well as causing large problems with separation. Due to the generally larger nature of the tank-based reactors a relatively large amount of catalyst is required for each test.

Fixed bed reactors generally consist of a sample tube packed with catalyst that is heated while reactant gases are flowed through the sample bed. Fixed bed reactors when employed on a

large scale can suffer from insufficient heat removal,[1] especially when used with reactions as exothermic as the Fischer Tropsch process. This problem is however greatly reduced when working on a smaller scale. They possess many advantages over stirred tank reactors such as the simplicity of operation and maintenance as well as the easy exchange of used catalyst.

As this thesis focused on the screening of a large range of catalysts the ease of catalyst exchange was of vital importance and as such a fixed bed tubular reactor was chosen for all catalyst tests. As the reactors were constructed specifically for this project the simplicity of construction and maintenance also played a large part in the decision for its use over a stirred tank reactor based system.

As screening was carried out on a small scale it was envisaged that problems due to heat removal would be minimal. For the reduction of carbon dioxide the endothermic reverse water-gas shift reaction should also help in limiting the influence of this problem.

Bukur *et al*.[2] conducted a study on the effects of reactor type on the performance of an industrially employed catalyst. They found that there was no significant difference in product distribution between tests carried out in a fixed bed reactor and a stirred tank reactor. Their work suggested that a fixed bed reactor is ideal for screening catalysts intended for use in both reactor types when used on much larger scales.

For the work reported in this thesis three reactors were constructed, one designed for low pressure testing of catalysts for direct hydrogenation of carbon dioxide, a second for testing the Fischer-Tropsch activity of catalysts with a CO/H_2 feed-gas and a third reactor capable of both CO/H_2 and CO_2/H_2 fed reactions at elevated pressures. All three reactors were purpose built for this project in collaboration with Dr. Justin O'Byrne and Mr. Daniel Minett.

2.2.1 Reactor 1

Reactor 1 was designed for the atmospheric pressure testing of catalysts for the direct hydrogenation of carbon dioxide. The tubular fixed bed reactor is constructed mainly of Swagelok stainless steel consisting of several sections which will be described in more detail below.

The gas supply system consists of three gas lines permanently connected to cylinders of argon (BOC – Pureshield, 99.998% purity), hydrogen (BOC – High Purity, 99.995% purity) and carbon dioxide (99.9% purity). The pressure of each gas was individually controlled using the two-stage regulator attached to the neck of each bottle. Each cylinder was connected to an Omega FMA-2600A series mass flow controller (MFC) (max working pressure 10 bar) by ¼ inch external diameter Swagelok stainless steel tubing. A connected PC controlled each MFC through the use of LabView software. After flow is regulated individually all gas lines are connected and merged into a single line. After each MFC all gas lines were equipped with a Swagelok ball valve to prevent back flow of gases through closed mass flow controllers.

The single gas line was directly connected to the sample cell of tubular fixed bed reactor, shown in more detail in Figure 2.1. It consists of a stainless steel tube 130 mm long with a 4.6 mm internal diameter, packed with catalyst. Quartz wool was employed to keep the powdered catalyst sample in place under gas flow. The sample cell is encapsulated in a 3-zone Carbolite furnace (1200 ^{o}C max operating temperature); the temperature of each zone can be controlled individually by a two Eurotherm 213 control panels and a Eurotherm 3216 temperature controller for the central stage. For the reactions reported within this thesis all stages were set to the same temperature, this functionally does, however, provide the possibility in future tests to either have a range of temperatures across a single sample cell or test a two catalyst system with each at a different temperature.

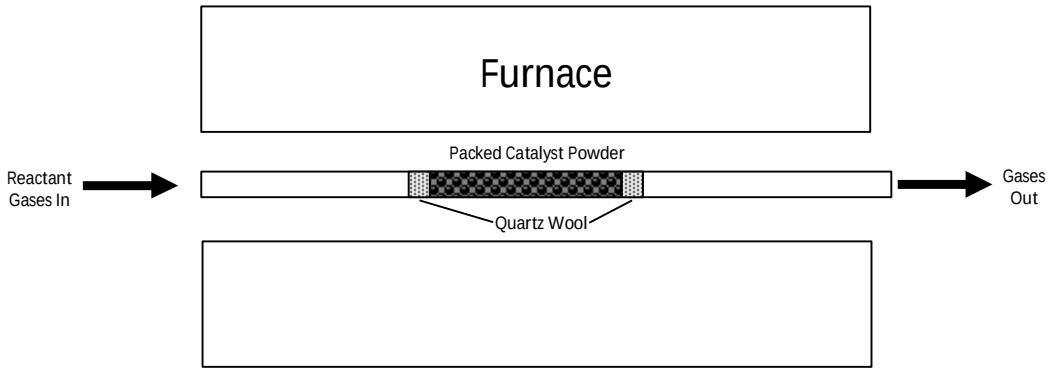

Figure 2.1 – Schematic showing the sample cell of Reactor 1

An in-line, 0.5 micron pore size, particulate filter was positioned at the end of the reactor in order to ensure no catalyst particles are collected when sampling. The filter was then connected to a water-cooled condenser and collection flask *via* two Swagelok three-way ball values to allow for product analysis *via* either an *in situ* gas chromatograph (GC) equipped with a flame ionisation detector (FID) or an isolated GC-MS system. Exhaust gases then pass through a silicon oil bubbler before being connected to the labs extraction system. A schematic representation of Reactor 1 is shown in Figure 2.2

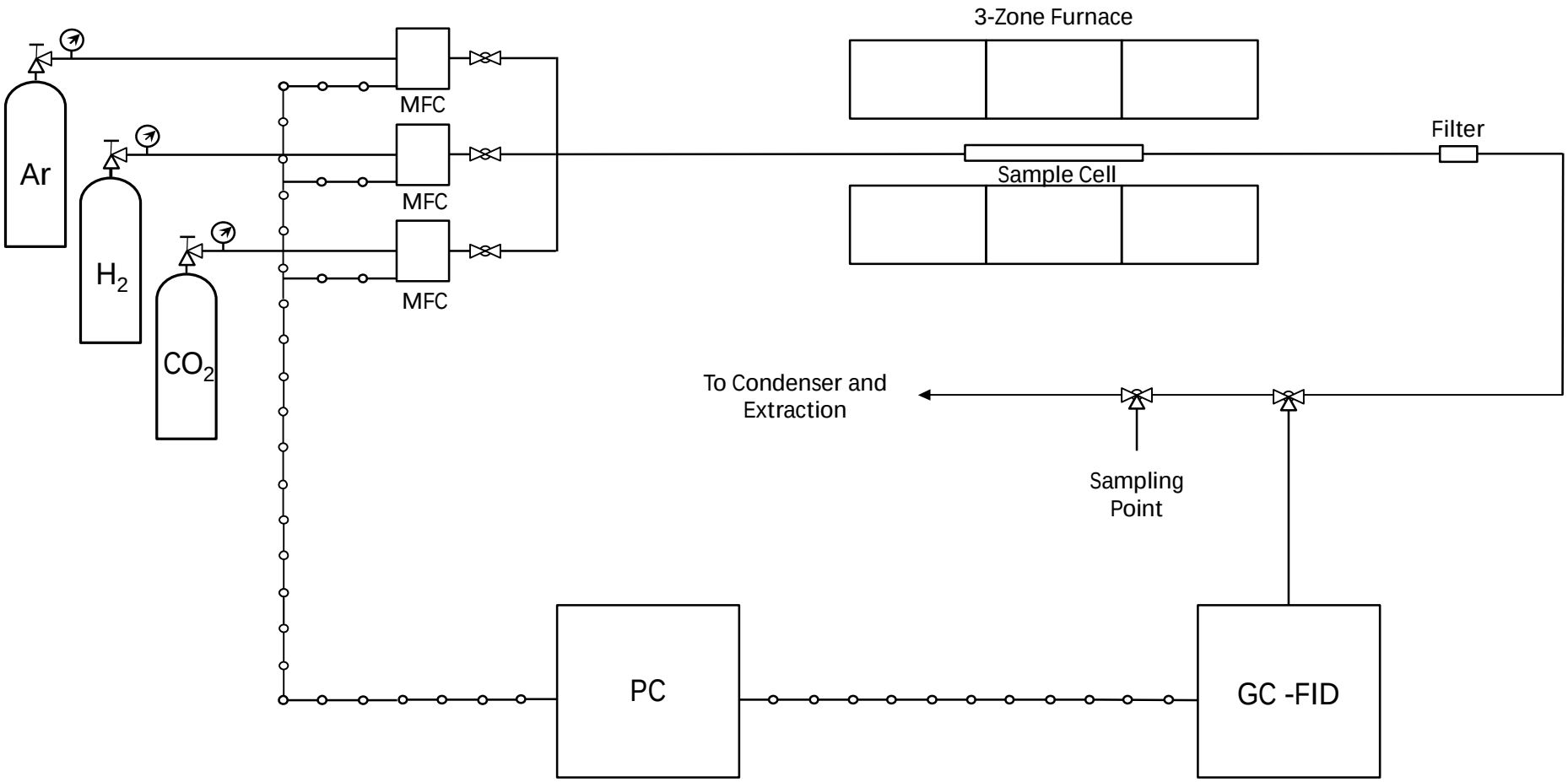

Figure 2.2 – Schematic showing the construction of Reactor 1

2.2.2 Reactor 2

The second reactor was constructed for testing catalysts with the ability to introduce a feed-gas of CO/H_2, CO_2/H_2 or various mixtures/ratios of $CO/CO_2/H_2$. As with Reactor 1 it was constructed mainly of ¼ inch Swagelok stainless steel tubing, a schematic is shown in Figure 2.3.

The same cylinders used with Reactor 1, all fitted with high-pressure regulators provide argon, hydrogen and carbon dioxide. Carbon monoxide was provided by a 20 L Research grade (99.9% purity) cylinder placed on the bench top next to the reactor for ease of access. A small cylinder was used to limit the amount of CO released and the time taken to reduce levels to a safe limit should a leak occur. CO detectors were placed both by the CO cylinder and by the entrance to the lab.

Four Omega FMA 5400/5500 MFCs again operated *via* the LabVeiw computer program provide individual control over each gas stream and allow a range of different feed gas compositions to be used. Each mass flow controller used in this system is rated to 35 bar pressure with a flow range of 10 – 500 sccm. A Swagelok ball valve is placed after each MFC to prevent back diffusion through closed MFCs. All gas lines are then connected into a single pipe that is connected to the reactor *via* a flexible braided hose.

The reactor sample cell consisted of a 130 mm long, 4.6 mm internal diameter stainless steel tube of the same construction as that used in Reactor 1 and illustrated in Figure 2.1. This sample cell was contained within a single stage Carbolite vertical furnace (1200 ^oC max temp). Another braided hose connected the reactor to a 0.5-micron pore size particulate filter which then connected the reactor to two three-way Swagelok ball valves. These valves allowed for either sample collection by a gas syringe for analysis by GC/MS or diverting the gas stream to the on-line FID-GC. All exhaust gases pass through a silicone oil bubbler before being extracted by the lab extraction system

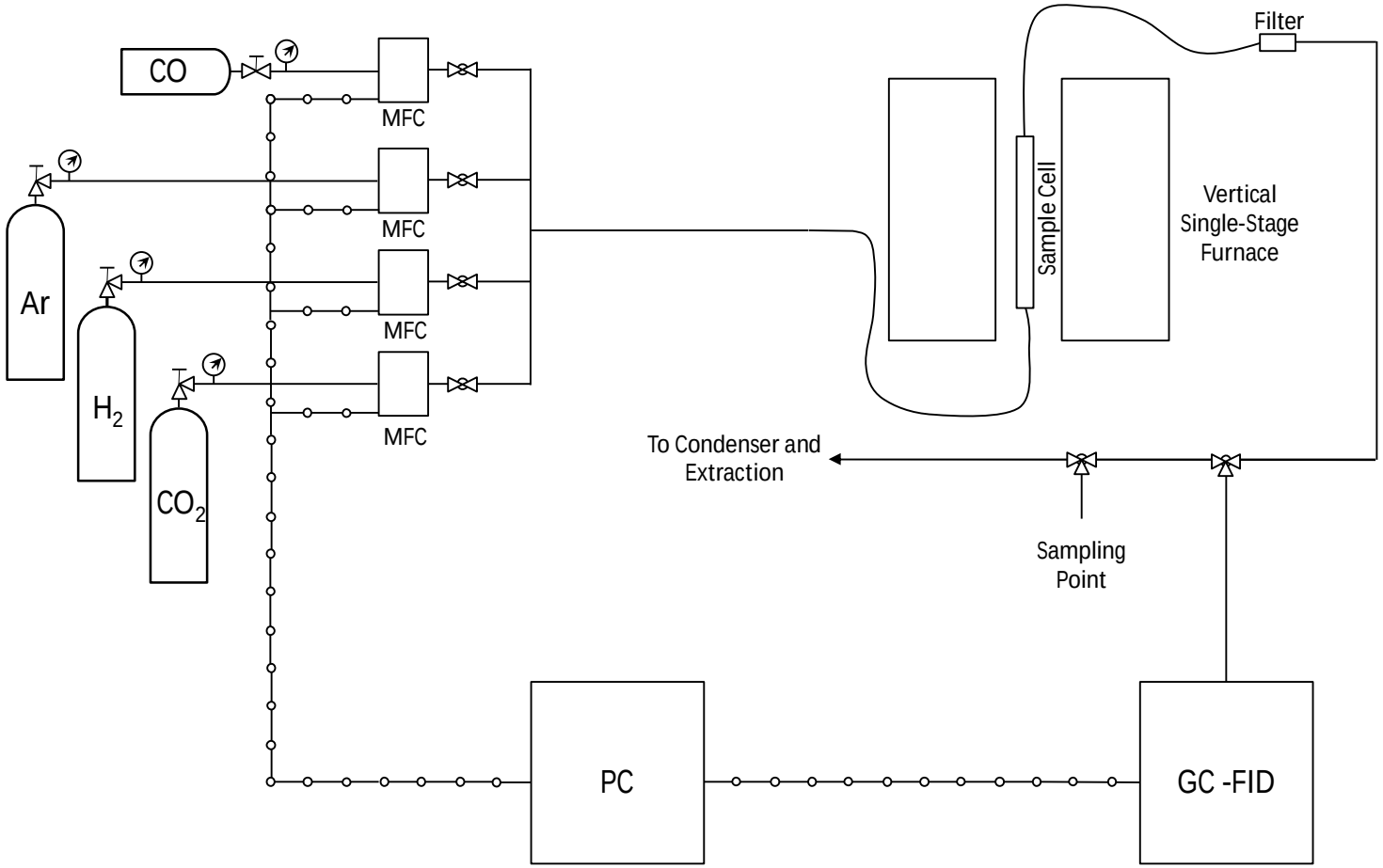

Figure 2.3 – Schematic illustrating the construction of Reactor 2

2.2.3 Reactor 3

Reactor 3 was designed and constructed for the high pressure testing of catalyst both for CO_2/H_2 fed direct hydrogenation of CO_2 and CO/H_2 fed FT type reactions. The tubular fixed bed reactor is constructed mainly of Swagelok stainless steel tubing and Swagelok braided hosing. The reactor was capable of running at pressures up to 20 bar. The entire reactor system was constructed within a 'walk-in' fume-hood in order to minimise risk and aid containment should a leaks or any failures occur.

The gas supply system consisted of three cylinders, namely hydrogen (BOC – High Purity, 99.995 % purity), CO_2 (99.9 % purity) and carbon monoxide (20 L, Research grade, 99.9% purity). The pressure of each gas was controlled individually by high pressure two-stage regulators at the neck of each cylinder. Flash back arrestors were fitted to both hydrogen and carbon monoxide cylinders. The CO_2 and CO cylinders were connected to a three-way valve so that either CO or CO_2 could be chosen as a carbon source. The hydrogen and carbon source lines were both controlled through the use of two MFCs, one for a high flow rate (0-500 sccm, Omega FMA 5400/5500) mainly used to rapidly pressurise the system and another for a low flow rate (0-20 sccm Bronkhurst EL-FLOW) these are generally used maintain lower flow rates during reaction. Which MFCs is used can be selected *via* a three way valve.

After flow control using the MFCs both the hydrogen and carbon source lines were connected into a single gas line. This is then connected to the reactor sample cell within which the catalyst sample is contained. In order to ensure that no connections were contained within the 40 cm furnace a 60 cm stainless steel tube was used. This prevents the repeated heating and cooling of Swagelok joints which may result in leaks particularly at higher reaction pressures. Figure 2.4 shows an illustration of the sample cell used in Reactor 3. In order to have a catalyst bed length of *ca.* 130 mm (as with Reactors 1 and 2) yet still keep all joints outside of the furnace the majority of the tube must be packed with an inert substance. The second half of the sample cell is packed with quartz wool which keeps the bed in place. The contamination of this quartz wool by the catalyst powder is prevented by 1 cm of inert SiC which was replaced every time the catalyst is replaced. To keep the catalyst bed in place the first half of the reactor is packed with SiC, this allows for easy removal so that the catalyst can easily be replaced.

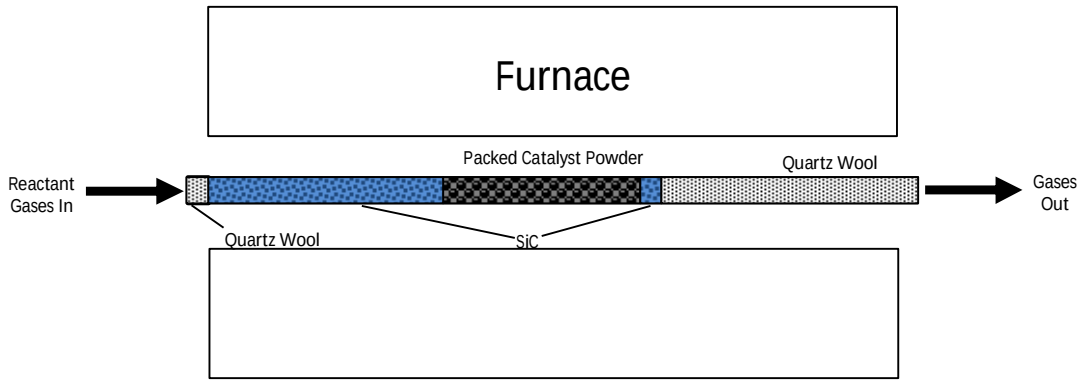

Figure 2.4 – Schematic showing the sample cell of Reactor 3

The sample cell was contained within a 40 cm PyroTherm furnace (1200 ^{o}C max temperature). After passing through the furnace the system is connected to an EL-PRESS Bronkhurst back pressure regulator (pressure 1-40 bar, max flow 40 sccm) which can be used to regulate and measure the pressure of the reactor system. A pressure transducer is also placed before the sample cell so that the pressure drop across the catalyst bed can be monitored. The backpressure regulator was connected to a three way valve with one connection used as a sampling point and the other passing through a silicone oil bubbler before feeding through to the labs extraction system.

The two high flow Omega MFCs and pressure transducer are monitored and controlled by the connected PC through the use of LabView software. All Bronkhurst components (the two low flow MFCs and back pressure regulator) are also controlled using the attached PC only through the use of Bronkhurst's 'Flow DDE' software rather than LabView.

In the interests of safety a burst valve (rated to 30 bar) was located prior to the sample cell to enable release of any unintentional pressure build up. An emergency release needle valve connected directly to the extraction system was also included so that the pressure in the reactor could be safely and rapidly released (pressure release through back pressure regulator is relatively slow and requires electrical power to operate so is not suitable for use in an emergency). A schematic representation of Reactor 3 is shown in Figure 2.5 and a photographs of the rig as set up is shown in Figure 2.6.

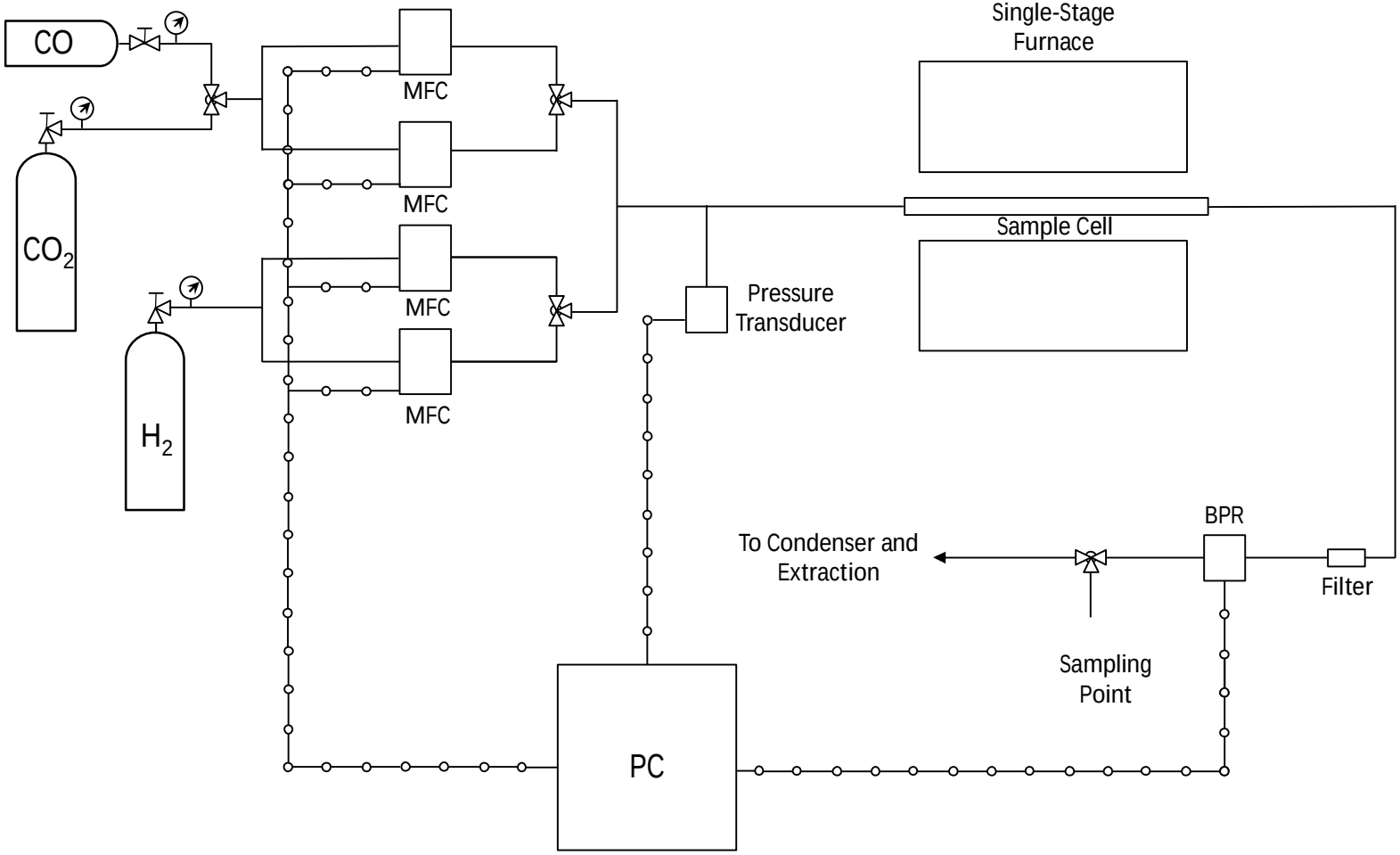

Figure 2.5 - Schematic showing the construction of Reactor 3

Figure 2.6 – Photographs of Reactor 3

2.3 Catalyst Testing Procedure

2.3.1 General Catalyst Testing Procedure: Reactor 1.

The same general catalyst testing procedure was repeated for all catalyst tests conducted in Reactor 1, this is detailed below.

- 0.7 g of the chosen catalyst was packed into the reactor sample cell, Quartz wool is used to hold the sample in place under flow conditions.
- The sample cell is placed in the centre of a tubular furnace and connected to the rest of the reactor.
- The furnace was heated to the pre-treatment temperature of 300 ^{o}C under a flow of argon at a ramp rate of 30 ^{o}C min^{-1}.
- Once at temperature the argon flow is replaced with a flow of hydrogen and left to reduce for 2 hours.
- With pre-treatment completed the hydrogen flow is replaced with argon and the furnace is heated or cooled to the reaction temperature.
- With the reaction temperature reached hydrogen and carbon dioxide are introduced in a 3:1, H_2:CO_2 ratio with a total flow of 8 sccm.
- After one hour on stream a gas sample is collected from the sampling point with a gas tight syringe.

- The sample is then analysed with an off line GC-MS system (details given in Section 2.4).
- Sample collection is repeated every hour until the catalyst test is completed.
- Once testing is complete hydrogen and carbon dioxide flow is stopped and replaced with a flow of argon which remains on until the furnace has cooled to a safe temperature.

Any deviations from this experimental procedure are given in the appropriate results chapter.

2.3.2 General Catalyst Testing Procedure: Reactor 2.

The same general testing procedure was used for the majority of catalyst tests conducted in Reactor 2. This is detailed below.

- 0.7 g of the chosen catalyst is packed into the reactor sample cell, Quartz wool is used to hold the sample in place under flow conditions.
- The sample cell is placed in the centre of a tubular furnace, connected to the rest of the reactor and clamped in place.
- Argon is introduced at a flow rate of 50 sccm. The reactor is then heated to 300 ^{o}C for pre-treatment at a rate of 30 ^{o}C min^{-1}.
- Once at pre-treatment temperature argon flow is stopped and replaced with 50 sccm hydrogen and reduced for 2 hours.
- With the reduction stage completed the hydrogen flow is replaced with 50 sccm argon and the reactor heated or cooled to reaction temperature.
- Once reaction temperature is achieved the flow of argon is replaced with 10 sccm CO and 30 sccm H_2.
- After one hour under reaction conditions a sample is collected using a gas tight syringe and analysed using an *ex-situ* GC-MS. Full details of product analysis are given in Section 2.4.
- Sample collection is then repeated every hour until the catalyst testing is completed.
- After the final sample has been taken CO and H_2 flow is stopped and argon is flowed through the reactor at 50 sccm until the furnace has reached a safe temperature.

Any deviation from the above procedure is detailed in the appropriate chapter.

2.3.3 General Catalyst Testing Procedure: Reactor 3.

The same general catalyst test procedure was used for all catalyst tests conducted using Reactor 3. This procedure is detailed below.

- First enough SiC (200-450 mesh, Sigma Aldrich) was added to give a packed bed approximately 1 cm in length (0.3 g). This was done to prevent the contamination of quartz wool used to pack half of the 60 cm sample cell.
- 0.7 g of the chosen catalyst was packed into the sample cell giving a catalyst bed approximately 130 mm in length.
- The remainder of the sample cell was then packed with SiC to hold the catalyst bed in place.
- The filled sample cell was loaded into the reactor and the reactor pressurised to 2 bar greater than the desired reaction pressure.
- The system was then tested for leaks. If any were found the pressure was released, the leak sealed and the reactor re-pressurised and tested again for leaks. This process was repeated until no further leaks were found. The reactor was then de-pressurised.
- The reactor was then heated to the pre-treatment temperature of 300 ^{o}C under a flow of hydrogen. Once at temperature the system was pressurised to the desired reduction pressure.
- After two hours under pre-treatment conditions the reactor pressure was reduced to atmospheric pressure and heated/cooled to the desired reaction temperature.
- Once the reaction temperature was reached the system was then re-pressurised to the required reaction pressure under a high flow of 3:1 H_2:CO_2 feed gas mix.
- With the pressure reached the flow of H_2 and CO_2 was reduced to reaction flow and maintained using the low-flow MFCs.
- A sample was collected using a gas tight syringe after an hour under reaction conditions and analysed using on off-line GC-MS system (detailed in Section 2.4).
- Samples were taken every hour until the catalyst test was completed. At this point the pressure is slowly released, all flow is stopped and the furnace cooled.

Any deviation from the above procedure is detailed in the appropriate results Chapter.

2.4 Product Analysis Utilising Gas Chromatography

Product analysis was conducted using an Agilent 7890A gas chromatography mass spectrometer (GC-MS) equipped with a HP-PLOT/Q, 30 m long 0.530 mm diameter column. Typically a 50 cm^3 sample of gas was collected from the reactor's sampling point and injected into the GC-MS. A large volume was used in order to flush out the system and ensure that the 0.25 cm^3 sample loop was not contaminated from the previous samples.

The Agilent 7890A is equipped with three detectors, a flame ionisation detector (FID), a thermal conductivity detector (TCD) and a mass spectrometer. For the purposes of this report calculations were based on the results from the FID and MS detectors. FIDs are highly sensitive

to hydrocarbons and as such are the detectors of choice for hydrocarbon identification but do possess drawbacks. Due to their nature of operation, non-combustible gases such as carbon dioxide and carbon monoxide are not detectible and so the traces obtained from the MS are used to calculate conversions and other values that require knowledge of amount of CO and CO_2 present.

With water as one of the main reaction products for both the reverse water gas shift reaction and the Fischer Tropsch process the results from the TCD were not used as the presence of H_2O and O_2 tend to cause a noisy baseline and as such can reduce the sensitivity of the detector. Despite the decrease in sensitivity the TCD was used as a 'back-up' detector confirming what was seen in both the FID and MS traces.

2.4.1 GC Method

A helium carrier gas was used with a flow of 1.2 ml min^{-1}. The sample contained within a 0.25 cm^3 sample loop was injected with a split ratio of 10:1 and an injector temperature of 250 ^oC. The temperature program for the GC oven is illustrated in Figure 2.7. An initial temperature of 40 ^oC was held for 5 minutes before being heated to 250 ^oC at a ramp rate of 15 ^oC min^{-1}. Once at 250 ^oC it was held for a further 5 minutes.

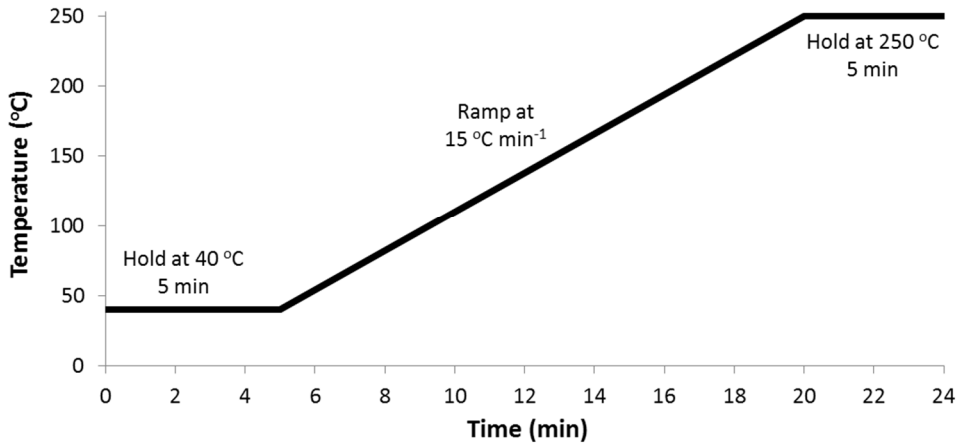

Figure 2.7 – Oven temperature variation with time for the GC method used for product analysis

2.4.2 GC Calibration

The GCMS system was calibrated using an 8-gas mix obtained from BOC. It consisted of, by volume, 1% carbon dioxide, 1% carbon monoxide, 1% methane, 1% ethane, 1% propene, 1% propane and 1% n-butane with nitrogen as a balance. Typical chromatogram traces obtained for the calibration gas recorded using the MS and FID detectors are shown in Figure 2.8.

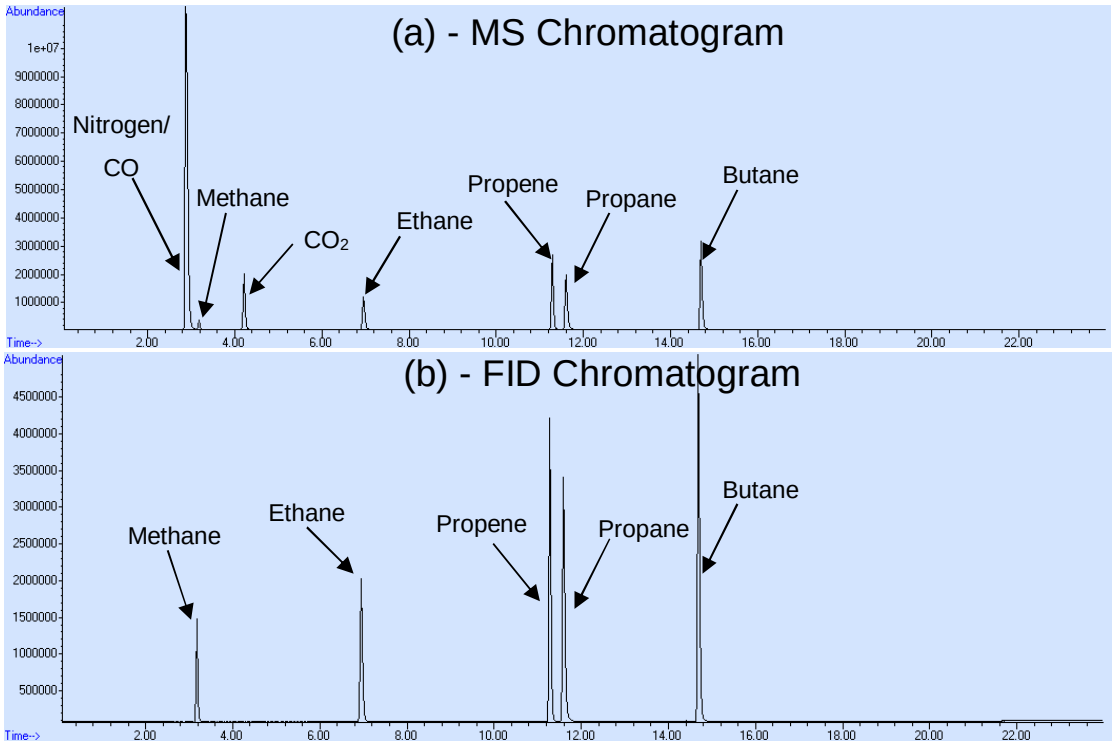

Figure 2.8 – Typical chromatograms recorded for the calibration gas using (a) the MS detector and (b) the FID.

As illustrated in Figure 2.8 the retention time (RT) for both carbon monoxide and nitrogen is too close to distinguish between peaks. This means that the gas obtained from BOC cannot be used to calibrate to CO using the HP-PLOT/Q column. Typical retention times and areas for each component of the calibration gas are shown in Table 2.1.

Table 2.1 – Typical Retention times and peaks areas recorded for the calibration gas

Calibration Gas Component	Retention Time (mins)	MS Peak Area	FID Peak Area
N_2/CO	2.9	4.82×10^8	N.D.
CH_4	3.2	7.77×10^6	3.32×10^7
CO_2	4.2	5.61×10^7	N.D.
C_2H_6	7.0	4.35×10^7	7.04×10^7
C_3H_6	11.3	7.74×10^7	9.57×10^7
C_3H_8	11.6	7.02×10^7	1.07×10^8
C_4H_{10}	14.7	1.01×10^8	1.56×10^8

N.D. Component not detected due to the limitation of the detector

The area of a peak obtained in each trace is proportional to the amount of compound present. As can be seen in the chromatograms in Figure 2.8, although each compound (with the exception of nitrogen) is present in the same amount different peak heights and areas are

observed. This is due to the fact that each molecule responds differently to each detector. To overcome this problem the response factor (RF) must be calculated. The RF compensates for the differing intensities observed upon detection of different molecules. By running a sample of a known concentration and dividing the area obtained by the % volume present in the sample as shown in Equation 2.1 the RF for each component can be calculated.

$$Response\ Factor = \frac{Measured\ Area\ of\ Component\ Peak}{\%\ Volume\ of\ Component\ Injected}$$

Equation 2.2 – Equation for the calculation of response factor

For initial calibration, an average area was taken based on four calibration runs and used to calculate the RF for each component. As the % volume present for each sample was 1 % the measured area is, in this case, equivalent to the RF and as such the areas listed in Table 2.1 were used as the RF values. A calibration sample was run each morning before any samples were run in order to take into account any variations that may occur with time due to, for example, the ageing of the MS filament.

As the response factors calculated for the FID should be approximately proportional to the hydrocarbon chain length a graph of RF against carbon number (C_n) was plotted for all linear saturated hydrocarbons present in the calibration gas mix, Figure 2.9. The plot shows a linear relationship between the carbon chain length and the RF. The response factors for heavier hydrocarbons can be extrapolated based on these plots. The process was repeated for the RFs calculated from the mass spectrometer detector, Figure 2.9 shows the resulting plot. Again a linear relationship is observed allowing for the extrapolation of response factors for the heavier hydrocarbons.

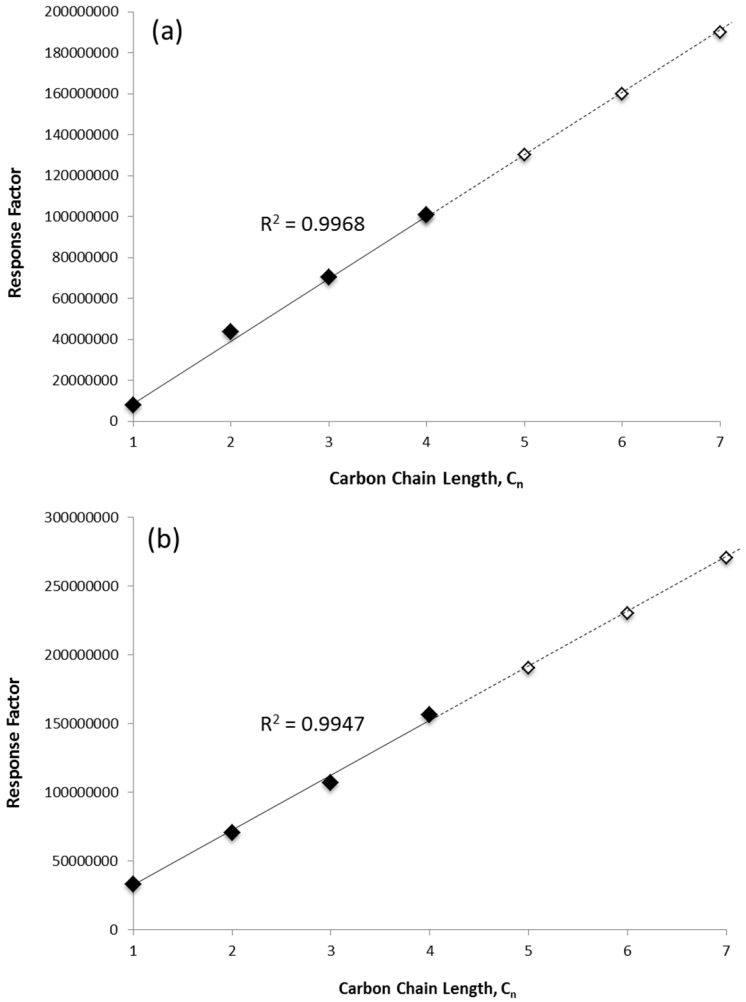

Figure 2.9 – Plots showing the relationship between response factor and carbon chain length for (a) the MS detector and (b) the FID. Dotted lines represent the extrapolation line used for calculation of response factors for C_4+ hydrocarbons.

With the retention time of CO and the N_2 nitrogen make-up gas being too close to distinguish between peaks, a common problem with smaller gas molecules, an alternative way to calculate its RF was required. To combat this problem Reactor 1 was assembled without any catalyst loaded and the MFCs were set to so that the exhaust gas consisted of 10 % (by volume) CO and 90 % CO_2. A high rate of flow of gas was used in order to minimise error. Several samples were collected over a three-hour period and analysed by the GCMS. The process was then repeated to cover a range of differing CO:CO_2 ratios.

As with previous calibration runs the area of the peaks were recorded and through the use of Equation 2.1 the response factor for both carbon dioxide and carbon monoxide was calculated. Both were found to be equal within expected error and as such the response factor calculated for carbon dioxide from the BOC calibration gas was used for carbon monoxide in all calculations.

Using the measured peak area and response factor it is possible to calculate the moles of each component formed per hour using Equation 2.3. By dividing the measured peak area for

each component by its calibrated response factor a % vol may be obtained. This can then be multiplied by the volumetric flow ($\dot{V}$) to give the volume of component formed per hour. This is converted to moles formed per hour by dividing by the molar volume.

$$Moles = \frac{Measured\ Peak\ Area}{Response\ Factor} * \frac{\dot{V}}{V_m}$$

Equation 2.3 – Equation for calculation of moles (mol h^{-1}) where $\dot{V}$ is the volumetric flow ($cm^3\ h^{-1}$) and V_m is the molar volume ($cm^3\ mol^{-1}$)

2.5 Calculations

2.5.1 Calculation of Crystallite Size from pXRD

The crystallite size, d (nm), was calculated from pXRD based on the broadening of diffraction peaks using the Sherrer equation (Equation 2.4). *K* is a dimensionless shape factor assumed to be 0.9. β is the line broadening (FWHM) and θ is the Bragg angle. It should be noted that the Sherrer equation is limited to nano-scale particle and is not applicable for crystallite sizes greater than *ca.* 1 μm.

$$d = \frac{K\lambda}{\beta\ cos\theta}$$

Equation 2.4 – The Sherrer equation

2.5.2 Calculation of Conversion

Conversion of CO_2, ${}^{x}{}_{CO_2}$, was calculated according to Equation 2.5.

$${}^{x}{}_{CO_2} = \frac{Moles\ of\ CO_{2\ in} - Moles\ of\ CO_{2\ out}}{Moles\ of\ CO_{2\ in}} \times 100$$

Equation 2.5 – Equation for the calculation of CO_2 conversion

2.5.3 Calculation of Product Selectivity

The product selectivity, S_i, was calculated on a moles of carbon basis as shown in Equation 2.6. Where $[nC]_i$ is the moles of carbon contained in product *i* and $[nC]_{prod\ tot}$ is the total moles of carbon contained within the products.

$$S_i = \frac{[nC]_i}{[nC]_{prod\ tot}} \times 100$$

Equation 2.6 – Equation used for the calculation of product selectivity

2.5.4 Calculation of Carbon Balance

The carbon balance, $C_{Balance}$, was calculated according to Equation 2.7. All carbon balances for reported data were found to be acceptable.

$$C_{Balance} = \frac{Total\ Moles\ of\ Carbon\ Out}{Total\ Moles\ of\ Carbon\ In} \times 100$$

Equation 2.7 – Equation used for the calculation of carbon balance

2.5.5 Calculation of Rate

The rate of CO_2 consumption/conversion, $-r_{CO_2}$(mol s^{-1} g^{-1}) was calculated according to Equation 2.8 where $\dot{V}_{CO_2 in}$ is the volumetric flow of CO_2 into the reactor in $cm^3 min^{-1}$, χ_{CO_2} is the CO_2 conversion value, m_{cat} is the mass of catalyst in g and V_m is the standard molar volume in $cm^3\ mol^{-1}$.

$$-r_{CO_2} = \frac{\dot{V}_{CO_2 in}\ \chi_{CO_2}}{60\ m_{cat}\ V_m}$$

Equation 2.8 – Equation for the calculation of rate of CO_2 conversion

The rate of CO consumption/conversion $-r_{CO}$(mol s^{-1} g^{-1}) was calculated according to Equation 2.9.

$$-r_{CO} = \frac{\dot{V}_{CO\ in}\ \chi_{CO}}{60\ m_{cat}\ V_m}$$

Equation 2.9 – Equation for the calculation of rate of CO conversion

2.5.6 Calculation of Chain Growth Probability

The Anderson-Schulz-Flory (ASF) distribution discussed in Chapter 1 Section 1.3.3 can be employed to calculate the chain growth probability, α. Equation 2.10 describes the ASF distribution where the constant α is the ratio between rate of chain propagation and the sum of the rates of propagation and termination. W_n is the weight fraction of a hydrocarbon with carbon chain length *n*.

$$log\left(\frac{W_n}{n}\right) = n \log \alpha + constant$$

Equation 2.10 - The Anderson Schulz Flory distribution

In order to calculate the chain growth probability the moles of each hydrocarbon constituent formed per hour was first calculated using Equation 2.3. The mole fraction, x_i , for each component was then calculated using Equation 2.11 where n_i in this particular case is moles/hour of hydrocarbon *i* in a system containing a total hydrocarbon moles/hour value of n_{tot}.

$$x_i = \frac{n_i}{n_{tot}}$$

Equation 2.11 – Equation for the calculation of mole fraction

The weight fraction of each hydrocarbon was then calculated using Equation 2.12, where W_i is the weight fraction of hydrocarbon *i* with a molecular weight of M_i. $\bar{M}$ represents the average molecular mass of the mixture, calculated using Equation 2.13.

$$w_i = x_i \left(\frac{M_i}{\bar{M}}\right)$$

Equation 2.12 – Equation for the calculation of weight fraction

$$\bar{M} = \sum x_i M_i$$

Equation 2.13 – Equation for the calculation of the average molecular mass

A plot of carbon number, n, against $\log(w_n/n)$ should give a linear series with a gradient equivalent to $\log(\alpha)$ widely known as a Anderson-Schulz Flory plot.

2.6 Experimental Error

The experimental error associated with the calculation of quantities of products from the use of gas chromatography in the manner discussed in Section 2.4 was determined through the repeated analysis of samples of calibration gas using the same gas tight syringe technique used for reaction analysis. The standard deviation was found to be equivalent to 4 % error. All repeated reactions showed results within this expected error.

2.7 Catalyst and Support Preparation Methods

2.7.1 Preparation of MgO – 2. (Chapter 3)

MgO – 2 was prepared by the calcination of $Mg(NO_3)_2 \cdot 6H_2O$ (Sigma Aldrich). Typically 3g of $Mg(NO_3)_2 \cdot 6H_2O$ was placed in a calcination crucible and placed inside the furnace. The sample was heated to 450 ^oC at a ramp rate of 5 ^oC/min and left to calcine in air for 16 hours.

2.7.2 Preparation of MgO – 3. (Chapter 3)

MgO – 3 was prepared *via* a wet precipitation technique similar to that employed by Chen *et al*.[4] An ammonium carbonate solution was prepared by dissolving ammonium carbonate ($(NH_4)_2CO_3$, Sigma Aldirch) into distilled water to give a 1.5 M solution with the pH adjusted to 10.5 by the addition of ammonium hydroxide. To 25 cm^3 of this solution 50 cm^3 of a 0.5 M magnesium nitrate ($Mg(NO_3)_2 \cdot 6H_2O$, Sigma Aldrich) solution was added drop-wise under vigorous stirring producing a white precipitate. The precipitate was aged for 24 hours before being filtered, washed with water and ethanol and dried at 80 ^oC for 12 hours. The resulting powder ($Mg_5(OH)_2(CO_3)_4 \cdot XH_2O$) was then placed in a calcination crucible, placed inside a furnace and heated to 450 ^oC at a ramp rate of 5 ^oC/min. The powder was calcined at this temperature for 16 hours under air giving MgO – 3.

2.7.3 Preparation of MgO – 4. (Chapter 3)

MgO – 4 was prepared by the calcination of magnesium carbonate hydroxide hydrate ($Mg_5(OH)_2(CO_3)_4 \cdot XH_2O$), 99% Sigma Aldrich. Typically 10 g of ($Mg_5(OH)_2(CO_3)_4 \cdot XH_2O$) was placed in a calcination crucible and placed inside the furnace. The sample was heated to 450 ^oC at a ramp rate of 5 ^oC/min and left to calcine in air for 16 hours.

2.7.4 Preparation of 20wt%M/MgO, where M = Fe, Co or Ni. (Chapter 3)

Typically 2 g of MgO was suspended in the minimum amount of deionised water. To this suspension an appropriate volume of an aqueous solution of $Fe(NO_3)_3 \cdot 9H_2O$, $Co(NO_3)_2 \cdot 6H_2O$ or $Ni(NO_3)_2 \cdot 6H_2O$ was added drop-wise. The resulting mixture was left to stir for 10 min after which it was sonicated for 2 hours to ensure thorough mixing. The mixture was then left stirring at room temperature until all solvent had evaporated. The obtained powder was then calcined at 450 ^oC for 16 hours.

2.7.5 Preparation of 20wt%M/1wt%Pd/MgO, where M = Fe and Co. (Chapter 3)

Typically 2 g of MgO was suspended in the minimum amount of methanol. The desired amount of a methanol solution of $Fe(NO_3)_3 \cdot 9H_2O$ or $Co(NO_3)_2 \cdot 6H_2O$ was added drop-wise. A methanolic solution of $Pd(OAc)_2$ was then also added slowly. The resulting mixture was left to stir for 10 min after which it was sonicated for 2 hours to ensure thorough mixing. The mixture was then left stirring at room temperature until all solvent had evaporated. The obtained powder was then calcined at 450 ^oC for 16 hours.

2.7.6 Preparation of 20wt%M/1wt%Pd/1wt%K/MgO, where M = Fe and Co. (Chapter 3)

Generally 2 g of MgO was suspended in the minimum amount of methanol. The desired amount of a methanol solution of $Fe(NO_3)_3 \cdot 9H_2O$ or $Co(NO_3)_2 \cdot 6H_2O$ was added drop-wise. Proceeding this methanolic solutions of $Pd(OAc)_2$ and K(OAc) were then also added slowly. The resulting mixture was left to stir for 10 min after which it was sonicated for 2 hours to ensure thorough

mixing. The mixture was then left stirring at room temperature until all solvent had evaporated. The obtained powder was then calcined at 450 ^{o}C for 16 hours.

2.7.7 Preparation of Mixed MgO:SiO_2 Oxide Supported Catalyst Systems. (Chapter 3)

Mixed MgO:SiO_2 supports were prepared using a wet kneading technique similar to that used by Kvisle[5] and co-workers. The desired molar ratio of MgO (as prepared in Section 2.7.3) and SiO_2 (35-70 μm particle size, 60Å pore diameter, Sigma Aldrich) were added together and deionised water added to form a slurry. This mixture was then heated to 50 ^{o}C while being stirred and the water left to evaporate. The resulting dry powder was used as a catalyst support.

Catalyst preparation was carried out using the same procedure detailed in Section 2.7.6 only with the MgO support typically used replaced with either silica or a mixed MgO-SiO_2 support.

2.7.8 Preparation of Xwt%Fe/Ywt%Pd/SiO_2, where X = 10, 20, 30, 40, 50 and 60 and Y = 1, 2, 3 and 4. (Chapter 4)

The same general catalyst preparation technique was used for all the catalyst systems reported within Chapter 4. The only difference in the method used for each catalyst was the amount of iron and palladium precursors added which varied depending on the desired catalyst composition. For investigations into the effect of catalyst support no change in catalyst preparation were made other than the replacement of the silica support with an equal quantity of the required SiO_2.

Each catalyst was prepared using a wet impregnation technique. First 2 g of the silica support was suspended in the minimum amount of methanol. This was then stirred vigorously as a methanol solution of $Fe(NO_3)_3 \cdot 9H_2O$ was added drop-wise. Next a solution of $Pd(OAc)_2$, also in methanol was also added drop-wise (note: for systems containing larger quantities of palladium larger volumes of methanol were required). The resulting mixture was left to stir for 10 mins before being sonicated for 2 hours. The methanol solvent was removed at 65 ^{o}C under vacuum on a rotary evaporator. The resulting dry powders were then calcined in a furnace under air. Furnace ramp rate: 5 ^{o}C/min. Calcination temperature 450 ^{o}C. Duration: 16 hours.

2.7.9 The Wet Impregnation Method. (Chapter 5)

The same general procedure was used for all catalysts prepared using the wet impregnation method detailed in Chapter 5. 2 g of the silica support (35-70 μm particle size, 250Å pore diameter, Davisil) was suspended in the minimum amount of methanol. To which the appropriate amount of each metal salt (Salts used were $Fe(NO_3)_3 \cdot 9H_2O$, $Cu(OAc)_2 \cdot H_2O$, $Zn(OAc)_2 \cdot 2H_2O$ and $AgNO_3$) dissolved in 20 cm^3 of methanol was added drop-wise to the stirred suspension of support. The resulting mixture was then stirred for 10 minutes before being sonicated for 60 minutes. The solvent was then removed under vacuum while being heated through the use of a

rotary evaporator until a powder of constant mass was obtained. This powder was then calcined in air for 16 hours at 450 ^{o}C under air.

2.7.10 Schlenk Line Method for Preparation of Air Sensitive Catalysts. (Chapter 5)

Due to the air and moisture sensitive nature of some of the precursors, any samples containing aluminium, gallium or indium were prepared using Schlenk line techniques. 2 g of the Silica support (35-70 μm particle size, 250Å pore diameter, Davisil) was first dried under vacuum for 4 hours before a solution of $GaCl_3$, $InCl_3$ or $AlCl_3$ in dried THF was added slowly to the stirred support using a cannula transfer. The formed suspension was then stirred for 10 minutes before the addition of the required volume of $Fe(NO_3)_3{\cdot}9H_2O$ solution again *via* cannula transfer. The slurry was left to stir for a further 2 hours before the solvent was removed under high vacuum. The resulting dry powder was then slowly exposed to air while being agitated with a magnetic stirrer. After a day exposed to air the sample was then calcined at 450 ^{o}C for 16 hours. For catalysts containing palladium a solution of $Pd(OAc)_2$ in methanol was introduced after the addition of the $Fe(NO_3)_3{\cdot}9H_2O$ solution in the same manner, with the rest of the preparation method remaining the same.

2.7.11 The Precipitation Method. (Chapter 5)

For the preparation of gold containing catalysts a co-precipitation method was employed. A solution of $Fe(NO_3)_3{\cdot}9H_2O$ in water (20 cm^3) was added to a suspension of silica (35-70 μm particle size, 250Å pore diameter, Davisil) in the minimum amount of deionised water and stirred. A solution of the required amount of $HAuCl_4{\cdot}3H_2O$ in water (20 cm^3) was also added. To this mixture an ammonia solution (*ca.* 4 M) was added drop-wise until a pH of approximately 8.5 was achieved. The resulting mixture was then stirred for 2 hours before being filtered and dried. The powder obtained was then calcined at 450 ^{o}C for 16 hours. For catalyst also containing palladium an aqueous solution of $PdCl_2$ was added before the addition of the ammonia solution.

2.7.12 Preparation of 20wt%Fe/SiO_2-X where X = 60, 150, 250, 500 or 60_b (with various particle sizes). (Chapter 6)

The same catalyst preparation method is utilised for all the catalyst systems reported within Chapter 6 with only the silica used as a support varied. 2 g of the desired silica is generally suspended in the minimum volume of methanol. To this suspension a methanol solution of $Fe(NO_3)_3{\cdot}9H_2O$ equating to a 20wt% loading is added drop-wise. The resulting mixture is stirred for 10 min before being sonicated for 2 hours. The solvent is then removed by heating to 65 ^{o}C under vacuum on a rotary evaporator. The resulting dry powder is then calcined at 450 ^{o}C for 16 hours.

2.7.13 Preparation of Cobalt-Based Catalysts (Chapter 7)

All of the cobalt based catalysts reported within Chapter 7 were all prepared using the same general procedure detailed below.

2 g of the desired silica support (SiO_2 with a pore size of 60, 250 or 500 Å and a particle size of 35-70 µm or 1-2 mm) was suspended in the minimum amount of methanol. To this suspension the appropriate mass of $Co(NO_3)_3 \cdot 6H_2O$ in 20 cm^3 methanol was added drop-wise while being stirred. Following this step the required amount of each promoter's precursor ($Pd(OAc)_2$, K(OAc), Li(OAc), $Na(OAc) \cdot 3H_2O$, $PtCl_2$, $RuCl_3 \cdot xH_2O$, $CrCl_3$, $(NH_4)_6Mo_7O_{24} \cdot 4H_2O$ and $Mn(OAc)_3 \cdot 2H_2O$) dissolved in methanol (note: for $(NH_4)_6Mo_7O_{24} \cdot 4H_2O$, which is not soluble in methanol, the minimum amount of deionised water was used) was also added slowly to afford the desired cobalt:promoter ratio. The resulting mixture was stirred for 10 minutes before being sonicated for 60 minutes. The solvent was then removed under vacuum while being heated through the use of a rotary evaporator until a powder of constant mass was obtained. The resulting powder was then calcined in air for 16 hour at 450 ^oC

2.8 References

[1] S. T. Sie, R. Krishna, *Appli. Catal., A* **1999**, *186*, 55-70.
[2] D. B. Bukur, S. A. Patel, X. Lang, *Appl. Catal.* **1990**, *61*, 329-349.
[3] J. Knochen, R. Güttel, C. Knobloch, T. Turek, *Chem. Eng. Process.* **2010**, *49*, 958-964.
[4] D. Chen, E. H. Jordan, *Mater. Lett.* **2009**, *63*, 783-785.
[5] S. Kvisle, A. Aguero, R. P. A. Sneeden, *Appl. Catal.* **1988**, *43*, 117-131.

3 Magnesium Oxide as a Catalyst Support for Carbon Dioxide Hydrogenation Catalysts

The use of magnesium oxide as a possible catalyst support was investigated. Iron, cobalt and nickel catalysts were tested along with the use of palladium and potassium as promoters. The use of silica as a co-support was also studied. It was found that magnesium oxide can be an effective catalyst support with the MgO preparation method having a significant influence on the properties of the support. Palladium and potassium addition was found to enhance catalyst performance with both CO_2 conversion and product selectivity improved.

3.1 Magnesium Oxide Preparation and its Use as a Catalyst Support for Carbon Dioxide Hydrogenation

Magnesium Oxide (MgO) is a thermally stable, easily obtainable and cheap inorganic oxide making it an ideal candidate for use as a heterogeneous catalyst support. The utilisation of MgO as a catalyst support has been investigated for both WGS[1] and FT processes[2] with it proving successful as a support in both cases. Its use in CO_2 hydrogenation catalysis has, however, been limited.[3] Studies by Cagnoli *et al.*[2a] have shown that when basic catalyst supports such MgO are used in FT catalysis improved selectivity towards the more valuable olefin products can be obtained. Work by Kishan *et al.*[3] has shown that use of MgO can have a similar impact on CO_2 hydrogenation over an Fe-K catalyst with methane selectivity also reduced when combined with Al_2O_3 as the catalyst's support. To determine magnesium oxide's suitability as a sole catalyst support for the CO_2 hydrogenation process a range of catalysts were prepared and tested.

3.1.1 Preparation of Magnesium Oxide.

One of the main reasons likely behind the relatively low interest in the use of MgO as a catalyst support in CO_2 hydrogenation is the large dependence of the structure and surface area on the preparation method employed. Commercial MgO generally shows a very low surface area, reducing its effectiveness as a catalyst support. The initial work focused on the use of commercial MgO purchased from Sigma Aldrich, the high density of the oxide however made working with the material difficult. When tested in a fixed bed reactor system the low porosity meant no flow through the reactor could be obtained without either significant pressure drop across the catalyst bed or dilution with SiC. As a result of these tests a range of different methods for MgO preparation were investigated to determine if a material more suited for use as a catalyst support could be easily prepared.

Although a range of different preparation techniques have been reported the complexity and cost often means very few are suitable for scale up to industrial use. The preparation methods investigated were kept as non-complex as possible. The first of the preparation

techniques investigated involved the calcination of magnesium nitrate hexahydrate {$Mg(NO_3)_2 \cdot 6H_2O$}. The second involved a method similar to that employed by Chen *et al*.[4] where $Mg(NO_3)_2 \cdot 6H_2O$ was precipitated to give magnesium carbonate hydroxide hydrate {$Mg_5(OH)_2(CO_3)_4 \cdot XH_2O$} which was calcined to give MgO. Commercially prepared $Mg_5(OH)_2(CO_3)_4 \cdot XH_2O$ was also calcined and the resulting MgO compared with that prepared *via* the other techniques discussed as well as commercial MgO.

$Mg_5(OH)_2(CO_3)_4 \cdot XH_2O$-**1** was prepared by *via* a wet precipitation process. A solution of $Mg(NO_3)_2 \cdot 6H_2O$ was added drop-wise to a $(NH_4)_2CO_3$ solution, pH 10.5 giving a white precipitate. The precipitate was then aged for 24 h before being filtered, washed and dried. A SEM image recorded for the resulting material is shown in Figure 3.1 (a). The precipitate was identified as $Mg_5(OH)_2(CO_3)_4 \cdot XH_2O$ by pXRD studies, Figure 3.1 (c). The morphology observed for $Mg_5(OH)_2(CO_3)_4 \cdot XH_2O$-**1** shows a distinct difference to that obtained for the commercially prepared $Mg_5(OH)_2(CO_3)_4 \cdot XH_2O$-**2** {Figure 3.1 (b)}. $Mg_5(OH)_2(CO_3)_4 \cdot XH_2O$-**1** shows irregular particles with a range of different diameters whereas $Mg_5(OH)_2(CO_3)_4 \cdot XH_2O$-**2** shows the presence of microspheres of an irregular size between 3 – 15 μm in diameter. Needle like structures are also witnessed for $Mg_5(OH)_2(CO_3)_4 \cdot XH_2O$-**1**. $Mg_5(OH)_2(CO_3)_4 \cdot XH_2O$-**1**, prepared *via* precipitation, was observed to have a larger surface area (32.61 m^2g^{-1} *Vs.* 22.67 m^2g^{-1}, Table 3.1) than the commercial $Mg_5(OH)_2(CO_3)_4 \cdot XH_2O$-**2**.

Table 3.1 - BET surface areas recorded for MgO materials and their precursors

Material	**Material Precursor**	**BET Surface Area (m^2g^{-1})**	**MgO Crystallite Size (nm)[c]**
$MgCO_3OH$ – 1[a]	$Mg(NO_3)_2 \cdot 6H_2O$	32.61	-
$MgCO_3OH$ – 2[b]	-	22.07	-
MgO – 1	-	3.16	22.3
MgO – 2	$Mg(NO_3)_2 \cdot 6H_2O$	2.74	8.9
MgO – 3	$Mg_5(OH)_2(CO_3)_4 \cdot XH_2O$ – 1[a]	54.86	22.3
MgO – 4	$Mg_5(OH)_2(CO_3)_4 \cdot XH_2O$ – 2	222.05	14.9

[*a*] – prepared by precipitation of $Mg(NO_3)_2.6H_2O$. [*b*] – Commercially obtained $Mg(OH)_2(CO_3)_4 \cdot XH_2O$ purchased from Sigma Aldrich. [*c*] – Crystallite size as determined by pXRD using Sherrer equation

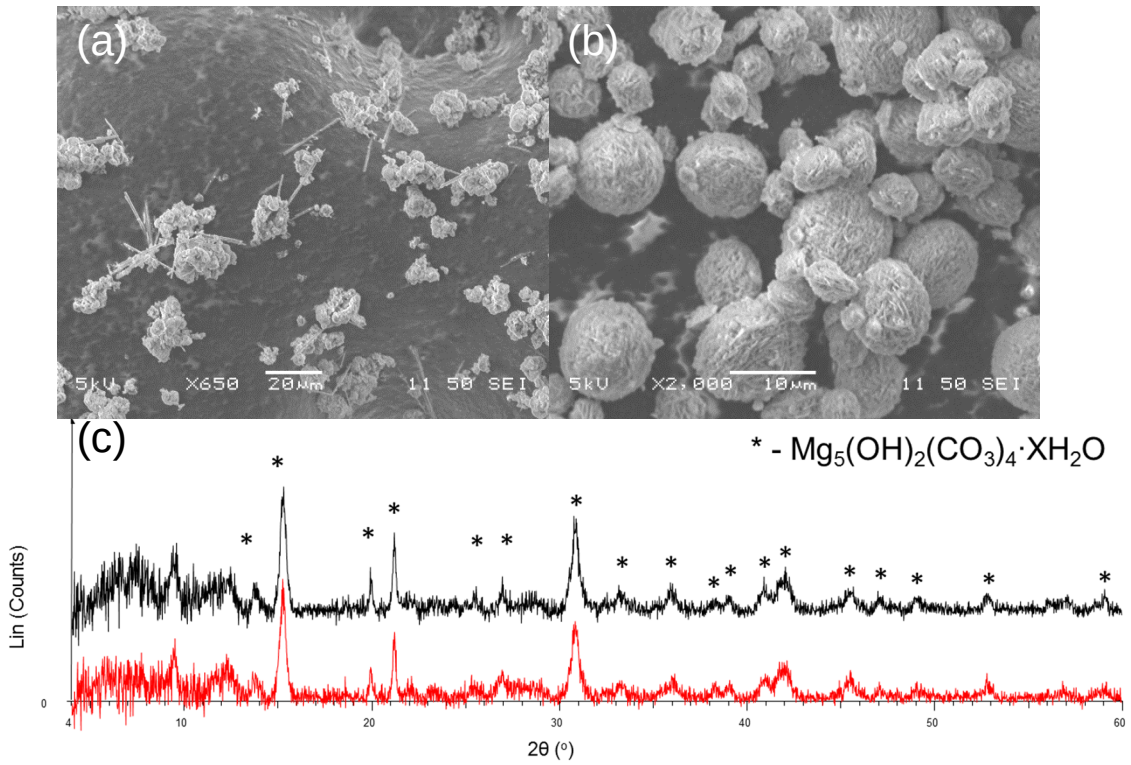

Figure 3.1 - (a) SEM image recorded for $Mg_5(OH)_2(CO_3)_4$•XH_2O-1 prepared by precipitation method and (b) SEM image recorded for $Mg_5(OH)_2(CO_3)_4$•XH_2O-2, commercially prepared. (c) pXRD recorded for $Mg_5(OH)_2(CO_3)_4$•XH_2O-1 (red) and $Mg_5(OH)_2(CO_3)_4$•XH_2O-2 (black)

The thermal decomposition of the two $Mg_5(OH)_2(CO_3)_4 \cdot XH_2O$ materials was investigated by thermogravimetric analysis (TGA) over a temperature range of 50 - 600 ^oC, Figure 3.2. Both systems decompose to approximately 44 % of their original mass, equating to the decomposition to five equivalents of MgO, as expected. Decomposition proceeds through two major mass loses. Initially the waters of crystallisation are lost. This process is completed by a temperature of approximately 400 ^oC. $Mg_5(OH)_2(CO_3)_4 \cdot XH_2O$-**1** appears less thermally stable than the commercial equivalent with mass loss beginning at *ca*. 100 ^oC compared to 200 ^oC for $Mg_5(OH)_2(CO_3)_4 \cdot XH_2O$-**2**. The second major mass loss corresponds to the final decomposition to MgO. For comparison the thermal decomposition of $Mg(NO_3)_2 \cdot 6H_2O$ was also investigated {Figure 3.2 (a)}. Again two major mass loses are evident, first the loss of waters of crystallisation between 100 ^oC and 300 ^oC. Final decomposition from $Mg(NO_3)_2$ to MgO is observed at approximately 450 ^oC. With all three materials tested showing their final decomposition stage to MgO at approximately 450 ^oC this was chosen as the calcination temperature for the preparation of MgO from the three pre-cursors. Hutchings *et al.*[5] showed this temperature was found to give MgO with close to optimum surface area.

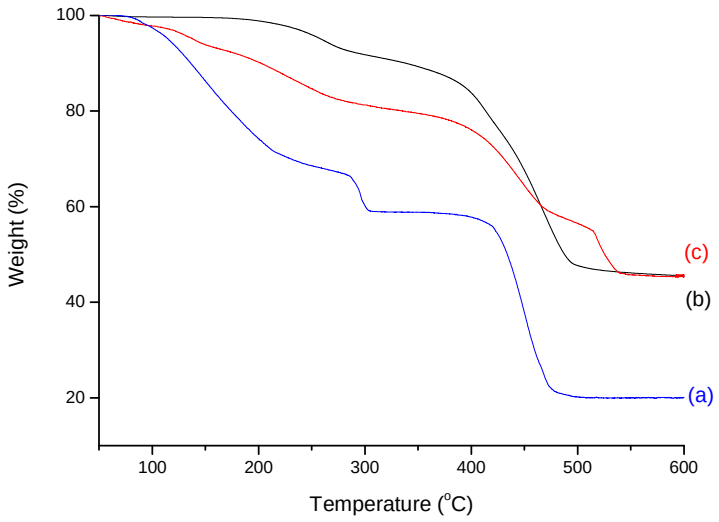

Figure 3.2 – TGA conducted over a temperature range of 50 - 600 °C, 10 °C/min ramp rate, for (a) $Mg(NO_3)_2$•$6H_2O$, (b) $Mg_5(OH)_2(CO_3)_4$•XH_2O-2 and (c) $Mg_5(OH)_2(CO_3)_4$•XH_2O-1

The resulting MgO materials formed *via* this calcination step were then analysed by SEM, N_2 physisorption and pXRD. pXRD patterns for each of the four MgO materials studied are shown in Figure 3.3. Peaks present at 2θ values of 36.85 ° and 42.76 ° indicate the successful formation of MgO. MgO-**2**, formed *via* the direct calcination of $Mg(NO_3)_2 \cdot 6H_2O$ shows only a weak peak at 2θ = 42.76 ° indicating that while MgO appears to have formed the material possesses a low degree of crystallinity. The remaining three materials all show peaks suggesting MgO with a crystalline structure. N_2 physisorption studies were used to analyse the surface area of the prepared MgO materials using the Brunauer–Emmett–Teller (BET) theory (Table 3.1). The surface area of MgO-**1** (commercially prepared) was calculated as 3.16 m^2g^{-1} a value much lower than desired for use as a catalyst support. The lowest calculated surface area was, however, found to be that of the poorly crystalline MgO-**2** (prepared *via* $Mg(NO_3)_2 \cdot 6H_2O$ calcination). The surface areas calculated for MgO-**3** and **4**, both prepared by the calcination of the $Mg_5(OH)_2(CO_3)_4 \cdot XH_2O$ precursor, were found to be significantly larger, MgO-**4** (prepared by calcination of $Mg_5(OH)_2(CO_3)_4 \cdot XH_2O$-**2**) showing the largest of all four MgO materials.

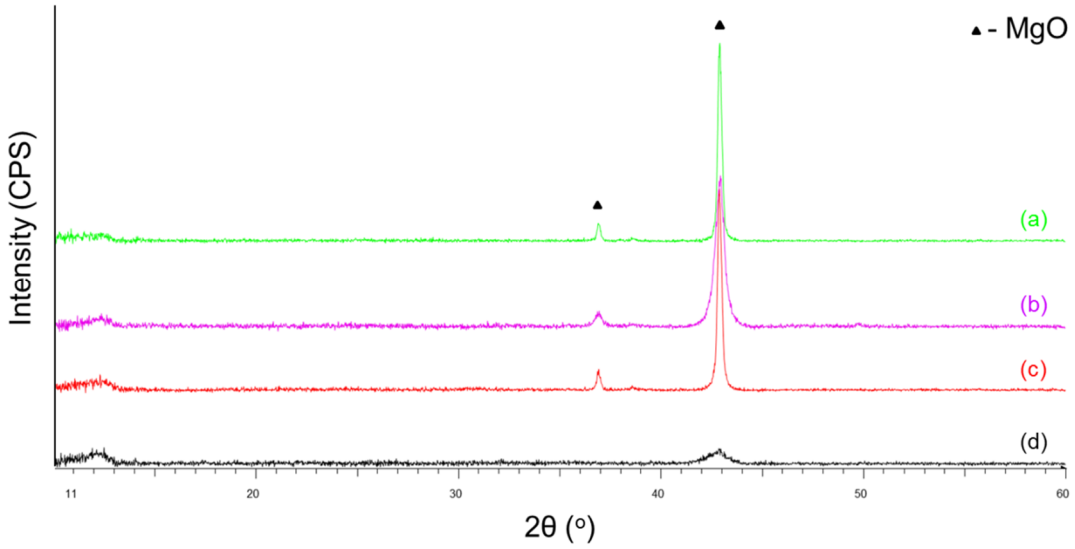

Figure 3.3 – XRD patterns for the MgO materials obtained *via* various preparation methods. (a) MgO-1, (b) MgO-4, (c) MgO-3 and (d) MgO-2.

Catalyst morphology was investigated by SEM analysis with the resulting images shown in Figure 3.4. The images reveal that the size and morphology of the oxide produced depends heavily on the oxide precursor. MgO-**3** and MgO-**4** {Figure 3.4 (c and d respectively)} retain a similar morphology to that observed for the $Mg(OH)_2(CO_3)_4 \cdot XH_2O$ precursors with no distinct change in size or shape. Whereas MgO-**4** consists of microspheres consisting of smaller crystallite sheets the MgO-**3** particles appear to be formed from the agglomeration of smaller irregular spherical particles. This could account for the significant difference in surface area observed. The morphology of MgO-**1** and MgO-**2** {Figure 3.4 (a and b respectively)} show a distinct difference to that observed for the other MgOs. MgO-**1** consists of several particles, generally spherical in nature in the size range of 1 – 4 µm. MgO-**2** appears to consist of a conglomeration of smaller (0.5 – 1.5 µm) particles, this may account for the low surface area observed.

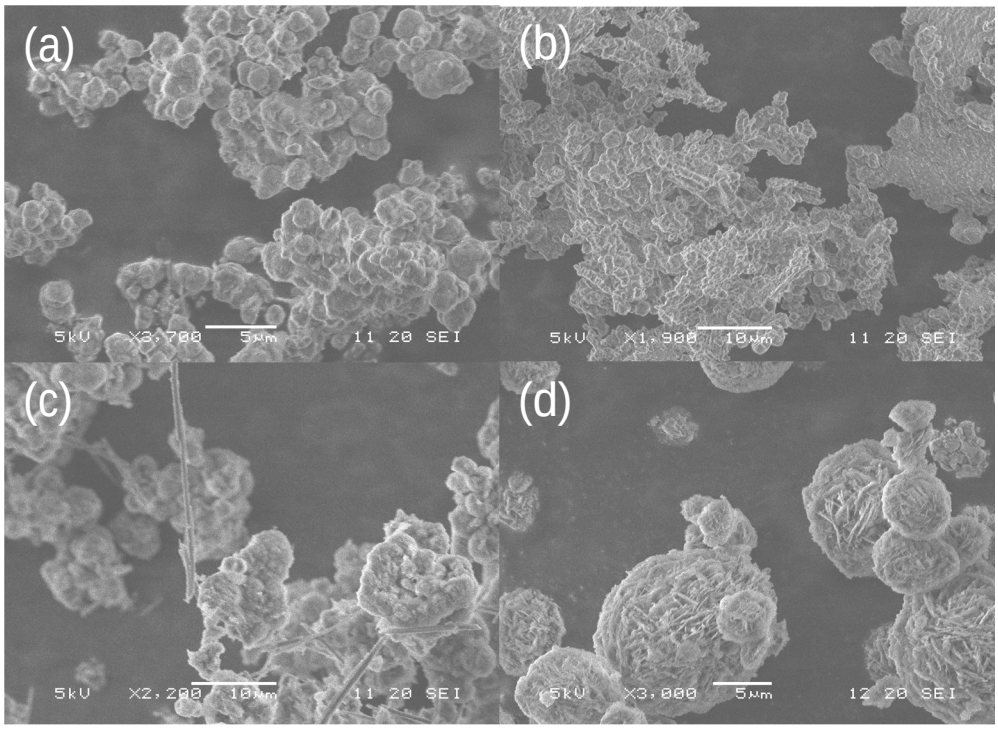

Figure 3.4 – SEM images recorded for MgO prepared by the range of methods discussed (a) MgO-1, (b) MgO-2, (c) MgO-3 and (d) MgO-4.

The preparation method used had a dramatic impact on the morphology and surface areas of the resulting magnesium oxide. Readily available commercial MgO, while showing a high degree of crystallinity, shows a low surface area and is not suitable for use as a catalyst support. Direct calcination of $Mg(NO_3)_2 \cdot 6H_2O$ resulted in a largely amorphous, low surface area MgO. Calcination of $Mg_5(OH)_2(CO_3)_4 \cdot XH_2O$ proved the most successful MgO preparation technique. MgO-**4** prepared *via* the thermal decomposition of the commercial $Mg_5(OH)_2(CO_3)_4 \cdot XH_2O$-**2** gave the highest surface area and when combined with the non-complex nature of its preparation makes an ideal candidate for use as a catalyst support. MgO-**4** was chosen to be taken forward for catalyst preparation and testing.

3.1.2 Catalyst Preparation

To test MgO's applicability and performance as a catalyst support for CO_2 hydrogenation to hydrocarbons a range of iron, cobalt and nickel based catalyst systems were prepared and tested. These metals were chosen for their balance between activity for the FT process and cost. A metal loading of 20 wt% was chosen as preliminary tests had shown little to no activity for the iron based catalysts at loadings below this value.

Catalysts were prepared using a simple aqueous deposition method similar to that used by Jones *et al.*[6] A suspension of magnesium oxide was formed in water and constantly agitated. A solution of the desired metal nitrate {$Fe(NO_3)_3 \cdot 9H_2O$, $Co(NO_3)_2 \cdot 6H_2O$ or $Ni(NO_3)_2 \cdot 6H_2O$} in 20 cm^3 deionised water was prepared and the required amount was then added drop-wise to the suspended MgO support. After stirring for 10 mins the resulting mixture was then sonicated for

1 hour to ensure thorough mixing. Water removal was achieved by slow evaporation of the stirred mixture at room temperature.

Metal loading was calculated relative to the initial mass of support used. For example, in a 20wt%Fe/MgO catalyst system, for every 0.8 g of MgO a mass of iron nitrate that equated to 0.2 g of metallic iron would be added. Since iron accounts for 13.82 wt% of $Fe(NO_3)_3 \cdot 9H_2O$ 1.44 g of the salt would be added during catalyst preparation.

TGA analysis was conducted on the pre-calcined materials in order to determine the temperature at which the various metal nitrates decompose under an oxygen atmosphere, see Figure 3.5. All three systems show two major mass loses the first, between *ca*. 50 ^oC and 200^oC, is due to the loss of water from the metal nitrate employed and any possible residual moisture from catalyst preparation. The second mass loss between 300 ^oC and 400 ^oC can be attributed to the decomposition of the anhydrous metal nitrates to their oxides. Total mass loses of 48 %, 56% and 58% are observed for iron, cobalt and nickel respectively. These values closely match the calculated mass loss expected for the formation of Fe_2O_3, Co_3O_4 and NiO. The similarity between calculated and observed values also confirms the metal loadings are within error of the 20 wt% targeted. All samples show that the main decomposition begins at a temperature of approximately 350 ^oC with all systems full decomposed between 400 – 450 ^oC. Based on these results a calcination temperature of 450^oC was chosen for all three catalyst systems.

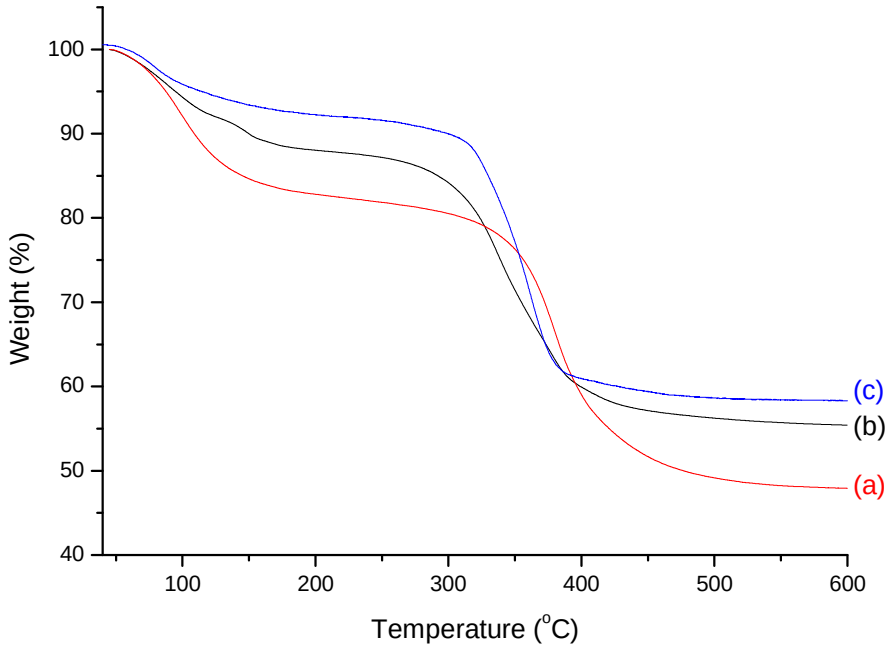

Figure 3.5 – TGA plots recorded for MgO impregnated with various metal nitrates (a) $Fe(NO_3)_3 \cdot 9H_2O$, (b) $Co(NO_3)_2 \cdot 6H_2O$ and (c) $Ni(NO_3)_2 \cdot 6H_2O$.

The formed catalyst systems were analysed after calcination using pXRD. Figure 3.6 shows the resulting diffraction patterns. MgO peaks are visible at 2θ values of 36.85 and 42.76. The 20wt%Fe/MgO catalyst {Figure 3.6 (d)} only shows a weak peak for MgO. A slight

broadening of peaks is also visible for MgO peaks in the 20wt%Ni/MgO system {Figure 3.6 (b)} and a slight narrowing of the MgO peak in 20wt%Co/MgO. No XRD peaks attributable to any of the iron, cobalt or nickel oxides are observed. This confirms that all metals are well dispersed on the supports surface and suggests any crystalline phases present are too small to detect.

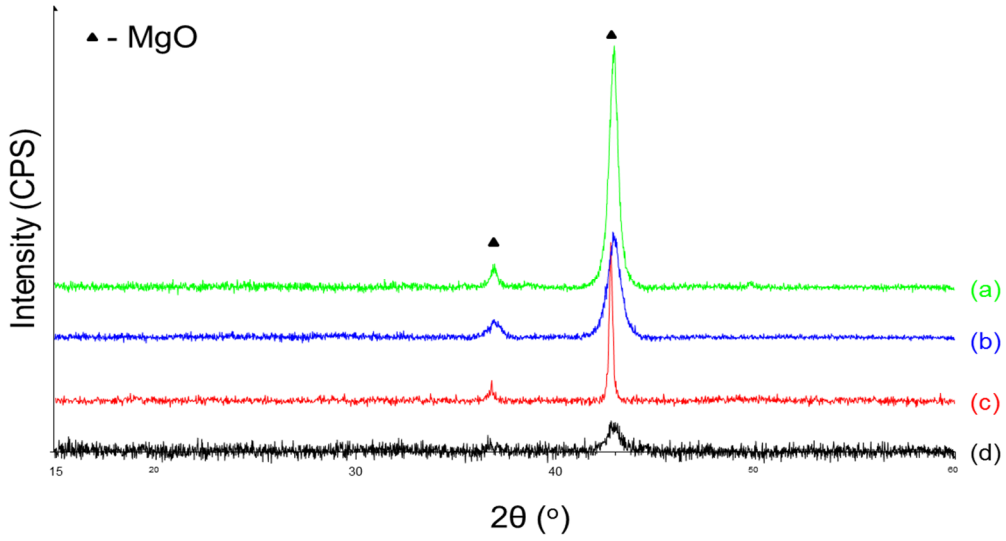

Figure 3.6 – pXRD traces recorded for MgO impregnated with various metal nitrates after calcination (a) MgO, (b) 20wt%Ni/MgO and (c) 20wt%Co/MgO and (d) 20wt%Fe/MgO.

3.1.3 Catalyst Testing

The prepared catalyst systems were tested for their ability to hydrogenate CO_2 at a range of different temperatures. For these initial catalyst tests Reactor-1 was used, see Chapter 2, Section 2.2 for full reactor information. Typically 0.7 g of catalyst was packed into the reactor sample cell, 130 mm in length, 4.6 mm internal diameter. Small plugs of quartz wool were used to hold the catalyst in place. With the catalyst loaded 50 standard cubic centimetres (sccm) of argon was flowed through the system, flow was checked and the reactor leak tested. The furnace was then heated to 300 ^{o}C at a rate of 30 ^{o}C/min for catalyst pre-treatment. Once the furnace had reached the programmed temperature gas flow was switched from argon to hydrogen with total flow remaining at 50 sccm. All catalyst systems were pre-treated under these conditions for 2 hours.

Once pre-treatment was completed, hydrogen flow was stopped and argon reintroduced at 50 sccm. The furnace temperature was then heated/cooled to the temperature required for the catalyst test. Once the temperature had stabilised argon flow was reduced to 2 sccm and CO_2 and H_2 were introduced at ratio of 1:3 with a total flow of 10 sccm.

The reaction temperature was varied for each of the catalyst systems in order to determine how hydrocarbon yield and product selectivity is altered with increasing reaction temperature; the results are summarised in Figure 3.7. It should be noted at this point that a sample of MgO support with no metal added was also investigated but showed no conversion to hydrocarbons under any reaction conditions tested. HC yield was observed to increase steadily with increasing temperature when 20wt%Fe/MgO was used as a catalyst. Yield increased from 0.45 % at a reaction temperature of 300 ^{o}C to 7.56 % at 400 ^{o}C. No plateau was observed in HC yield suggesting that higher reaction temperatures could potentially lead to a further increase in HC yield. The 20wt%Co/MgO system also shows a steady increase in HC yield with increasing temperature. No detectible hydrocarbons are formed at 300 ^{o}C however a HC yield of 9.4 % can be obtained when reaction temperature is increased to 400 ^{o}C. Again no obvious plateau in HC yield was shown indicating it is possible that CO_2 conversion could be increased further with higher temperatures. The 20wt%Ni/MgO system greatly outperforms the iron and cobalt based systems with HC yield increasing from 2.3 % at 300 ^{o}C to 55.6 % at 400 ^{o}C.

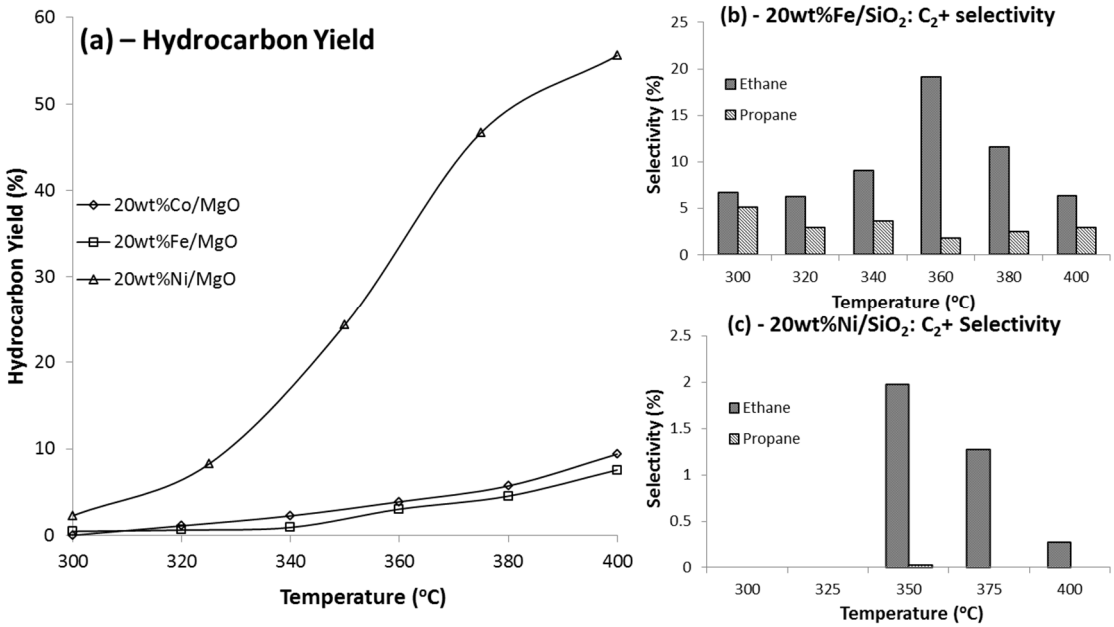

Figure 3.7 – (a) Hydrocarbon yield recorded over a range of temperatures for 20wt%Fe/MgO, 20wt%Co/MgO and 20wt%Ni/MgO. (b) Ethane and propane selectivity observed for 20wt%Fe/MgO with the remainder of hydrocarbons formed being methane. (c) Ethane and propane selectivity observed for 20wt%Ni/MgO with the remained of the hydrocarbons formed being methane.

The cobalt based catalyst system showed the formation of methane as the only hydrocarbon product at all temperatures investigated. The 20wt%Ni/MgO system showed a strong preference for methane formation at all reaction temperatures studied with small amounts of ethane and propane formed at higher temperature {Figure 3.7 (c)}. 350 ^{o}C gave the best selectivity to C_2+ products, methane selectivity was however still high at 98%. The 20wt%Fe/MgO showed the best selectivity towards C_2+ products with methane selectivity

dropping to 79 % at 360 ^{o}C {Figure 3.7 (b)}. This large difference in selectivity can most likely be attributed to iron's WGS activity allowing the formation of CO, the key reactant in the formation of longer hydrocarbons *via* the FT process. The methane selectivity observed in the cobalt and nickel systems could be due to the direct hydrogenation of CO_2 without proceeding *via* the RWGS and FT processes.

3.1.4 Summary

All catalysts tested proved effective for the conversion of CO_2 to hydrocarbons with HC yield generally increasing in the order 20wt%Fe/MgO < 20wt%Co/MgO < 20wt%Ni/MgO, following from left to right across the period. This trend varies from that observed for the silica supported iron, cobalt and nickel catalysts studied by Weatherbee and Bartholomew for CO_2 hydrogenation.[7] They found the Co/SiO_2 system to be more active than the Ni/SiO_2 while the Fe/SiO_2 remained least active. This difference can likely be attributed to the different support used. The nature of the oxide support used for cobalt based catalysts has been shown to have a significant impact on the Fischer-Tropsch activity of the catalyst.[8] Weatherbee and Bartholomew found that for the analogous silica supported catalysts only iron and cobalt produced C_2+ hydrocarbons with the nickel system producing almost exclusively methane.[7] The 20wt%Fe/MgO system showed a relatively high selectivity to C_2+ hydrocarbons under certain conditions in agreement with the results obtained by Weatherbee and Bartholomew, cobalt however formed exclusively methane. This suggests that MgO may not be as efficient a support for cobalt-based systems as SiO_2.

The activity of iron and cobalt catalyst for the formation of C_2+ hydrocarbons has been demonstrated with similar metal loadings over a range of supports when a CO/H_2 feed-gas is utilised[8-9] suggesting that the initial reduction of CO_2 to CO could be limiting the performance of the catalyst systems (in terms of C_2+ HC yield). While the 20wt%Ni/MgO systems proved particularly effective for CO_2 conversion even at high conversions HC distribution is almost exclusively methane.

3.2 Palladium Addition to Magnesium Oxide Supported Catalysts for Carbon Dioxide Hydrogenation.

3.2.1 Catalyst Preparation

The use of noble metal based systems are thought to be of pivotal importance for WGS catalysis[10] and have been shown to be equally adept at catalysing the RWGS reaction.[11] Work by Gorte *et al*.,[12] that investigated the effect of noble metal addition to Fe_2O_3 catalysts for the WGS reaction, found that palladium addition showed a significant improvement in WGS activity relative to the addition of equal amounts of platinum and ruthenium. For the purpose of

increasing the RWGS activity of the MgO supported catalysts discussed in Section 3.1 the addition of palladium was investigated.

Palladium has been widely used in hydrogenation reactions as it possesses high solubility of H_2 on the metal surface. Its introduction to FT catalyst systems has been shown to significantly enhance activity with little disadvantageous effects on methane selectivity.[13] The palladium promotion of iron catalysts has also been shown to increase the WGS activity of the catalyst system.[13a] Despite its success when used for in FT and RWGS catalysis its use in CO_2 hydrogenation has remained limited.

Due to the relative high cost and environmental footprint of palladium only small amounts (1 wt%) were introduced to the catalyst system. Palladium chloride ($PdCl_2$) was considered as the palladium precursor for catalyst preparation but with the addition of Cl^- anions proving detrimental to the performance of FT catalysts[14] palladium acetate {$Pd(OAc)_2$} was chosen instead. Catalysts were prepared using a similar method to that reported in Section 3.1, however, due to the solubility issues of $Pd(OAc)_2$ in water, methanol was used as a solvent for catalyst preparation.

Despite the high HC yield reported for 20wt%Ni/MgO in Section 3.1 it was decided not to take the system further due to the high methane selectivity observed even at high conversions. Nickel, when utilised for the FT process shows high methane selectivity[15] and so it is unlikely that the formation of more CO by the addition of palladium to the system would improve selectivity with the higher temperatures needed for the RWGS reaction likely to force hydrocarbon selectivity towards exclusive methane formation.[16] This system may warrant further investigation as a CO_2 methanation catalyst. Two catalyst systems were prepared for testing; 20wt%Fe/1wt%Pd/MgO and 20wt%Co/1wt%Pd/MgO.

3.2.2 Catalyst Characterisation

The prepared catalyst systems were characterised using a combination of SEM and energy dispersive X-ray spectroscopy (EDS), pXRD and X-ray photoelectron spectroscopy (XPS). As with the catalyst systems studied in Section 3.1 no diffraction attributable to iron, cobalt or palladium species were detected in pXRD studies. This suggests all metals are well dispersed on the surface of the catalyst support with any of the crystalline species likely to be too small for detection. Peaks corresponding to the catalyst support are however present for both systems.

An SEM image typical for the 20wt%Fe/1wt%Pd/MgO catalyst system is shown in Figure 3.8 (a). The morphology shows a significant difference to that observed for the MgO support alone {Figure 3.4 (d)} with particle sizes significantly larger. Microspheres are still observable however the majority appear to have combined with the metals present in the system resulting in the formation of larger particles. EDS mapping was conducted in conjunction with SEM, Figure 3.8 (b-e) shows the obtained images. Figure 3.8 (b) shows the positions at which magnesium from the MgO support can be detected. Iron and palladium can also be detected within the catalyst system confirming a successful loading of both metals. The lack of any iron

or palladium in areas without magnesium suggested that both are successfully supported on the MgO.

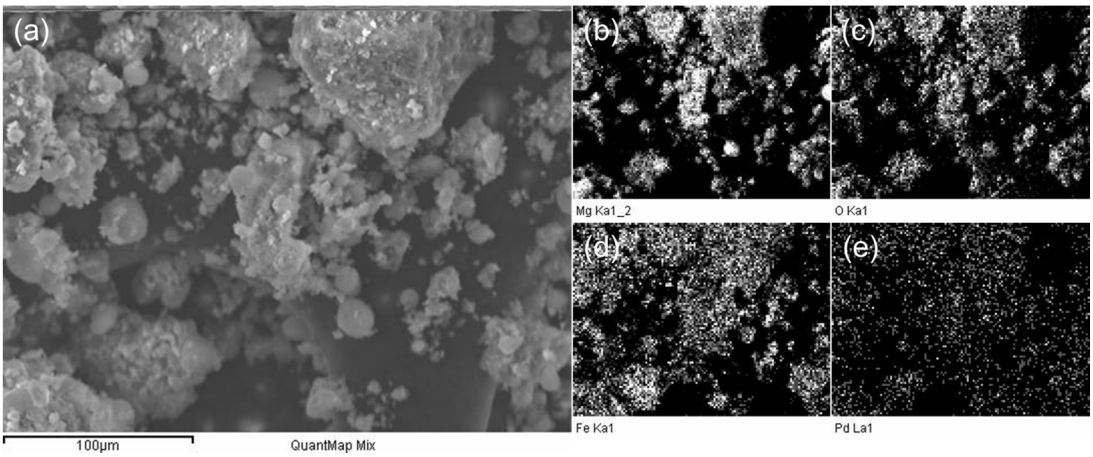

Figure 3.8 – (a) SEM image recorded for 20wt%Fe/1wt%Pd/MgO. EDS mapping performed in conjunction with SEM, mapping for (b) magnesium, (c) oxygen, (d) iron and (e) palladium.

XPS studies were conducted on 20wt%Fe/1wt%Pd/MgO to aid determination of the metal phases present on the catalyst surface. Figure 3.9 shows the spectra obtained from this analysis. Figure 3.9 (a) shows a survey spectrum obtained for the un-used, calcined catalyst between a binding energy ranging from 0 to 1200 eV. From the peak positions the presence of oxygen, iron and magnesium can be confirmed. The presence and/or oxidation state of the palladium within the system could not be determined. A peak would be expected at 337.0 eV for palladium (II) oxide (PdO) or 335.3 eV for metallic palladium (Pd^0).[17] The presence of an Mg KLL peak in this region, however, hinders the detection of the palladium 3d peak within the system. A more detailed scan with a smaller step size and longer dwell was performed between 700 eV and 745 eV to aid identification of the iron species, Figure 3.9 (b). The binding energy of 711 eV indicates the presence of iron in the +III oxidation state corresponding to Fe_2O_3. The satellite peak at 719 eV, characteristic of Fe^{3+} in Fe_2O_3 further confirms this.[18] A detailed scan of the O 1s region (Figure 3.9 (c)) reveals the presence of two O 1s subpeaks with binding energies of approximately 529 eV and 531 eV these peaks can be attributed to oxygen species in the form of oxide and hydroxyl groups respectively.[19] Based on the subpeak areas being of a similar size it can be suggested that the surface contains approximately equal quantities of hydroxyl and oxide functionality. While the subpeak at 529 eV can be attributed to the oxide species present in both the MgO support and the Fe_2O_3 phase that present at 531 eV is likely due to the hydroxylation of the MgO surface. The formation of hydroxyl groups upon the exposure of metal oxides to moisture due to the dissociative chemisorption of water is commonly observed.[19-20] The high isoelectric point[21] and strongly basic nature of MgO results in the increased likelihood of hydroxyl formation upon its surface.

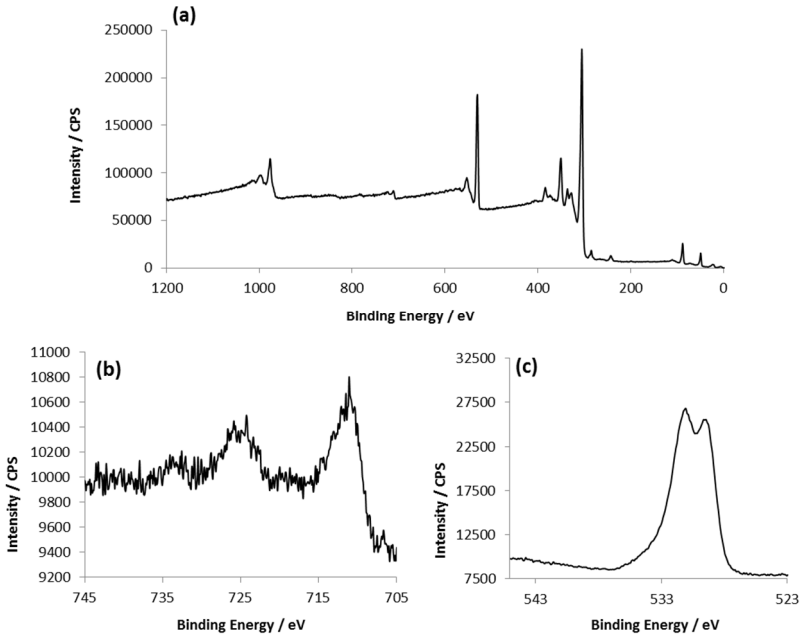

Figure 3.9 – XPS spectra recorded for a calcined 20wt%Fe/1wt%Pd/MgO sample. (a) Survey spectrum recorded between 0 eV and 1200 eV. (b) Detailed scan of the iron 2p region. (c) Detailed scan of the oxygen 1s region.

XPS studies were also conducted on the 20wt%Co/1wt%Pd/MgO system, the resulting spectra are shown in Figure 3.10. The survey spectrum {Figure 3.10 (a)} shows the presence of magnesium, oxygen and cobalt. As with the analogous iron system no peaks corresponding to palladium are detected due to the presence of large peaks from the MgO component of the catalyst. A more detailed scan was performed between 770 eV and 815 eV, the cobalt 2p region of the spectrum, Figure 3.10 (b) shows the resulting spectrum. Two major peaks are observed at 780.4 eV and 795.8 eV, these are characteristic of cobalt present as Co_3O_4,[22] and in good agreement with reported literature values.[23] A detailed scan of the oxygen 1s region again reveals the presence of two subpeaks attributable to oxide and hydroxyl oxygen species. Based on the areas of the two subpeaks there appears to be a slightly higher concentration of oxide species at the surface rather than hydroxyl species.

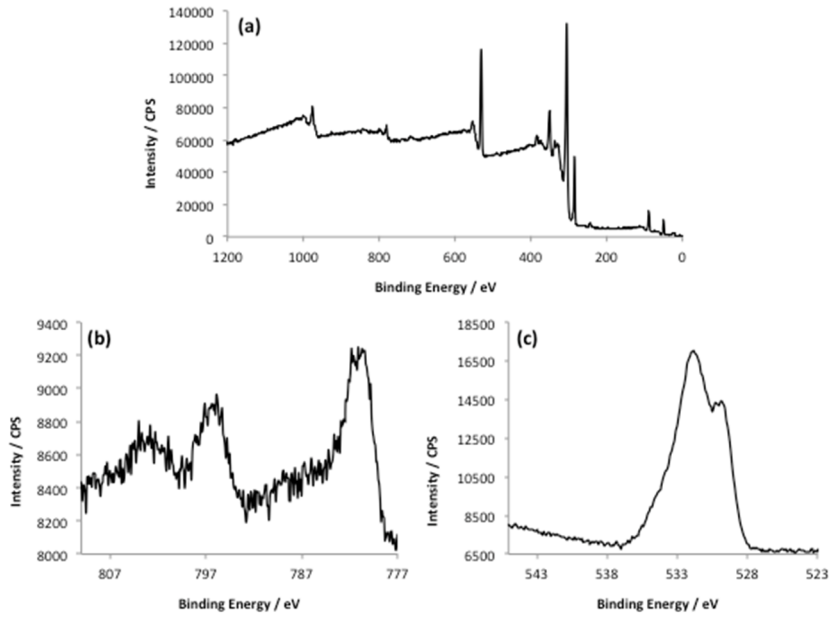

Figure 3.10 – XPS spectra recorded for a calcined 20wt%Co/1wt%Pd/MgO sample. (a) Survey spectrum recorded between 0 eV and 1200 eV. (b) Detailed scan of the cobalt 2p region. (c) Detailed scan of the oxygen 1s region

3.2.3 Catalyst Testing

The prepared and characterised catalyst systems were tested for their CO_2 hydrogenation ability. All systems were tested using the same general testing procedure as that utilised in Section 3.1.3. The catalytic test results for 20wt%Fe/1wt%Pd/MgO over a range of different temperatures are summarised in Table 3.2.

A significant increase in conversion is observed as the temperature is increased with the highest conversion observed at 420 ^{o}C. Product selectivity also shows a dependence on the reaction temperature with 360 ^{o}C found to be optimum in terms of hydrocarbon selectivity with up to C_5 HCs being formed and a methane selectivity of 53 %. The palladium promoted 20wt%Fe/1wt%Pd/MgO compares favourably with the non-promoted system. At a reaction temperature of 300 ^{o}C HC yield almost doubles from 0.5 % to 0.8 % with C_2+ selectivity increasing from 12 % to 37 % upon the introduction of palladium. Both systems show an optimum C_2+ selectivity at 360 ^{o}C with the Pd-promoted system still performing significantly better at this temperature with C_2+ selectivity increasing from 21 % with 20wt%Fe/MgO to 47 % for 20wt%Fe/1wt%Pd/MgO. This improved performance can most likely be attributed to the increased WGS activity of the catalyst system when palladium is present resulting in an increase in CO formation aiding the FT process. Palladium promotion is also likely to improve the performance of the catalyst for the FT synthesis component.[13] The HC products formed were found to be exclusively paraffins with no olefins present, this is presumably due to the high hydrogenating ability of the palladium which could be aiding the hydrogenation of any formed olefin products.

Table 3.2 - Catalytic data obtained for CO_2 hydrogenation tests using 20wt%Fe/1wt%Pd/MgO over a range of temperatures

Temperature (°C)	Hydrocarbon Yield (%)	Hydrocarbon Distribution (%)				
		C_1	C_2	C_3	C_4	C_5
300	0.8	62.9	22.1	10.1	4.8	0.0
330	1.4	56.4	27.3	12.4	3.9	0.0
360	5.3	53.2	28.6	13.7	3.8	0.7
390	10.7	56.4	29.0	12.2	2.4	0.1
420	12.8	66.5	25.9	6.9	0.7	0.0

Catalyst tests conducted at atmospheric pressure, $Ar:H_2:CO_2$ ratio 1:3:1, total flow – 10 sccm. 0.7g of catalyst.

The 20wt%Co/1wt%Pd/MgO catalyst system was also tested in order to determine its CO_2 hydrogenation ability. The same general catalyst test procedure was used however, since cobalt based catalyst systems are usually employed for low temperature FT processes, catalyst tests were started at 230 °C rather than 300°C. The resulting catalyst data is summarised in Table 3.3. As with all previous catalyst tests HC yield is observed to increase steadily with increasing reaction temperature. A maximum HC yield of 41 % is obtained at 440 °C, there is however little change above a temperature of 410 °C suggesting that a further increase in temperature is not likely to improve HC yield. The HC yield observed at 290 °C is significantly higher (by a factor of ~18) than that observed for the 20wt%Co/MgO system at 300 °C. This large improvement in HC yield can be attributed to the inclusion of palladium to the catalyst system, which is most likely acting as an active species in both the RWGS[24] and possibly the FT processes although palladium's FT activity has proved limited.[8] Addition of noble metals such as palladium to FT based cobalt catalysts have resulted in a higher reducibility of the cobalt species as well as increased cobalt dispersion.[25] Both properties that could also improve catalyst performance.

The catalyst shows a high selectivity for methane at all temperatures investigated. Generally a lower temperature leads to a better hydrocarbon selectivity with a temperature of 260 °C proving optimum for C_2+ selectivity. While C_2+ selectivity may seem poor relative to the 20wt%Fe/1wt%Pd/MgO system it has improved significantly from that observed for the 20wt%Co/MgO catalyst. This is can likely be attributed to the increased WGS activity resulting in the increased formation of CO that can be utilised for FT synthesis. The lack of WGS activity for the cobalt only catalyst means that methane is possibly being produced *via* a direct hydrogenation process. At the highest HC yield the HC products consist of exclusively methane, as a consequence a compromise between HC yield and HC selectivity is likely to be necessary when choosing the optimum reaction temperature.

Table 3.3 – Catalytic data obtained for CO_2 hydrogenation using the 20wt%Co/1wt%Pd/MgO catalyst over a range of temperatures

Temperature (°C)	Hydrocarbon Yield (%)	Hydrocarbon Distribution (%)				
		C_1	C_2	C_3	C_4	C_5
230	5.6	96.0	1.3	2.7	0.0	0.0
260	9.7	87.1	7.5	4.3	1.1	0.0
290	18.6	91.9	6.2	1.9	0.0	0.0
320	26.2	95.5	3.9	0.6	0.0	0.0
350	31.3	98.1	2.0	0.0	0.0	0.0
380	35.8	99.4	0.6	0.0	0.0	0.0
410	40.1	100.0	0.0	0.0	0.0	0.0
440	41.3	100.0	0.0	0.0	0.0	0.0

Catalyst tests conducted at atmospheric pressure, $Ar:H_2:CO_2$ ratio 1:3:1, total flow – 10 sccm. 0.7g of catalyst.

3.2.4 Characterisation of Used Catalysts

XPS studies have shown that both catalyst systems consist of the oxides of either iron or cobalt supported on an MgO support that has a high hydroxyl coverage on the surface after calcination. While Fe_2O_3 has been shown to be active for the RWGS reaction[26] the FT activity of Fe_2O_3 and Co_3O_4 is limited. As a consequence both catalysts are hydrogenated before use in order to reduce each species to phases more active for hydrocarbon production. As the reaction takes place under strongly hydrogenating conditions and the presence of water (one of the main reaction side products) the species present can be expected to change with time on stream. As a result it can be difficult to identify the active species. In an attempt to gain a further understanding of the system and the species present during reaction XPS studies were conducted on used catalyst systems. It should be noted at this point that the palladium species would also be expected to vary however with MgO present as a support it is not possible to assess these changes using XPS.

For the 20wt%Fe/1wt%Pd/MgO system, the catalyst tested at 360 °C was chosen for further investigation as this was seen as the best performing catalyst system, in terms of compromise between conversion and product selectivity. Figure 3.11 shows the XPS spectra obtained before and after catalyst use. Figure 3.11 (a and b) shows the Fe 2p region of the spectra for both samples, before and after use. The calcined sample shows a binding energy of 711 eV typically observed for Fe_2O_3. After a 2 hour reduction period followed by 5 hours on stream the XPS spectra shows a slight reduction in the satellite peak, characteristic for Fe_2O_3, at 719 eV along with a shift of 2p 3/2 peak to a slightly lower binding energy suggesting the presence of Fe_3O_4 as the main iron phase. This is further confirmed by the change in the catalyst system from a rust brown colour before use to a black colour after.

Figure 3.11 (c and d) shows the O 1s region with the peak at 531.2 eV corresponding to the oxygen present in hydroxyl groups on the MgO surface and the peak at 529.5 eV corresponding to oxygen present in an oxide form.[19] After the reductive pre-treatment and 5 hours on stream there is a clear reduction in the intensity of the peak at 531.2 eV. This suggests a significant reduction in the hydroxyl species present on the MgO surface after the reductive pre-treatment and 5 hours under reaction conditions.

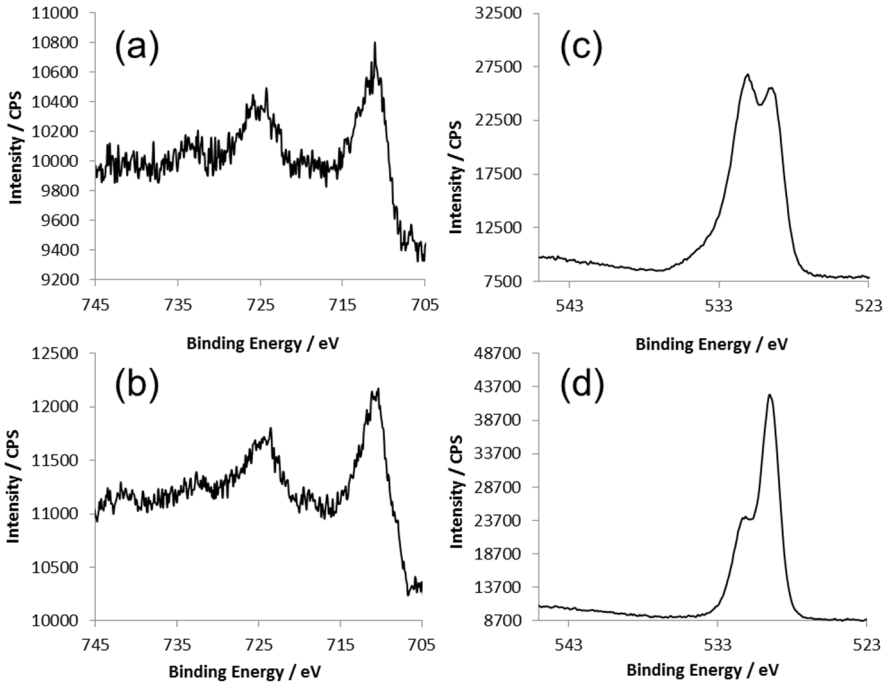

Figure 3.11 – XPS spectra recorded for the 20wt%Fe/1wt%Pd/MgO catalyst system both after calcination and after a 2 hour reduction followed by 5 hours on stream. (a) Spectra recorded in the Fe 2p region after calcination. (b) Spectra recorded in the Fe 2p region after use. (c) Spectra recorded in the O 1s region before use. (d) Spectra recorded in the O 1s region after use.

For the 20wt%Co/1wt%Pd/MgO system the catalyst tested at 300 ^{o}C was chosen for analysis by XPS as this reaction temperature was seen as the best compromise between HC yield and selectivity to C_2+ HCs. Figure 3.12 shows the XPS spectra obtained for the catalyst system after calcination and after a two hour reduction followed by 5 hours on stream. Figure 3.12 (a and b) shows the Co 2p region before and after reaction. For the calcined sample, a binding energy of 780.4 eV indicates the presence of Co_3O_4 as the main cobalt species present. After reduction and catalyst testing a slight increase in the $2p_{3/2}$ peak binding energy combined with the emergence of a more distinct satellite peak at 386 eV suggests an increase in the presence of Co^{2+}[23b] attributable to the reduction of Co_3O_4 to CoO.[22] Peaks attributable to the presence of metallic cobalt (Co^0) would be expected at 778.1 eV.[22] None are observed but they may be masked by the presence of the $2p_{3/2}$ peaks attributable to Co^{2+} and Co^{3+} and as such its presence can neither be confirmed of refuted by XPS. The main cobalt phase present can,

however, be confirmed as CoO. As observed with the analogous iron system the oxygen region of the spectrum {Figure 3.12 (c and d)} reveals the presence of oxygen in both the hydroxyl and oxide forms. After reaction a reduction in the surface MgO hydroxyl groups is observed.

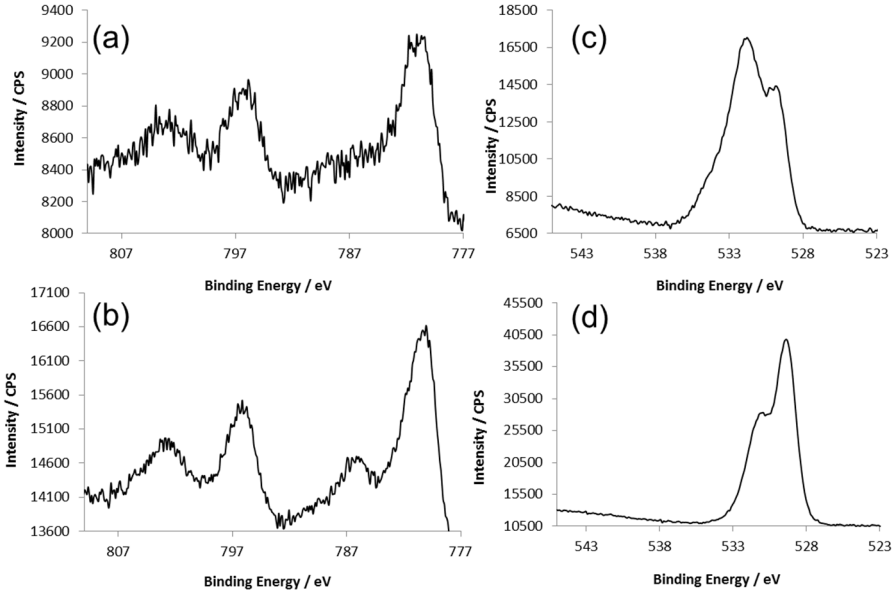

Figure 3.12 – XPS spectra recorded for the 20wt%Co/1wt%Pd/MgO catalyst system both after calcination and after a 2 hour reduction followed by 5 hours on stream. (a) Spectra recorded in the Co 2p region after calcination. (b) Spectra recorded in the Co 2p region after use. (c) Spectra recorded in the O 1s region before use. (d) Spectra recorded in the O 1s region after use.

3.2.5 Summary

The addition of palladium to the catalyst system proved successful in improving both the iron and cobalt based catalyst systems with an increase in HC yield and an improvement in HC selectivity observed for both systems upon its inclusion. The improved catalyst performance can be attributed to the increased RWGS activity of both systems along with the promotion of the FT step of CO_2 hydrogenation. XPS studies have shown the presence of iron as Fe_2O_3 and cobalt as Co_3O_4 before reaction these species are however reduced to Fe_3O_4 and CoO after the reductive pre-treatment and time under reaction conditions. The MgO support shows a high concentration of surface hydroxyl groups after calcination, these are however greatly reduced after the reductive pre-treatment and time under reaction conditions.

3.3 Palladium and Potassium Addition to Magnesium Oxide Supported Catalysts for Carbon Dioxide Hydrogenation.

Although the catalysts studied so far show selectivity to heavier hydrocarbons the selectivity to methane is still high with the products formed exclusively saturated HCs. The addition of a

potassium promoter to iron catalyst used in both CO and CO_2 fed hydrogenation processes has been shown to have a large influence on the reducing the methane selectivity and driving hydrocarbon distribution towards the heavier chained and unsaturated HC products.[27] Work conducted by O'Brien and co-workers suggested that for iron based catalyst systems the optimum potassium loading is equivalent to 4-5 wt% of the total iron loading.[27b] With the systems currently being investigated containing 20 wt% Fe a 1 wt% loading of potassium was chosen giving a catalyst composition of 20wt%Fe/1wt%Pd/1wt%K/MgO. An analogues 20wt%Co/1wt%Pd/1wt%K/MgO catalyst system was also prepared. The addition of potassium to cobalt based catalysts for CO_2 hydrogenation has not to our knowledge been investigated previously and while iron-potassium catalysts have been investigated the use of MgO as a support for these systems and in conjunction with palladium has not received any attention.

The preparation method remained similar to that used for the palladium only promoted catalyst systems reported in Section 3.2 only with the addition of a methanolic K(OAc) solution after the addition of the $Pd(OAc)_2$ solution. The remainder of the catalyst preparation remained unchanged.

3.3.1 Catalyst Characterisation

The 20wt%Fe/1wt%Pd/1wt%K/MgO and 20wt%Co/1wt%Pd/1wt%K/MgO catalyst systems were characterised using a combination of EDS, SEM, XPS and pXRD. As with previous pXRD studies conducted on this set of MgO supported catalyst systems only peaks attributable to the MgO support were observable with no peaks attributable to other metals or metal oxides.

To gain a further understanding of catalyst morphology SEM was employed to study the catalyst systems. Figure 3.13 (a) shows the SEM image recorded for 20wt%Fe/1wt%Pd/1wt%K/MgO. Particles are shown to be irregular in shape and size with no obvious difference in catalyst morphology when compared to the non-potassium promoted system. EDS studies were conducted in conjunction with SEM analysis. The resulting spectrum is shown in Figure 3.13 (b). Peaks that can be attributed to oxygen, magnesium, iron, palladium and potassium are shown demonstrating the successful loading of all components to the catalyst support with a good distribution.

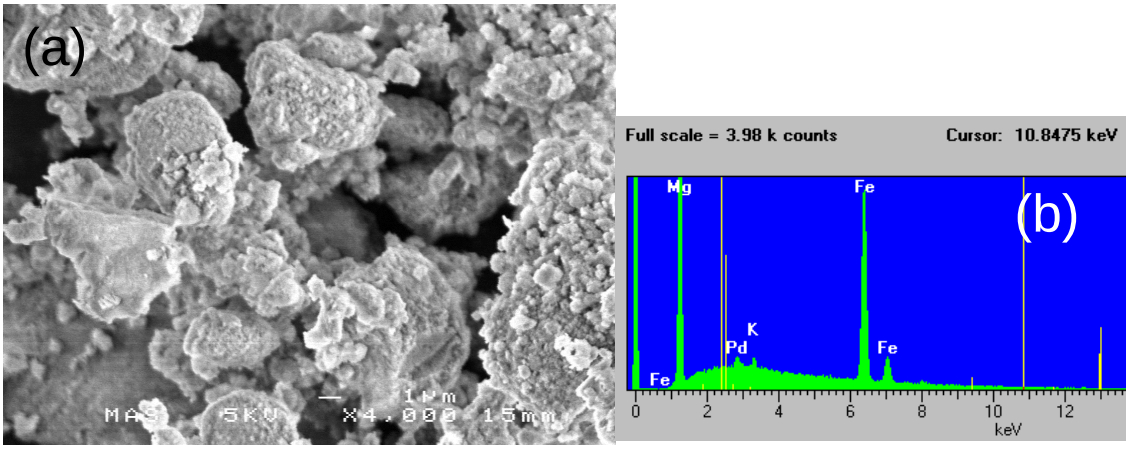

Figure 3.13 – Image and spectrum obtained from the EDS-SEM study of 20wt%Fe/1wt%Pd/1wt%K/MgO. (a) A SEM image typical for the catalyst system. (b) An EDX spectrum obtained in conjunction with SEM studies.

Figure 3.14 shows the images recorded from EDS-SEM studies conducted on the 20wt%Co/1wt%Pd/1wt%K/MgO catalyst system. An image typical of the morphology observed for the catalyst is shown in Figure 3.14 (a). As with the analogous iron system no observable morphology change is observed upon the addition of a potassium promoter to the system. EDX studies {Figure 3.14 (b)} showed the presence of oxygen, magnesium, palladium, potassium and cobalt confirming their presence in the catalyst system showing successful loading.

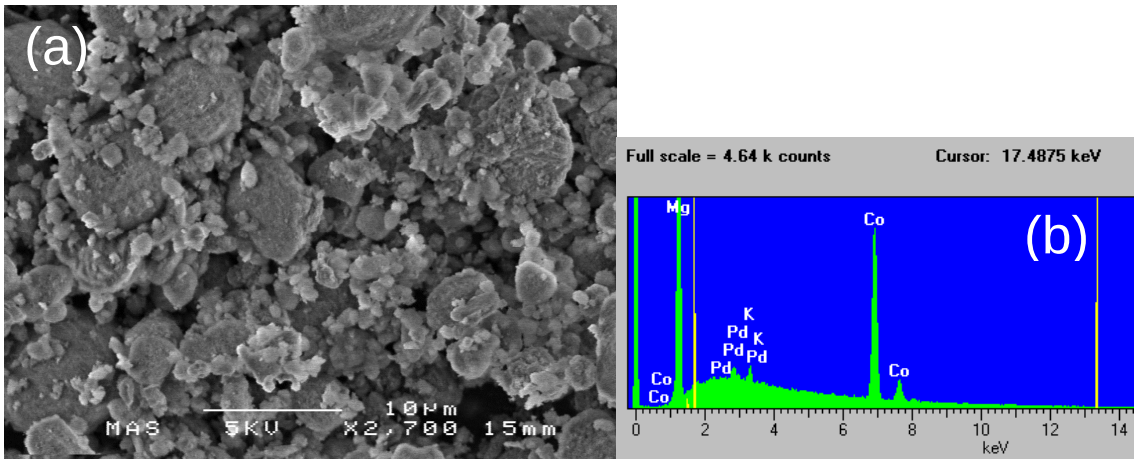

Figure 3.14 – Images and spectra obtained from the EDS-SEM study of 20wt%Co/1wt%Pd/1wt%K/MgO. (a) A SEM image typical for the catalyst system. (b) An EDX spectrum obtained in conjunction with SEM studies.

XSP studies were also carried out on the catalyst systems. Figure 3.15 shows the spectra recorded for 20wt%Fe/1wt%Pd/1wt%K/MgO. The survey scan shown in Figure 3.15 (a) confirms the presence of iron, magnesium and oxygen. Palladium cannot be detected again due to the Pd 3d region being blocked by the Mg KLL peak. A more detailed scan was obtained for the 700 eV – 745 eV, iron 2p region {Figure 3.15 (b)}. The signal recorded does not appear as strong as that recorded for the 20wt%Fe/1wt%Pd/MgO and as a result the peaks shape is not as

clear. The binding energy of *ca.* 711 eV suggests that the introduction of potassium to the system has no effect on the nature of iron species with Fe_2O_3 still representing the main iron phase present in the calcined catalyst system. As with the analogous catalysts without potassium the O 1s region shows the presence of two peaks attributable to oxides and hydroxyls. In contrast to the Fe/Pd/MgO catalyst a higher quantity of hydroxyl species is present in the potassium containing system rather than approximately equal amounts of each as observed with the system not containing potassium.

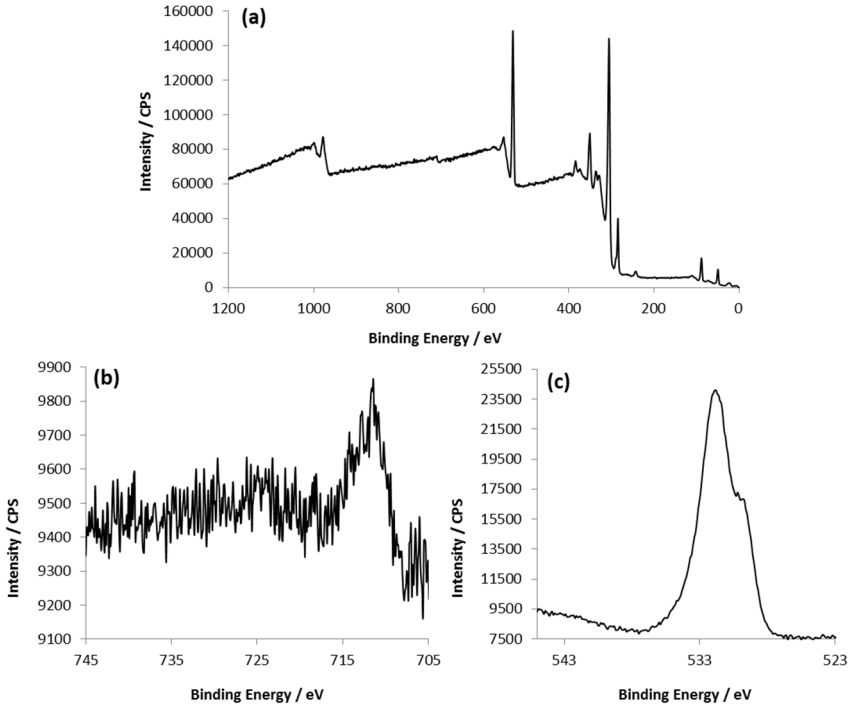

Figure 3.15 – XPS spectra recorded for a calcined 20wt%Fe/1wt%Pd/1wt%K/MgO sample. (a) Survey spectrum recorded between 0 eV and 1200 eV. (b) Detailed scan of the iron 2p region. (c) Detailed scan of the oxygen 1s region.

Figure 3.16 shows the results of XPS analysis carried out on the 20wt%Co/1wt%Pd/1wt%K/MgO catalyst system. The survey spectrum recorded for the system shows the presence of magnesium, oxygen and cobalt. Again, due to the Mg KLL peak palladium cannot be detected. Potassium is not detected although it is unclear as to the reason why. 1 wt% is well within the detection limit of the technique. Detailed scans of the Co 2p region {Figure 3.16 (b)} indicated that after calcination the main cobalt phase present in the system is Co_3O_4 with no noticeable change in phase upon the addition of potassium to the system. A detailed scan of the oxygen 1s region (Figure 3.16 (c)) reveals the presence of oxygen both in the oxide and hydroxyl form with an approximately equal distribution between the two.

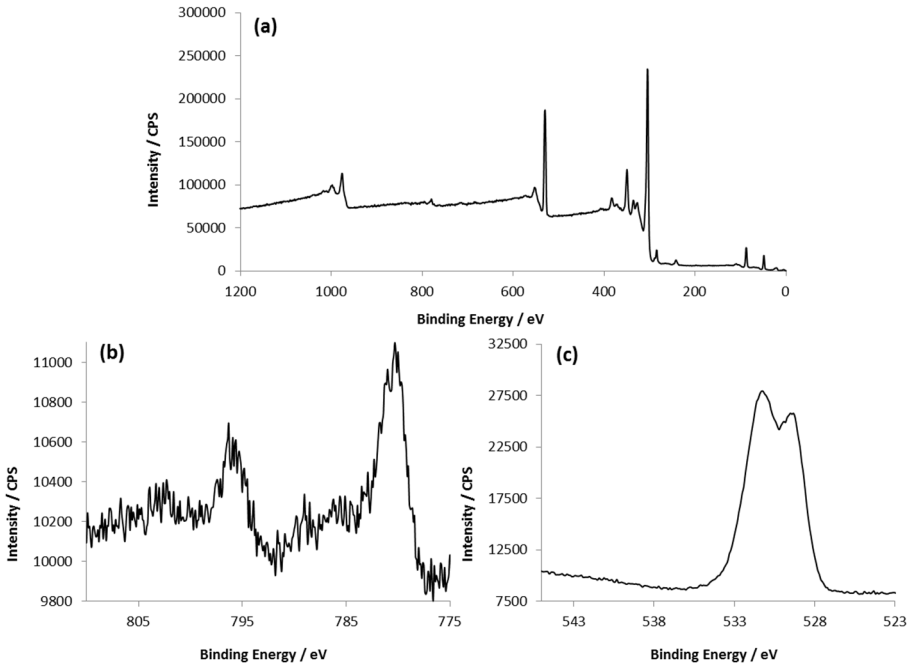

Figure 3.16 – XPS spectra recorded for a calcined 20wt%Co/1wt%Pd/1wt%K/MgO sample. (a) Survey spectrum recorded between 0 eV and 1200 eV. (b) Detailed scan of the cobalt 2p region. (c) Detailed scan of the oxygen 1s region.

3.3.2 Catalyst Testing

The effect of potassium promotion was first tested on the Fe/Pd/MgO system investigated in Section 3.2. The 20wt%Fe/1wt%Pd/1wt%K/MgO catalyst was loaded into Reactor 1 and tested under using the same procedure detailed previously for MgO supported catalyst systems. Testing was conducted over a range of temperatures from 230 ^{o}C to 410 ^{o}C at 30 ^{o}C intervals, Table 3.4 summarises the results obtained.

As with previous catalyst tests as the temperature was increased HC yield was observed to increase up to *ca.* 29 % at 360 ^{o}C, above this temperature no discernable increase is observed. A significant improvement in HC yield is observed for the potassium containing system over that observed for the Fe/Pd/MgO system tested in Section 3.2.3. The highest CO_2 conversion to HCs without potassium present was 12.8 %, significantly lower than that observed for the Fe/Pd/K/MgO system. This increase in HC yield can likely be attributed to an increased CO_2 chemisorption capacity when potassium is introduced into iron based catalysts[28] due to increased basicity of the surface which favours CO_2 adsorption.

Table 3.4 – Catalytic data obtained for CO_2 hydrogenation using 20wt%Fe/1wt%Pd/1wt%K/MgO over a range of temperatures.

Temperature (°C)	HC Yield (%)	Hydrocarbon Distribution (%)							
		C_1	C_2	C_3	C_4	C_5	C_6	C_7	C_8
300	4.7	27.0	24.8	25.8	11.0	4.9	6.6	0.0	0.0
320	9.9	26.1	24.8	24.5	13.6	7.1	2.8	1.1	0.0
340	22.1	23.9	21.8	22.9	14.0	8.2	6.1	3.0	0.1
360	29.3	29.7	22.3	22.2	11.3	8.2	4.9	1.4	0.0
380	29.5	38.4	24.1	21.0	9.0	3.9	1.8	1.7	0.0
400	27.4	48.9	22.6	17.6	6.4	2.2	1.0	1.3	0.0

Catalyst tests conducted at atmospheric pressure, Ar:H_2:CO_2 ratio 1:3:1, total flow – 10 sccm. 0.7g of catalyst.

The introduction of potassium also plays an important role in altering the hydrocarbon distribution as observed with other iron based catalysts for CO_2 hydrogenation.[27a] Methane selectivity is greatly reduced from the 50-60 % observed with the Fe/Pd/MgO system to as low as 24 %. This values compares favourably with literature[29] with few reports of lower selectivities of methane reported.[30] A temperature of 340 °C appears to be optimum in terms of HC distribution with the lowest methane selectivity and up to C_8 hydrocarbons being formed, albeit at low levels. Whereas all previous catalysts tested have formed exclusively paraffins the introduction of potassium has aided the production of olefins. The increased olefin content and reduction in methane selectivity observed for the reaction products can be attributed to a poorer H_2 adsorption ability upon potassium promotion[28] which leads to a less reductive surface favouring the formation of unsaturated HCs along with chain growth over termination. Figure 3.17 shows a typical FID chromatogram obtained at 340 °C illustrating the range of HC products formed. As well as the formation of linear olefins and paraffins the product stream also contained a range of monomethyl branched HCs, common with HCs formed through the FT process. The majority of monomethyl branching occurs at the 2-position again a typical attribute of FT produced HCs, a phenomenon that can be explained using the FT mechanism proposed by Dry[15] (see Chapter 1, Section 1.3.2 for further details).

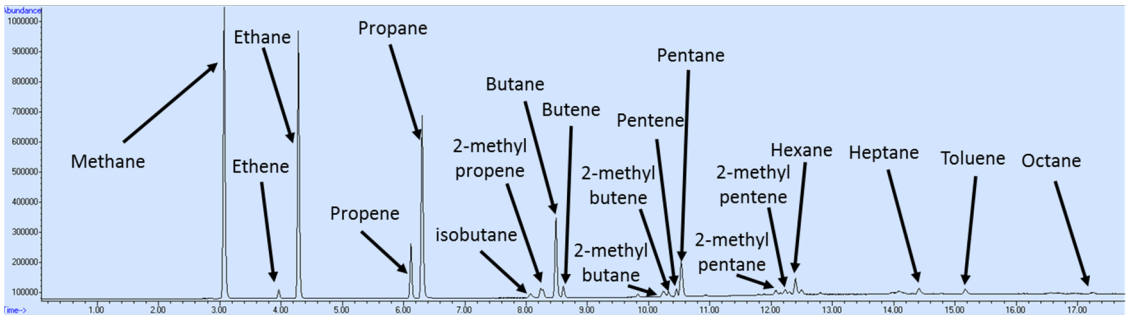

Figure 3.17 – GC-FID trace recorded at 340 ^{o}C for CO_2 hydrogenation over 20wt%Fe/1wt%Pd/1wt%K/MgO illustrating the range of hydrocarbon products produced with the largest peaks identified.

The effect of potassium addition to the 20wt%Co/1wt%Pd/MgO catalyst system was investigated. Reaction conditions were kept the same as those used for the analogous 20wt%Fe/1wt%Pd/1wt%K/MgO system with the same temperature range covered at 30 ^{o}C intervals however an initial temperature of 230 ^{o}C was chosen for comparison to the Co/Pd/MgO system. The resulting data is summarised in Table 3.5. Increasing reaction temperature is observed to lead to an increased HC yield. The HC yield values obtained compare favourably relative to the analogous system without the presence of potassium (Table 3.3). At a reaction temperature of 230 ^{o}C HC yield was observed to increase from 5.6 % to 7.0 % upon potassium addition. The trend continues at higher temperatures with HC yield increasing from 31.3 % to 39.0 % at 350 ^{o}C. This improved HC yield could be due to either an increase in RWGS activity of the catalyst as previously witnessed for upon the addition of potassium to a Co/CeO_2 RWGS catalyst[31] or possibly an improvement in the FT stage of reaction, this however seems unlikely as potassium addition has in the past been shown to reduce the activity of cobalt systems for the FT process.[32] There appears to be little change in the maximum HC yield achievable using both the Co/Pd/MgO and Co/Pd/K/MgO catalysts with both showing a maximum HC yield of *ca.* 40 %. The potassium containing system does reach this at a reaction temperature of approximately 320 ^{o}C compared to 410 ^{o}C as observed for the Co/Pd/MgO catalyst.

Table 3.5 – Catalytic data obtained for CO_2 hydrogenation suing 20wt%Co/1wt%Pd/1wt%K/MgO over a range of temperatures

Temperature (^oC)	Hydrocarbon Yield (%)	Hydrocarbon Distribution (%)				
		C_1	C_2	C_3	C_4	C_5
230	7.0	68.1	13.3	10.9	5.3	2.4
260	17.4	75.7	12.6	8.2	2.5	1.0
290	31.8	92.1	6.6	1.3	0.0	0.0
320	37.3	96.6	3.1	0.3	0.0	0.0
350	39.0	98.1	1.9	0.0	0.0	0.0

Catalyst tests conducted at atmospheric pressure, $Ar:H_2:CO_2$ ratio 1:3:1, total flow – 10 sccm. 0.7g of catalyst.

The addition of potassium also shows a large effect on the HC distribution. Methane selectivity was reduced to 68.1 % at 230 ^oC a value much lower than that observed for the majority of cobalt catalysts used for CO_2 hydrogenation[33] and similar to some of the lowest methane selectivities.[34] In conjunction with the decreased methane selectivity HCs of a chain length of up to C_5 are now formed compared to lower amounts of C_4 observed for the Co/Pd/MgO system. As temperature is increased beyond 230 ^oC methane selectivity increases to a value of approximately 98 % at the highest conversion, observed at 350 ^oC. This means that in order to obtain a catalyst system with a high HC yield and good HC selectivity a compromise on reaction temperature will need to be made. This shows that unlike cobalt catalysts utilised for FT processes[32] the addition of potassium to systems used for CO_2 hydrogenation is beneficial both in terms of product selectivity and HC yield.

3.3.3 Characterisation of Used Catalysts

The main iron and cobalt phases present after calcination are Fe_2O_3 and Co_3O_4 as shown by XPS studies (Section 3.3.1), however, as shown with the previous palladium promoted systems in Section 3.2.4 after the reductive pre-treatment and some time under reaction conditions the metal phases change. In order to determine if potassium has any influence on the changing metal phases of the catalyst systems XPS studies were conducted on used catalyst samples and compared to that of the catalysts after calcination.

The 20wt%Fe/1wt%Pd/1wt%K/MgO catalyst tested at 360 ^oC was chosen for further XPS studies as this system afforded best compromise between conversion and selectivity. Figure 3.18 shows the XPS spectra obtained from this study. As discussed earlier before use the catalyst system shows the presence of Fe_2O_3 as the main iron phase. After a 2-hour reduction followed by 5 hours on stream this species appears to be reduced to Fe_3O_4 {Figure 3.18 (a)}. A shift in binding energy from 710.6 eV to 709.8 eV is observed which would confirm this

change. The lack of an observable satellite at 719 eV also supports this suggestion along with a colour change from rust-brown before use to black after. This suggests that the addition of potassium to the system has little effect on the iron phases after catalyst testing. Figure 3.18 (b) shows the O 1s region recorded before and after catalyst use. Two oxygen environments are clearly observed at 532.1 eV and 530.2 eV attributable to MgO hydroxyl species and oxygen present oxide species. A decrease in the intensity of the peak at 531.2 eV as observed after reaction suggests a reduction in the number of hydroxyl sites present on the MgO surface. In contrast to what is observed with the Fe/Pd/MgO catalyst even after reaction the quantity of hydroxyl species present on the MgO surface is still higher quantity than the oxygen present in oxide forms. It is possible that this suggested increase in surface basicity could influence the catalyst selectivity.[2a]

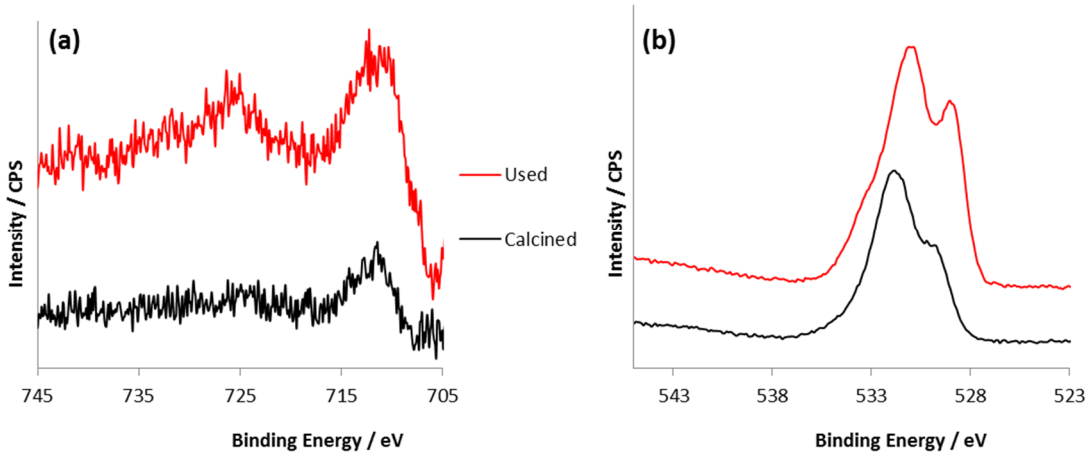

Figure 3.18– XPS spectra recorded for the 20wt%Fe/1wt%Pd/1wt%K/MgO catalyst system both after calcination and after a two hour reduction followed by 5 hours on stream. (a) Spectra recorded in the Fe 2p region. (b) Spectra recorded in the O 1s region.

The 20wt%Co/1wt%Pd/1wt%K/MgO system was also studied before and after reaction utilising XPS. The catalyst tested at a temperature of 290 ^{o}C was decided to be the best compromise between conversion and product distribution and as such was chosen for these further tests. Figure 3.19 (a) shows the Co 2p region of the spectra before and after use. After calcination Co_3O_4 is shown to be present as the main cobalt species. After the reductive pre-treatment and 5 hours on stream the shift in binding energy to 780.3 eV along with the appearance of more pronounced satellite signals at 786 eV and 802 eV[23b] suggests the reduction to CoO, the first step on the full reduction to metallic Co^0.[35] The presence of metallic Co^0 is unclear as the expected peak at 778.1 eV[22] could be masked by the Co^{2+} $2p_{3/2}$ peak. Figure 3.19 shows a detailed scan of the oxygen 1s region, before reaction there is slightly more hydroxyl species present than oxide species, after reaction a reduction in hydroxyl oxygens results in a slightly higher amount of oxide oxygens than hydroxyl species. The reduction in intensity of the hydroxyl peak is not as extensive as that recorded for the Co/Pd/MgO catalyst

suggesting that potassium could be influencing the hydroxyl species present on the catalyst surface.

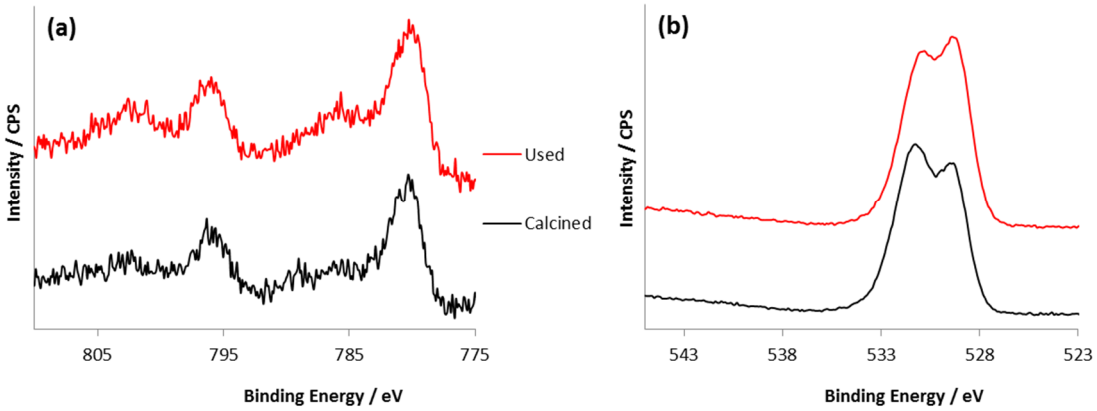

Figure 3.19 – XPS spectra recorded for the 20wt%Co/1wt%Pd/1wt%K/MgO catalyst system both after calcination and after a two hour reduction followed by 5 hours on stream. (a) Spectra recorded in the Co 2p region. (b) Spectra recorded in the O 1s region.

3.3.4 Summary

The addition of potassium to the catalyst system proved successful in improving both the iron and cobalt based catalyst systems with both an increase in HC yield and an improvement in HC selectivity observed for both systems upon its inclusion. Methane selectivity is found to reduce to 24 % upon the introduction of potassium to the iron based system comparing favourably with literature values when combined with the high HC yield this results in a promising catalyst system. Potassium introduction to the cobalt system results in an increase in HC yield, the opposite to what is observed for a CO/H_2 feed and an improved C_2+ selectivity that again compares favourably with literature values although this occurs at a much lower HC yield than reported with previous catalyst systems.[33a, 33c, 33d] XPS studies revealed little to no influence of potassium on the main iron and cobalt phases present in the catalyst system both before and after reaction. An increase in the presence of hydroxyl species on the catalyst surface after reaction was however observed. This increased basicity could play an important role in the changing hydrocarbon distribution.

3.4 Effect of SiO_2 Introduction as a Co-Support

Previous work by Cangnoli *et al.*[2a] has shown that the use of basic supports such as MgO can improve selectivity to light olefins and away from methane during FT synthesis. The use of MgO alone though has been shown to lead to poor iron dispersion.[36] Work by Kishan *et al.*[3] found that for a Fe-K catalyst system supported on MgO the introduction of Al_2O_3 to the catalyst system could improve CO_2 conversion, reduce methane selectivity and increase olefin

content of the products with the best performing CO_2 hydrogenation catalyst containing a mixture of Al_2O_3 and MgO as a catalyst support. In order to determine if similar affects could be achieved for a Fe-Pd-K catalyst system with a mixed support containing SiO_2:MgO a range of catalyst systems were prepared and tested.

3.4.1 Catalyst Preparation

A range of catalyst supports were prepared containing MgO:SiO_2 molar ratios of 1:0, 3:1, 2:1, 1:1, 1:2, 1:3 and 0:1. The mixed oxide supports were prepared using a wet kneading technique of the MgO support with SiO_2 (35-70 µm particle size 60 Å pore size, chromatography grade, Sigma Aldrich), a technique similar to that used by Kvisle *et al*.[37] This method varies from that used by Kishan for MgO:Al_2O_3 studies where the supports were co-precipitated.[3] The catalyst preparation method was kept the same as that used previously within this chapter with the exception that different mixed MgO:SiO_2 materials were used as a catalyst support instead of MgO alone.

3.4.2 Catalyst Characterisation

The resulting catalyst systems were characterised using a range of techniques. Figure 3.20 shows the pXRD patterns obtained for the prepared supports and prepared catalysts. For the pure SiO_2 support no diffraction peaks are observed showing the amorphous nature of the silica support used {Figure 3.20 (left, g)}. Pure MgO, not subjected to the wet kneading procedure shows the presence of peaks typical for MgO {Figure 3.20 (left, a)}. For the mixed oxide systems prepared *via* the wet kneading {Figure 3.20 (left, b-f)} diffraction peaks present at 2θ values of 18, 38, 50 and 59 ^{o} show the presence of $Mg(OH)_2$ with no peaks attributable to MgO.[38] This shows that the rehydration of MgO is occurring under the wet kneading conditions. At higher silica contents (above 50 %) diffraction peaks attributable to any magnesium species are no longer visible. After impregnation with the various metal salts required for catalyst preparation the oxides are calcined. The diffraction patterns obtained for the calcined catalyst systems are shown in Figure 3.20 (right). The emergence of a peak at a 2θ value and 43 ^{o} attributable to MgO[5] is observed. This indicates that the calcination of the catalyst system is sufficient to convert the $Mg(OH)_2$ observed previously back to MgO and as such this is the phase present as a catalyst support during reaction.

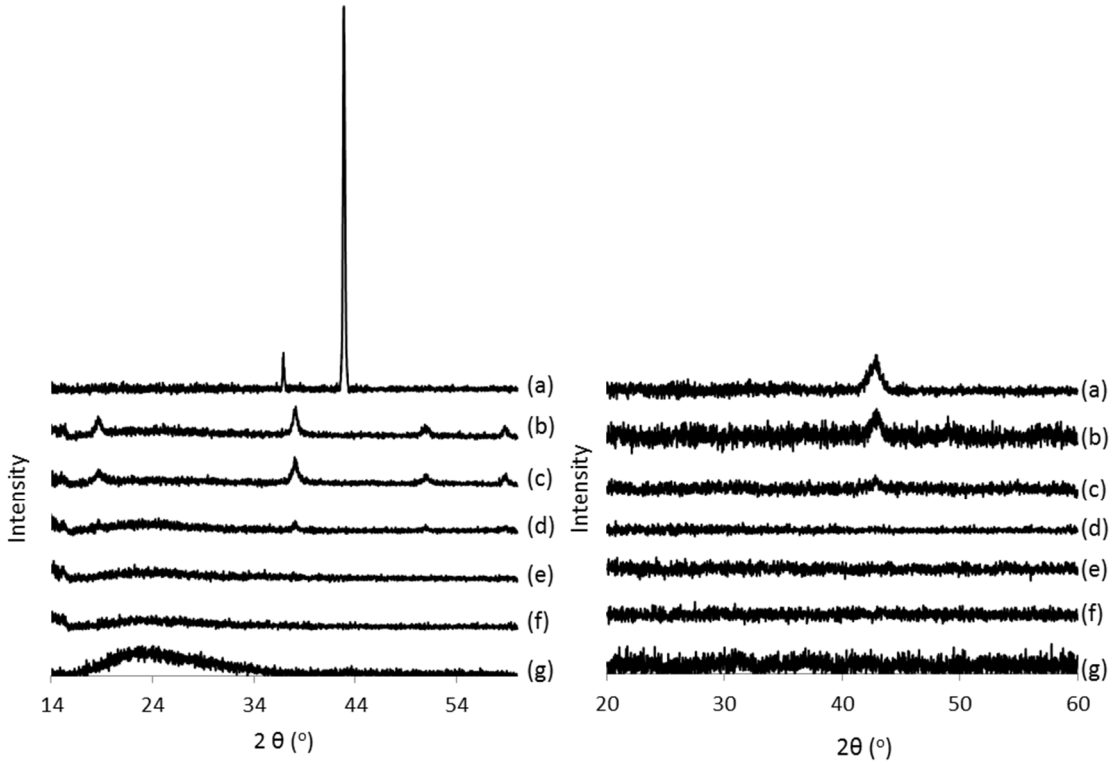

Figure 3.20 – pXRD patterns recorded for mixed MgO:SiO_2 supports (left) and 20wt%Fe/1wt%Pd/1wt%K supported on mixed MgO:SiO_2 supports (right). (a) MgO, (b) 3:1, (c) 2:1, (d) 1:1, (e) 1:2, (f) 1:3 and (g) SiO_2

The MgO peaks observed in the catalyst system decrease in intensity as the MgO content of the mixed oxide support is reduced, above a silica content of 33.3 % the peak present at 43 ^{o} is no longer detected. No further magnesium or silica phases are observed. No peaks corresponding to iron, palladium or potassium oxides are observed for any of the catalyst systems indicating a good distribution of the metals throughout the support.

XPS studies were conducted on both 20wt%Fe/1wt%Pd/1wt%K/MgO and 20wt%Fe/1wt%Pd/1wt%K/SiO_2 systems. The Fe 2p region for both systems is shown in Figure 3.21 (a). The MgO and SiO_2 systems show binding energies of 710.6 eV and 710.7 eV respectively this indicats the presence of Fe_2O_3 as the main iron phase present in both systems[18] with little effect of support evident on the binding energy of iron. When SiO_2 is used as the sole catalyst support the inability to see the Pd 3d band as with MgO supported systems is no longer an issue and as such this region can be studied in more detail. Palladium shows a binding energy of 337.1 eV typical for PdO[17] indicating this is the main palladium species present in the system after calcination {Figure 3.21 (b)}. XPS studies also reveal the presence potassium within the system supported on SiO_2, something not observed with the MgO based system. A binding energy of 293.6 eV indicates that potassium is present as K_2O {Figure 3.21(c)}.

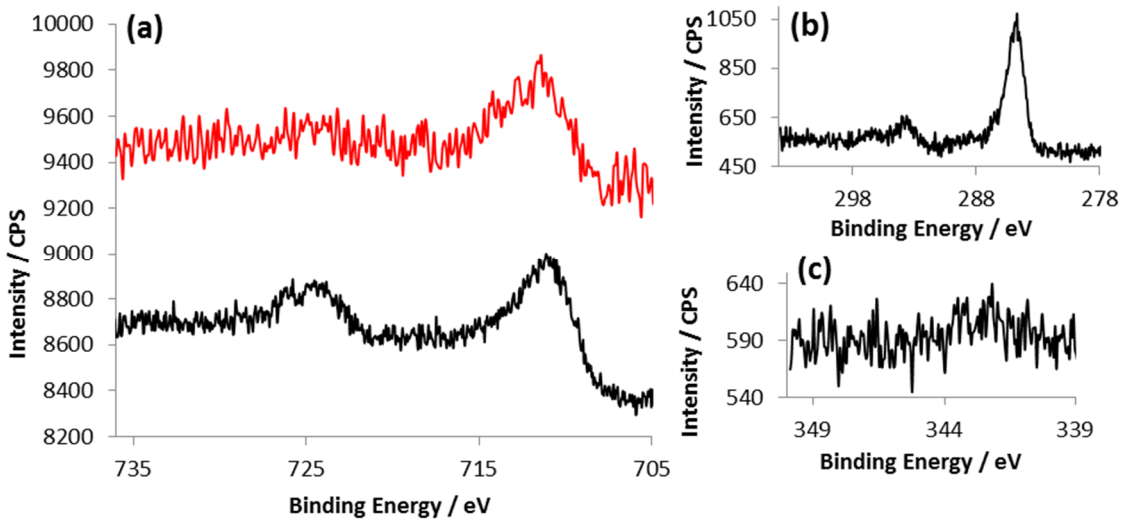

Figure 3.21– XPS spectra recorded for 20wt%Fe/1wt%Pd/1wt%K supported on SiO_2 or MgO. (a) Detailed scan of the Fe 2p region for both SiO_2 (black) and MgO (red) supported systems. (b) Detailed scan of K 1s region for SiO_2 supported system. The peaks present at 284.7 can be attributed to C 1s and the smaller peak at 293.6 eV is due to potassium. (c) Detailed scan of Pd 3d region for SiO_2 supported system.

BET surface areas were determined for each of the catalyst systems to be tested. The resulting surface areas are shown in Table 3.6. The highest surface area recorded is observed for the SiO_2 only supported system and the lowest for the MgO only supported system. Of note is the fact that the surface areas calculated for the catalyst systems are significantly lower than that of the supports alone. This could be due to a number of reasons such as the conglomeration of MgO particles as observed in previous SEM studies and/or the filling of SiO_2 pores upon metal loading. As SiO_2 content is increased in the mixed MgO:SiO_2 support the surface area as calculated by BET methods is seen to increase.

Table 3.6 – BET Surface areas recorded for 20wt%Fe/1wt%Pd/1wt%K supported on various mixed MgO:SiO_2 ratios

Catalyst Support (MgO:SiO_2 ratio)	BET Surface Area (m^2g^{-1})
MgO (1:0)	34.8
MgO:SiO_2(3:1)	42.3
MgO:SiO_2(2:1)	103.6
MgO:SiO_2(1:1)	190.8
MgO:SiO_2(1:2)	179.4
MgO:SiO_2(1:3)	276.9
SiO_2(0:1)	339.1
SiO_2 (support only)	490.0
MgO (support only)	222.1

3.4.3 Catalyst Testing

The prepared catalyst systems were assessed for their catalytic activity using the same catalyst test procedure used to test all catalysts within this chapter. The only exception being the removal of argon from the feed-gas giving a total flow 8 sccm with a 3:1 H_2:CO_2 ratio. The removal of argon allows for the measurement of CO formation (previously not possible due to argon and CO possessing the same retention time during GC analysis). A temperature of 370 ^{o}C was chosen for the catalysts tests as it was felt this value should give a good compromise between high conversion and good product distribution. Table 3.7 summarises the catalytic data obtained from these catalyst tests.

All of the catalyst systems studied were observed to be stable with time on stream. After 1 hour under reaction conditions no further changes in conversion or product selectivity were observed. The data reported in Table 3.7 corresponds to an average over the course of 4 hours after catalysts stabilisation. The catalyst performance both in terms of conversion and product selectivity is influenced by the support composition. As the silica content of the catalyst support is increased an increase in HC yield is observed up to a 50 molar per cent content. Above this point the conversion is seen to decrease again. Methane selectivity is also seen to increase with increasing silica content with up to a silica content of 50 % above this value methane selectivity again beings to decrease. The catalyst supported only on SiO_2 does, however, appear to show a slightly higher methane selectivity than that observed upon the introduction of a small amount of MgO.

The olefin content of the product streams appear to be dependent on the amount of MgO present in the catalyst support. The amount of olefins formed decreases as silica content is increased with only the MgO supported system showing any significant selectivity to alkenes. This change in selectivity is likely due to the relatively high basicity of the MgO support which has been shown to favour the formation of unsaturated hydrocarbons.[2a]

Table 3.7 – Catalytic data obtained for CO_2 hydrogenation using 20wt%Fe/1wt%Pd/1wt%K catalysts supported on mixed oxides consisting of various ratios of magnesia and silica.

$MgO:SiO_2$ ratio	Conversion (%)	HC Yield (%)	CO Yield (%)	Hydrocarbon Distribution									
				C_1	C_2=	C_2	C_3=	C_3	C_4	C_5	C_6	C_7	C_8
1:0	45.0	29.8	15.2	38.5	1.5	22.6	10.5	10.6	9.0	3.9	1.8	1.7	0.0
3:1	40.7	31.0	9.6	43.7	0.0	24.7	1.4	16.7	7.5	3.1	1.7	1.2	0.0
2:1	41.3	32.1	9.3	46.7	0.0	25.4	0.2	16.2	6.5	2.4	1.6	1.0	0.0
1:1	45.7	34.6	11.1	53.4	0.0	23.6	0.5	13.2	4.6	2.1	1.4	1.1	0.0
1:2	43.9	34.2	9.7	43.7	0.0	24.5	0.0	17.1	7.1	3.3	2.1	1.9	0.3
1:3	37.9	27.5	10.4	43.9	0.0	24.2	0.5	16.6	7.6	3.1	2.2	1.8	0.1
0:1	35.8	23.5	12.3	47.9	0.0	24.5	0.0	14.9	6.7	3.0	1.4	1.6	0.0

Catlyst tests conducted at atmospheric pressure, $H_2:CO_2$ ratio 3:1, total flow – 8 sccm. 0.7g of catalyst.

The chain growth probabilities for each catalyst system were calculated from ASF plots with the resulting α values shown in Table 3.8. The catalyst supported solely on MgO shows the highest chain growth probability indicating that the basicity of the support is not only suppressing the formation of methane but also increasing selectivity to longer chained hydrocarbons. There is a drop in α when silica is introduced as a co-support with the silica only supported catalyst showing the lowest chain growth probability.

In summary the introduction of silica as a co-support can result in an increase in HC yield with a maximum value obtained at a MgO: SiO_2 ratio of 1:1. This increase in HC yield does, however, also result in an increased selectivity to methane and a lowering in the amount of olefins formed. The introduction of only small amounts of silica can greatly reduce the selectivity towards alkene formation suggesting a strong influence of the MgO component on their formation.

Table 3.8 – Calculated chain growth probabilities for 20wt%Fe/1wt%Pd/1wt%K supported on mixed MgO:SiO_2 support with varying ratios

Catalyst Support (MgO:SiO_2 ratio)	Chain Growth Probability, α
MgO (1:0)	0.40
MgO:SiO_2(3:1)	0.38
MgO:SiO_2(2:1)	0.36
MgO:SiO_2(1:1)	0.36
MgO:SiO_2(1:2)	0.38
MgO:SiO_2(1:3)	0.36
SiO_2(0:1)	0.34

3.5 Chapter Conclusions

From the studies conducted within this chapter we have seen that the nature of the MgO preparation method can drastically affect the morphology and properties of the resulting MgO. Catalysts containing 20 wt% of the most commonly used FT catalytic metals were trialled for their CO_2 hydrogenation ability. The HC yield obtained from each system was found to increase in the order 20wt%Fe/MgO < 20wt%Co/MgO < 20wt%Ni/MgO. Despite the impressive performance of the nickel system under the catalyst conditions tested it appears to act as a methanation catalyst with only minimal amounts of C_2+ hydrocarbons formed even at high CO_2 conversion.

The addition of 1 wt% palladium to both the iron and cobalt based MgO supported catalysts was shown to have a significant impact on catalyst performance with both an increase in HC yield and an improved hydrocarbon distribution obtained. The catalyst performance can be enhanced further by the addition of 1 wt% potassium in combination with palladium. The inclusion of both promoters simultaneously results in impressive HC distributions for both systems with methane selectivity dropping to 23 % for the iron based system which compares very favourably with the majority of results obtained for CO_2 hydrogenation studies. A methane selectivity of 69 % was recorded for the cobalt based catalyst similar to the lowest CH_4 selectivity reported for cobalt based CO_2 hydrogenation reactions.

Characterisation techniques have shown that the iron and cobalt are mainly present as Fe_2O_3 and Co_3O_4 after catalyst preparation. When studied after use these oxides appear to have been reduced to Fe_3O_4 and CoO. Studies on mixed SiO_2-MgO supports show that while the CO_2 conversion value can be increased upon the introduction of SiO_2 as a co-support with MgO this occurs at the cost of selectivity to both C_2+ HCs and alkenes. The large decrease in olefins observed upon SiO_2 inclusion suggests that the MgO is playing an important role in the higher selectivity observed.

3.6 Future Work

Magnesium oxide shows promise as a support for iron and cobalt based CO_2 hydrogenation catalysts. The addition of silica can increase the CO_2 conversion values obtainable this does, however, occur at the cost of product distribution with higher methane selectivities observed. The preparation of the mixed silica-magnesia supports warrants further investigation. It is possible that an increase in CO_2 conversion may be obtained without loss of product selectivity if the two component oxides are co-precipitated in the manner shown by Kishan *et al*.[3] Alternatively MgO may be prepared by first depositing a pre-cursor on a silica support followed by calcination prior to the addition of any active components. This may impart the basic properties of the MgO on the silica without a significant loss in the high silica surface area.

The addition of other oxides instead of silica may also be investigated. One possibility is a mixed ceria-magnesia support. Ceria shows a great deal of promise as a support for RWGS catalyst and work by Dorner *et al*. has shown that the addition of ceria to an alumina support prior to the addition of the active components can result in an increased CO_2 conversion.[39] Other reducible oxides such as titania are other possible options.

3.7 References

[1] D. G. Rethwisch, J. A. Dumesic, *Appli. Catal.* **1986**, *21*, 97-109.

[2] (a) M. V. Cagnoli, S. G. Marchetti, N. G. Gallegos, A. M. Alvarez, A. A. Yeramian, R. C. Mercader, *Mater. Chem. Phys.* **1991**, *27*, 403-418; (b) N. G. Gallegos, A. M. Alvarez, M. V. Cagnoli, J. F. Bengoa, S. G. Marchetti, R. C. Mercader, A. A. Yeramian, *J. Catal.* **1996**, *161*, 132-142.

[3] G. Kishan, M. W. Lee, S. S. Nam, M. J. Choi, K. W. Lee, *Catal. Lett.* **1998**, *56*, 215-219.

[4] D. Chen, E. H. Jordan, *Mater. Lett.* **2009**, *63*, 783-785.

[5] J. K. Bartley, C. Xu, R. Lloyd, D. I. Enache, D. W. Knight, G. J. Hutchings, *Appli. Catal., B* **2012**, *128*, 31-38.

[6] M. D. Jones, C. G. Keir, C. D. Iulio, R. A. M. Robertson, C. V. Williams, D. C. Apperley, *Catal. Sci. Technol.* **2011**, *1*, 267-272.

[7] G. D. Weatherbee, C. H. Bartholomew, *J. Catal.* **1984**, *87*, 352-362.

[8] M. A. Vannice, *J. Catal.* **1977**, *50*, 228-236.

[9] M. A. Vannice, *J. Catal.* **1975**, *37*, 449-461.

[10] A. Faur Ghenciu, *Curr. Opin. Solid State Mater. Sci.* **2002**, *6*, 389-399.

[11] G. S. Yablonsky, R. Pilasombat, J. P. Breen, R. Burch, S. Hengrasmee, *Chemical Engineering Science* **2010**, *65*, 2325-2332.

[12] R. J. Gorte, S. Zhao, *Catal. Today* **2005**, *104*, 18-24.

[13] (a) M. Luo, R. O'Brien, B. Davis, *Catal. Lett.* **2004**, *98*, 17-22; (b) M. Minnermann, S. Pokhrel, K. Thiel, R. Henkel, J. Birkenstock, T. Laurus, A. Zargham, J. I. Flege, V. Zielasek, E. Piskorska-Hommel, J. Falta, L. Mädler, M. Bäumer, *J. Phys. Chem., C* **2010**, *115*, 1302-1310.

[14] (a) J. Zhang, X. Guo, W. Cao, *J. Nat. Gas Chem.* **2007**, *16*, 377-381; (b) V. Ragaini, R. Carli, C. L. Bianchi, D. Lorenzetti, G. Vergani, *Appli. Catal., A* **1996**, *139*, 17-29.

[15] M. E. Dry, *Applied Catalysis A: General* **1996**, *138*, 319-344.

[16] H. Schulz, *Appli. Catal., A* **1999**, *186*, 3-12.

[17] M. Peuckert, *J. Phys. Chem.* **1985**, *89*, 2481-2486.

[18] L. Peng, E. Y. Jiang, H. L. Bai, *J. Phys. D: Appl. Phys.* **2011**, *44*, 075003.

[19] W. Zhang, H. L. Tay, S. S. Lim, Y. Wang, Z. Zhong, R. Xu, *Applied Catalysis B: Environmental* **2010**, *95*, 93-99.

[20] C. Sun, J. C. Berg, *Adv. Colloid Interface Sci.* **2003**, *105*, 151-175.

[21] M. E. Labib, *Colloids Surf.* **1988**, *29*, 293-304.

[22] P. Shi, R. Su, F. Wan, M. Zhu, D. Li, S. Xu, *Appli. Catal., B* **2012**, *123-124*, 265-272.

[23] (a) J. Yan, T. Wei, W. Qiao, B. Shao, Q. Zhao, L. Zhang, Z. Fan, *Electrochim. Acta* **2010**, *55*, 6973-6978; (b) C. C. Li, X. M. Yin, T. H. Wang, H. C. Zeng, *Chem. Mater.* **2009**, *21*, 4984-4992.

[24] D. J. Pettigrew, D. L. Trimm, N. W. Cant, *Catal. Lett.* **1994**, *28*, 313-319.

[25] A. Y. Khodakov, W. Chu, P. Fongarland, *Chem. Rev.* **2007**, *107*, 1692-1744.

[26] A. Basinska, L. Kepinski, F. Domka, *Appli. Catal., A* **1999**, *183*, 143-153.

[27] (a) P. S. Sai Prasad, J. W. Bae, K. W. Jun, K. W. Lee, *Catal. Surv. Asia* **2008**, *12*, 170-183; (b) R. J. O'Brien, L. Xu, R. L. Spicer, S. Bao, D. R. Milburn, B. H. Davis, *Catal. Today* **1997**, *36*, 325-334.

[28] P. Choi, K. W. Jun, S. J. Lee, M. J. Choi, K. W. Lee, *Catal. Lett.* **1996**, *40*, 115-118.

[29] (a) R. W. Dorner, D. R. Hardy, F. W. Williams, H. D. Willauer, *Appli. Catal., A* **2010**, *373*, 112-121; (b) P. S. Sai Prasad, J. W. Bae, K. W. Jun, K. W. Lee, *Catal. Surv. Asia* **2008**, *12*, 170-183.
[30] J. Hong, J. S. Hwang, K. Jun, J. C. Sur, K. W. Lee, *Appli. Catal., A* **2001**, *218*, 53-59.
[31] L. Wang, H. Liu, Y. Chen, R. Zhang, S. Yang, *Chem. Lett.* **2013**, *42*, 682-683.
[32] (a) E. Blekkan, A. Holmen, S. Vada, *Acta. Chem. Scand.* **1993**, *47*, 275-280; (b) J. K. Jeon, C. J. Kim, Y. K. Park, S. K. Ihm, *Korean J. Chem. Eng.* **2004**, *21*, 365-369.
[33] (a) R. W. Dorner, D. R. Hardy, F. W. Williams, B. H. Davis, H. D. Willauer, *Energy Fuels* **2009**, *23*, 4190-4195; (b) A. N. Akin, M. Ataman, A. E. Aksoylu, Z. I. Önsan, *React. Kinet. Catal. Lett.* **2002**, *76*, 265-270; (c) M. K. Gnanamani, W. D. Shafer, D. E. Sparks, B. H. Davis, *Catal. Commun.* **2011**, *12*, 936-939; (d) C. G. Visconti, L. Lietti, E. Tronconi, P. Forzatti, R. Zennaro, E. Finocchio, *Appli. Catal., A* **2009**, *355*, 61-68; (e) T. Riedel, M. Claeys, H. Schulz, G. Schaub, S. S. Nam, K. W. Jun, M. J. Choi, G. Kishan, K. W. Lee, *Appli. Catal., A* **1999**, *186*, 201-213; (f) Y. Yao, D. Hildebrandt, D. Glasser, X. Liu, *Ind. Eng. Chem. Res.* **2010**, *49*, 11061-11066.
[34] Y. Zhang, G. Jacobs, D. E. Sparks, M. E. Dry, B. H. Davis, *Catal. Today* **2002**, *71*, 411-418.
[35] B. Ernst, S. Libs, P. Chaumette, A. Kiennemann, *Appli. Catal., A* **1999**, *186*, 145-168.
[36] N. G. Gallegos, A. M. Alvarez, M. V. Cagnoli, J. F. Bengoa, S. G. Marchetti, R. C. Mercader, A. A. Yeramian, *J. Catal.* **1996**, *161*, 132-142.
[37] S. Kvisle, A. Aguero, R. P. A. Sneeden, *Appli. Catal.* **1988**, *43*, 117-131.
[38] J. Temuujin, K. Okada, K. J. D. MacKenzie, *J. Solid State Chem.* **1998**, *138*, 169-177.
[39] R. W. Dorner, D. R. Hardy, F. W. Williams, H. D. Willauer, *Catal. Commun.* **2011**, *15*, 88-92.

4 Palladium Promoted Iron Catalysts for Carbon Dioxide Hydrogenation and Life Cycle Analysis of Their Use

The use of palladium in conjunction with iron-silica catalysts for CO_2 hydrogenation was investigated. The three component system was further optimised for the production of heavier hydrocarbons and higher CO_2 conversion by the variation of iron and palladium loading and changing the properties of the silica support. The environmental impacts associated with the preparation of each catalyst was assessed and related to the catalyst performance through the use of life cycle assessment.

While both iron and cobalt are used industrially for the FT process[1] the lack of WGS activity possessed by cobalt[2] means that the majority of CO_2 hydrogenation studies have focused on the use of iron as the main active catalyst component.[3] Despite iron-based catalysts being some of the most effective for the CO_2 hydrogenation process when used alone they do not show sufficient CO_2 conversion values or product distributions and as a result additional chemical and structural promoters are required to improve catalyst performance.

Noble metals are thought to be of vital importance for the future of WGS catalysis[4] and have been shown to be equally capable catalysts for the RWGS reaction.[5] Nobel metals have also been shown to enhance the catalytic performance of a number of FT catalysts.[6] For the following studies the addition of palladium to an iron catalyst system was chosen due to a number of factors. Work by Gorte *et al*.[7] has shown that for the WGS reaction palladium was particularly effective when used in conjunction with iron oxide, outperforming analogous ruthenium and platinum systems. It was hoped that the addition of palladium to an iron catalyst system would aid the initial reduction of CO_2 to CO resulting in CO_2 conversion values and product selectivities closer to those obtained for CO/H_2 feedstocks. In combination with the envisioned improvement of RWGS activity palladium has been shown to effectively promote iron-based catalysts when used under FT conditions (in conjunction with increased WGS activity)[8] which would further improve catalyst performance.

While palladium addition has received limited attention for iron-based FT catalysis, to the author's knowledge it has not been used in conjunction with iron for CO_2 hydrogenation catalysis. When considering the use of catalysts for green processes such as that envisioned for CO_2 hydrogenation it is important to consider the environmental impacts of the materials used for catalyst preparation, a factor often overlooked. The focus of this chapter is to investigate how varying each the iron and palladium loadings affects the catalyst performance while also relating any improvement in catalyst performance to any increase in environmental impact associated with using larger quantities of each material or increased energy usage. This has been

achieved through the use of life cycle assessment techniques in collaboration with Dr. M. McManus' group in the Department of Mechanical Engineering at the University of Bath.

In order to gain a better understanding of what role each component plays each catalyst system was also studied under a CO/H_2 feed so that the effects on FT process could be assessed in more detail.

4.1 Silica Supported Iron-Palladium Catalysts

Although some iron based catalysts are used unsupported this can lead to problems with physical degradation and low surface areas. The introduction of a catalyst support can result in a higher catalyst surface area[9] and improved catalyst stability with a lower deactivation rate.[10] Silica was chosen as a catalyst support as it has proved successful with iron catalyst both for the FT process[11] and CO_2 hydrogenation.[12] It has been shown to give a 40 % increase in activity over a non-supported system with an activity 50 % greater than an equivalent Al_2O_3 supported system.[13] Palladium can easily be observed by XPS, a problem when MgO is used as a structural promoter due to the position of the Mg KLL peak as observed in Chapter 3.

4.1.1 Catalyst Preparation

The iron-palladium-silica catalyst system was prepared using a wet impregnation technique similar to that used by Jones *et al*.[14] The silica support (35-70 nm particle size, 60 Å pore size, Sigma Aldrich) was suspended in the minimal amount of methanol. To this suspension methanol solutions containing the desired amount of $Fe(NO_3)_3 \cdot 9H_2O$ and $Pd(OAc)_2$ were added drop-wise. The resulting mixture was then dried at 65 ^oC under vacuum and the dried powder calcined at 450 ^oC in air for 16 hours. In order to minimise error standard solutions of each metal salt were prepared and the appropriate volume of each added. A starting loading of 20 wt% iron and 1 wt% palladium was chosen.

4.1.2 Catalyst Characterisation

The starting catalyst; 20wt%Fe/1wt%Pd/SiO_2 was characterised using a range of different techniques. N_2 physisorption at 77 K was used to determine the specific BET surface area. A value of 281.1 m^2g^{-1} was calculated using this technique, lower than that reported for the silica support before iron loading (490 m^2g^{-1}). This decrease in surface area observed upon the addition of iron to the catalyst support is observed in similar systems.[10b] XRD showed no diffraction peaks indicating that any metal phases present are well dispersed across the catalyst support or any crystalline phases present are too small to be detected. No peaks attributable to silica were observed confirming the amorphous nature of the support.

SEM was utilised to investigate the catalyst morphology of the 20wt%Fe/1wt%Pd/SiO_2 catalyst system, Figure 4.1 (a) and (b). The particles are of an irregular shape, however, they show a relatively consistent particle size by SEM. EDS was conducted in conjunction with the recording of the SEM images, a typical spectrum obtained is shown in Figure 4.1 (c). The

largest peaks are labelled and show the presence of silicon, iron and palladium. The peak present at approximately 0 keV can be attributed to the presence of oxygen in the system.

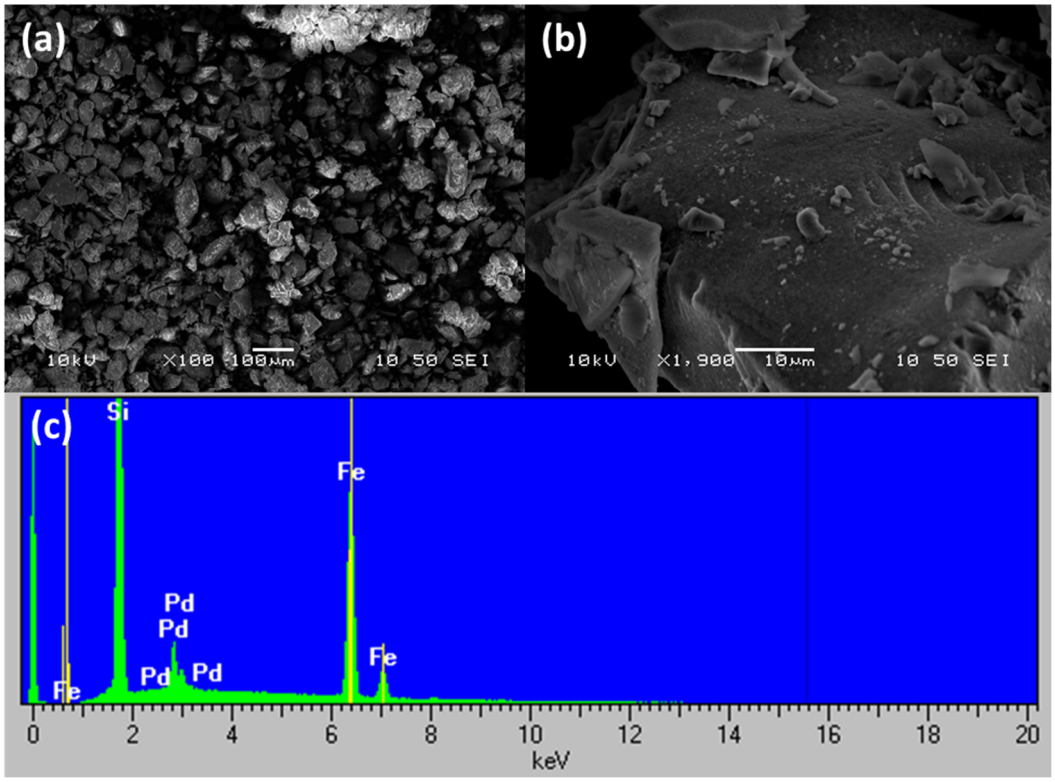

Figure 4.1– (a-b) SEM images recorded for 20wt%Fe/1wt%Pd/SiO_2 at different magnifications. (c) EDX spectrum recorded in conjunction with SEM investigations showing the presence of iron, palladium, silicon and oxygen.

Transmission electron microscopy (TEM) was employed in order to obtain further, more detailed information on the catalyst morphology along with any information about metal particle present on the surface. Figure 4.2 (a) shows a typical TEM image obtained for the 20wt%Fe/1wt%Pd/SiO_2 catalyst system with Figure 1.02 (b) showing the distribution of particle sizes observed indicating a mean nano-particle size of approximately 3.6 nm.

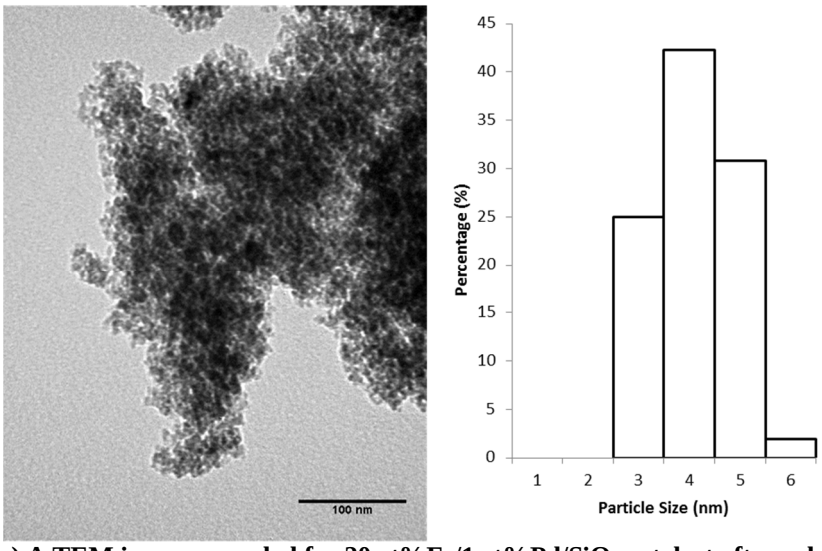

Figure 4.2 – (a) A TEM image recorded for 20wt%Fe/1wt%Pd/SiO_2 catalyst after calcination. (b) A graph showing the apparent nano-particle size distribution as measured by TEM analysis.

XPS studies were conducted on the 20wt%Fe/1wt%Pd/SiO_2 system in order to determine the metal species present after the calcination of the catalyst. A survey scan {Figure 4.3 (a)} indicates the presence of silicon (103 eV[15]), oxygen (533 eV[15]) and iron (711 eV[16]) as expected. A peak attributable to palladium is also detected. A detailed scan in the 705 eV to 735 eV, Fe 2p range {Figure 4.3 (b)} shows a peak at 710.9 eV with a satellite peak at *ca.* 719 eV typical for Fe^{3+} indicating the presence of iron in the Fe_2O_3 form[16] as seen previously with the 20wt%Fe/1wt%Pd/MgO catalyst (Chapter 3, Figure 3.11). A detailed scan in the 330 eV to 350 eV, Pd 3d range shows a peak at 337.0 eV indicating the presence of palladium in its PdO oxide form,[17] Figure 4.1 (c).

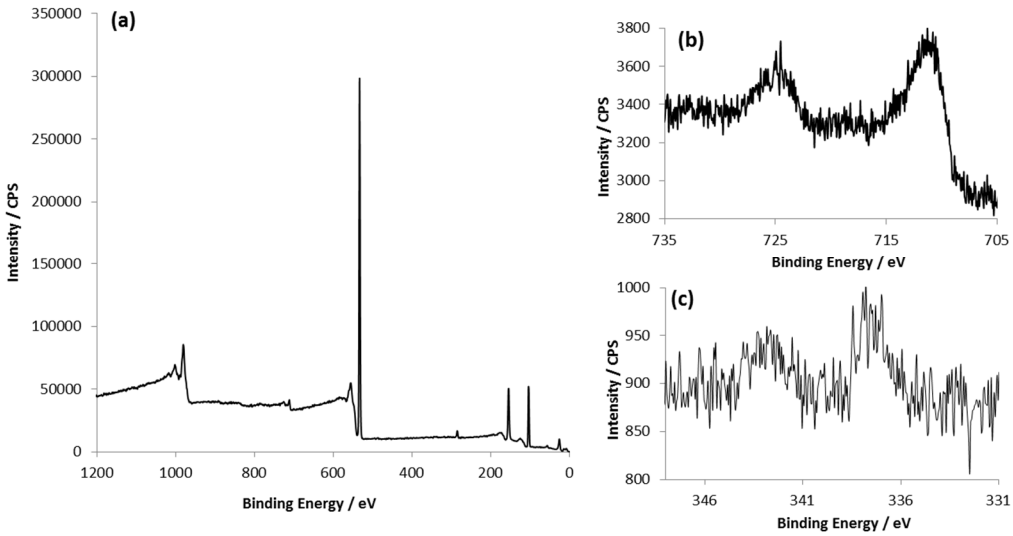

Figure 4.3 – XPS spectra recorded for 20wt%Fe/1wt%Pd/SiO_2. (a) Survey spectrum. (b) Fe 2p region. (c) Pd 3d region.

4.1.3 Catalyst Testing

The 20wt%Fe/1wt%Pd/SiO_2 catalyst system was tested for the hydrogenation of carbon dioxide in Reactor 1 (See Chapter 2, Section 2.2 for full details). 0.7 g of catalyst was packed into a sample cell, 130 mm in length, 4.6 mm internal diameter with the catalyst held in place with quartz wool. All catalysts were tested using the catalyst testing procedure outlined for Reactor 1 in Chapter 2, Section 2.3.

The 20wt%Fe/1wt%Pd/SiO_2 catalyst was trialled over a range of five temperatures from 250 ^oC to 410 ^oC at 30 ^oC intervals. Figure 4.4 (Top) shows a plot of CO_2 conversion, HC yield and CO yield against temperature. CO_2 conversion is observed to increase steadily with increasing temperature from approximately 20 % at 250 ^oC to *ca.* 40 % at 410 ^oC. CO yield is observed to stay relatively constant across the temperature range. In contrast HC yield is low at reduced temperatures with very little HCs formed between 250 and 290 ^oC with the majority of CO_2 converted to CO. Above 290 ^oC HC formation increases steadily with rising temperature. CO remains the main product.

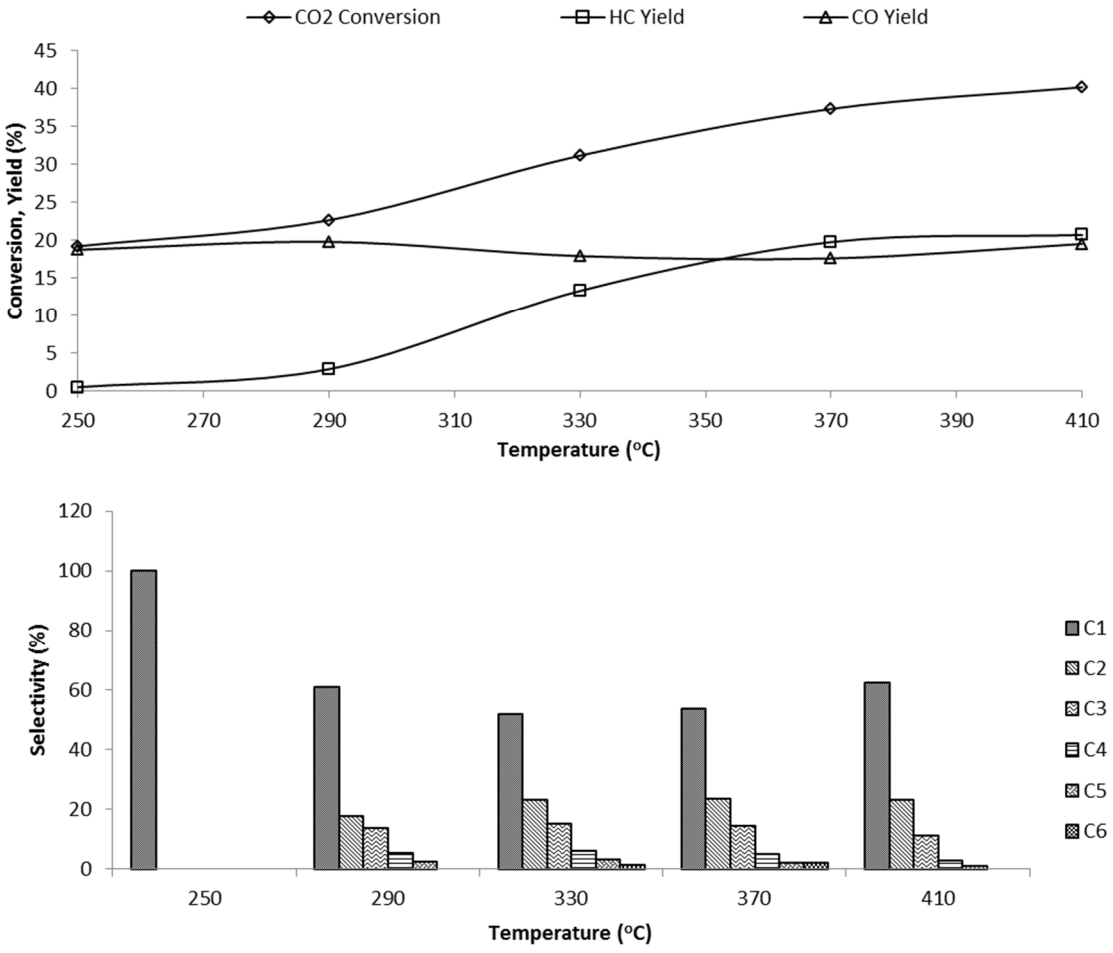

Figure 4.4 - (Top) a plot showing how conversion varies with increasing temperature over the 20wt%Fe/1wt%Pd/SiO_2 catalyst system. (Bottom) The variation in hydrocarbon distribution with varied temperature. Reaction conditions; H_2:CO_2 ratio- 3:1, Total flow – 8 sccm, Pressure – atmospheric.

The hydrocarbon distribution observed for the 20wt%Fe/1wt%Pd/SiO_2 across a range of temperatures is shown in Figure 4.4 (bottom). At the low HC yield observed at 250 ^oC methane accounts for 100 % of the hydrocarbon products. With increasing temperature selectivity to C_2+ hydrocarbons is seen to increase until a temperature of 330 ^oC is reached, above this point methane selectivity again begins to rise. In order to gain a better understanding of how temperature effects the HC distribution the chain growth probability for each catalyst was calculated from the Anderson Schulz Flory plot (Figure 4.5). The chain growth probability, α, values mirrors the selectivity observed in Figure 4.4 (bottom) with a temperature of 330 ^oC giving the best selectivity to heavier HCs and highest chain growth probability. Although the catalyst test performed at 370 ^oC shows a slightly lower α value relative to 330 ^oC it exhibits a 20 % increase in CO_2 conversion with no increase in CO yield. As such a temperature of 370^oC was chosen for catalyst optimisation investigations.

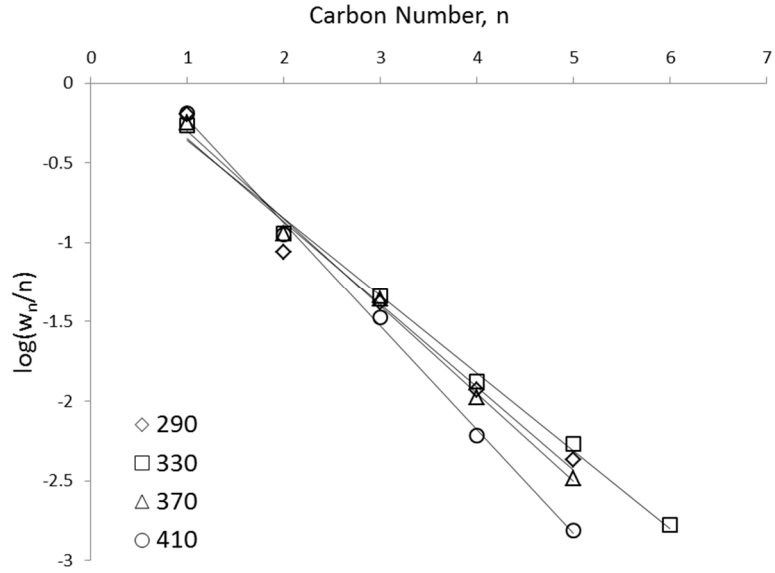

Reaction Temperature (°C)	Chain Growth Probability, α
250	0.00
290	0.30
330	0.33
370	0.28
410	0.22

Figure 4.5 – An Anderson Schulz-Flory plot for 20wt%Fe/1wt%Pd/SiO_2 at each temperature with the calculated chain growth probabilities, α, show in the table.

4.1.4 Summary

Temperature has been shown to have a large effect on the performance of a 20wt%Fe/1wt%Pd/SiO_2 catalyst when tested for CO_2 hydrogenation. Higher temperatures were found to give the highest conversions, however, above temperatures of 370 ^oC little improvement was observed suggesting this may be at the limit of the catalysts ability. The increase in CO_2 conversion does come at the cost of chain growth probability. This trade-off is due to the two stages, RWGS and FT preferring different temperatures. As such a compromise must be made in order to obtain a good conversion with a good selectivity towards heavier HCs.

4.2 Catalyst Optimisation: Variation of Iron Loading

The effect of iron loading on the Fe-Pd-SiO_2 catalyst system was investigated. The same silica used for previous catalyst tests (35-70 nm particle size, 60 Å pore size, Sigma Aldrich) was employed and the loading of palladium was kept constant at 1 wt% with only mass of iron used in preparation altered.

4.2.1 Catalyst Preparation

Seven catalyst systems were prepared using the wet impregnation method detailed in Chapter 2 Section 2.7.8. Iron loading was varied from 0 wt% Fe (1wt%Pd/SiO_2) through to 60 wt% Fe (60wt%Fe/1wt%Pd/SiO_2) at 10 wt% intervals.

4.2.2 Catalyst Characterisation

The prepared catalyst systems were characterised using a range of techniques. N_2 physisorption studies conducted at 77 K allowed the calculation of specific BET surface areas. The calculated values are shown in Table 4.1. The introduction of 1wt% palladium and 10 wt% iron to system results in a drop in surface area to 378.8 m^2g^{-1}. The specific surface area then drops further as iron loading is increased most likely due to the filling of the SiO_2 pores with high iron loadings and/or the conglomeration of support particles. The same effect has been observed previously for similar catalyst systems.[10b]

Table 4.1 – BET surface areas calculated for Fe-Pd-SiO_2 catalysts with various iron loadings

Catalyst	BET Surface Area (m^2g^{-1})
Unused SiO_2 support	490.0
10wt%Fe/1wt%Pd/SiO_2	378.8
20wt%Fe/1wt%Pd/SiO_2	281.1
30wt%Fe/1wt%Pd/SiO_2	269.5
40wt%Fe/1wt%Pd/SiO_2	249.1
50wt%Fe/1wt%Pd/SiO_2	215.8
60wt%Fe/1wt%Pd/SiO_2	153.0

The morphology of each catalyst system was investigated using field emission scanning electron microscopy (FE-SEM). Images typical for 20wt%Fe/1wt%Pd/SiO_2 and 40wt%Fe/1wt%Pd/SiO_2 are shown in Figure 4.6. Both (a) and (b) appear to show a good distribution of iron across the surface of the support even at higher loadings. An increase in apparent surface irregularity/roughness is observed as iron loading is increased presumably due to larger quantities of iron coating the surface of the silica support. Higher magnifications (c and

d) show a distinct difference in surface morphology for the two catalyst systems. With a higher iron loading (40 wt%) the formation of small sheets/platelets is observed whereas with a lower loading (20 wt%) no further surface morphology is observed with a higher magnification. EDS measurements were conducted in conjunction with SEM studies. Spectra typical for each catalyst system are shown in Figure 4.6 (e and f). Both spectra show the presence of iron, oxygen, silicon and palladium with higher iron loadings resulting in significantly larger peaks for iron. Peaks attributable to palladium are less intense with higher iron loadings suggesting that higher loadings are attenuating palladium signals. Mapping techniques showed both iron and palladium are well distributed across the catalyst surface.

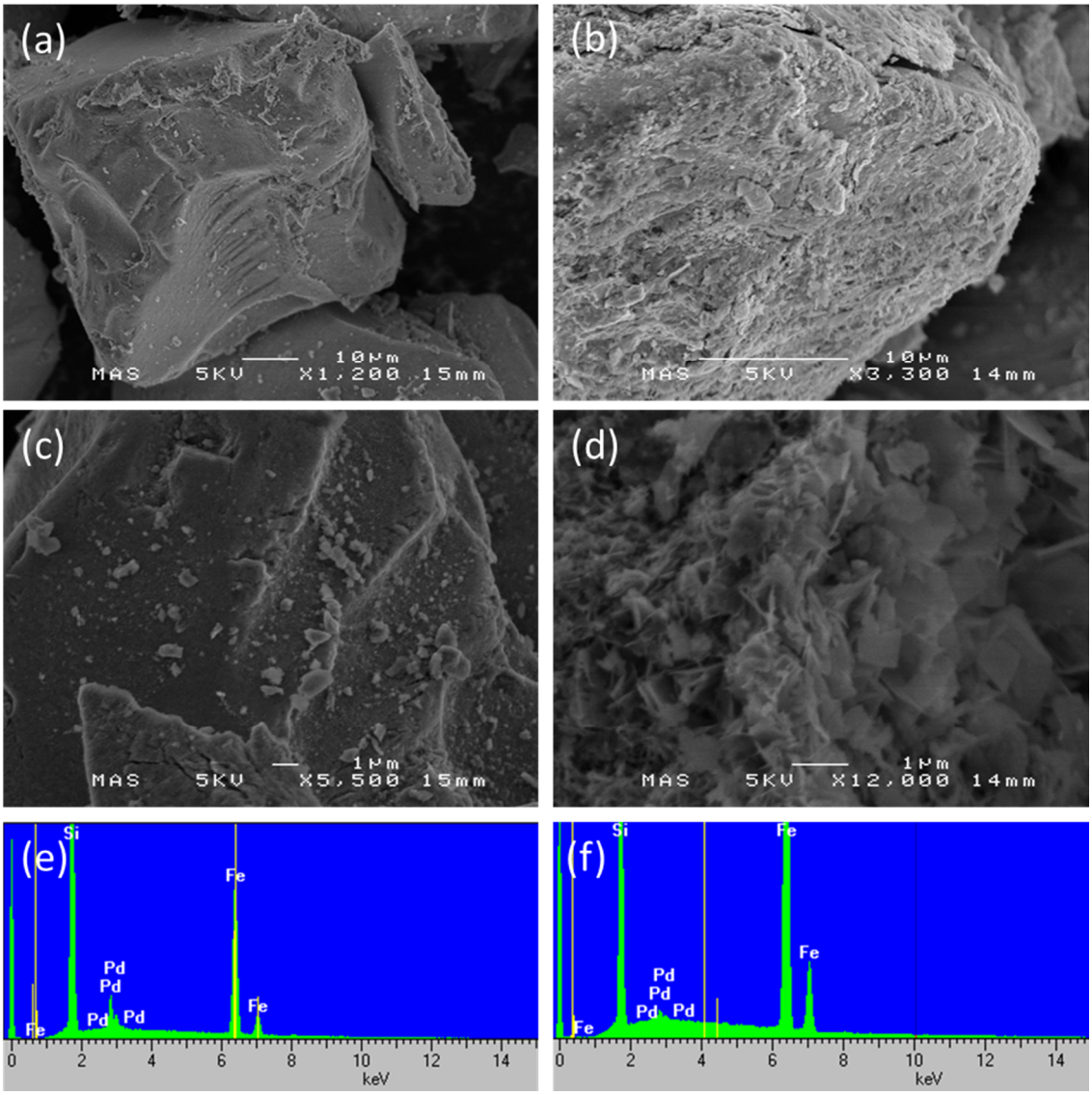

Figure 4.6 – (a) FE-SEM image typical for 20wt%Fe/1wt%Pd/SiO_2, a greater magnification shown in (c). (b) FE-SEM image typical for 40wt%Fe/1wt%Pd/SiO_2 with a higher magnification shown in (d). EDX studies conducted in conjunction with FE-SEM are shown for 20wt%Fe/1wt%Pd/SiO_2 (e) and 40wt%Fe/1wt%Pd/SiO_2 (f).

TEM studies were conducted on the prepared catalysts to further investigate the catalyst morphology. Figure 4.7 shows TEM images recorded for 1wt%Pd/SiO_2, 20wt%Fe/1wt%Pd/SiO_2 and 40wt%Fe/1wt%Pd/SiO_2 catalyst systems. Metal nano-particles are observed in the 10-25 nm size range for the 1wt%Pd/SiO_2 catalyst system {Figure 4.7 (a)}, larger than that observed when iron is added to the system as observed for the 20wt%Fe/1wt%Pd/SiO_2 system {Figure 4.7 (b)}. An increase in the iron content of the catalyst system results in the formation of larger particles in the size range of 10-15 nm. While the nano-particles observed for 1wt%Pd/SiO_2 and 20wt%Fe/1wt%Pd/SiO_2 appear well dispersed those detected for catalysts containing higher iron loadings appear in clusters/groups suggesting that with larger iron content dispersion is slightly reduced within the support.

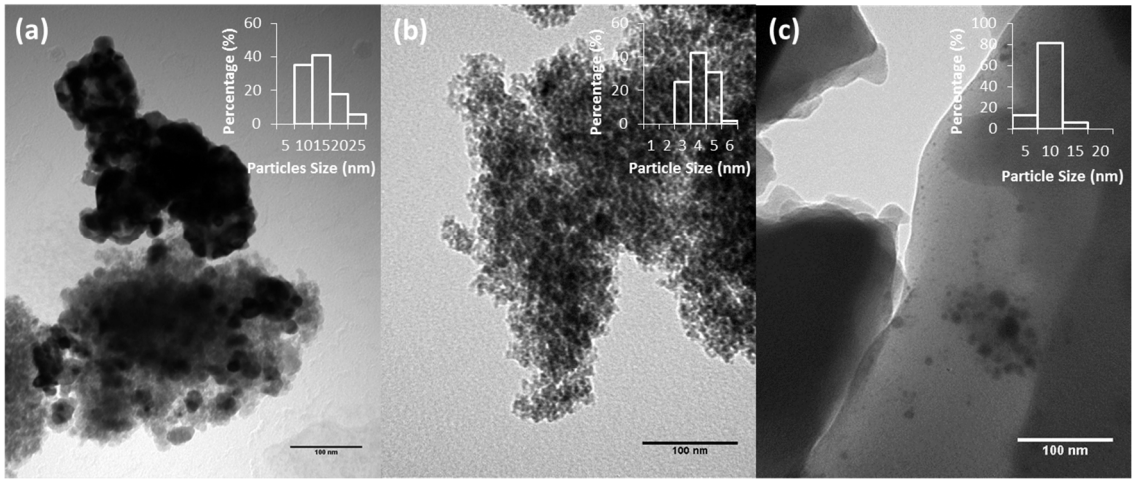

Figure 4.7 – TEM images typical for (a) 1wt%Pd/SiO_2, (b) 20wt%Fe/1wt%Pd/SiO_2 and (c) 40wt%Fe/1wt%Pd/SiO_2. Inserts - histograms showing the nano-particle size distribution as measured by TEM for each system.

4.2.3 Catalyst Testing

The prepared catalyst systems were tested for their CO_2 hydrogenation ability in Reactor 1 (see Chapter 2, Section 2.2 for full details). Each catalyst was first reduced at 300 ^oC for 2 hours under a stream of pure hydrogen. After completion of the pre-treatment the reactor was heated to 370 ^oC under an argon atmosphere. Once at temperature CO_2 and H_2 were introduced at 2 sccm and 6 sccm respectively. Gas samples were collected ever hour and analysed using gas chromatography.

After an initial decrease in CO_2 conversion and CO yield for the first 2 hours on stream all catalyst systems tested stabilised showing relatively consistent values for CO_2 conversion, HC yield and CO yield for the remaining time on stream. CO_2 conversion, HC yield and CO yield were calculated as an average of four hours on stream once the catalyst system had stabilised. Table 1.02 summarises the catalyst test results of the seven studied catalyst systems.

Table 4.2 – Catalytic data obtained for CO_2 hydrogenation tests using Fe-1wt%Pd/SiO_2 catalysts systems containing various iron loadings

Catalyst	Conversion (%)	HC Yield (%)	CO Yield (%)	Hydrocarbon Distribution									
				C_1	C_2=	C_2	C_3=	C_3	C_4	C_5	C_6	C_7	C_8
1wt%Pd/SiO_2	22.1	2.4	19.7	95.9	0.0	4.1	0.0	0.0	0.0	0.0	0.0	0.0	0.0
10wt%Fe/1wt%Pd/SiO_2	32.2	12.1	20.1	61.6	0.0	23.2	2.6	8.9	3.0	0.8	0.0	0.0	0.0
20wt%Fe/1wt%Pd/SiO_2	37.4	14.4	23.1	57.4	0.1	23.5	0.8	12.1	4.0	1.9	0.3	0.0	0.0
30wt%Fe/1wt%Pd/SiO_2	40.1	23.1	17.0	52.7	0.1	23.5	1.3	14.6	5.5	2.3	0.0	0.0	0.0
40wt%Fe/1wt%Pd/SiO_2	45.8	33.2	12.6	46.9	0.0	22.1	3.8	13.4	8.0	3.5	1.6	0.3	0.5
50wt%Fe/1wt%Pd/SiO_2	38.0	27.0	11.0	55.9	0.0	21.0	0.0	12.4	3.9	2.1	2.3	2.4	0.0
60wt%Fe/1wt%Pd/SiO_2	26.4	15.8	10.6	57.1	0.0	22.0	0.1	13.4	4.4	1.5	0.6	1.1	0.0

Catlyst tests conducted at atmospheric pressure, H_2:CO_2 ratio 3:1, total flow – 8 sccm. 0.7g of catalyst. Conversions, yields and product distributions calculated as an average of 4 hours on stream after catalyst stabilisation.

The 1wt%Pd/SiO_2 catalyst system shows a moderate CO_2 conversion, the majority of CO_2 is however converted to CO, this indicates that under the reaction conditions studied the palladium present within the system is active for the RWGS reaction whereas its FT ability is limited with a low HC yield with selectivity almost exclusively to methane. The introduction of 10 wt% iron to the system significantly improves catalyst performance with both a boost in CO_2 conversion and HC yield.

As iron loading is increased CO_2 conversion values and HC yields are seen to increase with the CO yield observed to decrease after iron loading is increased beyond 20 wt%. The optimal iron loading was found to be 40 wt%. Above this value and CO_2 conversion and HC yield was found to decrease.

Product selectivity improves drastically towards C_2+ hydrocarbons upon the introduction of 10 wt% iron to the 1wt%Pd/SiO_2 catalyst system. Methane selectivity decreases as iron content is increased. The optimum iron loading in terms of selectivity towards heavier hydrocarbons is observed with an iron loading of 40 wt% mirroring what is seen with CO_2 conversion. Above this optimal loading methane selectivity increases with a reduction in C_2+ HCs. Of the HC products formed a high selectivity to paraffins is observed with little to no olefin selectivity observed for the majority of catalysts. This is likely due to the hydrogenating ability of the palladium within the system which could be hydrogenating any olefins formed. In order to gain a deeper understanding of how the distribution of the HC products is effected by iron loading, the chain growth probability of each system was calculated using an Anderson Schulz-Flory plot as shown in Figure 4.8.

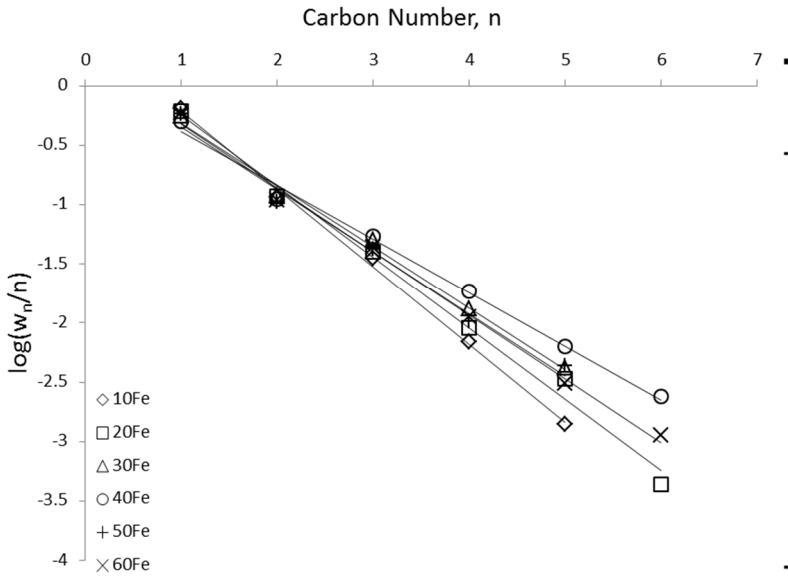

Catalyst's Iron Loading (wt%)	Chain Growth Probability, α
10	0.22
20	0.25
30	0.30
40	0.35
50	0.41
60	0.34

Figure 4.8 – An Anderson-Schulz-Flory plot for each catalyst with different iron loadings, calculated α values are tabulated.

Although it is possible to calculate an α value for 1wt%Pd/SiO_2 (0.02) it is not certain as to whether the ASF distribution applies to this catalyst as only two products are formed and

as such it is not possible to ascertain if HC production is occurring *via* FT synthesis. It is possible that the formation of each could be *via* a process other than FT such as direct hydrogenation. For each of the iron containing catalyst systems a linear relationship is observed for a plot of carbon number *vs.* $\log(w_n/n)$ proving that HC formation is occurring *via* the FT process[18] thus suggesting CO_2 hydrogenation to HCs through a CO not a MeOH mediated mechanism. The calculated chain growth probability increases with increasing iron loading until an iron loading of 50 wt%. Above this loading the introduction of further iron to the system no longer improves α with a slight decrease observed.

In order to determine the influence of iron loading on the FT process alone each of the catalyst systems was tested using a CO/H_2 (syngas) feed. For these catalyst tests Reactor 2 (see Chapter 2 Section 2.2 for full details) was utilised. A similar general procedure for catalyst testing was employed (see Chapter 2 Section 2.3 for full details) only with a higher total flow (40 sccm Vs. 8 sccm) due to the limitations of the mass flow controllers used on this reactor. This higher flow is also a benefit as a higher flow results in a lower residence time and as such conversion is limited so that all products formed are gaseous and easier to quantify and study.

The reaction temperature was kept constant at 370 ^oC with a H_2:CO ratio of 3:1. The results from the syngas fed FT reactions are summarised in Table 4.3. In contrast to the results obtained for the CO_2/H_2 fed reactions all catalysts show a much lower stability with no consistent period of catalyst activity observed during the time on stream. As a result of the unstable nature of each catalyst system CO conversion, HC yield and CO_2 yield after 1 hour on stream are used for comparison of catalyst performance.

Table 4.3 – Catalytic data obtained for CO hydrogenation tests using Fe-1wt%Pd/SiO_2 catalyst systems containing various iron loadings

Catalyst	CO Conversion (%)	HC Yield (%)	CO_2 Yield (%)	Hydrocarbon Distribution									
				C_1	C_2=	C_2	C_3=	C_3	C_4	C_5	C_6	C_7	C_8
1wt%Pd/SiO_2	10.0	5.4	4.6	89.7	0.0	3.7	0.0	6.6	0.0	0.0	0.0	0.0	0.0
10wt%Fe/1wt%Pd/SiO_2	83.2	52.7	30.5	47.6	0.0	21.7	2.1	15.7	8.2	3.1	1.7	0.0	0.0
20wt%Fe/1wt%Pd/SiO_2	85.7	55.9	29.8	46.0	0.0	23.3	0.7	16.6	7.1	3.6	1.9	0.9	0.0
30wt%Fe/1wt%Pd/SiO_2	86.0	56.0	30.3	43.3	0.0	22.4	0.3	17.2	9.6	4.2	2.1	1.0	0.0
40wt%Fe/1wt%Pd/SiO_2	90.1	57.8	32.3	38.4	0.0	20.3	0.0	19.2	11.3	6.0	3.5	1.4	0.0

Catlyst tests conducted at atmospheric pressure, H_2:CO ratio 3:1, total flow – 40 sccm. 0.7g of catalyst. Conversions, yields and product distributions calculated after 1 hour on stream.

A distinct difference is observed between the catalyst containing only 1wt% Pd and that also containing iron. The palladium only system shows a low CO conversion and the hydrocarbon products formed consist mainly of methane. This indicates that at this loading and under these conditions palladium is relatively ineffective as a FT catalyst. The introduction of 10 wt% iron shifts the HC distribution drastically towards a more typical FT distribution while also significantly increasing CO conversion. As the iron loading is increased a steady increase in both CO conversion and HC yield is observed mirroring the results obtained for the CO_2 fed catalyst tests (Table 4.2). A high quantity of CO_2 is observed in the product stream for all catalysts test implying that they all possess a high activity for the WGS reaction. While RWGS activity is desired for CO_2 hydrogenation these results obtained under the same reaction conditions using a CO feed indicate that some of the CO formed through the RWGS reaction can be converted back to CO_2 through the WGS reaction although the CO concentration present in the CO_2 hydrogenation process is unlikely to reach as high levels as is present within this study. Higher temperatures could be utilised to limit this CO_2 formation this would however interfere with the HC selectivity directing product distribution towards methane.

An Anderson Schulz-Flory plot for each catalyst is shown in Figure 1.09 along with the calculated α value for each system. All catalysts were found to follow the ASF distribution as expected for HCs formed *via* the FT process. A steady increase in chain growth probability is observed with increasing iron loading. This mirrors what is observed for the CO_2 fed reaction over the same catalyst systems. This indicates that while the increased iron content may affect the formation of CO it also plays an important role in improving the FT performance of the catalyst system, directing selectivity away from methane and towards heavier hydrocarbons.

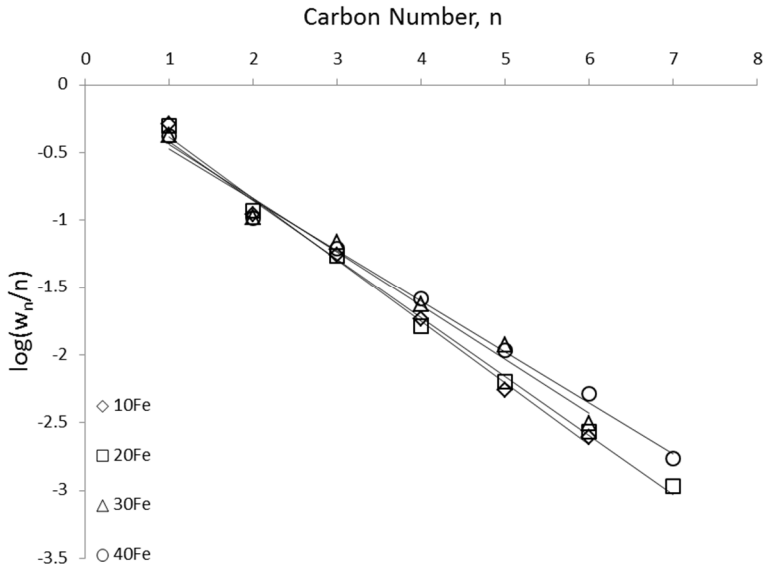

Catalyst's Iron Loading (wt%)	Chain Growth Probability, α
10	0.35
20	0.37
30	0.40
40	0.42

Figure 4.9 – An Anderson Schulz-Flory plot for each catalyst with different iron loadings, calculated α values are tabulated.

4.2.4 Summary

In summary the introduction of larger quantities of iron leads to a reduction in surface area of the catalysts with distinct changes in catalyst morphology for systems containing higher loadings. A catalyst containing only palladium supported on silica with no iron present showed a moderate CO_2 conversion but product selectivity was almost exclusively to CO indicating that the palladium component is active for the RWGS reaction under these conditions. Its FT activity is limited with a low HC yield and the HCs produced were almost exclusively methane. The introduction of 10 wt% iron to the system results in a large shift in product selectivity away from CO towards hydrocarbons with a large reduction in the amount of methane formed and significantly more C_2+ HCs detected. This confirms that the iron component is the main active metal for the FT process. As iron loading is increased CO_2 conversion was found to increase suggesting a role in the initial reduction of CO_2 to CO. Selectivity towards heavier C_2+ HCs is also increased suggesting that increasing iron loading improved the FT performance of the catalyst system, this is further confirmed by CO/H_2 fed catalyst tests. An iron loading of 40 wt% was found to be optimum both in terms of CO_2 conversion and selectivity to heavier HCs

4.3 Catalyst Optimisation: Variation of Palladium Loading

The effect of palladium loading on the Fe-Pd-SiO_2 catalyst system was investigated. The same silica used for previous catalyst tests (35-70 nm particle size, 60 Å pore size, Sigma Aldrich) was employed and the loading of iron was kept constant at 20 wt% with only the amount of palladium varied between catalyst preparations. Palladium loading was varied from 0 wt% Pd (20wt%Fe/SiO_2) through to 4 wt% Fe (20wt%Fe/4wt%Pd/SiO_2).

4.3.1 Catalyst Preparation

Generally the same catalyst preparation procedure was kept as had been used in the previous section (detailed in Chapter 2, Section 2.7.8) however due to solubility issues with the palladium acetate precursor larger volumes of methanol were utilised in the preparation of catalysts containing larger loadings of palladium.

4.3.2 Catalyst Characterisation

N_2 physisorption studies conducted at 77 K allowed the calculation the specific BET surface area, the values obtained from these experiments are summarised in Table 4.4. A decrease in surface area is observed upon the introduction of palladium to the system. When palladium content is increased a slow increase in catalyst surface area is observed.

Table 4.4 – BET Surface areas calculated for the Fe-Pd-SiO_2 catalyst systems with varying palladium loadings

Catalyst	BET Surface Area (m^2g^{-1})
20wt%Fe/SiO_2	368.9
20wt%Fe/1wt%Pd/SiO_2	281.1
20wt%Fe/2wt%Pd/SiO_2	311.3
20wt%Fe/3wt%Pd/SiO_2	325.2
20wt%Fe/4wt%Pd/SiO_2	330.7

The morphology of each catalyst system was investigated using SEM. Images typical of those recorded for 20wt%Fe/SiO_2, 20wt%Fe/1wt%Pd/SiO_2, and 20wt%Fe/4wt%Pd/SiO_2 are shown in Figure 4.10 (top a, b and c). Little difference is observed between catalyst samples suggesting that low loadings of palladium have little effect on morphology at the scale observed *via* SEM.

EDS spectra were recorded in conjunction with SEM studies, Figure 4.10 (bottom a, b and c). The resulting spectra show the presence of oxygen, silicon and iron for all systems. Peaks attributable to the presence of palladium are also observed confirming successful loading/impregnation of metals on to the silica support with a good distribution.

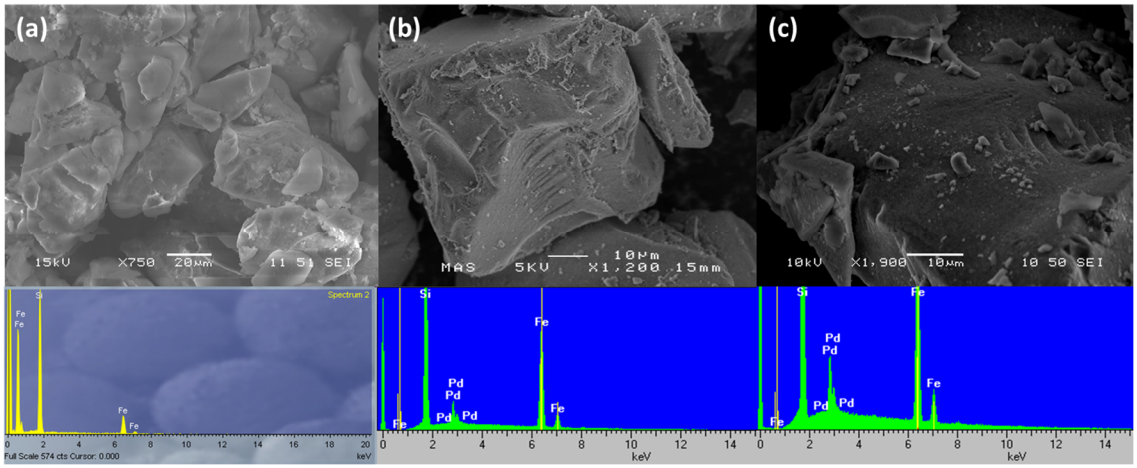

Figure 4.10– (a) SEM image typical for 20wt%Fe/SiO_2 with EDS spectrum. (b) SEM image typical for 20wt%Fe/1wt%Pd/SiO_2 with EDS spectrum. (c) SEM image typical for 20wt%Fe/4wt%Pd/SiO_2 with EDS spectrum.

Further studies on catalyst morphology were conducted utilising TEM. Figure 4.11 shows typical TEM images recorded for 20wt%Fe/SiO_2, 20wt%Fe/1wt%Pd/SiO_2 and 20wt%Fe/4wt%Pd/SiO_2 along with the distribution of nanoparticles observed for each system. A slight decrease in particle size distribution is observed when 1 wt% palladium is introduced to

the system, however, when palladium loading is increased to 4 wt% particle size distribution slightly increases.

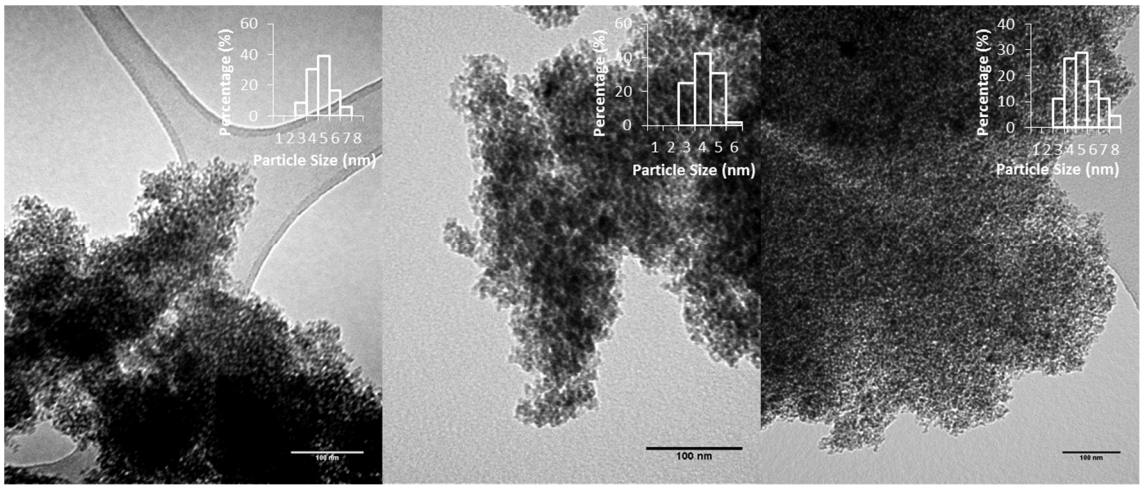

Figure 4.11 – TEM images typical for (a) 20wt%Fe/SiO_2, (b) 20wt%Fe/1wt%Pd/SiO_2 and (c) 20wt%Fe/4wt%Pd/SiO_2. Inserts: histograms showing the nano-particle size distributions.

4.3.3 Catalyst Testing

The prepared catalyst systems were tested for their CO_2 hydrogenation ability in Reactor 1 (see Chapter 2, Section 2.2 for full details). Each catalyst was first reduced at 300 ^oC for 2 hours under a stream of pure hydrogen. After completion of the pre-treatment the reactor was heated to 370 ^oC under an argon atmosphere. Once at temperature CO_2 and H_2 were introduced at 2 sccm and 6 sccm respectively. Gas samples were collected every hour and analysed using gas chromatography.

After 2 hours on stream each of the catalyst systems studied showed stable values for CO_2 conversion, HC and CO yield for the remainder of their time on stream. CO_2 conversion, HC Yield and CO yield were calculated as an average of four hours on stream once the catalyst system had stabilised. Table 4.5 summarises the catalyst test results of the 5 studied catalyst systems.

The 20wt%Fe/SiO_2 catalyst system showed activity for CO_2 hydrogenation under the reaction conditions studied proving that the iron component of the system is active for both the RWGS and FT processes. The introduction of a small loading of palladium to the system (1 wt%) significantly improves both CO_2 conversion values and HC yield. A steady increase in HC yield is observed with increasing palladium content of the catalyst systems. CO_2 conversion appears to level out somewhat at palladium loadings of 2 wt% and above while CO yield reaches its highest values between 1 and 2 wt% palladium content before beginning to decrease with high loadings. Previous work by Lou *et al.*[8a] has shown that the introduction of palladium to an iron FT catalyst system significantly enhances FT synthesis activity as well as boosting WGS activity these phenomenon could explain the increased HC yield observed as palladium loading is increased.

The 20wt%Fe/SiO_2 catalyst shows a high selectivity to methane with HCs of up to C_3 chain length formed. Upon the introduction of palladium to the system a significant improvement in hydrocarbon distribution is observed consistent with what is observed for the addition of palladium to iron systems under FT conditions.[8a] In contrast to what is observed with the variation of iron loading when palladium content is increased little change in HC selectivity is shown. An Anderson Schulz-Flory plot along with calculated α values for each catalyst are shown in Figure 4.12. The calculated α values show little variance with increasing palladium loading suggesting that the palladium content has a more significant influence on the RWGS reaction rather than the chain growth of HCs occurring through the FT process.

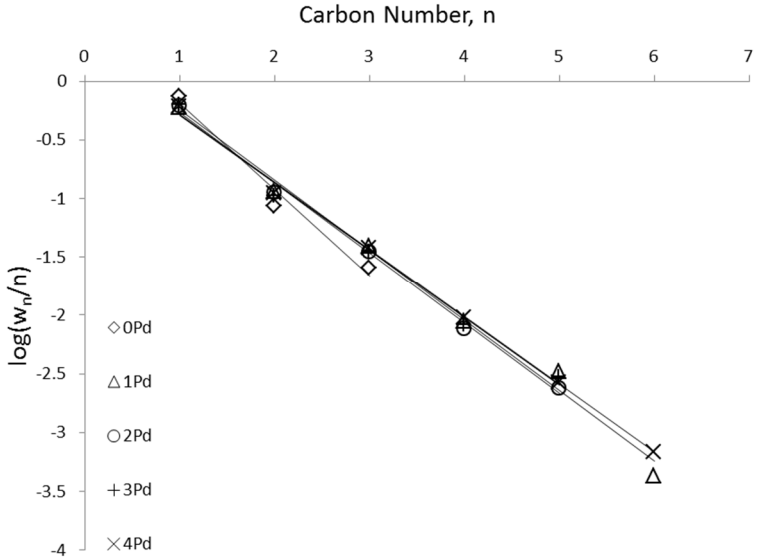

Palladium Content of Catalyst (wt%)	Chain Growth Probability, α
0	0.18
1	0.26
2	0.25
3	0.27
4	0.26

Figure 4.12 – A Anderson Schulz-Flory plot for each catalyst with different palladium loadings, calculated α values are tabulated.

Table 4.5 – Catalytic data obtained for CO_2 hydrogenation using Pd-20wt%Fe/SiO_2 catalyst systems containing various palladium loadings.

Catalyst	CO_2 Conversion (%)	HC Yield (%)	CO Yield (%)	Hydrocarbon Distribution									
				C_1	C_2=	C_2	C_3=	C_3	C_4	C_5	C_6	C_7	C_8
20wt%Fe/SiO_2	13.6	3.6	10.0	75.1	2.3	15.2	4.4	3.1	0.0	0.0	0.0	0.0	0.0
20wt%Fe/1wt%Pd/SiO_2	37.4	14.4	23.1	57.4	0.1	23.5	0.8	12.1	4.0	1.9	0.3	0.0	0.0
20wt%Fe/2wt%Pd/SiO_2	39.6	18.5	21.0	60.3	0.0	23.1	0.1	11.6	3.5	1.4	0.1	0.0	0.0
20wt%Fe/3wt%Pd/SiO_2	46.5	23.7	22.8	61.0	0.0	21.7	0.0	11.6	3.7	1.7	0.2	0.0	0.0
20wt%Fe/4wt%Pd/SiO_2	42.9	25.7	17.1	58.4	0.0	22.8	0.0	12.4	4.4	1.6	0.5	0.0	0.0

Catlyst tests conducted at atmospheric pressure, H_2:CO_2 ratio 3:1, total flow – 8 sccm. 0.7g of catalyst. Conversions, yields and product distributions calculated as an average of 4 hours on stream after catalyst stabilisation.

The introduction of palladium to the catalyst system greatly decreases olefin selectivity with only small amounts observed with a 1 wt% loading and none detected for palladium content above this value. A similar effect as previously been observed under Fischer-Tropsch reaction conditions.[8a]

To study the effect of palladium loading on the FT process alone each catalyst system was tested using a syngas (CO/H_2) feed. For this collection of catalyst tests Reactor 2 (See Chapter 2 Section 2.2 for full details) was employed. A catalyst testing procedure similar to that used for CO_2 hydrogenation tests was utilised (see Chapter 2 Section 2.3 for full details). Reaction temperature was kept constant at 370 ^oC, a $CO:H_2$ ratio of 1:3 with a total flow of 40 sccm was employed for all tests.

The results from the syngas fed tests are summarised in Table 4.6. As was observed with the CO/H_2 fed catalyst tests for varying iron loading a low catalyst stability is observed. While the CO_2/H_2 fed reactions (Table 4.5) appear stable after 2 hours on stream the same is not observed for CO/H_2 fed catalyst systems.

A significant jump in CO conversion is observed upon the introduction of palladium to the catalyst system, however, when palladium content is increased further little effect on CO conversion values are observed. This suggests that palladium's introduction improves the catalyst in such a way that 1 wt% is sufficient to achieve and any increase does not further improve the system. HC yield is shown to follow the same trend as that observed for CO conversion with little effect apparent with increasing palladium loading.

Table 4.6 – Catalytic data obtained for CO hydrogenation studies using Pd-20wt%Fe/SiO_2 catalyst systems containing various palladium loadings

Catalyst	CO Conversion (%)	HC Yield (%)	CO_2 Yield (%)	Hydrocarbon Distribution										α
				C_1	C_2=	C_2	C_3=	C_3	C_4	C_5	C_6	C_7	C_8	
20wt%Fe/SiO_2	20.54	6.40	14.14	88.1	0.0	11.9	0.0	0.0	0.0	0.0	0.0	0.0	0.0	0.06
20wt%Fe/1wt%Pd/SiO_2	85.70	55.88	29.82	46.0	0.0	23.3	0.7	16.6	7.1	3.6	1.9	0.9	0.0	0.37
20wt%Fe/2wt%Pd/SiO_2	85.93	53.40	32.53	42.3	0.0	22.2	0.5	18.2	8.4	4.9	2.5	1.0	0.0	0.39
20wt%Fe/3wt%Pd/SiO_2	86.44	53.96	32.47	39.2	0.0	21.1	0.0	19.4	11.0	5.7	2.6	1.1	0.0	0.40
20wt%Fe/4wt%Pd/SiO_2	88.79	57.67	31.12	38.7	0.0	20.2	0.0	19.7	11.4	5.9	2.9	1.2	0.0	0.41

Catlyst tests conducted at atmospheric pressure, H_2:CO ratio 3:1, total flow – 40 sccm. 0.7g of catalyst. Conversions, yields and product distributions calculated after 1 hour on stream.

The high CO_2 yields under these reaction conditions show that the system is highly WGS active with palladium introduction doubling the CO_2 yield. This suggests that palladium's inclusion has a more significant effect on the WGS component of CO_2 hydrogenation rather than that of the FT process. At this reaction temperature it also suggests that under CO_2 hydrogenation conditions while we are producing CO through the RWGS the WGS reaction is also competing with the FT for CO consumption, which could negatively affect the HC yield.

Figure 4.13 shows an Anderson Schulz Flory plot for each catalyst system after an hour on stream with the calculated α values summarised in the associated table. Increasing palladium loading appears to improve catalyst selectivity towards heavier hydrocarbons with a decrease in methane selectivity combined with a steady increase in the chain growth probability

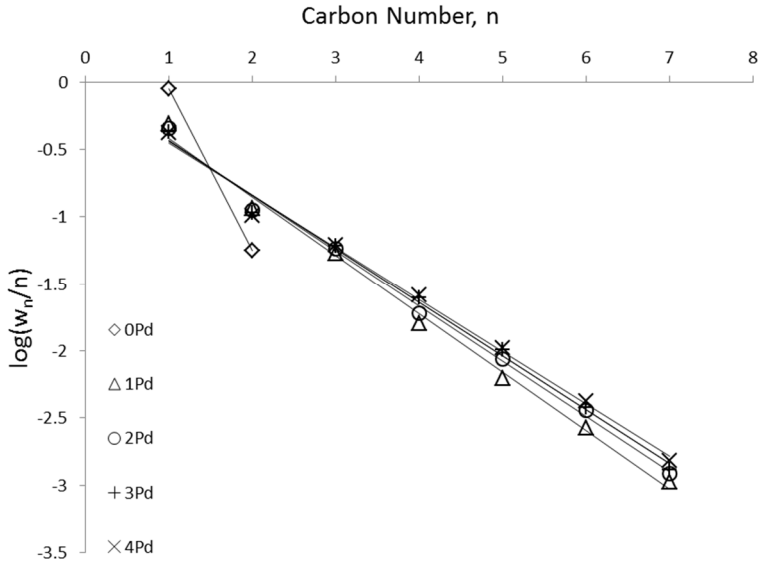

Palladium Content of Catalyst (wt%)	Chain Growth Probability, α
0	0.06
1	0.37
2	0.39
3	0.40
4	0.41

Figure 4.13 – An Anderson Schulz-Flory plot for each catalyst with different palladium loadings, calculated α values are tabulated.

4.3.4 Summary

Palladium addition greatly enhances the performance of iron-silica catalysts for both the FT reaction and the hydrogenation of CO_2. Under FT conditions palladium introduction greatly increases the WGS ability of the catalysts. Increasing loadings resulted in increased α values. When utilised for CO_2 hydrogenation little change in α is observed when palladium loading is increased above 1 wt%. There is, however, a steady increase in HC yields with higher palladium content. Product distributions for both the CO and CO_2 fed catalysts tests show a reduction in olefin formation upon palladium inclusion in the catalyst.

4.4 Influence of Silica Support Properties

The nature of catalyst support has been shown to have a large impact on catalyst performance.[9, 19] The acid/basic nature of the support can influence product selectivity[20] as well as activity as illustrated by the studies conducted in Chapter 3. Other support properties that can effect

catalyst performance include the interactions between the support and the active phase of the catalyst[21] as well as the particle size, surface area and pore size.[22] With iron and palladium loading shown to have a large impact on catalyst performance the final component left to investigate is the catalyst support, in this case silica. For the sake of this study a range of silica were chosen that allowed the investigation into the effects of pore size and particle size, both properties that have been shown to have a strong influence on the performance of a catalyst system.

4.4.1 Catalyst Preparation

For investigations into the effects of silica properties on a 20wt%Fe/1wt%Pd/SiO_2 catalyst system for CO_2 hydrogenation four different silica were chosen. The properties of each silica are shown in Table 4.7. SiO_2-60 (Sigma Aldrich) is the silica that has been utilised for the preparation of all catalyst systems up to this point. SiO_2-250 and SiO_2-500 (Grace Davison) are the same particle size with larger pores allowing the effect of pore size to be investigated. SiO_2-60_b possesses a pore size of 60 Å but with a much larger particle. All catalysts were prepared using the same preparation method utilised for all systems reported within this chapter with only the silica used varied between each.

Table 4.7 – Reported properties of each silica used as a catalyst support

Silica Denotement	Pore Size (Å)	Particle Size (µm)	Surface Area (m^2g^{-1})
SiO_2-60	60	35-70	550
SiO_2-250	250	35-70	285
SiO_2-500	500	35-70	80
SiO_2-60_b	60	1000-2000	525[a]

[a] – Surface area calculated by BET as no value was reported by Davisil.

4.4.2 Catalyst Testing

The prepared catalyst systems were tested for their CO_2 hydrogenation ability in Reactor 1 (see Chapter 2, Section 2.3 for full details). Each catalyst was first reduced at 300 ^oC for 2 hours under a stream of pure hydrogen. After completion of the pre-treatment the reactor was heated to 370 ^oC under an argon atmosphere. Once at temperature CO_2 and H_2 were introduced at 2 sccm and 6 sccm respectively. Gas samples were collected every hour and analysed using gas chromatography.

The four catalyst systems; 20wt%Fe/1wt%Pd/SiO_2-60, 20wt%Fe/1wt%Pd/SiO_2- 250, 20wt%Fe/1wt%Pd/SiO_2-500 and 20wt%Fe/1wt%Pd/SiO_2-60_b showed little variation in CO_2 conversion, HC yield and CO yield with increasing time on stream. Each system was investigated for 5 hours with little to no drop in CO_2 conversion over this period. The average

CO_2 conversion, HC yield, CO yield and hydrocarbon distributions for each system are shown in Table 4.8.

Despite the SiO_2-60 supported catalyst possessing the highest surface area of the systems tested within this section it shows the lowest CO_2 conversion, it is also the only silica to result in a catalyst that shows a higher selectivity to CO over HCs. Upon increasing the pore diameter of the silica support (SiO_2-250 and SiO_2-500) while keeping particle size constant, a significant increase in CO_2 conversion and HC yield are observed along with a reduction in CO yield. The SiO_2-250 supported catalyst system shows a slightly higher CO_2 conversion and HC yield than the SiO_2-500 supported system suggesting that the increased pore diameter alone is not responsible for the improved catalyst performance. The SiO_2-500 silica possesses a significantly lower surface area (80 m^2g^{-1} *vs.* 285 m^2g^{-1}) so it is possible that CO_2 conversion values are dependent upon both these properties with the SiO_2-250 system showing 'goldilocks' conditions with a larger pore diameter than SiO_2-60 and higher surface area SiO_2-500.

When pore diameter of the silica support is kept constant at 60 Å and particle size increased from 35-70 nm to 1000-2000 nm the product distribution is observed to remain similar whereas CO_2 conversion and HC yield values are reduced. This reduction is likely due to the larger particle size which may cause mass transport issues.

Product distribution is also observed to vary depending on the properties of the silica support used. Figure 4.14 shows the Anderson Schulz Flory plot for each of the different silica supported catalysts along with the calculated chain growth probabilities. When the pore diameter is increased from 60 Å through 250 Å to 500 Å methane selectivity is seen to decrease with selectivity towards heavier hydrocarbons increasing. The increasing chain growth probability with larger pore sizes suggests that the pore size of the catalyst support plays an important role in product selectivity of the Fischer-Tropsch process.

When pore size is kept constant at 60 Å and instead particle size increased product distribution shows little change. Methane selectivity remains similar for both 20wt%Fe/1wt%Pd/siO_2-60 and 20wt%Fe/1wt%Pd/SiO_2-60_b catalysts. Only a slight variance in α is observed between the two catalysts providing further proof that pore diameter plays an important role in product selectivity as when kept constant little change is observed. This shows that the increase in particle size only affects the amount of CO_2 converted.

Table 4.8 - Catalytic data obtained for CO_2 hydrogenation using 20wt%Fe/1wt%Pd/SiO_2 catalysts supported on various silica.

Catalyst[a]	CO_2 Conversion (%)	HC Yield (%)	CO Yield (%)	Hydrocarbon Distribution									
				C_1	C_2=	C_2	C_3=	C_3	C_4	C_5	C_6	C_7	C_8
20wt%Fe/1wt%Pd/SiO_2-60	37.4	14.4	23.1	57.4	0.1	23.5	0.8	12.1	4.0	1.9	0.3	0.0	0.0
20wt%Fe/1wt%Pd/SiO_2-250	52.5	38.4	14.1	54.9	0.0	21.8	5.4	7.3	4.8	2.2	1.5	2.3	0.0
20wt%Fe/1wt%Pd/SiO_2-500	49.8	36.3	13.5	46.6	0.7	20.9	0.2	16.7	8.2	3.6	2.3	0.1	0.0
20wt%Fe/1wt%Pd/SiO_2-60_b	24.8	9.3	15.5	59.8	0.0	24.0	0.4	11.3	3.5	0.8	0.2	0.0	0.0

[a] See Table 4.7 for full silica properties. Catlyst tests conducted at atmospheric pressure, H_2:CO_2 ratio 3:1, total flow – 8 sccm. 0.7g of catalyst. Conversions, yields and product distributions calculated as an average of 4 hours on stream after catalyst stabilisation.

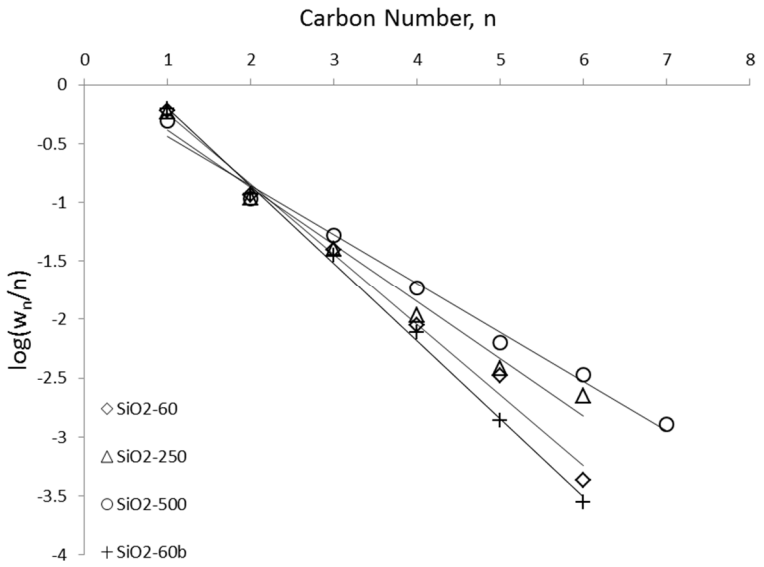

Silica Support Used	Chain Growth Probability, α
SiO_2-60	0.25
SiO_2-250	0.33
SiO_2-500	0.38
SiO_2-60[b]	0.22

Figure 4.14 – An Anderson Schulz-Flory plot for each catalyst with different silica supports, calculated α values are tabulated.

4.4.3 Summary

The properties of the catalyst support has a dramatic effect on the overall catalyst performance. Catalysts supported on silica with a larger pore diameter possess increased chain growth probability with a higher selectivity towards heavier hydrocarbons an effect similar to that observed for cobalt based FT catalysts when supported on silica. The relationship between silica properties and CO_2 conversion and HC yield appears slightly more complex with both surface area and pore diameter appearing to play a role. Larger support particle sizes resulted in a reduction in CO_2 conversion, however, little to no effect was observed on the product distribution.

4.5 Influence of Reaction Pressure

So far all reactions have been conducted at atmospheric pressure. In order to determine if catalyst performance could be improved further the influence of reaction pressure was investigated. Previous studies have shown that increasing pressure can have an effect on catalyst conversion/product distribution under Fischer-Tropsch conditions.[23] For these reasons the FT process is carried out industrially at elevated pressure.[24] As the base catalyst for optimisation studies, the 20wt%Fe/1wt%Pd/SiO_2-60 catalyst was chosen for pressure tests.

4.5.1 Catalyst Testing

The selected catalyst was tested for its CO_2 hydrogenation abilities in Reactor 3 (see Chapter 2 Section 2.2 for full details). 0.7 g of catalyst was loaded into the reactor and held in place with SiC and quartz wool. Pre-treatment was conducted under atmospheric pressure at 300 ^oC for 2 hours under a flow of pure hydrogen. Once the reduction phase was completed the reactor was heated to the desired temperature and the pressure increased to that required for the reaction.

The system was pressurised under a high flow of H_2 and CO_2 (3:1 ratio). Once the target pressure had been obtained H_2 and CO_2 flow was reduced to give a total flow of 8 sccm maintaining the same ratio.

The results obtained are summarised in Table 4.9. A high catalyst stability was observed for the catalyst at each pressure over the 5 hour test period with no significant deactivation observed.

As reaction pressure was increased from 0 bar(g) to 5 bar(g) an increase in CO_2 conversion was observed. Combined with an increase in selectivity to HCs over CO this resulted in a HC yield increase of 5%. A further increase in conversion was observed as reaction pressure was increased to 10 bar(g) when pressure is increased above this point to 15 bar(g) conversion dropped slightly. This suggests that a reaction pressure of 10 bar(g) is optimum for CO_2 hydrogenation using the Fe-Pd-SiO_2 catalysts studied.

Reaction pressure was also observed to have an impact on the product distribution. As pressure was increased from 0 bar(g) to 5 and 10 bar(g) along with the improved conversion and HC yield an increase in methane selectivity is observed with selectivity to C_7 hydrocarbons dropping from 2.3 % at 0 bar (g) to 0.4 % at optimum conversion {10 bar(g)}. The chain growth probability calculated for each system (Figure 4.15) was observed to decrease with increasing pressure. This contradicts what is observed for FT fed catalyst systems which suggests that the pressure increase is having an impact on more than the FT process which is aiding the formation of methane. It is also possible this difference can be attributed to the palladium present in the catalyst system, which is a more effective hydrogenation catalyst at higher pressures which could lead to a reduction in chain growth probability.

Table 4.9 – Catalytic data obtained for CO_2 hydrogenation using 20wt%Fe/1wt%Pd/SiO_2-60 over a range of reaction pressures.

Catalyst	Reaction Pressure (bar(g))	CO_2 Conversion (%)	HC Yield (%)	CO Yield (%)	Hydrocarbon Distribution									
					C_1	C_2=	C_2	C_3=	C_3	C_4	C_5	C_6	C_7	C_8
20wt%Fe/1wt%Pd/SiO_2-60	0	23.6	9.8	13.8	49.0	0.0	24.5	0.0	14.4	5.0	2.7	2.2	2.3	0.0
20wt%Fe/1wt%Pd/SiO_2-60	5	26.8	7.9	18.9	60.5	0.0	20.2	0.0	10.9	3.8	2.1	1.1	1.6	0.0
20wt%Fe/1wt%Pd/SiO_2-60	10	32.6	8.6	24.0	68.8	0.0	19.0	0.0	7.9	2.2	1.3	0.4	0.4	0.0
20wt%Fe/1wt%Pd/SiO_2-60	15	25.0	9.3	15.6	68.3	0.0	19.9	0.0	8.3	2.2	1.0	0.4	0.0	0.0

Catlyst tests conducted at atmospheric pressure, H_2:CO_2 ratio 3:1, total flow – 8 sccm. 0.7g of catalyst.

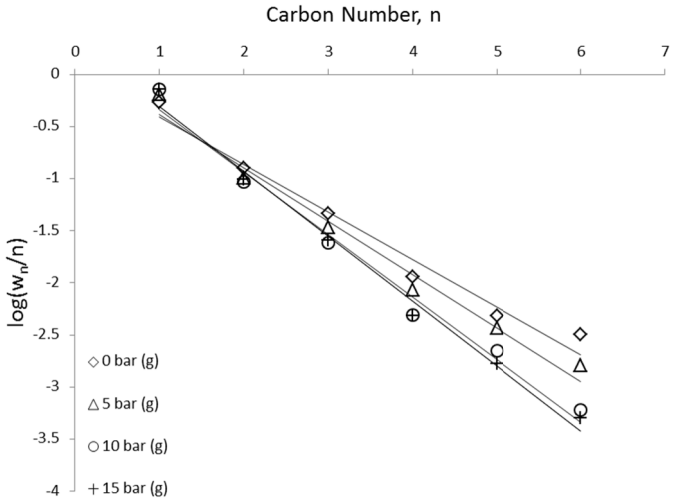

Reaction Pressure (bar (g))	Chain Growth Probability, α
0	0.35
5	0.30
10	0.25
15	0.24

Figure 4.15 – An Anderson Schulz-Flory plot for the catalyst tested at different reaction pressures, calculated α values are tabulated.

4.5.2 Summary

Reaction pressure has a significant impact on the performance of a Fe-Pd-SiO_2 catalyst system. 10 bar (g) appears the optimum pressure for high CO_2 conversion values and high HC yields. Unlike what has been previously observed with catalysts under FT conditions[23a] as pressure is increased a higher selectivity towards heavier HCs is observed. As with temperature when deciding upon reaction conditions a compromise must be made between CO_2 conversion and product distribution.

4.6 Influence of Pre-Treatment Pressure

While the Fe_2O_3 phase detected during catalyst characterisation is active for the RWGS reaction its activity for the Fischer-Tropsch process is limited. As a result, before catalyst testing all systems reported so far have been reduced under a stream of pure hydrogen for 2 hours. The majority of literature both for CO based FT catalysis and the hydrogenation of CO_2 report pre-treatment time of 12 hours and above although pre-treatment generally takes place under a stream of hydrogen (~ 10 %) diluted with nitrogen, as opposed to the pure H_2 utilised within this report. The reducibility of iron has been shown to play an important role in the catalyst performance.[25] As a result the effect of pre-treatment pressure was investigated. It was envisaged that a high pre-treatment pressure, effectively increasing hydrogen concentration, would lead to a more effective reduction of the iron species possibly improving catalyst performance. To our knowledge no previous studies have investigated the effect of pre-treatment pressure.

4.6.1 Catalyst Testing

For catalyst testing the 20wt%Fe/1wt%Pd/SiO_2-60 system was chosen. 0.7 g of catalyst was loaded and packed into Reactor 3 (see Chapter 2 Section 2.2 for full details). The reactor was first pressurised and leak tested. The system was then pressurised to the desired pre-treatment pressure under a high flow of hydrogen and heated to 300 ^oC. Once pressurised H_2 flow was reduced to 20 sccm and the system left for 2 hours. After pre-treatment was completed the reactor was depressurised to 0 bar(g) before being re-pressurised to the desired reaction pressure under a high flow of 3:1 H_2:CO_2. Once reaction pressure was reached the flow rates of CO_2 and H_2 were reduced, giving a total flow of 8 sccm with the ratio of H_2:CO_2 maintained at 3:1.

For each pre-treatment pressure tested the catalyst was evaluated at four different reaction pressures {0, 5, 10 and 15 bar (g)} in order to ascertain if the pre-treatment pressure had the same effect on catalyst performance under all reaction conditions. The catalytic results obtained are summarised in Figure 4.16.

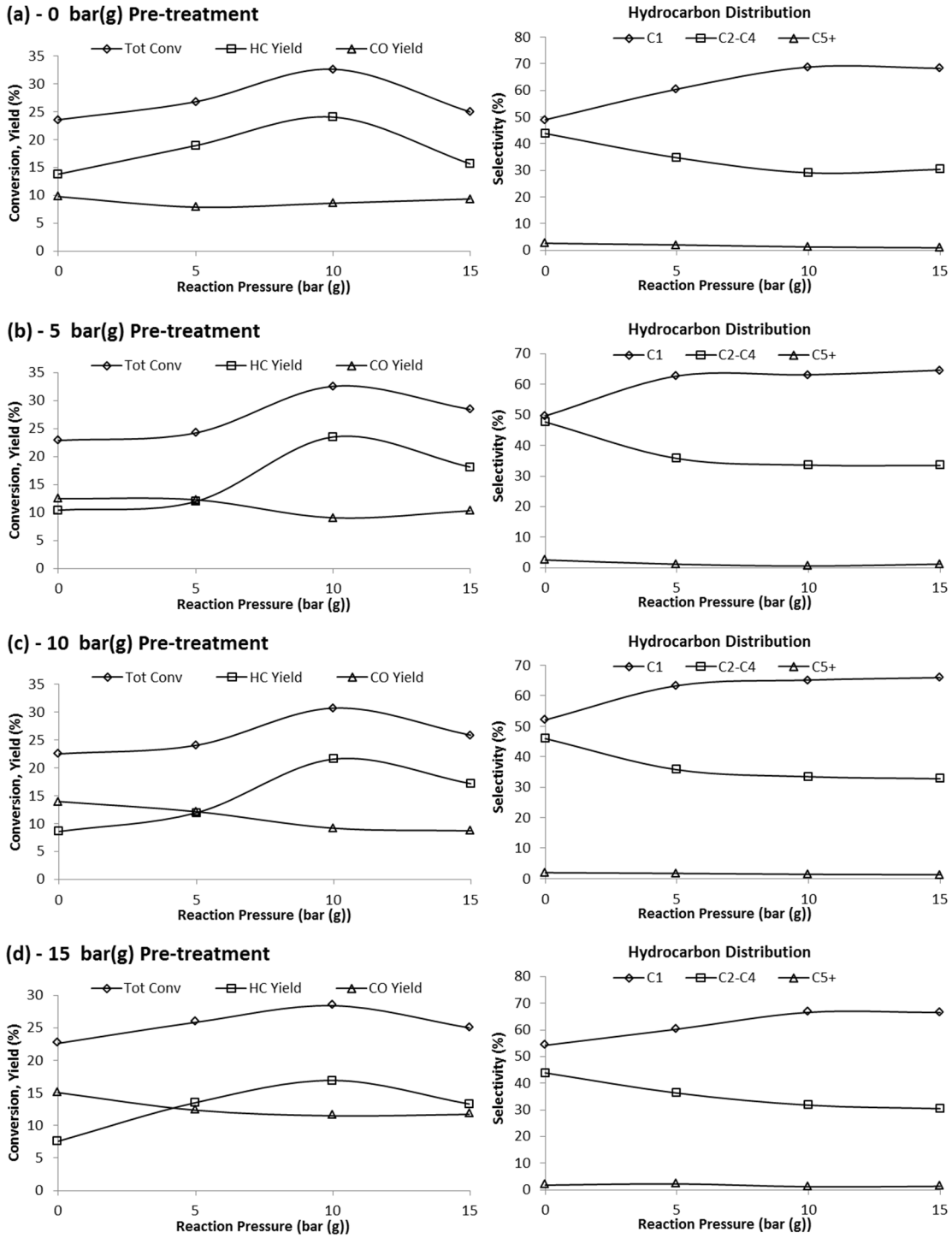

Figure 4.16 – Conversion and Product selectivity plots for (a) 0 bar(g) pre-treatment, (b) 5 bar(g) pre-treatment, (c) 10 bar(g) pre-treatment and (d) 15 bar(g) pre-treatment.

All catalyst systems were also shown to possess the same trend in reactivity observed for the 0 bar(g) pre-treatment, where conversion increases with increasing pressure until 10 bar(g), above this point CO_2 conversion begins to drop. Product distribution after pre-treatment at all pressures also mirrors that observed for the 'regular' atmospheric pre-treatment with increasing pressure resulting in increased selectivity to methane and a decrease in selectivity to C_5+ hydrocarbons.

With an atmospheric reaction pressure the pre-treatment pressure shows little influence on CO_2 conversion with the values remaining constant (within error) at approximately 24 %. HC yield is seen to drop with increasing reduction pressure, this is coupled with an increase in CO yield. At the optimum reaction pressure for high CO_2 conversion {10 bar (g)} CO_2 conversion shows a slight drop as pre-treatment pressure is increased. The HC yield follows the same trend whereas CO yield remains relatively constant.

The pre-treatment pressure also shows an influence on the HC distribution. With the catalyst tests performed with atmospheric reaction pressure an increasing pre-treatment pressure appears to increase selectivity towards methane, decreasing the selectivity towards heavier hydrocarbons. With an increase in reaction pressure to 10 bar (g) to give an optimal conversion only a slight alteration in hydrocarbon distribution was noted. A reduction in methane content from 70 % at 0 bar(g) pre-treatment temperature to 65 % at 5 bar(g) reduction pressure. At pre-treatment pressures above this value little change in product selectivity is observed. The 65 % methane selectivity is still significantly higher than that recorded at a reaction pressures of 0 bar(g).

4.6.2 Summary

The effect of pre-treatment pressure acts on the catalyst system slightly differently depending on the reaction pressure. At a reaction pressure of 0 bar (g) CO_2 conversion remains constant but a decrease in HC yield is observed, an increase in selectivity to methane is recorded with increasing pre-treatment pressure. At higher reaction pressures a slight reduction in selectivity to methane is observed at higher pre-treatment pressures.

For this catalyst system there is no advantage in increased pre-treatment pressure when the reaction is run at atmospheric pressure. For reactions run at higher pressures (>5 bar) a slight improvement in hydrocarbon distribution can be obtained, however, methane selectivity still remains much higher than that observed at atmospheric reaction conditions, although a significantly higher conversion is observed.

4.7 Further Catalyst Studies

In order to gain a deeper understanding of the catalyst process the 20wt%Fe/1wt%Pd/SiO_2-60 catalyst system was characterised further. As mentioned previously although Fe_2O_3 is detected as the main iron phase after catalyst calcination, it is unlikely this remains the main phase after

the reductive pre-treatment and under reaction conditions. As such the reduction of iron and palladium was investigated along with how catalysts vary with time on stream.

4.7.1 Catalyst Reduction Studies

Before each catalyst test the system to be studied was reduced in pure H_2 for 2 hours at 300 ^oC. In order to study the effect this pre-treatment has on the active phases of the metals present *in situ* XPS reduction studies were undertaken in the facilities at Cardiff University. [*] For this process a small amount of catalyst was placed within a specialised sample cell in the X-ray photoelectron spectrometer and a survey spectrum recorded along with detailed scans of the Fe 2p and Pd 3d regions. After a 2 hour reduction under an atmosphere of 1 bar hydrogen at 300 ^oC the catalyst was re-analysed by XPS. The resulting spectra are shown in Figure 4.17.

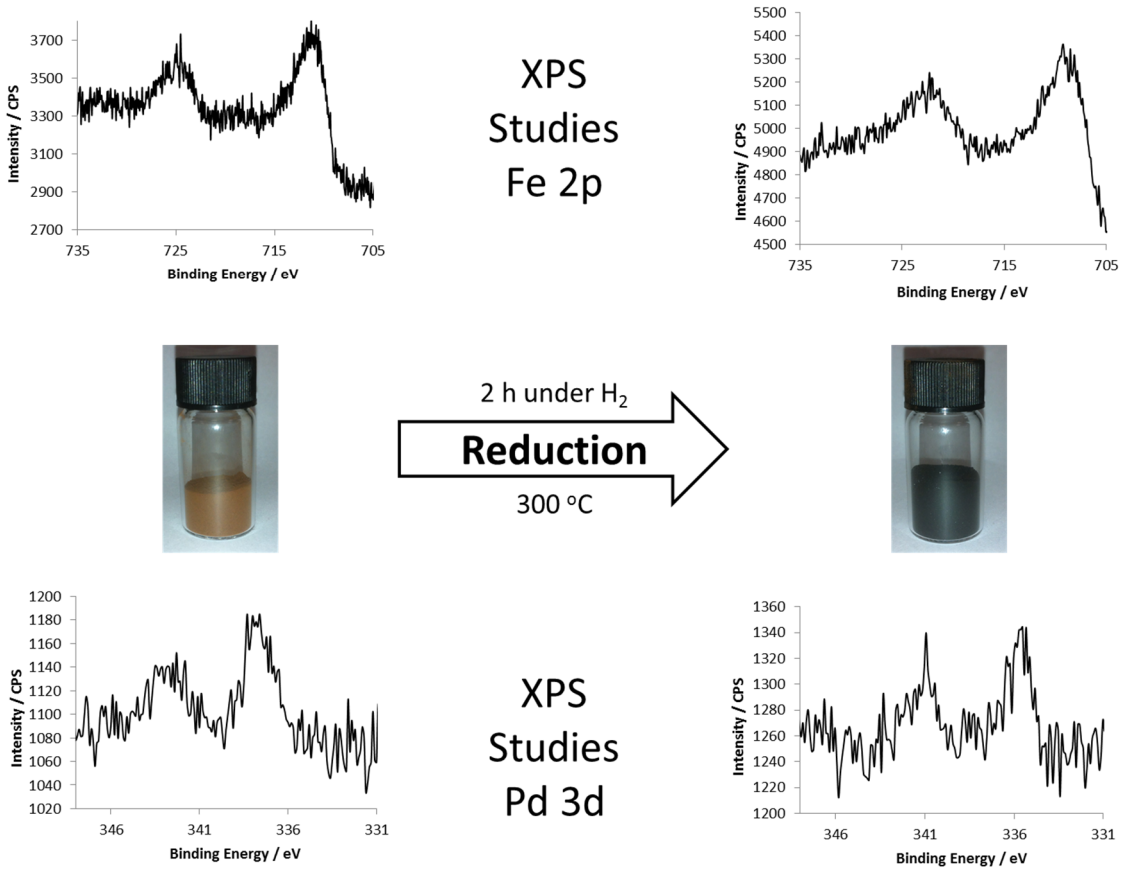

Figure 4.17 – Results for *in situ* XPS reduction experiments including detailed scans for the Fe 2p and Pd 3d regions before and after reduction as well as photographs showing the appearance of the catalyst system before and after reduction.

XPS spectra recoded before catalyst pre-treatment shows the presence of iron as Fe_2O_3 and palladium as PdO. The rust-brown colour of the catalyst system matches what would be expected for a system containing large quantities of Fe_2O_3. pXRD studies were attempted to further confirm the presence of iron as Fe_2O_3 however no peaks were observed suggesting that

[*] Dr. David Morgan at Cardiff University is gratefully acknowledged for his help with these studies

the iron is either amorphous or the crystalline phases are too small to be observed. After the 2 hour reduction had been completed further XPS spectra were recorded (Figure 4.17). The shift observed for palladium's binding energy from 337.6 eV to 335.3 eV suggests that the palladium oxide present in the calcined catalyst system had been fully reduced resulting in the formation of metallic palladium (Pd^0).[17]

A shift in the peak position from 711.0 eV to 709.21 eV observed in the Fe 2p region combined with a reduction in intensity of the satellite peak at 719 eV suggests that the Fe_2O_3 phase is being reduced to Fe_3O_4.[16] The colour change to black seen for the catalyst after reduction further supports the formation of Fe_3O_4 with the catalyst powder also becoming magnetic after reduction. Fe_3O_4 has been shown to be active for both the RWGS reaction[26] and the FT process[27] and so is likely responsible for the catalytic activity observed initially. Iron carbide, specifically the Hägg form (Fe_5C_2), is thought to be the main active phase for iron catalysts during FT synthesis[23a] with it being produced by the further reduction of Fe_3O_4 to metallic iron followed by the reaction of metallic iron with CO present either in the pre-treatment phases (where CO/H_2 gas mixes are used) or under reaction conditions as would be likely here. The active phase for iron catalysts is still however a matter of great debate. The fact no metallic iron signal is observed for the iron species (expected at 707 eV[28]) after reduction and the lower WGS activity of Fe_5C_2[29] suggests that Fe_3O_4 acts as the main phase for RWGS reaction and, at least initially, the FT process.

4.7.2 Used Catalyst Analysis

TEM studies were conducted in order to determine the effect of exposure to reaction conditions on the morphology of the catalyst system. Figure 4.18 shows TEM images recorded before and after reaction with the distribution of iron nanoparticles shown as an insert in the form of a histogram. For the 20wt%Fe/1wt%Pd/SiO_2 catalyst {Figure 4.18 (a) and (b)} the mean nano-particle size is observed to increase slightly after reaction with a shift in the particle size distribution to larger nano-particles. This suggests that the sintering of the catalyst nano-particles could be playing a role in initial drop in catalyst activity observed over the first 1 – 2 hours on stream before a steady CO_2 conversion is obtained. A more significant increase in particle size is observed with the 20wt%Fe/4wt%Pd/SiO_2 catalyst {Figure 4.18 (c) and (d)} the average particle size tripling in size over the course of reaction. This may suggest that increasing palladium loading aids the sintering of catalyst nanoparticles.

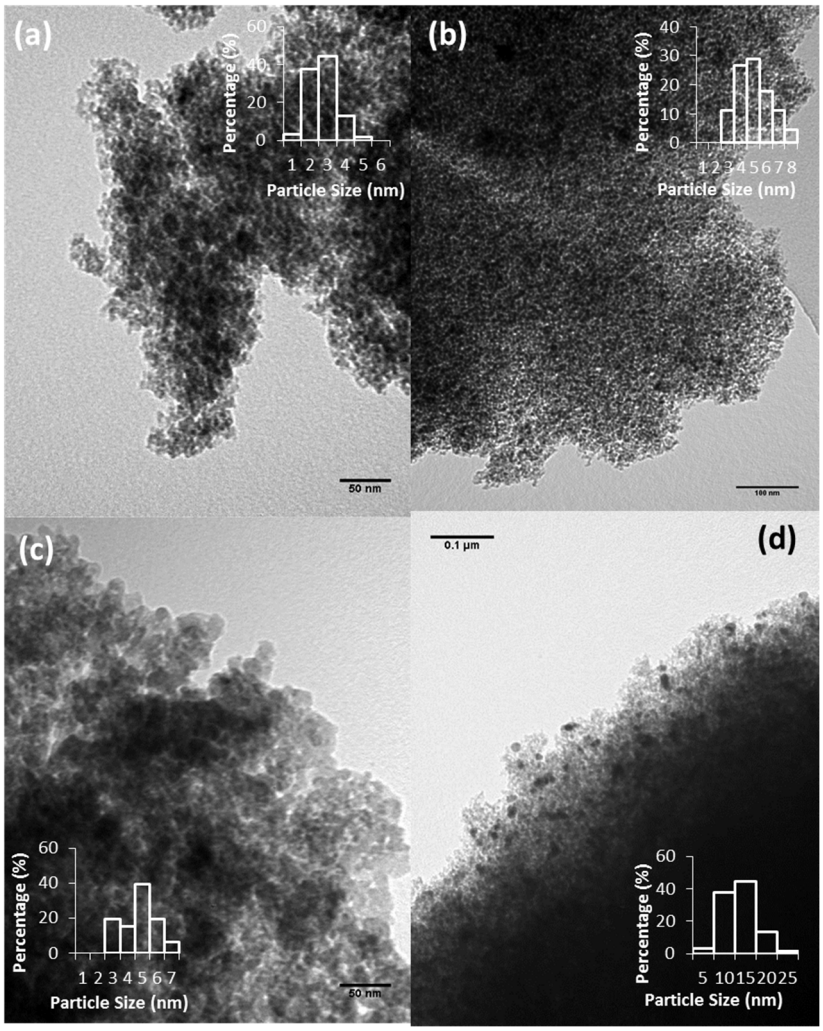

Figure 4.18 – TEM images recorded for 20wt%Fe/1wt%Pd/SiO_2 before (a) and after (c) reaction with TEM images recorded for 20wt%Fe/4wt%Pd/SiO_2 before (b) and after reaction (d).

4.7.3 Summary

From the catalyst characterisation performed it can be concluded that any active phase formed that is not Fe_3O_4 must be formed under reaction conditions. It is however possible that Fe_3O_4 is in fact the active phase, having been shown to be active for both the RWGS and FT processes. TEM studies of used catalysts indicate an increase in nano-particle size after the catalyst is exposed to reaction conditions. It is possible that this sintering is responsible for the slight reduction in catalytic activity over the course of the first *ca.* 1 hour under reaction conditions. The fact that catalysts appear stable after this initial period suggests that there is little change in morphology after this initial stabilisation period.

4.8 Life Cycle Assessment Studies[†]

CO_2 utilisation (CDU) has the ultimate goal of reducing the volume of CO_2 released into the atmosphere in the short term with the long-term goal of reducing the amount of fossil fuels and other petrochemical products derived from depleting fossil fuel reserves, a process currently very harmful to the environment. If CDU processes are to compete with current technology the processes must be evaluated both in terms of energy used (vital for a renewable process) and the impact on the environment. If a replacement process utilises more energy and results in a greater degree of damage to the environment then there is little point in pursing that particular route. Life cycle assessment/analysis (LCA) allows for the calculation of the energy use and environmental impacts of processes so that they are more easily compared. For the sake of this report the impact on catalyst performance upon increased loading of both iron and palladium is studied in order to determine if the increased environmental impact of higher metal content in catalyst preparation is outweighed by the improved catalyst performance. The lab scale process currently used for catalyst testing is also compared to the industrial processes currently employed to obtain petrochemical products so targets needed to be obtained can be calculated.

While there is currently a great upsurge in the study of environmentally friendly 'green' processes a very small amount of these take into account all factors associated with the overall process. As a result this can lead to the misinterpretation that a process may be 'green' and environmentally friendly when in fact part of the process (such as extraction of a particular metal) may be environmentally damaging to the point where the overall process is no longer viable. Previous LCA studies have already been used to show environmental gains through the use of alternative catalysis processes.[30] There is, however, a shortage of life cycle data on nanomaterials and this can be a barrier for their assessment relative to excising technologies.

4.8.1 What is Life Cycle Assessment (LCA)?

Life cycle assessment/analysis is a tool for assessing the environmental impacts of a process across its entire life cycle from the initial design through to the disposal at the end of its life. This is often termed a 'cradle-to-grave' analysis; more limited studies are, however, common such as the 'cradle-to-gate' analysis more suited for a continuous process as envisioned here. The 'cradle-to-gate' analysis studies the impacts associated with the extraction of the raw resources required right up to the 'factory gate' i.e. the production of the hydrocarbons but not their use after leaving the factory as this varies greatly and would be difficult to calculate leading to a high potential error and making it more difficult to compare with existing processes.

LCA studies involve the collection and analysis of quantitative data on all the inputs and outputs of a process from the materials used, the waste formed and the energy inputs and

[†] O. Glyn Griffiths is gratefully acknowledged for the life cycle assessment work.

outputs associated within the scope of the study. These impacts may be beneficial or adverse and combine to give the environmental footprint of the overall process (Figure 4.19).

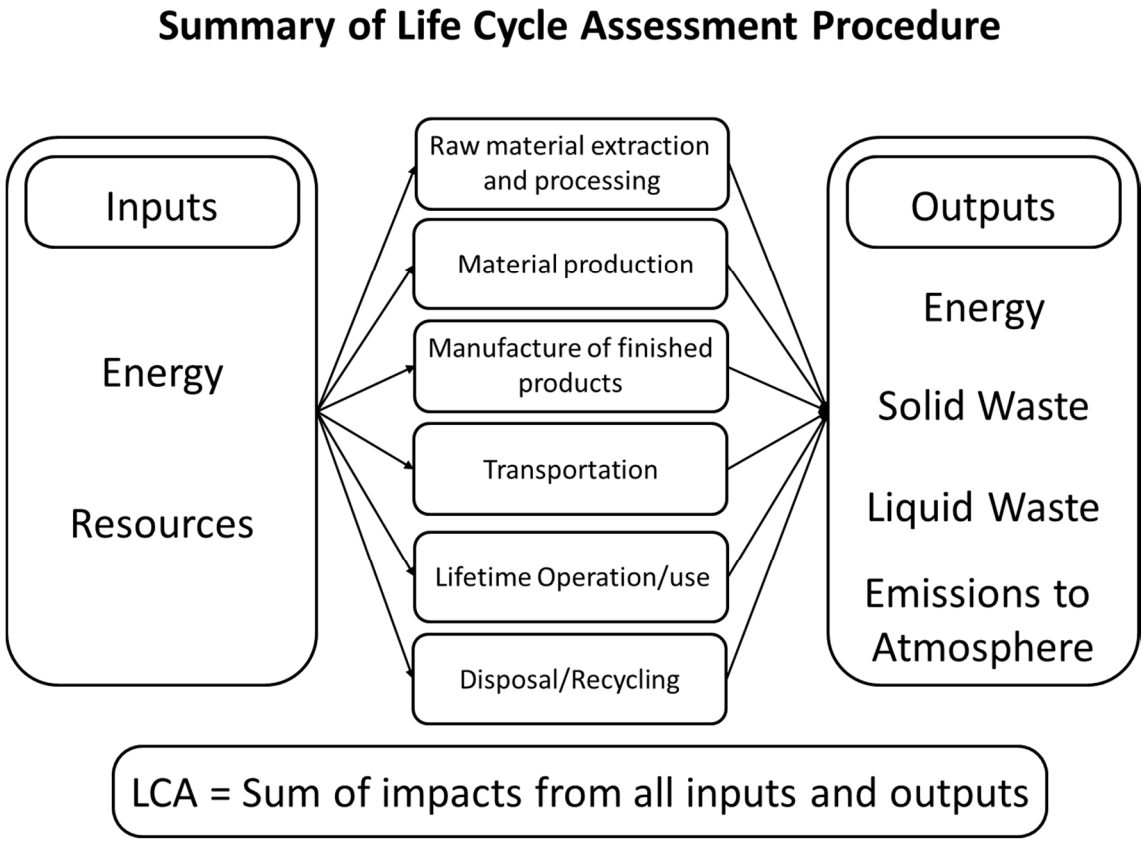

Figure 4.19 – A summary of the life cycle assessment procedure, adapted from [31]

LCAs rely heavily on the interpretation of the results obtained along with accurate data and as such it is possible that they can be used to reach pre-determined conclusions, i.e. say a process or product is green when it is not. In order to stop this and avoid their misuse the British Standards Institution and International Standards Organisation have published a set of guide lines, a LCA standard, which must be followed in order to obtain reliable results.[32]

According to the ISO 14040: 2006 environmental management standards[32a] the LCA process is carried out in four interdependent phases. Each phases is distinct but the results influence the other phases. These four main stages are summarised in Figure 4.20, adapted from ISO14040: 2006.[32a] The first phase is the definition of the goal and scope of the study to be carried out. This sets out the context of the study, it should include the system boundary, the functional unit (a definition of exactly what is being studied), any assumptions made and the limitations of the study.

The second phase is the inventory analysis and the formation of a detailed life cycle inventory (LCI). This involves creating an inventory of all the flows (within the scope of the study) to and from nature for a product or a process. The inventory should contain information on the inputs of energy, water and raw materials as well as the outputs such as releases to air,

water and land. LCI data can be obtained from existing databases such as the Ecoinvent Database,[33] or measured directly.

The next stage is the impact assessment, where the significance of the potential environmental impacts are evaluated. This phase generally includes the selection of impact assessment methodology, the grouping of data into their specific environmental impact categories, the classification stage and the characterisation stage where the emissions are weighted with respect to the environmental damage.

The final stage of the LCA process is the interpretation stage where the conclusions of the overall process are drawn and recommendations made. According to the ISO 14040: 2006[32a] this interpretation stage should include the identification of any significant issues determined in previous stages, an evaluation of the completeness and limitations of the study and the conclusions and recommendations.

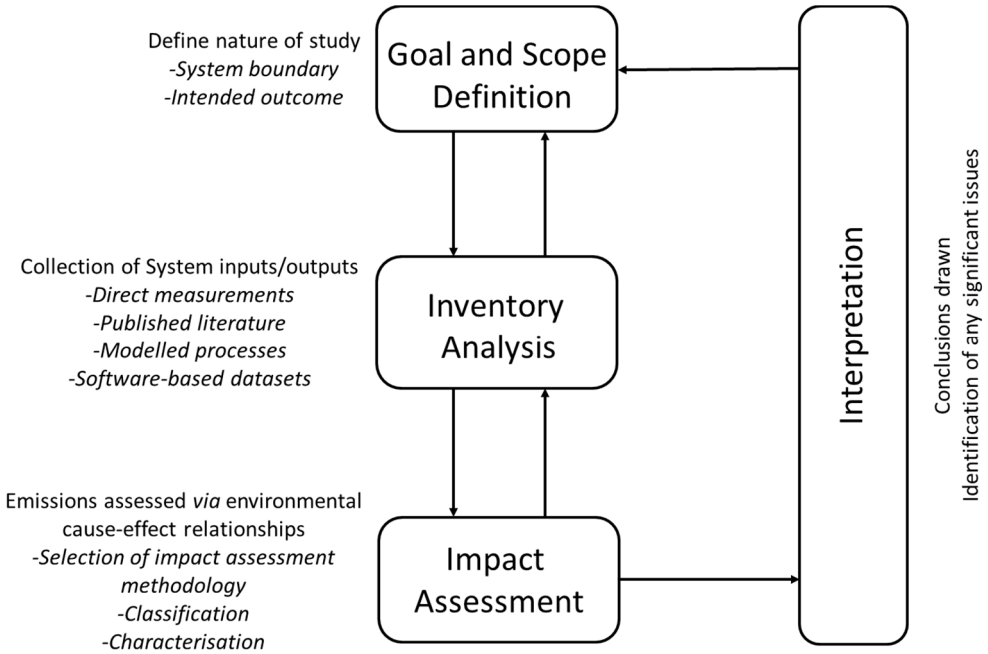

Figure 4.20 – A summary of the four main stages of the life cycle assessment procedure, adapted from ISO14040:2006[32a].

4.8.2 LCA Methodology

4.8.2.1 LCA

The LCA study was conducted in accordance with the ISO methodology standards for the principles and framework along with the requirements and guidelines.

4.8.2.2 Goal and scope definition

The goal of this LCA study is to investigate the environmental impact of producing HCs from CO_2 using the iron-palladium-silica catalysts studied so far within this chapter. This was

achieved by establishing the impacts inherent in making each catalyst and their related catalyst performance as summarised in Table 4.2 (page 139) and Table 4.5 (page 148). The impacts of this lab scale process were then compared to the impacts associated with traditional HC production routes. This gives a more instructive account rather than the LCA results alone and also allows the setting of targets that need to be met in order to compete with current processes.

The study can be considered a 'cradle-to-gate' assessment taking into account all the raw materials required for both catalyst preparation and reactor construction, processing, pre-cursor chemical synthesis and the in-use phase of the catalysts. The system boundaries corresponding to this study are shown in Figure 4.21. The catalyst test procedure will be compared to existing, fossil fuel based, HC production methods. The system boundaries for the study of these processes are shown in Figure 4.21 (c).

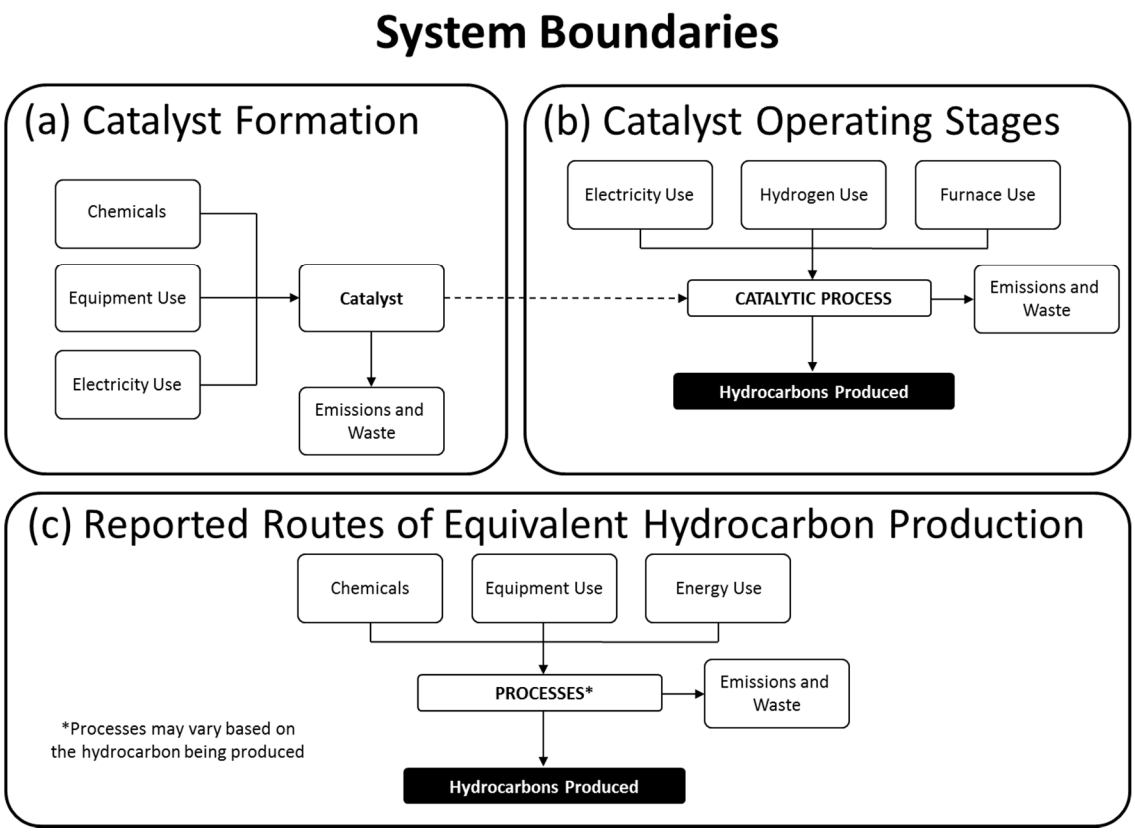

Figure 4.21 - The system boundaries for (a) catalyst preparation, (b) catalyst operating stage and (c) the boundary set for the reported routes for equivalent hydrocarbon production.

The functional unit (FU) chosen for the LCA of the catalyst performance was a combined measure of the kilograms of C_1 to C_7 HCs formed, kgHCs. Depending on the catalyst composition the conversion and HC selectivity was varied (see Table 4.2 {page 139} and Table 4.5 {page 148}) as a result the allocation of impacts is assessed on a mass basis.

4.8.2.3 Inventory data collection

The embodied impacts of each catalyst and the products formed are the sum of the impacts of the chemicals used in catalyst synthesis, materials used for the laboratory equipment and reactor

along with the energy consumption. The data used within this study has come from directly measured processes and existing life cycle inventories.

Where the inventory data was not available for particular chemicals (eg. Iron nitrate, palladium acetate and silica gel) datasets of the precursor chemicals were combined to give the impacts of the formed compounds based on known industrial production routes. The data for current, published, hydrocarbon manufacturing routes were obtained from the EcoInvent life cycle inventory.[33] As data sets were not available for all chemicals produced some assumptions were necessary and as such isomers of each carbon chain length are treated as having similar impacts. For this study hydrogen was modelled based on the current global hydrogen production mix with the data obtained from the EcoInvent life cycle inventory.[33]

As the equipment used for catalyst testing is at laboratory scale it does not represent the most efficient performance obtainable in terms of energy efficiency and infrastructure footprint compared to larger industrial processes. The materials used and their masses for each piece of equipment were estimated based on manufacturer specifications and the datasets of the major components were obtained from the EcoInvent life cycle inventory.[33]

4.8.2.4 Impact assessment

Each catalyst's environmental impact was assessed using the IPCC 100a global warming potential (GWP) impact methodology.[34] The values are expressed as kilograms of CO_2 equivalent atmospheric emissions ($kgCO_2$ eq.). In order to take into account both local and global environmental factors further impacts were assessed using the ReCiPe midpoint impact assessment methodology.[35] This ensures that the capture and conversion of CO_2 to hydrocarbons does not occur at the expense of other environmental factors. Calculations were performed using Simapro software.

For full details of the methodology please refer to [36] or [37].

4.8.3 LCA Studies: Results

The results obtained from the LCA study can be separated into two categories; 1) intrinsic impacts, which are unlikely to change when used at different scales (eg. the metals used) and 2) variable impacts which are likely to show a more significant change as the process is scaled up and includes impacts such as infrastructure and energy usage.

Each catalyst system is prepared using a wet impregnation method fully detailed in Chapter 2 Section 2.7.8. The GWP resulting from the preparation of 1g of each catalyst is shown in Figure 4.22. For the purpose of this graph it has been broken down into four distanced inputs: 1) The active metals used in the catalyst (Iron and palladium), 2) the chemicals used in the catalyst preparation including the silica support used, 3) the electricity used and finally 4) the infrastructure, containing the impacts from all laboratory equipment and their use. The largest impacts, in terms of GWP, for the preparation of each catalyst is the electricity

consumed by the equipment. The furnace responsible for the calcination of each catalyst system results in the largest contribution with the initial heating to calcination temperature the most energy intensive stage. The electrical impact has been modelled based on the UK electricity mix however if this were to be replaced by renewable sources a great reduction in GWP would be expected.

The environmental impacts associated with the active metals present in each catalyst contributed the second highest impact to the GWP of catalyst preparation. This can be attributed almost solely to the palladium present within the catalyst (see metal contribution of 20wt%Fe/SiO_2 *vs.* 20wt%Fe/1wt%Pd/SiO_2, Figure 4.22). This is due to the overwhelmingly large impacts of extraction and processing of the much rarer palladium metal whereas iron is readily available from normal scrap and recycling routes. As the mass of support is kept constant for the preparation of all catalysts those containing higher iron loadings result in a higher yield of calcined catalyst and so result in a lower, per gram impacts. For the systems containing higher palladium loadings the GWP of including larger quantities results in rapidly increasing GWP.

The impacts on GWP calculated for the other chemicals (methanol, silica and water) and infrastructure are negligible in comparison to the other contributions during catalyst preparation.

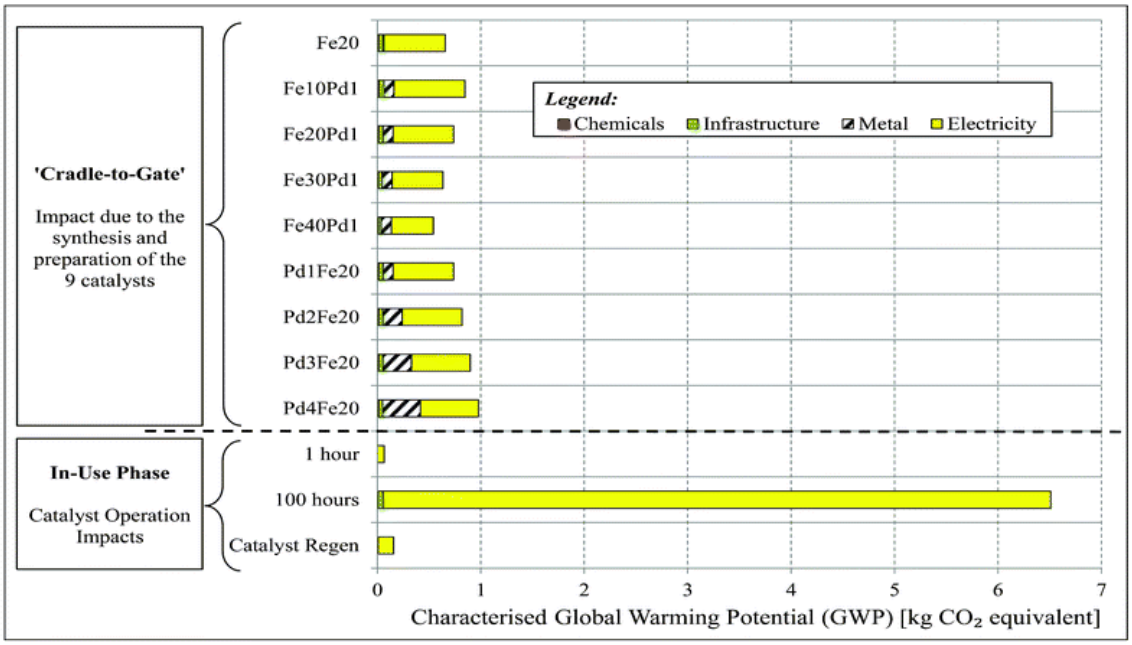

Figure 4.22 – The GWP contributions per gram of catalyst formed and impacts associated with catalyst operation.[36]

Three additional environmental impacts, as determined using the ReCiPe methodology, for the preparation of each catalyst system are shown in Figure 4.23. These include the metal depletion, fossil depletion and human toxicity. When impacts are calculated for these three factors it is the palladium addition and not electricity usage that accounts for the largest

contribution towards human toxicity and metal depletion. This serves as a fine example of why additional indicators should always be considered as well as carbon impacts when completing a life cycle analysis.

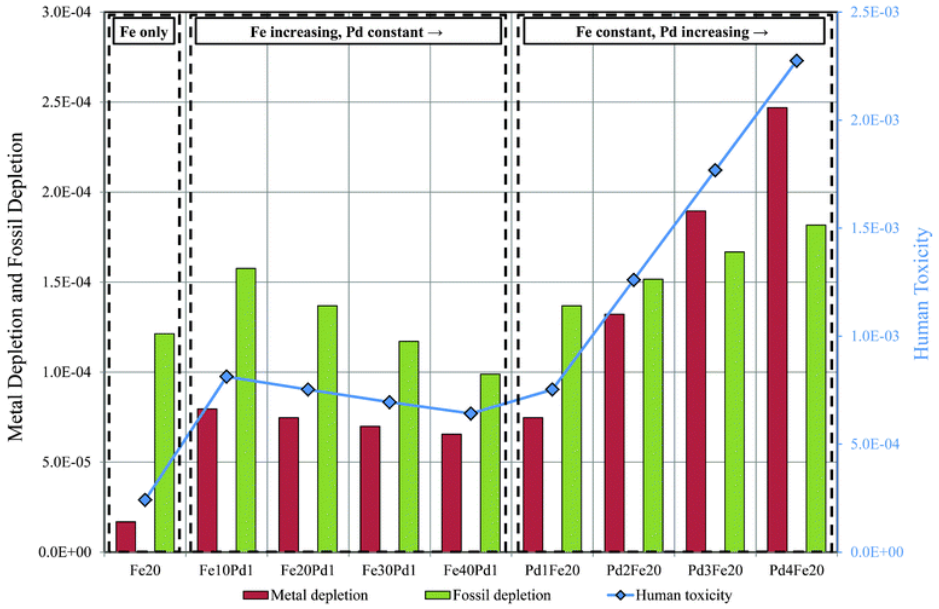

Figure 4.23– The normalised ReCiPe midpoint scores for the metal depletion, fossil depletion and human toxicity impacts of the prepared catalyst systems.[36]

The reaction impacts for the in-use catalyst remain constant for all catalyst systems. The GWP potential for 1 hour and 100 hours of catalyst use are shown in Figure 4.22. It must be stressed at this point that this is for a lab scale process and these calculated values could be improved significantly if the process was scaled up to that used industrially. While the reaction impacts remain constant for each of the systems tested the performance of the catalyst (see Table 4.2{page 139} and Table 4.5{page 148}) has the most significant impact on the environmental footprint of the hydrocarbons produced. Improved catalyst performance should lead to a direct reduction in the impacts of the HCs produced.

While Table 4.2 (page 139) and Table 4.5 (page 148) provide details of catalyst performance, through the use of LCA a more insightful account of catalyst performance may be obtained. The improvement observed for a catalyst system upon the increasing content of either iron or palladium can be compared to the environmental impact associated with the preparation of each catalyst system in order to help determine if the improved catalyst performance outweighs the potential increased environmental impact. Figure 4.24 shows, as a percentage, the impacts offset from HCs not being formed *via* traditional routes *vs*. the embodied impacts in forming the same amount of HCs using the catalysts studied within this chapter. For this figure reaction inputs have not been taken into account.

From Figure 4.24 it is possible to tell that increasing iron loadings do result in increasingly better environmentally performing catalysts, meaning the increased environmental

impact of adding increasing iron to the catalyst system is outweighed by the improved catalyst performance. The addition palladium to the catalyst system is necessary in order to produce hydrocarbons larger than propane and as a result the addition of 1 wt% palladium to the system results in a 50 % improvement in environmental impact. When the palladium loading is increased beyond this, despite the improved catalyst performance, it is not sufficient to counteract the increased environmental impact of catalyst preparation which in turn results in a lower relative HC environmental performance. While in terms of catalyst performance 20wt%Fe/SiO_2 appears to be the poorest performing (in terms of conversion and selectivity, Table 4.5 {page 148}) LCA studies suggest that the 20wt%Fe/4wt%Pd/SiO_2 system is in fact the worst performing system based on environmental impacts.

From the LCA findings we can conclude that the addition of palladium to a 20wt%Fe/SiO_2 system is beneficial to the overall catalyst performance. There is, however, an upper limit at which the increased environmental impact of palladium addition no longer outweighs the improved performance. For the addition of increasing iron loading to the system the opposite is true with increasing loading resulting in an improved environmental impact. Catalysts with iron loadings above 40wt% were not studied as increasing loading beyond this point was found to be detrimental to catalyst performance (Table 4.5, page 148).

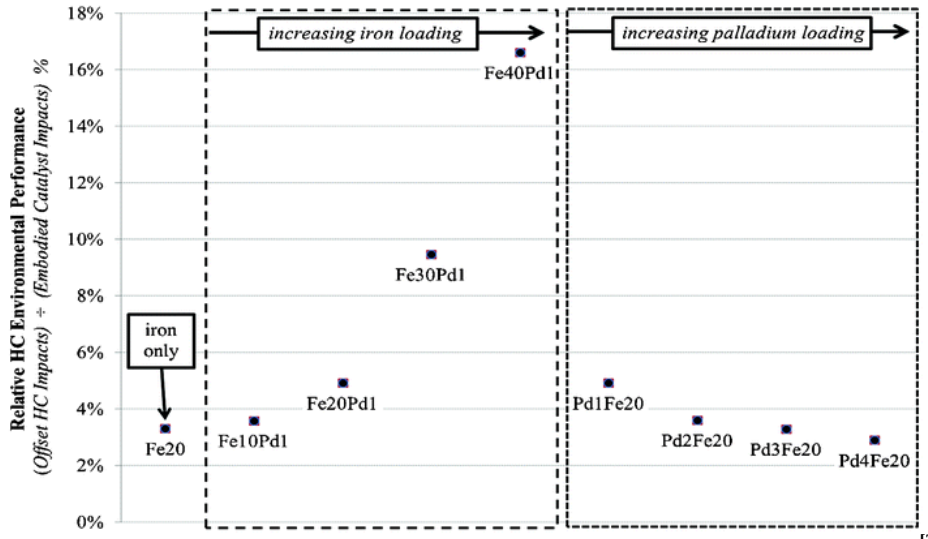

Figure 4.24 – The relative HC environmental performance of each catalyst system.[36]

As Figure 4.24 measures catalyst performance relative to established industrial process currently used for hydrocarbon production it shows that HCs prepared using Fe-Pd catalyst are more impactful. This also excludes the impacts of the in-use phase inputs such as electricity. The comparison of a small scale laboratory batch process such as this to an established and optimised large volume process is an unrealistic prospect and unlikely to ever compete with well-known industrial processes until this method is scaled up.

During the 'in-use' phase of catalysis 95 % of the reaction impact can be attributed to electricity usage. For the purpose of this study electricity has been modelled based on the current UK electricity mix, largely dependent on fossil fuel use which results in significant embodied impacts of electricity generation. In order to obtain as green a process as possible it is envisioned that electricity used for the process would be obtained from renewable sources (burning fuels to create fuels is not sustainable). If the current UK grid mix of electricity was replaced by photovoltaic, off-shore wind or hydropower derived electricity it could result in a 70 %, 90 % and 71- 93 % reduction in impacts respectively. This highlights the importance of renewable electricity for the success of the overall process as mentioned in Chapter 1. The use of renewable energy sources such as those discussed also offers the opportunity for HC production in remote areas which lack access to the electricity grid.

4.8.4 LCA of the CO_2 Hydrogenation Process.

Further work by Griffiths[37] has investigated the overall CO_2 hydrogenation process based on the thermochemical means studied within this chapter. Results have shown that unsurprisingly as performed now, on a laboratory scale, the process is not viable with the CO_2 offset through the production of hydrocarbons in this manner is not high enough to outweigh the CO_2 produced by the process as a whole. However, if the energy used in the process is replaced by renewable electricity (wind) and the recycling of unconverted CO_2 conducted as would be envisaged for the scaled up process then this difference in CO_2 offset can be greatly reduced.

If the excess heat produced by the exothermic Fischer-Tropsch portion of the reaction is utilised to generate electricity, as achieved industrially with many processes, then the difference in CO_2 offset can become minimal. While the GWP of the preparation of the catalyst system represents a relatively small portion (eg. *ca*. 5 % for 20wt%Fe/4wt%Pd/SiO_2) of the overall CO_2 produced by the process careful consideration of catalyst composition and preparation method can play an important in the minimisation of this impact. The catalysts performance plays a more significant role. If catalyst selectivity can be directed towards the more traditionally environmentally harmful to produce hydrocarbons then this can aid the reduction in difference between the GWP of traditional processes and CO_2 hydrogenation methods.

Two other process that are expected to change in the coming future, along with an improvement in catalyst performance, is the effectiveness of carbon capture technology and the difficulty of obtaining HCs through traditional methods. Extensive research is currently ongoing into carbon capture technologies and as such the GWP of the portion of the process is expected to drop drastically. For example Jess *et al*.[38] have already demonstrated that CO_2 can be captured from flue gas and from the atmosphere with reasonable energy requirements and the effectiveness of these processes are expected to increase with further research. As oil supplies continue to dwindle the energy required to extract them is expected to increase. If we predict

that the CO_2 capture technologies become a third as impactful as they are currently and that the formation of hydrocarbons *via* current methods become 3 times more impactful then HC production through CO_2 hydrogenation using some of the more successful catalysts within this study beings to become viable. Further improvements in catalyst performance would increase the amount of CO_2 being offset using CO_2 hydrogenation methods relative to currently used methods.

4.8.5 Summary

The Fe-Pd catalysts tested within this chapter were analysed using LCA in order to establish their embodied environmental impacts. Through LCA it was found that the most significant impacts for catalyst preparation were due to the use of palladium as a promoter and the energy requirements for the process, specifically the electricity required. The usage of iron, silica, other chemicals such as solvents and infrastructure contribution were minimal in comparison. The impact of the in-use phase of reaction could be reduced by as much as 93 % if renewable energy was used to replace the current UK electricity mix highlighting the importance of renewable energy for CDU processes.

Increasing iron loading resulted in an increased conversion and better selectivity to heavier more valuable HCs, this enhanced catalyst performance outweighs the negative environmental impacts associated with larger iron content. While the introduction of palladium is essential to achieve a catalyst that shows a sufficient CO_2 conversion and product selectivity when increased above a 1 wt% loading the improvements in catalyst performance observed are not significant to outweigh the increased environmental impacts with the 20wt%Fe/4wt%Pd/SiO_2 catalyst the poorest performing system in terms of environmental impact.

Although LCA studies show as the process currently stands on a lab scale it is not viable, producing more CO_2 than is offset by the production of HCs in this manner, if the use of renewable energies and excess heat recovery are taken into account this can be counteracted. If the effectiveness of carbon capture is improved in the near future and the formation of HCs through traditional methods becomes more impactful then the process should become viable even with some current catalysts. The further improvement of catalyst performance along with careful control of the embodied impacts of catalyst preparation should aid the reduction in timeframe until the process can become viable.

4.9 Chapter Conclusions

This chapter focused on the optimisation of a 20wt%Fe/1wt%Pd/SiO_2 catalyst system for CO_2 hydrogenation. The work was complimented by LCA analysis investigating the environmental impacts of the overall process with a focus on the embodied impacts of catalyst preparation and their relationship to performance.

The iron content of the catalyst system was found to have a significant impact on the catalyst performance with both CO_2 conversion and selectivity towards heavier hydrocarbons increased when a loading of 40 wt% was utilised. CO/H_2 catalyst tests indicate that this is related to an improved FT activity. The addition of palladium to an Fe/SiO_2 system was shown to significantly improve catalyst performance with higher palladium content resulting in increasing chain growth probabilities. The addition of palladium is seen to reduce the catalyst selectivity towards unsaturated HCs.

The effect of catalyst support properties was also investigated with the physical properties of the silica used having the largest impact on the catalyst performance of the three catalyst components. Large silica pore sizes are observed to result in increased chain growth probability and increased selectivity towards heavier hydrocarbons. The relationship between silica properties and HC yield/CO_2 conversion is slightly more complex with increased conversion appearing to be dependent on a combination of both pore size and surface area.

While an increased reaction pressure can enhance the catalysts CO_2 hydrogenation ability this occurs at the cost of C_2+ selectivity. TEM analysis of used catalysts showed an increased nano-particle size after catalyst use. It is possible that this morphology change is responsible for the initial stabilisation period observed.

LCA studies indicated that the most significant impacts in catalyst preparation were due to the use of palladium as a promoter and the electricity required. While the improved performance observed with increasing iron loading was seen to outweigh the increased environmental impact associated with using more iron the same was not true for palladium. The initial introduction of 1 wt% palladium is necessary to provide a catalyst with a high enough performance however if palladium content is increased beyond this 1 wt% loading the improvement in catalyst performance does not outweigh the increased environmental impacts associated with use of higher quantities of palladium.

While the lab scale process reported within this chapter are, as expected, not viable from an environmental standpoint further LCA work has shown that should the electricity and hydrogen be obtained from renewable means and the process scaled up it has the potential to become environmentally viable. Further improvements in catalyst performance with careful consideration of the components used in catalyst preparation are required.

4.10 Future Work

The use of palladium has proved successful as a promoter for iron-based catalysts utilised for CO_2 hydrogenation. While noble metals have attracted significant attention in FT catalysis their use in iron-based CO_2 hydrogenation has been limited with only studies on ruthenium reported thus far. As such the expansion of the work reported within this chapter to include a range of other noble metals such as platinum and rhodium is worth investigating. The use of LCA proved useful in determining if the addition of palladium enhanced the catalyst performance sufficiently

enough to outweigh the increased environmental impact associated with its use. Similar studies should be conducted with other noble metals in order to ascertain if the same is true.

The life cycle assessment of CO_2 hydrogenation catalysts containing promoters known to be less environmentally harmful than palladium, such as potassium, should also be conducted in order to determine how far current catalyst are from reaching the targets required, from a catalyst performance point of view.

4.11 References

[1] R. L. Espinoza, A. P. Steynberg, B. Jager, A. C. Vosloo, *Appl. Catal., A* **1999**, *186*, 13-26.

[2] T. Riedel, G. Schaub, K. W. Jun, K. W. Lee, *Ind. Eng. Chem. Res.* **2001**, *40*, 1355-1363.

[3] (a) J. P. O'Byrne, R. E. Owen, D. R. Minett, S. I. Pascu, P. K. Plucinski, M. D. Jones, D. Mattia, *Catal. Sci. Tech.* **2013**, *3*, 1202-1207; (b) P. S. Sai Prasad, J. W. Bae, K. W. Jun, K. W. Lee, *Catal. Surv. Asia* **2008**, *12*, 170-183.

[4] A. Faur Ghenciu, *Curr. Opin. Solid State Mater. Sci.* **2002**, *6*, 389-399.

[5] G. S. Yablonsky, R. Pilasombat, J. P. Breen, R. Burch, S. Hengrasmee, *Chem. Eng. Sci.* **2010**, *65*, 2325-2332.

[6] (a) J. W. Niemantsverdriet, D. P. Aschenbeck, F. A. Fortunato, W. N. Delgass, *J. Mol. Catal.* **1984**, *25*, 285-293; (b) F. Diehl, A. Y. Khodakov, *Oil Gas Sci. Technol.- Rev. IFP* **2009**, *64*, 11-24.

[7] R. J. Gorte, S. Zhao, *Catal. Today* **2005**, *104*, 18-24.

[8] (a) M. Luo, R. O'Brien, B. Davis, *Catal. Lett.* **2004**, *98*, 17-22; (b) M. Minnermann, S. Pokhrel, K. Thiel, R. Henkel, J. Birkenstock, T. Laurus, A. Zargham, J. I. Flege, V. Zielasek, E. Piskorska-Hommel, J. Falta, L. Mädler, M. Bäumer, *J. Phys. Chem., C* **2010**, *115*, 1302-1310.

[9] D. B. Bukur, X. Lang, D. Mukesh, W. H. Zimmerman, M. P. Rosynek, C. Li, *Ind. Eng. Chem. Res.* **1990**, *29*, 1588-1599.

[10] (a) T. Herranz, S. Rojas, F. J. Pérez-Alonso, M. Ojeda, P. Terreros, J. L. G. Fierro, *Appl. Catal., A* **2006**, *308*, 19-30; (b) C. Pirola, C. L. Bianchi, A. Di Michele, S. Vitali, V. Ragaini, *Catal. Commun.* **2009**, *10*, 823-827.

[11] A. A. Adesina, *Appl. Catal., A* **1996**, *138*, 345-367.

[12] P. S. Sai Prasad, J. Bae, K. W. Jun, K. W. Lee, *Catal. Surv. Asia* **2008**, *12*, 170-183.

[13] D. B. Bukur, C. Sivaraj, *Appl. Catal., A* **2002**, *231*, 201-214.

[14] M. D. Jones, C. G. Keir, C. D. Iulio, R. A. M. Robertson, C. V. Williams, D. C. Apperley, *Catal. Sci. Technol.* **2011**, *1*, 267-272.

[15] N. Yan, F. Wang, H. Zhong, Y. Li, Y. Wang, L. Hu, Q. Chen, *Sci. Rep.* **2013**, *3*.

[16] L. Peng, E. Y. Jiang, H. L. Bai, *J. Phys., D: Appl. Phys.* **2011**, *44*, 075003.

[17] M. Peuckert, *J. Phys. Chem.* **1985**, *89*, 2481-2486.

[18] M. Fujiwara, H. Ando, M. Matsumoto, Y. Matsumura, M. Tanaka, Y. Souma, *Chem. Lett.* **1995**, *24*, 839-840.

[19] Ø. Borg, S. Eri, E. A. Blekkan, S. Storsæter, H. Wigum, E. Rytter, A. Holmen, *J. Catal.* **2007**, *248*, 89-100.

[20] M. V. Cagnoli, S. G. Marchetti, N. G. Gallegos, A. M. Alvarez, A. A. Yeramian, R. C. Mercader, *Mater. Chem. Phys.* **1991**, *27*, 403-418.

[21] C. H. Zhang, H. J. Wan, Y. Yang, H. W. Xiang, Y. W. Li, *Catal. Commun.* **2006**, *7*, 733-738.

[22] A. Y. Khodakov, A. Griboval-Constant, R. Bechara, V. L. Zholobenko, *J. Catal.* **2002**, *206*, 230-241.
[23] (a) G. P. Van Der Laan, A. A. C. M. Beenackers, *Catal. Rev.* **1999**, *41*, 255-318; (b) Z. Yan, Z. Wang, D. B. Bukur, D. W. Goodman, *J. Catal.* **2009**, *268*, 196-200; (c) V. A. de la Pena O'Shea, M. C. Alvarez-Galvan, J. M. Campos-Martin, J. L. G. Fierro, *Catal. Lett.* **2005**, *100*, 105-116.
[24] R. L. Espinoza, A. P. Steynberg, B. Jager, A. C. Vosloo, *Appl. Catal., A* **1999**, *186*, 13-26.
[25] E. de Smit, F. M. F. de Groot, R. Blume, M. Havecker, A. Knop-Gericke, B. M. Weckhuysen, *PCCP* **2010**, *12*, 667-680.
[26] A. N. Pour, M. R. Housaindokht, S. F. Tayyari, J. Zarkesh, *J. Nat. Gas Chem.* **2010**, *19*, 362-368.
[27] E. de Smit, B. M. Weckhuysen, *Chem. Soc. Rev.* **2008**, *37*, 2758-2781.
[28] C. D. Wagner, G. E. Muilenberg, *Handbook of x-ray photoelectron spectroscopy: a reference book of standard data for use in x-ray photoelectron spectroscopy*, Physical Electronics Division, Perkin-Elmer Corp., **1979**.
[29] S. T. Oyama, *Chemistry of Transition Metal Carbides and Nitrides*, Springer, **1996**.
[30] (a) P. A. Holman, D. R. Shonnard, J. H. Holles, *Ind. Eng. Chem. Res.* **2009**, *48*, 6668-6674; (b) K. G. Harding, J. S. Dennis, H. von Blottnitz, S. T. L. Harrison, *J. Clean. Prod* **2008**, *16*, 1368-1378.
[31] I. Wrightson, S. Cooper , M. Crookes, N. King, P. Lewis, J. Larner, D. Lohmann, C. Maxwell, D. Sanderson, S. Lipworth, *RSC: Environmental,Health and Saftey Committee Note on: Life Cylce Asscessment*, 3 ed., **15 Feb 2010**.
[32] (a) ISO, *in ISO 14040:2006. Environmental Management - Life Cycle Assessment - Principles and Framework*, BSI, **2006**; (b) ISO, *In Environmental Management- Life Cycle Assessment - Requirements and Guidelines*, BSI, **2006**.
[33] *Ecoinvent Database v2.2*, May 2010 ed.
[34] IPCC, *International Panel on Climate Change, Fourth assessment report: Climate change 2007*, **2007**.
[35] M. Goedkoop, R. Heijungs, M. Huijbergts, A. Schryver, J. Struijs, R. Zelm, *ReCiPe: A life cylce impact assessment method which comprises harmonised category indicators at the midpoint and the endpoint level*, **2009**.
[36] O. G. Griffiths, R. E. Owen, J. P. O'Byrne, D. Mattia, M. D. Jones, M. C. McManus, *R. Soc. Chem. Adv.* **2013**, *3*, 12244-12254.
[37] O. G. Griffiths, *PhD Thesis, University of Bath* **2014**.
[38] A. Jess, P. Kaiser, C. Kern, R. B. Unde, C. von Olshausen, *Chem. Ing. Tech.* **2011**, *83*, 1777-1791.

5 Introduction of Group 11, 12 and 13 Promoters for Iron-Silica Catalysts and Their Influence on Product Distribution

The promotional effects of Group 11, 12 and 13 metals on iron-silica catalyst systems have been investigated. While high loadings of copper, zinc and gallium proved to inhibit catalyst activity the introduction of low (1 wt%) loadings other Group 11 and 13 metals proved more successful with indium and gold both giving catalysts with larger CO_2 conversion values and higher selectivities to olefins.

With both iron and cobalt catalysts being utilised industrially for the Fischer-Tropsch (FT) process the majority of attention on CO_2 hydrogenation catalysts has been focused on catalysts utilising these two metals as the main active component.[1] Initial investigations have however shown cobalt to be largely unsuitable due to high selectivity towards methane,[2] a property attributed to the low water-gas shift (WGS) activity possessed by cobalt based systems.[3] Iron systems have been shown to be active for both the RWGS and FT processes, when combined with its lower cost, relative to cobalt, this makes iron the ideal starting point for investigations into CO_2 hydrogenation. Iron based systems have, as a result, been the focus of a significant proportion of catalyst studies.[4]

A larger proportion of research has thus far focused on the formation of liquid (C_5+) HCs[5] with the idea of utilising them as replacement fuels in the transport industry. There is also a renewed interest in the formation of lower (C_2-C_4) olefins.[6] There is currently a high demand for unsaturated C_2-C_4 HCs as they are important chemical building blocks used extensively in the manufacture of polymers, solvents, drugs, cosmetics and detergents.[7] The use of lower olefins for the production of jet fuel through their oligomerisation over solid acid catalysts has also been attracting the attention of the U.S. Navy.[8]

So far many of the schemes for the renewable production of lower olefins rely on multistep processes such as the formation of methanol followed by the methanol to olefin (MTO) process.[9] As a result there has been renewed interest in the single step Fischer-Tropsch to olefin (FTO) process,[6b] whereby CO is converted directly into lower olefins. Studies have shown that a similar process is also possible using a CO_2/H_2 feed, a process denoted CO_2LO. Relatively little attention has, however, been focused in this area. In order to direct selectivity towards shorter chained HCs FTO is generally conducted at higher temperatures than traditional FT (> 300 ^oC); these conditions should also favour the formation of CO through the RWGS reaction if CO_2 is used as a reaction feedstock. Recently Centi *et al.*[10] investigated the economic factors associated with the use of CO_2 as a possible feedstock for the formation of lower olefins and their studies suggest that the process is close to becoming environmentally viable and as such detailed studies in the field should *"not be delayed"*.

When used alone iron catalysts possess several problems[4] such as a high selectivity to undesired products such as methane and they can also undergo rapid deactivation under reaction conditions. Catalysts utilised for FT synthesis often contain additives to promote structural and chemical properties while also stabilising the active phases present during catalysis. A similar approach has been used with CO_2 hydrogenation catalysts with several studies investigating the effects of additives on catalyst activity, product distribution and catalyst stability having been undertaken.[4]

One promoter that has shown promise in the field of CO_2LO is the addition of potassium to iron based catalysts. Work by Xu *et al.*[11] investigated the addition of potassium to Fe-Mn-SiO_2 catalyst systems and found that the addition of 10 wt% potassium led to a 13.5 mol % increase in selectivity towards C_2-C_4 olefins. New promoters are still required for CO_2 hydrogenation with the ability to increase conversion and direct HC selectivity towards more valuable products. The aim of this chapter is a fundamental study into the effects of promoters on iron-based catalyst systems and their impacts on CO_2 conversion and product distribution.

5.1 Addition of Copper, Zinc and Gallium to Iron-Silica Catalysts

Silica was utilised as a structural promoter for each iron based catalyst system studied within this chapter as it has been shown to improve catalyst stability[12] and increase catalyst surface area.[13] For all tests conducted within this chapter the support used was kept constant; Davisil, particle size 35-70 µm, pore size 250 Å.

Copper and zinc have both been shown to be active for the RWGS[14] and so in an attempt to improve the initial reduction of CO_2 to CO *via* the RWGS reaction their addition to an iron-silica catalyst system was investigated. While both copper and zinc have been used in conjunction with iron systems for CO_2 hydrogenation previously these systems have generally been tested at high pressures typically in the range 1.5 MPa – 5 MPa[15] with no studies conducted at atmospheric pressure. Gallium has also been shown to be RWGS active,[16] however, it has not been employed in conjunction with iron catalysts for the hydrogenation of CO_2.

5.1.1 Catalyst Preparation

Each catalyst system was prepared with a 2:1 iron to additional metal ratio giving four catalyst systems; 20wt%Fe/10wt%Cu/SiO_2, 20wt%Fe/10wt%Zn/SiO_2, 20wt%Fe/10wt%Ga/SiO_2 and a non-promoted 20wt%Fe/SiO_2 catalyst for comparison. Catalysts containing zinc and copper were prepared using a wet impregnation (WI) technique (detailed in Chapter 2 Section 2.7.9) similar to that used by Jones *et al.*[17] using $Fe(NO_3)_3 \cdot 9H_2O$, $Cu(OAc)_2 \cdot H_2O$ and $Zn(OAc)_2 \cdot 2H_2O$ as precursors for each of the metals used, all catalyst systems prepared using this method are denoted hereafter with the suffix '-WI'. Due to the air sensitive nature of the gallium precursor ($GaCl_3$) the catalyst system containing gallium was prepared using standard

Schlenk line techniques as detailed in Chapter 2 Section 2.7.10. In order to determine the influence of catalyst preparation and as a comparison for the 20wt%Fe/10wt%Ga/SiO_2 system a 20wt%Fe/SiO_2 system was also prepared using Schlenk line (SL) techniques, all systems prepared using this technique are denoted with the suffix '-SL'.

5.1.2 Catalyst Characterisation

Each of the prepared catalyst systems were analysed using a range of different characterisation techniques. Table 5.1 shows the BET surface areas calculated for each catalyst system. Addition of any metals to the surface of the catalyst results in a reduction of the measured surface area relative to the silica support alone. The values calculated for the 20wt%Fe/SiO_2 system prepared using the wet impregnation method is higher than that for the analogous system prepared *via* the Schlenk line method. The addition of copper to the catalyst system results in a slight increase relative to the iron only system whereas zinc addition results in a reduction in surface area. Gallium addition was observed to lead to a reduction in the surface area measured for the catalyst system relative to the 20wt%Fe/SiO_2-SL system.

Table 5.1 – BET surface areas determined for each catalyst system

Catalyst[a]	**BET Surface Area (m^2g^{-1})**
Unused SiO_2 support	287.6
20wt%Fe/SiO_2-WI	218.7
20wt%Fe/10wt%Cu/SiO_2-WI	223.3
20wt%Fe/10wt%Zn/SiO_2-WI	190.3
20wt%Fe/SiO_2-SL	195.5
20wt%Fe/10wt%Ga/SiO_2-SL	180.2

[a] – Suffix indicates the preparation method used for each catalyst. WI: wet impregnation method and SL: Schlenk line method

The morphology of each catalyst system was investigated through the use of SEM. Representative images typical for 20wt%Fe/SiO_2-WI, 20wt%Fe/10wt%Cu/SiO_2-WI, 20wt%Fe/10wt%Zn/SiO_2-WI and 20wt%Fe/10wt%Ga/SiO_2 are shown in Figure 5.1 along with EDX spectra recorded in conjunction with SEM imaging. Peaks attributable to silicon, oxygen and iron are observed in all EDX spectra showing the successful loading of iron to the support in all cases. Peaks for copper, zinc and gallium are also observed in the appropriate samples showing that the promoter metals are successfully loaded. The observation of similar spectra across the catalyst surfaces suggests all metals are well and evenly distributed for each catalyst sample. No distinct change in catalyst morphology is observed upon the introduction of copper and zinc to the iron-silica catalyst. The gallium system {Figure 5.1 (d)} does, however, show a

change in morphology relative to the samples prepared using the wet impregnation method with smaller catalyst particles. This change in morphology can be attributed to the Schlenk line methods used in catalyst preparation with an extended period of stirring using this method possibly leading to the break-up of the silica support particles. The method of solvent removal may also play a role.

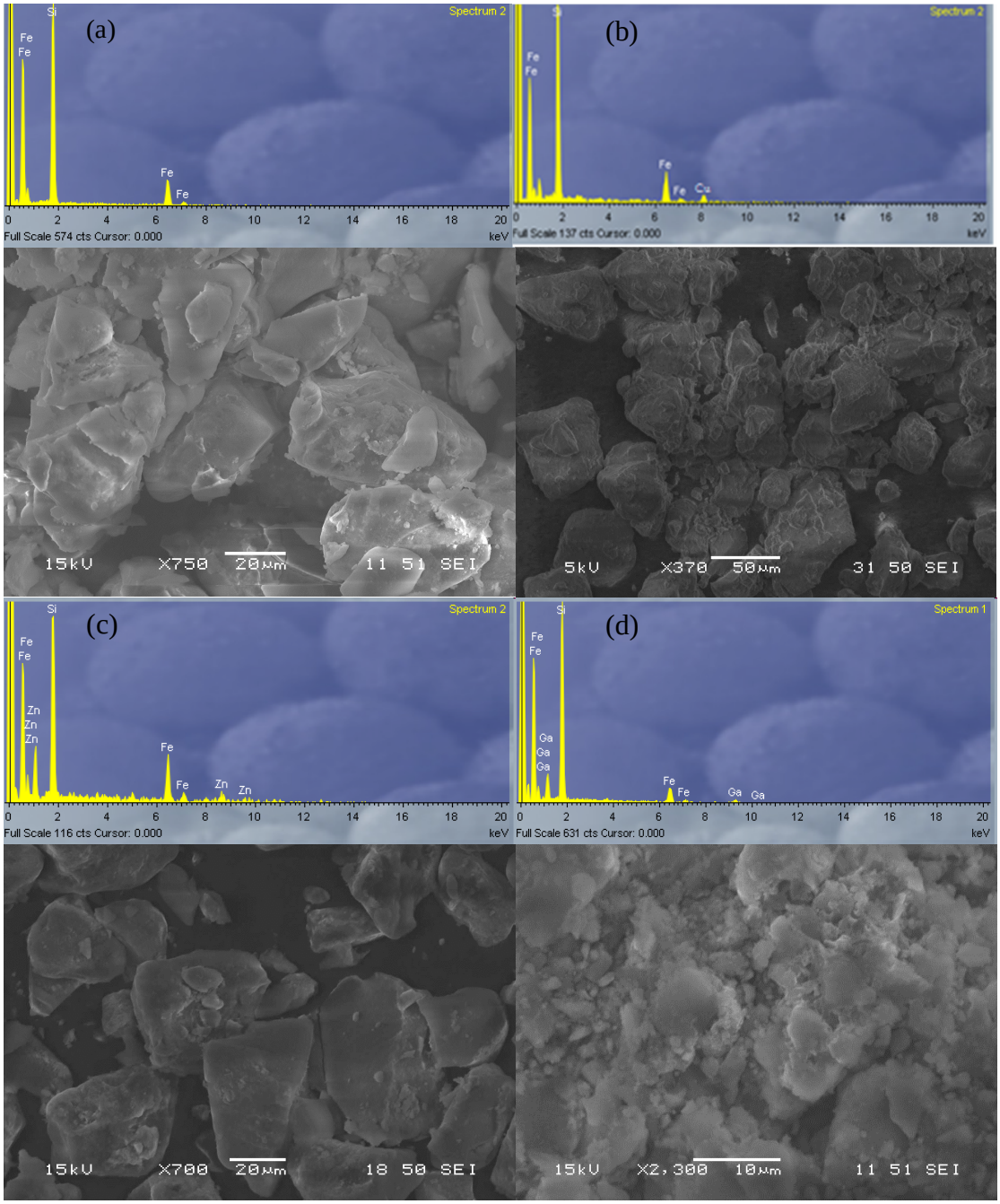

Figure 5.1 - SEM images and EDX spectra recorded for: (a) 20wt%Fe/SiO_2-WI, (b) 20wt%Fe/10wt%Cu/SiO_2-WI, (c) 20wt%Fe/10wt%Zn/SiO_2-WI, (d) 20wt%Fe/10wt%Ga/SiO_2-SL.

Each catalyst system was studied using XRD, however, no peaks attributable to any copper, zinc or gallium phase were observed. XPS studies were conducted in order to gain a deeper understanding of the metal phases present in each catalyst system. Figure 5.2 shows the

spectra recorded from these studies. Figure 5.2 (a) shows the Fe 2p region for four of the catalysts tested. 20wt%Fe/SiO_2-WI shows a binding energy of 710.3 eV with a satellite peak at 719 eV representative Fe^{3+} likely in its Fe_2O_3 oxide form.[18] Little change is observed upon the introduction of copper, zinc and gallium to the system with Fe_2O_3 remaining the main iron phase present. Detailed scans of the Cu 2p, Zn 2p and Ga 2p regions shows the presence of peaks at 933.0 eV, 1022.2 eV and 1117.9 eV respectively which can be attributed to CuO,[19] ZnO[20] and Ga_2O_3.[21]

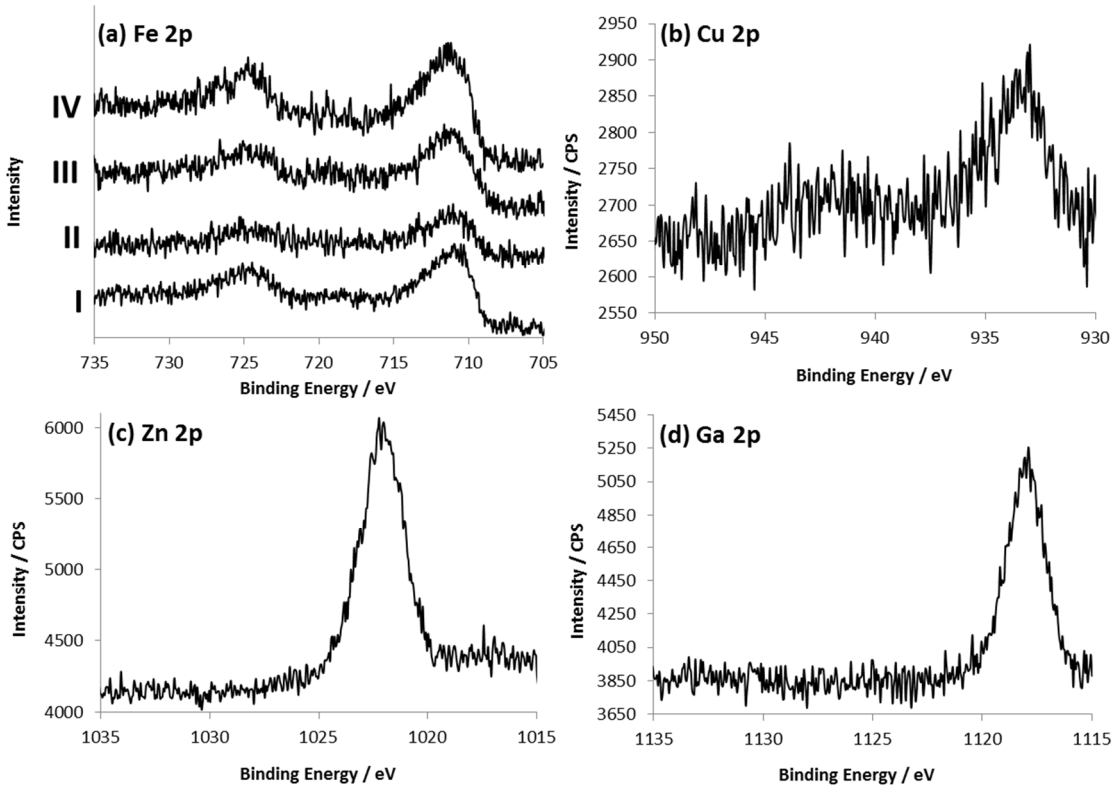

Figure 5.2 – XPS spectra recorded for (a i) Fe2p region of 20wt%Fe/SiO_2-WI, (a ii) Fe2p region of 20wt%Fe/10wt%Cu/SiO_2-WI, (a iii) Fe2p region of 20wt%Fe/10wt%Zn/SiO_2-WI, (a iv) Fe2p region of 20wt%Fe/10wt%Ga/SiO_2-SL, (b) Cu 2p region of 20wt%Fe/10wt%Cu/SiO_2-WI, (c) Zn 2p region of 20wt%Fe/10wt%Zn/SiO_2-WI and (d) Ga 2p region of 20wt%Fe/10wt%Ga/SiO_2-SL.

5.1.3 Catalyst Testing

All prepared catalyst systems were tested for their CO_2 hydrogenation ability at atmospheric pressure. Typically 0.7 g of catalyst was packed into Reactor 1 (See Chapter 2 Section 2.2 for full details). All catalysts were pre-treated under a flow of pure hydrogen at 300 ^oC for 2 hours. Once the reduction stage was completed the reactor was heated to 370 ^oC under a flow of argon before CO_2 and H_2 were introduced at flows of 2 sccm and 6 sccm respectively. Full details of the catalyst testing procedures can be found in Chapter 2 Section 2.3.

Table 5.2 summarises the catalytic data obtained from these catalyst tests. The catalyst preparation method was found to influence the performance of the catalyst both in terms of conversion and selectivity. A comparison of 20wt%Fe/SiO_2-WI and 20wt%Fe/SiO_2-SL shows that the wet impregnation method is more effective with a slightly increased hydrocarbon yield and slightly higher selectivity towards C_2+ HCs. The difference between catalyst performance is, however, only small and likely attributable to the different catalyst morphology with the lower surface area calculated for 20wt%Fe/SiO_2-SL possibly playing a role.

Table 5.2 – Catalytic data obtained for Fe-M-SiO_2 catalysts (where M = Cu, Zn, Ga or no metal)

Catalyst[a]	**CO_2 Conv. (%)**	**CO Yield (%)**	**HC Yield (%)**	**HC Selectivity (%)**			O/(O+P)[b] in C_2-C_4
				C_1	**C_2-C_4**	**C_5+**	
20wt%Fe/SiO_2-WI	34.8	9.3	25.6	64.5	35.3	0.2	6.0
20wt%Fe/10wt%Cu/SiO_2-WI	24.9	14.2	10.7	67.6	32.3	0.1	5.0
20wt%Fe/10wt%Zn/SiO_2-WI	7.9	7.0	0.9	100.0	0.0	0.0	0.0
20wt%Fe/SiO_2-SL	30.1	7.2	22.9	68.9	30.8	0.3	2.4
20wt%Fe/10wt%Ga/SiO_2-SL	6.5	5.8	0.7	100.0	0.0	0.0	0

[a] – Suffix indicates the preparation method used for each catalyst. WI – wet impregnation method and SL – Schlenk line method [b] - Olefin content (mol percentage) for C_2-C_4 hydrocarbons, calculated as [olefin(O) / (olefin(O) + paraffin(P)) × 100]. Catalyst tests conducted at atmospheric pressure, H_2:CO_2 ratio 3:1, total flow – 8 sccm. 0.7 g of catalyst. Conversions, yields and product distributions calculated after 5 hours on stream.

Under the ambient pressure utilised in catalyst tests the addition of 10 wt% copper, zinc and gallium is observed to decrease the CO_2 conversion values and direct selectivity away from the desired heavier hydrocarbons and towards methane. No improvement in olefins selectivity is observed for any catalyst system. The performance of the copper and zinc containing catalysts appear to contradict the results observed by Ando *et al.*[15a] and Nam *et al.*[15b] respectively where similar loadings of both copper and zinc were found to be beneficial to catalyst performance. This difference is likely due to the higher pressures (5 MPa and 1 MPa, respectively) under which their catalyst systems were tested.

The HC distribution obtained with the 20wt%Fe/10wt%Cu/SiO_2 catalyst was found to obey the Anderson Schulz Flory (ASF) distribution as seen with the 20wt%Fe/SiO_2-WI catalyst (Figure 5.3) showing that HC formation occurs *via* the FT process.[22] This confirms that the systems are both forming HCs based on the CO mediated mechanism and not the methanol mediated process. No methanol was observed in the products of any of the catalyst systems tested, methanol has been observed for copper containing systems at higher pressures.[15a] With the zinc and gallium containing systems methane is formed exclusively and as such it is not possible to determine whether HCs are formed by the FT process or not based on an ASF plot.

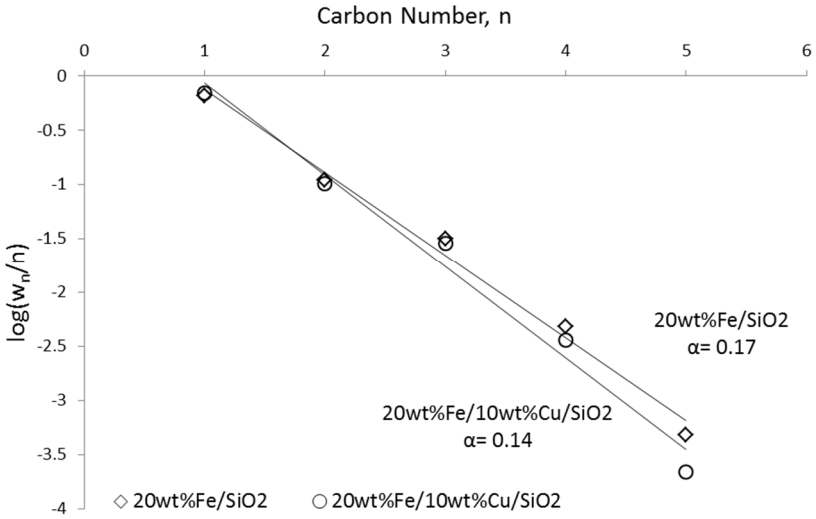

Figure 5.3 –ASF plots for (a) 20wt%Fe/SiO_2-WI and (b) 20wt%Fe/10wt%Cu/SiO_2-WI

The reduction in catalytic activity observed upon the introduction of high loadings of copper, zinc and gallium could be due to the coating of the iron present on the catalyst surface and hence blocking of active sites. Each additional metal, M, (where M = Cu, Zn and Ga) was introduced in such an amount as to give a Fe:M ratio of 2:1. XPS studies conducted on each catalyst showed that the surface Fe:M ratio for each system was 2:2.34, 2:6.22 and 2:1.7 for the copper, zinc and gallium systems respectively. This ratio being lower than expected indicates a lower concentration of iron present at the catalyst surface supporting the suggestion that each of the additional metals may be coating the surface iron and preventing access during reaction. If no favourable interactions for catalysis are occurring between the added metal and iron and each is simply acting as a diluent, blocking or reducing the number of active sites then both the copper and gallium catalyst would be expected to have a similar reduction in activity as both show a surface Fe:M ratio of approximately 1:1. This is, however, not the case as a significant reduction in catalytic activity is observed upon gallium addition whereas the introduction of copper results in only a slight decrease in CO_2 conversion. This suggests that while the copper system may possess promotional properties the effect could be over shadowed by the high loading that at atmospheric pressure appears to be inhibiting catalyst activity. An alternative possibility is that the gallium is actively inhibiting iron's activity for CO_2 hydrogenation.

5.2 Promotion of Iron-Silica Catalysts with Group 11 Metals

There are some suggestions of the promotional effects of copper possibly being masked by the high loadings trialled thus far (Table 5.2). As such, investigations were conducted in order to determine whether the promotional properties of copper can be utilised at ambient pressures by its introduction in lower amounts (1 wt%). In this case it would be expected that any blocking/inhibiting effects likely caused by the high amounts of copper present in the catalyst

system would be greatly reduced. The investigation was extended to include silver and gold in order to determine how the promotional abilities varied down Group 11.

5.2.1 Catalyst Preparation

1 wt% of copper, silver and gold were introduced to an iron-silica system containing 20 wt% iron giving four different catalyst compositions; 20wt%Fe/SiO_2, 20wt%Fe/1wt%Cu/SiO_2, 20wt%Fe/1wt%Ag/SiO_2 and 20wt%Fe/1wt%Au/SiO_2. Catalyst systems containing copper and silver {$Cu(OAc)_2$ H_2O and $AgNO_3$ metal precursors} were prepared using the wet impregnation method as utilised for some catalyst in Section 5.1.1 (See Chapter 2 Section 2.7.9 for full details) and are denoted by the suffix 'WI'. Owing to the use of chloroauric acid as the catalyst precursor for the gold containing catalyst systems a co-precipitation method more suited to this precursor was employed (See Chapter 2 Section 2.7.11 for full details). All catalysts prepared using this technique are denoted by the suffix 'PPT' hereafter. The 20wt%Fe/1wt%Au/SiO_2-PPT catalyst cannot be directly compared to the 20wt%Fe/SiO_2-WI system due to the differing preparation methods employed so in order to ascertain the promotional ability of gold a 20wt%Fe/SiO_2-PPT system was also prepared

5.2.2 Catalyst Characterisation

Each catalyst system was investigated using a range of characterisation techniques. N_2 physisorption studies were conducted and used to calculate the specific BET surface area for the each of the catalyst system, the results are summarised in Table 5.3. Generally the catalysts prepared through the wet impregnation technique give a lower surface area than those prepared *via* the precipitation method. The addition of copper and silver to each system results in a slight increase in surface area. The addition of 1 wt% gold to the 20wt%Fe/SiO_2-PPT system however results in a decrease in catalyst surface area. Figure 5.4 shows SEM images for 20wt%Fe/SiO_2-WI and 20wt%Fe/SiO_2-PPT which are representative for the catalyst morphology observed for catalysts prepared *via* each of the methods. A distinct difference in catalyst morphology is observed for each preparation method with the catalyst prepared using the co-precipitation method appearing to give a much more irregular surface relative to the wet impregnation method. This difference in catalyst morphology could account for the higher surface area calculated for the catalysts prepared using the precipitation method.

TEM studies conducted on each of the 20wt%Fe/SiO_2 systems (Figure 5.4) also reveals a significant change in catalyst morphology. The systems prepared *via* a wet impregnation method show a mean particle diameter of 54 nm with an even distribution of particle sizes from 20 nm up to 100 nm. TEM images recorded for the systems prepared using a precipitation technique show the presence of significantly smaller particles with an average size of approximately 3 nm, a narrower distribution is also noted.

Table 5.3 – BET areas determined for each catalyst system

Catalyst[a]	BET Surface Area (m^2g^{-1})
20wt%Fe/SiO_2-WI	218.7
20wt%Fe/1wt%Cu/SiO_2-WI	233.0
20wt%Fe/1wt%Ag/SiO_2-WI	227.0
20wt%Fe/SiO_2-PPT	324.4
20wt%Fe/1wt%Au/SiO_2-PPT	283.1

[a] – Suffix indicates the preparation method used for each catalyst. WI: wet impregnation method and PPT: precipitation method

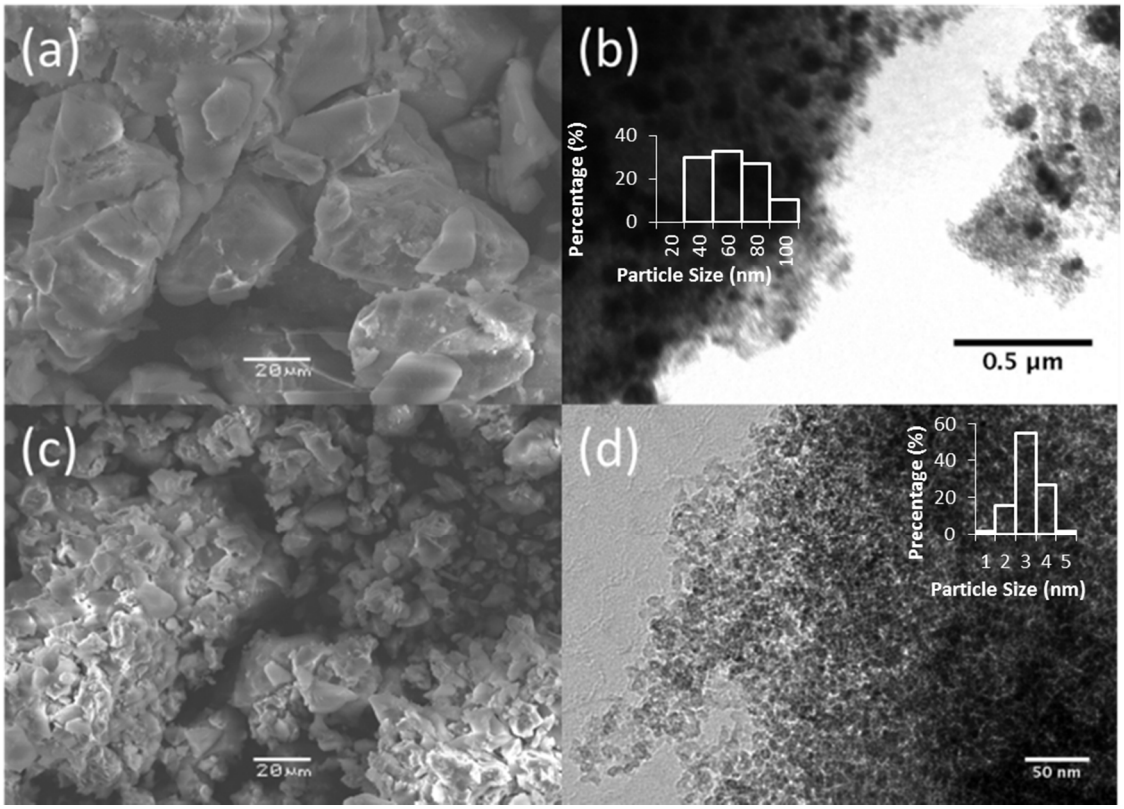

Figure 5.4 – (a) SEM image recorded for 20wt%Fe/SiO_2-WI representative of all catalyst systems prepared using the wet impregnation technique. (b) TEM image recorded 20wt%Fe/SiO_2-WI again representative of all catalysts prepared using the wet impregnation technique. Insert – particle size distribution. (c) A typical SEM image recorded for 20wt%Fe/SiO_2-PPT representative for all catalysts prepared using the precipitation method. (d) TEM image recorded 20wt%Fe/SiO_2-PPT again representative of all catalysts prepared using the precipitation method. Insert – particle size distribution.

pXRD studies were conducted on each of the catalyst systems. Figure 5.5 (a) shows example diffraction patterns obtained from these studies. The 20wt%Fe/SiO_2 system prepared using the wet impregnation technique shows weak peaks at 33, 36, 41, 50 and 54 ^{o} characteristic for α-Fe_2O_3.[23] When the same catalyst system was prepared using the precipitation technique no diffraction peaks were observed suggesting that any crystalline phases are too small to be

detected. Raman studies on samples prepared using both methods were conducted with the spectra obtained from 20wt%Fe/SiO_2-WI and 20wt%Fe/SiO_2-PPT shown in Figure 5.5 (b). Major resonances were observed at 225, 239, 290, 408, 487, 608 and 1312 cm^{-1} for both samples characteristic of iron oxide in its α-Fe_2O_3 form.[24] This further confirms what is observed by pXRD for the wet impregnation prepared catalyst and confirms that iron is present in the same form for the precipitation sample even if this phase is not detected by pXRD.

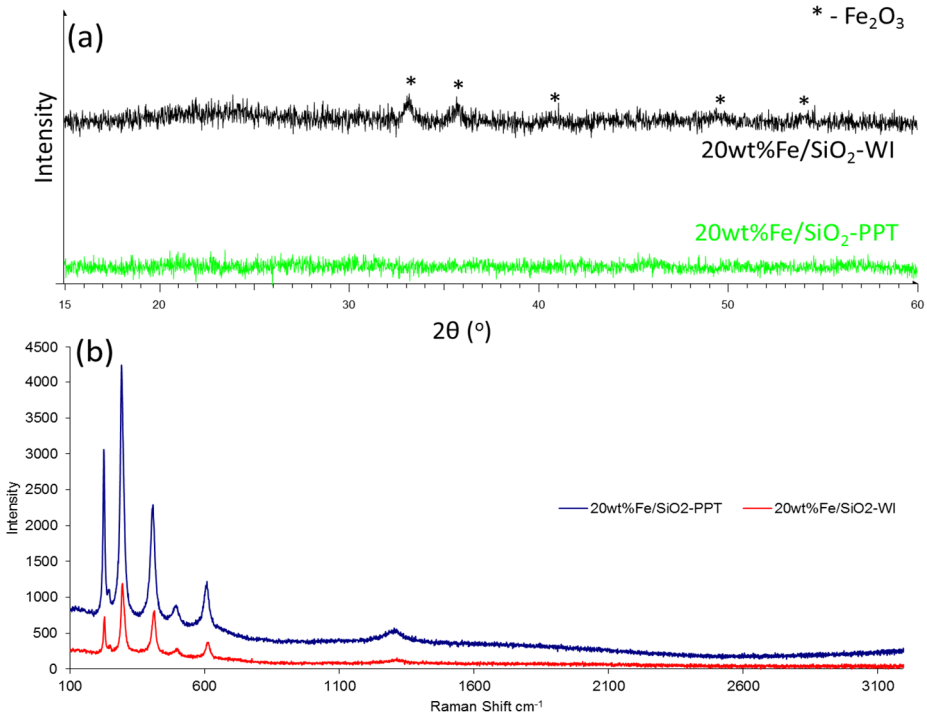

Figure 5.5 – (a) XRD patterns recorded for the 20wt%Fe/SiO_2 samples are prepared using the wet impregnation and precipitation methods. (b) Raman spectra recorded for 20wt%Fe/SiO_2 as prepared using both the wet impregnation and precipitation techniques.

XPS studies were conducted on each of the prepared samples in order to investigate the effect of the promoter metals on the oxidation of the iron present and each promoter. Figure 5.6 shows a selection of the spectra recorded. Detailed scans of the Fe 2p region indicates iron is present as Fe_2O_3 with little effect on the binding energy observed upon the introduction of any promoter species. A scan in the 365 to 380 eV range reveals a peak at 368.4 eV typical for the presence of silver in its metallic Ag^0 form.[25]

Detailed scan of the Au 4f region show no peaks attributable to the presence of any gold species. The 1 wt% loading is well within the limits of XPS detection of *ca.* 0.1 at%. A 1wt%Au/SiO_2-PPT system was also prepared and analysed in order to confirm that the preparation method was effective and no gold is being lost during the filtration step. The resulting XPS studies show a peak at 83.9 eV attributable to the presence of gold in its metallic, Au^0 form,[25] indicating that gold should be present within the 20wt%Fe/1wt%Au/SiO_2-PPT system. This suggests that the iron present in the mixed metal catalyst system could be coating

any gold present and therefore, preventing detection; an effect previously observed for mixed cobalt gold systems.[26]

To confirm that the high iron loading was accountable for the inability to detect gold within the system using XPS a catalyst containing a lower iron loading was also prepared and tested. The Fe 2p region is shown in Figure 5.6 (c II) and shows no change in the iron species with Fe_2O_3 still present as the main species. With the lower iron loading a detailed scan on the Au 4f region does, however, reveal the presence of gold with a binding energy of 84 eV confirming that gold is present as Au^0 with the presence of iron, further indicating that the high iron loading is contributing to the inability to detect gold in the 20wt%Fe/1wt%Au/SiO_2-PPT catalyst system.

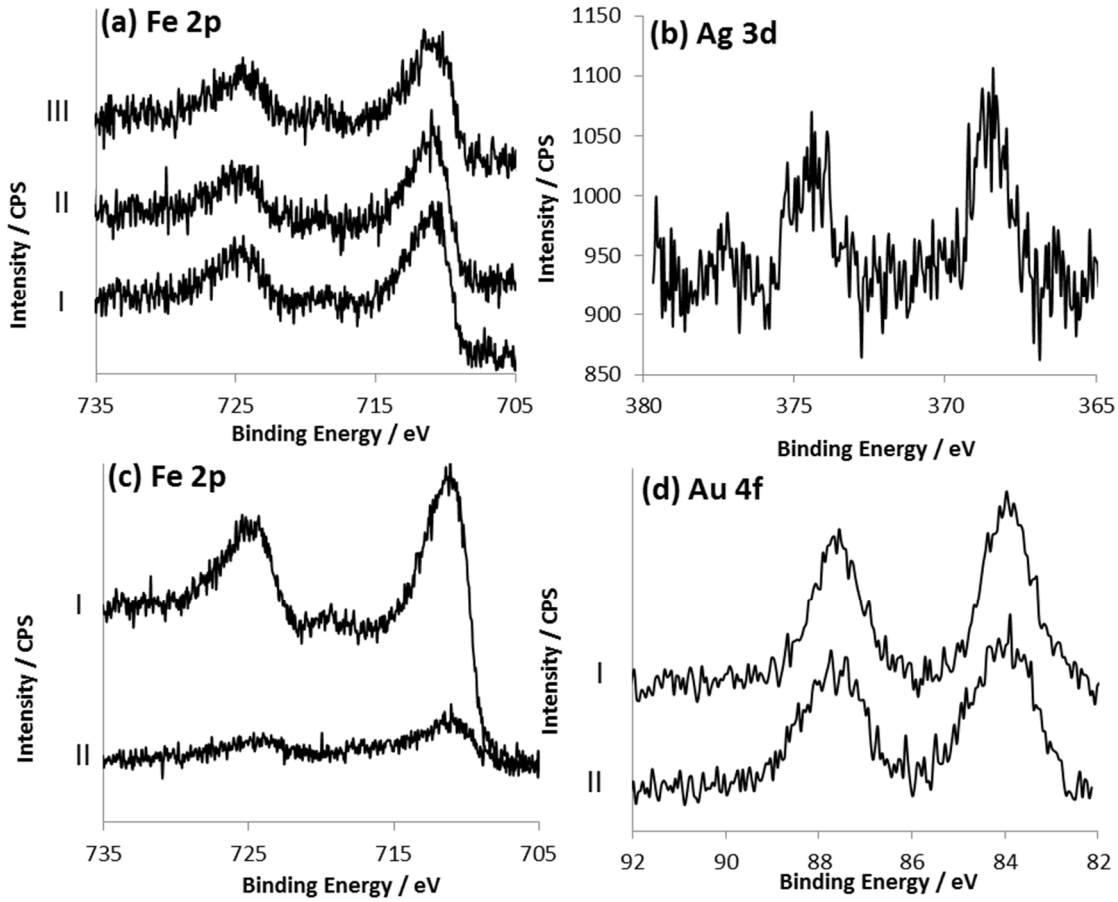

Figure 5.6 – (a) XPS spectra recorded in the Fe 2p region for 20wt%Fe/SiO_2-WI (I), 20wt%Fe/1wt%Cu/SiO_2-WI (II) and 20wt%Fe/1wt%Ag/SiO_2-WI (III), (b) Detailed scan of the Ag 3d region recorded from 20wt%Fe/1wt%Ag/SiO_2-WI. (c) Detailed scan of the Fe 2p region for (I) 20wt%Fe/1wt%Au/SiO_2-PPT and (II) 1wt%Fe/1wt%Au/SiO_2. (d) Detailed scan of the Au 4f region for (I) 1wt%Au/SiO_2-PPT and (II) 1wt%Fe/1wt%Au/SiO_2.

XPS studies on the 20wt%Fe/1wt%Cu/SiO_2 catalyst system did not indicate the presence of copper within the system. However, when a catalyst containing a higher loading (10 wt%) of copper was tested {Figure 5.2 (b)} the peaks observed indicated the presence of CuO. This suggests a similar problem to that observed for the gold containing catalyst system

where a high iron loading leads to signal attenuation possibly due to the coating of any copper present with iron oxide.

5.2.3 Catalyst Testing

The CO_2 hydrogenation ability of each catalyst was tested at atmospheric pressure using Reactor 1 (see Chapter 2 Section 2,2 for full details). Typically 0.7 g of catalyst was packed into the reactor sample cell and reduced under a stream of pure hydrogen at 300 ^oC for 2 hours. Reactions were conducted at 370 ^oC, atmospheric pressure with a H_2:CO_2 ratio of 3:1, total flow 8 sccm. The results obtained are summarised in Table 5.4.

The addition of copper even at a low, 1 wt% loading still results in a decrease in CO_2 conversion along with a slight increase in CO yield giving a decreased HC yield. No significant change in hydrocarbon distribution in observed other than a minor decrease in C_2-C_4 olefin selectivity is observed. These results appear to contradict what was observed by Ando *et al*.[15a] who found the introduction of copper to unsupported iron systems under high pressure reaction conditions improved both CO_2 conversion and selectivity. This difference is likely due to a combination of the introduction of a catalyst support and a significantly higher (5 MPa *vs*. 0.1 MPa) reaction pressure. Their work also reported that for copper/iron ratios below 0.11 resulted in product distributions that no longer followed the ASF distribution. In contrast the copper-iron-silica system tested here (Cu/Fe ratio 0.05) resulted in a product distribution that still follows the ASF distribution (Figure 5.7 (a)) indicating that hydrocarbons are still being formed *via* the FT process.[22]

The addition of a small amount of silver to the iron-silica system gave a slight increase in CO_2 conversion this however, occurs in conjunction with an increase in selectivity towards CO which in turn results in a slight reduction in HC yield. The HC product distribution remains similar with a reduction in selectivity towards lower olefins. C_2-C_4 olefins percentage was calculated to be lower than both the iron only system and the iron-copper system.

The performance of the iron-silica catalyst is greatly reduced when the catalyst is prepared using the precipitation technique; there is a significant reduction in both CO_2 conversion and selectivity to hydrocarbons. The only HC products detected are methane and ethane with a high preference for the former. The difference in catalyst performance can likely be attributed to the change in catalyst morphology observed by SEM {Figure 5.4 (c)} and the significantly smaller nanoparticles observed by TEM {Figure 5.4 (d)}.

Table 5.4 – Catalytic data obtained for CO_2 hydrogenation tests using Fe-M-SiO_2 catalysts (M = Cu, Ag, Au or no metal)

Catalyst[a, b]	Conversion (%)	HC Yield (%)	CO Yield (%)	Hydrocarbon Distribution							O/(O+P)[c] in C_2-C_4
				C_1	C_2=	C_2	C_3=	C_3	C_4	C_5+	
20wt%Fe/SiO_2-WI	34.8	25.6	9.3	64.5	0.7	22.0	1.8	8.7	2.1	0.2	6.0
20wt%Fe/1wt%Cu/SiO_2-WI	26.1	18.4	7.7	62.1	0.3	22.7	1.4	10.2	2.7	0.6	4.4
20wt%Fe/1wt%Ag/SiO_2-WI	36.8	23.5	13.2	63.9	0.3	22.0	0.9	10.0	2.2	0.4	3.6
20wt%Fe/SiO_2-PPT	8.8	2.4	6.3	95.9	0.0	4.1	0.0	0.0	0.0	0.0	0.0
20wt%Fe/0.5wt%Au/SiO_2-PPT	16.1	7.9	8.2	86.3	0.0	8.8	1.2	2.8	0.9	0.0	6.1
20wt%Fe/1wt%Au/SiO_2-PPT	17.5	8.1	9.4	82.9	1.5	10.1	2.6	2.1	0.7	0.1	21.6
20wt%Fe/2wt%Au/SiO_2-PPT	13.8	5.1	8.7	83.1	2.3	9.0	4.2	1.2	0.3	0.0	34.2
20wt%Fe/3wt%Au/SiO_2-PPT	14.0	7.2	6.8	90.9	0.0	6.8	0.8	1.5	0.0	0.0	6.4
20wt%Fe/4wt%Au/SiO_2-PPT	15.3	7.3	8.0	89.9	0.0	10.1	0.0	0.0	0.0	0.0	0.0
20wt%Fe/1*wt%Au/SiO_2-PPT	16.0	6.0	10.0	85.0	2.5	7.7	2.9	1.8	0.0	0.0	32.4

[a] – Suffix indicates the preparation method used for each catalyst. WI: wet impregnation method and PPT: precipitation method. [b] - * indicates catalyst calcined between the addition of iron and gold precursors before the final calcination step. [c] – Olefin content (mol percentage) for C_2-C_4 hydrocarbons, calculated as [olefin(O) / (olefin(O) + paraffin(P)) × 100]. Catlyst tests conducted at atmospheric pressure, H_2:CO_2 ratio 3:1, total flow – 8 sccm. 0.7 g of catalyst. Conversions, yields and product distributions calculated after 5 hours on stream.

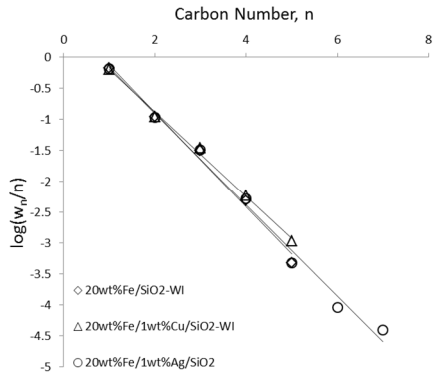

Promoter and loading	Chain Growth Probability, α
No Promoter-WI	0.17
1wt%Cu -WI	0.20
1wt%Ag-WI	0.18
0.5wt%Au-PPT	0.11
1wt%Au-PPT	0.12
2wt%Au-PPT	0.10

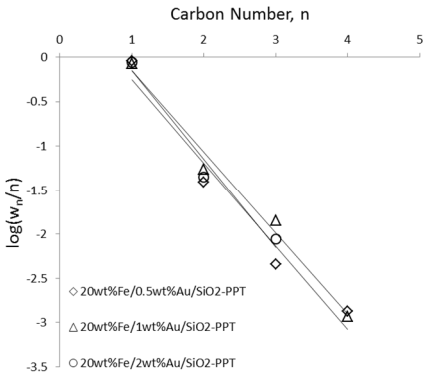

Figure 5.7 – ASF plots for copper and silver promoted catalysts (a) and gold promoted catalysts (b). Calculated alpha values are tabulated.

The introduction of a low loading of gold to the catalyst system results in a large improvement in catalyst performance with CO_2 conversion observed to nearly double. When this increase in conversion is combined with the decreased selectivity to CO this leads to an overall increase in HC yield from 2.4 to 8.1 %. A beneficial effect is also observed for the hydrocarbon selectivity. Methane selectivity is decreased and HCs with a change length of up to C_4 are detected. Of the C_2-C_4 hydrocarbons formed 22.3 % are olefins, a significant improvement over the non-promoted catalyst system.

Despite the overall performance of the 20wt%Fe/1wt%Au/SiO_2-PPT catalyst comparing poorly with some previous catalysts reported within this chapter this can be attributed to the preparation method used. The enhanced catalyst performance shown upon the introduction of gold to the catalyst system indicates that gold acts as an effective promoter for iron catalysts utilised for CO_2 hydrogenation with a large influence on C_2-C_4 olefin selectivity. As a result of these findings, investigations into the iron-gold-silica catalyst systems were extended.

Furthermore, Jalama *et al.*[26-27] investigated the effect of gold addition on cobalt based catalysts used for the FT process and found that small amounts were beneficial to catalyst activity. Sakuri and co-workers[28] investigated gold nanoparticles supported on Fe_2O_3 for the hydrogenation of CO_2 to methanol and found that small amounts of methane were formed in initial catalyst test as well as CO and methanol. No studies were conducted on the Fe_2O_3 support alone however and as such it is not clear as to the promotional effects of the introduction of gold.

TEM images showing the catalyst morphology before gold addition (20wt%Fe/SiO_2-PPT) and after (20wt%Fe/1wt%Au/SiO_2-PPT) are shown in Figure 5.8. Little change in morphology is observed upon the inclusion of gold to the catalyst system. A slight decrease in the nano-particle size is, however, observed with the average size decreasing from *ca*. 3 nm to *ca*. 2 nm distribution is also slightly narrowed.

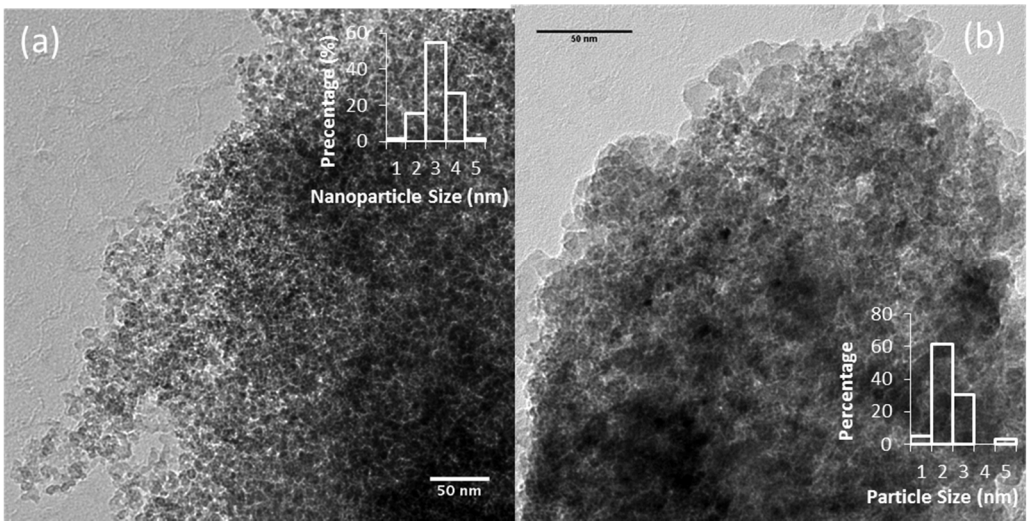

Figure 5.8 – TEM images recorded for (a) 20wt%Fe/SiO_2-PPT and (b) 20wt%Fe/1wt%Au/SiO_2. Inserts: Histograms showing the particle size distribution for each catalyst.

In order to gain a deeper understanding of the influence of gold on the iron-gold catalyst system several catalysts were prepared containing a range of iron:gold ratios and tested under CO_2 hydrogenation conditions. The data obtained from these tests are summarised in Table 5.4. The introduction of 0.5 wt% gold had a similar effect to the addition of 1 wt% of gold with a significant increase in CO_2 conversion and HC yield. HC selectivity was also observed to improve with a reduction in methane selectivity and improved selectivity to C_2-C_4 olefins. This was not to the same extent as the enhanced catalyst performance observed with 1 wt% gold. When gold loading doubled to 2 wt% a slight reduction in CO_2 conversion is observed, however, the C_2-C_4 olefin selectivity increases further to 34.2 % significantly higher than that observed for the non-promoted system. When gold content is increased beyond this point the CO_2 conversion remains constant, within experimental error, the methane selectivity increases and selectivity to lower olefins decreases. Form this it can determine that in terms of conversion 1 wt% gold is the optimum loading but for the highest selectivity to lower olefins a 2 wt% loading is most efficient.

With the XPS studies suggesting that the gold present within the catalyst system may be coated by iron, further investigations were conducted in an attempt to determine what influence this may have on the catalyst performance. During the preparation of all previous gold containing catalysts the iron and gold precursors are added together and precipitated at the same time. In order to prevent the coating of any gold present the iron component of the system was precipitated first and the system calcined before the subsequent addition of gold. The 20wt%Fe/1*wt%Au/SiO_2 catalyst system (* indicating that gold was added after the calcination of the iron component) was then tested under the same reaction conditions with the resulting data shown in Table 5.4. The CO_2 conversion value obtained was found to be much closer to that observed for the gold promoted catalyst rather than the non-promoted iron-silica system.

The product distribution was also found to be much closer to the promoted rather than non-promoted system however the catalyst enhancement was not quite as significant. One property that appeared to be improved when prepared using this method was the selectivity to lower olefins with a selectivity of 32.4 % rather than 21.6 %. This suggests while the coating of the gold within the system by iron does play a role in catalyst performance it is not essential with the other catalyst system performing almost as well.

In order to determine how each of the metal oxide phases alters under reaction conditions XPS studies were conducted on a used catalyst sample. Due to the difficulty in detection of gold by XPS when present in lower loadings the 20wt%Fe/4wt%Au/SiO_2 samples was chosen. Figure 5.9 shows detailed scan of the Fe 2p and Au 4f region of the XPS spectra. A peak at 711.0 is observed in the Fe 2p region, the lack of a satellite peak at 719 eV characteristic of Fe^{3+},[18] easily observed in the 20wt%Fe/1wt%Au/SiO_2-PPT catalyst before reaction, suggests the presence of iron mainly as Fe_3O_4 after five hours under reaction conditions resulting from the reduction of the Fe_2O_3 phase observed before reaction. This reduction is also supported by the colour change from rust brown to black observed for the catalyst system before and after use. The detailed scan of the Au 4f region after reaction reveals a peak present at 84.1 eV indicating the gold is still present in its metallic, Au^0,[25] form after being under reaction conditions for 5 hours.

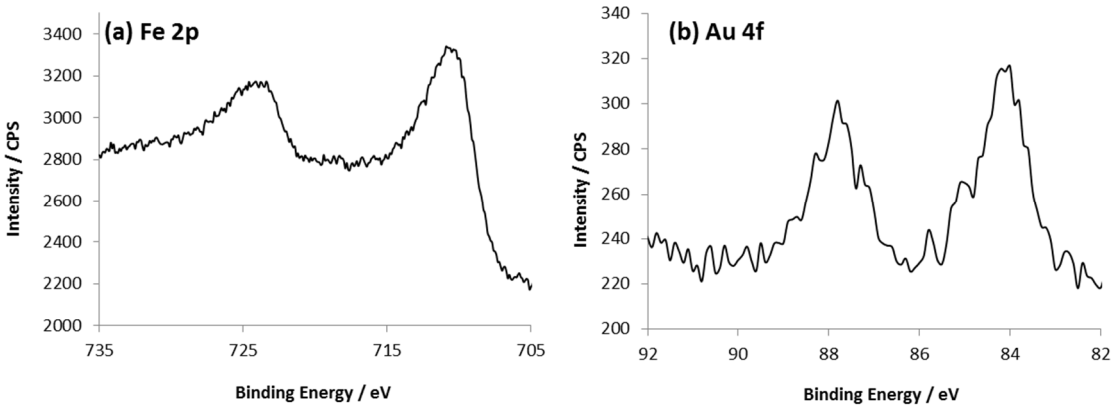

Figure 5.9 – XPS spectra recoded for 20wt%Fe/4wt%Au/SiO_2 after subjection to reaction conditions. (a) Detailed scan of the Fe 2p region. (b) Detailed scan of the Au 4f region.

The improved catalyst performance upon the introduction of gold could be due to an improved WGS shift activity of the catalyst systems. Mixed iron gold systems have recently been attracting significant attention as promising WGS catalysts[29] with the catalysts also proving successful for the RWGS reaction. This increased conversion of CO_2 to CO could aid the formation of higher chain length hydrocarbons due to a high CO:H_2 ratio which can lead to high chain growth probability and an increased likelihood of alkene formation. Another possibility is a reduction in support-iron interactions when gold is present, an effect similar to that postulated by Jalama *et al*. for mixed cobalt-gold systems.[26] This reduction in support-iron

interactions can lead to an increased reducibility of the iron species which can aid the formation of the active species and so enhance catalyst performance.

XPS analysis of the 20wt%Fe/SiO_2-PPT and 20wt%Fe/1wt%Au/SiO_2-PPT was used to calculate the Fe:Si atomic ratio in order to aid determination of the surface concentration of iron present in each catalyst. A significant increase in this ratio from 0.02 to 0.07 upon the inclusion of gold indicates an enrichment of iron at the catalyst surface, an increase in iron dispersion. An effect similar to this has been witnessed with Co/Au/TiO_2 catalysts by Jalama *et al*.[27] and could play an important role in the improved catalyst performance upon the introduction of gold to the iron-silica catalyst system.

5.3 Promotion of Iron-Silica Catalysts with Group 13 Metals

With the studies down Group 11 revealing some interesting and promising promoters it was decided to conduct an extended study down Group 13. Although gallium did not prove successful when added in high loadings with almost all catalytic activity inhibited upon its introduction (Table 5.2) its content was lowered to 1 wt% in order to determine if any promotional abilities could be observed without high gallium concentrations inhibiting the catalytic activity of the iron-silica system. The addition of low loadings of gallium has been shown to improve the performance of a Ni/SiO_2 CO_2 methanation catalyst[30] with the addition of Ga_2O_3 to the silica support aiding the activation of adsorbed CO_2 resulting in higher CO_2 conversions.

With catalyst tests extended to include an investigation into the promotional abilities down Group 13 20wt%Fe/1wt%Al/SiO_2 and 20wt%Fe/1wt%In/SiO_2 catalysts were also prepared. The use of alumina has been investigated extensively in high loadings as a structural support both for the FT process[31] and CO_2 hydrogenation.[32] The investigations herein, however, focus on the use of small quantities with the oxide formed during the catalyst calcination process and with silica present to act as the catalyst support. Wan *et al*.[33] have shown that for a multi-promoted iron based FT catalyst altering the ratio of SiO_2 to Al_2O_3 can have a beneficial influence on catalyst performance by reducing some unfavourable SiO_2 - iron interactions. Significantly higher amounts than used here were employed and to the best of the author's knowledge no similar study has been performed with Fe/SiO_2 CO_2 hydrogenation catalyst particularly with the formation of Al_2O_3 *in situ* during the formation of the iron oxide phase.

Although both aluminium and gallium have both attracted some attention in the field of CO_2 hydrogenation catalysis, focus on the use of indium has so far been very limited.[34]

5.3.1 Catalyst Preparation

Owing to the air and moisture sensitive nature of the promoter precursors ($AlCl_3$, $GaCl_3$ and $InCl_3$) all catalyst systems were prepared under a nitrogen atmosphere using standard Schlenk

line procedures as detailed in Section 2, Chapter 2.7.10. All catalysts prepared using this method are denoted by the suffix –SL.

5.3.2 Catalyst Characterisation

The catalyst systems were analysed using a range of techniques. N_2 physisorption experiments were used to calculate the BET surface area of the prepared catalysts with the results summarised in Table 5.5. Little influence is observed on the surface area upon the introduction of gallium and indium, aluminium however, results in an increased catalyst surface area.

Table 5.5 – Surface areas for each catalyst system as determined by BET

Catalyst[a]	**BET Surface Area (m^2g^{-1})**
20wt%Fe/SiO_2-SL	195.5
20wt%Fe/1wt%Al/SiO_2-SL	222.4
20wt%Fe/1wt%Ga/SiO_2-SL	197.4
20wt%Fe/1wt%In/SiO_2-SL	198.3

[a] – Suffix indicates the preparation method used for each catalyst. SL: Schlenk line technique

XPS studies were conducted in order to determine the metal oxide present for each catalyst with detailed scan for selected regions of each catalyst shown in Figure 5.10. The studies reveal that all catalyst systems possess iron present mainly in the Fe_2O_3 oxide form with little to no change observed for each system upon the introduction of each promoter. The aluminium and indium containing catalyst systems were observed to contain peaks at 74.1 eV and 444.8 eV respectively, indicating their presence in the form of their 3+ oxides: Al_2O_3[25] and In_2O_3[35] {Figure 5.10 (b and c)}. No signals attributable to any gallium species were detected for the 20wt%Fe/1wt%Ga/SiO_2 system. A 1wt%Ga/SiO_2-SL system was tested and yielded a peak at 1118.1 eV attributable to the presence of Ga_2O_3[21] indicating that gallium is in a high enough concentration for detection and that the preparation method is effective which suggests that the lack of a gallium signal could be attributable to the high iron loading attenuating the gallium signal. When a catalyst containing a higher gallium loading was tested Ga_2O_3 was also detected (Figure 5.2) further confirming this possibility.

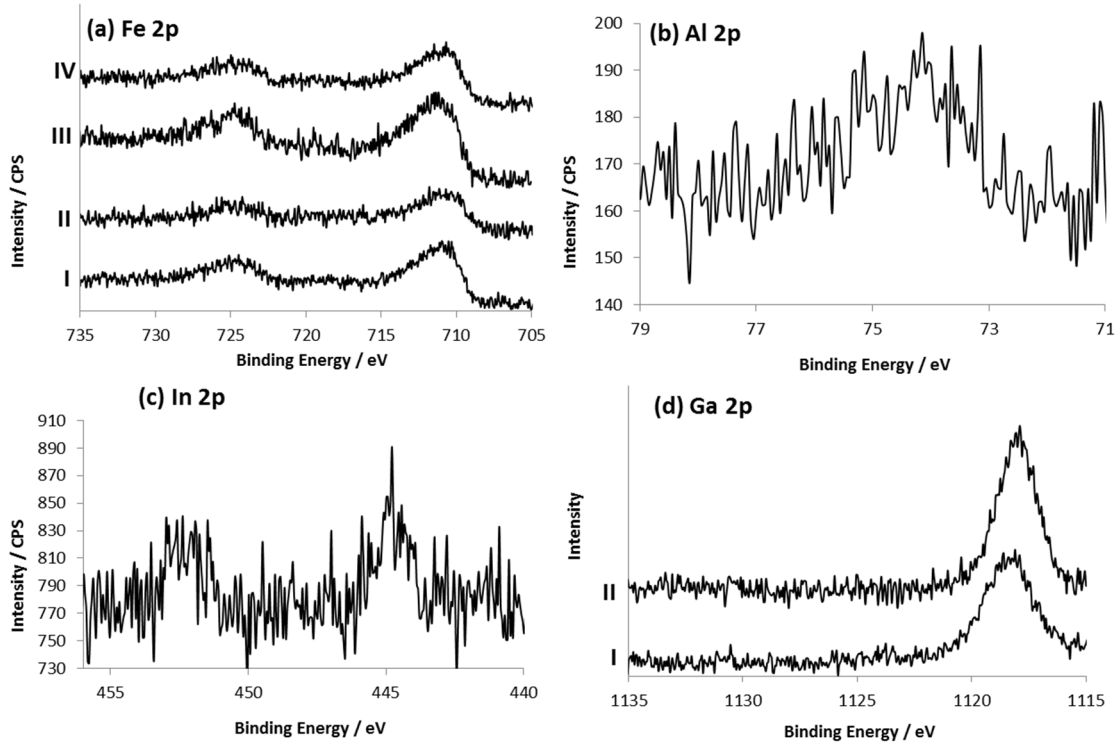

Figure 5.10 – (a) XPS spectra recorded in the Fe 2p region for 20wt%Fe/SiO_2-SL (I), 20wt%Fe/1wt%Al/SiO_2-SL (II), 20wt%Fe/1wt%Ga/SiO_2-SL (III) and 20wt%Fe/1wt%In/SiO_2-SL. (b) Detailed scan of the Al 2p region recorded from 20wt%Fe/1wt%Al/SiO_2-SL. (c) Detailed scan of the In 3d region for 20wt%Fe/1wt%In/SiO_2-SL. (d) Detailed scan of the Ga 2p region for (I) 1wt%Ga/SiO_2-PPT and (II) 20wt%Fe/10wt%Ga/SiO_2.

5.3.3 Catalyst Testing

The CO_2 hydrogenation ability of each catalyst was tested at atmospheric pressure using Reactor 1 (see Chapter 2 Section 2.2 for full details). Typically 0.7 g of catalyst was packed into the reactor sample cell and reduced under a stream of pure hydrogen at 300 ^oC for 2 hours. Reactions were conducted at 370 ^oC, atmospheric pressure with a H_2:CO_2 ratio of 3:1, total flow 8 sccm. The results obtained are summarised in Table 5.6.

The addition of 1 wt% aluminium to the iron-silica catalyst system appears to have little influence on CO_2 conversion. A dramatic change in product selectivity is observed, however, with CO selectivity increasing greatly resulting in a large drop in HC yield. Product selectivity is also influenced with aluminium inclusion, methane selectivity is increased and no C_5+ hydrocarbons are formed. This alteration in product distribution does result in a slight increase in the olefin selectivity observed for C_2-C_4 hydrocarbons. It is possible that the Al_2O_3 is not present in high enough quantities to give similar effects to those observed by Wan *et al.*[33] or that the formation of Al_2O_3 during the same calcination process as Fe_2O_3 formation resulted in the inactive Al_2O_3 blocking the iron active sites

No effect on catalyst performance in terms of CO_2 conversion was observed upon the addition of 1 wt% gallium to the iron-silica catalyst system. A slight change in the CO/HC product ratio is observed, however, this has minimal effect on the HC yield and is within

experimental error. The hydrocarbon distribution varies to a larger extent with an increase in C_2-C_4 olefin selectivity observed over the non-promoted system this does however occur along with an increase in methane selectivity.

The inclusion of 1 wt% indium in the Fe/SiO_2 catalyst system leads to an increase in CO_2 conversion with little change in CO/HC product distribution. No discernible difference in methane selectivity is observed however a higher C_5+ selectivity is observed. More significantly, a large improvement in alkene selectivity was observed; the C_2-C_4 olefin selectivity increased from 4 % in the non-promoted system to 22 % with indium present. This indicates that indium is an efficient catalyst promoter for the hydrogenation of CO_2 over iron-silica catalysts.

ASF plots for each of the catalyst systems are shown in Figure 5.11. All catalyst systems show straight line plots for a plot of $ln(w_n/n)$ *vs.* carbon number, n indicating that all systems produce HCs *via* the FT process showing that the addition of promoters has no effect on the overall reaction mechanism, which is still occurring through the CO mediated and not methanol mediated process.

Table 5.6 – Catalytic data obtained for CO_2 hydrogenation tests using Fe-M-SiO_2 catalysts (M = Al, Ga, In or no metal)

Catalyst[a]	Conversion (%)	HC Yield (%)	CO Yield (%)	Hydrocarbon Distribution							O/(O+P)[b] in C_2-C_4
				C_1	C_2=	C_2	C_3=	C_3	C_4	C_5+	
20wt%Fe/SiO_2-SL	30.1	22.9	7.2	68.9	0.0	19.4	0.9	8.6	2.0	0.3	2.4
20wt%Fe/1wt%Al/SiO_2-SL	27.6	5.0	22.7	80.3	0.0	14.1	1.7	3.4	0.5	0.0	5.6
20wt%Fe/1wt%Ga/SiO_2-SL	29.6	22.0	7.6	72.4	0.1	17.8	1.3	7.0	1.4	0.0	4.0
20wt%Fe/0.5wt%In/SiO_2-SL	46.1	39.3	6.8	64.3	1.1	14.4	5.0	7.3	5.3	2.7	22.3
20wt%Fe/1wt%In/SiO_2- SL	35.5	26.4	9.1	68.4	1.7	11.6	7.4	4.2	4.8	1.8	35.3
20wt%Fe/2wt%In/SiO_2- SL	29.9	22.4	7.6	67.2	2.9	8.4	10.6	2.3	6.3	2.3	52.4
20wt%Fe/3wt%In/SiO_2- SL	25.7	20.0	5.7	65.7	4.7	6.6	12.9	1.8	6.3	2.1	65.2
20wt%Fe/4wt%In/SiO_2- SL	20.4	14.6	5.8	78.9	2.8	4.3	8.3	1.0	4.1	0.7	65.1

[a] – Suffix indicates the preparation method used for each catalyst. SL: Schlenk line method [b] – Olefin content (mol percentage) for C_2-C_4 hydrocarbons, calculated as [olefin(O) / (olefin(O) + paraffin(P)) × 100]. Catlyst tests conducted at atmospheric pressure, H_2:CO_2 ratio 3:1, total flow – 8 sccm. 0.7 g of catalyst. Conversions, yields and product distributions calculated after 5 hours on stream.

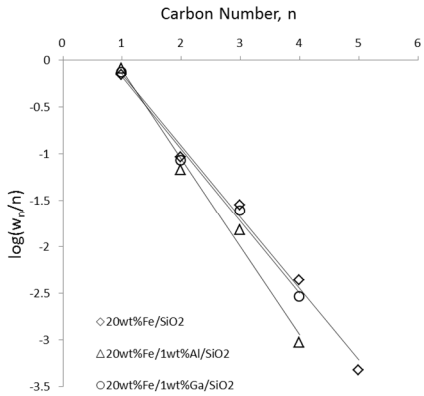

Promoter and loading	Chain Growth Probability, α
No Promoter-SL	0.17
1wt%Al-SL	0.11
1wt%Ga-SL	0.17
0.5wt%In-SL	0.26
1wt%In-SL	0.26
2wt%In-SL	0.26
3wt%In-SL	0.26
4wt%In-SL	0.24

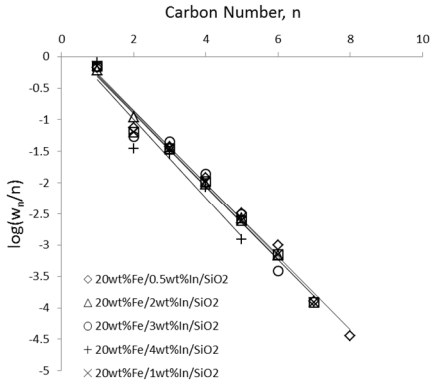

Figure 5.11 – ASF plots for the iron-silica catalyst along with the aluminium and gallium promoted catalysts (a) and indium promoted catalysts (b). Calculated alpha values are tabulated.

Theoretical investigations conducted by Ye *et al*.[34] suggested that In_2O_3 was effective for CO_2 activation and also adsorbs hydrogen dissociatively; both properties that could be responsible for the increased CO_2 conversion observed upon indium incorporation. In_2O_3 is also active for the dehydrogenation of propane utilising CO_2 as a mild oxidant,[36] hence the high levels of propane observed in this case. Ga_2O_3 is more traditionally employed in dehydrogenation reactions such as these[37] which could account for the increased preference for olefins observed when gallium is used in low loadings. However, when used in conjunction with iron under the reaction conditions studied indium proves far more effective.

As a result of the initial 20wt%Fe/1wt%In/SiO_2-SL catalyst results this system was chosen for further investigation. A range of catalysts were prepared with varying indium loadings. Their CO_2 hydrogenation abilities were then examined and the results summarised in Table 5.6. Although the addition of 1 wt% indium improved catalyst performance the benefits of 0.5 wt% indium are significantly larger with CO_2 conversion greatly increased. A drop in CO selectivity results in the HC yield increasing from 22.9 % in the non-promoted iron system to 39.3 % with the addition of 0.5 wt% indium. When the indium loading is increased beyond this point the CO_2 conversion begins to drop with a 2 wt% loading resulting in conversion values similar to that observed for the non-promoted catalyst system.

The hydrocarbon distribution is also improved greatly upon the addition of 0.5 wt% indium with C_5+ HC selectivity increasing to 2.6 %. While the olefin selectivity is observed to increase when 0.5 wt% indium is added this is to a lesser extent than observed with 1 wt% indium addition. As indium loading is increased beyond 1 wt% the selectivity towards lower olefins is seen to continue to increase with indium loadings of 3 and 4 wt% resulting in C_2-C_4 olefin selectivities of 65.2 and 65.1 % respectively.

The trends in selectivity and conversion observed suggest that above a loading of 1 wt% indium is present in too high a concentration to effectively promote the iron-silica system and instead begins to block active sites inhibiting CO_2 conversion. Since olefin selectivity continues

to increase with higher indium loadings this suggests that the trends observed with CO_2 conversion and product selectivity are unrelated. Instead the increased In_2O_3 present in catalysts with higher indium loadings means there is a higher quantity of active sights for the dehydrogenation reaction it is active for resulting in increasing amounts of olefin products.

In order to determine how the iron and indium metal oxides varied under reaction conditions XPS studies were conducted on a used catalyst sample. The 20wt%Fe/4wt%In/SiO_2 system was chosen as it was envisioned that the relatively high indium loading would give clearer indium signals. Figure 5.12 shows detailed scans of the Fe 2p and In 3d regions of the spectrum. In the iron region of the spectrum an Fe $2p_{3/2}$ peak is observed at 711.0 eV, the lack of a satellite peak at 719 eV, characteristic of Fe^{3+},[18] suggests that this peak can be mainly attributed to Fe_3O_4 formed by the reduction of the Fe_2O_3 observed before reaction. This is further supported by the colour change from rust brown to black observed for the catalyst system before and after use. An indium $3d_{5/2}$ peak observed at 444.3 eV matches well with literature values observed for In_2O_3[35] and indicates that the indium oxide component of the system is not reduced under reaction conditions and is available as In_2O_3 both for CO_2 activation as suggested by Ye *et al*.[34] and as an active site for the dehydrogenation of paraffins as reported by Chen *et al*.[36]

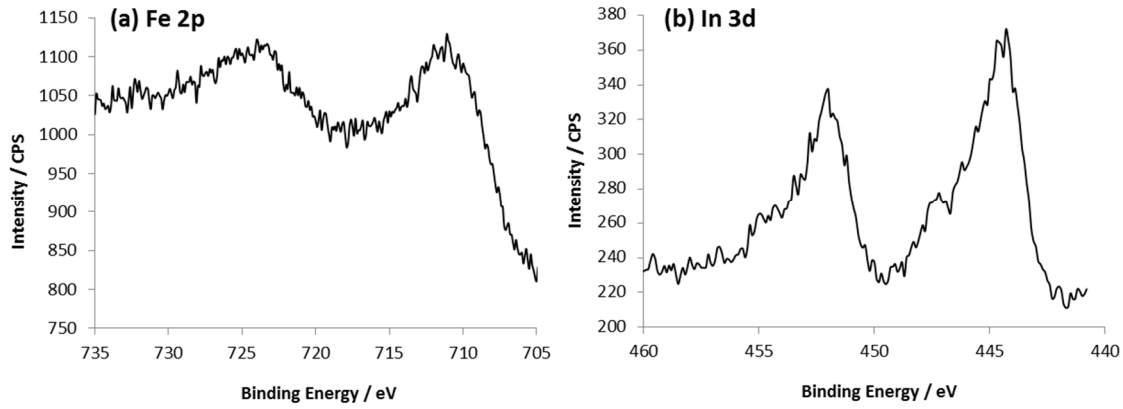

Figure 5.12 – XPS spectra recorded for (a) Fe 2p and (b) In 3d regions for 20wt%Fe/1wt%In/SiO_2-SL after catalyst use.

5.4 Co-Promotion with Pd-Ga and Pd-Au

Mixed gallium-palladium systems have been shown to successfully hydrogenate CO_2 for the formation of methanol at elevated pressures.[38] As such studies were conducted on the introduction of gallium and palladium simultaneously to the iron-silica catalysts studied so far in order to determine if this could enhance the catalytic activity.

The use of palladium–gold based catalyst systems has also been gaining significant attention as a promising hydrogenation catalyst.[39] Despite this increased interest they have not so far been employed either as promoter or as a standalone system for the hydrogenation of CO_2.

5.4.1 Catalyst Preparation

The catalyst systems studied within this section were prepared *via* one of two preparation methods. Due to the air sensitive nature of the gallium precursor ($GaCl_3$) any system containing gallium and the associated systems for comparison were prepared using standard Schlenk line techniques as detailed in Chapter 2 Section 2.7.10.

As with the gold systems investigated in Section 5.2 any catalyst system containing gold, or prepared for comparison with the gold-based systems were prepared using the co-precipitation preparation method detailed in Chapter 2 Section 2.7.11.

For each of the 20wt%Fe/1wt%Ga/1wt%Pd/SiO_2-SL and 20wt%Fe/1wt%Au/1wt%Pd/SiO_2-PPT systems tested catalysts containing 20wt%Fe/SiO_2 and 20wt%Fe/1wt%Pd/SiO_2 were prepared and tested using the co-precipitation and Schlenk line based techniques for comparison.

5.4.2 Catalyst Characterisation

N_2 physisorption experiments were utilised for the determination of the BET surface areas for the prepared catalysts. The 20wt%Fe/1wt%Ga/1wt%Pd/SiO_2-SL catalyst was found to have a surface area of 218.2 m^2g^{-1}, higher than that observed for the iron only and gallium promoted catalyst systems indicating that palladium can aid an increase in surface area. The 20wt%Fe/1wt%Au/1wt%Pd/SiO2-PPT was found to possess a surface area of 288.7 m^2g^{-1} intermediate between the iron only and gold promoted catalyst systems.

The prepared catalyst systems were also investigated using XPS analysis with detailed scans of selected areas shown in Figure 5.13. Studies on the 20wt%Fe/1wt%Ga/1wt%Pd/SiO_2-SL system revealed iron present mainly in the Fe_2O_3 oxide form as indicated by a $2p_{3/2}$ peak present at 710.9 eV and a satellite peak at *ca.* 719 eV. Peaks attributable to palladium were observed at 337.3 eV indicating the presence of palladium as PdO. As with the 20wt%Fe/1wt%Ga/SiO_2 system discussed in Section 5.3.2 no peaks due the presence of gallium could be detected suggesting that a high iron loading could again be attenuating the gallium signal.

The 20wt%Fe/1wt%Au/1wt%Pd/SiO_2-PPT catalyst system again showed the presence of iron as Fe_2O_3 {Figure 5.13 (c I)} however no peaks attributable to the presence of gold or palladium were detectible. Again this suggests similar problems to those observed with the 20wt%Fe/1wt%Au/SiO_2-PPT system discussed in Section 5.2.2. When a catalyst system containing higher loadings of both palladium and gold (20wt%Fe/4wt%Au/4wt%Pd/SiO_2-PPT) was analysed under the same conditions a palladium peak at 337.5 eV was observed along with a peak at 83.4 eV attributable to gold. This indicates the presence of gold in the metallic Au^0 form[25] and palladium as PdO.[40] This further confirms that iron could be blocking the signal at lower loadings. The Fe 2p region for the 20wt%Fe/4wt%Au/4wt%Pd/SiO_2-PPT catalyst system

{Figure 5.13 (c II)} showed little change from the system containing lower gold and palladium loadings indicating they have little effect on the iron species within the system after calcination.

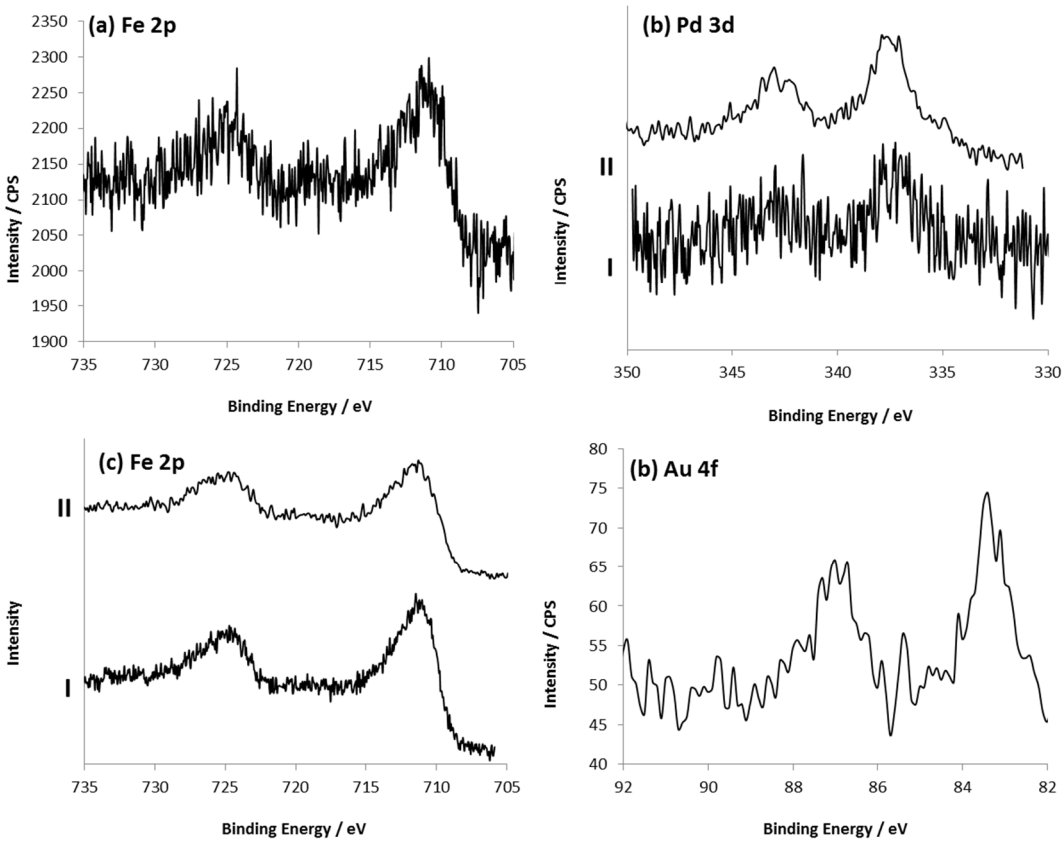

Figure 5.13– (a) XPS spectra recorded in the Fe 2p region for 20wt%Fe/1wt%Ga/1wt%Pd/SiO_2-SL. (b) Detailed scan of the Pd 3d region recorded for 20wt%Fe/1wt%Ga/1wt%Pd/SiO_2-SL(I) and 20wt%Fe/4wt%Au/4wt%Pd/SiO_2-PPT (II). (c) Fe 2p region for 20wt%Fe/1wt%Au/1wt%Pd/SiO_2-PPT (I) and 20wt%Fe/4wt%Au/4wt%Pd/SiO_2-PPT (II). (d) Detailed scan of the Au 4f region for 20wt%Fe/4wt%Au/4wt%Pd/SiO_2-PPT.

5.4.3 Catalyst Testing

The Fe-Ga-Pd-SiO_2 and Fe-Au-Pd-SiO_2 and related catalyst systems were investigated for their CO_2 hydrogenation ability, the data obtained from these tests is summarised in Table 5.7. The promotion of the 20wt%Fe/SiO_2-SL catalyst system with gallium and palladium resulted in an increased CO_2 conversion and HC yield. A strong influence on HC distribution was also observed; methane selectivity dropped with an increase in C_5+ hydrocarbons. A large reduction in olefin selectivity was observed with all products formed being saturated hydrocarbons. Despite the reported effectiveness of Ga-Pd catalyst systems for methanol formation[41] no oxygenates were detected in the products stream. The formed HCs still follow the ASF distribution as shown in Figure 5.14, showing HCs are still being formed by the FT process i.e. CO_2 hydrogenation is occurring *via* the CO mediated mechanism. This lack of methanol formation is likely a combination of high iron loading and perhaps more significantly the much lower reaction pressures used for catalyst testing. A similar effect is noted at lower pressures with the copper and zinc catalysts studied in Section 5.1.3.

Table 5.7 – Catalytic data obtained for CO_2 hydrogenation tests for dual promoted Au-Pd and Ga-Pd catalyst and associated systems

Catalyst[a]	Conv. (%)	HC Yield (%)	CO Yield (%)	Hydrocarbon Distribution							O/(O+P)[b] in C_2-C_4
				C_1	C_2=	C_2	C_3=	C_3	C_4	C_5+	
20wt%Fe/SiO_2-SL	30.1	22.9	7.2	68.9	0.0	19.4	0.9	8.6	2.0	0.3	2.4
20wt%Fe/1wt%Pd/SiO_2-SL	52.5	38.4	14.1	54.9	0.0	21.8	5.4	4.8	4.8	5.9	11.9
20wt%Fe/1wt%Ga/1wt%Pd/SiO_2-SL	37.1	30.5	6.6	55.9	0.0	25.5	0.0	3.5	3.5	0.8	0.0
20wt%Fe/SiO_2-PPT	8.8	2.4	6.3	95.9	0.0	4.1	0.0	0.0	0.0	0.0	0.0
20wt%Fe/1wt%Pd/SiO_2-PPT	20.7	7.3	13.4	78.8	0.0	14.4	0.2	1.7	1.7	0.5	1.0
20wt%Fe/1wt%Au/1wt%Pd/SiO_2-PPT	37.4	19.8	17.7	83.1	0.0	12.7	0.0	0.2	0.2	0.0	0.0

[a] – Suffix indicates the preparation method used for each catalyst. SL: Schlenk line method and PPT: precipitation method [b] – Olefin content (mol percentage) for C_2-C_4 hydrocarbons, calculated as [olefin(O) / (olefin(O) + paraffin(P)) × 100]. Catlyst tests conducted at atmospheric pressure, H_2:CO_2 ratio 3:1, total flow – 8 sccm. 0.7 g of catalyst. Conversions, yields and product distributions calculated after 5 hours on stream.

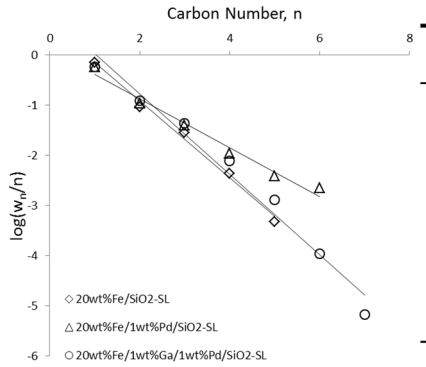

Promoter and loading	Chain Growth Probability, α
No Promoter-SL	0.17
1wt%Pd-SL	0.33
1wt%Pd/1wt%Ga-SL	0.16
No Promoter-PPT	0.03
1wt%Pd-PPT	0.19
1wt%Pd/1wt%Au-PPT	0.20

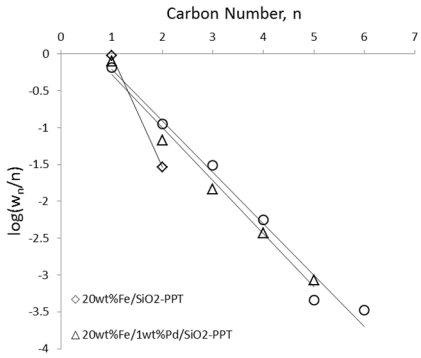

Figure 5.14 – ASF plots for the iron-silica catalyst along with the palladium and mixed palladium-gallium promoted catalysts (a) and palladium and mixed palladium-gold promoted catalysts (b). Calculated alpha values are tabulated.

The catalyst results obtained *via* co-promotion with gallium and palladium compare favourably with the system promoted only with gallium (Table 5.6) with a higher CO_2 conversion, lower methane selectivity and higher chain growth probability. The increased selectivity to lower olefins observed for the Fe-Ga-SiO_2 is, however, lost upon palladium introduction.

When the 20wt%Fe/1wt%Ga/1wt%Pd/SiO_2-SL catalyst system is compared the palladium only promoted system the results are less favourable. The addition of palladium alone results in a more significant enhancement both in terms of CO_2 conversion and hydrocarbon selectivity. CO_2 conversion is increased to 52.5 % which is combined with a reduction in methane selectivity to 55 %, more significantly this also results in a significant increase in selectivity to C_5+ hydrocarbons increasing from 0.3 % to 5.9 %. The percentage olefin products in C_2-C_4 HCs is also improved. This suggests that under the reaction conditions tested gallium inhibits the promotional abilities of palladium in the Fe-Ga-Pd-SiO_2 system.

The addition of 1 wt% palladium to the 20wt%Fe/SiO_2-PPT resulted in a significant increase in CO_2 conversion along with a reduction in methane selectivity and a slightly higher proportion of C_2-C_4 olefins. This catalyst performance compares favourably with the addition of 1wt% gold (Table 5.4) with a slightly higher CO_2 conversion and C_2+ selectivity.

Upon the combination of gold and palladium as co-promoters for the precipitation prepared 20wt%Fe/SiO_2 catalyst a large improvement in CO_2 conversion is observed from 8.8 % to 37.4 %, higher than the enhancement observed when gold and palladium are used alone. The selectivity towards methane remains similar to that observed for the gold only promoted system at *ca.* 83 %. This is slightly higher than that observed for the Fe-Pd-SiO_2-PPT system, the superior product distribution does however occur at the cost of a much lower hydrocarbon yield relative to the Fe-Au-Pd-SiO_2-PPT. Both palladium and gold-palladium promoted systems continue to follow the ASF distribution (Figure 5.14) indicating little effect on the overall reaction mechanism upon their introduction.

5.5 Chapter Conclusions

The promotional ability of several metals on a mixed iron-silica catalyst has been investigated. High loadings (10wt%) proved to generally inhibit the activity of the iron system with XPS suggesting this could be due to the blocking of the active iron component of the catalyst. The introduction of 1 wt% of Group 11 metals was investigated with the addition of 1 wt% gold proving the most successful of the Group 11 metals added resulting in an increased CO_2 conversion, a higher selectivity to lower olefins and a larger quantity of heavier hydrocarbons. A range of gold loadings were tested with 1 wt% proving optimum in terms of conversion and 2 wt% giving the highest selectivity to lower olefins. The improved catalyst activity can likely be attributed to an increased WGS activity of the catalyst system and a higher iron distribution upon the inclusion of gold. The dual promotion of iron-silica systems with a combination of gold and palladium resulted in a significant increase in CO_2 conversion from 8.8 % to 37.4 % outperforming both the gold and palladium only promoted systems.

An investigation into the effect of the introduction of 1 wt% of three Group 13 metals was also undertaken. The addition of gallium resulted in a slight increase in selectivity to lower olefins. The inclusion of indium however proved far more effective with low loadings resulting in a significant increase in CO_2 conversion likely due to In_2O_3 aiding the activation of CO_2. The selectivity to lower olefins was also significantly improved upon the addition of indium, with higher loadings resulting in increasing selectivity towards C_2-C_4 olefins. This increase in quantity of olefins can be attributed to the dehydrogenation of paraffins across the In_2O_3 component of the catalyst system.

5.6 Future Work

With the large improvement in CO_2 conversion obtained upon the dual promotion of the Fe/SiO_2-PPT with palladium and gold, this system warrants further investigation. Thus far only a 1:1 ratio of gold to palladium has been trailed with total promoter loading of 2 wt%. Optimisation of this catalyst system through variation of both the Pd:Au ratio and overall loading may result in further improvements to the catalyst performance.

The significant increase in selectivity to lower olefins observed upon the addition of indium to the iron-silica catalyst system suggests further investigations into the use of indium as a promoter for CO_2 hydrogenation should be carried out. The addition of indium in combination with other well-known promoters for iron-based CO_2 hydrogenation catalysts, such as potassium, could yield further improvements both in terms of CO_2 conversion values and selectivity to lower olefins.

5.7 References

[1] R. L. Espinoza, A. P. Steynberg, B. Jager, A. C. Vosloo, *Appl. Catal., A* **1999**, *186*, 13-26.

[2] R. W. Dorner, D. R. Hardy, F. W. Williams, B. H. Davis, H. D. Willauer, *Energy Fuels* **2009**, *23*, 4190-4195.

[3] T. Riedel, G. Schaub, K. W. Jun, K. W. Lee, *Ind. Eng. Chem. Res.* **2001**, *40*, 1355-1363.

[4] P. S. Sai Prasad, J. W. Bae, K. W. Jun, K. W. Lee, *Catal. Surv. Asia* **2008**, *12*, 170-183.

[5] P. Kaiser, R. B. Unde, C. Kern, A. Jess, *Chem. Ing. Tech.* **2013**, *85*, 489-499.

[6] (a) G. Kishan, M. W. Lee, S. S. Nam, M. J. Choi, K. W. Lee, *Catal. Lett.* **1998**, *56*, 215-219; (b) H. M. Torres Galvis, J. H. Bitter, C. B. Khare, M. Ruitenbeek, A. I. Dugulan, K. P. de Jong, *Science* **2012**, *335*, 835-838.

[7] B. Hu, S. Frueh, H. F. Garces, L. Zhang, M. Aindow, C. Brooks, E. Kreidler, S. L. Suib, *Appl. Catal., B* **2013**, *132–133*, 54-61.

[8] R. W. Dorner, D. R. Hardy, F. W. Williams, H. D. Willauer, *Energy & Environmental Science* **2010**, *3*, 884-890.

[9] (a) D. Chen, K. Moljord, A. Holmen, *Microporous Mesoporous Mater.* **2012**, *164*, 239-250; (b) K. Hemelsoet, J. Van der Mynsbrugge, K. De Wispelaere, M. Waroquier, V. Van Speybroeck, *ChemPhysChem* **2013**, *14*, 1526-1545.

[10] G. Centi, G. Iaquaniello, S. Perathoner, *ChemSusChem* **2011**, *4*, 1265-1273.

[11] L. Xu, Q. Wang, D. Liang, X. Wang, L. Lin, W. Cui, Y. Xu, *Appl. Catal., A* **1998**, *173*, 19-25.

[12] T. Herranz, S. Rojas, F. J. Pérez-Alonso, M. Ojeda, P. Terreros, J. L. G. Fierro, *Appl. Catal., A* **2006**, *308*, 19-30.

[13] D. B. Bukur, X. Lang, D. Mukesh, W. H. Zimmerman, M. P. Rosynek, C. Li, *Ind. Eng. Chem. Res.* **1990**, *29*, 1588-1599.

[14] (a) K. H. Ernst, C. T. Campbell, G. Moretti, *J. Catal* **1992**, *134*, 66-74; (b) N. Schumacher, A. Boisen, S. Dahl, A. A. Gokhale, S. Kandoi, L. C. Grabow, **2005**, *229*, 265-275; (c) T. Shido, Y. Iwansawa, *J. Catal* **1993**, *140*, 575-584; (d) T. Shido, Y. Iwasawa, *J. Catal* **1991**, *355*, 343-355.

[15] (a) H. Ando, Q. Xu, M. Fujiwara, Y. Matsumura, M. Tanaka, Y. Souma, *Catal. Today* **1998**, *45*, 229-234; (b) S. S. Nam, S. J. Lee, H. Kim, K. W. Jun, M. J. Choi, K. W. Lee, *Energy Convers. Manage.* **1997**, *38*, S397-S402; (c) Q. Xu, D. He, M. Fujiwara, M. Tanaka, Y. Souma, H. Yamanaka, *J. Mol. Catal. A: Chem.* **1998**, *136*, 161-168.

[16] W. Jochum, S. Penner, R. Kramer, K. Föttinger, G. Rupprechter, B. Klötzer, *J. Catal* **2008**, *256*, 278 - 286.

[17] M. D. Jones, C. G. Keir, C. D. Iulio, R. A. M. Robertson, C. V. Williams, D. C. Apperley, *Catal. Sci. Technol.* **2011**, *1*, 267-272.

[18] L. Peng, E. Y. Jiang, H. L. Bai, *J. Phys. D: Appl. Phys.* **2011**, *44*, 075003.

[19] S. Yuji, N. Satoshi, H. Kenzo, *Surf. Interface Anal.* **2012**, *44*, 938-941.

[20] A. Bulusu, H. Kim, D. Samet, J. S. Graham, *J. Phys. D: Appl. Phys.* **2013**, *46*, 084014.

[21] X. Zhou, J. Qu, F. Xu, J. Hu, J. S. Foord, Z. Zeng, X. Hong, S. C. Edman Tsang, *Chem. Commun.* **2013**, *49*, 1747-1749.

[22] M. Fujiwara, H. Ando, M. Matsumoto, Y. Matsumura, M. Tanaka, Y. Souma, *Chem. Lett.* **1995**, *24*, 839-840.

[23] Y. Yang, H. W. Xiang, Y. Y. Xu, L. Bai, Y. W. Li, *Appl. Catal., A* **2004**, *266*, 181-194.

[24] (a) W. Qing, Z. Zhengjun, L. Zhengcao, Z. Qin, Z. Yu, *J. Phys. D: Appl. Phys.* **2008**, *41*, 202002; (b) E. de Smit, B. M. Weckhuysen, *Chem. Soc. Rev.* **2008**, *37*, 2758-2781.
[25] C. D. Wagner, G. E. Muilenberg, *Handbook of X-ray Photoelectron Spectroscopy: A Reference Book of Standard Data for Use in X-ray Photoelectron Spectroscopy*, Physical Electronics Division, Perkin-Elmer Corp., **1979**.
[26] K. Jalama, N. J. Coville, H. Xiong, D. Hildebrandt, D. Glasser, S. Taylor, A. Carley, J. A. Anderson, G. J. Hutchings, *Appl. Catal., A* **2011**, *395*, 1-9.
[27] K. Jalama, N. J. Coville, D. Hildebrandt, D. Glasser, L. L. Jewell, J. A. Anderson, S. Taylor, D. Enache, G. J. Hutchings, *Top. Catal.* **2007**, *44*, 129-136.
[28] (a) H. Sakurai, M. Haruta, *Appl. Catal., A* **1995**, *127*, 93-105; (b) H. Sakurai, S. Tsubota, M. Haruta, *Appl. Catal., A* **1993**, *102*, 125-136.
[29] (a) J. Hua, K. Wei, Q. Zheng, X. Lin, *Appl. Catal., A* **2004**, *259*, 121-130; (b) S. Kudo, T. Maki, T. Fukuda, K. Mae, *Catalysts* **2011**, *1*, 175-190.
[30] Y. X. Pan, P. Kuai, Y. Liu, Q. Ge, C. J. Liu, *Energy Environ. Sci.* **2010**, *3*, 1322-1325.
[31] H. J. Wan, B. S. Wu, C. H. Zhang, H. W. Xiang, Y. W. Li, B. F. Xu, F. Yi, *Catal. Commun.* **2007**, *8*, 1538 - 1545.
[32] Z. H. Suo, Y. Kou, J. Z. Niu, W. Z. Zhang, H. L. Wang, *Appl. Catal., A* **1997**, *148*, 301 - 313.
[33] H. J. Wan, B. S. Wu, C. H. Zhang, B. T. Teng, Z. C. Tao, Y. Yang, Y. L. Zhu, H. W. Xiang, Y. W. Li, *Fuel* **2006**, *85*, 1371 - 1377.
[34] J. Ye, C. Liu, Q. Ge, *J. Phys. Chem., C* **2012**, *116*, 7817-7825.
[35] H. Y. Lai, C. H. Chen, C. F. Lee, *Plasmonics* **2010**, *5*, 233-239.
[36] M. Chen, J. Xu, Y. M. Liu, Y. Cao, H. Y. He, J. H. Zhuang, *Appl. Catal., A* **2010**, *377*, 35 - 41.
[37] B. Zheng, W. Hua, Y. Yue, Z. Gao, *J. Catal* **2005**, *232*, 143 - 151.
[38] D. L. Chiavassa, J. Barrandeguy, A. L. Bonivardi, M. A. Baltanás, *Catal. Today* **2008**, *133-135*, 780-786.
[39] (a) X. Yang, L. Du, S. Liao, Y. Li, H. Song, *Catal. Commun.* **2011**, 1-22; (b) J. A. Lopez-Sanchez, N. Dimitratos, P. Miedziak, E. Ntainjua, J. K. Edwards, D. Morgan, A. F. Carley, R. Tiruvalam, C. J. Kiely, G. J. Hutchings, *PCCP* **2008**, *10*, 1921.
[40] M. Peuckert, *J. Phys. Chem.* **1985**, *89*, 2481-2486.
[41] (a) S. E. Collins, D. L. Chiavassa, A. L. Bonivardi, M. A. Baltanás, *Catal. Lett.* **2005**, *103*, 83-88; (b) H. Kong, H. Y. Li, G. D. Lin, H. B. Zhang, *Catal. Lett.* **2011**, *141*, 886-894.

6 Further Investigations into CO_2 hydrogenation over an Fe/SiO_2 catalyst.

Further studies in to the effects of the silica support properties on the performance of an iron-silica catalyst have been conducted with both the pore size and particle diameter having a large effect on catalyst performance both in terms of CO_2 conversion and product selectivity. Investigations were extended to include the influence of reaction conditions such as WHSV, pressure and temperature. From these studies information on activation energies, mass transfer limitations and reaction mechanisms was derived.

While the catalyst composition can have a drastic impact on the CO_2 hydrogenation reaction (as observed in previous chapters) there are a number of other factors that must also be taken into account. These include the reaction conditions; temperature, pressure, flow rate and ratio of the reactants, H_2 and CO_2. The morphology of the catalyst particles used can also influence the reaction.

This chapter focuses on the effects each of the reaction conditions and the morphology of the catalyst particles have on the hydrogenation of CO_2 over an iron catalyst. Studies are also extended to include a basic kinetic investigation in order to gain a deeper understanding of the processes occurring and what may be limiting the conversion of CO_2. For all studies conducted within this chapter a 20wt%Fe/SiO_2 catalyst was used in order to keep the system as non-complex as possible, eliminating any influence a promoter may have.

There are seven main steps typically involved in a reaction over a heterogeneous catalyst. A simplified illustration of these seven steps is shown in Figure 6.1. The first step involves the diffusion of any reactants from the bulk gas-phase to the surface of the solid catalyst this is referred to as external diffusion.

In order to obtain a high catalyst surface area, giving a better dispersion of the active component, heterogeneous catalysts tend to be supported on porous supports. As a result of the catalyst's porous nature the largest part of the active surface is in the interior of the catalyst. This means that in order to reach the active component of the catalyst the majority of the reactants must first diffuse into the catalyst; this is the second step and is referred to as internal diffusion. The third step involves the adsorption of the reactants to the catalyst surface. Once completed the surface reaction can take place, this is the fourth step. After the reaction is completed the products must then desorb from the catalyst surface, diffuse through the porous structure of the catalyst and away from the surface back to the bulk gas phase, steps 5, 6 and 7 respectively, as shown in Figure 6.1.

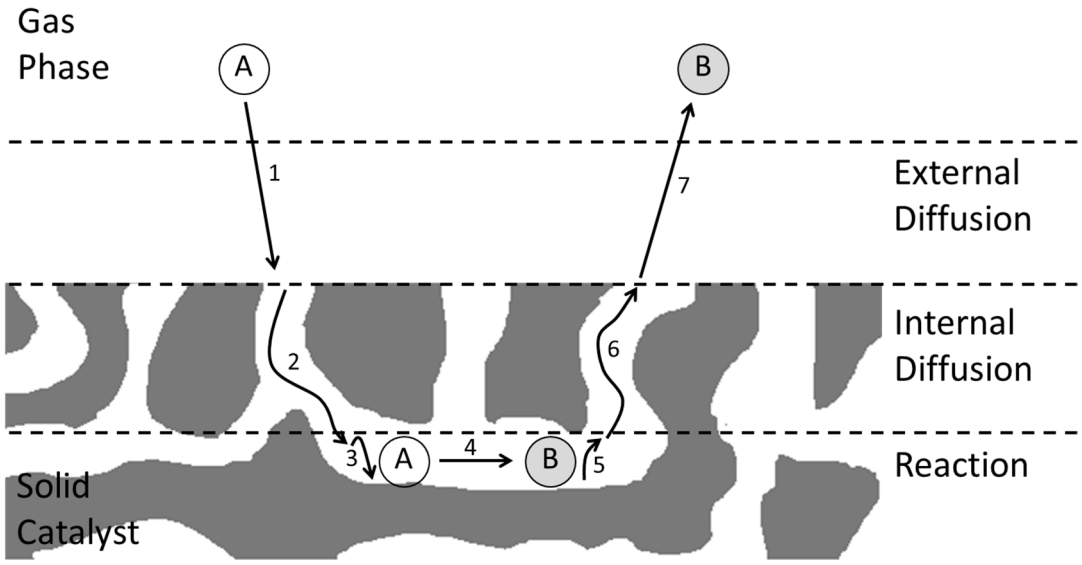

Figure 6.1 – A simplified illustration of the seven main steps involved in a simple reaction occurring over a heterogeneous catalyst

In order to obtain optimum performance form a catalyst system it is of vital importance to understand which of the above steps are responsible for limiting the conversion be it a mass transfer effect, the adsorption/desorption of reactant and products or the surface reaction itself. In the same vein of thought it is important to gain an understanding of the kinetics of the reaction as this can lead to insights into what is limiting the catalyst/reaction performance while also giving us the ability to investigate reaction mechanisms both of which can aid the development of more efficient and better performing systems while also allowing simulation of the reactions.

With the industrial interest shown in both the FT and WGS reactions, kinetic investigations into both of these processes has received a great deal of attention in the literature.[1] Despite the significant interest in the WGS reaction kinetic studies of the RWGS reaction have so far remained limited.[2] Kinetic studies for the overall process of CO_2 hydrogenation have attracted even less attention with very few studies published.[3]

6.1 Investigations into Silica Support Effects on Fe/SiO_2

From the studies conducted on Fe-Pd catalysts in Chapter 4 we know that the particle and pore size of the silica support used can have a dramatic effect on the performance of the catalyst even if the composition of the catalyst is kept constant. Studies in Section 4.4, Chapter 4 in fact showed that the silica properties had the largest influence on the performance of the catalyst in terms of CO_2 conversion and HC distribution.

Both the particle size and pore diameter can have a large influence on the mass transfer properties of the catalyst with smaller particle sizes meaning there are more active sites

available on the particle surface relative to internally and as such the internal diffusion stage becomes less significant. The pore diameter of the silica support can also influence the ease of diffusion and as such the mass transfer.

6.1.1 Catalyst Preparation

In order to investigate the influence of the silica support properties a range of catalysts were prepared using various silica with different particle sizes and pore diameters. The properties of each silica utilised for these tests are summarised in Table 6.1. Each catalyst was prepared using the standard wet impregnation method detailed in full in Chapter 2 Section 2.7.12. The iron content was kept constant for all catalysts with only the silica used altered, the rest of the preparation technique was kept constant. Catalysts are herein labelled 20wt%Fe/SiO_2-X where X indicates the pore size of the silica support used as defined in Table 6.1.

Table 6.1 – Reported properties of each silica used within this chapter as a catalyst support

Silica Denotement	**Pore Size (Å)**	**Particle Size (µm)**	**Surface Area (m^2g^{-1})**
SiO_2-60	60	35-70	550
SiO_2-250	250	35-70	285
SiO_2-500	500	35-70	80
SiO_2-150	150	250-500	300
SiO_2-60_b[a]	60	1000-2000	525[b]

[a] – Subscript b indicates a larger particle size and is used to distinguish between the two silica with 60 Å pores. [b] – Surface area calculated by BET as no value was reported by Davisil.

6.1.2 Catalyst Characterisation

The surface areas of each of the prepared catalysts were determined by N_2 physisorption studies with the results summarised in Table 6.2. The addition of 20wt% iron to the silica support generally results in a decreased surface area most likely due to the filling of pores an effect often observed with similar catalyst systems.[4] The extent of surface area reduction upon iron introduction decreases with larger pore sizes which further supports this theory with the SiO_2-500 supported catalysts showing no decrease in surface area with iron addition. Generally a larger pore diameter silica shows a lower surface area. A smaller particle size, however, appears to have little effect on the catalyst's surface area with both catalysts supported on a silica with a 60 Å pore diameter giving similar surface areas with little difference in the reduction observed when iron is incorporated into the system.

Table 6.2 – BET surface areas calculated for each Fe/SiO_2 catalysts with various silica supports

Catalyst	BET Surface Area (m^2g^{-1})
20wt%Fe/SiO_2-60	371.9
20wt%Fe/SiO_2-250	215.7
20wt%Fe/SiO_2-500	82.0
20wt%Fe/SiO_2-150	222.5
20wt%Fe/SiO_2-60_b	396.6

TEM analysis was also carried out on each sample with the results summarised in Figure 6.2 the apparent particle size observed for each system is shown as an inset in the form of a histogram. Increasing the silica pore size from 60 to 150 to 250 Å increases the apparent particle size as assessed using TEM studies. A slight increase is observed between 60 and 150 Å followed by a significant jump when increased to 250 Å. The catalyst supported on this silica shows relatively large nano-particles evenly distributed between 30 and 90 nm. No distinct nano-particles were observed upon TEM analysis of the SiO_2-500 supported system. The silica particle size appears to have little influence on particle distribution with both silica possessing a 60 Å pore diameter giving very similar nano-particle distributions.

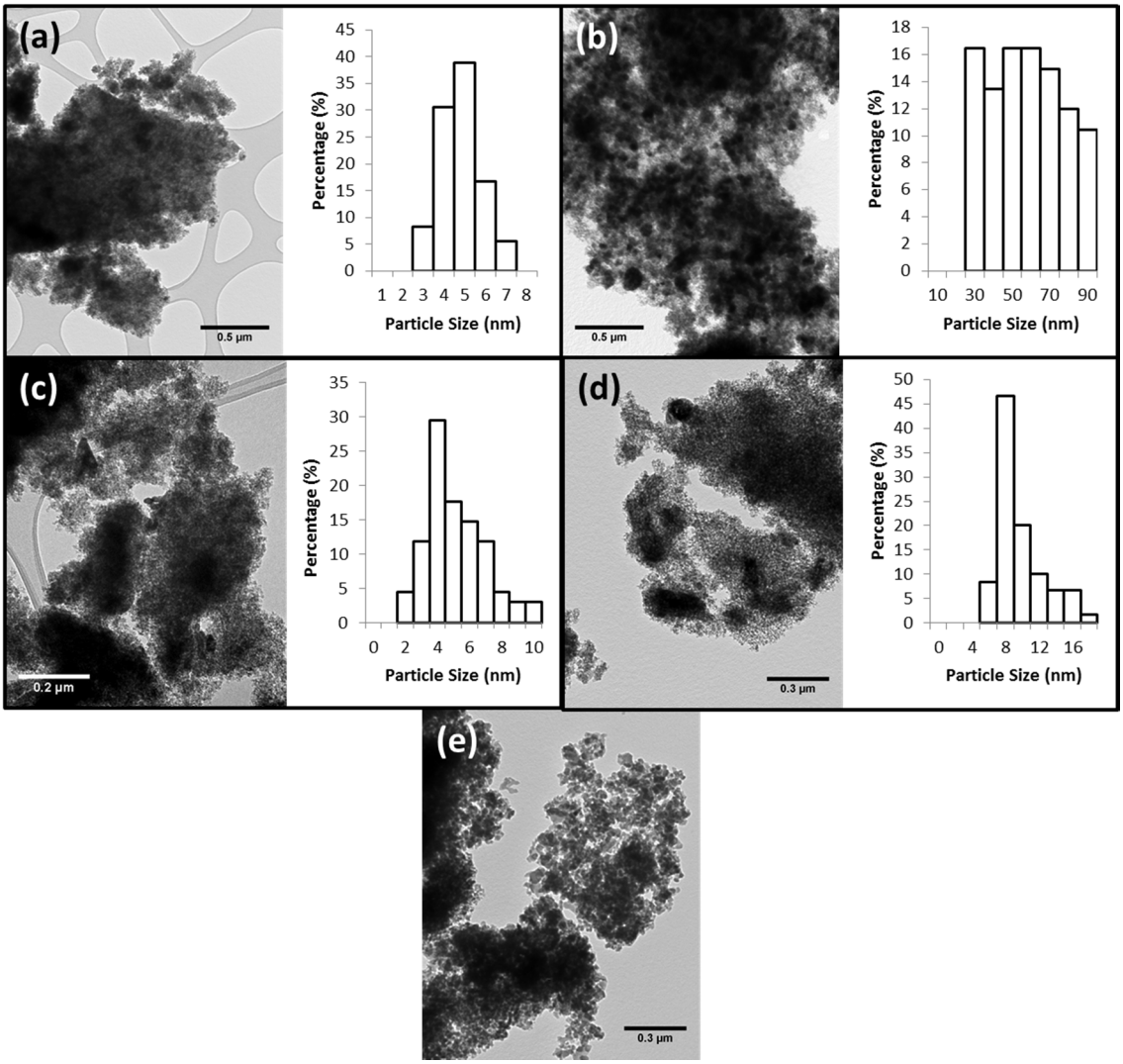

Figure 6.2 – Representative TEM images recorded for (a) 20wt%Fe/SiO_2-60, (b) 20wt%Fe/SiO_2-250, (c) 20wt%Fe/SiO_2-60$_b$, (d) 20wt%Fe/SiO_2-150 and (e). 20wt%Fe/SiO_2-500

6.1.3 Catalyst Testing

For initial tests 1.0 g of each catalyst was mechanically mixed with 10 g of inert silicon carbide so the packing of the catalyst bed would not play a significant role. This mix was then loaded into a ½ inch external diameter, 10 cm length stainless steel tube and held in place using quartz wool. This sample cell was then loaded into Reactor 1. Full details of this set up are given in Chapter 2 Section 2.2. All catalysts were pre-treated at 300 ^oC for 2 hours under a flow of 50 sccm pure hydrogen. With the reduction phase completed the reactor was heater to reaction temperature under a flow of argon before the feed-gas was replaced with a 3:1 ratio of H_2:CO_2. For more information on reaction procedure please refer to Section 2.3, Chapter 2. Conversions, yields and product selectivities were calculated as an average of the last four hours on stream. The data is summarised in Table 6.3

Table 6.3 – Catalytic data obtained for CO_2 hydrogenation tests using 20wt%Fe/SiO_2 catalysts systems with various support properties

Catalyst[a]	CO_2 Conversion (%)	HC Yield (%)	CO Yield (%)	Hydrocarbon Distribution									
				C_1	C_2=	C_2	C_3=	C_3	C_4	C_5	C_6	C_7	C_8
20wt%Fe/SiO_2-60 (Diluted)	11.4	1.8	9.5	80.7	8.6	4.5	5.9	0.1	0.2	0.0	0.0	0.0	0.0
20wt%Fe/SiO_2-250 (Diluted)	14.9	2.3	12.6	73.6	9.02	10.7	6.2	0.4	0.0	0.0	0.0	0.0	0.0
20wt%Fe/SiO_2-500 (Diluted)	21.7	8.4	13.3	63.7	4.4	18.0	6.8	4.4	1.9	0.1	0.1	0.7	0.0
20wt%Fe/SiO_2-60_b (Diluted)	12.0	1.2	10.8	78.8	10.1	2.4	7.7	0.1	0.9	0.0	0.0	0.0	0.0
20wt%Fe/SiO_2-150 (Diluted)	12.2	1.8	10.5	74.1	13.2	2.5	9.4	0.3	0.5	0.0	0.0	0.0	0.0
20wt%Fe/SiO_2-60	19.0	6.7	12.3	69.4	4.4	16.1	6.4	2.9	0.8	0.0	0.0	0.0	0.0
20wt%Fe/SiO_2-250	34.8	25.6	9.3	64.5	0.7	22.0	1.8	8.7	2.1	0.2	0.0	0.0	0.0
20wt%Fe/SiO_2-500	36.1	17.1	19.0	61.5	2.6	21.6	5.4	5.6	2.5	0.8	0.0	0.0	0.0
20wt%Fe/SiO_2-60_b	13.6	3.6	10.0	75.1	2.3	15.2	4.4	3.1	0.0	0.0	0.0.	0.0	0.0
20wt%Fe/SiO_2-150	13.8	4.8	9.0	69.5	1.8	19.6	3.8	4.9	0.3	0.0	0.0	0.0	0.0

[a] Catalyst were either diluted in SiC (1 g catalyst in 10 g SiC) and packed into a 100 mm in length ½ inch external diameter catalyst bed, labelled diluted, or were tested in a non diluted packed bed 130 mm in length ¼ inch external diamter. Catlyst tests conducted at atmospheric pressure, H_2:CO_2 ratio 3:1, total flow – 8 sccm. 0.7g of catalyst. Conversions, yields and product distributions calculated as an average of 4 hours on stream after catalyst stabilisation.

Upon comparison of the results obtained from the catalysts supported on SiO_2-60, SiO_2-250 and SiO_2-500 it is possible to see the influence of the pore diameter as all possess the same particle size. Figure 6.3 (a) shows how the CO_2 conversion value obtained increases steadily with increasing silica pore diameter. Product distribution is also strongly influenced as shown in Figure 6.3 (b). As the diameter of the pore is increased methane selectivity drops with a concurrent increase in selectivity to heavier C_2+ HCs. Despite the fact that SiO_2-150 has a different silica particle size when plotted on the same axis as the SiO_2-60, SiO_2-250 and SiO_2-500 supported systems it shows only a slight deviation from the trend observed (white markers, Figure 6.3) indicating that for a diluted catalyst test such as this the catalyst particle size does not play a significant role. This is further confirmed by comparing the results obtained from the SiO_2-60 and SiO_2-60_b supported catalyst systems which despite large differences in particle size show very similar catalytic results.

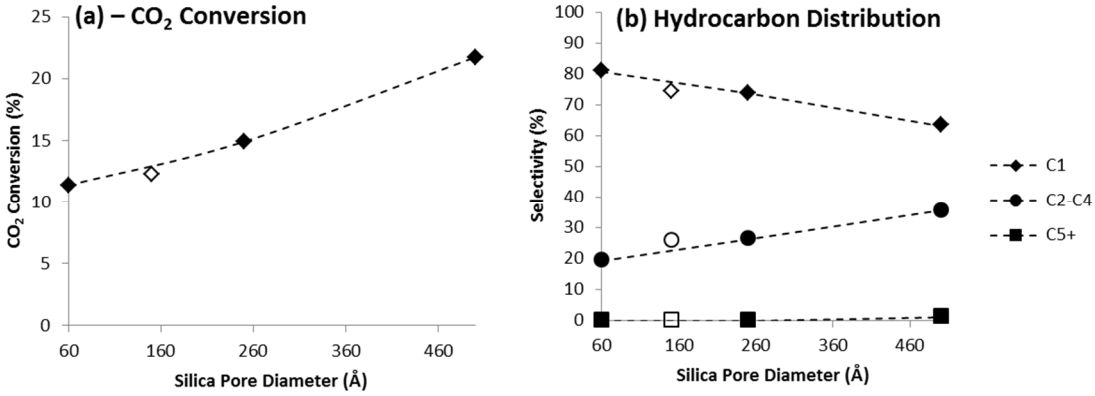

Figure 6.3 – Plots showing (a) the variation of CO_2 conversion with increasing pore diameter and (b) the differing hydrocarbon distribution observed with larger pore diameters. Solid black markers represent silica particles with a same average size, white markers show SiO_2-150 with a larger particle diameter.

Based on the minimal difference in catalyst performance based on silica particle size it suggests that under these test conditions the reaction is not limited by internal diffusion. This suggests that the differences observed for catalysts with differing pore diameters is not due entirely to their effects on internal diffusion. Similar results have been observed with cobalt-based Fischer-Tropsch catalysts and in these instances the enhanced catalyst performance observed with larger pore diameters has been attributed to the larger cobalt crystallites formed in the presence of larger pores.[5] It is entirely possible that a similar effect is occurring here with these iron-silica catalysts. While the crystallite size cannot be determined by XRD as the catalysts tested showed no diffraction peaks attributable to the iron phases, the TEM studies conducted (Figure 6.2) do however show a difference in particle size which support this.

With all catalyst tests conducted in previous chapters being carried out in an un-diluted packed bed reactor each of the catalysts were tested again in this manner. 0.7 g of catalyst was

packed into a 130 mm long, ¼ inch external diameter reactor. The remainder of the catalyst test procedure remained the same. For the full experimental procedure please refer to Section 2.3, Chapter 2.

As with the diluted catalyst tests there was no significant deviation in the CO_2 conversion or the product selectivity with time on stream with all catalysts appearing stable over the 5 hour period of the test. The catalytic data obtained is summarised in Table 6.3.

All catalyst tests conducted in a non-diluted packed bed show a significantly higher CO_2 conversion. The CO_2 conversion is observed to increase with increasing silica pore diameter as observed with the diluted tests as shown in Figure 6.4 (a). The increase observed between SiO_2-250 and SiO_2-500 is however not as significant. A higher selectivity to CO over HCs is also observed for the SiO_2-500 catalyst system resulting in a drop in HC yield when the silica pore size is increased from 250 Å to 500 Å. The hydrocarbon distribution improves with larger silica pore diameters with a reduction in methane selectivity and a larger amount of C_2+ HCs formed {Figure 6.4 (b)}. This is the same trend observed for the diluted catalyst tests.

Unlike the catalyst tests conducted in a diluted bed when SiO_2-150 is plotted on the same axis {white marker Figure 6.4 (a)} as SiO_2-60, SiO_2-250 and SiO_2-500 the CO_2 conversion shows a distinct difference from the trend observed indicating that for a non-diluted catalyst test the particle size plays a far more important role. When product selectivity is compared however {Figure 6.4 (b)} the difference is significantly smaller. A similar trend in conversion is observed when comparing SiO_2-60 and SiO_2-60_b with a lower CO_2 conversion observed with a larger silica particle size.

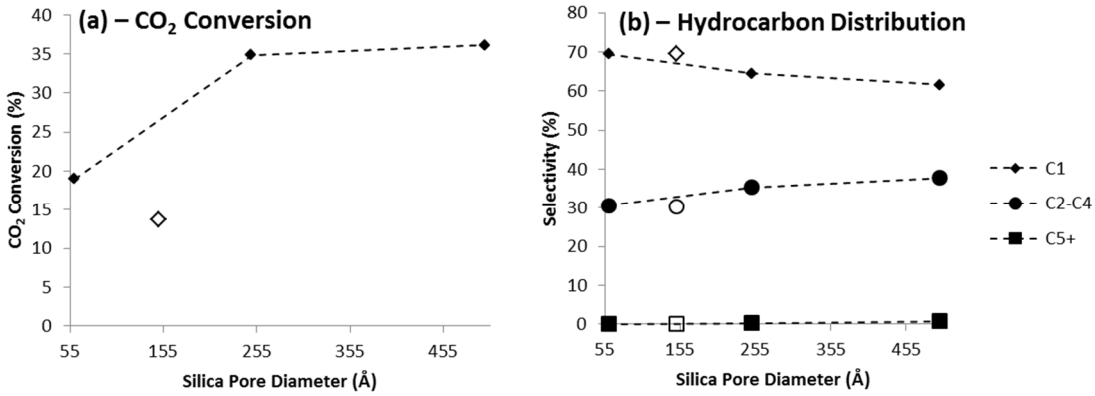

Figure 6.4 – Plots showing (a) the variation of CO_2 conversion with increasing pore diameter and (b) the differing hydrocarbon distribution observed with larger pore diameters. Solid black markers represent silica particles with a same average size, white markers show SiO_2-500 with a larger particle diameter.

The above results illustrate that properties of the silica support can strongly affect the performance of the catalyst. The effect of pore size on internal diffusion cannot be determined simply by varying the diameter of the silica pore size as this can influence other properties of

the catalyst such as the nano-particle size. The influence of the silica particle size appears to have more of an influence on an un-diluted packed bed suggesting that this could be due to the packing efficiency in combination with mass transfer effects. Further studies are required to investigate these effects in more detail.

6.2 Influence of Reaction Temperature

The reaction temperature can significantly influence the reaction. With the hydrogenation of CO_2 consisting of a two-step process, the endothermic RWGS reaction (Equation 6.1) followed by the exothermic FT process (Equation 6.2) this adds further complications.[6] Studies have shown that the effects of temperature on the Fischer-Tropsch are significant with a higher temperature generally leading to a poorer product distribution with high methane selectivity.[1a] Generally, with the RWGS reaction being endothermic, higher reaction temperatures lead to larger conversions. This means that in order to get high CO_2 conversion and good selectivity towards the heavier hydrocarbons a compromise on temperature must be reached illustrating the importance of reaction temperature particularly with CO_2 hydrogenation.

$$CO_2 + H_2 \rightleftharpoons CO + H_2O,\ \Delta_R H^0_{298} = 41\ kJ\ mol^{-1}$$

Equation 6.1 – The reverse water-gas shift reaction

$$CO + 2\ H_2 \rightarrow -(CH_2)- + H_2O,\ \Delta_R H^0_{298} = -152\ kJ\ mol^{-1}$$

Equation 6.2 – The Fischer-Tropsch process

The CO_2 conversion obtainable over the iron catalysts tested thus far is dependent on the effectiveness of the RWGS reaction as CO_2 must first be converted to CO before HCs can be formed. The RWGS reaction is an equilibrium process (Equation 6.1) and so the equilibrium position will affect the maximum CO_2 conversion possible. Gibbs free energy calculations indicate that in the temperature range under investigation equilibrium constraints exist as such the equilibrium conversion of CO_2 has been calculated.

The calculated CO_2 equilibrium conversion values are shown to increase with increasing temperature, as would be expected with the endothermic nature of the reaction (see Figure 6.5). A maximum conversion of *ca*. 20 % is observed at 300 ^oC and is just above 40 % at 450 ^oC, a temperature above that normally utilised in FT catalysis in order to obtain good product selectivity. These initial conversion calculations only take into account the RWGS component of the process and since the overall process also includes a second FT step which consumes CO a second calculation was also conducted to take this into account. A measurable increase in equilibrium CO_2 conversion is observed when 90 % of the formed CO is removed. This shifts the equilibrium position and as a result the CO_2 conversion values obtainable up to *ca*. 50 % at 300 ^oC and close to 80 % at 450 ^oC.

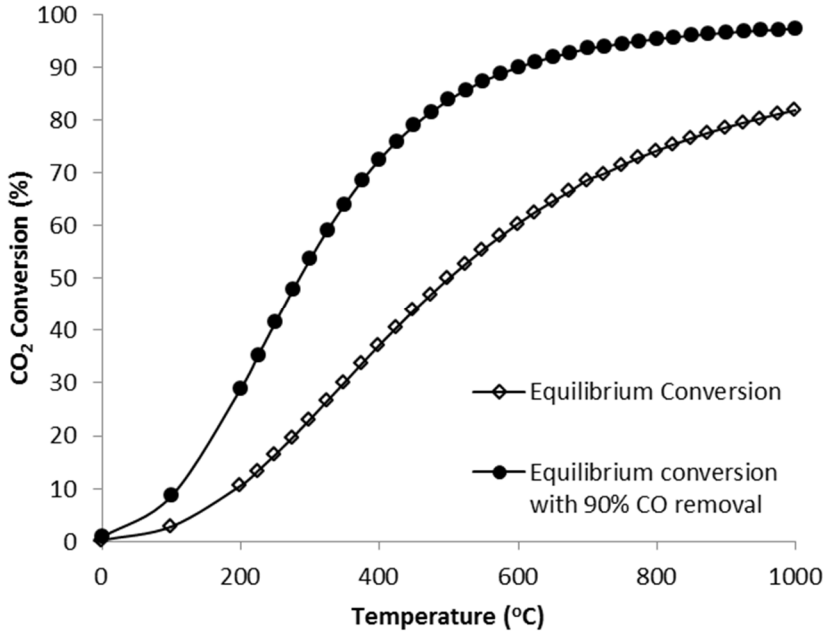

Figure 6.5 – Calculated equilibrium conversion of CO_2 as a function of temperature

6.2.1 Catalyst Testing

For investigations into the effect of temperature on CO_2 hydrogenation the 20wt%Fe/SiO_2-250 catalyst system was chosen as it showed the highest HC yield of the catalysts tested. Catalyst tests were conducted in Reactor 1 in an undiluted packed bed. Full details of the general procedure are detailed in Section 2.3, Chapter 2. The test was repeated seven times at various temperatures from 230 ^oC to 430 ^oC. The results obtained from these catalyst tests are summarised in Table 6.4.

Table 6.4 – Catalytic data obtained for CO_2 hydrogenation tests using 20wt%Fe/SiO_2-250 catalysts over a range of temperatures

Temperature (^oC)	CO_2 Conversion (%)	HC Yield (%)	CO Yield (%)	Hydrocarbon Distribution									
				C_1	C_2=	C_2	C_3=	C_3	C_4	C_5	C_6	C_7	C_8
230	4.1	0.9	3.2	100.0	0.0	0.0	0.0	0.0	0.0	0.0	0.0	0.0	0.0
250	8.5	1.7	6.8	70.1	0.0	13.8	0.0	8.5	3.7	1.9	2.2	0.0	0.0
280	16.2	9.2	6.9	56.9	0.0	18.7	0.0	13.0	5.2	3.8	2.3	0.0	0.0
300	23.8	17.3	6.5	44.1	0.3	23.2	1.2	16.7	8.0	3.7	2.2	0.6	0.0
330	37.2	31.2	6.1	46.0	0.7	21.5	1.8	13.9	6.8	3.6	3.4	2.2	0.0
380	38.3	29.6	8.7	59.5	1.5	22.5	3.2	9.1	3.3	0.9	0.0	0.0	0.0
430	36.4	23.8	12.6	81.2	1.2	14.0	1.1	2.4	0.0	0.0	0.0	0.0	0.0

Catlyst tests conducted at atmospheric pressure, H_2:CO_2 ratio 3:1, total flow – 8 sccm. 0.7g of catalyst.

CO_2 conversion values are observed to increase with increasing temperature as predicted by the thermodynamic calculations discussed earlier. A comparison plot showing how the measured CO_2 conversion compares to the calculated equilibrium conversion is shown in Figure 6.6. At temperatures below 280 ^oC the rate of RWGS reaction is slow and the equilibrium conversion is not reached. At a temperature of 280 ^oC the measured CO_2 conversion value matches the equilibrium conversion however at temperatures above this CO_2 conversion values exceed the calculated equilibrium conversions for the RWGS reaction alone. At these temperatures the rate of HC formation is high and so CO consumption should be taken into account, giving a higher possible CO_2 conversion. This was found to be higher than the CO_2 conversion values obtained suggesting that either the CO consumption is not as high as the 90 % modelled or there are processes other than the equilibrium constraints limiting CO_2 conversion. At temperatures about 300 ^oC conversion shows no further increase.

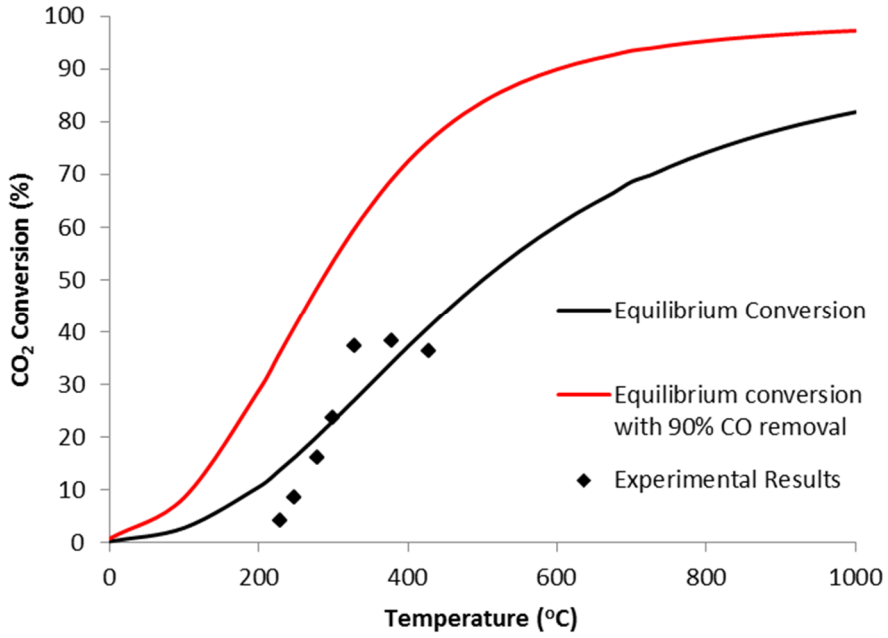

Figure 6.6 – Measured CO_2 conversion values resulting from CO_2 hydrogenation over 20wt%Fe/SiO_2-250 (0.7g catalyst, 3:1 H_2:CO_2 ratio, total flow 8 sccm). Calculated equilibrium conversion curves shown for comparison.

Product selectivity is significantly influenced by the temperature of the reaction. Generally a lower reaction temperature in the FT process favours the formation of longer chained HCs.[1a] Figure 6.7 (a), showing the variation of hydrocarbon distribution with temperature, illustrates that the same is not initially the case with CO_2 hydrogenation. Initially a high methane selectivity is observed this can likely be attributed to the low rate of the RWGS reaction which means although CO is being formed the H_2/CO ratio is relatively high so a poor selectivity to heavier HCs is observed. As the temperature is increased and a larger amount of CO is formed the H_2/CO ratio is lowered and the formation of heavier hydrocarbons is favoured.

ASF plots for each temperature are also shown in Figure 6.7 (b) with the calculated chain growth probabilities tabulated in Figure 6.7 (c).

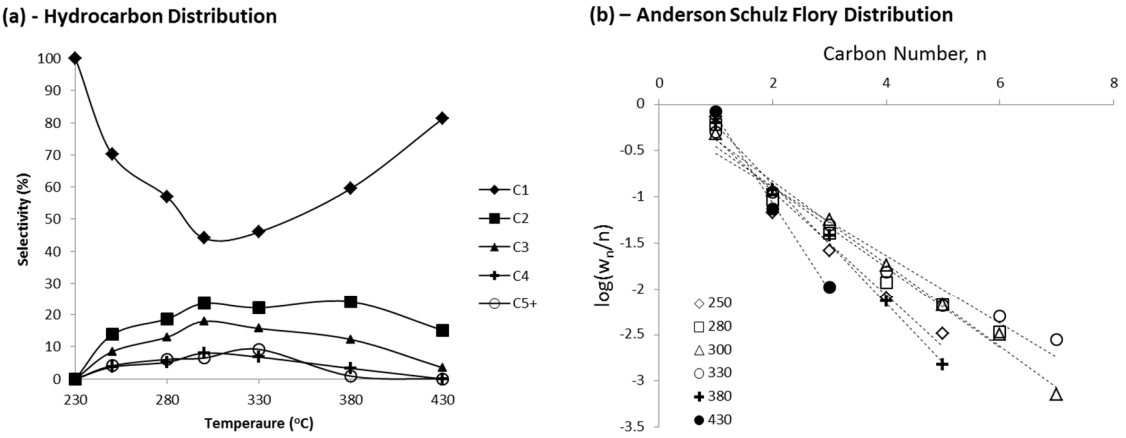

(c) – Chain growth probabilities

Temperature (°C)	230	250	280	300	330	380	430
Chain Growth Probability, α	0.00	0.27	0.37	0.36	0.43	0.23	0.11

Figure 6.7 – (a) Plot showing the variation of hydrocarbon distribution with temperature. (b) ASF plots recorded for each temperature. (c) Calculated chain growth probabilities.

A reaction temperature of 330 °C gives the highest chain growth probability (0.43) with the highest selectivity to C_5+ hydrocarbons. When the reaction temperature is increased beyond this point selectivity to methane increases as has been seen previously with FT systems.[1a] A concurrent decrease in calculated α values is also observed.

The effect of temperature was further investigated using the Arrhenius equation (Equation 6.3). It allows the calculation of the activation energy of CO_2 hydrogenation which in this instance corresponds to the activation energy of the RWGS reaction as all CO_2 converted whether to HCs or CO must first proceed *via* the RWGS reaction. It is also possible to calculate the activation energy for the hydrogenation of CO_2 to hydrocarbons based on the HC yield results. According to the Arrhenius equation a plot of ln(k) against 1/T should give a straight line with a gradient of $-E_a/R$ from which the activation energy can be calculated.

$$k = A\, e^{\frac{-E_a}{(RT)}}$$

Equation 6.3 – The Arrhenius equation

Since the rate of reaction is proportional to the conversion and yield this allows the calculation of activation energy based on a plot of the natural log of conversion/yield {ln(X)/ln(Y)} against 1/T. It must be noted, however, that under these conditions the intercept is no longer equivalent to the Arrhenius pre-exponential factor. Figure 6.8 shows the Arrhenius plot for the process based on conversion of CO_2 and HC yield.

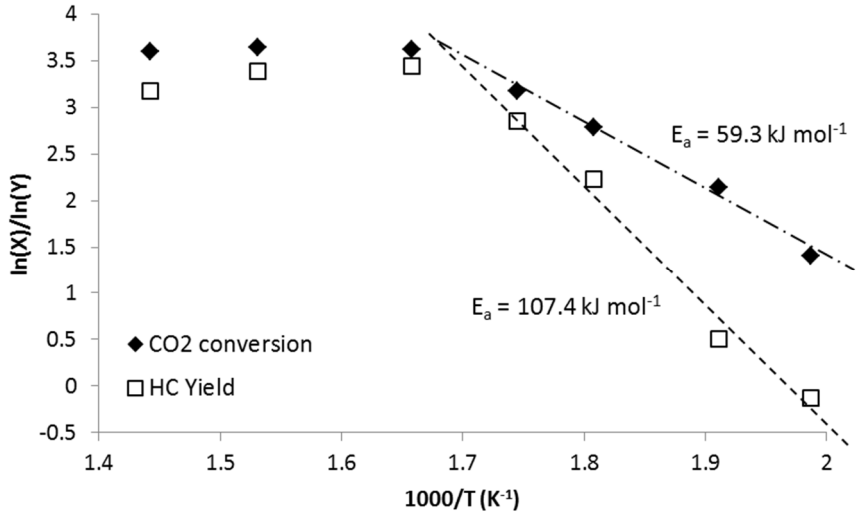

Figure 6.8 – Arrhenius plot for 20wt%Fe/SiO_2-250 (3:1 H_2:CO_2, total flow 8 sccm)

As stated if the reaction obeyed the Arrhenius equation a linear relationship would be expected. The plot shown in Figure 6.8 however shows two distinct sections. At lower temperatures (between 230 ^oC and 300 ^oC) a linear relationship is observed indicating that the overall rate of CO_2 conversion and HC yield is controlled by the rate of the surface reaction and as such the plot can be used to calculate the activation energies associated with each process in this region. At higher temperatures (> 300 ^oC) both plots plateau. This is likely due to a higher rate of surface reaction due to an increased temperature which in turn leads to a mass transfer limitation of the overall process. This mass transfer limitation observed provides an explanation for the levelling off of the CO_2 conversion values observed in Table 6.4 and Figure 6.6.

The activation energies for CO_2 conversion and HC formation were calculated from the lower temperature data points and are shown in Figure 6.8. As mentioned earlier due to the fact that all CO_2 must first be converted to CO *via* the RWGS reaction regardless of final product, the activation energy of 59.3 $kJmol^{-1}$ obtained from the CO_2 conversion is the activation energy of the FT process over this particular catalyst. This value of 59.3 $kJmol^{-1}$ is close to literature values previously reported for this reaction over iron-based catalysts.[7] An activation energy of 107.4 $kJmol^{-1}$ was calculated for the conversion of CO_2 to hydrocarbons.

In order to gain a better understanding of the effect of temperature on the processes involved in the overall hydrogenation of CO_2 catalyst tests were conducted over a range of temperatures with a CO/H_2 feed to fully establish the effect on the FT component of the process. For the catalyst tests all reaction conditions were kept the same as the analogous CO_2 hydrogenation temperature range tests with the exception of the feed-gas. For all CO fed tests the H_2/CO ratio was changed to 2:1 to reflect the ratio that would be present had all CO_2 been converted to CO. ($CO_2 + 3H_2 \rightleftharpoons CO + 2H_2 + H_2O$). For these experiments the effects of water formed from the RWGS reaction have not been taken into account although it has been shown

to negatively affect the performance of iron based FT catalysts.[8] Full details of the catalyst testing procedure are shown in Section 2.3, Chapter 2. The data obtained from these studies is summarized in Table 6.5.

CO conversion is seen to steadily increase with increasing temperatures with values much larger than CO_2 hydrogenation observed, as would be expected, since the FT process does not first have to proceed *via* RWGS reaction. The fact the FT reaction does not involve the RWGS reaction means that the process is also not equilibrium controlled like CO_2 hydrogenation. Conversion values and HC yields are not seen to stabilize at higher temperature as observed with the analogous, CO_2 fed, reaction. This suggests that the FT process is not mass transfer limited even at higher temperatures.

The results summarised in Table 6.5 show a large CO_2 yield with the higher temperatures showing a selectivity to CO_2 over HCs of just over 50 %. This indicates that the catalysts show a good activity for the WGS reaction. This is often observed with iron-based FT catalysts and this WGS activity is one of the main reason iron was chosen as the main active component as WGS catalysts are often also active for the RWGS reaction. This does, however, indicate that under the reaction conditions studied thus far a larger quantity of the CO formed from the RWGS reaction under CO_2 hydrogenation conditions may be converted back to CO_2.

Table 6.5 – Catalytic data obtained for CO hydrogenation tests using 20wt%Fe/SiO_2-250 catalysts over a range of temperatures

Temperature (^oC)	CO Conversion (%)	HC Yield (%)	CO_2 Yield (%)	Hydrocarbon Distribution									
				C_1	C_2=	C_2	C_3=	C_3	C_4	C_5	C_6	C_7	C_8
230	2.0	0.0	2.0	0.0	0.0	0.0	0.0	0.0	0.0	0.0	0.0	0.0	0.0
250	3.9	0.0	3.9	0.0	0.0	0.0	0.0	0.0	0.0	0.0	0.0	0.0	0.0
280	14.9	6.7	8.2	44.1	6.1	11.3	16.0	4.3	6.1	6.6	0.0	0.0	0.0
300	20.7	9.8	10.9	37.0	6.1	15.5	15.2	5.5	6.1	6.4	2.2	0.0	0.0
330	34.1	16.5	17.5	30.9	9.9	16.3	17.7	4.9	9.9	6.4	2.1	0.6	0.0
380	51.4	24.4	27.0	32.6	12.7	13.5	19.2	3.6	12.7	5.1	2.9	0.7	0.0
430	82.3	40.9	41.4	44.7	5.1	18.7	12.0	5.7	5.1	2.1	2.6	3.1	0.0

Catlyst tests conducted at atmospheric pressure, H_2:CO ratio 2:1, total flow – 8 sccm. 0.7g of catalyst.

Figure 6.9 (a) shows the variation of hydrocarbon distribution with increasing temperature. At temperatures below 280 ^{o}C no hydrocarbons are formed. As temperatures are increased the selectivity to methane is reduced until 330 ^{o}C where the highest selectivity to C_2+ HCs is observed. This appears to contradict what has been reported previously where lower reaction temperatures give better selectivity to heavier HC products.[1a] An Anderson Schulz Flory plot {Figure 6.6 (b)} was utilised to calculate the chain growth probabilities for the 20wt%Fe/SiO_2-250 catalyst at the various reaction temperatures investigated; the results a tabulated in Figure 6.6 (c). As the temperature is increased the chain growth probability decreases as would be expected based on previous FT studies.[1a] This suggests that the lower selectivity towards heavier hydrocarbons observed at 280 and 300 ^{o}C could possibly be an artefact of the poor conversion observed at these temperatures.

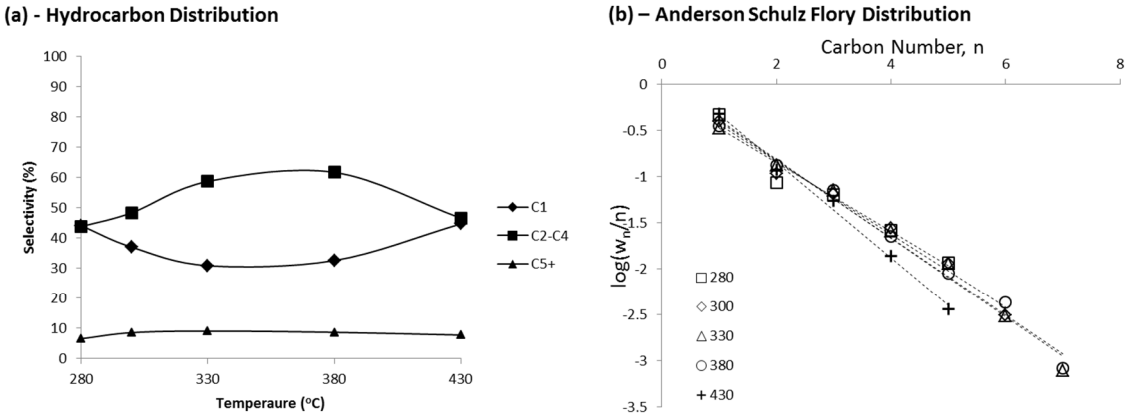

(c) – Chain growth probabilities

Temperature (°C)	280	300	330	380	430
Chain Growth Probability, α	0.42	0.40	0.37	0.37	0.30

Figure 6.9 - (a) The variation of hydrocarbon selectivity with temperature. (b) ASF plots recorded for each temperature (c) Calculated chain growth probabilities.

Figure 6.10 shows Arrhenius plots for (a) the formation of hydrocarbons from the FT process and (b) the formation of CO_2 from the WGS reaction. Figure 6.10 (a) shows a linear relationship between the natural log of the HC yield and 1/T indicating that the system follows Arrhenius behaviour with no mass transport limitations at higher temperatures as observed with the CO_2 hydrogenation process. From this the activation energy of FT can be calculated as 39.4 kJmol^{-1}. This value is lower than the majority of values reported in the literature for the FT process.[3a] Activation energy has however been demonstrated to show a strong dependence on the catalyst used.[9] The fact there is no observable mass transfer limit over the range of temperatures investigated suggests that it is a mass transfer limit on the RWGS reaction that is inhibiting CO_2 conversion in Figure 6.6. The activation energy for the conversion of CO_2 to hydrocarbons (107.4 kJmol^{-1}) appears closely related to the sum of the activation energies of

CO formation from the RWGS reaction (59.3 kJmol^{-1}) and the conversion of CO to HCs *via* the FT process (39.4 kJmol^{-1}).

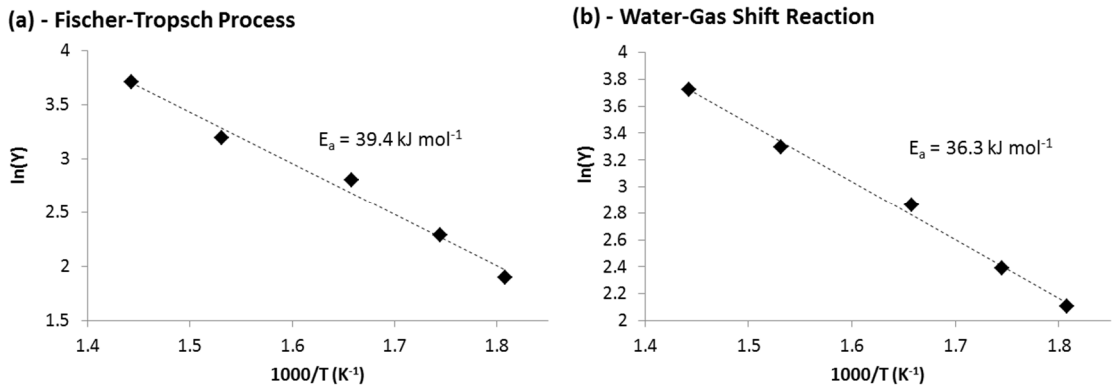

Figure 6.10 - Arrhenius plots for 20wt%Fe/SiO_2-250 (2:1 H_2:CO, total flow 8 sccm). (a) Hydrocarbon formation *via* the Fischer-Tropsch process. (b) CO_2 formation *via* the WGS reaction.

Figure 6.10 (b) shows the Arrhenius plot for the WGS reaction calculated from the CO_2 yield. A linear relationship is observed again suggesting that there are no mass transport limitations on the reaction as observed with the RWGS reaction in the CO_2 hydrogenation studies. An activation energy of 36.3 kJ mol^{-1} was calculated for CO_2 formation *via* the WGS reaction over this catalyst system.

6.3 Influence of External Diffusion

External diffusion can play an important role in the reaction. It determines how fast reactants can get to the catalyst and how fast products can get away. As such if the external diffusion is slow relative to the rate of the reaction taking place on the catalyst surface it can limit the overall reaction rate.

6.3.1 Influence of Flow Rate

In order to investigate the effects of external diffusion in more detail further catalyst tests were conducted to study the influence of feed-gas flow rate. For these studies the 20wt%Fe/SiO_2-250 catalyst used for the previous investigations into the effects of temperature was utilised. Full catalyst test details are given in Section 2.3, Chapter 2. All parameters were kept consistent with previous tests with the exception of the total flow of the CO_2/H_2 feed gas. H_2/CO_2 ratio was kept at 3:1 with total flow increased from 8 sccm through 12 and 16 to 20 sccm.

The variation of flow showed little to no influence on the catalyst stability with CO_2 conversion values and product selectivity remaining relatively unchanged with increasing time on stream. The data obtained from each catalyst test is summarised in Table 6.6.

Table 6.6 – Catalytic data obtained for CO_2 hydrogenation tests using 20wt%Fe/SiO_2-250 catalysts over a range of flows/residence times

Total Flow (sccm)	WHSV (h^{-1})	CO_2 Conversion (%)	HC Yield (%)	CO Yield (%)	Hydrocarbon Distribution									
					C_1	C_2=	C_2	C_3=	C_3	C_4	C_5	C_6	C_7	C_8
8	0.35	35.4	24.8	10.6	54.7	1.5	20.8	4.1	10.6	7.1	1.2	0.0	0.0	0.0
12	0.52	26.0	15.0	11.1	58.8	2.4	19.5	5.8	7.7	4.7	1.1	0.0	0.0	0.0
16	0.69	19.5	8.8	10.7	63.5	3.2	18.1	6.5	5.3	2.1	1.3	0.0	0.0	0.0
20	0.87	16.9	7.0	9.9	68.2	3.7	15.7	6.0	4.3	2.2	0.0	0.0	0.0	0.0

Catlyst tests conducted at atmospheric pressure, H_2:CO ratio 2:1, total flow – 8 sccm. 0.7g of catalyst.

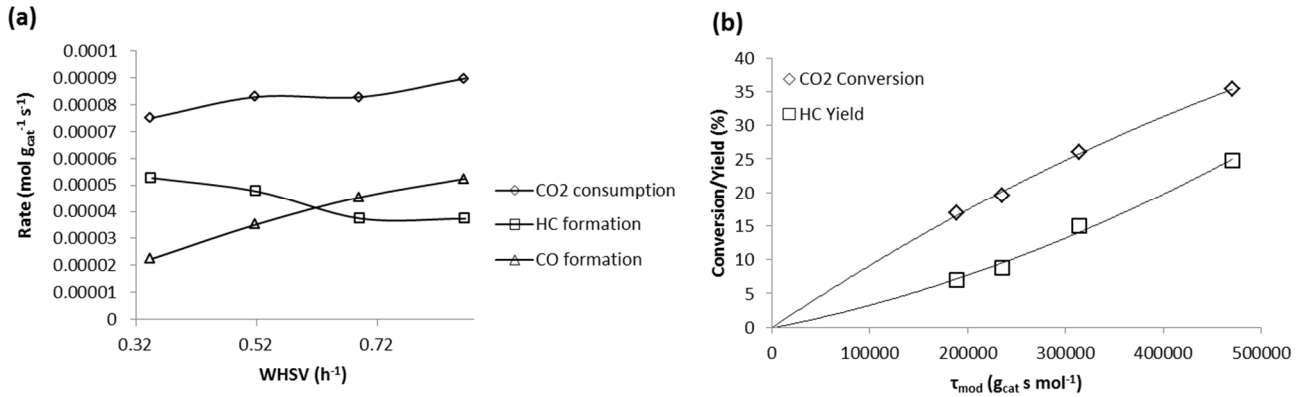

Figure 6.11 – (a) A plot showing the variation in rate with increasing WHSV (b) A Plot showing the variation in CO_2 conversion/HC yield with increasing τ_{mod}

Generally as the flow of the CO_2/H_2 feed gas is increased CO_2 conversion is observed to decrease steadily, a trend also observed with the HC yield. With increasing flow HC selectivity is shifted towards methane and away from the more desirable, heavier HCs. Figure 6.11 (a) shows a plot of average reaction rate over the course of each catalyst test against the weight hourly space velocity (WHSV). The rate of CO_2 consumption shows little change with increasing WHSV indicating that the effect of external mass transfer on catalyst performance is small.

The modified residence time, τ_{mod} was calculated according to Equation 6.4. A plot of τ_{mod} against CO_2 conversion and HC yield is shown in Figure 6.11 (b) An increasing modified residence time results in an increased CO_2 conversion and HC yield. The same trend is observed by Riedel *et al*. over a K-promoted iron catalyst at relatively low residence times.[3a] From the gradient of the plot the rate of CO_2 consumption can be determined. The initial gradient at low conversion values corresponds to the rate under initial conditions (no mass transfer effects and partial pressures of products equal to zero) similar to a differential reactor. The rate determined from this plot was found to be 9.61×10^{-5} $molg^{-1}s^{-1}$, which corresponds well with the average reaction rate observed in Figure 6.11 (a).

$$\tau_{mod} = \frac{Mass_{cat}}{\dot{N}}$$

Equation 6.4 – Modified residence time, τ_{mod}. Where $Mass_{cat}$ – is the catalyst mass utilised and $\dot{N}$ is the molar flow rate

6.4 Influence of Internal Diffusion

For the majority of catalysts, such as those discussed within this chapter, the largest part of active surface area is located within the porous structure of each catalyst particle. As such it is not only the mass transfer involved in the external diffusion that plays a role in catalyst performance. The diffusion of reactants to the active sites within each catalyst particle also plays an important role. In order to study the effects that the internal diffusion has on the catalyst performance a number of catalyst tests were carried out on catalysts with varying particle diameters, d_p.

6.4.1 Catalyst Preparation and Characterisation

In order to examine a wide range of particle sizes SiO_2-60_b was chosen as a catalyst support as, possessing the largest diameter (1000-2000 μm), it allowed for the preparation of the largest range of particle diameters. Initially the catalysts were sieved using 1000 and 2000 μm sized sieves to ensure only particles between these diameters were present. The support was then ground in a pestle and mortar and sieved further between various mesh sizes to give SiO_2-60_b with the following particle diameter ranges; 1000-2000 μm, 355-500 μm, 180-250 μm, 106-

125 μm, 53-75 μm and <20 μm. Catalysts were prepared using the standard wet impregnation technique as detailed in Chapter 2, Section 2.7.12 with the particle size of the SiO_2-60_b support used varied giving catalysts with the composition 20wt%Fe/SiO_2-60_b only with a range of catalyst particle sizes.

N_2 physisorption experiments were conducted to calculate the specific BET surface areas of each catalyst system. The data from these experiments is shown in Table 6.7. Generally there is a slight increase in surface area with larger silica particle sizes.

Table 6.7 – BET surface areas for 20wt%Fe/SiO_2-60_b catalysts with varying particle sizes

Particle size of the SiO_2-60_b support used (μm)	BET Surface Area (m^2g^{-1})
<20	334.5
53-75	333.4
106-125	363.6
180-250	361.8
355-500	378.5
1000-2000	396.7

6.4.2 Catalyst Testing

Catalyst tests were conducted in Reactor 1 using the regular procedure as detailed in Section 2.3, Chapter 2 with only the catalyst tested changed between runs. The mass of catalyst was kept constant. For all catalyst tests CO_2 conversion and hydrocarbon selectivities over the course of the reaction were found to be stable with no apparent effect of particle size on the catalyst stability. The catalytic data obtained from each test is summarised in Table 6.8.

As the particle size is reduced there is a significant influence on the catalyst performance. CO_2 conversion increases with a smaller diameter with the smaller particles generally leading to a lower methane selectivity and higher quantity of C_2+ HCs formed. This large impact of particle size strongly suggests that the internal mass transfer is having a large impact on the catalyst performance.

Table 6.8 – Catalytic data obtained for CO_2 hydrogenation over a 20wt%Fe/SiO_2-60$_b$ with varying particle sizes

Particle diameter range (μm)	CO_2 Conversion (%)	HC Yield (%)	CO Yield (%)	Hydrocarbon Distribution									
				C_1	C_2=	C_2	C_3=	C_3	C_4	C_5	C_6	C_7	C_8
<20	41.9	34.0	7.9	66.3	0.6	19.6	1.1	8.6	2.9	0.7	0.2	0.0	0.0
53-75	24.6	14.7	9.9	59.4	2.2	21.4	4.5	8.3	3.2	0.6	0.0	0.0	0.0
106-125	15.4	5.2	10.2	69.8	8.5	13.0	7.7	0.9	0.3	0.0	0.0	0.0	0.0
180-250	15.0	5.3	9.7	73.6	10.2	8.8	7.4	0.0	0.0	0.0	0.0	0.0	0.0
355-500	14.0	4.3	9.7	74.4	10.7	7.1	7.9	0.0	0.0	0.0	0.0	0.0	0.0
1000-2000	13.1	3.3	9.8	80.3	11.0	2.8	5.8	0.0	0.1	0.0	0.0	0.0	0.0

Catlyst tests conducted at atmospheric pressure, H_2:CO_2 ratio 3:1, total flow – 8 sccm. 0.7g of catalyst.

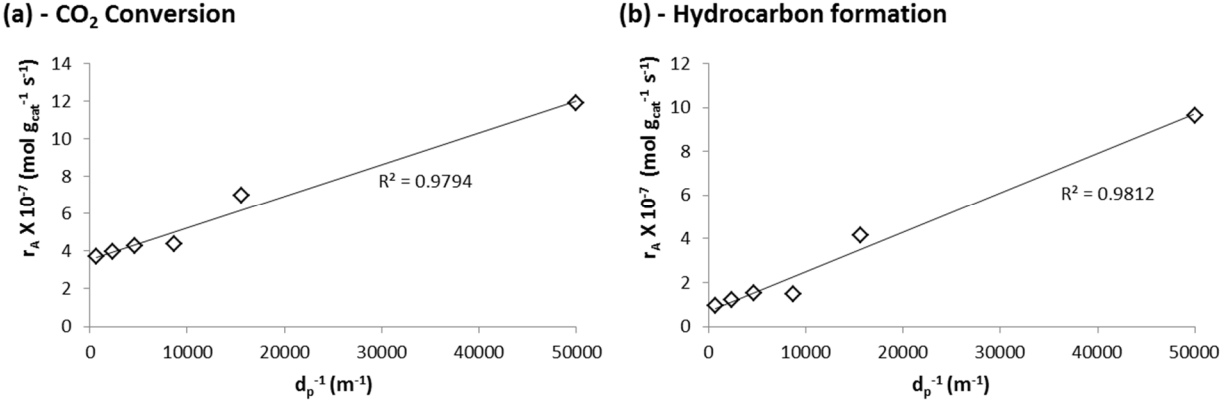

Figure 6.12 – Plots of r_A against d_p^{-1} for (a) CO_2 consumption and (b) HC formation

Studies contained within the previous section suggest that the external mass transfer effects (transfer of reactant species from the bulk flow to the surface of the catalyst) are minimal which indicates that it is the internal diffusion (transfer of reactant species from the surface of a catalyst particle to the interior) that is limiting the reaction and resulting in the alteration of CO_2 conversion values observed.

For reactions that are diffusion limited in this manner the concentration of reactant is lower inside each catalyst particle than at the surface and as such the reaction rate in the interior of each particle will likely also be lower. This decrease in reaction rate inside each particle relative to the surface can be described by the effectiveness factor (Equation 6.5) where r_A is the observed/actual reaction rate and r_{As} is the rate of reaction at the surface of each particle (i.e. without any mass transfer limitations). The effectiveness factor, μ, usually takes a value between 0 and 1 where a value of 1 indicates that the reaction rate inside each particle is equal to that observed on the surface, i.e. there are no mass transfer limitations. Lower μ values indicate an increasing mass transfer limitation.

$$\mu = \frac{r_A}{r_{As}}$$

Equation 6.5 – The effectiveness factor

The relative ratio of the rate of reaction to the rate of diffusion can be described by the Thiele modulus, Φ. If the reaction is diffusion limited as the results in Table 6.8 suggest then the Thiele modulus for the reaction should be large. For high Φ values the approximation that $\mu = 3/\Phi$ can be used.[10] If this is substituted into Equation 6.5 then the observed rate of reaction can be expressed as Equation 6.6.

$$r_A = \frac{3}{\Phi} r_{As}$$

Equation 6.6 – Observed rate of reaction in terms of Thiele modulus

The Thiele modulus for an nth order reaction is shown in Equation 6.7 where D_e is the effective diffusivity, k_n is the rate constant for the reaction, S_a is the surface area per unit mass of catalyst, ρ_c is the catalyst density, R is the particle radius and C_{As}^{n-1} is the surface concentration of reactant. If this is substituted into Equation 6.6 along with the expression for rate of surface reaction; $r_{As} = k_n S_a \rho_c C_{As}^{n}$ then the observed rate of reaction can be written as Equation 6.8.

$$\frac{1}{\Phi} = \sqrt{\frac{D_e}{k_n R^2 S_a \rho_c C_{As}^{n-1}}}$$

Equation 6.7 – The Thiele modulus for the nth order of reaction

$$r_A = 3\sqrt{\frac{D_e}{k_n R^2 S_a \rho_c C_{As}^{n-1}}}\; k_n S_a \rho_c C_{As}^n$$

Equation 6.8 – The observed rate of reaction

Therefore, according to Equation 6.8, the observed rate of reaction is proportional to the inverse of the particle radius, R. From this we can say the reaction rate observed for CO_2 consumption should be proportional to 1 over the catalyst particle diameter d_p. As such a plot of observed rate against d_p^{-1} should give a straight line with an intercept of 0. Plots for CO_2 consumption and HC formation are shown in Figure 6.12.

Both show a linear relationship that indicates that the reactions are being mass transfer limited by internal diffusion. Despite the linear relationship shown the intercept value for both CO_2 conversion and HC formation is not zero as predicted. This indicates that while the reaction is limited by internal diffusion there are also other contributing factors.

The catalyst tests were repeated under the same reaction conditions with a CO/H_2 feed in order to ascertain the impact of internal diffusion on the FT component of the CO_2 hydrogenation process. As with the previous CO fed tests within this chapter the ratio of carbon source to hydrogen was altered from 3:1 to 2:1 with the overall flow kept constant. The data obtained is summarised in Table 6.9.

Table 6.9 – Catalytic data obtained for CO hydrogenation over a 20wt%Fe/SiO_2-60$_b$ with varying particle sizes

Particle diameter range (μm)	CO Conversion (%)	HC Yield (%)	CO_2 Yield (%)	Hydrocarbon Distribution									
				C_1	C_2=	C_2	C_3=	C_3	C_4	C_5	C_6	C_7	C_8
<20	82.7	56.9	25.8	41.7	1.0	25.2	3.9	14.2	7.8	3.8	1.9	0.4	0.0
53-75	42.2	22.3	19.9	39.5	11.0	16.3	16.6	4.1	7.8	3.5	1.2	0.0	0.0
106-125	30.9	14.8	16.1	46.1	8.1	17.2	13.5	4.4	6.8	3.2	0.8	0.0	0.0
180-250	21.8	8.3	13.5	63.4	9.6	10.2	11.3	1.2	3.6	0.7	0.0	0.0	0.0
355-500	19.8	6.3	13.5	60.4	13.8	7.7	13.5	1.0	2.9	0.7	0.0	0.0	0.0
1000-2000	24.5	8.1	16.5	65.5	8.5	6.9	8.8	1.6	3.9	2.2	1.9	0.4	0.0

Catlyst tests conducted at atmospheric pressure, H_2:CO ratio 2:1, total flow – 8 sccm. 0.7g of catalyst.

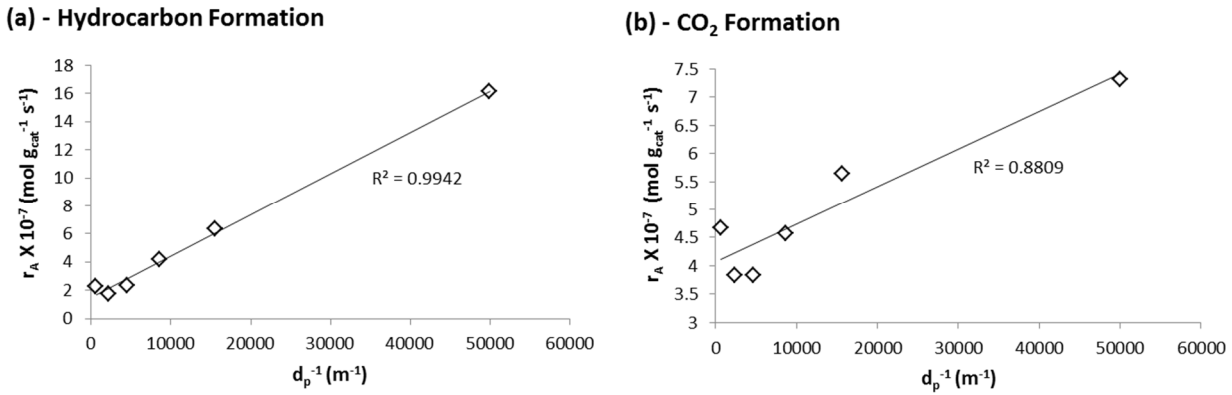

Figure 6.13 – Plots of r_A against d_p^{-1} for (a) HC formation (FT) (b) CO_2 formation (WGS)

CO conversion and HC yield are both observed to increase with smaller silica particle size, a similar trend to that observed with a CO_2 feed. Again, as with previous CO tests conversion is significantly higher than the equivalent CO_2 tests as CO conversion is not being limited by the equilibrium conversion of the RWGS reaction. Both HC and CO_2 formation appear to be occurring at the same time under the same reaction conditions. The reducing CO conversion and yields observed with larger particle sizes again suggests that mass transfer limitations are playing an important role.

If the CO hydrogenation is being limited by mass transfer limitations then the same assumptions made for the analogous CO_2 tests can be made and as such Equation 6.8 should still hold true. From this we can determine that if the reaction is limited by internal diffusion then the observed rate should be proportional to the inverse of the catalysts particle diameter. Figure 6.13 shows plots of r_A against $1/d_p$ for (a) HC formation *via* the FT process and (b) CO_2 formation *via* the WGS reaction.

The linear relationship observed in Figure 6.13 (a) indicates that the rate of HC formation appears to be diffusion limited. As with the analogous CO_2 hydrogenation experiments however the intercept is not zero suggesting the contribution of other factors. Figure 6.13 (b) shows that CO_2 formation by the WGS reaction roughly shows linear relationship between the observed rate of CO_2 formation and $1/d_p$ the coefficient of determination (R^2 value) is however relatively small suggesting that while there may be a mass transfer component to the reaction limitation it is likely affected by other factors too. The reaction relies on the formation of H_2O by the FT process and as such this is likely also playing an important role the limitation of CO_2 formation.

6.5 Influence of Reaction Pressure

The reaction pressure can have a large influence on the performance of both FT and WGS catalysts and as such its influence on CO_2 hydrogenation reactions is also significant.[1a] Generally an increasing reaction pressure during FT reactions leads to a lower methane selectivity and a higher chain growth probability.

6.5.1 Catalyst Testing

In order to determine the influence of reaction pressure on CO_2 hydrogenation the 20wt%Fe/SiO_2-250 catalyst was tested under a range of different reaction pressures. Catalyst tests were conducted in Reactor 3. Full details of reactor and catalyst test procedures are given in Section 2.3, Chapter 2.

Under CO_2 hydrogenation conditions the reaction pressure appears to have little influence on the catalyst stability with CO_2 conversion and product distributions remaining relatively consistent with increasing time on stream. The data obtained from each catalyst test is summarised in Table 6.10.

Table 6.10 – Catalytic data obtained for CO_2 hydrogenation over a 20wt%Fe/SiO_2-250 with varying reaction pressure

Reaction Pressure (bar (g))	CO_2 Conversion (%)	HC Yield (%)	CO Yield (%)	Hydrocarbon Distribution									
				C_1	C_2=	C_2	C_3=	C_3	C_4	C_5	C_6	C_7	C_8
0	30.2	22.8	7.3	48.2	0.0	25.0	1.4	15.0	5.8	2.7	1.8	0.0	0.0
5	34.5	31.2	3.3	49.6	0.0	24.0	0.3	15.4	6.0	3.5	1.2	0.1	0.0
10	40.5	37.6	2.9	56.7	0.0	23.2	0.2	12.6	4.3	2.3	0.7	0.1	0.0
15	31.1	27.6	3.6	54.1	0.0	24.3	0.3	13.3	4.7	2.5	0.8	0.0	0.0

Catlyst tests conducted at 370 ^oC, H_2:CO_2 ratio 3:1, total flow – 8 sccm. 0.7g of catalyst.

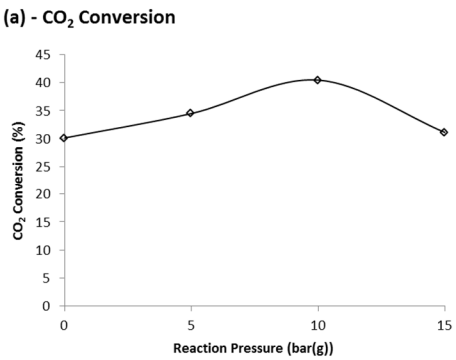

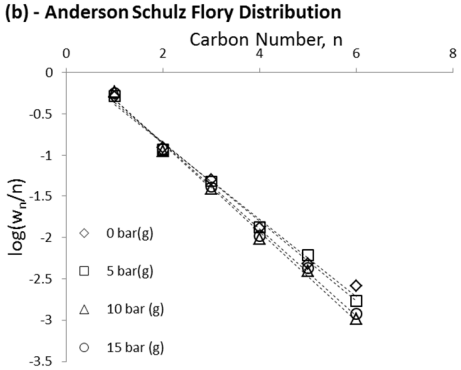

(c) – Chain growth Probability

Reaction Pressure (bar (g))	Chain Growth Probability, α
0	0.34
5	0.33
10	0.29
15	0.30

Figure 6.14 – (b) A plot showing the influence of reaction pressure on CO_2 conversion. (b) ASF plot showing the influence of reaction pressure on product selectivity. (c) Tabulated chain growth probabilities.

Initially an increase in reaction pressure results in an increased CO_2 conversion, a higher HC yield and a reduction in the amount of CO produced. When the reaction pressure is increased beyond 10 bar(g) CO_2 conversion drops again back to a value similar to that observed for the reaction conducted at atmospheric pressure. A plot showing the variation in CO_2 conversion *via* a maximum against reaction pressure is shown in Figure 6.14 (a).

An increase in reaction pressure results in an increasing selectivity to methane with a lower amount of C_2+ HCs formed. Figure 6.14 (a) shows the ASF plots for each reaction pressure. Although there appears to be a slight increase in methane selectivity with increasing pressure this appears to have little effect on the chain growth probability with higher pressure only giving a slight decrease in alpha value. This change in selectivity with pressure contradicts that generally observed with the FT reaction illustrating the difference between the reactions where CO_2 and CO are used as carbon sources.

6.5.2 Reaction Mechanism

There are two main reaction mechanisms that can be used to describe bimolecular surface reactions over heterogeneous catalysts. These are the Langmuir-Hinshelwood and the Eley-Rideal mechanisms.

The Langmuir-Hinshelwood describes a reaction in which both reactants first adsorb to the catalyst surface before reacting with one another. The rate of this chemical reaction is proportional to the concentration of each reactant present on the catalyst surface, described by the term coverage, θ. As such the rate can be described by Equation 6.9, where θ_A is the coverage of component A, θ_B is the coverage of reactant B and k_{fR} is the rate constant of the surface reaction.[11]

$$Rate = k_{fR}\theta_A\theta_B$$

Equation 6.9 - The rate of a surface reaction according to Langmuir Hinshelwood theory

The coverage of each reactant A and B can be expressed in the form of a modified Langmuir isotherm as shown in Equation 6.10. The Langmuir isotherm is a method of expressing the surface coverage of an adsorbed molecule in terms of its partial pressure. The traditional Langmuir isotherm is slightly modified for competitive molecular adsorption with the addition of a third term in the denominator taking into account the surface already covered by the other reactant present.

$$\theta_A = \frac{aP_A}{1+aP_A+bP_B} \text{ and } \theta_B = \frac{bP_B}{1+aP_A+bP_B}$$

Equation 6.10 - The surface coverage in terms of the partial pressures of each reactant

The substitution of Equation 6.10 into Equation 6.9 allows for the rate of the surface reaction to be expressed in terms of the partial pressures of the reactants rather than coverage which is far more complex to determine. This gives the standard form of the Langmuir Hinshelwood equation, Equation 6.11.

$$Rate = \frac{k_{fR}\ a\ b\ P_A P_B}{(1 + aP_A + bP_B)^2}$$

Equation 6.11 – The Langmuir Hinshelwood equation

For the purposes of mechanistic studies Equation 6.11 is slightly complex and as such a simplified versions based on a few assumptions are often preferred.[12] If we first assumed that under reaction conditions there is a reasonable coverage of both reactants but one is a stronger adsorber then the rate of reaction can be written as Equation 6.12. This is a slightly modified version of Equation 6.9 where the coverage of one component, *A*, is expressed as θ_A and the coverage of the less strongly adsorbing species, *B*, is assumed to be equivalent to the remaining sites (based on the assumption of good coverage) which can be expressed in terms of θ_A as $(1 - \theta_A)$.

$$Rate = k_{fR}\theta_A(1 - \theta_A)$$

Equation 6.12 - The rate of reaction in terms of surface coverage of one reactant

The Langmuir isotherm can be substituted into Equation 6.12 in order to express the rate of reaction in terms of partial pressures rather than surface coverage. This gives Equation 6.13.

$$Rate = k_{fR}\ \frac{aP_A}{1 + aP_A}\left(1 - \frac{aP_A}{1 + aP_A}\right)$$

Equation 6.13 – The rate of reaction in terms of pressure

This equation can then be simplified to give Equation 6.14. This equation has a simplified denominator as one component is considered to be a weak adsorber. This simplifies the equation for use in mechanistic studies.

$$Rate = \frac{k_{fR} aP_A}{(1 + aP_A)^2}$$

Equation 6.14 – Simplified equation for rate of reaction in terms of pressure

The Eley-Rideal mechanism describes a surface reaction in which only one of the two reactants must be adsorbed to the surface with the second reactant reacting with the surface bound species from the gas phase. The rate of reaction according to this mechanism is proportional to the surface coverage of the bound species, A, and the partial pressure of the un-bound species, B. As such the rate of reaction can be expressed as Equation 6.15.[11]

$$Rate = k\, P_b \theta_A$$

Equation 6.15 – The rate of surface reaction in terms of partial pressure of B and coverage of A

Equation 6.15 can be expressed in terms of partial pressures by the substitution of θ_A using the Langmuir isotherm to give Equation 6.16.

$$Rate = \frac{k_{fR} a P_A P_B}{1 + a P_A}$$

Equation 6.16 - The Eley-Rideal equation

The applicability of Equation 6.14 and Equation 6.16 and hence the likely mechanism of reaction can be tested by linearising each equation and plotting the obtained experimental data in order to see if either equation will show the expected linear relationship. Equation 6.14 can be linearised to give Equation 6.17 and Equation 6.16 to give Equation 6.18.

$$\sqrt{\frac{P_A}{-r_a}} = \frac{1}{\sqrt{k_{fR} a}} + \frac{a}{\sqrt{k_{fR} a}} . P_A$$

Equation 6.17 – The linear form of Equation 6.14

$$\frac{r_a}{P_B} = k_{fR} a P_A + k_{fR}$$

Equation 6.18 – The linear form of Equation 6.16

Therefore a plot of Plot $(P_A/-r_a)^{0.5}$ against P_A should give a linear relationship if the reaction proceeds *via* a Langmuir Hinshelwood mechanism or a linear plot of $(-r_a/P_B)$ against P_A would suggest the reaction proceeds *via* the Eley Rideal mechanism. These two plots are shown in Figure 6.15.

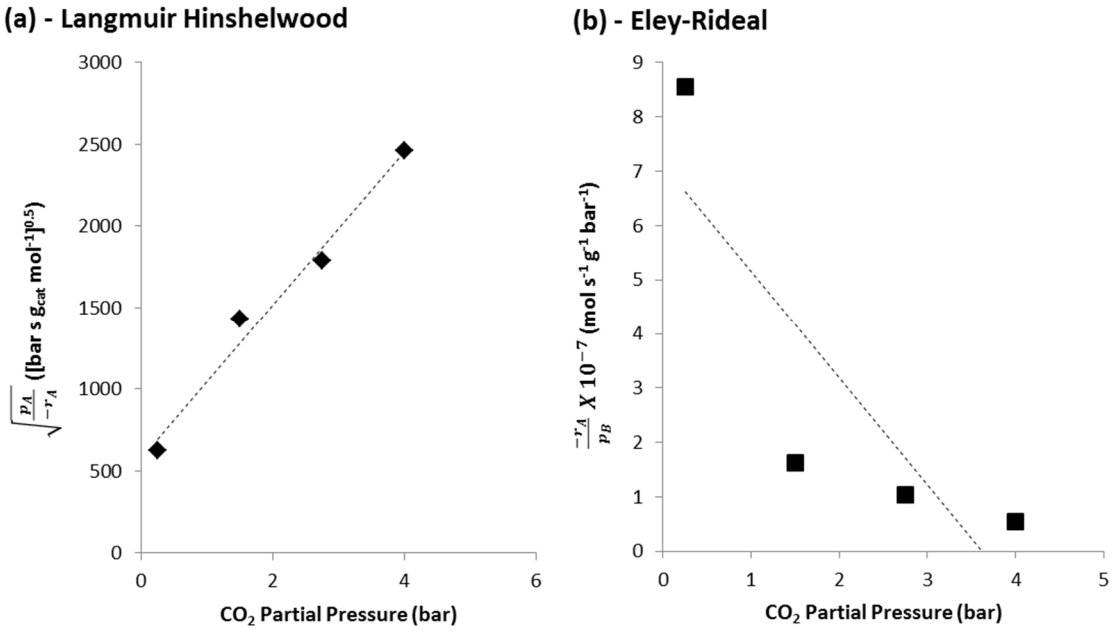

Figure 6.15 – Test of experimental results with (a) Equation 6.17 and (b) Equation 6.18

From the plots we can see that Langmuir Hinshelwood plot {Figure 6.15 (a)} affords a linear relationship with an R^2 value of 0.9809 whereas Eley-Rideal plot {Figure 6.15 (b)} does not give a straight line. A linear line of best fit gives an R^2 value of only 0.7112. This suggests that the reaction proceeds *via* the Langmuir Hinshelwood mechanism. This is in correlation with the suggested RWGS and FT mechanisms (Chapter 1 Section 1.2.2 and 1.3.2) that have been previously proposed, which involve the adsorption of both reactants to the surface.

The results above report only a very basic investigation into the reaction mechanism and further, more detailed, kinetic studies are required to confirm this work. A 'detailed' kinetic study should also reveal more significant mechanistic details.

6.6 Chapter Conclusions

This chapter has shown that properties of the silica support used in an Fe/SiO_2 catalyst for CO_2 hydrogenation can have a large influence on the morphology of the prepared catalyst which likely contributes to the significantly different catalyst performances observed depending on the silica used.

Temperature studies have shown that at lower temperatures the reaction is limited by the rate of surface reaction. At higher temperatures, however, mass transfer appears to play an important role. Under the conditions tested the external diffusion appears to show little influence on the rate of CO_2 consumption. The role of internal diffusion appears to play a more important role with a proportional relationship between the inverse catalyst particle diameter and the rate of CO_2 conversion. Evidence for the influence of other factors is also observed.

Basic mechanistic studies indicate that the reaction proceeds *via* a Langmuir-Hinshelwood type mechanism rather than a Eliey-Rideal type mechanism. Further more detailed studies are however required to confirm this.

6.7 Future Work

This chapter covers only a basic study into the kinetics of the CO_2 hydrogenation reaction over an Fe/SiO_2 catalyst and in order to confirm the results obtained and gain a better understanding of the processes involved investigations into a detailed kinetic model should be undertaken.

6.8 References

[1] (a) G. P. Van Der Laan, A. A. C. M. Beenackers, *Catal. Rev.* **1999**, *41*, 255-318; (b) A. N. Pour, M. R. Housaindokht, S. F. Tayyari, J. Zarkesh, *J. Nat. Gas Chem.* **2010**, *19*, 362-368; (c) A. N. Pour, M. R. Housaindokht, S. F. Tayyari, J. Zarkesh, *J. Nat. Gas Chem.* **2010**, *19*, 441-445; (d) I. C. Yates, C. N. Satterfield, *Energy Fuels* **1991**, *5*, 168-173; (e) D. C. Grenoble, M. M. Estadt, D. F. Ollis, *J. Catal.* **1981**, *67*, 90-102; (f) R. Smith, M. Loganathan, M. S. Shantha, *Int. J. Chem. Reactor Eng.* **2010**, *8*.

[2] T. Osaki, N. Narita, T. Horiuchi, T. Sugiyama, H. Masuda, K. Suzuki, *J. Mol. Catal. A: Chem.* **1997**, *125*, 63-71.

[3] (a) T. Riedel, G. Schaub, K. W. Jun, K. W. Lee, *Ind. Eng. Chem. Res.* **2001**, *40*, 1355-1363; (b) H. D. Willauer, R. Ananth, M. T. Olsen, D. M. Drab, D. R. Hardy, F. W. Williams, *Journal of CO2 Utilization* **2013**, *3–4*, 56-64.

[4] C. Pirola, C. L. Bianchi, A. Di Michele, S. Vitali, V. Ragaini, *Catal. Commun.* **2009**, *10*, 823-827.

[5] D. Song, J. Li, *J. Mol. Catal. A: Chem.* **2006**, *247*, 206-212.

[6] U. Rodemerck, M. Holeňa, E. Wagner, Q. Smejkal, A. Barkschat, M. Baerns, *ChemCatChem* **2013**, *5*, 1948-1955.

[7] J. Kaspar, M. Graziani, A. M. Rahman, A. Trovarelli, E. J. S. Vichi, E. C. da Silva, *Appl. Catal., A* **1994**, *117*, 125-137.

[8] C. N. Satterfield, R. T. Hanlon, S. E. Tung, Z. M. Zou, G. C. Papaefthymiou, *Ind. Eng. Chem. Prod. Res. Dev.* **1986**, *25*, 407-414.

[9] A. N. Pour, M. R. Housaindokht, S. F. Tayyari, J. Zarkesh, M. R. Alaei, *J. Nat. Gas Sci. Eng.* **2010**, *2*, 61-68.

[10] H. S. Fogler, *Elements of chemical reaction engineering*, Prentice-Hall, **1986**.

[11] M. Bowker, *The Basis and Applications of Heterogeneous Catalysis*, Oxford University Press, Incorporated, **1998**.

[12] M. J. Shah, B. Davidson, *Ind. Eng. Chem.* **1965**, *57*, 18-23.

7 Cobalt Based Catalysts for the Hydrogenation of CO_2 to Hydrocarbons.

This chapter outlines the investigations carried out into the use of cobalt as the main catalytic component of a CO_2 hydrogenation catalyst. The influence of support and a range of different noble, alkali and transition metal promoters were studied. These studies allowed the development and optimisation of cobalt based catalyst which showed a good selectivity towards C_2+ hydrocarbons combined with high CO_2 conversion.

Iron based catalyst systems have attracted the majority of attention for the hydrogenation of CO_2.[1] Their ability to catalyse both the RWGS reaction and the FT process, both thought to be important steps in the CO_2 hydrogenation process, combined with their relatively low cost appears to make them an ideal starting point for catalyst development. Iron catalysts have however been shown to possess problems with rapid deactivation under reaction conditions and high selectivity towards undesirable products such as methane as a result of low chain growth probabilities.[2] While one possibility to overcome these downfalls is the addition of dopant metals to alter the catalyst activity, selectivity and stability (as investigated in Chapters 3, 4 and 5) another alternative is the use of a different metal as the main catalyst component.

Cobalt based systems are the catalysts most commonly used industrially for the Fischer-Tropsch process. Despite their higher cost they show a higher catalytic activity with a higher CO conversion per pass and an enhanced catalyst stability.[3] As a result of their improved performance they do in fact represent the best performance to cost ratio when utilised for FT catalysis. Cobalt based system also tend to show higher chain growth probabilities than iron based catalyst systems.

Studies on the use of cobalt-based catalyst systems for CO_2 hydrogenation have been limited. The majority have focused on the effect of the introduction CO_2 into the regular CO/H_2 FT feed.[4] Studies have shown that as CO in the syngas feed gas is replaced with CO_2 conversion generally decreases and a dramatic increase in methane selectivity is observed. Not all of these papers report the study of reactions involving CO_2 as the only carbon source.[5] Those that do generally observe a significantly high selectivity to methane, typical values reported for methane selectivity are generally higher than 90 %.[4] To the best of the author's knowledge the lowest methane selectivity for CO_2 hydrogenation over a cobalt catalyst was that observed by Zhang *et al.* over a Co-Pt-Al_2O_3 catalyst at 70 % this occurs when CO_2 conversion is limited to *ca.* 40 %.[6]

Studies have also been conducted purely on the hydrogenation of CO_2. These studies have generally focused on traditional FT catalysts. Examples of such work include the studies of Dorner *et al*. who found that the addition of platinum can be beneficial with a Co-Pt-Al_2O_3

system proving effective although high methane selectivities of >90% were still observed.[7] Other catalysts studied thus far include those reported by Somorjai and co-workers with cobalt nano-particles supported on MCF-17.[8] Again methane selectivity was exceedingly high (typically >95 %). Generally the use of cobalt based catalysts has been unsuccessful for the formation of C_2+ with each system acting as a methantion catalyst under a CO_2/H_2 feed. This change in catalyst behaviour, which is not observed with iron based catalysts, can likely be attributed to cobalt's lack of activity for the RWGS reaction.[9]

7.1 Dual Promotion of Cobalt Catalysts with a Combination of Alkali and Noble Metals

Chapter 3 reported the use of a 20wt%Co/1wt%Pd/1wt%K/MgO catalyst. The system performed well giving a methane selectivity of *ca*. 68 % at a HC yield of *ca*. 7 %. While the methane selectivity here compares favourably with what has been reported previously[6] this occurs with at a relatively low HC yield. An increase in reaction temperature can increase HC yield (See Table 3.5, Chapter 3) however this also results in an increase in methane selectivity. This Chapter focuses on the development of a cobalt catalyst that is active for the hydrogenation of CO_2 producing C_2+ hydrocarbons based on the optimisation of this Co-K-Pd catalyst system.

The addition of noble metals to cobalt based catalyst utilised for the FT process have been shown to have a large impact on the structure and dispersion of cobalt species.[3] Improved cobalt reducibility is also observed upon their introduction. Palladium has been shown to be active for the RWGS reaction[10] and its introduction to the Co/MgO system studied in Chapter 3 showed a significant improvement in terms of HC yield and selectivity to C_2+ hydrocarbons. This improvement can likely be attributed to a combination of both the improved FT activity and increase in CO production *via* an increased activity for the RWGS reaction.

While the addition of alkali metals is common with iron catalysts both for the FT process[11] and the hydrogenation of CO_2[12] its use in conjunction with cobalt catalyst has been extremely limited. Of the limited investigations conducted on the addition of alkali metals to cobalt based FT catalysts all have so far shown that while selectivity towards C_5+ hydrocarbons can be increased this occurs at a significant decrease in catalyst activity and CO conversion.[13] No studies have thus far reported the addition of alkali metals to cobalt catalysts used for CO_2 hydrogenation. Recently, positive results have however been observed when potassium was used in conjunction with cobalt for RWGS catalysis.[14] The addition of potassium to the Co-Pd-MgO catalyst system studied in Chapter 3 resulted in both an increase in HC yield and a further increase in C_2+ selectivity with the Co-Pd-K-MgO catalyst showing significant promise.

While the basicity of the MgO support may play a role in the impressive catalyst selectivity observed in Chapter 3 previous studies have shown that the low interaction strength between silica and cobalt can result in an effective catalyst support.[3] With this in mind the use of silica (Sigma Aldrich, mesh: 35-70 µm, pore size: 60 Å) was first investigated.

7.1.1 Catalyst Preparation

A silica supported analogue of the MgO supported Co-Pd-K catalyst reported in Chapter 3 was prepared. As with each catalyst reported within this chapter it was prepared using a wet impregnation method similar to that used by Jones *et al*.[15] The catalyst support was suspended in the minimum amount of methanol, to which the appropriate amount of methanol solutions of $Co(NO_3)_2 \cdot 6H_2O$ and the precursors for any promoters {KOAc and $Pd(OAc)_2$} were added drop-wise. The resulting mixture was then sonicated for 60 min and the solvent removed before calcination at 450 ^oC for 16 hours. For full details of the catalyst test procedure please refer to Chapter 2, Section 2.3.

7.1.2 Catalyst Characterisation

The prepared 20wt%Co/1wt%Pd/1wt%K/SiO_2 was characterised using a range of different characterisation techniques. N_2 physisorption studies allowed the calculation of the BET surface area as 248 m^2g^{-1}, lower than that of the unused support (490 m^2g^{-1}). Catalyst morphology was investigated using scanning electron microscopy. Figure 7.1 shows typical SEM images recorded for the 20wt%Co/1wt%Pd/1wt%K/SiO_2 catalyst system. Silica particle size is relatively regular with the average size generally in the 35-70 µm range as reported. With the use of silica as a support the catalyst shows a drastically different morphology to the MgO supported system reported in Section 3.14, Chapter 3.

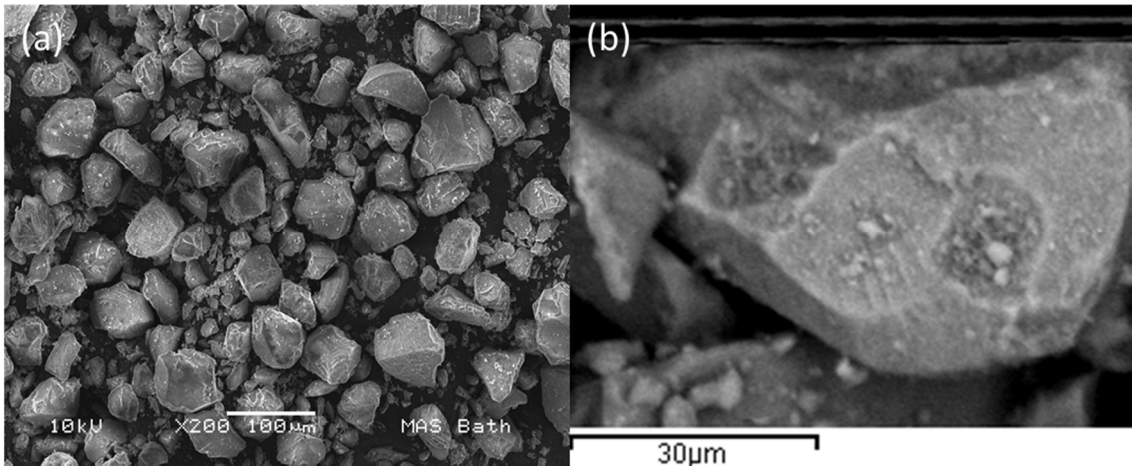

Figure 7.1 – SEM images recorded for 20wt%Co/1wt%Pd/1wt%K/SiO_2. (a) image showing over all catalyst morphology. (b) Same catalyst system shown at a higher magnification

Field emission SEM (FE-SEM) was used to investigate the elemental composition of the catalyst. Figure 7.2 shows a FE-SEM image of a single catalyst particle with a morphology typical for the overall system. Figure 7.2 (b-g) shows the mapping results. Figure 7.2 (c and d) shows the presence of silicon and oxygen which can mainly be attributed to the silica catalyst support. Figure 7.2 (e) indicates the presence of cobalt within the catalyst system and indicates a

successful loading with good distribution. Potassium and palladium are also detected with a good distribution across the catalyst surface.

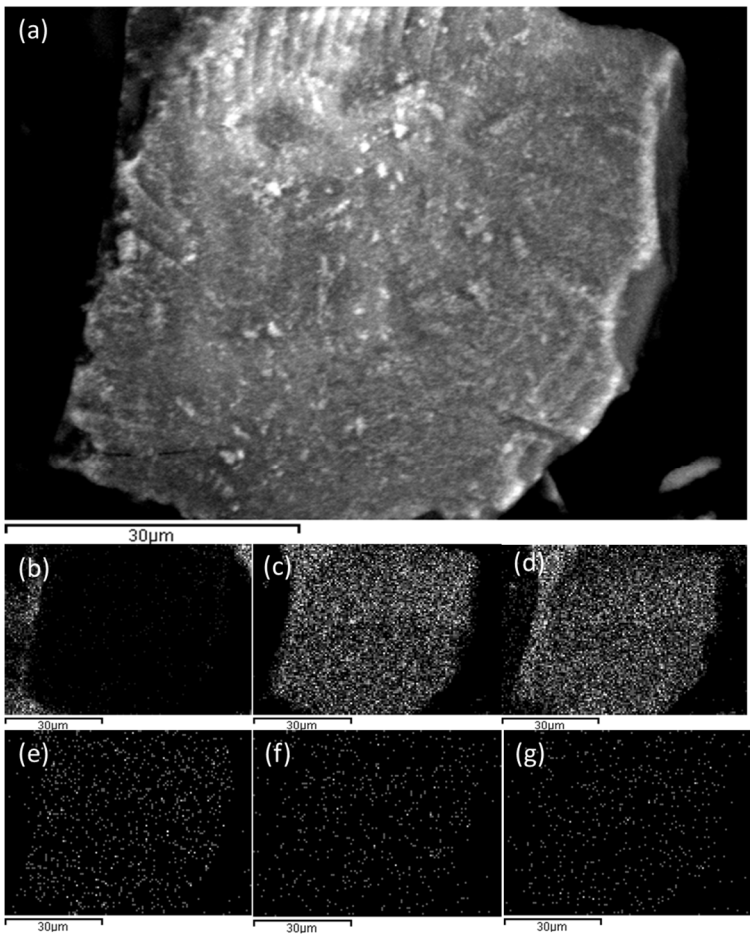

Figure 7.2 – (a) FE-SEM image recorded of a single 20wt%Co/1wt%Pd/1wt%K/SiO_2 catalyst particle. EDX was used in conjunction with FE-SEM in order to give elemental mapping. (b) C K*α*, (c) Si K*α*, (d) O K*α*, (e) Co K*α*, (f) Pd K*α* and (g) K K*α*.

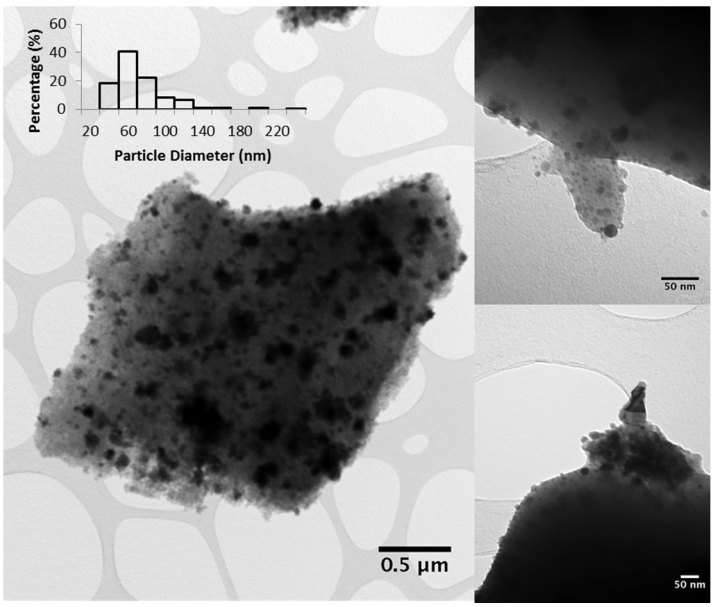

Figure 7.3 – TEM images recorded for 20wt%Co/1wt%Pd/1wt%K/SiO_2. Insert: histogram showing the nano-particle size distribution.

TEM analysis was conducted on the calcined catalyst sample. Images typical for those obtained from the system are shown in Figure 7.3. Nano-particles of a range of different sizes are observed with the particle diameter distribution shown as a histogram in Figure 7.3. A mean particle diameter of 63 nm is observed although a wide size range from *ca*. 30 nm to 240 nm is observed. The nano-particles appear well dispersed across the catalyst surface.

XPS analysis was utilised to investigate the nature of each metal species present on the catalyst surface. A wide survey spectrum was recorded in order to determine the elements present in the system along with any possible contaminants. Detailed scans with a smaller step size and longer time per step were also recorded for the Co 2p, Pd 3d and K 2p regions. The resulting spectra from these studies are shown in Figure 7.4.

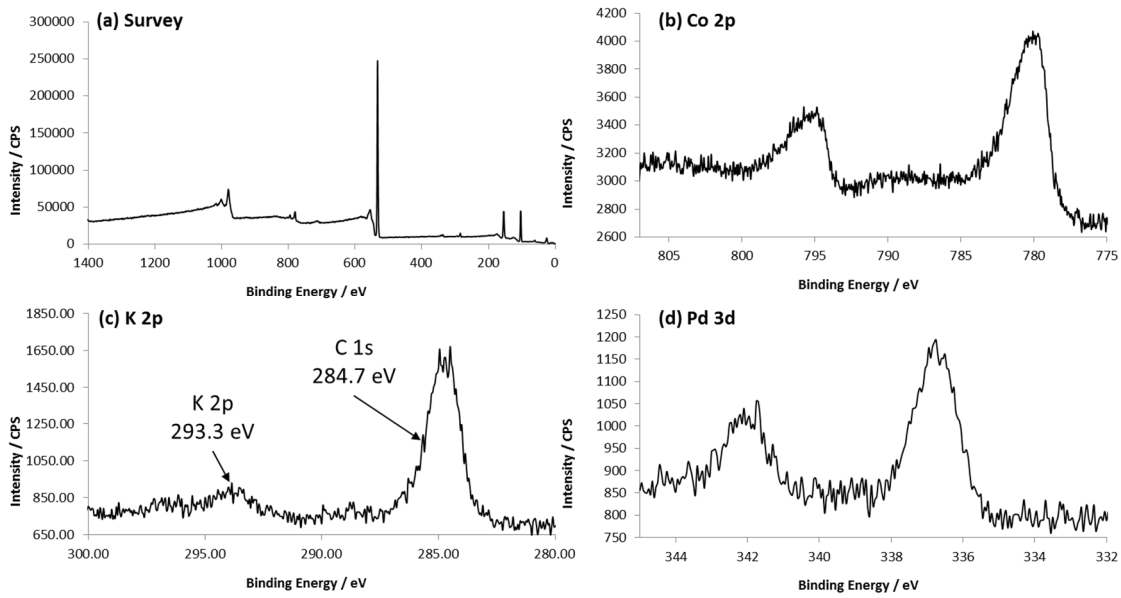

Figure 7.4 – XPS spectra recorded for the 20wt%Co/1wt%Pd/1wt%K/SiO_2 catalyst system. (a) Survey spectrum. (b) Co 2p region. (c) K 2p region. (d) Pd 3d region.

The survey spectrum indicates the presence of silicon, oxygen, cobalt, palladium, potassium and carbon as expected. Carbon is only present in a low quantity and is likely from the carbon tape used to secure the sample to the sample holder during analysis. The Co 2p spectrum shows the presence of a peak at 779.7 eV typical for the presence of cobalt in the Co_3O_4 oxide form.[16] This is further confirmed by XRD analysis where a peak at a 2θ value of 37 ^{o} is observed, characteristic of the Co_3O_4 (311) peak.[17] Scans of the K 2p region reveal a peak at 293.3 eV characteristic for potassium in its K^+ form likely as K_2O. Scans of the Pd 3d region reveals a peak at 336.7 attributable to the $3d_{5/2}$ peak of palladium indicating the presence of PdO.[18]

7.1.3 Catalyst Testing

The prepared catalyst system was tested for its CO_2 hydrogenation ability in Reactor 1 (see Chapter 2 Section 2.2 for full details. Typically 0.7 g of catalyst was packed into Reactor 1 and pre-treated under a stream of pure H_2 for 2 hours at 300 ^{o}C. Once the reduction stage was completed the reactor was either heated or cooled to the catalyst testing temperature under a flow of argon. CO_2 and H_2 were then introduced at the desired ratio with a total flow of 8 sccm. For full details on catalyst test procedure refer to Section 2.3, Chapter 2.

7.1.3.1 The influence of reaction temperature

Initial tests focused on the influence of temperature on the performance of the catalyst system both in terms of CO_2 conversion and the product selectivity. For these initial investigations a H_2:CO_2 ratio of 3:1 was chosen as this matches that used in Chapter 3 for catalyst tests

performed on the analogous MgO supported system. The obtained catalyst results are summarised in Figure 7.5.

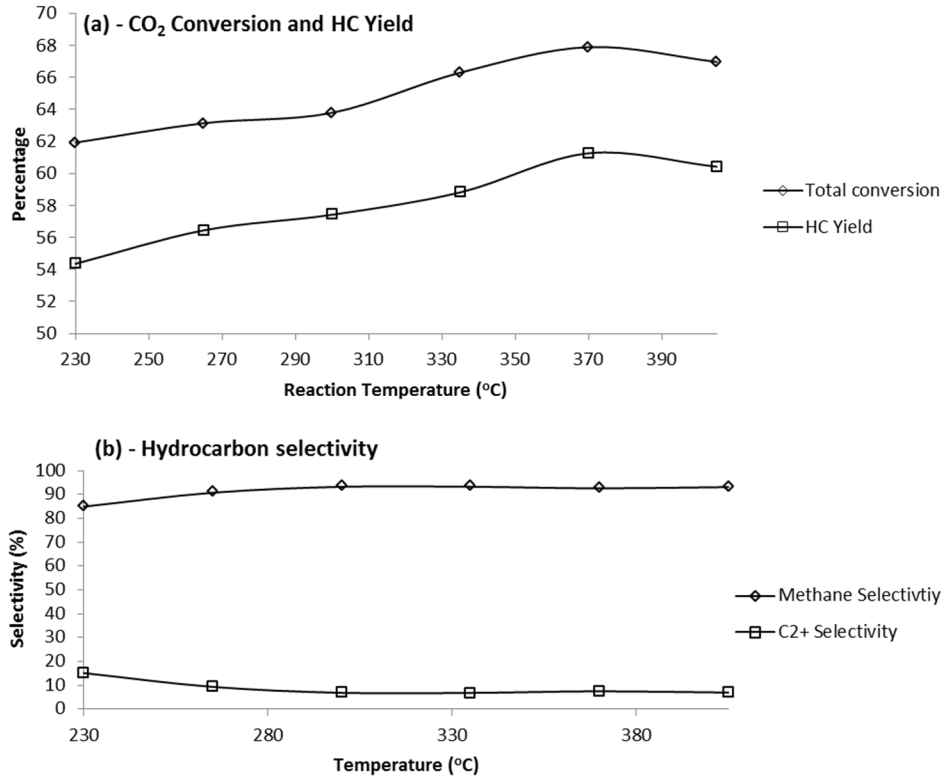

Figure 7.5 – 20wt%Co/1wt%Pd/1wt%K/SiO_2 catalyst test investigating the influence of temperature. Pressure: atmospheric, H_2:CO_2 3:1, total flow 8 sccm. (a) Plot showing how CO_2 conversion and HC yield varies with temperature. CO Yield is omitted for clarity. (b) The variation in product selectivity observed with increasing temperature.

CO_2 conversion and HC yield is observed to increase with increasing temperature until a temperature of 370 °C above this point no further increase in HC yield is observed. Little variation in CO yield is observed with varying temperature remaining relatively constant at *ca.* 7 %. In the interest of clarity it is omitted from Figure 7.5. The highest HC yield observed (*ca.* 61 %) is significantly higher than that observed with the analogous MgO supported system (39 %).

While higher reaction temperatures do result in increasing CO_2 conversion values and higher HC yields this does occur at the cost of hydrocarbon selectivity with the lowest methane selectivity observed at 230 °C. While this value is higher than that observed for the analogous MgO supported system (68 % *vs.* 85 %) the HC yield is significantly higher (7 % *vs* 62 %). This indicates that while the use of silica as a support may hinder selectivity to the more desirable C_2+ HCs a significant improvement in HC yield is obtainable.

7.1.3.2 The influence of H_2:CO_2 ratio on catalyst performance

The influence of H_2:CO_2 ratio on the performance the catalyst system was investigated. A reaction temperature of 300 ^oC was chosen as this was thought to give the best compromise between CO_2 conversion and product distribution based on results from the previous section. Figure 7.6 summarises the catalytic data obtained.

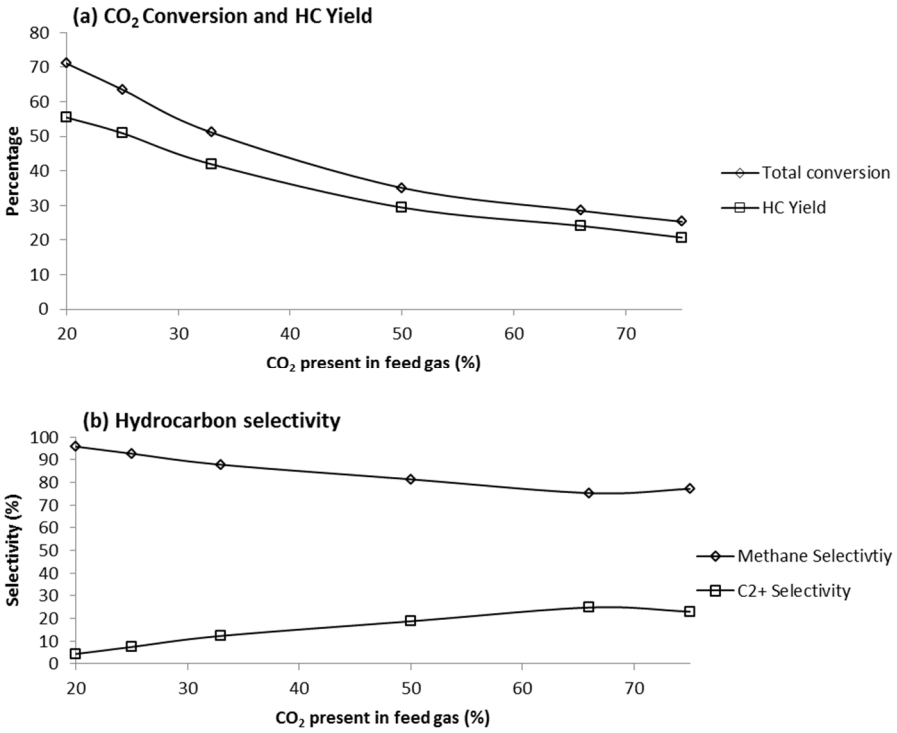

Figure 7.6 – 20wt%Co/1wt%Pd/1wt%K/SiO_2 catalyst test investigating the influence of H_2:CO_2 ratio. Pressure: atmospheric, temperature: 300 ^oC, total flow 8 sccm. (a) Plot showing how CO_2 conversion and HC yield vary with temperature. (b) The variation in product selectivity observed with increasing temperature.

As the content of CO_2 in the feed gas is increased CO_2 conversion and HC yield is drastically effected. An increasing hydrogen content results in a steady increase in CO_2 conversion from approximately 25 % up to 75 %. This shift is expected since when the CO_2 content is reduced the environment effectively becomes more reductive favouring the hydrogenation of CO_2. The same trend was observed by Dorner *et al*. when the ratio of CO_2 to H_2 was varied over a Co-Pt/Al_2O_3 catalyst however over the Co-K-Pd/SiO_2 system studied here the effect on conversion appears less pronounced.[7]

Dorner *et al*.[7] predicted that as the CO_2 concentration in the feed gas was increased a larger selectivity to longer chained hydrocarbons would be observed as the less hydrogenating environment would favour chain growth over chain termination resulting in an increased chain growth probability. While Dorner *et al*. did witness this phenomenon the effect was minimal with only a slight reduction in methane selectivity. The effects observed over our catalyst

appear significant in relation with a lower H_2 content leading to an increased selectivity to higher hydrocarbons as originally postulated by Dorner and co-workers.[7] With a H_2:CO_2 ratio of 1:3 a methane selectivity of *ca*. 77% is obtained albeit at a low CO_2 conversion value.

As with the influence of temperature H_2:CO_2 ratio benefits CO_2 conversion and product selectivity in an opposite manner meaning a compromise must be made. A H_2:CO_2 ratio of 3:1 appears to give the highest conversion while still retaining some selectivity to heavier hydrocarbon as such all catalyst tests conducted hereafter use this ratio.

7.2 Influence of Cobalt Loading on Co-Pd-SiO_2

The influence of cobalt loading on the base 20wt%Co/1wt%Pd/1wt%K/SiO_2 catalyst was investigated. The same silica support utilised thus far was used for all catalysts and the palladium and potassium loading kept constant with only the mass of cobalt used in catalyst preparation altered.

7.2.1 Catalyst Preparation

Four catalysts were prepared with the same wet impregnation method used in Section 7.1.1 employed. Cobalt loading was varied from 10 wt% to 40 wt% at 10 wt% intervals to give four different catalyst compositions: 10wt%Co/1wt%Pd/1wt%K/SiO_2, 20wt%Co/1wt%Pd/1wt%K/SiO_2, 30wt%Co/1wt%Pd/1wt%K/SiO_2 and 40wt%Co/1wt%Pd/1wt%K/SiO_2.

7.2.2 Catalyst Characterisation

XRD studies were conducted on each catalyst system, the resulting diffraction patterns are shown in Figure 7.7. A peak at a 2θ value of 37 ^{o} is observed for all catalyst system a value characteristic of the Co_3O_4 (311) peak.[17] This is expected to be the most intense of the Co_3O_4 diffraction pattern peaks and so with the weakly diffracting nature of the cobalt species it is not unexpected that this is the only detectable peak. No peaks attributable to the silica are observed confirming its amorphous nature. No palladium or potassium species are detected, however, this is likely due to their low loading. No change in cobalt phase is observed with increasing cobalt loading the intensity of the Co_3O_4 peak however, appears to be reduced.

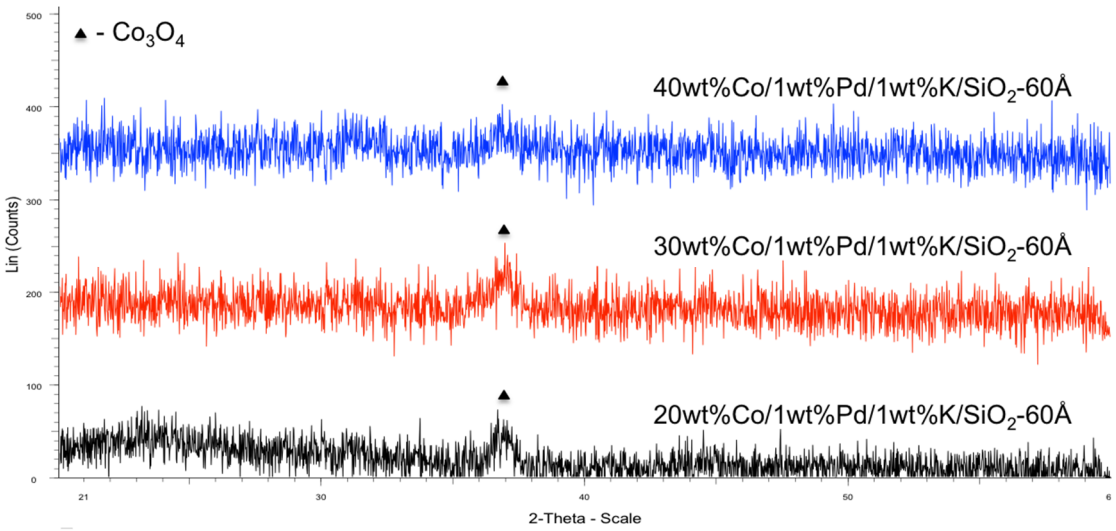

Figure 7.7 – pXRD patterns recorded between 2θ values of 20 and 60 ° for the catalyst systems containing various cobalt loadings.

7.2.3 Catalyst Testing

The prepared catalyst systems were each tested for their CO_2 hydrogenation ability in Reactor 1. Each catalyst was first pre-treated under a flow of pure hydrogen for 2 hours at 300 °C. After the reduction stage the reactor temperature was kept constant at 300 °C and CO_2 and H_2 were introduced in a 1:3 ratio with a total flow of 8 sccm. Gas samples were collected every hour and analysed using gas chromatography. Full details of the catalyst test procedure are outlined in Chapter 2 Section 2.3.

The tested catalyst systems appeared stable with little change in CO_2 conversion and product selectivity with increasing time on stream. CO_2 conversion, HC yield, CO yield and product distribution were calculated as an average over a five hour period. The obtained data is summarised in Table 7.1. CO_2 conversion increases drastically when cobalt loading is doubled from 10 wt% to 20 wt% with a concurrent increase in HC yield also observed. When cobalt loading is increased beyond this point, however, a decrease in CO_2 conversion and HC yield is observed. The CO yield follows the trend observed for CO_2 conversion with the highest CO produced at a cobalt loading of 20 wt%. This indicates that the catalyst systems are active for the RWGS reaction, a property most likely attributable to the addition of palladium and potassium as cobalt-based catalysts are generally not active for WGS shift processes.

The HC distribution is also influenced by the cobalt content of the catalyst system. Generally, as the cobalt loading is increased a decrease in methane selectivity is observed. This suggests that the cobalt present within the system is the main active phase for the FT process with a higher cobalt loading leading to a higher FT activity. Of the HC products produced all were saturated HCs with no olefin products detected.

Table 7.1 – Catalytic data obtained for CO_2 hydrogenation tests using Co-1wt%Pd/1wt%K/SiO_2 catalyst systems containing various cobalt loadings

Catalyst	CO_2 Conv. (%)	CO Yield (%)	HC Yield (%)	HC Selectivity (%)				
				C_1	C_2	C_3	C_4	C_5+
10wt%Co/1wt%Pd/1wt%K/SiO_2	36.4	2.9	33.5	97.0	2.7	0.3	0.0	0.0
20wt%Co/1wt%Pd/1wt%K/SiO_2	63.4	8.8	54.6	93.2	5.4	1.2	0.2	0.0
30wt%Co/1wt%Pd/1wt%K/SiO_2	39.4	3.5	35.9	88.9	7.9	2.4	0.5	0.2
40wt%Co/1wt%Pd/1wt%K/SiO_2	39.1	3.7	35.4	91.6	6.4	1.7	0.3	0.1

Catalyst tests conducted at atmospheric pressure, H_2:CO_2 ratio 3:1, total flow – 8 sccm, Temperature: 300 ^oC 0.7g of catalyst. Conversions, yields and product distributions calculated as an average of 5 hours on stream after catalyst stabilisation.

7.3 Influence of Potassium Loading on Co-Pd-K-SiO_2

The influence of potassium loading on the base 20wt%Co/1wt%Pd/1wt%K/SiO_2 catalyst was investigated. The same silica support utilised thus far was used for all catalyst and the cobalt and palladium loading kept constant with only the mass of potassium used in catalyst preparation altered.

7.3.1 Catalyst Preparation

Five catalysts were prepared using the same wet impregnation method used in Section 7.1.1. The potassium loading was varied giving catalysts containing 0.5, 1, 1.5, 2 and 3 wt% potassium.

7.3.2 Catalyst Testing

Each of the prepared catalyst systems were tested for their CO_2 hydrogenation ability in Reactor 1 under the same reaction conditions used thus far; temperature: 300 ^oC, pressure: atmospheric, H_2:CO_2 ratio 3:1, total flow 8 sccm. Full details of the catalyst test procedure are outlined in Section 2.3, Chapter 2.

Generally all catalyst systems tested within this section showed a good catalyst stability over the time period investigated with no significant change in CO_2 conversion or product distribution. The catalytic data obtained from these investigations are summarised in Table 7.2. CO_2 conversion values show little variation when potassium loading is increased from 0.5 wt% to 1 wt% when increased beyond this point however CO_2 conversion begins to decreases with increasing potassium content. A concurrent decrease in HC yield is observed with CO yield increasing slightly. This suggests that when potassium content is above 1 wt% the detrimental effects on CO conversion observed for FT based systems overcome the improved WGS shift activity that has been observed with other cobalt systems upon potassium introduction.

Table 7.2 – Catalytic data obtained for CO_2 hydrogenation tests using K-20wt%Co/1wt%Pd/SiO_2 catalyst systems containing various potassium loadings

Catalyst	CO_2 Conv. (%)	CO Yield (%)	HC Yield (%)	HC Selectivity (%)				
				C_1	C_2	C_3	C_4	C_5+
20wt%Co/1wt%Pd/0.5wt%K/SiO_2	62.8	9.6	53.3	89.5	7.3	2.6	0.6	0.0
20wt%Co/1wt%Pd/1wt%K/SiO_2	63.4	8.8	54.6	93.2	5.4	1.2	0.2	0.0
20wt%Co/1wt%Pd/1.5wt%K/SiO_2	59.1	9.6	49.5	77.2	10.6	7.6	3.1	1.5
20wt%Co/1wt%Pd/2wt%K/SiO_2	50.0	13.6	36.3	68.2	12.3	13.5	4.3	1.8
20wt%Co/1wt%Pd/3wt%K/SiO_2	43.2	10.5	32.7	70.1	10.9	10.3	5.2	3.6

Catalyst tests conducted at atmospheric pressure, H_2:CO_2 ratio 3:1, total flow – 8 sccm, Temperature: 300 ^oC 0.7g of catalyst. Conversions, yields and product distributions calculated as an average of 5 hours on stream after catalyst stabilisation.

Increasing potassium content of the catalyst system is also observed to have a significant impact on product distribution. While all of the HCs formed are still saturated a significant reduction in methane selectivity is observed with higher potassium content. Significant increases in selectivity to heavier (C_5+) hydrocarbons are observed at potassium loadings of 1.5 and above. The methane selectivity drops to approximately 70 %, similar to the lowest value previously reported for any CO_2 hydrogenation reactions over cobalt catalysts. While CO_2 conversion values are lower at these preferential selectivities they still compare favourably with current values reported for most iron based catalyst systems.[2]

If hydrocarbon formation is occurring *via* the FT process a plot of carbon number, *n*, against *log* (w_n/n) would give a straight line as product formation is expected to follow the ASF distribution. This has been the case for all catalyst systems studied within previous chapters. When ASF graphs are plotted for the cobalt based catalyst systems reported within Table 7.2 they display a double α phenomenon as shown in Figure 7.8. This is commonly observed with cobalt based catalyst systems when used for CO_2 hydrogenation [1, 7] and indicates that not all HCs are being formed *via* the FT process and suggests that there may be two active sites for HC production.[19]

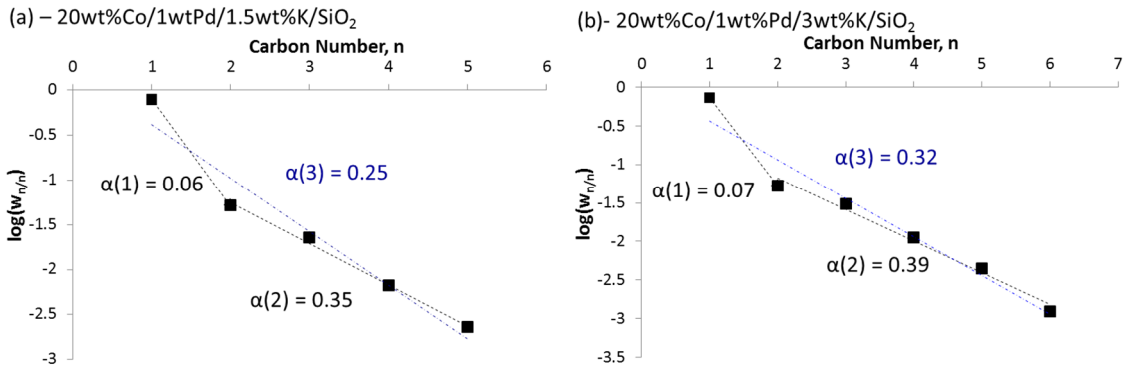

Figure 7.8 – ASF plots for (a) 20wt%Co/1wt%Pd/1.5wt%K/SiO_2 and (b) 20wt%Co/1wt%Pd/3wt%K/SiO_2 showing the double α phenomenon observed

Methane content is higher than predicted by the ASF distribution and as such does not lie on the same trend line as the C_2+ hydrocarbons. The fact that all C_2+ HCs produced do give a linear relationship suggest they are indeed formed *via* the FT process over the same active site. While methane is likely formed *via* the same FT process forming the C_2+ HCs its higher than predicted content suggests that methane is also being formed through another parallel process such as the direct hydrogenation of CO_2 to form CH_4 with no CO intermediate through the equation $CO_2 + 4H_2 \rightarrow CH_4 + 2H_2O$, possibly over a second active site.[9] Although the α(3) value cannot be used to reliably calculate the chain growth probability for the catalyst systems there is a general increase in the α(3) value as potassium loading is increased (Table 7.3). This can be attributed to the an increasing α(2) value which is most likely more representative of the chain growth probability for the FT process occurring over each catalyst system as it excludes the anomalous methane result. The values calculated for α(2) (see Table 7.3) generally increase as potassium content is increased as would be expected based on the increased selectivity towards heavier HCs observed upon the introduction of potassium to cobalt FT catalysts.[20]

Table 7.3 – Chain growth probabilities calculated for the Xwt%K/20wt%Co/1wt%Pd/SiO_2 catalyst system with various potassium loadings

Potassium Loading (wt%)	**0.5**	**1**	**1.5**	**2**	**3**
α(3) *[a]*	0.12	0.08	0.25	0.28	0.32
α(2) *[b]*	0.19	0.13	0.35	0.35	0.39

[a] – Overall 'chain growth probability' calculated while including the anomalous methane point. [b] – Chain growth probability calculated for C_2+ HCs excluding the anomalous methane point. See Figure 7.8.

7.4 Variation of Catalyst Support on the 20wt%Co/1wt%Pd/1wt%K/SiO_2 System

The nature of the catalyst support used has been shown to have a large influence on catalyst performance both in terms of activity and product selectivity.[21] While the composition of the

catalyst support plays an important role so do the physical properties of the oxide such as surface area, particle size and pore size.[22]

7.4.1 Catalyst Preparation

For the investigations into the effects of silica properties on the 20wt%Co/1wt%Pd/1wt%K/SiO_2 four different silica supports were chosen: SiO_2-60, SiO_2-250 and SiO_2-500 each with a particle size of 35-70 nanometres and a varying pore size as indicated by the number proceeding each (measured in angstroms). A catalyst system with a 60 Å pore size but a 1 – 2 mm particle size was also investigated to study the influence of catalyst particle size on catalyst performance. Full details of silica properties are given in Table 6.1, Chapter 6. All systems were prepared using the standard wet impregnation method detailed in Section 2.7.13, Chapter 2. Masses of all catalyst precursors were kept constant with the only the silica changed and the rest of the catalyst preparation method remaining the same.

7.4.2 Catalyst Characterisation

Each catalyst system was characterised using a range of different characterisation methods. N_2 physisorption methods were used to calculate the specific BET surface area, the values obtained are summarised in Table 7.4. Surface area is observed to decrease with increasing pore size, matching the decreasing surface area reported for the bare silica supports (550, 285 and 80 m^2g^{-1} for SiO_2-60, SiO_2-250 and SiO_2-500 respectively). The decrease in surface area upon the loading of metals is reduced as pore size increases, this is likely due to the fact the reduced surface area can be attributed to the filling of support pores with the added metal, an effect that is reduced as pore size is increased.

Table 7.4 – BET surface areas calculated for 20wt%Co/1wt%Pd/1wt%K/SiO_2 supported on a range of different silica

Catalyst[a]	BET Surface Area (m^2g^{-1})
20wt%Co/1wt%Pd/1wt%K/SiO_2-60	248
20wt%Co/1wt%Pd/1wt%K/SiO_2-250	186
20wt%Co/1wt%Pd/1wt%K/SiO_2-500	66
20wt%Co/1wt%Pd/1wt%K/SiO_2-60_b	286

[a] – SiO_2-X where X is the pore size of the silica support in Å and b indicates a particle size of 1 – 2 mm. All other silica systems have a particle size of 35 – 70 μm.

XRD studies for the SiO_2-60, SiO_2-250 and SiO_2-500 supported catalyst are shown in Figure 7.9. As the pore size of the silica support is increased the XRD peaks present become more intense and defined. All indicate the presence of cobalt in the Co_3O_4 phase.[17] Whereas only the (311) peak at 37 ^{o} is observed for the SiO_2-60 supported system as support pore size is

increased the (220), (400) and (511) peaks at 31, 45 and 59 ^{o} respectively are also observed. The Scherrer equation was used to calculate the crystallite size for each system and indicated that as silica support pore size was increased the cobalt (Co_3O_4) crystallite size increased (Figure 7.9). This is most likely the cause of the more distinct XRD diffraction patterns observed for the higher pore sized supports. A similar effect of support pore size on crystallite size has been observed on both Al_2O_3[23] and SiO_2[22a] supported cobalt FT catalysts.

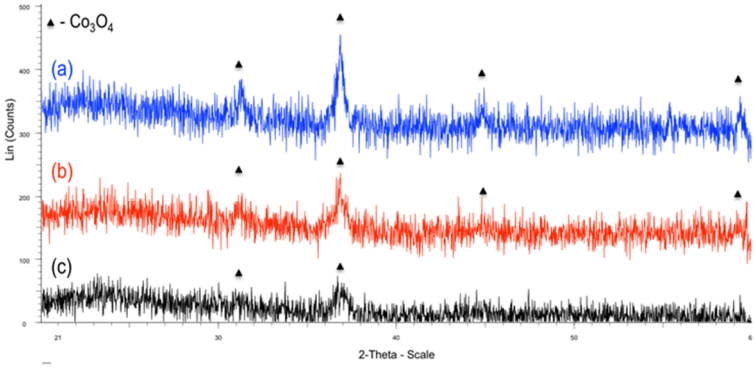

SiO_2 Pore Size (Å)	Crystallite Size[a] (nm)
60	8.4
250	9.4
500	14.0

[a] – Crystallite size calculated from XRD using the Scherrer equation

Figure 7.9 –XRD patterns recorded for (a) 20wt%Co/1wt%Pd/1wt%K/SiO_2-500, (b) 20wt%Co/1wt%Pd/1wt%K/SiO_2-250 and (c) 20wt%Co/1wt%Pd/1wt%K/SiO_2-60. Crystallite sizes calculated using the Scherrer equation are tabulated.

TEM analysis was conducted on each of the SiO_2-60, SiO_2-250 and SiO_2 500 supported catalyst systems in order to investigate catalyst morphology, representative images are shown in Figure 7.10. The most obvious difference between samples is the size of nano-particles. Nano-particles are clearly observed for the SiO_2-60 supported system, however, they appear smaller and less numerous for the SiO_2-250 and SiO_2-500 supported systems. These measurements suggest particle diameter falls from an average of 62.9 nm to 47.4 nm to 30.8 nm as pore size increases. With the particle size measured from TEM significantly larger than that calculated from the Scherrer equation based on XRD results this suggests that these particles are either conglomerations of much smaller particles or consist of several smaller crystalline phases a phenomenon similar to that observed with cobalt based systems by Feller *et al.*[24]

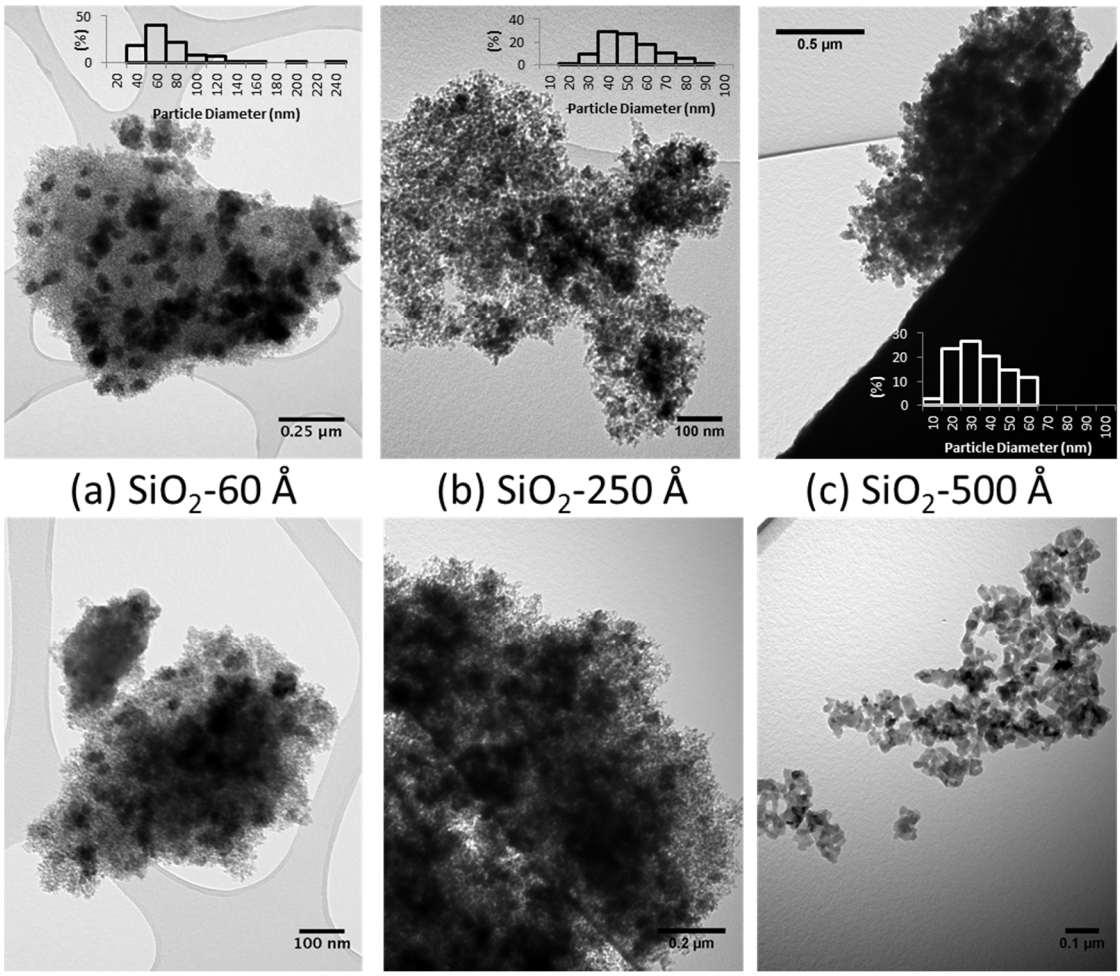

Figure 7.10 – TEM images recorded for (a) 20wt%Co/1wt%Pd/1wt%K/SiO_2-60, (b) 20wt%Co/1wt%Pd/1wt%K/SiO_2-250 and (c) 20wt%Co/1wt%Pd/1wt%K/SiO_2-500. Inserts – histograms showing particle size distribution as determined by TEM.

7.4.3 Catalyst Testing

Each of the prepared catalyst systems were tested for their CO_2 hydrogenation ability in Reactor 1 under the same reaction conditions utilised thus far; temperature: 300 ^oC, pressure: atmospheric, H_2:CO_2 ratio 3:1, total flow 8 sccm. Full details of the catalyst test procedure are outlined in Section 2.3, Chapter 2.

All the catalyst systems studied within this section show a good stability with time on stream with no significant change in CO_2 conversion or product distribution observed over the course of the catalyst test. The results obtained are summarised in Table 7.5. The porosity of the silica support was shown to have a significant impact on the performance of each catalyst system. A large drop in CO_2 conversion was evident when pore size was increased from 60 Å to 250 Å. A further, albeit far less significant drop in CO_2 conversion and resulting HC yield was observed when the pore size was increased to 500 Å.

Despite this drop in CO_2 conversion and HC yield the conversions observed still compare favourably with most iron based catalyst systems.[2] The silica properties also show a

significant impact on product distribution with a large increase in C_5+ hydrocarbon formation from 0 % with 60 Å silica pores to 3.7 % with SiO_2-500 Å supported system. Methane selectivity also decreases with the SiO_2-500 supported system giving a CH_4 selectivity of 62.8 % lower than any previously reported. Not only is this selectivity better than that obtained for the 20wt%Co/1wt%Pd/1wt%K/MgO system at 230 ^oC reported in Chapter 3 Section 3.3, it occurs at a significantly higher HC yield (42 % *vs.* 7 %).

The improved C_5+ selectivity can be attributed to the larger crystallite size formed when a silica support with a larger pore size is utilised. De Jong *et al*. observed the same effect of cobalt crystallite size on cobalt catalysts utilised for the FT process.[25] Studies on the effect of pore size on Co-SiO_2 catalysts for FT reactions by Khodakov *et al*. also observed larger Co_3O_4 crystallite sizes with larger diameter silica pores.[22a] Their investigations also revealed that the larger particles are more easily reduced through a combination of the effect of particle size and the fact that smaller pores tend to stabilise the oxide species. It is likely a similar reducibility effect is occurring with the 20wt%Co/1wt%Pd/1wt%K/SiO_2 catalyst systems and this is also contributing towards the improved hydrocarbon distribution.

ASF plots of the three catalyst systems are shown in Figure 7.11. All systems show evidence of a double alpha phenomenon as discussed in Section 7.3.2, however the phenomenon appears less dramatic as the pore size of the catalyst support is increased. The difference between the overall chain growth probability α(3) and α(2) gives an idea as to the magnitude or extent of the double alpha phenomenon as caused by excess methane formation. Figure 7.11 shows the tabulated α values, a decrease in Δα with increasing pore size suggests that the parallel methane formation reaction postulated in Section 7.3 is decreasing relative to the C_2+ formation with the SiO_2-500 supported system only showing a slight double alpha phenomenon indicating almost all methane is formed *via* the FT process that is responsible for all C_2+ hydrocarbon formation.

Table 7.5 – Catalytic data obtained for CO_2 hydrogenation tests using 20wt%Co/1wt%Pd/1wt%K/SiO_2 and related catalyst systems supported on various silica

Catalyst	Conv. (%)	HC Yield (%)	CO Yield (%)	Hydrocarbon Distribution										$O/(O+P)^{[a]}$ in C_2-C_4
				C_1	C_2=	C_2	C_3=	C_3	C_4	C_5	C_6	C_7	C_8	
20wt%Co/1wt%Pd/1wt%K/SiO_2-60	63.4	54.6	8.8	93.2	0.0	5.4	0.0	1.2	0.0	0.0	0.0	0.0	0.0	0
20wt%Co/1wt%Pd/1wt%K/SiO_2-250	44.9	41.9	3.0	76.9	0.0	13.0	0.0	7.0	2.0	0.8	0.3	0.0	0.0	0
20wt%Co/1wt%Pd/1wt%K/SiO_2-500	41.6	36.8	5.7	62.8	0.0	17.0	0.0	11.6	4.7	2.4	1.0	0.3	0.0	0
20wt%Co/1wt%Pd/1wt%K/SiO_2-60_b	45.7	42.2	3.6	91.6	0.0	6.3	0.0	1.6	0.4	0.1	0.0	0.0	0.0	0
20wt%Co/SiO_2-500	64.3	60.0	4.3	98.2	0.0	1.8	0.0	0.1	0.0	0.0	0.0	0.0	0.0	0

[a] Olefin content (mol percentage) for C_2-C_4 hydrocarbons, calculated as [olefin(O) / (olefin(O) + paraffin(P)) × 100]. Catlyst tests conducted at atmospheric pressure, 300 ^oC H_2:CO_2 ratio 3:1, total flow – 8 sccm. 0.7g of catalyst. Conversions, yields and product distributions calculated as an average of 5 hours on stream.

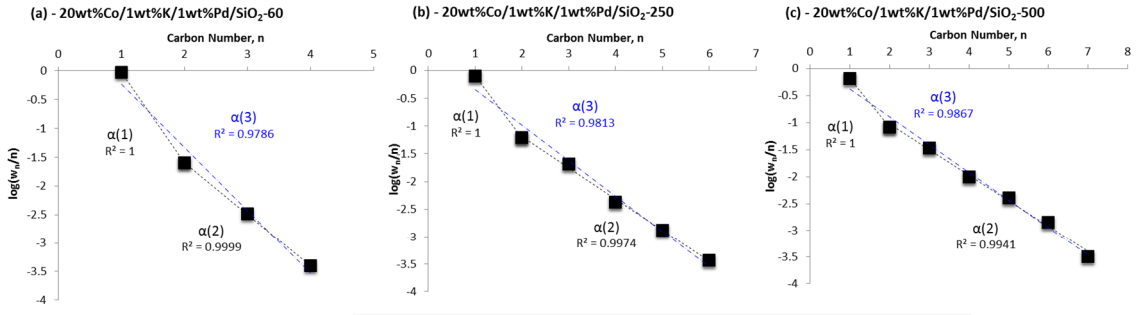

Silica Supported	α(2)	α(3)	$\Delta\alpha_{(2,3)}$[a]
SiO_2-60	0.13	0.08	0.05
SiO_2-250	0.27	0.23	0.04
SiO_2-500	0.34	0.31	0.03

[a] – The difference between α(1) and α(2) values

Figure 7.11 – ASF plots for 20wt%Co/1wt%Pd/1wt%K supported on (a) SiO_2-60, (b) SiO_2-250 and (c) SiO_2-500. Chain growth probabilities are tabulated.

A reduction in CO_2 conversion is observed when SiO_2-60_b is used as a catalyst support relative to the smaller particle sized SiO_2-60. This can potentially be attributed to diffusional effects. The HC distribution is observed to remain similar for both catalysts supported on silica with a 60 Å pore size.

In order to determine if the effect of support pore size alone was enough to significantly influence the product distribution a catalyst system containing only 20 wt% cobalt supported on the best performing of the supports, SiO_2-500, was prepared and tested the results are shown in Table 7.5. A significant reduction in selectivity to C_2+ hydrocarbons is observed with methane selectivity increasing to 98 %. This shows that the influence of the increased catalyst support pore size alone is not enough to have any significant effect on the product selectivity.

With the 20wt%Co/1wt%Pd/1wt%K/SiO_2-500 catalyst system proving very promising, giving the best performance of any cobalt-based catalyst used for CO_2 hydrogenation, in terms of C_2+ selectivity further XPS studies were used to investigate the metal phases after calcination and after the reductive catalyst pre-treatment. Figure 7.12 shows the resulting spectra obtained for the Co 2p and Pd 3d regions.

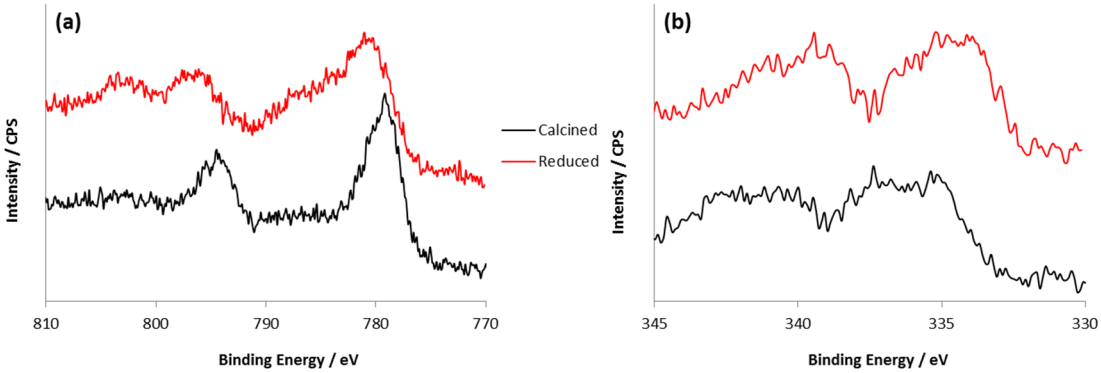

Figure 7.12 – XPS studies of the 20wt%Co/1wt%Pd/1wt%K/SiO_2-500 catalyst before use (black) and after reductive pre-treatment (red). (a) Co 2p region. (b) Pd 3d region.

After calcination the presence of a Co $2p_{3/2}$ peak with a binding energy of 780.0 eV suggests the presence of cobalt in the Co_3O_4 phase.[26] After reduction under a stream of hydrogen at 300 ^oC for 2 hours the catalyst was reanalysed using XPS. The resulting Co 2p spectrum shows a shift in the Co $2p_{3/2}$ peak to a higher binding energy of 781.13 eV which suggests the reduction of the Co_3O_4 species to CoO. This is further confirmed by the emergence of satellite peaks, attributable to Co^{2+}, at *ca*. 785 eV. No peaks attributable to the presence of Co^0, the active phase for FT, are detected these are however possibly masked by the CoO peaks.

After calcination the Pd 3d region shows a peak at 336.0 eV attributable to the presence PdO. A shift in binding energy to 335.1 after the reductive pre-treatment indicates that during the reaction palladium is present in its metallic, Pd^0, form.

7.5 Variation of Noble Metal

Several studies conducted on cobalt based catalyst have shown that the addition of a noble metal to the system has a large impact on the performance of the resulting catalyst system.[3] This change in catalyst performance can largely be attributed to a change in cobalt dispersion and an increase in reducibility. The addition of palladium to the cobalt based CO_2 hydrogenation catalyst studies in Chapter 3 showed a significant improvement upon its introduction.

Although the addition of noble metals (Ru, Rh, Pt and Pd) generally affects the same catalyst properties the extent to which each property is affected can change drastically depending on the particular metal used. Studies have shown that the FT catalytic activity decreases in the order Co-Ru > Co-Pd > Co-Pt > Co, with platinum and palladium leading to an increased methane selectivity.[27] For catalyst systems used for CO_2 it is expected that the noble metal component may also play an important role as an active site for the initial reduction of CO_2 to CO *via* the RWGS process and so which noble metal is chosen could result in a larger impact on catalyst performance.

In order to investigate how it affects the catalyst performance the noble metal used in the 20wt%Co/1wt%M/1wt%K/SiO_2 (where M = Pd, Pt and Ru) catalyst system was varied and the influence on catalyst performance investigated.

7.5.1 Catalyst Preparation

All catalyst systems were prepared using the standard wet impregnation method described in detail in Section 2.7.13 Chapter 2. Based on the promising catalyst results in Section 7.4 the silica support with a 500 Å pore size was employed for all catalysts. $Pd(OAc)_2$, $PtCl_2$ and $RuCl_3{\cdot}xH_2O$ were used as the precursors for each noble metal.

7.5.2 Catalyst Characterisation

The properties of each catalyst system were investigated using a range of different characterisation techniques. N_2 physisorption experiments were used to calculate the specific

BET surface area. The values shown Table 7.6 indicate that the noble metal used does have an influence on the surface area although the difference between each system is relatively small. The surface areas were observed to increase in the order Co-Pd-K < Co-Ru-K < Co-Pt-K.

Table 7.6 – BET surface area, Co/Si ratio calculated from XPS and Co_3O_4 crystallite size calculated from XRD for each of the catalyst systems

Catalyst	BET Surface Area (m^2g^{-1})	Co/Si Ratio[a]	Co_3O_4 crystallite size (nm) [b]
20wt%Co/1wt%Pd/1wt%K/SiO_2-500	66.1	0.028	14.0
20wt%Co/1wt%Pt/1wt%K/SiO_2-500	83.5	0.062	10.5
20wt%Co/1wt%Ru/1wt%K/SiO_2-500	71.9	0.066	12.0

[a] – The Co/Si atomic ratio on catalyst surface calculated using XPS. [b] – Crystallite size calculated from XRD using the Scherrer equation

XRD studies on each catalyst system indicated the presence of Co_3O_4 as the main cobalt phase with the (220), (311) and (400) peaks observed at 31, 37 and 45 ^{o} for each catalyst system (Figure 7.13). No peaks attributable to any noble metal species were observed. The Sherrer equation was used to calculate the cobalt oxide crystallite size based on the broadening of the (311) Co_3O_4 peak. The calculated crystallite sizes are shown in Table 7.6. There appears to be an influence of the noble metal promoter on the Co_3O_4 crystallite with the size decreasing in the order: Co-Pd-K > Co-Pt-K > Co-Ru-K.

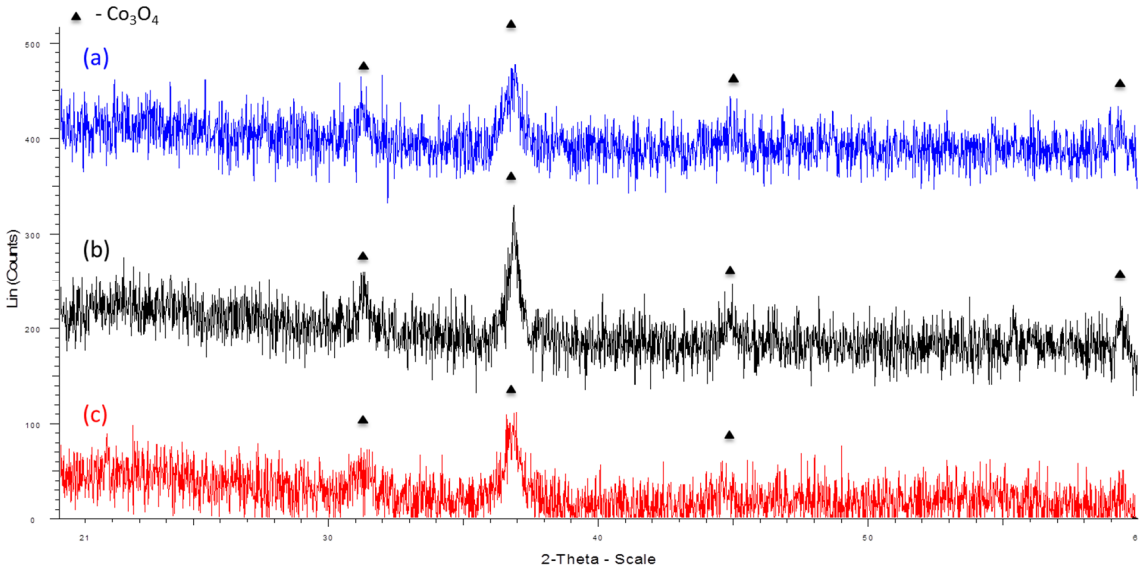

Figure 7.13 – XRD diffraction patterns recorded for (a) 20wt%Co/1wt%Pd/1wt%K/SiO_2-500, (b) 20wt%Co/1wt%Pt/1wt%K/SiO_2-500 and (c) 20wt%Co/1wt%Ru/1wt%K/SiO_2-500

Figure 7.14 shows selected spectra obtained from detailed scans on specific regions of each catalyst system. Figure 7.14 (a) shows the Co 2p region for all catalysts. Each system shows the Co $2p_{3/2}$ peak with a binding energy of *ca*. 780 eV this value is typical for cobalt

present in the Co_3O_4 form, this is further confirmed as the main cobalt phase by XRD (Figure 7.13). Figure 7.14 (b) shows the spectra obtained from a detailed scan of the K 1s region with the peaks from each system indicating the presence of potassium in the K^+ form most likely as the oxide, K_2O. No obvious variation is observed with the alteration of the noble metal present. Spectra obtained from the detailed scans of the Pd 3d and Pt 4d regions revealed palladium and platinum are present in their PdO and PtO_2 oxide forms. No peaks were however detected in the Ru 3d region of the spectrum. This suggests that the cobalt could be coating any ruthenium present an effect similar to that previously observed with Au-Co catalysts.[28]

The Co/Si atomic ratio on the surface of each catalyst as calculated by XPS are shown in Table 7.6. As the noble metal is changed from palladium to platinum to ruthenium the ratio increases suggesting cobalt enrichment at the catalyst surface consistent with an increase in cobalt dispersion.[29]

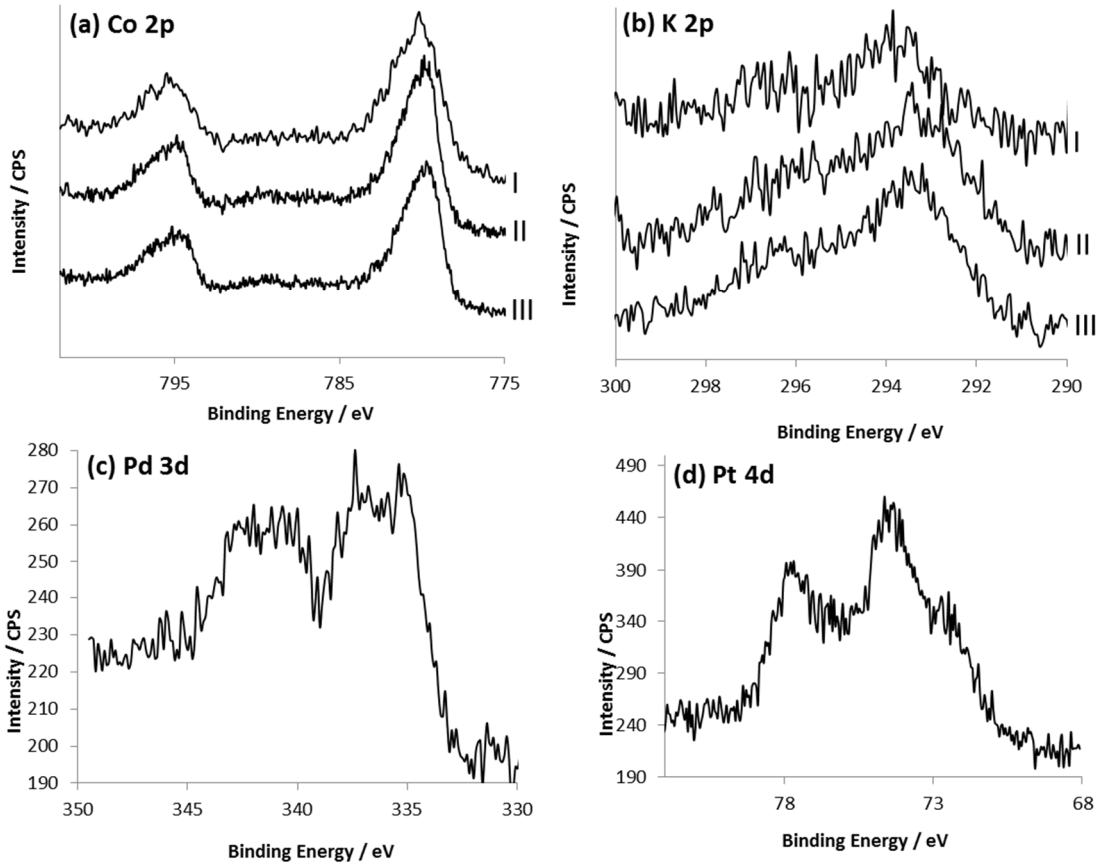

Figure 7.14 – XPS spectra obtained for the 20wt%Co/1wt%M/1wt%K/SiO_2-500 catalyst systems. (a) Detailed scan of the Co 2p region; (i) 20wt%Co/1wt%Pd/1wt%K/SiO_2-500, (ii) 20wt%Co/1wt%Pt/1wt%K/SiO_2-500 and (iii) 20wt%Co/1wt%Ru/1wt%K/SiO_2. (b) Detailed scan of the K 1s region; (i) 20wt%Co/1wt%Pd/1wt%K/SiO_2-500, (ii) 20wt%Co/1wt%Pt/1wt%K/SiO_2-500 and (iii) 20wt%Co/1wt%Ru/1wt%K/SiO_2. (c) Detailed scan of 20wt%Co/1wt%Pd/1wt%K/SiO_2-500 Pd 3d region (d) Detailed scan of 20wt%Co/1wt%Pt/1wt%K/SiO_2-500 Pt 3d region

TEM studies were conducted in order to investigate the changing catalyst morphology upon the alteration of the noble metal used in catalyst preparation. Figure 7.15 shows TEM images typical for each catalyst system. As with the catalyst discussed in Section 7.4 the nano-

particle sizes measured by TEM are larger than the crystallite size calculated by XRD although the average size does follow the same trend. No distinct particles were observed for the ruthenium promoted system, this could be due to the smaller particle size suggested by XRD or the higher dispersion indicated by XPS studies.

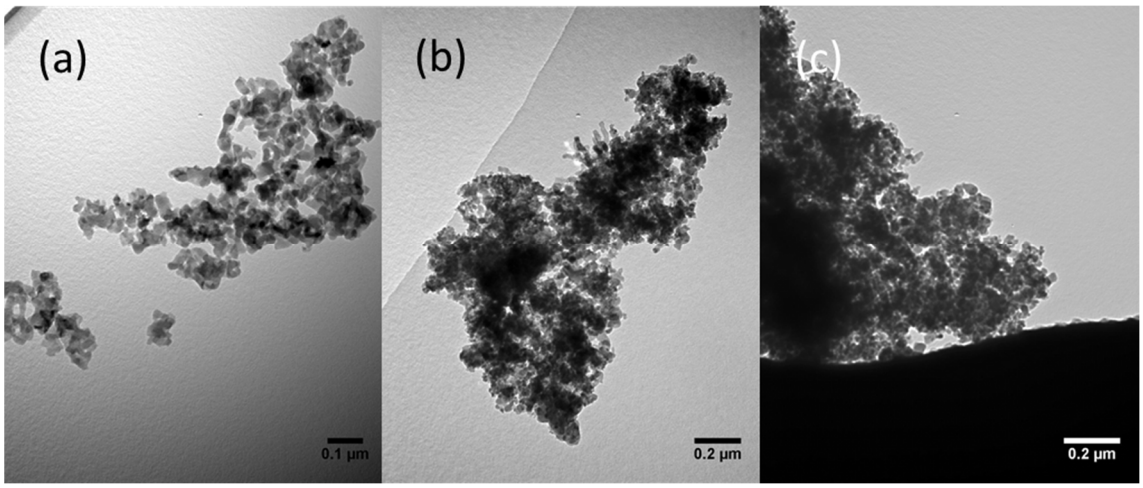

Figure 7.15 – TEM images recorded for (a) 20wt%Co/1wt%Pd/1wt%K/SiO_2-500, (b) 20wt%Co/1wt%Pt/1wt%K/SiO_2-500 and (c) 20wt%Co/1wt%Ru/1wt%K/SiO_2-500.

7.5.3 Catalyst Testing

Each of the prepared catalyst systems were tested for their CO_2 hydrogenation ability in Reactor 1 under the following reaction conditions; temperature: 300 ^oC, pressure: atmospheric, H_2:CO_2 ratio 3:1, total flow 8 sccm. Full details of the catalyst test procedure are outlined in Section 2.3, Chapter 2.

Each of the three catalyst systems showed good stability of the course of the catalyst test with no significant changes in HC distribution. No evidence of catalyst deactivation was observed with CO_2 conversion values showing little change. The catalytic data obtained from these catalyst tests is summarised in Table 7.7.

The nature of the noble metal used in catalyst preparation is shown to have a significant impact on catalyst performance. CO_2 conversion values increase in the order Co-Pt-K < Co-Pd-K < Co-Ru-K with the resulting HC yield matching this trend. Despite the platinum containing system showing the lowest CO_2 conversion it gives the highest CO yield this suggests that the platinum promoted system could have the poorest FT activity of the three systems or alternatively the highest RWGS activity.

Table 7.7 – Catalytic data obtained for CO_2 hydrogenation tests using 20wt%Co/1wt%M/1wt%K/SiO_2-500 (where M = Pd, Pt and Ru)

Catalyst	Conv. (%)	HC Yield (%)	CO Yield (%)	Hydrocarbon Distribution										O/(O+P)[a] in C_2-C_4
				C_1	C_2=	C_2	C_3=	C_3	C_4	C_5	C_6	C_7	C_8	
20wt%Co/1wt%Pd/1wt%K/SiO_2-500	41.6	36.8	5.7	62.8	0.0	17.0	0.0	11.6	4.7	2.4	1.0	0.3	0.0	0
20wt%Co/1wt%Pt/1wt%K/SiO_2-500	36.5	28.9	7.6	52.4	0.3	15.5	2.9	9.9	6.9	4.8	3.7	2.4	1.1	9.6
20wt%Co/1wt%Ru/1wt%K/SiO_2-500	45.1	39.4	5.7	60.2	0.5	13.3	6.7	5.9	7.0	3.7	2.1	0.6	0.1	24.1

[a] Olefin content (mol percentage) for C_2-C_4 hydrocarbons, calculated as [olefin(O) / (olefin(O) + paraffin(P)) × 100]. Catlyst tests conducted at atmospheric pressure, 300 ^oC H_2:CO_2 ratio 3:1, total flow – 8 sccm. 0.7g of catalyst. Conversions, yields and product distributions calculated as an average of 5 hours on stream.

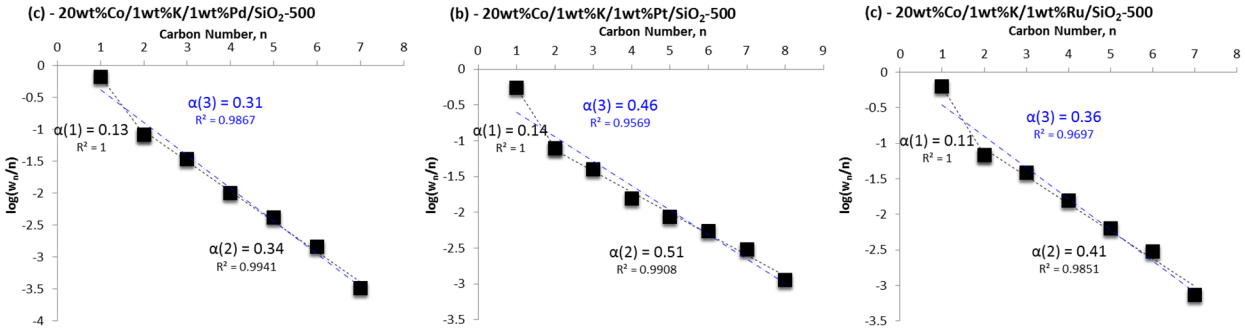

Figure 7.16 – ASF plots for (a) 20wt%Co/1wt%Pd/1wt%K/SiO_2-500, (b) 20wt%Co/1wt%Pt/1wt%K/SiO_2-500 and (c) 20wt%Co/1wt%Ru/1wt%K/SiO_2-500

There is also a pronounced influence on the HC distribution. Methane selectivity is observed to drop further from 63 % to 60 % to 52 % when the noble metal is changed from palladium to ruthenium to platinum. The increased amount of C_5+ mirrors this trend with the platinum promoted system giving a C_5+ selectivity of 12 %. Significantly better than any cobalt based catalyst reported previously or so far studied within this chapter. The enhanced cobalt dispersion upon the replacement of palladium with platinum and ruthenium may play an important role in the reduced methane selectivity observed for these two systems.

ASF plots for each catalyst system are shown in Figure 7.16. Each system shows the double alpha phenomenon to varying extents. The α(2) value for the palladium promoted system is closest to the α(3) value indicating this system shows the lowest formation of excess methane. The chain growth probability α(2), calculated from C_2+ HCs, increases from 0.34 for the Co-Pd-K system to 0.51 for the Co-Pt-K catalyst.

The lack of correlation between cobalt dispersion and the oxide particle size with the CO_2 conversion and HC distributions suggests that these properties alone are not responsible for the alteration in catalyst properties with other factors such as RWGS activity also playing an important role.

7.6 Variation of Alkali Metal

Investigations into the effects of alkali metal addition to cobalt catalysts for FT have been limited.[21] To our knowledge no studies on CO_2 hydrogenation with alkali containing cobalt catalysts have been conducted. Although their addition to cobalt-based FT catalysts has been studied attention has been limited due to the sharp decrease in catalytic activity observed upon their inclusion.[13] Previous studies within this thesis (Chapter 3, Section 3.3) have shown that the addition of potassium to a Co-Pd-MgO catalyst enhanced performance both in terms of an increased HC yield and improved selectivity to heavier hydrocarbons.

Studies conducted by Wang *et al*. have shown a large increase in RWGS activity when potassium (1 wt%) is used in conjunction with a Co-CeO_2 catalyst.[30] The introduction of potassium also reduces the formation of methane, an undesired side product in the RWGS reaction, and aids the reduction of cobalt oxide species. It is likely that this improvement in RWGS activity is the major cause for the improved CO_2 hydrogenation ability.

An investigation conducted by Lillebø and co-workers on the effect of alkali metal on cobalt-based FT catalysts show a distinct difference in catalyst performance depending on the nature of the alkali metal introduced.[20] For iron based FT and CO_2 hydrogenation catalysts potassium has been observed to perform as the best Group 1 alkali metal promoter[13a] however for the cobalt based-catalyst systems studied by Lillebø[20] the introduction of lithium gave the highest selectivity to heavier hydrocarbons and the lowest selectivity to methane. Lithium also resulted in the lowest reduction in catalyst activity relative to the potassium and sodium containing systems. As a result of these observations the replacement of the potassium

component of the 20wt%Co/1wt%Pd/1wt%K/SiO_2-500 with an equal loading of lithium and sodium and the resulting difference in catalyst performance was investigated.

7.6.1 Catalyst Preparation

All catalyst systems were prepared using the standard wet impregnation method described in detail in Section 2.7.13 Chapter 2. Based on the promising catalyst results in Section 7.4 the silica support with a 500 Å pore size was employed for all catalysts. LiOAc, $NaOAc \cdot 3H_2O$ and KOAc were used as precursors for each alkali metal. Three catalyst systems were prepared: 20wt%Co/1wt%Pd/1wt%M/SiO_2-500 (where M = Li, Na and K).

7.6.2 Catalyst Characterisation

Several characterisation techniques were used to probe the properties of each catalyst system. Table 7.8 shows the specific BET surface areas calculated using N_2 physisorption techniques. All show a decrease in surface area relative to the black silica support (80 m^2g^{-1}) the largest decrease was observed for the sodium promoted system with the potassium containing system showing the highest surface area of the three catalyst systems.

Table 7.8 - BET surface area and Co_3O_4 crystallite size calculated from XRD for each of the catalyst systems

Catalyst	BET Surface Area (m^2g^{-1})	Co_3O_4 crystallite size (nm) [a]
20wt%Co/1wt%Pd/1wt%Li/SiO_2-500	60.8	10.1
20wt%Co/1wt%Pd/1wt%Na/SiO_2-500	56.2	14.0
20wt%Co/1wt%Pd/1wt%K/SiO_2-500	66.1	14.0

[a] – Crystallite size was calculated based on the (311) Co_3O_4 peak observed from XRD measurements using the Sherrer equation.

The diffraction patterns obtained from XRD studies are show in Figure 7.17. All systems show the presence of peaks attributable to the presence of cobalt in its Co_3O_4 form. With the sodium and potassium promoted system peaks are observed at 2θ values of 31, 37, 45 and 59 ^{o} corresponding to the Co_3O_4 (220), (311), (400) and (511). The lithium promoted catalyst system however only shows the (220) and (311) peaks. No other peaks attributable to the formation of any other phases or attributable to the promoters are observed. The Scherrer equation was used to calculate the crystallite size for each catalyst based on the Co_3O_4 peaks, the calculated values are show in Table 7.8. The sodium and potassium containing systems both show crystallite sizes of 14 nm with the introduction of lithium to the system resulting in the formation of smaller cobalt oxide crystallites.

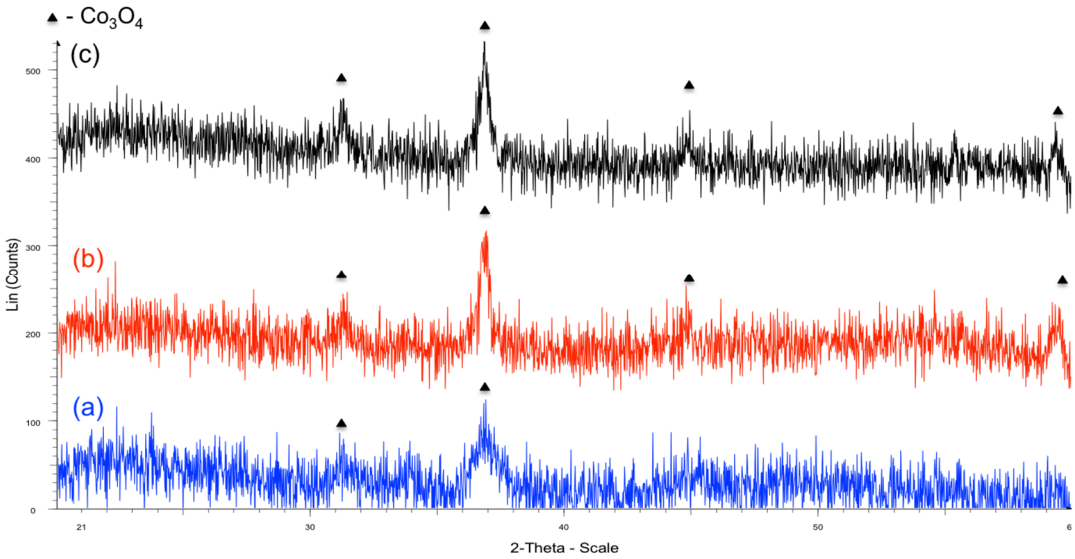

Figure 7.17 – XRD diffraction patterns recorded for (a) 20wt%Co/1wt%Pd/1wt%Li/SiO_2-500, (b) 20wt%Co/1wt%Pd/1wt%Na/SiO_2-500 and (c) 20wt%Co/1wt%Pd/1wt%K/SiO_2-500

TEM was utilised to investigate the catalyst morphology for the three systems. Images typical for each system are shown in Figure 7.18. While nano-particles are observed with the potassium and lithium promoted systems no distinct particles are observable at this magnification for the sodium containing catalyst. As with the systems discussed in Sections 7.4 and 7.5 TEM measurements suggest the formation of much larger nano-particles than calculated by XRD (Table 7.8), this could be due to the conglomeration of smaller nano-particles or larger nano-particles consisting of many smaller crystalline phases.

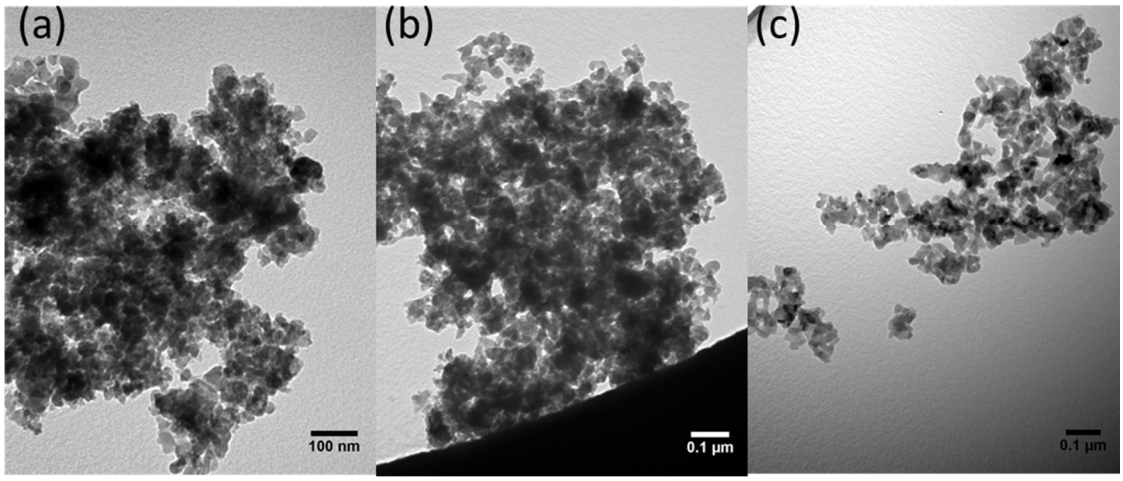

Figure 7.18 – TEM images typical for (a) 20wt%Co/1wt%Pd/1wt%Li/SiO_2-500, (b) 20wt%Co/1wt%Pd/1wt%Na/SiO_2-500 and (c) 20wt%Co/1wt%Pd/1wt%K/SiO_2-500

XPS studies were conducted to further investigate the composition of each catalyst. Selected detailed spectra are shown in Figure 7.19. The detailed scan of the Co 2p region shows little change upon the changing of the alkali metal component of the catalyst system. A Co $2p_{3/2}$

peak present at *ca*. 780 eV for all three systems indicates the presence of cobalt as Co_3O_4[31] further confirming what was observed by XRD studies. Figure 7.19 (b) shows a detailed scan of the Pd 3d region for all catalyst systems. Again little change is observed with the changing alkali metal with each showing a peak at approximately 337 eV indicative of palladium in its PdO form.[18] The K 1s {Figure 7.19 (c)} and Na 1s {Figure 7.19 (d)} show the presence of potassium and sodium as K^+ and Na^+ most likely as their oxides K_2O and Na_2O. No peak attributable to any lithium species was detected possibly suggesting that cobalt may be coating it and preventing detection.

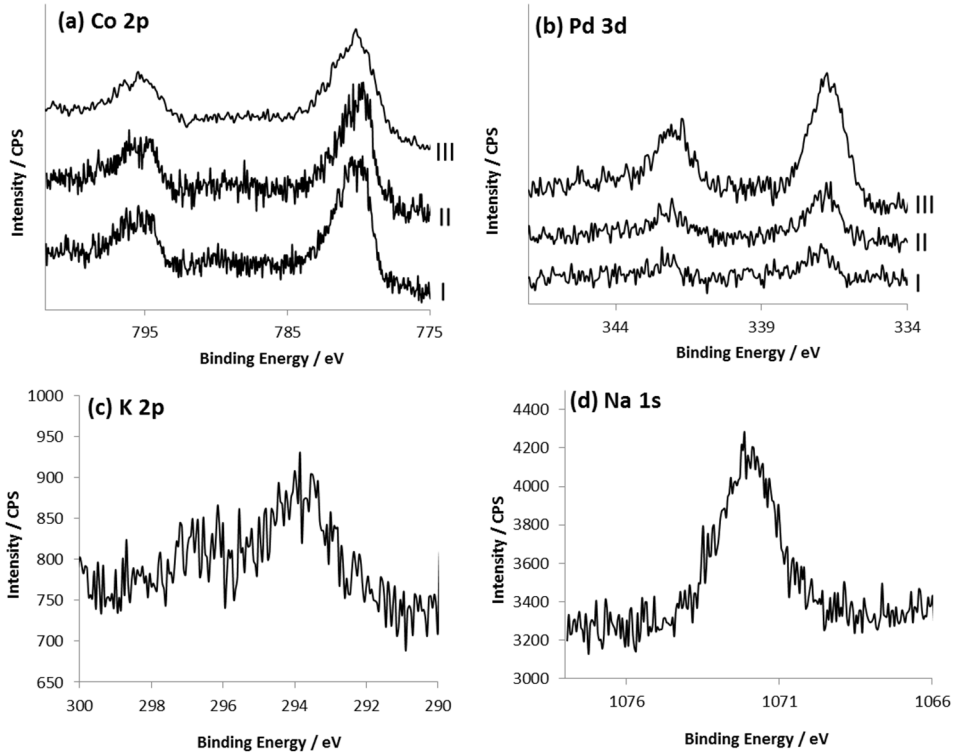

Figure 7.19 - XPS spectra obtained for the 20wt%Co/1wt%Pd/1wt%M/SiO_2-500 catalyst systems. (a) Detailed scan of the Co 2p region; (i) 20wt%Co/1wt%Pd/1wt%Li/SiO_2-500, (ii) 20wt%Co/1wt%Pd/1wt%Na/SiO_2-500 and (iii) 20wt%Co/1wt%Pd/1wt%K/SiO_2. (b) Detailed scan of the Pd 3d region; (i) 20wt%Co/1wt%Pd/1wt%Li/SiO_2-500, (ii) 20wt%Co/1wt%Pd/1wt%Na/SiO_2-500 and (iii) 20wt%Co/1wt%Pd/1wt%K/SiO_2-500. (c) Detailed scan of 20wt%Co/1wt%Pd/1wt%K/SiO_2-500 K 2p region (d) Detailed scan of 20wt%Co/1wt%Pd/1wt%Na/SiO_2-500 Na 1s region

7.6.3 Catalyst Testing

Each of the prepared catalyst systems were tested for their CO_2 hydrogenation ability in Reactor 1 under the following reaction conditions; temperature: 300 ^oC, pressure: atmospheric, H_2:CO_2 ratio 3:1, total flow 8 sccm. Full details of the catalyst test procedure are outlined in Section 2.2, Chapter 2.

All three catalyst systems showed good catalyst stability with little change in CO_2 conversion, HC or CO yield with time on stream. While product selectivity remained relatively consistent for potassium promoted catalyst the same was not observed for the lithium and sodium systems. Figure 7.20 shows how the product distribution for each catalyst varies with

time on stream. The lithium containing catalyst showed a decrease in methane selectivity with a shift towards heavier HCs over the first 2-3 hours after this period HC distribution appears to stabilise.

With the sodium containing catalyst the HC distribution varies to a greater extent again with selectivity towards heavier hydrocarbons improving with time on stream. With this system stability is not achieved until *ca*. 4-5 hours under reaction conditions. With all systems appearing relatively stable after 5 hours on stream the CO_2 conversion, HC and CO yields and HC distribution at this time were chosen for comparison of catalyst performance. Table 7.9 summarises the data obtained.

Very little change is observed in CO_2 conversion when the alkali metal component of the catalyst is changed. HC yield does, however, increase steadily, if not significantly, as you descend the group from lithium to potassium this results in a concurrent decrease in CO yield.

The product selectivities observed for each system varies to a greater extent. The replacement of potassium with lithium results in an increase in methane selectivity and decrease in the selectivity towards C_5+ hydrocarbons. This appears to contradict the trend observed for cobalt based FT catalysts, where the use of lithium resulted in the largest increase in selectivity towards heavier hydrocarbons. This could, however, be due to a number of reasons such as higher temperature, much lower pressure and the use of CO_2 not CO as a feed-gas with the effect on RWGS activity likely to have a significant effect.

When the potassium within the Co-Pd-K-SiO_2 system is replaced with an equal loading of sodium a decrease in methane selectivity is observed with C_5+ HC selectivity increasing from 3.7 % to 9.2 %. The olefin to paraffin ratio shows a slight increase, however, the majority of products formed are still fully saturated.

Table 7.9 – Catalytic data obtained for CO_2 hydrogenation tests using 20wt%Co/1wt%Pd/1wt%M/SiO_2-500 (where M = Li, Na and K)

Catalyst	Conv. (%)	HC Yield (%)	CO Yield (%)	Hydrocarbon Distribution										O/(O+P)[a] in C_2-C_4
				C_1	C_2=	C_2	C_3=	C_3	C_4	C_5	C_6	C_7	C_8	
20wt%Co/1wt%Pd/1wt%Li/SiO_2-500	39.5	31.9	7.6	69.5	0.0	18.9	0.2	6.9	2.2	1.0	0.8	0.5	0.1	0.5
20wt%Co/1wt%Pd/1wt%Na/SiO_2-500	41.9	33.4	8.5	60.7	0.0	14.9	2.0	8.5	4.7	4.1	3.3	1.6	0.2	7.0
20wt%Co/1wt%Pd/1wt%K/SiO_2-500	41.6	36.8	5.7	62.8	0.0	17.0	0.0	11.6	4.7	2.4	1.0	0.3	0.0	0

[a] Olefin content (mol percentage) for C_2-C_4 hydrocarbons, calculated as [olefin(O) / (olefin(O) + paraffin(P)) × 100]. Catlyst tests conducted at atmospheric pressure, 300 ^oC H_2:CO_2 ratio 3:1, total flow – 8 sccm. 0.7g of catalyst. Conversions, yields and product distributions calculated after 5 hours on stream.

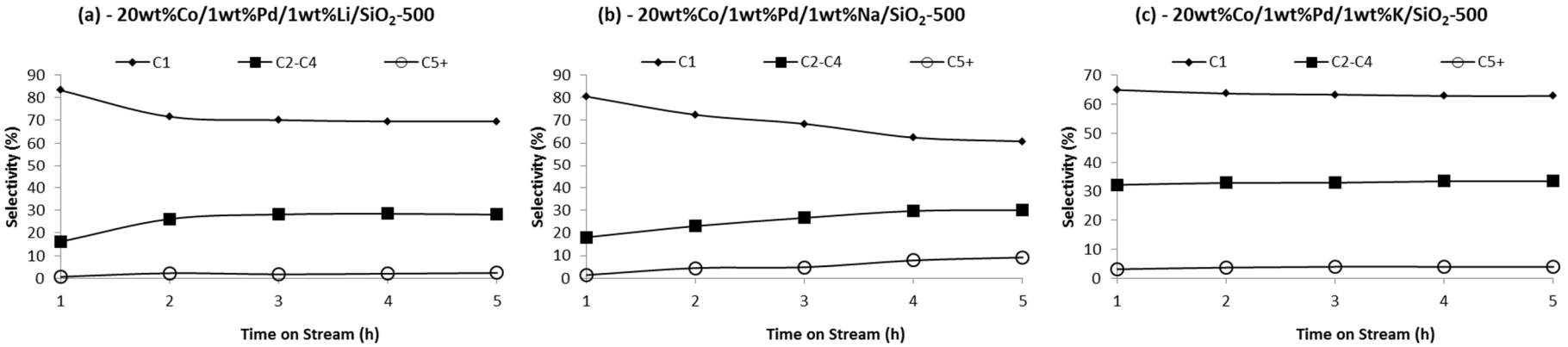

Figure 7.20 – Variation of HC distribution with time on stream as observed for (a) 20wt%Co/1wt%Pd/1wt%Li/SiO_2, (b) 20wt%Co/1wt%Pd/1wt%Na/SiO_2 and (c) 20wt%Co/1wt%Pd/1wt%K/SiO_2

The ASF plots for each catalyst system are shown in Figure 7.21. The lithium containing catalyst system differs from the sodium and potassium systems as the double alpha phenomenon observed cannot be explained by the formation of excess methane. The C_1-C_5 HCs appear to give a different chain growth probability to the C_5-C_7 HCs. This type of double alpha phenomenon has been observed previously[32] and several reasons have been suggested. The most common explanations are the two active site model and models relating to the readsorption of olefins.[19] Both the potassium and sodium promoted systems show a higher methane content than predicted by the ASF distribution likely due to the parallel formation of methane by the direct hydrogenation of CO_2 and such α(2) gives a more accurate chain growth probability for the FT process. The replacement of potassium with sodium results in a significant increase in chain growth probability for C_2+ hydrocarbons with the α(2) value increasing from 0.34 to 0.50.

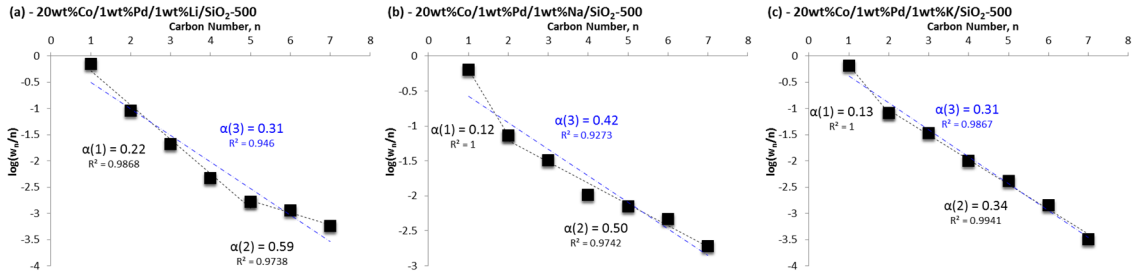

Figure 7.21 – ASF distribution plots for (a) 20wt%Co/1wt%Pd/1wt%Li/SiO_2-500 (b) 20wt%Co/1wt%Pd/1wt%Na/SiO_2-500 and (c) 20wt%Co/1wt%Pd/1wt%K/SiO_2-500

Although the smaller crystallite may be responsible for the poorer performance observed by the lithium containing system. The difference in catalyst performance for sodium and potassium catalysts cannot be attributed to particle size as there is no distinguishable change in crystallite size as calculated by XRD this shows that this is not the only property dictating catalyst performance with other important properties at play such as electronic effects. The work conducted by Lillebø and co-workers[20] on the effect of alkali metal on cobalt-based FT catalysts shows that at higher loadings the sodium containing catalyst system shows the highest selectivity to CO_2 indicating a higher WGS activity. This higher WGS activity observed under FT conditions may translate to a higher RWGS ability under the reaction conditions studied within this Chapter. The CO_2 selectivity reported decreases in the order Na > K > Li, the same trend observed for higher C_5+ selectivity as shown in Table 7.9. With no significant effect observed on CO_2 conversion values it is possible that this suggested increase in RWGS activity is responsible for an increase in CO formation which leads to a high CO:H_2 ratio which has been shown to aid selectivity towards heavier hydrocarbons (see Section 7.1.3.2).

7.7 Removal of Noble Metal

Although the effect of palladium and potassium addition to cobalt on a MgO support was discussed in Chapter 3 no studies were conducted to establish the effect of potassium addition

alone or if the effects were the same on a silica supported catalyst system. Several catalyst systems were prepared in order to determine the answers to these questions. It was hoped that these investigations may also lead to a deeper understanding of the role of each promoter.

7.7.1 Catalyst Preparation

The standard wet impregnation method detailed in Chapter 2 Section 2.7.13 was employed to prepared all catalyst system. For the initial investigations into promoter effects on silica supported catalysts SiO_2-60 was chosen as the catalyst's structural promoter. A cobalt only catalyst (20wt%Co/SiO_2) was prepared along with systems promoted only with palladium or potassium (20wt%Co/1wt%Pd/SiO_2-60 and 20wt%Co/1wt%K/SiO_2-60) these were then compared to a catalyst system promoted by both palladium and potassium (20wt%Co/1wt%Pd/1wt%K/SiO_2).

7.7.2 Catalyst Characterisation

The effect of palladium and potassium addition to the Co-SiO_2 on the catalyst properties were investigated by XRD and BET. The specific BET surface areas for each system are shown in Table 7.10. The surface area of the silica support (490 m^2g^{-1}) is reduced upon the addition of cobalt to the system. The surface area of the Co-SiO_2 system is further reduced upon the introduction of potassium and the palladium potassium combination. Palladium introduction however results in a slight increase in the surface area as calculated by BET.

XRD studies were conducted on each catalyst with the diffraction patterns recorded shown in Figure 7.22. A peak at a 2θ value of 37 ^{o} is viewed for all catalyst systems this is characteristic for the (311) Co_3O_4 peak and indicates this is the main cobalt phase in all systems.

Table 7.10 - BET surface area for each of the catalyst systems

Catalyst	BET Surface Area (m^2g^{-1})
20wt%Co/SiO_2-60	340
20wt%Co/1wt%Pd/SiO_2-60	389
20wt%Co/1wt%K/SiO_2-60	294
20wt%Co/1wt%Pd/1wt%K/SiO_2-60	248

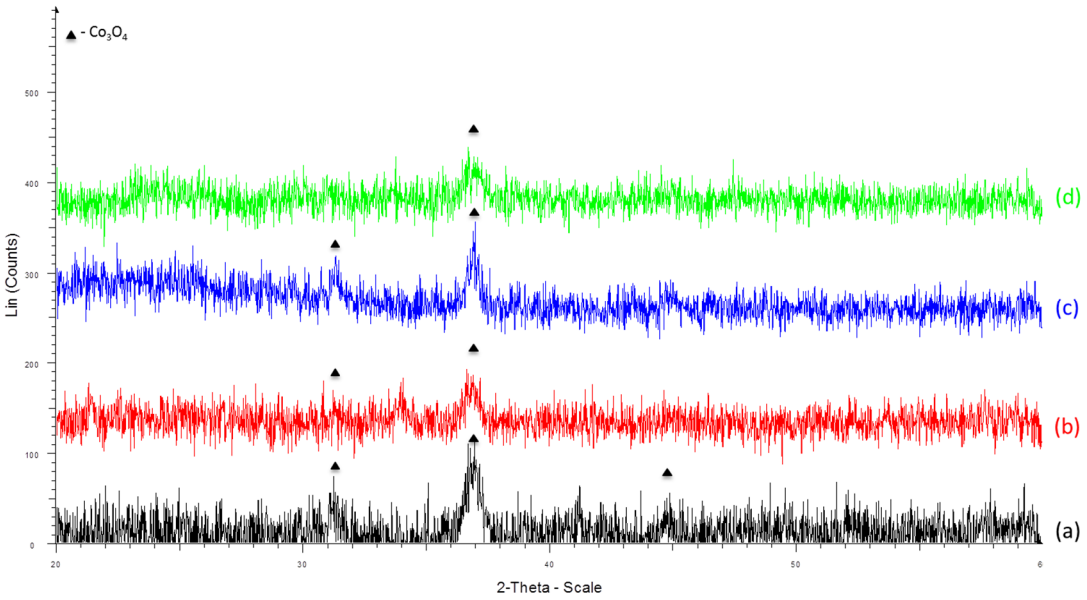

Figure 7.22 – pXRD patterns recorded for (a) 20wt%Co/SiO_2-60, (b) 20wt%Co/1wt%Pd/SiO_2-60, (c) 20wt%Co/1wt%K/SiO_2-60 and (d) 20wt%Co/1wt%Pd/1wt%K/SiO_2-60.

7.7.3 Catalyst Testing

The prepared catalyst system were all tested for their hydrogenation ability in Reactor 1 (See Chapter 2 Section 2.2 for full details). Reaction conditions were kept constant for all tests with a temperature of 300 ^{o}C, atmospheric pressure and a H_2:CO_2 ratio of 3:1 with a total flow of 8 sccm. Full details of the catalyst test procedure are outlined in Section 2.3, Chapter 2.

The catalyst evaluation results for the four systems are summarised in Table 7.11. The 20wt%Co/SiO_2 catalyst shows a relatively high CO_2 conversion with a high selectivity to hydrocarbons. The products, however, consist of almost exclusively methane with only a very small amount of ethane also formed. This SiO_2 supported catalyst system significantly outperforms the analogous MgO supported system reported in Chapter 3 where a maximum HC yield of *ca*. 10 wt% was observed. Product distribution remains similar for both systems though with the MgO supported system also showing an exceptionally high selectivity to methane.

The addition of a low loading of palladium to the system, resulting in a 20wt%Co/1wt%Pd/SiO_2 catalyst resulted in a drop in CO_2 conversion and HC yield. No change is observed in HC distribution with methane still making up the majority of HCs formed. These results appear to contradict those obtained for the MgO supported system investigated in Chapter 3 where the addition of palladium to the catalyst system resulted in an improvement in both HC yields and selectivity to C_2+ HCs. This confirms that the nature of the oxide support used can have a significant influence on catalyst performance with the basic nature of the MgO support likely playing an important role in the selectivity to heavier HCs.[33] It is possible that this change in behaviour of the palladium promoter could be due to the MgO inhibiting the activity of the cobalt by, for example, reducing the metal dispersion a problem previously observed with MgO catalysts.[34] The addition of palladium (which has been shown to increase

cobalt dispersion[3]) to the MgO supported system could then aid the counteraction of the dispersion inhibiting properties of the MgO. With the silica system showing a much higher dispersion initially the effect of palladium addition is greatly decreased. This would not, however, explain the reduced CO_2 conversion.

The addition of a potassium promoter to the Co-SiO_2 catalyst system results in a large decrease in CO_2 conversion and HC yield. The CO content of the product stream is increased. The decrease in CO_2 conversion mirrors that which is observed in the CO fed FT process when alkali metals are added.[20] The increase in CO yield hints at an increase in RWGS activity, a reduction in FT activity or a combination of both. The introduction of potassium to the system does result in a significant reduction in methane selectivity with a concurrent increase in C_5+ selectivity. The addition of potassium also aids the formation of olefins with a significant increase in their yield observed upon its inclusion. This increase in C_5+ and olefins selectivity can be attributed to electronic effects where the addition of potassium to cobalt increases the surface to molecule charge transfer effectively increasing the strength of CO binding which can result in an increased surface coverage[35] and as such an increased chain growth probability.

When the cobalt-silica system is dual promoted with 1 wt% palladium and potassium the CO_2 conversion is significantly higher than the potassium and palladium only promoted system and only slightly lower than the 20wt%Co/SiO_2 catalyst. While the catalyst selectivity shows improvement over the Co-SiO_2 system with a drop in methane selectivity and increase in C_2+ yield this enhancement is significantly less impressive than the addition of potassium alone. The addition of palladium to the Co-K-SiO_2 system also results in a loss of selectivity towards olefins with only saturated HCs detected in the product stream.

Table 7.11 – Catalytic data obtained for CO_2 hydrogenation tests investigating the influence of palladium and potassium addition to a Co/SiO_2-60 catalyst and studies using 20wt%Co/1wt%M/SiO_2-500 (where M = Li, Na and K)

Catalyst	Conv. (%)	HC Yield (%)	CO Yield (%)	Hydrocarbon Distribution										O/(O+P)[a] in C_2-C_4
				C_1	C_2=	C_2	C_3=	C_3	C_4	C_5	C_6	C_7	C_8	
20wt%Co/SiO_2-60	67.4	64.4	2.8	99.7	0.0	0.3	0.0	0.0	0.0	0.0	0.0	0.0	0.0	0
20wt%Co/1wt%Pd/SiO_2-60	50.7	47.5	3.2	99.7	0.0	0.3	0.0	0.0	0.0	0.0	0.0	0.0	0.0	0
20wt%Co/1wt%K/SiO_2-60	36.1	29.9	6.1	54.7	2.0	11.5	10.7	3.8	2.5	5.5	3.2	0.7	0.1	39.2
20wt%Co/1wt%Pd/1wt%K/SiO_2-60	63.4	54.6	8.8	93.2	0.0	5.4	0.0	1.2	0.0	0.0	0.0	0.0	0.0	0
20wt%Co/1wt%Li/SiO_2-500	39.3	30.9	8.4	74.3	0.6	14.8	2.6	4.7	2.5	0.6	0.0	0.0	0.0	12.2
20wt%Co/1wt%Na/SiO_2-500	51.2	40.1	11.1	53.7	2.1	13.4	11.1	5.1	8.2	3.8	2.1	0.8	0.0	35.4
20wt%Co/1wt%K/SiO_2-500	47.6	39.5	8.1	60.4	1.4	13.0	9.0	5.2	6.6	3.0	1.3	0.1	0.0	31.1

[a] Olefin content (mol percentage) for C_2-C_4 hydrocarbons, calculated as [olefin(O) / (olefin(O) + paraffin(P)) × 100]. Catlyst tests conducted at atmospheric pressure, 300 ^oC H_2:CO_2 ratio 3:1, total flow – 8 sccm. 0.7g of catalyst. Conversions, yields and product distributions calculated after 5 hours on stream.

These results suggest that while there is an improvement in CO_2 conversion with palladium there is no benefit in terms of HC selectivity upon its introduction. With this in mind the effect of removal of palladium from the Co-Pd-M-SiO_2-500 (where M = Li, Na and K) catalysts was investigated to see if HC distribution could be improved further compared to what was observed with palladium present (Table 7.9). A summary from the catalyst results is shown in Table 7.11.

All three of the alkali metal only promoted catalyst systems show consistent CO_2 conversion values over the course of catalyst testing with little to no change in HC and CO yield. A more significant variation is observed with the hydrocarbon distribution with a stabilisation period as observed with some previous catalyst systems (See Figure 7.20) recorded. Figure 7.23 shows how the HC distribution varies with time on stream. For all systems methane selectivity drops initially with a concurrent increase in selectivity to C_2-C_4 and C_5+ hydrocarbons. These values stabilise after varying periods under reaction conditions with the sodium promoted system the quickest to stabilise after *ca*. 3 hours. Both the potassium and lithium systems stabilise after approximately 4 hours on stream. With all systems appearing stable after 5 hours on stream this time was chosen for catalyst comparison.

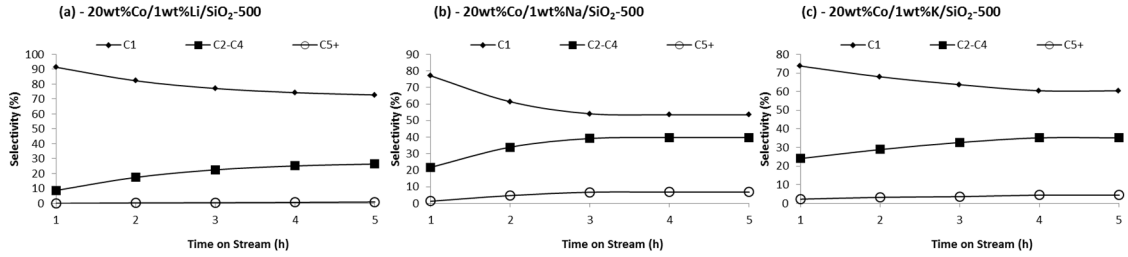

Figure 7.23 – Variation of HC distribution with time on stream as observed for (a) 20wt%Co/1wt%Li/SiO_2, (b) 20wt%Co/1wt%Na/SiO_2 and (c) 20wt%Co/1wt%K/SiO_2

The lithium containing catalyst system shows the lowest conversion of the three alkali metal promoted catalysts, there is little difference between the potassium and sodium containing systems with a slightly higher CO_2 conversion observed for the Co-Na-SiO_2 sample. HC yield was shown to follow the same trend with the Co-Li-SiO_2 system lowest. The CO_2 conversion values were all found to be higher than those recorded for the analogues systems that also contained palladium (Table 7.9) with the exception of the lithium containing system where CO_2 conversion values remained similar.

The HC distribution was observed to vary to a greater extent with the lithium containing catalyst showing the lowest selectivity to C_2+ HCs. The methane selectivity decreases in the order Co-Li-SiO_2 > Co-K-SiO_2 > Co-Na-SiO_2. While the catalysts discussed here follow the same trend observed for their palladium containing analogues the potassium and sodium promoted systems show a greater reduction in methane selectivity with a concurrent increase in the yield of C_5+ HCs compared to the systems also containing palladium (Table 7.9). The

20wt%Co/1wt%Na/SiO_2-500 system shows a methane selectivity of 54 % lower than any other cobalt based catalyst studied so far within this thesis and significantly better than any cobalt-based CO_2 hydrogenation catalysts previously reported within the literature. The removal of palladium giving catalysts promoted only by alkali metals results in the formation of some olefin products whereas with a noble metal present the HCs formed are exclusively saturated.

The ASF plots for each of the catalyst systems are shown in Figure 7.24. In contrast to what has been observed with the majority of previous cobalt catalyst systems both within this chapter and previously reported in the literature[1, 7] the product distribution obeys what is predicted by ASF with no double alpha phenomenon caused by a higher selectivity to methane than predicted. This indicates that all hydrocarbon are being produced *via* the FT process. There is a slight anomaly for the C_2 hydrocarbons in each system with the point lying slightly off the trend line, this phenomenon is however often observed for HCs produced by the FT process[36] and can be explained by Dry's mechanism (see Chapter 1 Section 1.2.2 for more details).[37]

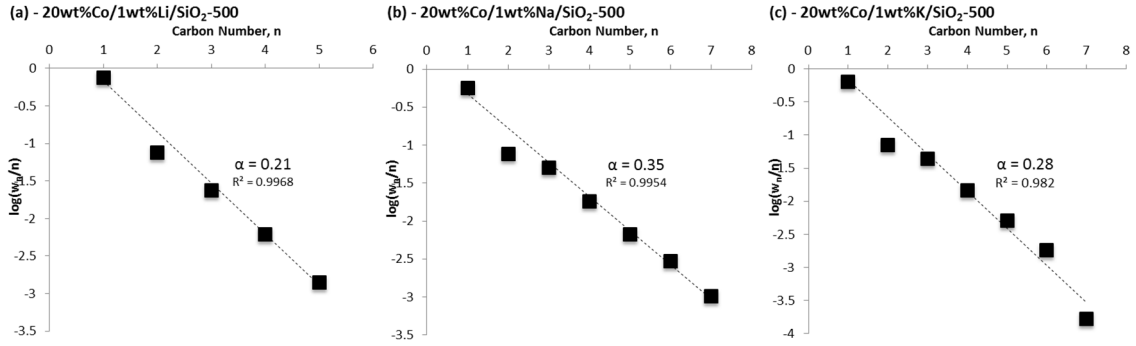

Figure 7.24 – ASF plots for (a) 20wt%Co/1wt%Li/SiO_2-500, (b) 20wt%Co/1wt%Na/SiO_2-500 and (c) 20wt%Co/1wt%K/SiO_2-500

N_2 physisorption measurements were used to calculate the BET surface areas of each catalyst system, the results are shown in Table 7.12. There appears to be little to no influence on the catalyst surface area with the changing of the alkali metal with values showing little change even relative to the non-promoted 20wt%Co/SiO_2-500 (62.8 m^2g^{-1}) system. XRD studies were also conducted on each catalyst with the resulting diffraction patterns shown in Figure 7.25. All catalysts show the presence of peaks at 2θ values of 31, 37, 45 and 59 ^{o}, characteristic for Co_3O_4[17] indicating this is the main cobalt phase present with the introduction of differing alkali metals having little effect on the phase of cobalt present. The Sherrer equation was used to calculate the Co_3O_4 based on the (311) Co_3O_4 diffraction peak with the results shown in Table 7.12. As with the analogous catalysts that also contain palladium the sodium and potassium containing systems show the same crystallite size with the lithium promoted system producing slightly smaller particles. A slight reduction in crystallite size is observed in the absence of palladium (Table 7.8). No obvious relationship between particle size, surface area and catalyst

performance is observed suggesting that other factors such as electronic effects also play an important role.

Table 7.12 - BET surface area and Co_3O_4 crystallite size calculated from XRD for each of the catalyst systems

Catalyst	BET Surface Area (m^2g^{-1})	Co_3O_4 crystallite size (nm) [a]
20wt%Co/1wt%Li/SiO_2-500	58.3	9.3
20wt%Co/1wt%Na/SiO_2-500	58.1	12.0
20wt%Co/1wt%K/SiO_2-500	62.8	12.0

[a] – Crystallite size was calculated based on the (311) Co_3O_4 peak observed from XRD measurements using the Sherrer equation.

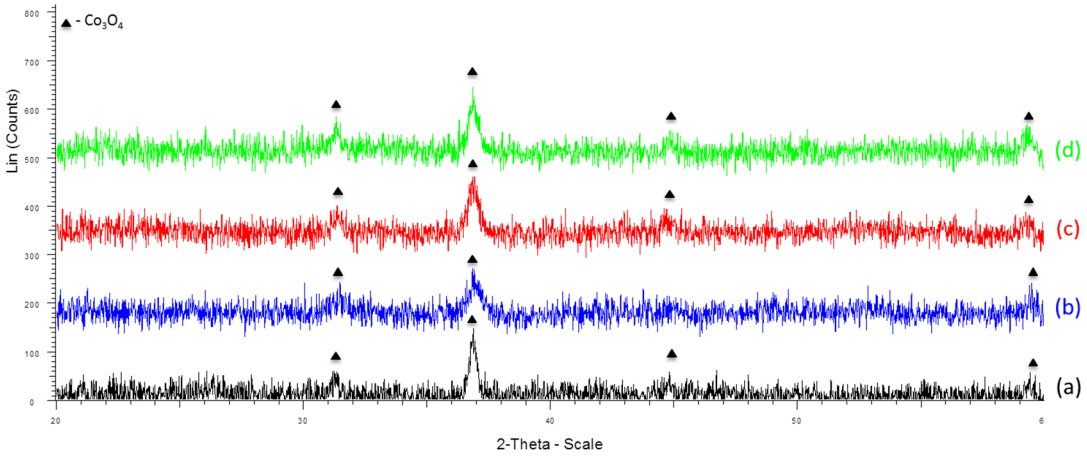

Figure 7.25 – XRD patterns recorded for (a) 20wt%Co/SiO_2-500, (b) 20wt%Co/1wt%Li/SiO_2-500, (c) 20wt%Co/1wt%Na/SiO_2-500 and (d) 20wt%Co/1wt%K/SiO_2-500.

7.8 The Addition of Transition Metal Promoters to Cobalt Catalysts

With the results of the previous section showing that the addition of expensive noble metals offers no benefits in terms of selectivity towards C_2+ hydrocarbons some cheaper transition metal alternatives were investigated.

Although molybdenum is not traditionally thought of as an FT transition metal catalyst work by Dun and co-workers[38] has previously shown that under certain conditions it can be used as an effective FT catalyst. The selectivity shown was also found to be quite desirable with a low methane content and high selectivity to the more valuable alkene products. The addition of molybdenum to cobalt based FT catalysts was investigated by Chen *et al.* where they found that its incorporation into the catalyst composition resulted in an enhanced catalyst performance with the selectivity to both C_2+ and olefins increased upon its introduction.[39] Investigations have shown that mixed cobalt molybdenum oxide catalysts are active for the WGS reaction[40] suggesting that molybdenum's incorporation could also lead to an improved RWGS activity.

The addition of chromium as a promoter for cobalt based FT catalyst has also been investigated.[41] This showed that the addition of low loadings of chromium to the cobalt FT catalysts resulted in a desirable increase in selectivity to heavier, longer chained hydrocarbons. Work by Copperthwaite and co-workers has also shown that mixed cobalt-chromium oxide catalysts are active for the WGS reaction[42] and as such the addition of chromium to the cobalt-silica catalyst system may also result in an increased RWGS activity.

Manganese-cobalt oxides have also been employed successfully for WGS catalysis[43] and as such it was decided that investigations should be extended across the period to include it. The addition of manganese to cobalt based FT catalyst has also received some attention with increased WGS activity reported[44] while this can be undesirable for FT catalysis, increased WGS activity may aid the formation of CO under CO_2 hydrogenation conditions and as such may result in enhanced catalyst performance.

The addition of none of the aforementioned transition metals to cobalt based catalysts for CO_2 hydrogenation has been previously investigated. In order to test the affects each of these metals has on Co-SiO_2 catalysts for the CO_2 hydrogenation reaction catalysts systems were prepared of the general composition of 20wt%Co/1wt%M/SiO_2-500 where M = no metal, Mn, Cr and Mo.

7.8.1 Catalyst Preparation

Generally the same wet impregnation method utilised for all catalysts reported within this chapter was used for catalyst preparation with $(NH_4)_6Mo_7O_{24}\cdot 4H_2O$, $CrCl_3$ and $Mn(OAc)_3\cdot 2H_2O$ used as precursors for each of the promoters. Due to solubility issues with the molybdenum precursor in methanol the minimum amount of deionised water was used to dissolve $(NH_4)_6Mo_7O_{24}\cdot 4H_2O$ with the rest of the preparation method remaining unchanged. With the SiO_2-500 proving the most successful of the supports used so far it was chosen as the support for these catalyst tests. For full details on the catalyst preparation please refer to Chapter 2 Section 2.7.13.

7.8.2 Catalyst Characterisation

N_2 physisorption studies of each of the catalyst systems allowed the calculation of the specific BET surface areas. The values obtained are shown in Table 7.13. No change in surface area is observed when manganese is added to the Co-SiO_2 catalyst however the introduction of both chromium and molybdenum results in an increased surface area with the Co-Mo-SiO_2 system showing the highest surface area.

Table 7.13 - BET surface area for each of the 20wt%Co/1wt%M/SiO_2-500 catalyst systems where M = no metal, Mo, Cr and Mn

Catalyst	BET Surface Area (m^2g^{-1})
20wt%Co/SiO_2-500	62.8
20wt%Co/1wt%Mo/SiO_2-500	74.8
20wt%Co/1wt%Cr/SiO_2-500	68.4
20wt%Co/1wt%Mn/SiO_2-500	62.3

XRD studies were conducted on each of the 20wt%Co/1wt%M/SiO_2- catalysts 500 (where M = no metal, Mo, Cr and Mn) with the recorded diffraction patterns shown in Figure 7.26. The presence of peaks at 2θ values of 31, 37, 45 and 59 °, characteristic for Co_3O_4, indicate that this is the main cobalt phase present for each catalyst. There appears to be little influence on the cobalt phase present upon the introduction of the different transition metal promoters with no evidence for the formation of mixed oxides.

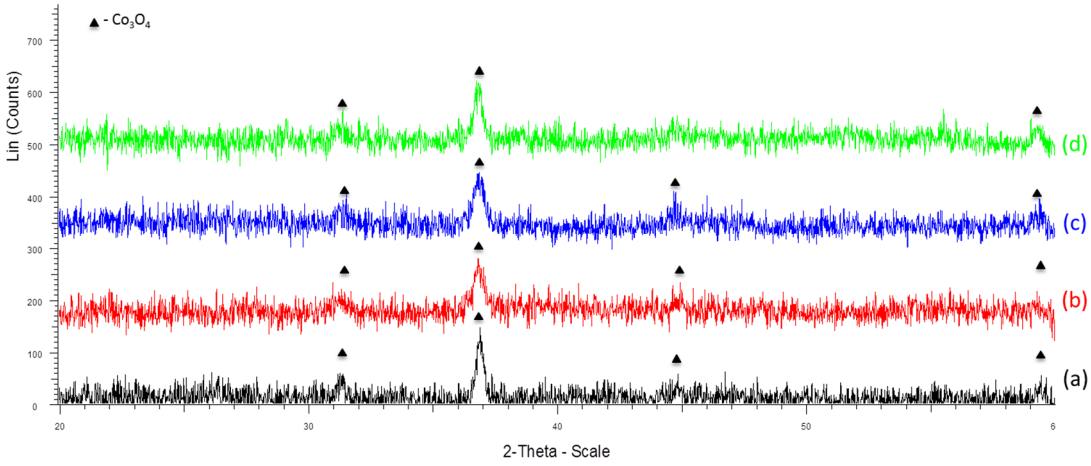

Figure 7.26 - pXRD patterns recorded for (a) 20wt%Co/SiO_2-500, (b) 20wt%Co/1wt%Mn/SiO_2-500, (c) 20wt%Co/1wt%Mo/SiO_2-500 and (d) 20wt%Co/1wt%Cr/SiO_2-500

7.8.3 Catalyst Testing

The prepared catalyst system were all tested for their hydrogenation ability in Reactor 1 (See Chapter 2 Section 2.2 for full details) reaction conditions were kept constant for all tests with all tests conducted at 300 °C under atmospheric pressure and a H_2:CO_2 ratio of 3:1 with a total flow of 8 sccm. Full details of the catalyst test procedure are outlined in Section 2.3, Chapter 2.

All of the transition metal promoted systems show a good catalyst stability over the entirety of time on stream. Little variation is observed both in terms of CO_2 conversion values and product selectivity. The results from these catalyst tests are summarised in Table 7.14.

The addition of 1 wt% chromium to the Co-SiO_2-500 system resulted in a slight reduction in CO_2 conversion. An increase in CO yield could be due either to an increased RWGS ability upon the inclusion of chromium or possibly an inhibition of the FT process. Little effect on CO_2 conversion is observed when both manganese and molybdenum are introduced to the Co-SiO_2-500 catalyst. Selectivity to CO also remains similar with no significant change in either CO or HC yield.

Little difference in CH_4 selectivity was observed for the Co-Cr-SiO_2-500 system relative to the non-promoted cobalt system with a high methane selectivity still observed. A more significant decrease in methane selectivity was, however, observed upon the addition of manganese and molybdenum. The introduction of 1 wt% molybdenum proved the most successful of the three transition metals trialled as it showed the largest drop in methane selectivity with no concurrent drop in CO_2 conversion.

Interestingly, despite the high selectivity towards methane, all of the transition metal promoted catalysts obey the ASF distribution with no anomalies suggesting that all hydrocarbons are being formed *via* the FT process albeit with a very low chain growth probability {between 0.01 (manganese promotion) and 0.06 (chromium promotion)}.

While there are some promotional effects observed upon the addition of the transition metals particularly with the addition of manganese and molybdenum these pale in comparison to those observed with the addition of alkali metals (Table 7.11). In order to ascertain if the promotional abilities of the alkali metals could be combined with the slight improvements observed with the molybdenum and manganese systems two dual promoted cobalt catalysts were prepared. These systems contained a combination of 1 wt% sodium (the best performing of the alkali metal promoters) with 1 wt% of each of the best performing transition metal promoters. Each system was prepared using the same wet impregnation method used earlier.

N_2 physisorption studies on each of the prepared catalyst showed there was little change in surface area upon the addition of sodium to give the Co-Na-Mn-SiO_2-500 catalyst system with a calculated surface area of 61.2 m^2g^{-1}. The addition of sodium to give the Co-Na-Mo-SiO_2-500 however resulted in a relatively large drop in surface area from 74.8 m^2g^{-1} to 56.6 m^2g^{-1}, one of the lowest surface areas calculated for the cobalt based catalyst tested within this chapter. XRD studies (Figure 7.27) show peaks characteristic of Co_3O_4 indicating this is the main cobalt phase present. No peaks attributable to any other metals are detected.

Table 7.14 – Catalytic data obtained for CO_2 hydrogenation tests using 20wt%Co/1wt%M/SiO_2-500 (where M = no metal Mo, Cr and Mn) and associated catalysts

Catalyst	Conv. (%)	HC Yield (%)	CO Yield (%)	Hydrocarbon Distribution										O/(O+P)[a] in C_2-C_4
				C_1	C_2=	C_2	C_3=	C_3	C_4	C_5	C_6	C_7	C_8	
20wt%Co/SiO_2-500	64.3	60.0	4.3	98.2	0.0	1.8	0.0	0.1	0.0	0.0	0.0	0.0	0.0	0
20wt%Co/1wt%Mo/SiO_2-500	64.8	60.7	4.2	94.7	0.0	5.0	0.0	0.3	0.0	0.0	0.0	0.0	0.0	0
20wt%Co/1wt%Cr/SiO_2-500	60.9	47.1	13.9	98.2	0.0	1.6	0.1	0.1	0.1	0.0	0.0	0.0	0.0	2.1
20wt%Co/1wt%Mn/SiO_2-500	62.0	57.7	4.3	97.9	0.0	2.0	0.0	0.1	0.0	0.0	0.0	0.0	0.0	0
20wt%Co/1wt%Na/1wt%Mn/SiO_2-500	42.7	34.3	8.4	72.4	0.8	13.1	4.4	4.9	3.5	0.9	0.0	0.0	0.0	20.5
20wt%Co/1wt%Na/1wt%Mo/SiO_2-500	43.9	37.0	6.9	45.5	1.7	15.8	11.1	6.4	9.1	4.9	3.1	1.9	0.4	33.0

[a] Olefin content (mol percentage) for C_2-C_4 hydrocarbons, calculated as [olefin(O) / (olefin(O) + paraffin(P)) × 100]. Catlyst tests conducted at atmospheric pressure, 300 ^oC H_2:CO_2 ratio 3:1, total flow – 8 sccm. 0.7g of catalyst. Conversions, yields and product distributions calculated as an after 5 hours on stream.

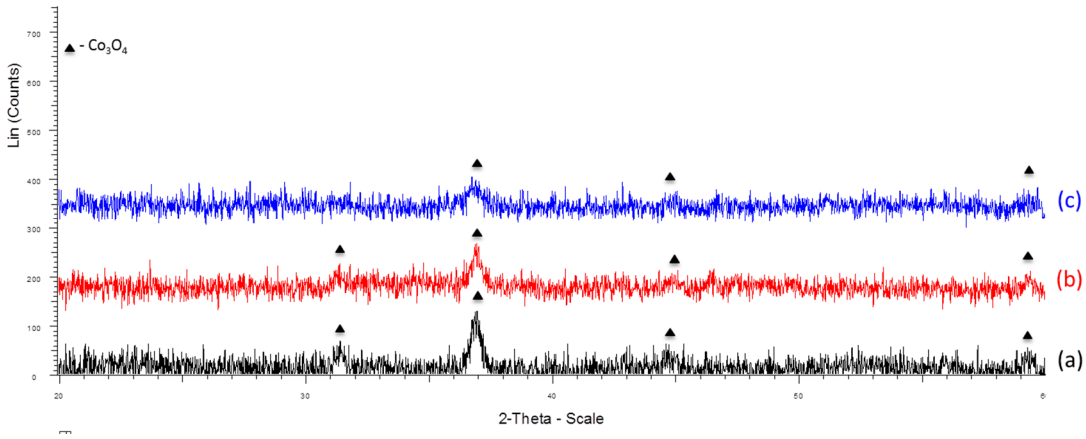

Figure 7.27 - pXRD patterns recorded for (a) 20wt%Co/1wt%Na/SiO_2-500, (b) 20wt%Co/1wt%Na/1wt%Mo/SiO_2-500Å and (c) 20wt%Co/1wt%Na/1wt%Mn/SiO_2-500Å.

Both of the dual alkali-transition metal promoted catalysts were tested for their CO_2 hydrogenation ability under the same reaction conditions as those detailed at the start of this chapter. Each shows a good catalyst stability over the course of the catalyst test with the little variation in CO_2 conversion values. Neither of the catalyst systems showed a stable HC distribution initially. Figure 7.28 shows how the hydrocarbon distribution varies with time on stream. Both systems see an initial drop in methane selectivity with a concurrent increase in the amount of C_2+ HCs produced. The manganese containing system stabilises after approximately 3 hours whereas the molybdenum system appears stable after 3-4 hours. With both systems stable after 5 hours conversion and selectivity values at this point were used to compare catalysts with the data obtained summarised in Table 7.14.

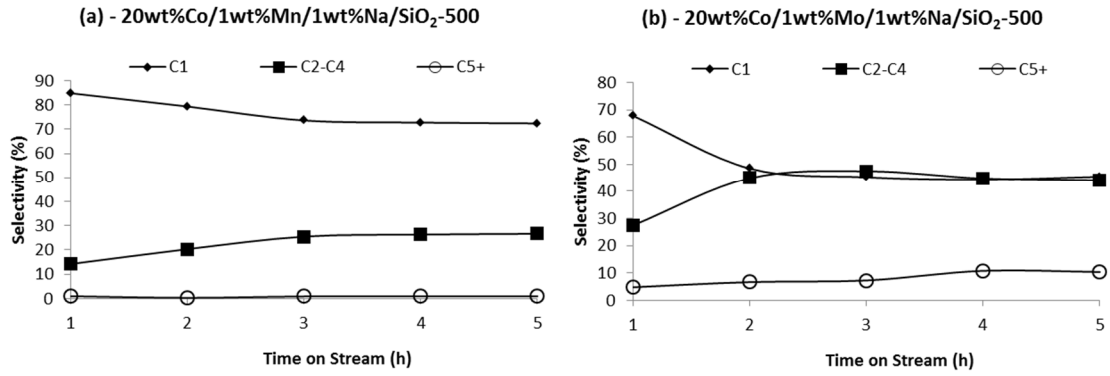

Figure 7.28 - Variation of HC distribution with time on stream as observed for (a) 20wt%Co/1wt%Mn/1wt%Na/SiO_2-500 and (b) 20wt%Co/1wt%Mo/1wt%Na/SiO_2-500

The combination of manganese and sodium as promoters for the Co-SiO_2-500 catalyst system resulted in CO_2 conversion values both lower than the non-promoted cobalt system and both individually promoted systems. The hydrocarbon selectivity recorded was found to be intermediate between the Co-Na-SiO_2-500 and Co-Mn-SiO_2-500 catalyst systems with a

methane selectivity lower than the manganese system but not as low as that observed for the sodium promoted system.

The dual promotion of the Co-SiO_2-500 catalyst with molybdenum and sodium proved far more successful. The system gave a much higher selectivity to C_5+ hydrocarbons similar to that observed for the Co-Pt-K-SiO_2 catalyst (Table 7.7), however, the conversion was found to be much higher. Methane selectivity was shown to be 45.5 % significantly lower than any previous catalyst and the lowest selectivity observed for any cobalt catalyst within this chapter thus far.

The ASF plots for both systems are shown in Figure 7.29 with the linear relationship observed clearly indicating that both obey the ASF distribution indicating that all HCs are being formed through the FT process. A slight deviation is again observed for C_2 HCs. As would be expected based on the HC distribution observed the Mo-Na system shows the higher of the two dual alkali-transition metal promoted cobalt system. An α of 0.41 is observed for the Co/Mo/Na/SiO_2-500 system, higher than the 0.35 observed for the Co/Na/SiO_2 catalyst.

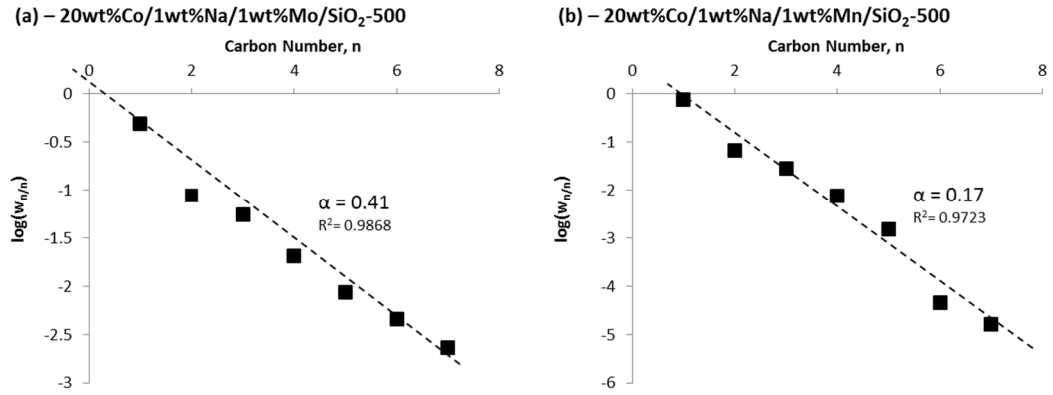

Figure 7.29 - ASF plots for (a) 20wt%Co/1wt%Na/1wt%Mo/SiO_2-500 and (b) 20wt%Co/1wt%Na/1wt%Mn/SiO_2-500

7.9 Further Investigations into the Co-Mo-Na-SiO_2 Catalyst

The novel 20wt%Co/1wt%Mo/1wt%Na/SiO_2-500 catalyst studied in the previous section shows a significant reduction in selectivity towards methane relative to any catalyst previously studied while also showing an impressive selectivity to heavier C_5+ hydrocarbons. While a reduction in CO_2 conversion and HC yield is observed upon the introduction of sodium to this system this is more than out-weighed by the improved selectivity with the conversion value still comparing favourably with the majority of iron catalysts studied for CO_2 hydrogenation[2] and previous cobalt systems that have shown lower than average (~75 %) methane selectivities.[6] For these reasons it was decided to investigate the system further in order to both gain a deeper understanding of promoter effects while also studying if performance can be further improved.

7.9.1 Further Catalyst Characterisation

In order to determine the oxidation state and phase of all metals present a sample of the 20wt%Co/1wt%Mo/1w%Na/SiO_2-500 was studied using XPS techniques. The spectra obtained from these studies are shown in Figure 7.30. The survey spectrum indicates the presence of silicon (103.0 eV) and oxygen (531 eV) the remainder of detected elements were scanned in more detail with a smaller step and longer time per step. The detailed scan of the Co 2p region is shown in Figure 7.30 (b). A Co $2p_{3/2}$ peak at a binding energy of 779.3 eV is characteristic of Co_3O_4,[16] this was further confirmed by XRD studies. Sodium is present within the catalyst system as Na^+, most likely in its Na_2O form as indicated by the presence of a Na 1s peak at 1071.6 eV. Molybdenum is detected in the MoO_3 oxide form with Mo $3d_{x/y}$ and Mo $3d_{x/y}$ peaks detected at 231.9 eV and 235.0 eV which are in good agreement with literature values of molybdenum in this oxidation state.[45] The crystallite size of the cobalt species was calculated from the Co_3O_4 (311) peak using the Sherrer equation. A crystallite size of 12 nm was calculated equal to that calculated for the Co-Na-SiO_2-500 system with the presence of molybdenum having little effect.

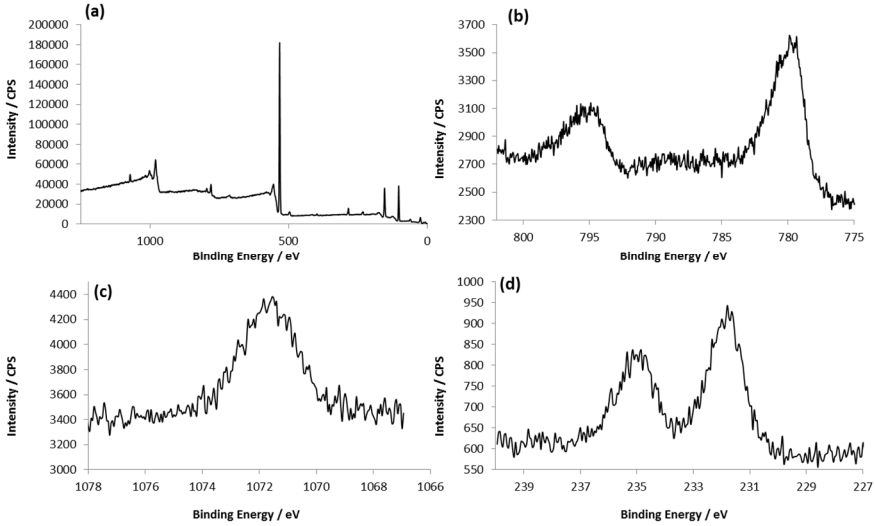

Figure 7.30 – XPS spectra recorded for 20wt%Co/1wt%Mo/1wt%Na/SiO_2-500. (a) Survey spectrum, (b) Detailed scan of Co 2p region, (c) Detailed scan of Na 1s region and (d) Detailed scan of Mo 3d region.

7.9.2 Gaining a Better Understanding of Promoter Effects

Initial tests into catalyst performance covered a 5 hour period under reaction conditions, in order to determine if the catalyst stability continued beyond this point an extended catalyst test was conducted. Under previous test conditions the catalyst required between 3 and 4 hours to stabilise, a common phenomenon,[41] this could be to a number of possible reasons. One of the most likely is the incomplete reduction of the Co_3O_4 to the FT active metallic cobalt phase during the catalyst pre-treatment. Several hours under the reductive reaction conditions may

then complete this reduction stage, which results in stabilisation of hydrocarbon distribution. This possible lack of full reduction may be due to the 2 hour reduction used not being sufficiently long and as such this pre-treatment step was extended to 15 hours with the rest of the catalyst testing conditions remaining constant. The results from this catalyst test are summarised in Figure 7.31.

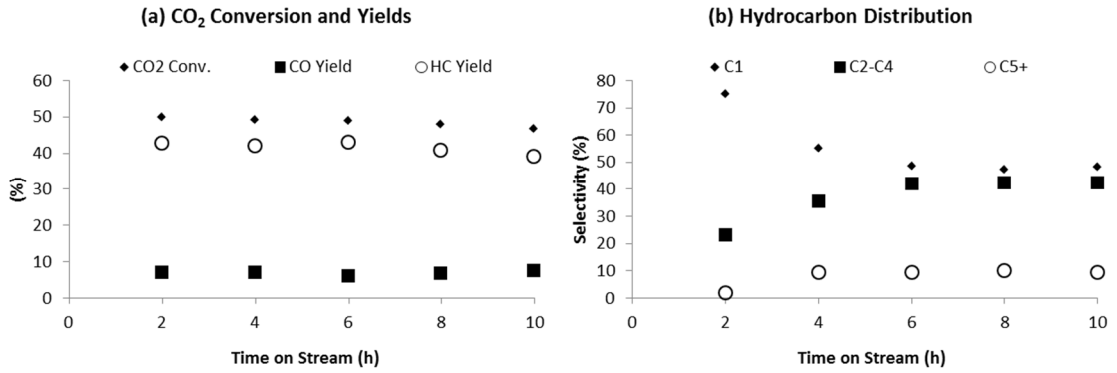

Figure 7.31 – Plots showing (a) how CO_2 conversion and yields vary with time on stream and (b) how hydrocarbon distribution varies with time on stream

Conversion was observed to remain relatively stable throughout the 10 hours on stream. The CO_2 conversion is higher than that observed for the previous, shorter test (49 % *vs*. 44 %) due to the extended pre-treatment stage. This suggests that the reduction of Co_3O_4 may indeed be incomplete with the longer reductive treatment allowing further reduction of any cobalt oxide species which has resulted in a higher CO_2 conversion and HC yield. The HC distribution takes 4-6 hours to stabilise indicating this is not related to the incomplete reduction of the cobalt oxide phase. Once HC distribution has stabilised little change is observed relative to the previous catalyst test with methane selectivity remaining at approximately 45% for both systems further indicating the increased reduction has little effect on HC selectivity.

7.9.2.1 Variation of sodium loading in the Co-Mo-Na-SiO_2 catalyst

While the addition of sodium to the Co-Mo-SiO_2-500 catalyst system resulted in significant improvements in terms of hydrocarbon selectivity no studies have thus far been conducted on catalysts containing any loadings other than 1 wt%. In order to determine if the promotional effects observed previously could be increased by utilising higher sodium loadings a range of catalyst systems containing 1, 2, 3, 4 and 5 wt% sodium were prepared. Each catalyst was prepared using the same wet impregnation technique used in Section 7.8 with only the relative amount of sodium acetate altered.

XRD studies conducted on the prepared catalysts (Figure 7.32) showed that increasing sodium content had little influence on the cobalt phase present with peaks observed at 2θ values of 31, 37, 45 and 59 ^{o} for all systems indicating the presence of Co_3O_4 as the main cobalt

phase.[17] No peaks attributable to any other species were observed even at high sodium loadings.

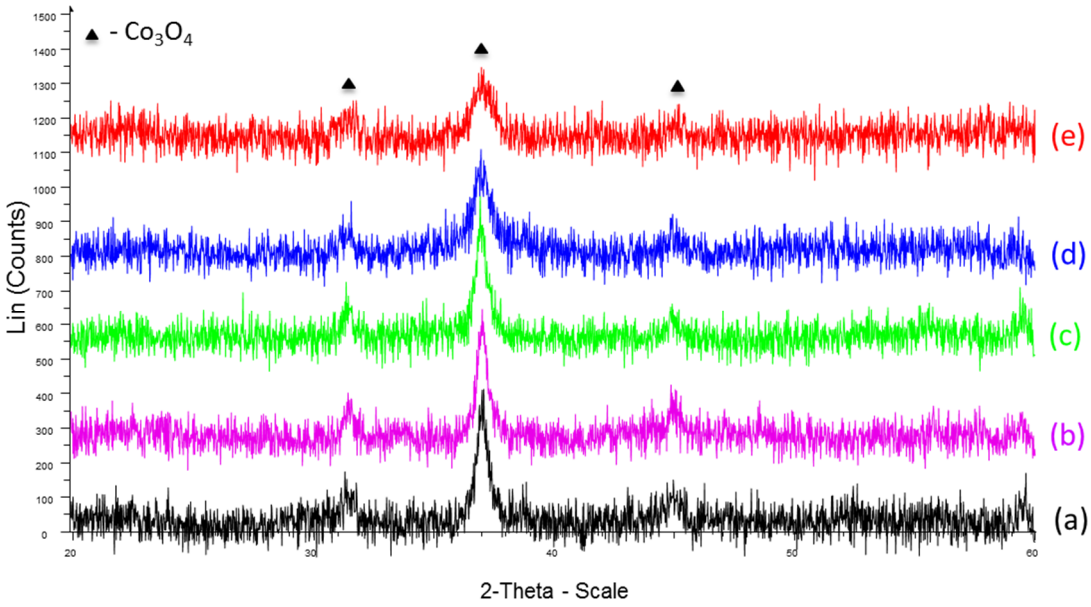

Figure 7.32 – XRD patterns for 20wt%Co/1wt%Mo/Xwt%Na/SiO_2-500 where X is (a) 1, (b) 2, (c) 3, (d) 4 and (e) 5.

Each of the prepared catalysts were tested under the standard reaction conditions (300 ^oC, 1 atm, 3:1 H_2:CO_2, 8 sccm total flow), the results are summarised in Table 7.15. For comparison the results shown were recorded at a time on stream where the lowest selectivity to methane was obtained. For the catalysts containing 1 and 2 wt% sodium this was after 5 hours on stream with both catalysts showing relativity good CO_2 conversion stability while HC distribution was optimum after stabilisation which took 3-4 hours on stream, as shown in Figure 7.33. When the sodium loading was increased beyond this point the catalyst stability was lost with CO_2 conversion values steadily decreasing with time on stream. For these systems HC distribution was at its optimum after 1 hour on stream with increasing time on stream generally leading to an increase in methane selectivity (Figure 7.33). As a result catalysts containing 3 wt% sodium and above the results shown in Table 7.15 were calculated after only 1 hour on stream.

When compared at optimum HC distribution no significant variation in CO_2 conversion is observed between the catalyst systems containing 1 and 2 wt% sodium, for loadings above this a slight decrease in CO_2 conversion is observed until a 5 wt% loading where a more dramatic drop is observed. This large drop observed with the 5 wt% sodium system could be due to a more rapid deactivation over the initial hour on stream before the first sample is taken.

The hydrocarbon distribution is also affected by the sodium content of the catalyst with an increasing sodium loading initially leading to a decreasing methane selectivity with the 3 wt% sodium system showing a methane selectivity as low as 32 %. When sodium content is increased beyond this methane selectivity again begins to rise.

Table 7.15 – Catalytic data obtained for CO_2 hydrogenation tests using 20wt%Co/Xwt%Na/1wt%Mo/SiO_2-500 (where X = 1, 2, 3, 4 and 5 wt%)

Catalyst	Conv. (%)	HC Yield (%)	CO Yield (%)	Hydrocarbon Distribution										O/(O+P)[a] in C_2-C_4
				C_1	C_2=	C_2	C_3=	C_3	C_4	C_5	C_6	C_7	C_8	
20wt%Co/1wt%Na/1wt%Mo/SiO_2-500	43.9	37.0	6.9	45.5	1.7	15.8	11.1	6.4	9.1	4.9	3.1	1.9	0.4	33.0
20wt%Co/2wt%Na/1wt%Mo/SiO_2-500	44.1	35.5	8.6	40.0	2.1	12.5	12.1	5.0	9.8	13.1	3.4	1.7	0.2	42.9
20wt%Co/3wt%Na/1wt%Mo/SiO_2-500	43.1	35.3	7.8	32.9	2.6	11.5	14.8	4.7	12.4	10.1	7.3	3.4	0.3	48.9
20wt%Co/4wt%Na/1wt%Mo/SiO_2-500	40.9	31.4	9.5	50.3	2.4	11.0	13.2	4.8	7.9	3.6	1.9	0.6	0.0	47.8
20wt%Co/5wt%Na/1wt%Mo/SiO_2-500	21.9	13.1	8.8	59.6	5.7	8.4	12.9	3.2	6.9	3.3	0.1	0.0	0.0	53.6

[a] Olefin content (mol percentage) for C_2-C_4 hydrocarbons, calculated as [olefin(O) / (olefin(O) + paraffin(P)) × 100]. Catlyst tests conducted at atmospheric pressure, 300 ^oC H_2:CO_2 ratio 3:1, total flow – 8 sccm. 0.7g of catalyst. Conversions, yields and product distributions calculated as an after 5 hours on stream for catalysts containing 1 and 2 wt% Na and after 1 hour on stream for catalysts containing 3, 4 and 5 wt% Na.

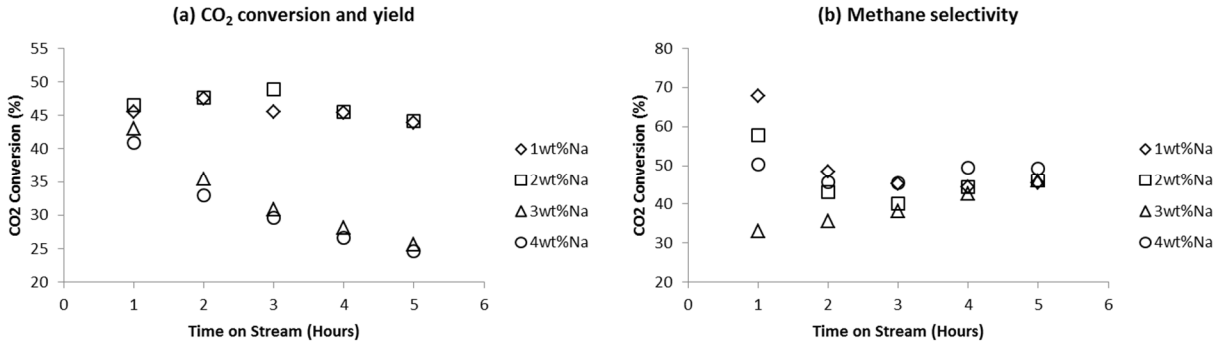

Figure 7.33 - Plots showing (a) how CO_2 conversion varies with time on stream and (b) how methane selectivity varies with time on stream

Although the catalyst containing 3 wt% initially looks promising with an exceptionally low methane selectivity the rapid deactivation observed (see Figure 7.33) means the system is not useful for any significant length of time. If the deactivation of the catalyst system is assumed to proceed exponentially where $r = r_0\, e^{-kt}$ (where r_0 is the initial rate and r is the rate at time t) then a plot of $ln(r/r_0)$ *vs. t* should give a straight line from which the rate constant, k_d for deactivation can be obtained. Figure 7.34 shows a plot of apparent deactivation rate for the catalysts containing 1, 2, 3, 4 and 5 wt% sodium with the calculated k_d values tabulated.

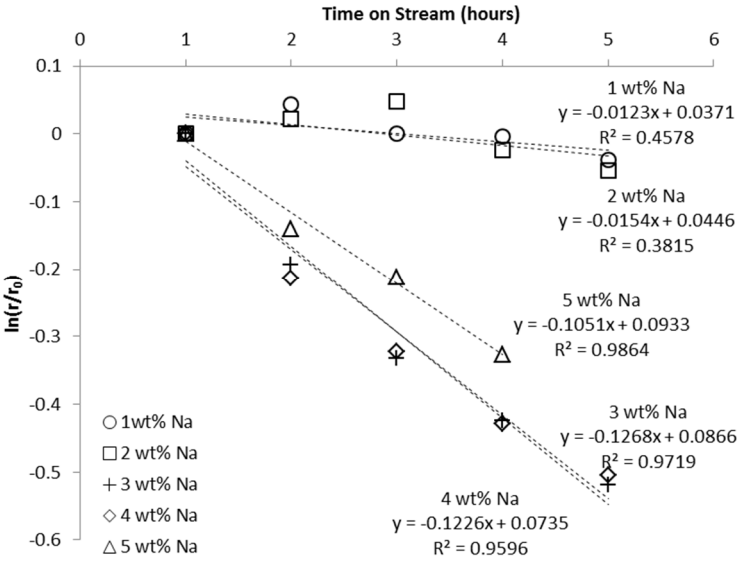

Sodium Loading (wt%)	k_d (h^{-1})
1	0.0123
2	0.0154
3	0.1268
4	0.1226
5	0.1051

Figure 7.34 – Apparent deactivation rates of catalysts containing 1, 2, 3, 4 and 5 wt% sodium calculated by assuming that $r = r_0\, e^{-kt}$.

The apparent stability of the catalysts containing 1 and 2 wt% sodium is further confirmed by the low k_d values calculated, they do however suggest a possible slow deactivation of these two catalysts with the system containing a higher sodium content deactivating at a slightly higher rate. A large jump in k_d values is observed as sodium content is increased to 3, 4 and 5 wt% with the apparent rate of deactivation increasing ten-fold. This indicates that at sodium loading larger than 2 wt% deactivation is rapid.

The deactivation of heterogeneous catalysts is generally caused *via* one or more of three main mechanisms; (1) the deposition of carbon on the catalyst surface, blocking active sites (2) the oxidation of active phases (3) surface reconstruction where a change in catalyst morphology such as sintering causes catalyst deactivation.

Previous studies have shown that the addition of alkali metals can increase the rate of carbon deposition on the catalyst surfaces[46] and since the rate of deactivation is increasing with higher sodium loadings this suggested that this may be the likely cause. In order to determine if any carbon was being deposited and coating the active phases Raman spectroscopy was conducted on catalysts before and after use. For these studies the catalysts containing the lowest

(1 wt%) and highest (5 wt%) loadings of sodium were chosen. The obtained spectra are shown in Figure 7.35.

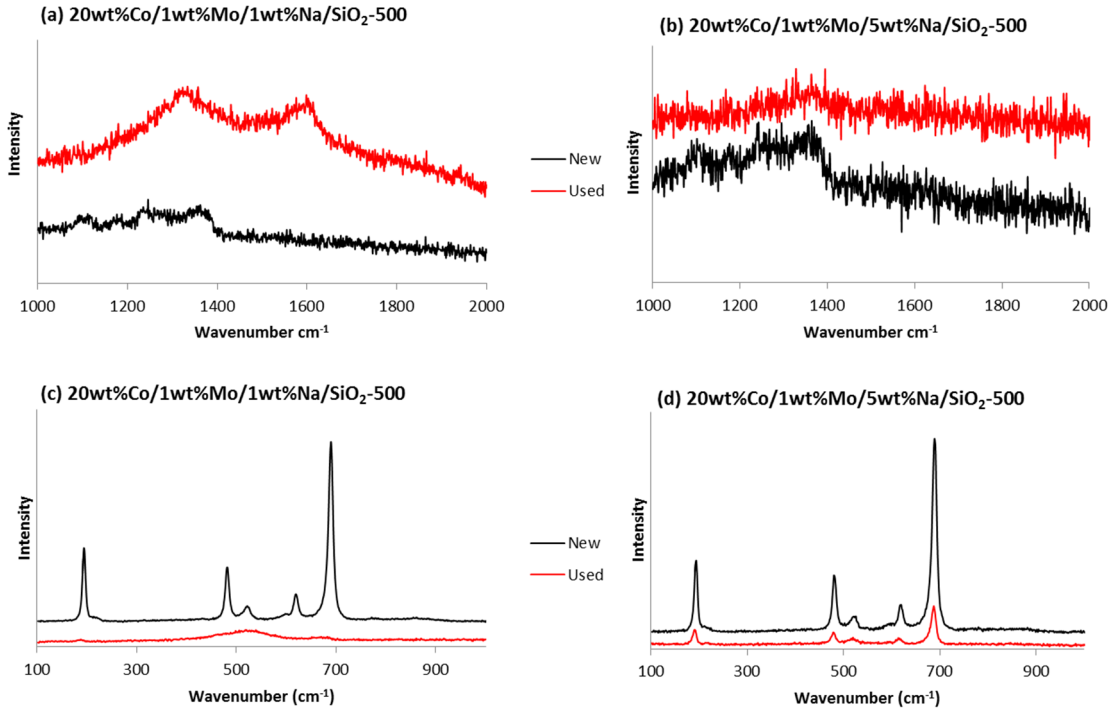

Figure 7.35 – Raman spectra studies on new and used catalysts for (a) carbon region of 20wt%Co/1wt%Mo/1wt%Na/SiO_2-500, (b) carbon region of 20wt%Co/1wt%Mo/5wt%Na/SiO_2-500, (c) cobalt region of 20wt%Co/1wt%Mo/1wt%Na/SiO_2-500 and (d) cobalt region of 20wt%Co/1wt%Mo/5wt%Na/SiO_2-500

The 1 wt% sodium system, as expected, showed no signs of any carbon species present after calcination. When the used catalyst system was tested however peaks of a low intensity were observed at 1327 cm^{-1} and 1600 cm^{-1}. These values are in good agreement with what has been observed in literature for carbon deposition.[47] The peak at 1327 cm^{-1} can be attributed to ordered (graphite) carbon and that observed at 1600 cm^{-1} distorted carbon species. These peaks are of a low intensity, however, and appear to have little effect on CO_2 conversion values. It is possible that this is accountable for the slight reduction in catalyst activity observed.

The Raman spectra for the carbon region show little difference before and after catalyst use with the 5 wt% sodium catalyst system with no peaks attributable to the presence of carbon observed for each system. This indicates that the deposition of carbon on the catalyst surface is not responsible for the large decrease in catalytic activity observed for systems with higher sodium contents.

The use of Raman spectroscopy can also reveal details about the cobalt phase present for each system and as such this region of the spectra was also investigated {Figure 7.35 (c) and (d)}. Before use the catalyst containing 1 wt% sodium shows major peaks at 194.3, 482.4, 522.1, 618.7 and 689.9 cm^{-1} characteristic for Co_3O_4[48] as suggested by both XRD and XPS studies. After the reductive pre-treatment and 5 hours under reaction conditions only broad

peaks at *ca*. 520 cm^{-1} and 690 cm^{-1} are observed indicating that the majority of Co_3O_4 has been successfully reduced to the FT active metallic phase which is not Raman active. The broad peaks present can likely be attributed to the silica support.

The Co_3O_4 spectrum observed for the 5 wt% sodium system indicates that this is also the main phase present before use, as expected. After the reductive pre-treatment and 5 hours under reaction conditions peaks attributable to either Co_3O_4 or CoO are observed with the resolution of the spectrometer not high enough to distinguish between the two. After use the system is no longer XRD active suggesting a phase change has occurred at some point and meaning the determination of which oxidation state is present is not possible. The presence of cobalt oxide after reaction suggests that oxidation of the active metallic cobalt phase may be occurring under reaction conditions which could be leading to rapid catalyst deactivation observed for the systems containing higher sodium content.

If the catalyst deactivation is occurring *via* the oxidation of the cobalt phase then a simple reduction treatment after used should result in reactivation of the catalyst. In order to test this theory the catalyst containing 3 wt% sodium was chosen. The variation of CO_2 conversion, HC yield and product distribution is shown in Figure 7.36.

Hour 1 to 5 shows the initial catalyst test as reported in Table 7.15 and Figure 7.33 and shows a relatively rapid deactivation with a concurrent loss in selectivity towards heavier hydrocarbons. After this period under reaction conditions CO_2 flow was stopped and the H_2 flow increased to 50 sccm for 2 hours. With the reductive pre-treatment completed CO_2 was reintroduced at 2 sccm and H_2 flow reduced to 6 sccm. A sample was taken after an hour under these conditions and then every hour until the catalyst had been on stream for a further 4 hours.

After this reductive regeneration the catalyst activity appears restored with CO_2 conversion and HC yield restored to higher than their initial values. This suggests that the oxidation of the active species may very well be responsible for the deactivation behaviour observed. The fact CO_2 conversion values are higher after a second reductive treatment indicates that for the initial run there may be incomplete reduction of the Co_3O_4 phase. A theory further supported by the increased conversion observed when a longer, 15 hour pre-treatment was employed for the 20wt%Co/1wt%Mo/1wt%Na/SiO_2-500 (Figure 7.31).

Despite the regained CO_2 conversion observed the selectivity to heavier hydrocarbons is not restored to initial levels and instead appears to only stabilise. This suggests the possibility of another deactivation mechanism possibly contributing to the changing HC distribution. In order to determine if the deposition of carbon could be accountable for this the catalyst system was subjected to a second regeneration procedure. This time the catalyst was first subjected to an *ex situ* calcination at 450 ^oC for in static air for 5 hours which should burn off any possible carbon depositions. The catalyst was then reloaded into the reactor and reduced again at 300 ^oC for 2 hours before again being subjected to reaction conditions.

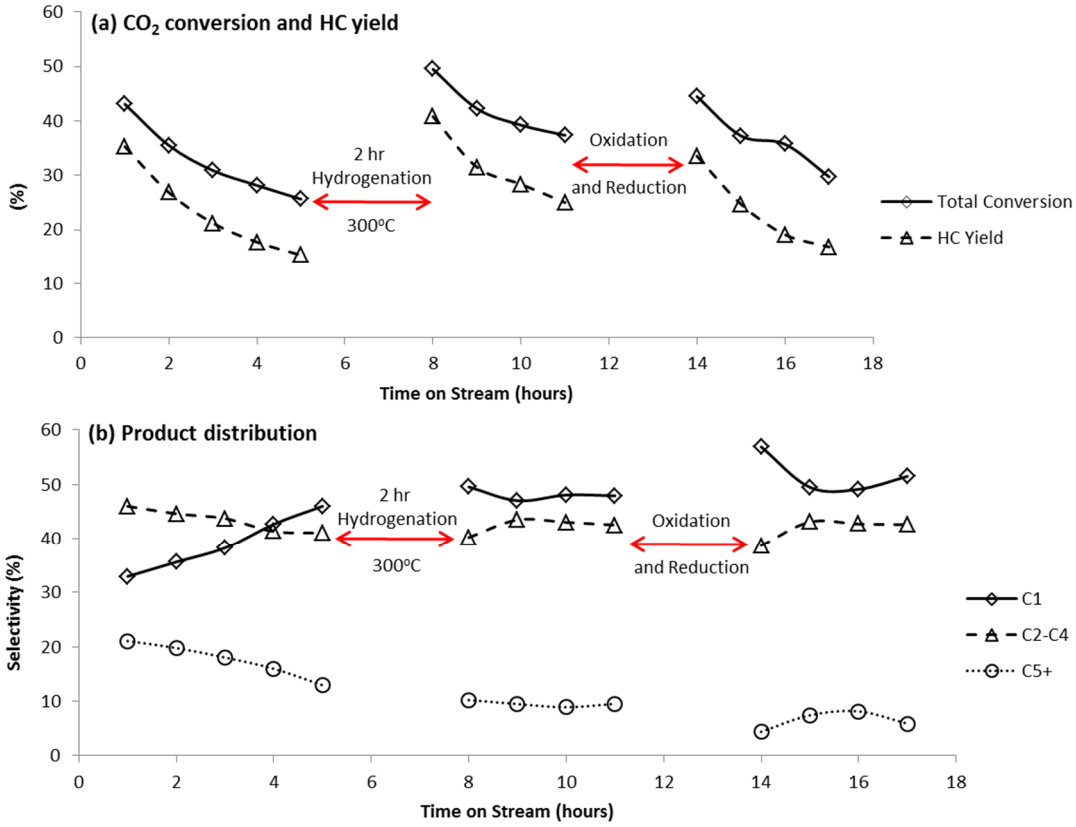

Figure 7.36 – (a) Plot showing the variation of CO_2 conversion and HC yield with time on stream and the effects of regeneration treatments. (b) Plot showing the effects of time on stream and regeneration treatments on the hydrocarbon distribution over a 20wt%Co/1wt%Mo/3wt%Na/SiO_2-500 catalyst

After the oxidative-reductive regeneration the CO_2 conversion ability of the catalyst was again restored although this could simply be due to the reductive part of the regeneration and not related to the oxidation step. HC distribution showed no improvement further indicating that it is unlikely that carbon deposition is responsible for any of the activity/selectivity changes observed. It is possible that the changing HC distribution observed could be due to an irreversible process such as sintering. Unfortunately, there was no method available to assess the particle size after reaction as the system is no longer XRD active and no nano-particles were clearly observed by TEM either before or after reaction.

7.9.2.2 Variation of molybdenum loading in the Co-Mo-Na-SiO_2 catalyst

With the studies into varying sodium content revealing some possibly interesting effects the study on catalyst optimisation was extended to include the variation of molybdenum loading. In order to determine if the promotional effects observed previously could be increased by utilising higher loadings of molybdenum a range of catalyst systems containing 1, 2, 3, 4 and 5 wt% molybdenum were prepared. Each catalyst was prepared using the same wet impregnation technique used in Section 7.8 with only the relative amount of molybdenum altered.

Each of the catalysts was analysed by XRD with the resulting diffraction patterns shown in Figure 7.37. Peaks at 2θ values of 31, 37, 45 and 59 ^{o} confirm cobalt is mainly present as Co_3O_4 in all catalyst systems. As the molybdenum content is increased a peak at a 2θ value of

approximately 26 ^{o} emerges. This value is in good agreement with literature values reported for the most intense peak observed for the mixed oxide β-$CoMoO_4$.[49]

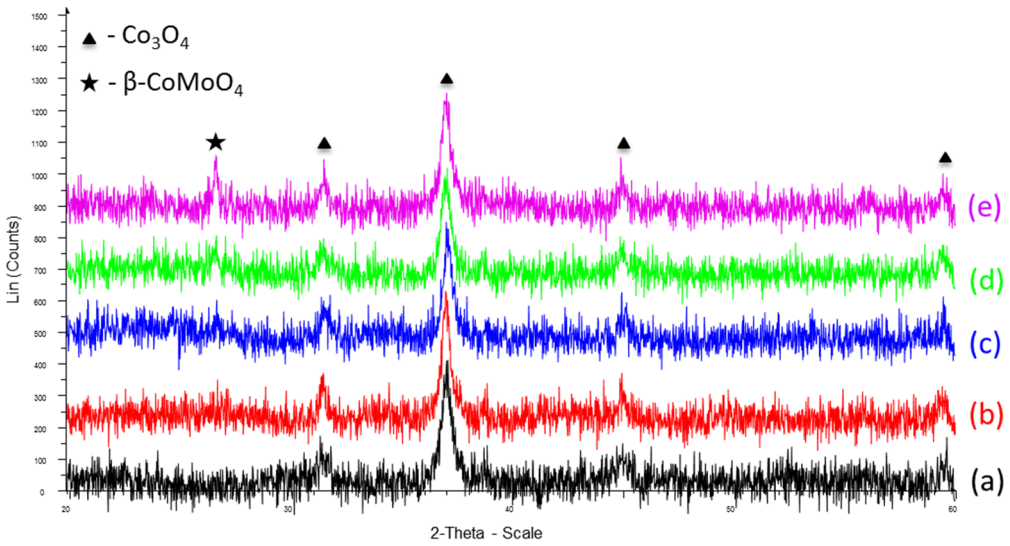

Figure 7.37 - XRD patterns for 20wt%Co/Xwt%Mo/1wt%Na/SiO_2-500 where X is (a) 1, (b) 2, (c) 3, (d) 4 and (e) 5.

In order to determine the effect of increasing molybdenum each of the prepared catalysts were tested for their CO_2 hydrogenation ability under standard reaction conditions (0.7 g catalyst, 1 atm, 300 ^{o}C, 3:1 H_2:CO_2, 8 sccm total flow).

Each of the catalyst systems showed good catalyst stability after an initial period (2-3 hours) of stabilisation. After this CO_2 conversion, HC yield and product distribution remains relatively constant. With all systems showing no significant deviations after the initial period of stabilisation catalysts were compared after 5 hours under reaction conditions. The result obtained are summarised in Table 7.16.

Table 7.16 – Catalytic data obtained for CO_2 hydrogenation tests using 20wt%Co/1wt%Na/Xwt%Mo/SiO_2-500 (where X = 1, 2, 3, 4 and 5 wt%)

Catalyst	Conv. (%)	HC Yield (%)	CO Yield (%)	Hydrocarbon Distribution										O/(O+P)[a] in C_2-C_4
				C_1	C_2=	C_2	C_3=	C_3	C_4	C_5	C_6	C_7	C_8	
20wt%Co/1wt%Na/1wt%Mo/SiO_2-500	43.9	6.9	37.0	45.5	1.7	15.8	11.1	6.4	9.1	4.9	3.1	1.9	0.4	33.0
20wt%Co/1wt%Na/2wt%Mo/SiO_2-500	42.5	6.7	35.7	39.8	2.6	14.0	13.1	4.2	10.1	7.1	5.0	3.4	0.8	41.6
20wt%Co/1wt%Na/3wt%Mo/SiO_2-500	56.6	6.7	49.9	37.5	0.9	14.8	9.6	9.2	11.2	7.0	5.4	3.6	0.8	28.0
20wt%Co/1wt%Na/4wt%Mo/SiO_2-500	51.6	6.8	44.7	46.5	0.8	16.5	6.6	9.1	8.6	5.8	4.0	1.6	0.5	21.0
20wt%Co/1wt%Na/5wt%Mo/SiO_2-500	35.3	8.8	26.5	57.2	1.1	14.4	7.6	6.4	6.6	3.7	2.8	0.2	0.0	30.0

[a] Olefin content (mol percentage) for C_2-C_4 hydrocarbons, calculated as [olefin(O) / (olefin(O) + paraffin(P)) × 100]. Catlyst tests conducted at atmospheric pressure, 300 ^oC H_2:CO_2 ratio 3:1, total flow – 8 sccm. 0.7g of catalyst. Conversions, yields and product distributions calculated as an after 5 hours on stream.

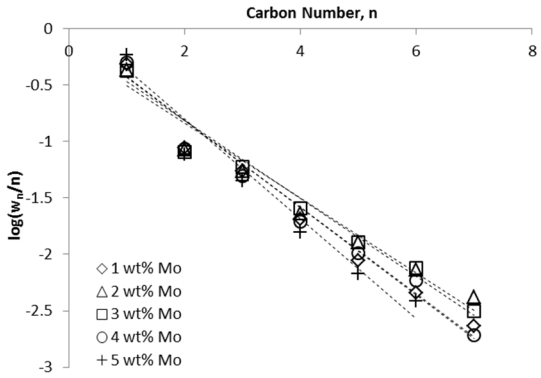

Molybdenum Loading (wt%)	Chain Growth Probability, α
1	0.41
2	0.47
3	0.45
4	0.41
5	0.36

Figure 7.38 – ASF plots for the catalysts containing various molybdenum loadings. Chain growth probabilities are tabulated

Generally as molybdenum loading is increased the CO_2 conversion is observed to increase with the 3 wt% molybdenum showing a CO_2 conversion of 57 % significantly higher than the 44 % observed for the 1 wt% molybdenum system. When the molybdenum content is increased beyond this point CO_2 conversion begins to decrease again. This decrease could be due to the formation of the mixed cobalt molybdenum oxide; $CoMoO_4$ as evidenced by XRD. No peak attributable to $CoMoO_4$ is observed for molybdenum contents below 4 wt%. The activity of $CoMoO_4$ for this reaction is not known however its formation could explain the variation in CO_2 conversion values observed.

As the content of molybdenum is increased form 1 wt% to 3 wt% the selectivity towards C_2+ HCs is also reduced with the 3 wt% molybdenum system showing a methane selectivity of only 38 %. When molybdenum content is increased further methane selectivity begins to increase again concurrent with the decreasing CO_2 conversion, again possibly due to the formation of $CoMoO_4$.

The ASF plots for each of the five catalyst systems are shown in Figure 7.38. Each system follows the trend predicted by ASF indicating that all hydrocarbons are being formed by the FT process. The double alpha phenomenon observed for cobalt systems studied earlier is not apparent suggesting all methane is being formed *via* the FT process and not by a parallel route. An anomaly is observed for C_2 HCs, this is however common for HCs produced by FT[36] and provides further evidence that their formation is occurring *via* the CO mediated route.

7.10 Chapter Conclusions

Work reported within this chapter has shown that with careful consideration of the support properties along with choice of appropriate promoters and loadings an affective cobalt-based catalyst can be developed for CO_2 hydrogenation showing a high CO_2 conversion value as well as good selectivity towards heavier hydrocarbons.

The pore size of the silica support utilised plays an important role in product selectivity. Higher pore sizes are observed to result in larger Co_3O_4 crystallite sizes which in turn gives a decreased selectivity towards methane and an increased chain growth probability. The addition of alkali metals had a negative effect on the CO_2 conversion values this is however counteracted by a significant increase in selectivity towards C_2+ hydrocarbons. Of the alkali metals tested sodium proves the most effective.

While the addition of a noble metal in conjunction with alkali metals can have a negative effect on catalyst performance the nature of the metal used can drastically alter the catalyst performance in terms of product selectivity and conversion. Ruthenium addition appears to give the highest CO_2 conversion whereas platinum addition results in the highest selectivity to heavier hydrocarbons.

A range of transition metal promoters were also investigated (Mn, Cr and Mo) and while when used alone their impact on performance was limited the combination of molybdenum with sodium (20wt%Co/1wt%Mo/1wt%Na/SiO_2-500) resulted in a particularly

effective Co-based catalyst. CO_2 conversion values of *ca.* 49 % were observed with a methane selectivity of 45 %, significantly lower than any previously reported Co-based systems. The catalyst appears relatively stable on stream with no significant deactivation observed over a 10 hour catalyst test.

The sodium and molybdenum content of this catalyst can significantly alter its performance. Increasing the sodium content can decrease methane selectivity to as low as 32 %, this sodium loading does however result in an increased rate of catalyst deactivation. An increased molybdenum loading was found to reduce methane selectivity to 38 % while also increasing CO_2 conversion to 57 % with no apparent negative effect on the catalyst stability. If molybdenum loading is increased beyond this point no further improvements in performance are observed possibly due to the formation of mixed Co-Mo oxides.

7.11 Future Work

This chapter has reported the development of an effective cobalt catalyst for CO_2 hydrogenation giving a relatively high conversion and good selectivity towards C_2+ hydrocarbons. As such this system warrants further investigation in order to determine if catalyst performance can be improved further.

The properties of the silica support showed a significant influence on the C_2+ selectivity and as such other metal oxide supports such as Al_2O_3 should be investigated with a particular focus on the effects of the porous nature of the Al_2O_3 used. Alternatively a range of metal oxides that have been shown to be effective supports for FT based cobalt catalyst such as TiO_2 and ZrO_2 could be investigated both as potential replacements for the silica or used in conjunction with the SiO_2-500 support in a manner similar to that investigated with the mixed SiO_2-MgO support investigated in Chapter 3.

7.12 References

[1] R. W. Dorner, D. R. Hardy, F. W. Williams, H. D. Willauer, *Energy Environ. Sci.* **2010**, *3*, 884-890.

[2] P. S. Sai Prasad, J. W. Bae, K. W. Jun, K. W. Lee, *Catal. Surv. Asia* **2008**, *12*, 170-183.

[3] A. Y. Khodakov, W. Chu, P. Fongarland, *Chem. Rev.* **2007**, *107*, 1692-1744.

[4] (a) C. G. Visconti, L. Lietti, E. Tronconi, P. Forzatti, R. Zennaro, E. Finocchio, *Appl. Catal., A* **2009**, *355*, 61-68; (b) M. K. Gnanamani, W. D. Shafer, D. E. Sparks, B. H. Davis, *Catal. Commun.* **2011**, *12*, 936-939.

[5] T. Riedel, G. Schaub, *Top. Catal.* **2003**, *26*, 145-156.

[6] Y. Zhang, G. Jacobs, D. E. Sparks, M. E. Dry, B. H. Davis, *Catal. Today* **2002**, *71*, 411-418.

[7] R. W. Dorner, D. R. Hardy, F. W. Williams, B. H. Davis, H. D. Willauer, *Energy Fuels* **2009**, *23*, 4190-4195.

[8] (a) S. Alayoglu, S. Beaumont, F. Zheng, V. Pushkarev, H. Zheng, V. Iablokov, Z. Liu, J. Guo, N. Kruse, G. Somorjai, *Top. Catal.* **2011**, *54*, 778-785; (b) V.

Iablokov, S. K. Beaumont, S. Alayoglu, V. V. Pushkarev, C. Specht, J. Gao, A. P. Alivisatos, N. Kruse, G. A. Somorjai, *Nano Lett.* **2012**, *12*, 3091-3096.
[9] T. Riedel, G. Schaub, K. W. Jun, K. W. Lee, *Ind. Eng. Chem. Res.* **2001**, *40*, 1355-1363.
[10] D. J. Pettigrew, D. L. Trimm, N. W. Cant, *Catal. Lett.* **1994**, *28*, 313-319.
[11] (a) H. Arakawa, A. Bell, *Ind. Eng. Chem. Process Des. Dev.;(United States)* **1983**, *22*; (b) W. Ngantsoue-Hoc, Y. Zhang, R. J. O'Brien, M. Luo, B. H. Davis, *Appl. Catal., A* **2002**, *236*, 77-89.
[12] (a) L. Xu, Q. Wang, D. Liang, X. Wang, L. Lin, W. Cui, Y. Xu, *Appl. Catal., A* **1998**, *173*, 19-25; (b) S. Krishnamoorthy, A. Li, E. Iglesia, *Catal. Lett.* **2002**, *80*, 77-86; (c) T. Riedel, G. Schaub, K. W. Jun, K. W. Lee, *Ind. Eng. Chem. Res* **2001**, *40*, 1355-1363.
[13] (a) J. Gaube, H. F. Klein, *Appl. Catal., A* **2008**, *350*, 126-132; (b) Ø. Borg, N. Hammer, B. C. Enger, R. Myrstad, O. A. Lindvåg, S. Eri, T. H. Skagseth, E. Rytter, *J. Catal.* **2011**, *279*, 163-173.
[14] L. Wang, H. Liu, Y. Chen, R. Zhang, S. Yang, *Chem. Lett.* **2013**, *42*, 682-683.
[15] M. D. Jones, C. G. Keir, C. D. Iulio, R. A. M. Robertson, C. V. Williams, D. C. Apperley, *Catal. Sci. Technol.* **2011**, *1*, 267-272.
[16] J. Yan, T. Wei, W. Qiao, B. Shao, Q. Zhao, L. Zhang, Z. Fan, *Electrochim. Acta* **2010**, *55*, 6973-6978.
[17] Y. Z. Wang, Y. X. Zhao, C. G. Gao, D. S. Liu, *Catal. Lett.* **2008**, *125*, 134-138.
[18] M. Peuckert, *J. Phys. Chem.* **1985**, *89*, 2481-2486.
[19] C. M. Masuku, D. Hildebrandt, D. Glasser, *Chem. Eng. Sci.* **2011**, *66*, 6254-6263.
[20] A. H. Lillebø, E. Patanou, J. Yang, E. A. Blekkan, A. Holmen, *Catal. Today* **2013**, *215*, 60-66.
[21] I. T. Ghampson, C. Newman, L. Kong, E. Pier, K. D. Hurley, R. A. Pollock, B. R. Walsh, B. Goundie, J. Wright, M. C. Wheeler, R. W. Meulenberg, W. J. DeSisto, B. G. Frederick, R. N. Austin, *Appl. Catal., A* **2010**, *388*, 57-67.
[22] (a) A. Y. Khodakov, A. Griboval-Constant, R. Bechara, V. L. Zholobenko, *J. Catal.* **2002**, *206*, 230-241; (b) D. Song, J. Li, *J. Mol. Catal., A: Chem.* **2006**, *247*, 206-212.
[23] H. Xiong, Y. Zhang, S. Wang, J. Li, *Catal. Commun.* **2005**, *6*, 512-516.
[24] A. Feller, M. Claeys, E. vam Steen, *J. Catal.* **1999**, *185*, 120-130.
[25] J. P. den Breejen, P. B. Radstake, G. L. Bezemer, J. H. Bitter, V. Frøseth, A. Holmen, K. P. de Jong, *J. Am. Chem. Soc.* **2009**, *131*, 7197-7203.
[26] C. C. Li, X. M. Yin, T. H. Wang, H. C. Zeng, *Chem. Mater.* **2009**, *21*, 4984-4992.
[27] N. Tsubaki, S. Sun, K. Fujimoto, *J. Catal.* **2001**, *199*, 236-246.
[28] K. Jalama, N. J. Coville, H. Xiong, D. Hildebrandt, D. Glasser, S. Taylor, A. Carley, J. A. Anderson, G. J. Hutchings, *Appl. Catal., A* **2011**, *395*, 1-9.
[29] K. Jalama, N. J. Coville, D. Hildebrandt, D. Glasser, L. L. Jewell, J. A. Anderson, S. Taylor, D. Enache, G. J. Hutchings, *Top. Catal.* **2007**, *44*, 129-136.
[30] L. Wang, H. Liu, Y. Chen, R. Zhang, S. Yang, *Chem. Lett.* **2013**, *42*, 682-683.
[31] P. Shi, R. Su, F. Wan, M. Zhu, D. Li, S. Xu, *Appl. Catal., B* **2012**, *123-124*, 265-272.
[32] D. D. Eley, H. Pines, P. B. Weisz, *Advances in Catalysis*, Elsevier Science, **1993**.
[33] M. V. Cagnoli, S. G. Marchetti, N. G. Gallegos, A. M. Alvarez, A. A. Yeramian, R. C. Mercader, *Mater. Chem. Phys.* **1991**, *27*, 403-418.
[34] G. Kishan, M. W. Lee, S. S. Nam, M. J. Choi, K. W. Lee, *Catal. Lett.* **1998**, *56*, 215-219.

[35] D. A. Wesner, G. Linden, H. P. Bonzel, *Appl. Surf. Sci.* **1986**, *26*, 335-356.
[36] (a) J. R. Anderson, M. Boudart, *Catalysis: science and technology*, Springer-Verlag, **1981, Chapter 4**; (b) R. B. Anderson, H. Kölbel, M. Rálek, *The Fischer-Tropsch synthesis*, Academic Press, **1984**.
[37] M. E. Dry, *Appl. Catal., A* **1996**, *138*, 319-344.
[38] J. W. Dun, E. Gulari, *Can. J. Chem. Eng.* **1986**, *64*, 260-266.
[39] H. Chen, A. A. Adesina, *Appl. Catal., A* **1994**, *112*, 87-103.
[40] M. Nagai, K. Matsuda, *J. Catal.* **2006**, *238*, 489-496.
[41] S. E. Colley, R. G. Copperthwaite, G. J. Hutchings, G. A. Foulds, N. J. Coville, *Appl. Catal., A* **1992**, *84*, 1-15.
[42] R. G. Copperthwaite, F. M. Gottschalk, T. Sangiorgio, G. J. Hutchings, *Appl. Catal.* **1990**, *63*, L11-L16.
[43] G. J. Hutchings, R. G. Copperthwaitet, F. M. Gottschalk, R. Hunter, J. Mellor, S. W. Orchard, T. Sangiorgio, *J. Catal.* **1992**, *137*, 408-422.
[44] M. J. Keyser, R. C. Everson, R. L. Espinoza, *Ind. Eng. Chem. Res* **1999**, *39*, 48-54.
[45] M. Anwar, C. A. Hogarth, R. Bulpett, *J. Mater. Sci.* **1990**, *25*, 1784-1788.
[46] H. P. Bonzel, H. J. Krebs, *Surf. Sci.* **1981**, *109*, L527-L531.
[47] J. M. G. Carballo, E. Finocchio, S. García-Rodriguez, M. Ojeda, J. L. G. Fierro, G. Busca, S. Rojas, *Catal. Today* **2013**, *214*, 2-11.
[48] V. G. Hadjiev, M. N. Iliev, I. V. Vergilov, *J. Phys. C.* **1988**, *21*, L199.
[49] A. P. De Moura, L. H. De Oliveira, P. F. S. Pereira, I. L. V. Rosa, S. L. Maximo, E. Longo, J. A. Varela, *Adv. Chem. Eng. Sci.* **2012**, *2*, 465-473.

8 Conclusion

A range of heterogeneous catalysts have been prepared, characterised and tested for the hydrogenation of carbon dioxide for the formation of hydrocarbons.

The use of MgO as a catalyst support was trailed and found to be effective for cobalt, iron and nickel based catalysts although selectivity to methane was high. The addition of palladium and dual promotion with palladium and potassium could increase CO_2 conversion and selectivity to C_2+ hydrocarbons. The 20wt%Co/1wt%Pd/1wt%K/MgO catalyst showed a methane selectivity of 68 %, close to the lowest value previously reported. While addition of silica as a co-support with 20wt%Fe/1wt%Pd/1wt%K/MgO catalyst could further improve CO_2 conversion this occurred at the expense of product selectivity which shifted towards methane.

The addition of palladium to iron-silica catalysts was found to greatly improve the catalyst's performance as a CO_2 hydrogenation catalyst for the formation of hydrocarbons. Both the iron and palladium loadings were found to have a significant impact on the catalyst performance. The effects of silica support properties were also studied with larger silica pore diameters found to give higher selectivities to heavier hydrocarbon products.

Life cycle assessment was utilised to study the preparation of the Fe-Pd/SiO_2 catalyst systems and found that most significant impacts associated were due to the use of palladium as a promoter and the electricity required. While the improved catalyst performance observed with increasing iron loading was seen to outweigh the increased environmental impact related to higher quantities of iron the same was not true for palladium. If palladium loading was increased beyond 1 wt% the observed enhancement in catalyst performance no longer outweighs the environmental impact associated with the use of larger quantities of palladium. The initial introduction of 1 wt% palladium is however necessary with its impact outweighed by the improved performance.

The lab scale process utilised for evaluation of the catalysts was, as expected, not viable in its current format from an environmental point of view. Further LCA work has shown that should the electricity and hydrogen for the process be obtained from renewable means and the overall process scaled up it has the potential to become environmentally viable.

A systematic investigation into the use of Group 11, 12 and 13 metals as potential promoters for iron-silica catalysts for CO_2 hydrogenation revealed several new and promising dopants. The effect of indium addition was two-fold with both an increase in CO_2 conversion and a significantly higher selectivity to desirable lower olefins. The addition of low loadings of gold was observed to have a similar effect with more lower olefins in the product stream and a higher CO_2 conversion. The dual promotion of the iron-silica system with both gold and palladium was found to significantly improve the catalyst performance beyond that observed when either gold or palladium were used alone as promoters.

The effect of reaction temperature on iron-silica catalysts was investigated and revealed that at lower temperatures the hydrogenation of CO_2 over these systems was limited by the rate of the surface reaction. When the temperature is increased however the reaction becomes mass transfer limited. Basic kinetic investigations suggested that the reaction is proceeding *via* the Langmuir-Hinshelwood mechanism.

Work conducted showed that with careful consideration of the support properties in combination with the correct promoter choice a cobalt-based catalyst can be developed for CO_2 hydrogenation that not only gives a high conversion but also a good selectivity to C_2+ hydrocarbons.

The pore size of the silica support used plays an important role in product selectivity with the larger pore diameter leading to larger Co_3O_4 crystallite sizes which gives a decreased methane selectivity and an increased chain growth probability. While the addition of an alkali metal can result in a decreased CO_2 conversion this is outweighed by a significant increase in selectivity towards heavier hydrocarbons with sodium performing best of the alkali metals tested.

The performance of Co-Na/SiO_2 can be improved further by the addition of molybdenum as a second promoter. Variation of both sodium and molybdenum loading showed that the optimum catalyst composition to be 20wt%Co/1wt%Na/3wt%Mo/SiO_2 which gave a CO_2 conversion of 57 % and a methane selectivity of 38 %, significantly lower than any value previously reported.